DOCTOR OF PHILOSOPHY

# Geochemical and mineralogical studies of the weathering of Silurian argillaceous rocks

Chapman, Paul

*Award date:*
1986

*Awarding institution:*
Bangor University

# GEOCHEMICAL AND MINERALOGICAL STUDIES

## OF THE WEATHERING OF SILURIAN ARGILLACEOUS ROCKS

by

Paul Chapman

A thesis presented for the degree of Ph.D. from the Department of Biochemistry and Soil Science, University College of North Wales, Bangor.

September 1986.

## SUMMARY

This work was carried out as part of the Natural Environment Research Council's geochemical cycling programme. Its aim was to identify the changes taking place in the constituent minerals as Silurian Gwestyn Shale weathers to a humic stagnopodsol soil at Plynlimon, mid Wales.

Hand specimen appearance and chemical analyses show that the rock groups present at Plynlimon are not homogeneous. The chlorites in different rocks are also shown to have significantly different chemical compositions, and are seen to be physically intergrown with mica. Another source of variation is that many of the soils are developed on glacial or periglacial deposits, rather than directly on rock.

Chlorite, the most rapidly altered mineral, was magnetically separated from the rock. It is characterised by microprobe analysis as a ripidolite, and is shown to be a IIb polytype by X-ray diffraction. It is shown to be high in octahedral Al, due to the presence of about 15% hydroxy interlayered vermiculite. The associated mica is a $2M_1$ polymorph.

Particle size separation coupled with quantitative X-ray diffraction analysis is used to demonstrate the changes in mineralogy with increasing weathering. The weathering of clay size chlorite and mica is studied in detail, with the favoured route for chlorite weathering being via hydroxy interlayered vermiculite and vermiculite. This suggests that the chlorite has suffered at least low grade metamorphism. The mica also alters via vermiculite.

The crystallinity of the mica, as measured by X-ray diffraction, apparently increases with increasing weathering. It is proposed that this is due to preferential dissolution of the least crystalline grains. On the basis of crystallinity and particle size data, it is proposed that some mica is illuviated from the Ea1 and Ea2 horizons to the Bsg. This finding is contrary to the accepted theories of podsol genesis.

ACKNOWLEDGEMENTS

My thanks are due: To Professors W.C. Evans and D.W. Ribbons for the provision of laboratory facilities and technical support within their department. To Drs. J.F.W. Bowles and A.R. Date at IGS, for providing analytical facilities in their laboratories. To the Natural Environment Research Council, who funded my post as Research Assistant at UCNW. To my colleagues on the geochemical cycling project for advice, encouragement and the provision of associated data: Ernie Biela at UCNW, Mike Hornung, Brian Reynolds, Aldyth Hatton and Paul Stevens at ITE, and Neil Breward and David Peachey at IGS.

To other colleagues in the Department of Biochemistry and Soil Science for advice on experimental procedures: Frank Price, Barrie Johnson and Ian Kelso. To John Conway, and particularly Chris Whittaker of the UCNW Statistics Advisory Service, for guidance on computing and statistical procedures. To David Jenkins, my supervisor, without whose direction this work could not have been either started or completed.

To Redland Technology Ltd., for the use of microscopy, image analysis, word processing and photocopying facilities. To Shirley Stevens, who has processed the words and typed the tables and diagrams for much of this thesis. Most of all to my wife, Denise, who has alternately supported and threatened me through a fraught first four years of marriage to both a husband and a thesis!

CONTENTS


| | PAGE |
|---|---|
| TITLE AND DECLARATION | i |
| SUMMARY | ii |
| ACKNOWLEDGEMENTS | iii |
| CONTENTS | iv |
| 1 INTRODUCTION | 1 |
| 2 LITERATURE REVIEW | 4 |
| 2.1 The Nature and Properties of Shales | 4 |
| 2.1.1 Classification | 5 |
| 2.1.2 Fabric | 7 |
| 2.1.3 Mineralogy and Geochemistry | 8 |
| 2.1.4 Geological Occurrence | 17 |
| 2.1.5 Particle Size Distribution | 18 |
| 2.1.6 Colour and Organic Matter Content | 19 |
| 2.1.7 Diagenesis and Metamorphism | 22 |
| 2.1.8 Porosity and Compaction | 24 |
| 2.2 Phyllosilicate Minerals | 25 |
| 2.2.1 Formation and Occurrence | 32 |
| 2.2.2 Kaolinites | 35 |
| 2.2.3 Micas and Expandable Minerals | 36 |
| 2.2.4 Chlorite Mineralogy and Classification | 46 |
| 2.2.5 Chlorite Occurrence | 56 |
| 2.2.6 Chlorite Identification | 57 |
| 2.2.7 Noncrystalline Clay Size Minerals | 59 |
| 2.3 The Weathering of Rocks and Minerals | 59 |
| 2.3.1 Physical Weathering | 61 |
| 2.3.2 Chemical Weathering | 61 |
| 2.3.3 The Weathering of Mica | 67 |
| 2.3.4 The Weathering of Chlorite | 73 |
| 3 PLYNLIMON SHALES AS A PARENT MATERIAL | 85 |
| 3.1 The Ideal Requirements for a Study of Weathering | 85 |
| 3.2 The Geography and Geology of Plynlimon | 88 |
| 3.2.1 Drift Deposits | 96 |
| 3.3 The Chemistry and Mineralogy of Plynlimon Shales | 97 |
| 3.4 The Soil Profiles Investigated | 106 |
| 4 SEPARATION OF MINERAL PHASES | 109 |
| 4.1 Introduction | 109 |
| 4.1.1 Magnetic Separation | 110 |
| 4.2 The Magnetic Separation of Chlorite from Suspension | 112 |
| 4.2.1 Separation from Finer than 2μm Starting Material | 117 |

4.2.2 Calgon Addition 122

4.3 A Critique of the Magnetic Separation Data of Rezk 130

4.4 The Separation of Illite 134

4.5 Conclusions 138

5 CHARACTERISATION OF MINERAL PHASES 139

5.1 The Electron Probe Microanalysis of Mineral Grains 139

5.1.1 Analytical Results 140

5.1.2 Discussion of the Mean Chlorite Analysis 141

5.1.3 Discussion of the Mean Mica Analysis 143

5.1.4 Statistical Analysis of Microprobe Data 144

5.1.5 Differences Between Chlorite Analyses 144

5.1.6 Differences Between Mica Analyses 148

5.2 The Chemical Analysis of Chlorite 148

5.3 Structural Formula Determination of Chlorite 150

5.3.1 c Axis Spacing Methods 152

5.3.2 b Axis Spacing Methods 157

5.3.3 Peak Intensity Methods 161

5.3.4 Investigation of Errors 170

5.3.5 Asymmetry Assessment 174

5.4 Polytype Determination of Chlorite 178

5.5 Polymorph Determination of Illite 180

5.6 Conclusions 182

6 QUANTITATIVE MINERALOGICAL ANALYSIS 185

6.1 Introduction 185

6.2 Particle Size Fractionation 186

6.2.1 Experimental Separation Procedure 187

6.2.2 Sample Preparation 189

6.2.3 Recalculation of Results 192

6.2.4 Interpretation of Particle Size Distributions 193

6.2.5 Breakdown of Shale Particles 208

6.2.6 Particle Size Distribution by the Bouyoucos Method 211

6.3 Quantitative Mineralogical Analysis by X-ray Diffraction 212

6.3.1 Chung's Method for Quantitative X-ray Diffraction Analysis 214

6.4 Experimental Techniques 217

6.4.1 Mineralogical Assumptions Made 222

6.4.2 Interpretation of Diffractometer Traces 224

6.5 Calculated Mineralogical Analyses 226

6.5.1 Mineralogy and Chemistry of Weathered Rock Surfaces 232

6.6 The Effects of Weathering on Mineral Distribution Patterns 233

7 COMPOSITIONAL VARIATION WITHIN MINERAL PHASES 236

7.1 The X-ray Diffraction Analysis of Clay Separates 236

7.1.1 Hydroxy Interlayered Vermiculite 244
7.1.2 Interpretation of Diffractometer Traces 245
7.1.3 Estimation of Vermiculite Content by X-ray Diffraction 259
7.2 The Chemical Determination of Vermiculite and Smectite 262
7.2.1 Interpretation of Results 266
7.3 The Effects of Weathering on Phyllosilicate Composition 270
8 CRYSTALLINITY DETERMINATION BY X-RAY DIFFRACTION 275
8.1 Introduction 275
8.2 Experimental Techniques 276
8.3 Illite Crystallinity Studies 281
8.4 The Effects of Interstratification on Crystallinity 289
8.5 Chlorite Crystallinity 296
8.6 The Effects of Other Factors on Crystallinity 299
8.7 The Effects of Weathering on Mineral Crystallinity 301
9 SURFACE AREA ESTIMATION 305
9.1 Introduction 305
9.1.1 Surface Area Determination Methods Using Adsorption of Alcohols 308
9.2 Experimental Techniques 313
9.3 Ethanl,2diol Adsorption Measurements 316
9.3.1 Variation of Surface Area with Particle Size 319
9.3.2 Comparison of Surface Area and Particle Size Data 322
9.4 The Effects of Weathering on Mineral Surface Area 326
10 CONCLUSIONS AND DISCUSSION 329
10.1 Shale Weathering at Plynlimon 329
10.1.1 Magnetic Separation 330
10.1.2 Mineralogical Investigation 331
10.1.3 Dithionite Pretreatment 332
10.1.4 Mineral Weathering 333
10.1.5 Crystallinity 336
10.1.6 Other Investigations 337
10.2 Plynlimon - Representative or Anomalous? 337
10.3 Building on Plynlimon 339
APPENDIX - TABLES, PROFILE DESCRIPTIONS AND FIGURES 341
REFERENCES 367

# CHAPTER 1

## INTRODUCTION

This thesis presents the results of work carried out as part of a co-operative project in the Natural Environment Research Council's geochemical cycling programme, which was set up in 1978. The project as a whole sought to investigate mineral weathering in terms of the links in the geochemical cycle between rock, soil and fresh water, and its co-operative nature enabled expertise in several related fields to be focussed on a single experimental site. The study involved workers from the Institute of Terrestrial Ecology (ITE), the Institute of Geological Sciences (IGS, now the British Geological Survey) and the Institute of Hydrology (IH), as well as from the University College of North Wales (UCNW).

The main objectives of the project as a whole were:

1. To investigate the breakdown of bedrock and its mineral components, and the consequent release of both major and nutrient elements to the overlying soils.

2. To investigate the movement of elements released by weathering within the soil profiles, and to relate elemental movement into drainage waters to the controlling environmental factors.

3. To relate the elemental contents of the rock to those of the associated drift, soils and stream sediments, and to investigate factors causing variation in the chemistry of the stream sediments.

Although some overlap was seen as inevitable, the responsibility for achieving these objectives lay respectively with UCNW, ITE and IGS.

IH's Wye experimental catchment at Plynlimon in mid Wales was chosen for the work by ITE because its bedrock, soils, climate, vegetation and land use are representative of similar areas throughout upland Britain, and because a large amount of background information on the climate, soils, geology and streamflow of the site were already available.

At UCNW, the effort was shared by two workers, with the responsibility of one being to investigate the effects of weathering on the rock and soils, and thus to determine the breakdown paths that were being followed, and that

of the other being to simulate these breakdown paths in the laboratory, to determine elemental release rates, and to apply these data to the findings on weathering in the field, in order to calculate the elemental release occurring under field conditions. This thesis presents the results of the investigation into the natural breakdown paths of the rock and soil minerals.

The Wye catchment includes a limited variety of sedimentary rock types, with shales being the dominant lithology, and an appropriate shale sample was thus chosen to be representative of the bedrock in the catchment. There is a much greater variety of soil types, but humic stagnopodsols are typical of the soils developed on periglacial deposits, rather than boulder clay, and thus a Hiraethog series soil was studied in most detail.

To define the starting material of the weathering sequence in detail, magnetic separation of the mineral phases and then quantitative chemical and microprobe analysis was carried out. Quantitative particle size analysis of the rock and soil horizons, and then quantitative mineralogical analysis of each of the separated size fractions, enabled the alteration paths of the major minerals to be followed from the rock to the upper soil horizon and from coarse to finest particles. The use of qualitative mineralogical techniques and the determination of the mineral crystallinity allowed subtle details of the alteration, which could not be observed by the quantitative techniques employed, to be examined. Surface area analysis of different size fractions from the soils provided further details of the alteration processes, and thus an overall picture of the breakdown of the component minerals of the shale, as it was transformed into the soil, was built up.

Following this introduction, Chapter 2 of the thesis provides a literature review of shales and phyllosilicate minerals in general, and then turns to the findings of previous workers in the fields of chlorite and mica weathering. To summarise these findings is particularly important, as two different views as to the major route for chlorite weathering have been put forward, and only in 1974 was a reconciliation between these two views suggested [227]. Chapter 3 then presents the background to the present study, providing descriptions of the geography and geology of the site at Plynlimon, and of the soil profiles sampled, together with a detailed study of the shales investigated.

Having described the materials collected in the field, Chapter 4 details how individual mineral phases were separated from the bulk samples, whilst

Chapter 5 covers the characterisation of these phases in terms of mineralogy and chemistry. Based on this coverage of the individual phases, Chapter 6 then works to quantify the occurrence of the different phases throughout the materials investigated.

As Chapter 6 reveals the variation in mineral distribution patterns, so Chapters 7, 8 and 9 respectively detail the accompanying variation in the chemical and mineralogical compositions of the phases, their crystallinity, and their surface areas. Finally, Chapter 10 summarises the findings of the thesis, compares them with the findings of other workers, and suggests further investigations that could usefully be carried out.

The results thus provide the detailed evidence for mineral breakdown required to be employed in the laboratory study of mineral breakdown rates, and in the investigation of the transport of released elements through the soil solution into the stream waters. Whenever possible, results have been compared with those of Rezk [219] and Adams and his colleagues [1,91-95,244,245], who have carried out important studies of the weathering of similar shales under similar environmental conditions elsewhere in Wales.

To conclude, it is believed that this thesis provides at least partial answers to the questions:

1. What is the mode of weathering of chlorite?

2. How are minerals distributed between different particle size fractions in soils undergoing weathering?

3. How does weathering affect mineral crystallinity?

# CHAPTER 2

# LITERATURE REVIEW

## 2.1 THE NATURE AND PROPERTIES OF SHALES

In the past many terms have been used to describe fine grained terrigenous rocks and sediments, and still there is little agreement over terminology [261]. "Shale" is used both as the class name for fine grained rocks and sediments that contain more than 50% of terrigenous clastic components that are finer than 62μm in maximum dimension [209], and also for only those rocks in the class which show fissility or are dominantly composed of phyllosilicates [206]. Mudrock is also used as the class name [206], with unconsolidated fine grained sediments being known as muds, clays or silts, depending on their grain size distribution. Mudstone, claystone and siltstone can be used for their consolidated equivalents, but are generally only used for rocks that show no fissility.

In this study, shale will be used as the class name, including both fissile and nonfissile rocks. When used in this sense, more than 60% of the sedimentary record consists of shale, which is estimated to constitute 44 to 56% of all rocks exposed at the continental surface. Utilising the British Standards Institution (BSI) system for particle size classification [35,42], on average modern muds consist of 15% sand, 45% silt and 40% clay size particles, whilst grain size analysis suggests that most shales contain more than 50% of silt size (2-62μm) particles; this observation is confirmed by thin section studies. Pettijohn estimated that the average shale was composed of two thirds silt and one third clay particles [206]. Geochemical considerations suggest that shale should constitute 80% of all sediments.

The study of shale lagged behind that of most other sedimentary rocks for two main reasons. Shales were once of less immediate economic interest than other sediments; sandstones and limestones were often used as building stones, and sandstones were found to be common reservoir rocks for oil and water. However, economic interest in shales has increased substantially now that shale is known to be the most common petroleum source rock. Secondly, the practical reason was that, until very recently, it was almost impossible to identify and study single particles in shales due to their small grain size, thus preventing a sedimentary history of the rock being built up. An

overview of the present knowledge of shales, together with an extensive bibliography, is provided by [209], and this, together with the relevant chapters in [29,206], provides the basis for this section, except where other references are cited.

### 2.1.1 Classification

There have been several attempts to classify shales [89,162,206,210, 261], but no one system has been widely accepted. Shales contain significant percentages of fine grained phyllosilicates and other clay size particles, whose properties dominate the properties of the rock as a whole because of their large specific surface areas. Wentworth defined clay size as finer than 1/256mm (3.9μm) [261], but most phyllosilicate particles are in fact finer than 2μm [209], except in well consolidated shales, where they may be silt size [261]. Any classification should recognise the importance of these components, but remove the confusion that has been caused by the term "clay" having both mineralogical and textural connotations [261]. In this study, clay will be used only as a textural term; "phyllosilicate" will be used instead of the often used phrase "clay mineral".

A classification based on description will outlast classifications based on changing genetic interpretations, as in shales it is difficult to identify the separate components, let alone account for their genesis. It is likely that a descriptive classification of shales will eventually be shown to have genetic significance, particularly with regard to the diagenetic and metamorphic history of the rock, as well as to source and sedimentary environments [261]. Genetic classifications based on whole rock criteria, such as the $Al_2O_3/Na_2O$ maturity index [206], or more sophisticated weathering indices [89], neglect the fact that the rock is a summation of its individual components and their individual histories, and not a single entity with a single history. They may provide a useful means of following chemical changes due to weathering in a series of closely related sediments, but are unable to provide an overall classification of argillaceous sediments, as they ignore the many variables that cannot be quantified by a chemical formula.

Many classifications, including that of Potter et al [209], incorporate thickness of stratification and degree of induration (Table 2.1), whilst emphasising that the classification must be based on lamination, rather than fissility [62]. On the other hand, Lewan [162] classifies

| Percentage of Clay Size Particles | | 0-33 | 33-67 | 67-100 |
|---|---|---|---|---|
| Field Description | | Gritty | Loamy | Fat |
| Nonindurated | Beds >10mm thick | Bedded Silt | Bedded Mud | Bedded Claymud |
| | Laminae <10mm thick | Laminated Silt | Laminated Mud | Laminated Claymud |
| Indurated | Beds >10mm thick | Bedded Siltstone | Mudstone | Claystone |
| | Laminae <10mm thick | Laminated Siltstone | Mudshale | Clayshale |
| Metamorphosed | Low grade | Quartz Argillite | Argillite | |
| | Medium grade | Quartz Slate | Slate | |
| | High grade | Phyllite or Mica Schist | | |

Table 2.1 Classification of Shales after Potter et al [209]

| Stratification Thickness (mm) | Stratification Description | | Parting Description | Composition |
|---|---|---|---|---|
| 30-300 | Thin | Bedding | Slabby | High sand, silt and carbonate contents |
| 10- 30 | Very thin | | | |
| 5- 10 | Thick | Lamination | Flaggy | |
| 1- 5 | Medium | | Platy | |
| 0.5- 1 | Thin | | Fissile | High clay & organic matter contents |
| <0.5 | Very thin | | Papery | |

Table 2.2 Classification of Shale Stratification after Potter et al [209]

shales without reference to bedding, lamination or fissility, believing that field evidence shows fissility to be a function of weathering, increasing with the degree of weathering. Instead, the content of material below the limit of optical resolution (taken as 5μm) is used to divide shales from mudstones, and further classification is based on the mineralogy of the whole rock, as determined by semiquantitative X-ray diffraction (XRD). Similarly, Weaver [261] avoids terms with structural connotations, basing his classification on the occurrence of phyllosilicates and clay size material. In both of these classifications, an optional descriptive term to emphasise particular characteristics of the shale is included in the nomenclature. A more esoteric classification utilises X-radiographs of fabric to place a shale into one of four categories, which reflect compositional as well as fabric variation [197]. Although it may be debatable whether fissility is a primary characteristic of shales [261], it is certainly a most useful, if not essential, criterion for any classification used in weathering studies.

### 2.1.2 Fabric

> "The thickness of stratification and parting in shales is related to many factors, including rates of sedimentation and compactional state. However, field observations suggest that the most obvious factors are composition, grain size and fabric. Stratification and parting generally decrease in thickness as the relative amounts of clay minerals and organic compounds increase, as the degree of orientation of platy minerals increases, and as the percentages of sand and silt sized mineral fragments decrease." [209]

Where stratification occurs on a scale of less than 10mm, it is defined as lamination [209], and is usually due to subparallel orientation of platy micaceous minerals. Random orientation may be due to bioturbation of the original sediment, authigenic mineral formation, deposition of the phyllosilicate particles as floccules, or extremely uniform sedimentation over a long period of time. Very thin laminations are of three main kinds: alternations of coarse and fine particles, of dark organic rich and light organic poor layers, or of carbonate and silicate material. Many of these laminations have a structure and thickness suggestive of yearly laminations, or varves, which can be seen forming at the present day and depend on the yearly climatic cycle. Shales with continuous thin laminae tend to contain coarser silt fractions than those that are unlaminated or have discontinuous lenticular laminations [197].

Fissility is the tendency of a shale to part along the plane of stratification, whilst the development of slaty cleavage is independent of stratification, being caused by metamorphic processes. Potter et al [209] suggest a refinement of previous schemes to classify stratification and parting (Table 2.2).

Increased fissility is favoured by high proportions of well crystallised silt size phyllosilicate grains [261], whose unbalanced charge is concentrated on faces rather than edges. Kaolinites have a small negative charge on their crystal faces due to a limited degree of isomorphous substitution [249], but a positive charge on crystal edges [242], resulting in the possibility of edge to face attraction between particles and, potentially, a massive rock. Because positive charges on crystal edges are less important for other phyllosilicates, their particles tend to form parallel arrangements, although montmorillonite may form cardhouse structures (Figure 2.1). Organic rich shales are often exceptionally fissile. They contain abundant straight chain hydrocarbons with terminal substitution of polar groups, which are attracted to the phyllosilicate surfaces. Fissility develops because of the lack of interaction between the ends of the organic molecules not attached to the phyllosilicates (Figure 2.2).

Shales are not commonly bonded by a chemical cement, as are coarser sediments, but the larger grains are embedded in a matrix of smaller grains, often of similar composition. Most shales have an internal stratigraphy defined primarily by variations in organic matter content, as revealed by colour, but also by changes in density, mineralogy, bedding, lamination, bioturbation and fossil content. Individual horizons can often be correlated over very wide areas, reflecting the fact that shales have a greater lateral continuity than their associated facies.

### 2.1.3 Mineralogy and Geochemistry

In contrast with the difficulty involved in studying individual grains in shales, their bulk mineralogical and geochemical properties have been extensively studied. Several schemes have been proposed to calculate shale mineralogy from the basis of a bulk chemical analysis, in the same way as normative calculations are used for igneous rocks [132,193]. These schemes suffer from a somewhat arbitrary choice of the calculated minerals, no doubt to suit the authors' particular needs, and also from the problem that phyllosilicates have very

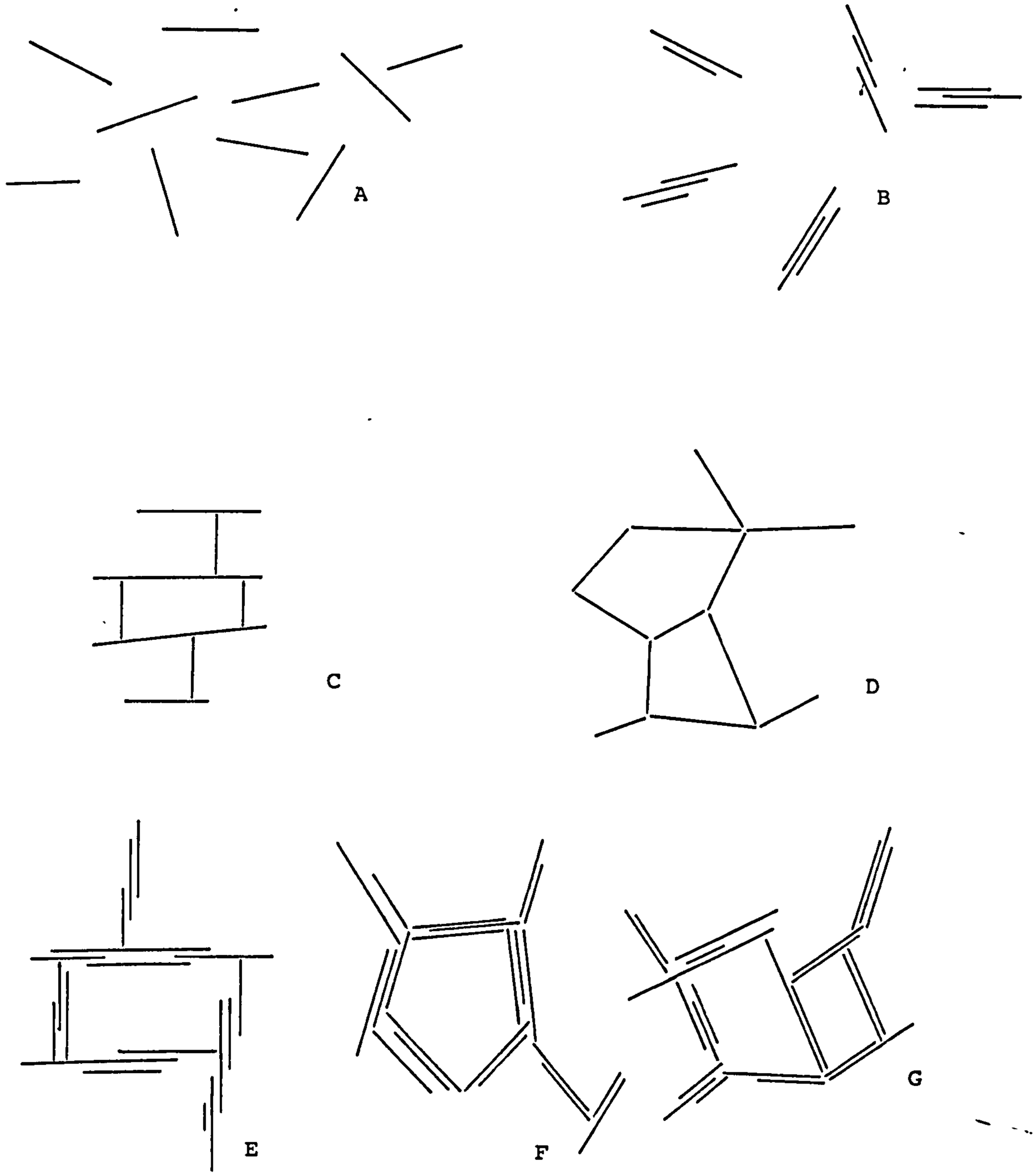


Figure 2.1 Modes of Particle Association in Clays after Van Olphen [249]

A - Dispersed and deflocculated; B - Face to face aggregated but deflocculated;
C - Dispersed but edge to face flocculated; D - Dispersed but edge to edge flocculated;
E - Aggregated and edge to face flocculated; F - Aggregated and edge to edge flocculated;
G - Aggregated and both edge to face and edge to edge flocculated.

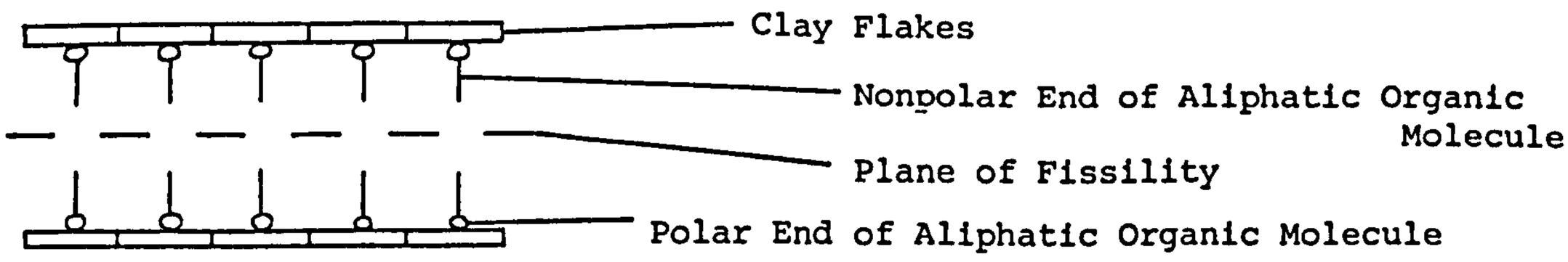


Figure 2.2 A Schematic Diagram Showing the Relationship Between Polar Aliphatic Molecules, Clay Flakes and Fissility in Paper Shales after Blatt et al [29]

variable compositions. Although these normative schemes may make no allowance for the presence of plagioclase [132], or even of feldspar at all [193], they can provide a useful basis on which to compare the potential mineralogy of fine grained sediments for which other information is limited, as phases such as feldspar usually only occur to the extent of a few percent or less.

The problems resulting from assigning fixed chemical compositions to normative minerals have been assessed [140], and it is suggested that semiquantitative XRD gives an estimate of mineralogy more closely correlated with the petrographic mode than that given by a norm calculated from chemical analysis, although chemical analysis is still required to estimate the contents of minor mineral phases such as rutile and apatite. For instance, the unreasonable postulate that no $Fe^{2+}$ occurs in illite or chlorite [132] can result in the miscalculation of Fe rich chlorite as montmorillonite, which is especially misleading if the normative mineralogy is used as an indicator, albeit a broad one, of the phyllosilicate assemblage of the rock.

Phyllosilicates and quartz make up the bulk of most shales, with feldspars, Fe oxides and carbonates being common minor minerals, although a wide range of other minerals can be found in different shales. Phyllosilicates will be reviewed in greater detail in Section 2.2, because of their relevance to this study, but the other minerals found in shales can usefully be considered here:

1. Quartz forms between 20 and 30% of the average shale, although optical studies generally underestimate its proportion. By weight, 12% is sand size, 73% silt size and 15% clay size, with a mean at 14μm [30], resulting in nearly all grains being monocrystalline. In thin section, grain boundaries appear fuzzy, due to the smearing of phyllosilicates, the presence of Fe oxides and the finite depth of focus of the microscope. The grains are angular and often appear to be elongate, but rounding increases with grain size. This may be due to derivation from foliated metamorphic rocks or, more likely, to shaping of larger grains by chipping during transport [222,239]. It has been suggested that much silt size quartz originates from glacial grinding [239,254], and some from aeolian attrition [239], but it now seems that most silt size grains are produced during soil formation [244]. Almost

all the quartz is detrital, and some may be of aeolian origin, although some authigenic quartz can be found. Silica may also occur in a noncrystalline form, or as chalcedony or opal, all of which may have a biogenic origin.

The common assumption, also made by Pettijohn [206], that silt size material in shales is dominated by quartz, is shown to be mistaken when the actual particle size and mineral distributions found in shales are examined more closely [261]. Average free silica contents from compilations of data on shales vary between 22.3 and 32.2% [93,261], with values for individual shales falling between 3 and 78% [30]. However, an analysis of 158 Ordovician shales gives an average of 3% sand, 59% silt and 38% clay size particles [261], indicating that, in general, quartz must compose less than 50% of the silt fraction of a shale. The quartz that is present is nevertheless mainly found in the silt fraction, with only 11.6% of the total quartz occurring as sand size grains and 15.4% as clay particles [30].

In 10 Lower Palaeozoic shales from mid Wales the free silica content varied from 26 to 37%, with a mean of 32.2%; 90% of the free silica occurred as silt size grains, and the remaining 10% as clay particles [93].

A good correlation can be found between the percentage of crystalline silica in a sediment, and the mean size of the silica particles. Extrapolation of the regression line so produced indicates that no quartz particles finer than 1.8μm will be found in the average shale, and that only 16% of all shales will contain any quartz finer than 0.6μm [30].

2. Feldspar is nearly always less abundant than quartz, but very little is known about its occurrence in shales. It is believed that plagioclase is more common than alkali feldspar, while some feldspar may be authigenic.

3. Zeolites are commonly found in shales which have a volcaniclastic component, where they are derived from the alteration of smectite, whilst authigenic phillipsite and clinoptilolite occur in modern marine sediments in amounts of up to a few percent.

4. Fe oxides and hydroxides commonly occur as coatings on phyllosilicate grains. Hematite is the most common oxide in shales, but during deposition, weathering and pedogenesis, hydrous oxides such as goethite, ferrihydrite and lepidocrocite are more common. Fe oxides form 6 to 7% of most shales, and rarely make up more than 10% of the total rock.

5. Carbonates in shales are little understood, except where they are related to usual morphologies such as concretions or cone-in-cone structures. Calcite is dominant, but dolomite, ankerite and siderite have also been reported. Calcite and its polymorph aragonite may occur in the form of a chemical precipitate or as biogenic detritus, but aragonite is not stable below 50°C and, on a geological time scale, is rapidly dissolved or replaced by calcite.

6. Pyrite of widely varying crystal size is commonly formed authigenically in organic rich shales. Both Fe and S are common in most depositional environments, and the presence of organic matter can bring about the reduction of sulphate to sulphide and the consequent production of Fe sulphides. Modern anoxic muds commonly contain noncrystalline Fe sulphides, but only crystalline $FeS_2$, as pyrite or marcasite, is found in ancient sediments. $FeS_2$ is much more abundant in marine than nonmarine shales, and both forms indicate strongly reducing conditions, either at the sediment/water interface or within the sediment.

7. Sulphates, including gypsum, anhydrite and barite, can occur as concretions, and may indicate hypersalinity during deposition or diagenesis. Sulphates can also form by atmospheric oxidation of sulphides during weathering.

8. Phosphates, especially apatite, form nodules in slowly deposited marine sediments in areas of high organic productivity. Rare earth element (REE) phosphates, such as monazite, can be surprisingly common as silt size grains in shales.

9. Heavy mineral assemblages are very variable, although zircon and tourmaline are two of the heavy minerals most commonly found. They are often best preserved in concretions, and may also be concentrated into specific horizons by sedimentary processes. The

average shale analysis contains more than 0.5% $TiO_2$, and this is mostly found in the heavy mineral fraction as rutile, anatase, sphene or ilmenite.

Many compilations of chemical analyses of shales have been published, and it is instructive to consider these analyses with regard to the mineralogy and depositional environment of the shales concerned. $SiO_2$ and $Al_2O_3$ are the dominant components of all nonexotic shales because of the preponderance of quartz and phyllosilicates in the rock. The $K_2O$ in a shale analysis is usually found in illite, the $Fe_2O_3$ in hematite, the CaO and $CO_2$ in calcite and dolomite, the FeO and MgO in chlorite and the $Na_2O$ in feldspar and smectite. Deviations of any oxide component in the analysis from an average value can usually be associated with raised or lowered levels of the corresponding minerals.

Defining the composition of an average shale is difficult, as many of the published compilations are not composed of randomly selected analyses, but Table 2.3 gives several analyses showing the variation in composition with age and degree of metamorphism. It is uncertain whether the increase of $K_2O$ content with age is simply due to increased diagenesis, or whether it is due to a change in earth surface chemistry, possibly related to the appearance of land plants. Within a single shale the chemical composition varies considerably between size fractions, reflecting the fact that phyllosilicates dominate the finer fractions and quartz the coarser fractions (Table 2.4). In fact there are also grain size differences between the phyllosilicates, which can be reflected in the chemical composition of different size fractions. Kaolinite forms the largest flakes, and illite commonly has flakes 0.1-0.3μm in length, whilst montmorillonite flakes are the smallest, but almost invariably occur in the form of floccules about the same size as single illite flakes.

Due to the fact that mineralogy is difficult to relate in more than a general way to chemical analysis, estimates of the average mineralogy of shales vary even more widely than estimates of shale chemistry (Table 2.5). Provenance has a dominant control over shale chemistry, but depositional environment can play a minor part, especially in the distribution of exchangeable cations in phyllosilicates. Diagenesis and metamorphism have little effect on the bulk chemical composition of shales, but exchangeable cations can be readily altered by circulating pore waters.

| Constituent | A | B | C | D | E | 1040 | 1039 |
|---|---|---|---|---|---|---|---|
| % $SiO_2$ | 58.10 | 55.43 | 60.15 | 60.64 | 56.30 | 63.39 | 59.50 |
| % $TiO_2$ | 0.65 | 0.46 | 0.76 | 0.73 | 0.77 | 1.13 | 1.31 |
| % $Al_2O_3$ | 15.40 | 13.84 | 16.45 | 17.32 | 17.24 | 17.63 | 23.25 |
| % $Fe_2O_3$ | 4.02 | 4.00 | 4.04 | 2.25 | 3.83 | 9.26 | 6.71 |
| % FeO | 2.45 | 1.74 | 2.90 | 3.66 | 5.09 | | |
| % MgO | 2.44 | 2.67 | 2.32 | 2.60 | 2.54 | 2.38 | 1.61 |
| % CaO | 3.11 | 5.96 | 1.41 | 1.54 | 1.00 | 0.13 | <0.05 |
| % $Na_2O$ | 1.30 | 1.80 | 1.01 | 1.19 | 1.23 | 1.17 | 1.12 |
| % $K_2O$ | 3.24 | 2.67 | 3.60 | 3.69 | 3.79 | 2.89 | 4.17 |
| % $H_2O^+$ | 5.00 | 3.45 | 3.82 | 3.51 | 3.31 | n.d. | n.d. |
| % $H_2O^-$ | | 2.11 | 0.89 | 0.62 | 0.38 | n.d. | n.d. |
| % $CO_2$ | 2.63 | 4.62 | 1.46 | 1.47 | 0.84 | n.d. | n.d. |
| % Organic Carbon | 0.80 | 0.69 | 0.88 | n.d. | 1.18 | n.d. | n.d. |
| % Miscellaneous | 0.81 | 1.04 | 0.77 | 0.38 | 2.50 | 0.24 | 0.12 |
| Total | 99.95 | 100.48 | 100.46 | 99.60 | 100.00 | 98.22 | 97.79 |

Table 2.3 Chemical Compositions of Average Shales and Plynlimon Shale and Boulder Clay

A = Average shale based on columns B and C [61]

B = Composite sample of 27 Mesozoic and Cenozoic shales [61]

C = Composite sample of 51 Palaeozoic shales [61]

D = Unweighted average of 36 analyses of slate (29 Palaeozoic, 1 Mesozoic and 6 early Palaeozoic or Precambrian) [86]

E = Unweighted average of 33 analyses of Precambrian slates [190]

1040 = Unweathered Plynlimon shale

1039 = Plynlimon boulder clay

n.d. = Not determined

| Constituent | Size Fraction (μm) | | |
|---|---|---|---|
| | <1 | 1-5 | 5-50 |
| % $SiO_2$ | 40.61 | 48.07 | 61.29 |
| % $TiO_2$ | 0.79 | 0.89 | 0.85 |
| % $Al_2O_3$ | 18.97 | 18.83 | 13.30 |
| % $Fe_2O_3$+FeO | 7.42 | 6.91 | 3.94 |
| % MgO | 3.19 | 3.56 | 3.31 |
| % CaO | 6.24 | 4.96 | 5.11 |
| % $Na_2O$ | 1.19 | 1.17 | 1.32 |
| % $K_2O$ | 2.62 | 2.57 | 2.33 |
| % Ignition Loss | 12.51 | 10.91 | 7.05 |
| % Kaolinite and Smectite | 23.2 | 17.0 | 7.5 |
| % Illite | 22.1 | 21.2 | 16.6 |
| % Quartz | 13.1 | 19.3 | 36.7 |
| % Chlorite | 7.3 | 10.3 | 8.2 |
| % Fe oxides and Pyrite | 8.0 | 5.5 | 3.0 |
| % Carbonates | 5.7 | 7.5 | 10.5 |
| % Feldspars | 7.3 | 7.2 | 12.6 |
| % Zeolites | 6.9 | 7.5 | 3.0 |
| % Heavy Minerals | 1.7 | 2.0 | 1.7 |
| % Carbonaceous Matter | 0.6 | 0.9 | 0.2 |
| % Moisture | 4.1 | 1.3 | 0.9 |
| Total | 100.0 | 99.7 | 100.9 |

Table 2.4 Chemical Analyses and Recalculated Mineralogy for Different Size Fractions, Based on an Average of 1 Ordovician Shale, 2 Cretaceous Clays, 1 Residual Clay and 8 Clays of Glacial or Recent Origin [117,206]

| Constituent | Source of Analysis | | | |
|---|---|---|---|---|
| | [61] | [157] | [271] | [236] |
| Quartz and chert | 22.3 | 32 | 20 | 31 |
| Feldspar | 30.0 | 18 | 8 | 4.5 |
| Phyllosilicates | 25.0 | 34 | 59 | 61 |
| Fe oxides | 5.6 | 5 | 3 | <0.5 |
| Carbonates | 5.7 | 8 | 7 | 3.6 |
| Other Minerals | 11.4 | 1 | 3 | - |
| Organic Matter | - | 1 | - | 1 |

Table 2.5 Estimates of Average Shale Mineralogy

| Particle Diameter (μm) | % of Total Sediment |
|---|---|
| 500-1000 | trace |
| 250- 500 | trace |
| 125- 250 | 6 |
| 62.5- 125 | 23 |
| 31.2-62.5 | 30 |
| 15.6-31.2 | 16 |
| 7.8-15.6 | 7 |
| 3.9- 7.8 | 7 |
| <3.9 | 11 |

Table 2.6 A Composite Particle Size Distribution of Mississippi Delta Sediment, Based on 300 Surface and Borehole Samples after Pettijohn [206]

| Constituent % | Source of Analysis | | | |
|---|---|---|---|---|
| | [61] | [157] | [271] | [236] |
| Quartz and chert | 22.3 | 32 | 20 | 31 |
| Feldspar | 30.0 | 18 | 8 | 4.5 |
| Phyllosilicates | 25.0 | 34 | 59 | 61 |
| Fe oxides | 5.6 | 5 | 3 | <0.5 |
| Carbonates | 5.7 | 8 | 7 | 3.6 |
| Other Minerals | 11.4 | 1 | 3 | - |
| Organic Matter | - | 1 | - | 1 |

Table 2.5 Estimates of Average Shale Mineralogy

| Particle Diameter (μm) | % of Total Sediment |
|---|---|
| 500-1000 | trace |
| 250- 500 | trace |
| 125- 250 | 6 |
| 62.5- 125 | 23 |
| 31.2-62.5 | 30 |
| 15.6-31.2 | 16 |
| 7.8-15.6 | 7 |
| 3.9- 7.8 | 7 |
| <3.9 | 11 |

Table 2.6 A Composite Particle Size Distribution of Mississippi Delta Sediment, Based on 300 Surface and Borehole Samples after Pettijohn [206]

The trace element geochemistry of shales has been widely studied, but may have more potential for stratigraphic correlation than for determining the depositional environment, although B has been used successfully to distinguish marine from nonmarine shales.

Shale is not simply a lithified residual clay weathering product, as in situ lithified weathering profiles are rare in the geological record. The components of shale have usually been transported, often over considerable distances, to their place of deposition. Shales have higher contents of silt size grains, and thus higher $SiO_2$ contents, and also have higher contents of $K_2O$, MgO and CaO than residual clays. These components are added to the products of weathering during deposition and diagenesis, when degraded phyllosilicate structures are at least partially reformed.

### 2.1.4 Geological Occurrence

Several generalisations can be made about the occurrence of shales in the sedimentary record:

1. Most shales are marine, and thus thick shale sequences are most common in marginal basins, rather than in cratonic or piedmont environments, although widespread thin shales can cover vast areas on cratons.

2. Most thick shales are related to distal turbidites, and thus were deposited in relatively deep water, although shales can be found accumulating in protected basins at any depth of water.

3. At the present day, shale is the dominant lithology of the deep ocean basins, in the form of thin, wide ranging units deposited slowly from suspension. Some particles may have been transported by wind, and interbedding with volcaniclastics is common near midocean ridges or marginal trenches. When deposited below the calcite compensation depth, shale is free from carbonates, unless they have been introduced into the sediment by turbidity currents.

4. Shale sequences usually have a clinoform structure, related to the original basin geometry. Faults, flowage structures and mud diapirs, generated by overpressuring in the unconsolidated sediment, are the dominant small scale structures in marginal basin shales.

5. Overpressuring, and shale deposition in general, implies a high rate of sediment supply, and thus the source land mass must have had high relief, high rainfall, or both. Because clay size particles can remain suspended in turbulent water indefinitely, the source of sediment supply may actually be far removed from the depositional site, and settling can only occur when the clay particles form flocculated aggregates. Kaolinite tends to flocculate at lower salinities than other phyllosilicates, and it is suggested that this is the cause of the kaolinite content of a shale often increasing towards the sediment source. However, kaolinite also tends to form larger single crystals than the other phyllosilicates, and this alone may account for its more rapid deposition.

6. Reconstruction of the depositional environment of a shale requires a study of the sedimentary structures of minor interbedded siltstones, sandstones and limestones, and an integrated study of the shale, its associated beds, and their lateral equivalents is essential in discovering the correct facies model.

### 2.1.5 Particle Size Distribution

Determining the particle size distribution of a shale is complicated both by the commonly used analytical methods and by the effects of diagenesis, and thus caution must be exercised in working back to an environment of deposition from a particle size distribution. Diagenesis can greatly alter the grain size distribution of a shale, especially amongst the finest clay size particles. These may be unstable under the conditions of diagenesis, and their very large specific surface areas allow any chemical alteration to proceed rapidly.

Particle size distributions of silt and clay fractions are commonly determined by methods based on quantifying the percentage of the total specimen that settles through a measured distance of water in a time equal to the settling time over the same distance of quartz spheres of a known diameter. The obvious problem is that not all particles have the same density and shape as quartz spheres; denser particles settle faster, and are falsely counted into a coarser size fraction. On the other hand, any deviation from a spherical shape increases the viscous drag on the particle, and thus its settling time, resulting in nonspherical particles being falsely counted into a finer size

fraction. Developing the concept of "equivalent spherical diameter" (esd), which is the actual physical size of a grain of a given mineral which settles at the same velocity as a quartz sphere of defined diameter, enables useful results to be obtained from specimens of similar mineralogy, even though in a given size fraction the mica flakes may be larger than the quartz grains. Fractions coarser than 20μm are usually separated by sieving, which tends to underestimate the size of nonspherical particles. The fraction that has its upper boundary determined by sieving and its lower boundary by sedimentation is particularly susceptible to inaccuracies, because the relationship between the real and the determined particle size distribution is different for the two methods of fractionation. This can result in inflexions appearing at the transitional grain size in particle size distributions [256]. The grain size distribution of sediments deposited in the Mississippi Delta (Table 2.6) is given as a possible representative of the grain size distribution of an average shale.

Before the determination of particle size distribution can be carried out, the material has to be disaggregated and dispersed. Disaggregation of indurated shales requires considerable grinding, and the resulting particle size distribution may be more related to the properties of the grinding mill than those of the sediment. Dispersion can be chemical or mechanical; either may seriously alter the natural size distribution of fine silt and clay particles, especially where the original sediment was flocculated or deposited as pellets.

### 2.1.6 Colour and Organic Matter Content

More emphasis is placed on the colour of shale than on that of other sedimentary rocks, as colour variation in shales is an excellent guide to stratigraphic subdivision and can also be used to indicate depositional environment. To a large extent, the colour of a shale is controlled by the content of organic C, both directly and through its effect on the $Fe^{3+}/Fe^{2+}$ ratio, although finely disseminated Fe sulphides can impart a strong black colour to shales with an organic C content less than 1%. Some shales may be coloured by Mn oxides, particularly in the form of dark stains on cleavage or bedding surfaces. Figure 2.3 shows that shales partition into two colour series. In the first series, from red through purple to greenish grey, the pigmentation is dominantly controlled by $Fe^{3+}$, but in the second series, from greenish grey through grey to black, all the Fe is reduced and pigmentation is predominantly due to the organic C content. Even

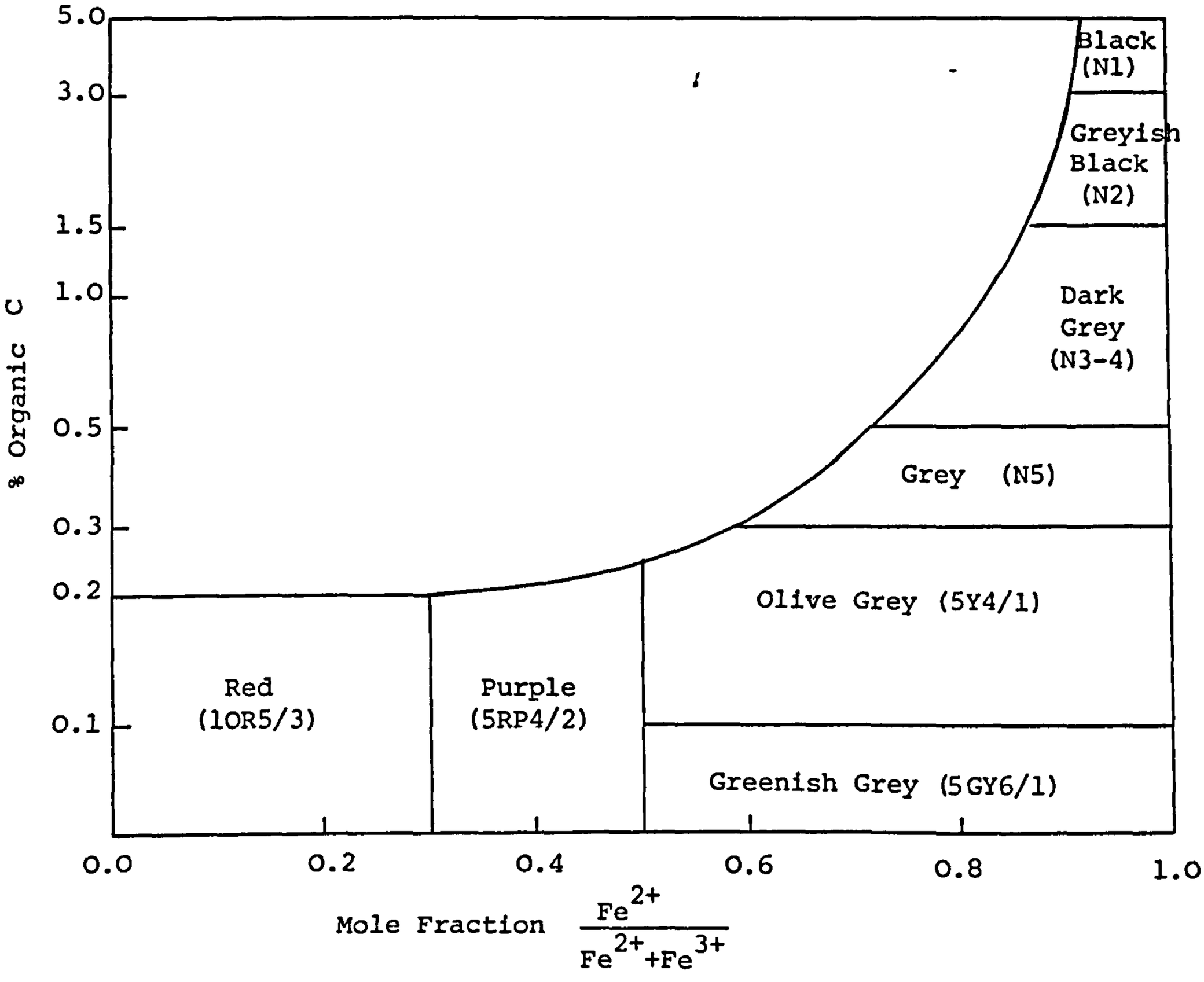


Figure 2.3 A Suggested Relationship Between Shale Colour, Carbon Content and Iron Oxidation State after Potter et al [209]

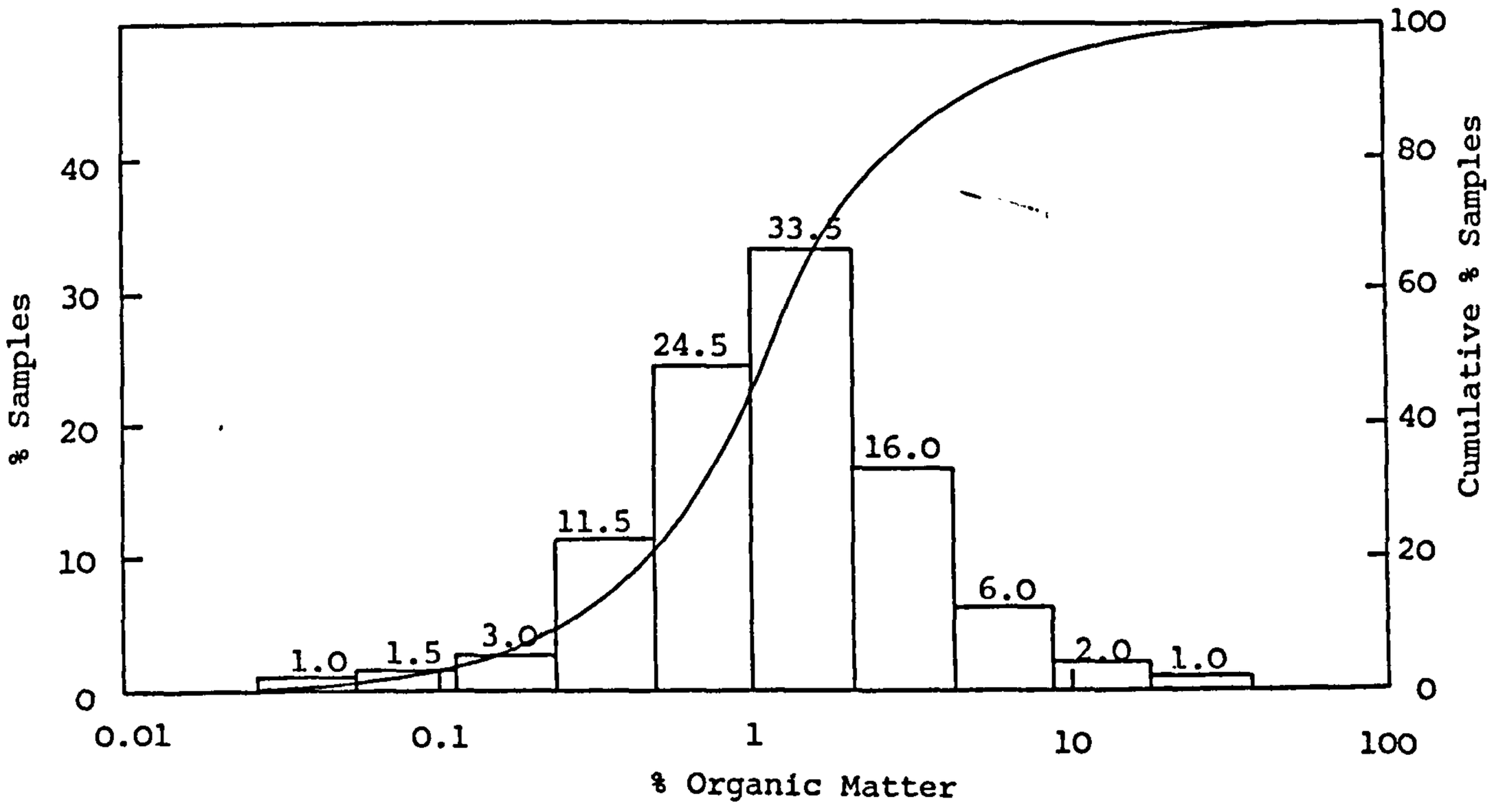


Figure 2.4 The Frequency Distribution of Shale Organic Matter Contents after Blatt et al [29]

small amounts of organic matter favour the reduction of Fe, and shale becomes darker with increasing organic matter content. The intermediate colours occur when the Fe is reduced but there is little organic C.

The prevailing opinion is that, as colour can be changed so easily, it is almost always of depositional or diagenetic origin. This means that red shales are most commonly produced in oxidising continental environments, often associated with evaporites, and black shales in restricted marine basins, although exceptions are deep sea clays which are reddish brown, and estuarine deposits which are often black.

Three factors can affect the amount of organic matter accumulating in a shale, and thus its eventual colour:

1. An increasing rate of organic production in overlying waters, or of transport of organic debris to those waters, tends to favour organic accumulation, and thus black shales.

2. Increasing the rate of inorganic sedimentation dilutes the organic matter, giving rise to green or grey shales.

3. Highly oxidising conditions in the sediment tend to destroy organic matter and lead to red shales.

Normal marine and fresh waters have an Eh of +0.3 volts, and thus a restricted water circulation is necessary to maintain the Eh of 0.0 volts or lower which is suggested to be consistent with organic matter accumulation [177]. Restricted circulation implies a lack of strong currents, and thus of arenaceous and carbonate sediments, resulting in the fact that 95% of the preserved organic matter in sediments is in shales.

Shales can contain up to 40% organic matter, but have an average content of 1.1% (Figure 2.4). The organic matter present in modern muds is in the form of complex molecules, but these are broken down to simpler molecules by micro-organisms in the early stages of diagenesis. As diagenetic temperature increases with depth of burial, these molecules interact to form humic and fulvic acids and eventually kerogen and hydrocarbons which, as they have no further nutrient value for micro-organisms, are preserved in the sediment until forced out by

compaction. If the temperature rises too much, hydrocarbons are destroyed and graphite formed. Humic and fulvic acids can be stabilised against further diagenetic alteration by reaction with phyllosilicate surfaces.

### 2.1.7 Diagenesis and Metamorphism

Unless a metamorphic temperature of 300°C is reached, the mineralogy of shales is rarely visibly reconstituted, although at about 200°C the highest pregreenschist facies reaction, the conversion of illite to $2M_1$ dioctahedral mica, coincides with the lithological change from shale to slate [125]. At temperatures below this it is only the most reactive of the unstable phases that begin to alter, and under earth surface conditions where illite is thermodynamically stable even smectite, one of the most reactive minerals in shales, could have survived from the Palaeozoic to the present day, although in practice it is usually only found in Mesozoic or younger rocks.

Kinetic considerations play an important part in determining the mineral assemblage; with reactions not being complete even after tens of millions of years, Pliocene shales show a much lower grade assemblage than shales buried under the same conditions of temperature and pressure since the Eocene. As depth of burial increases, one scenario suggests that, at temperatures as low as 50°C [261], smectite is converted to illite through a series of interstratified intermediaries, K feldspar is decomposed, and chlorite begins to form, according to the equation:

Smectite + K Feldspar $\longrightarrow$ Illite + Chlorite + Quartz [125].

The most sensitive indicators of pregreenschist metamorphic grade are the percentage of illite layers in the interstratified minerals and the degree of ordering of the layers, both of which increase with increasing grade. Kaolinite can stably co-exist with illite, but is decomposed before greenschist conditions are attained. Correlation of mineral assemblages with temperatures logged in boreholes (Figure 2.5) shows that all type I chlorites are pregreenschist; $Ib_d$ does not persist above 80°C, and Ib is converted to IIb at 200°C. Further explanation of chlorite polytypism is given in Section 2.2.4.

Perhaps one of the most important effects of diagenesis and low grade metamorphism on shales is that of a change in grain size. The majority

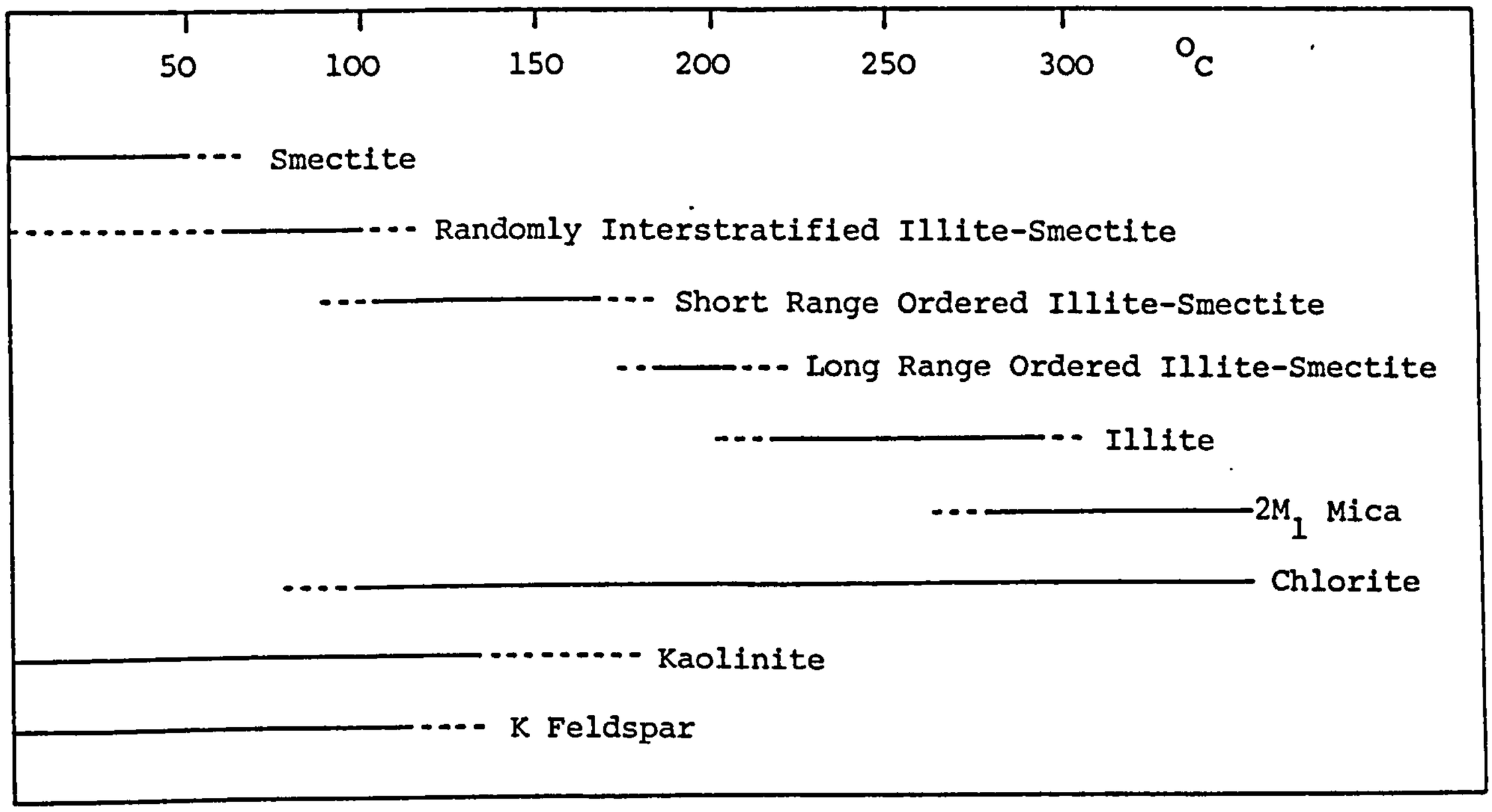


Figure 2.5 Correlation of Temperature-dependent Mineral Assemblages in Shales after Hoffman and Hower [125]

Temperatures do not represent equilibrium, but are applicable with caution to lower Tertiary and Mesozoic pregreenschist facies rocks.

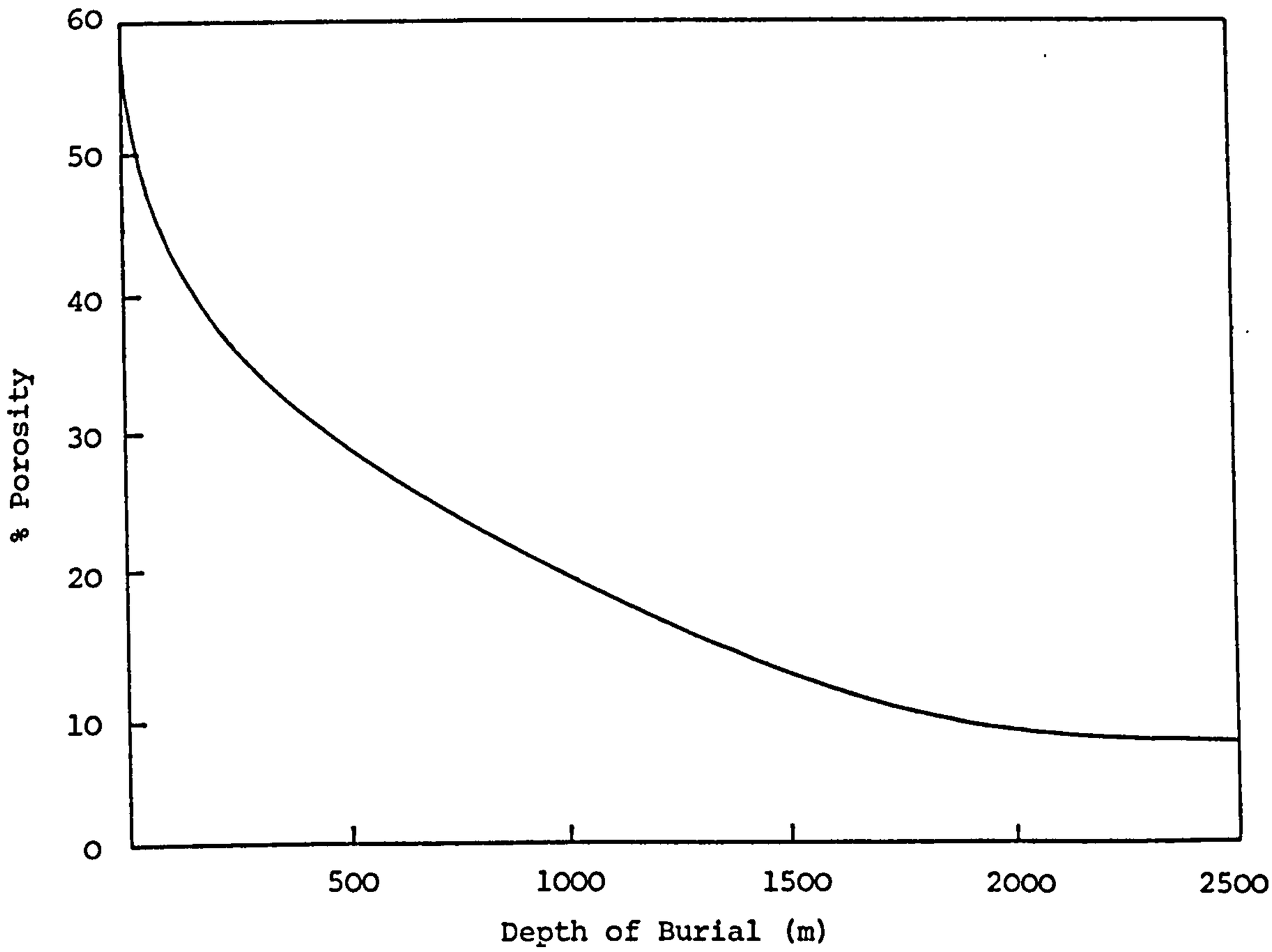


Figure 2.6 The Relationship Between Porosity and Depth of Burial of Shales after Pettijohn [206]

of phyllosilcates in unconsolidated sediments (except for detrital illite and chlorite from previous sedimentary cycles) are finer than 2μm in size. However, by the time these sediments have been buried sufficiently deeply to reach a temperature of 150°C, they have become siltstones in texture, due to growth in grain size of the phyllosilicates. This size increase seems to take place at the same time as montmorillonite is being converted through interstratified minerals to illite.

Chlorite formed during diagenesis may be both silt and clay sized, but as diagenesis becomes more advanced, its grain size also increases, until eventually chlorite grains become larger than those of illite [261].

Argillaceous marine sediments that have not been deeply buried usually contain 60% or more phyllosilicate minerals, and commonly consist of 50 to 80% clay size and 20 to 40% silt size material, the phyllosilicate content correlating well with the clay content. However, deeply buried rocks of similar chemical composition contain only 10 to 40% clay size material, yet maintain phyllosilicate contents of 60 to 80%, implying that grain size is not directly related to mineralogy, and that phyllosilicates coarser than clay size are common.

### 2.1.8 Porosity and Compaction

When deposited, some muds may have a water content of up to 90%, associated with a porosity of up to 80%, whilst an average porosity value is 35%. By the time the overburden pressure has reached 0.54kbar, water content has been reduced to 30%, of which only one third is pore water. The average shale has a porosity of 13%.

In sandstones loss of porosity is caused by infilling of pores with cement, but in shales it is due to compaction. Compaction begins at the moment of deposition and continues over a long period of time (Figure 2.6), taking place in three stages. Firstly, overburden pressure removes most pore water and all but two of the layers of water adsorbed onto the phyllosilicate particles. Beyond this stage, pressure alone is no longer effective, and dehydration proceeds by heating at about 100°C, which converts smectite to illite and leaves about 10 to 15% water in pores rather than as phyllosilicate interlayers. Finally, on a very long timescale, all interlayer water is removed, leaving only a few percent pore water. As compaction

proceeds, the fabric is progressively modified, bringing phyllosilicate particles into greater parallelism with the bedding [49].

Many factors can affect the initial porosity and early rate of compaction: high initial porosity is associated with high salinity, whilst rapid deposition leads to excess pore pressure and underconsolidation [49].

## 2.2 PHYLLOSILICATE MINERALS

Many useful reviews of the phyllosilicates, their structure, composition, occurrence, classification and interrelationships have been written, varying widely in their range and depth of investigation [40, 56,75,105,141,207,249]. Several have been consulted whilst preparing the present review which, however, is based in particular on [207]. Special attention is given to mica, chlorite and vermiculite, as these minerals are of particular relevance to this study.

Phyllosilicates are the most abundant group of minerals in sedimentary rocks, comprising about 40% of their total bulk, and are also found in soils and modern marine sediments. More than 50% of all phyllosilicates are micas, followed in decreasing abundance by smectite, chlorite, kaolinite and serpentine, vermiculite, palygorskite and sepiolite. All phyllosilicates are hydrous, and all except sepiolite and palygorskite, which have chain structures, are based on planes of octahedrally and tetrahedrally co-ordinated cations (Figures 2.7 to 2.9).

The tetrahedral sheets are composed of $SiO_4^{4-}$ tetrahedra, each connected by their basal O atoms to three other tetrahedra to form a planar hexagonal lattice, with all the free apices of the tetrahedra pointing in the same direction. The octahedral sheets are formed from two planes of hydroxyl ions, one on each side of a plane of cations, usually $Fe^{2+}$, $Fe^{3+}$, Mg or Al, which are octahedrally co-ordinated by the hydroxyl ions. Octahedral and tetrahedral sheets are structurally combined by the Os of the free apices in the tetrahedral sheet projecting into one of the hydroxyl planes of the octahedral sheet, and replacing two thirds of the hydroxyl ions in that plane. This plane of apical Os plus hydroxyl ions is structurally part of both a tetrahedral and an octahedral sheet, and thus neither sheet can be removed without disrupting the structure of the other.

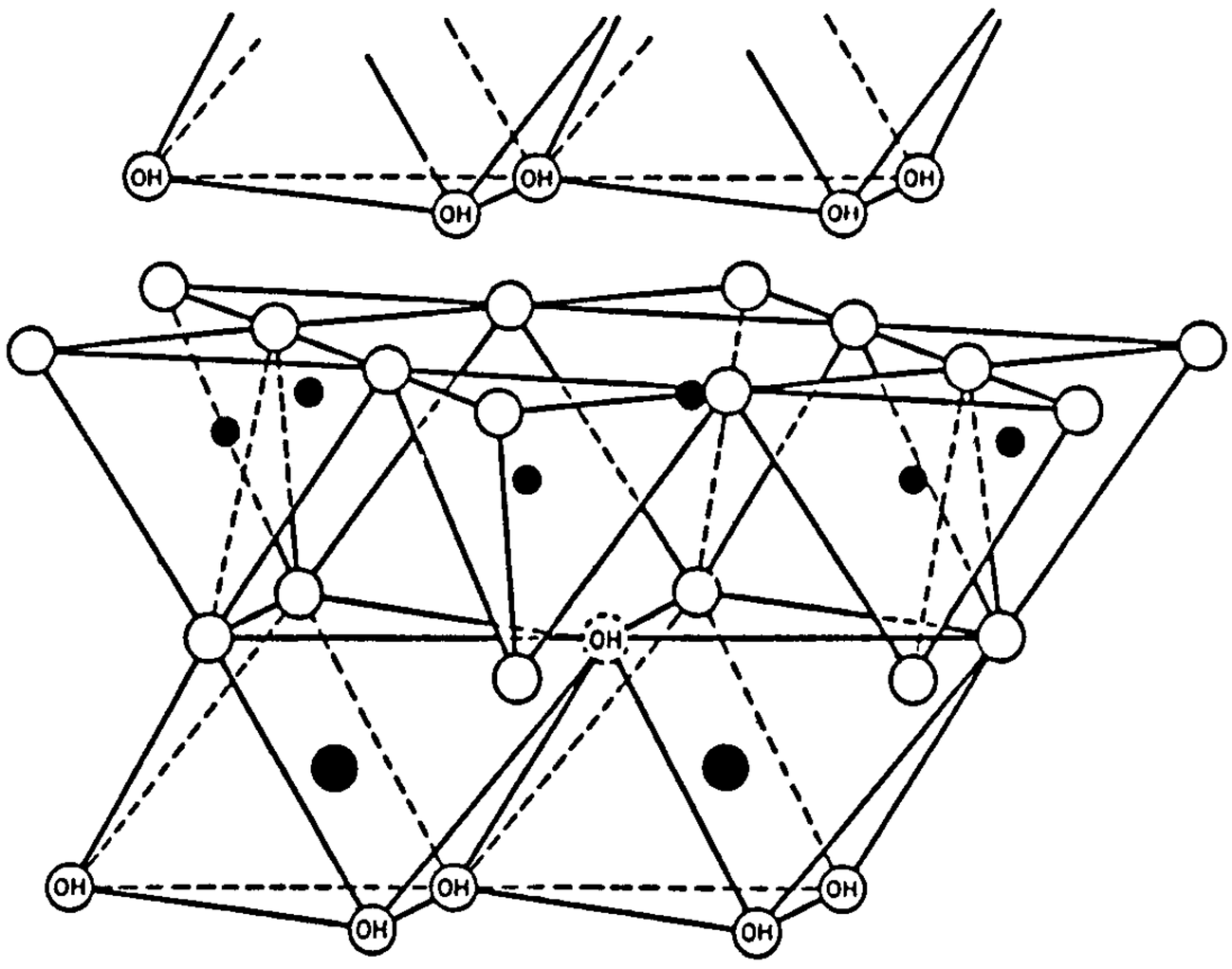


Figure 2.7 The Diphormic 1:1 Layer Structure of Kaolinite after Grim [115] Key as for Figure 2.9.

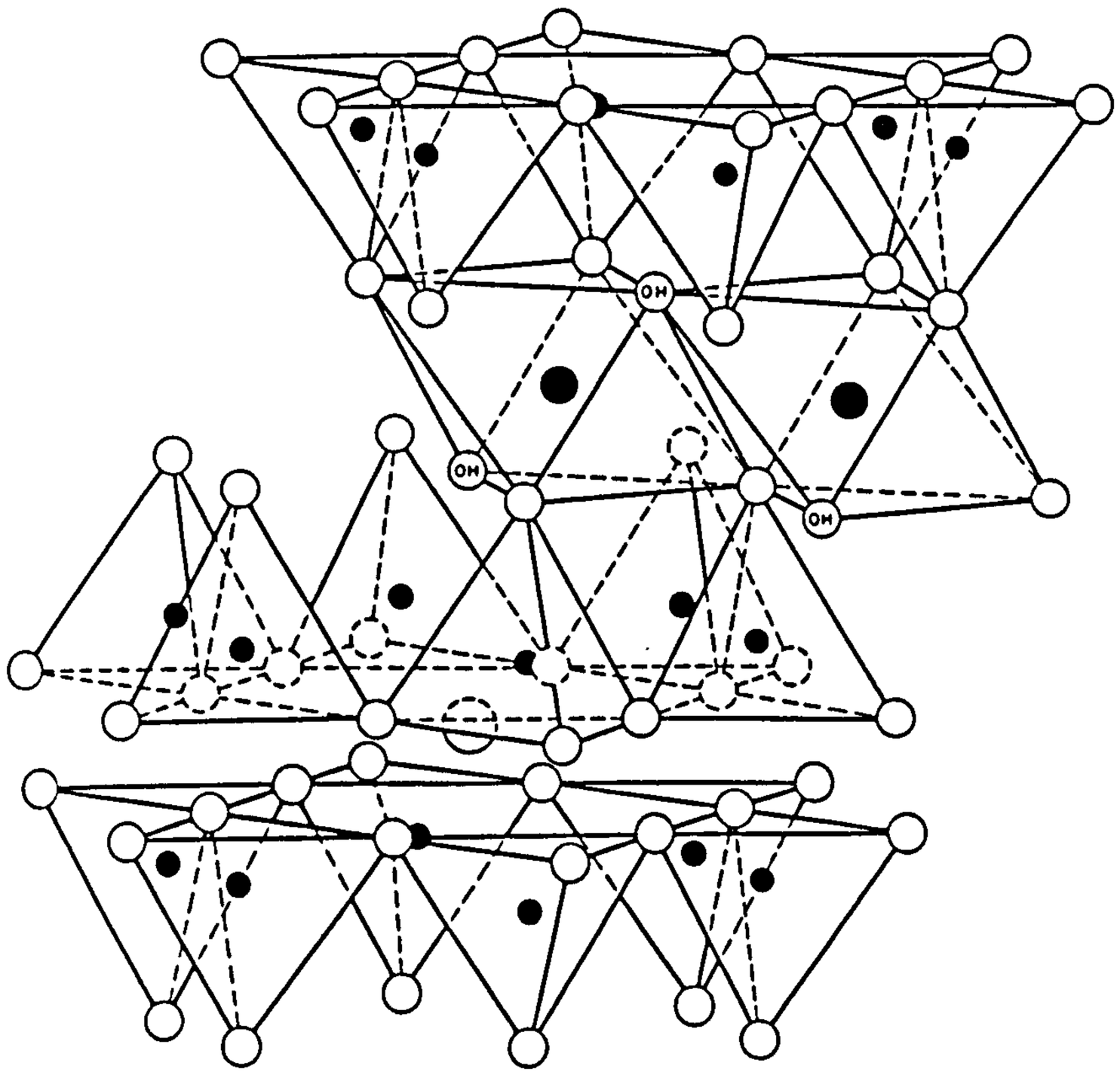


Figure 2.8 The Triphormic 2:1 Layer Structure of Mica after Grim [115] Key as for Figure 2.9.

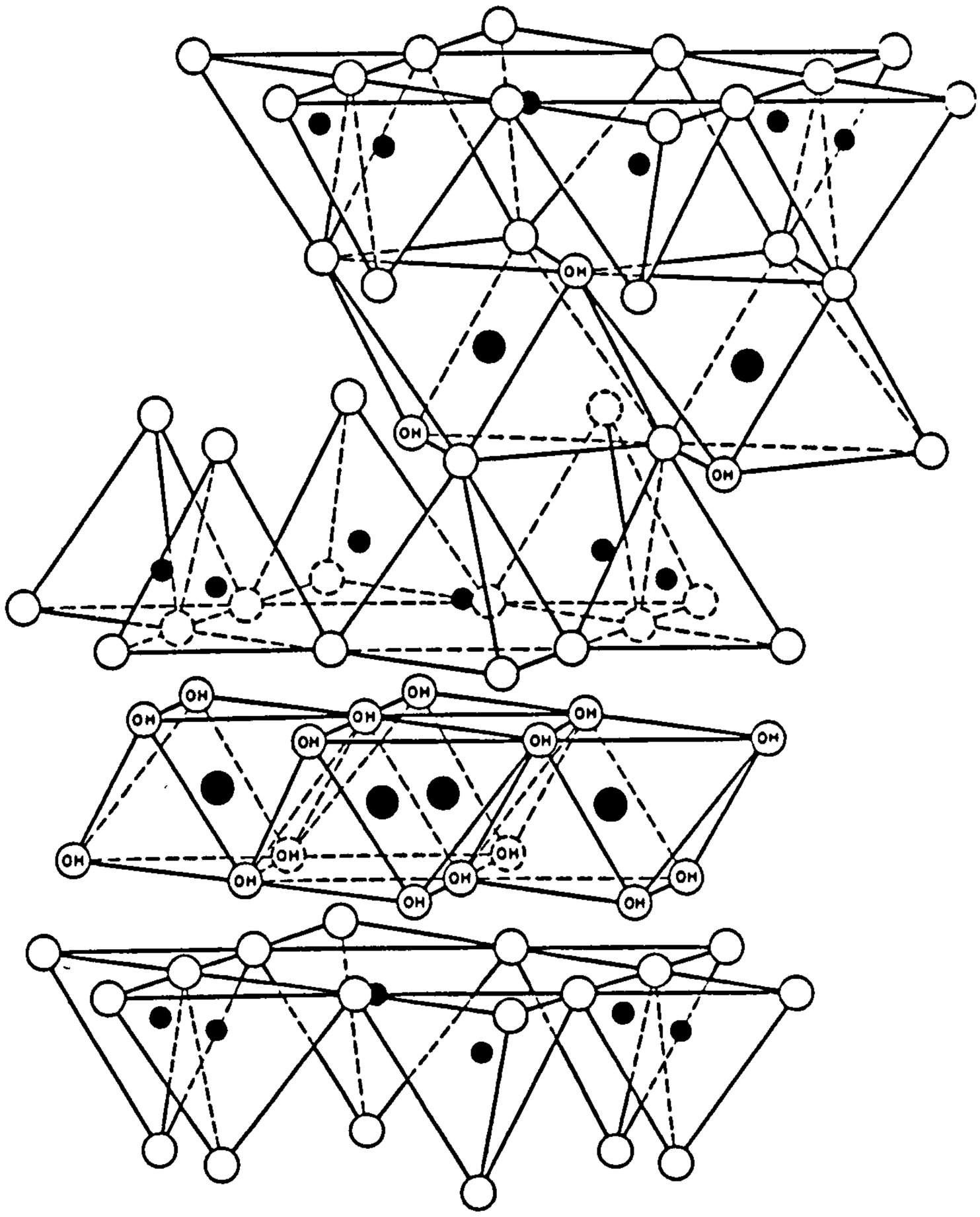


Figure 2.9 The Tetraphormic Structure of Chlorite with a 2:1 Layer and an Interlayer Hydroxide Sheeter after Grim [115]

Key:

- ○ Potassium
- ○ Oxygen
- (OH) Hydroxyl
- ● Octahedrally co-ordinated cation, usually $Mg^{2+}$, $Fe^{2+}$, $Al^{3+}$ or $Fe^{3+}$
- ● Tetrahedrally co-ordinated cation, usually $Si^{4+}$ or $Al^{3+}$

The phyllosilicates, as these layer silicate structures are called, are subdivided on the bases of (Table 2.7):

1. The arrangement of the octahedral and tetrahedral sheets into layers. One tetrahedral and one octahedral sheet together form the diphormic 1:1 layer of the kaolinites; one tetrahedral sheet on either side of a single octahedral sheet forms the triphormic 2:1 layer of the micas, smectites and vermiculites, and the alternation of a 2:1 layer with an interlayer hydroxide sheet forms the tetraphormic chlorite unit. This latter structure is often erroneously referred to as a 2:1:1 or 2:2 layer structure [11,12].

2. The number of cations per unit cell in each octahedral sheet. A structure with four cations per unit cell is dioctahedral, whilst one with six cations per unit cell, and thus all its octahedral sites occupied, is trioctahedral. Dioctahedral structures have octahedral sheets that are dominantly composed of trivalent cations, whilst trioctahedral minerals have mostly divalent cations in their octahedral sites. In dioctahedral structures, the unoccupied sites have an ordered distribution [97].

3. The method of stacking the structural layers on top of one another. There are usually several different stacking positions for the second and subsequent layers of a phyllosilicate structure relative to the first layer. Regularly ordered stacking arrangements are most common, repeating after every one, two, three or six layers, and these give rise to the polytypes of the phyllosilicates (see Sections 2.2.3 and 2.2.4 and Figure 2.10). Different stacking arrangements, and thus different polytypes, are stable under different environmental conditions, and can be used diagnostically.

4. The isomorphous substitution of cations within the octahedral and tetrahedral sheets. If the substitution involves replacing ions in the idealised formula with others of a different, usually lower, charge, a negative charge builds up on the layer surfaces, and is balanced by interlayer cations which may or may not be exchangeable. Variation in the surface charge density of the layers leads to variation in the physical properties of the minerals, and is thus an important characteristic for

Table 2.7 A Classification Scheme for Phyllosilicate Minerals after ~~McKenzie~~ Mackenzie [171] and Rezk [219]

| Lattice Type | Interlayer Material | Mineral Group | Electron Charge per Layer Unit Cell | Octahedrality | Typical Mineral Species | Idealised Formula |
|---|---|---|---|---|---|---|
| 2:1 | None | Pyrophyllite-talc | 0 | Dioctahedral | Pyrophyllite | $Al_4Si_8O_{20}(OH)_4$ |
| | | | | Trioctahedral | Talc | $Mg_6Si_8O_{20}(OH)_4$ |
| | Individual Cations or Hydrated Cations | Montmorillonite-saponite | 0.5-1.0 | Dioctahedral | Montmorillonite | $Na_{0.67}Al_{3.33}Mg_{0.67}Si_8O_{20}(OH)_4$ |
| | | | | Trioctahedral | Saponite | $Na_{0.67}Mg_6Si_{7.33}Al_{0.67}O_{20}(OH)_4$ |
| | | Vermiculite | 1.0-1.5 | Dioctahedral | Dioctahedral Vermiculite | $Na_{1.33}(Al,Fe)_4(Si,Al)_8O_{20}(OH)_4$ |
| | | | | Trioctahedral | Vermiculite | $Na_{1.33}(Mg,Fe)_6(Si,Al)_8O_{20}(OH)_4$ |
| | | Illite | 2 | Dioctahedral | Illite | $(K,H_3O)_2(Al,Fe)_4(Si,Al)_8O_{20}(OH)_4$ |
| | | | | Trioctahedral | Ledikite | $(K,H_3O)_2(Mg,Fe)_6(Si,Al)_8O_{20}(OH)_4$ |

Table 2.7 (continued)

| Lattice Type | Interlayer Material | Mineral Group | Electron Charge per Layer Unit Cell | Octahedrality | Typical Mineral Species | Idealised Formula |
|---|---|---|---|---|---|---|
| 2:1 | Individual Cations or Hydrated Cations | Mica | 2 | Dioctahedral | Muscovite | $K_2Al_4Si_6Al_2O_{20}(OH)_4$ |
| | | | | Trioctahedral | Biotite | $K_2(Mg,Fe)_6Si_6Al_2O_{20}(OH)_4$ |
| | | Brittle Mica | 4 | Dioctahedral | Margarite | $Ca_2Al_4Si_4Al_4O_{20}(OH)_4$ |
| | | | | Trioctahedral | Xanthophyllite | $Ca_2Mg_4Al_2Si_2Al_6O_{20}(OH)_4$ |
| | Hydroxide Sheet | Chlorite | Variable | Dioctahedral | Sudoite | $Al_8Si_8O_{20}(OH)_{16}$ |
| | | | | Trioctahedral | Ripidolite | $(Mg,Fe)_{12}(Si,Al)_8O_{20}(OH)_{16}$ |
| 1:1 | None or $H_2O$ | Kaolinite-serpentine | 0 | Dioctahedral | Kaolinite | $Al_4Si_4O_{10}(OH)_8$ |
| | | | | Trioctahedral | Amesite | $(Mg,Fe)_4Al_2Si_2Al_2O_{10}(OH)_8$ |
| 2:1 Chain | $H_2O$ | Hormite | 0.2 | Ditrioctahedral | Palygorskite | $Al_3Mg_{0.5}Si_8O_{20}(OH)_2 \cdot 4H_2O$ |
| | | | | Trioctahedral | Sepiolite | $Mg_8Si_{12}O_{30}(OH)_4 \cdot 4H_2O$ |

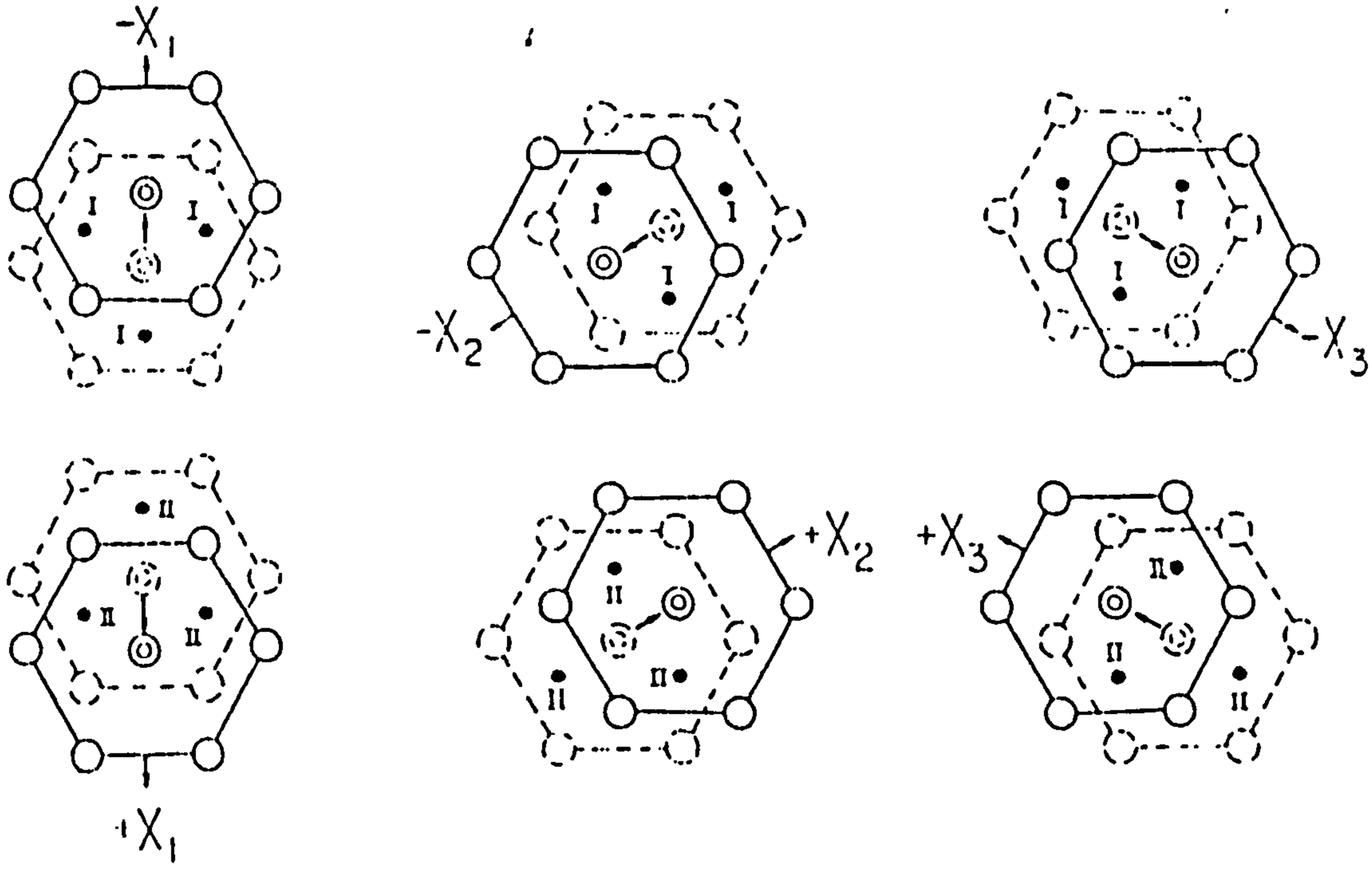


Figure 2.10 Possible Octahedral Cation Sites and Intralayer Shifts after Fanning and Keramidas [97]

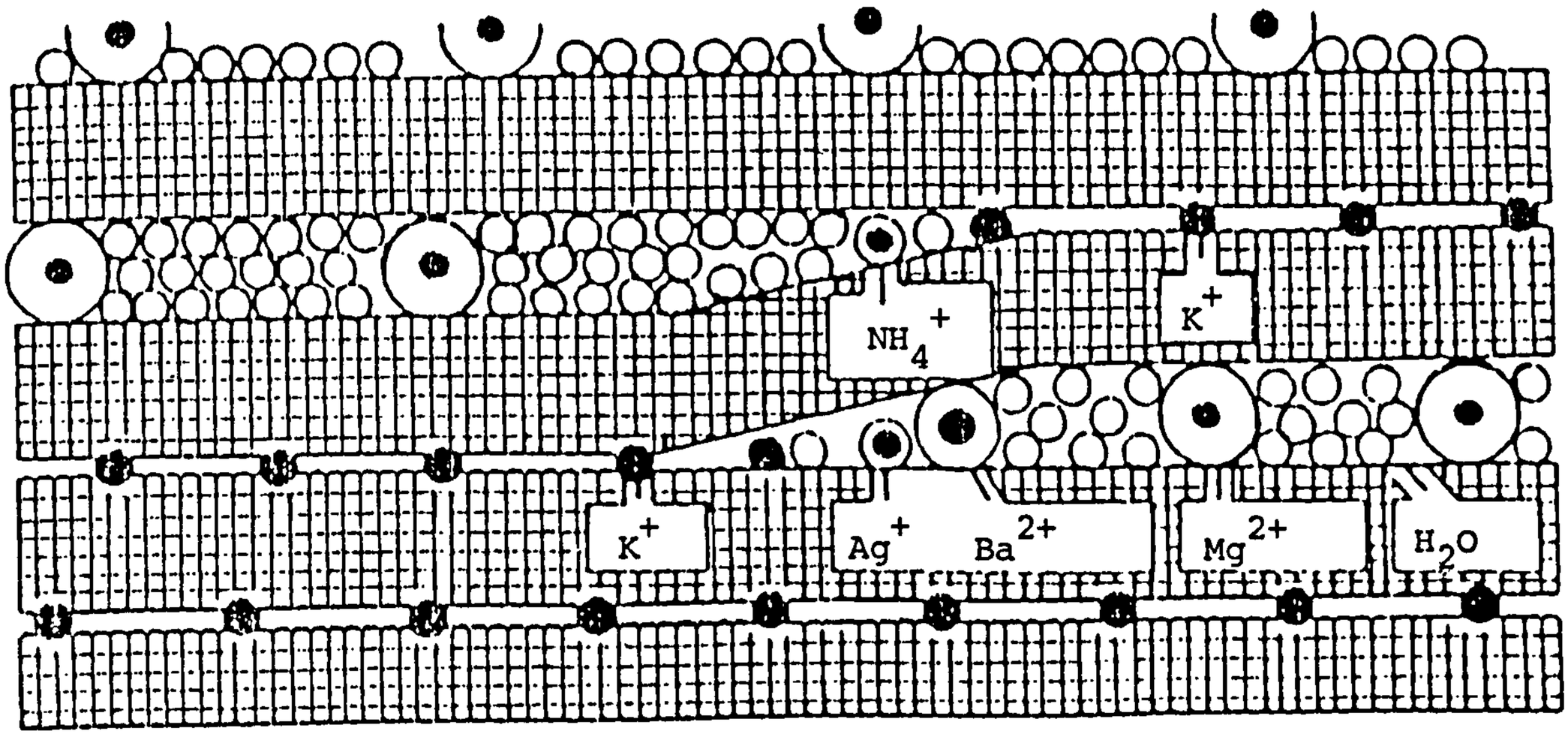


Figure 2.11 Wedge-shaped Vermiculite Zones in Mica, Showing the Fit of Several Cations in the Wedge after Douglas [77]

distinguishing between different minerals. Minerals in which the total layer charge is identical may have different proportions of that charge contributed by the octahedral and tetrahedral sheets. In some structures, such as that of chlorite, where trivalent cations can replace divalent cations in the interlayer hydroxide sheet, internal charge compensation can take place, reducing or removing the requirement for interlayer cations.

5. The presence or absence of interlayer cations or polar molecules, and their types when present. For example, muscovite is distinguished from paragonite by the fact that the interlayer cations are K in the former and Na in the latter.

Many phyllosilicates are not pure mineral types, but consist of interstratified units of different chemical composition and structure. Corrensite is the most common well defined interstratified mineral, consisting of a regular 1-1 chlorite-vermiculite or chlorite-montmorillonite interstratification. However, various interstratified illite-montmorillonite compositions make up about 90% of all interstratified minerals [207]. Interstratified minerals are often made up from one unit which is expandable and one that is not, although it is possible for more than two basic units to be interstratified, or for the type of interstratification to vary within a single crystal. Interstratified minerals are particularly important in the soil and in other environments where mineral transformations are taking place. Three basic types of interstratification are possible, but because these can be combined in many ways, and because of the large number of minerals that can combine with others to form an interstratification, classification is very difficult:

1. Random, for example BBABAABABBBBAAB..
2. Regular with long range ordering, for example [100A][100B][100A]..
3. Regular with short range ordering, for example ABABABABABABABA..

As well as interstratification of different layer structures, a single layer may show lateral heterogeneity. In particular, micas often have frayed vermiculitic edges, caused by a weathering front progressing from the edge towards the core of the mineral (Figure 2.11).

### 2.2.1 Formation and Occurrence

Phyllosilicates may form by:

1. Crystallisation of ions from solution.
2. Crystallisation of aluminosilicate colloids.
3. Alteration of silicate glasses.
4. Alteration of nonphyllosilicates.
5. Alteration of pre-existing phyllosilicates.

All of these mechanisms except the last produce primary, neoformed phyllosilicates with a one stage history, whilst those phyllosilicates produced by the alteration of other phyllosilicates, often as they occur in rocks such as shales, have a multi-stage history. When dealing with the latter, an attempt must be made to determine whether they are indicators of provenance, diagenesis, or both. Marine environments are very variable, and thus one mineral cannot be used as an indicator of a marine influence in a sediment, athough a lateral series of phyllosilicate assemblages may be able to give useful information, such as indicating the direction to the shore line. Different phyllosilicates respond in different ways when they are transported from a terrestrial environment to the ocean.

> "Environmental aspects of clay minerals may be considered from the viewpoint of the depositional environment, i.e., given a depositional environment, recent or ancient, what clay minerals actually occur there? The accounts of clay minerals actually occurring in the deposits are extremely valuable because of the realistic information they supply. On the other hand, their potential value for predicting either the environment or the kind of clay mineral from the other member of the pair is appreciably limited unless the clay minerals "formed here" are (or can be) differentiated from those "found here" - in other words the geochemical system differentiated from geological space. If such distinction is not made, it will be found that almost any or all kinds of clay minerals may occur in any major depositional environment." [141]

Which phyllosilicates form, and how they form, depends on pH, Eh, pressure, temperature, the activities of ions in solution and the presence of noncrystalline precursors, all integrated over a period of geological time. By definition, a primary mineral is found in situ in its environment of formation, and thus the origin of primary phyllosilicates is easiest to interpret. When a phyllosilicate is moved away from its environment of formation it will be in disequilibrium to a greater or lesser extent, as a result of which it will be altered and thus will no longer be a primary mineral. As well as being altered by their environment, phyllosilicates can be agents in altering the environment by means of cation exchange, adsorption of

species from solution, or dissolution of the mineral structure. Once a mineral is moved away from its environment of formation, it can have three possible subsequent histories:

1. The rate of alteration is so slow that the mineral appears to be unaltered, although it is not in equilibrium with its environment.

> "To illustrate the disparity that may occur between environments of origin and deposition of clay minerals, take an example of a clay mineral which, after being formed under hypersaline, hot, arid conditions in Death Valley, is then blown via a dust storm to snow and glaciers in Colorado or Wyoming. After mixing with glacial rock-flows (sic), the clay mineral may be deposited in fresh-water, outwash, or river sediments, and is then in an environment and association quite incompatible with that of its origin. Alternatively, it may be deposited in the Gulf of Mexico and build shale quite different from its source rock." [141]

2. The mineral may show alteration in progress, perhaps in the form of interstratification of the original and altered mineral structures, or by a zone of altered structure around a core of the original structure.

3. The mineral may be completely altered, or even dissolved, so that no evidence remains of its previous identity.

Formation by crystallisation from solution is exemplified by various well crystallised mica and kaolinite polymorphs found in vughs and geodes. In distilled water, kaolinite dissolves only to the extent of 0.1 parts per million (ppm) Al in solution, but some near surface environments with 120ppm Al in solution are known, and thus direct crystallisation could occur under hydrothermal conditions. In vughs in Carboniferous limestone from Kansas, close to an intrusion, dickite crystallises nearest to the intrusion and kaolinite further away, where the circulating water has cooled to a significant extent [141]. Minerals formed by direct crystallisation from solution have structural formulae very close to the ideal, and their XRD traces show almost all possible reflections.

At high temperature and high water pressure, phyllosilicates can replace earlier minerals and rocks; examples include glauconite replacing rhyolite and mica replacing quartz [141]. Phyllosilicate assemblages are characteristic of low temperature hydrous environments, and thus weathering is a very important phyllosilicate forming process. Almost all phyllosilicates can be formed in the weathering environment.

2.2.2 Kaolinites

The complete 1:1 structural unit of the kaolinites is characteristically 0.7nm thick. Kaolinites are all dioctahedral; the trioctahedral 1:1 minerals, the serpentines, are not usually considered together with the other phyllosilicates because of their different paragenesis. The composition of all kaolinites approximates to the ideal formula of $Al_4Si_4O_{10}(OH)_8$, with little isomorphous substitution. Different members of the kaolinite group, such as dickite and nacrite, are characterised by different stacking patterns of the 0.7nm units, and are thus kaolinite polytypes. 1.0nm-halloysite is a hydrated form of kaolinite, while 0.7nm-halloysite is a dehydration product of 1.0nm-halloysite [38]. The cation exchange capacity (CEC) of kaolinites and serpentines is about 5mEq $100g^{-1}$, and is mainly due to protonation or dissociation on particle edges, rather than to isomorphous substitution within the structure.

Kaolinite can form from the weathering of any aluminosilicate, provided that metal cations are leached, protons from water are added and a low Si/Al ratio is maintained. This latter is favoured by low pH conditions, where the solubility of $SiO_2$ is very much less than that of $Al_2O_3$. Formation from Na or K aluminosilicates, dominantly feldspars, is most common, as minerals that release Ca, Mg or Fe on weathering tend to flocculate silica, and thus prevent the Si/Al ratio decreasing sufficiently for kaolinite to form [141]. Leaching occurs where precipitation exceeds evaporation, in permeable rocks, or where water can percolate through the system. For kaolinite to form, the ratio $[K]/[H^+]$ must be below a critical value, and thus kaolinite formation is favoured by acid conditions. Fe can be effectively removed from the weathering system by precipitation as $Fe_2O_3$ upon oxidation, as in laterites, or as $FeS_2$ on reduction, as well as by leaching. Fresh water can provide $H^+$, as can oxidation of sulphides, solution of $CO_2$ (which is increased in soil air to several hundred times its value of 0.03% in the free atmosphere [35]), or by the oxidation of organic matter. In effect this means that kaolinite forms under conditions of high rainfall and acidity and good drainage, and is thus characteristically found in well drained soils developed by tropical weathering.

Changes in microenvironment can be very important in determining which minerals form on weathering; with varying [K], one side of a feldspar crystal may alter to kaolinite, whilst the other alters to mica.

Kaolinite may particularly be expected to form in the acid micro-environments surrounding plant roots [242].

Flint clays are thought to form by the crystallisation of aluminosilicate colloids. They form in nonmarine marshes, and have very different properties and structures from ball clays or kaolinite formed by weathering. They consist of randomly oriented kaolinite crystals, forming an isotropic, homogeneous nonplastic clay with good resistance to slaking.

1.0nm-halloysite seems to form in soils developed on volcanic ash deposits, or under conditions of extreme acidity or rainfall. In the Chattanooga Shale, Kentucky, oxidation of sulphides gives rise to percolating solutions of pH 1 which dissolve illite and then precipitate 1.0nm-halloysite when the pH rises to 3 to 3.5 on interaction with more rock [141].

In recent marine sediments kaolinite, often associated with gibbsite, indicates derivation from land areas experiencing lateritic weathering. Kaolinite dissolves more slowly in sea water than other phyllosilicates, but experiments show that after six months up to 2.2ppm $SiO_2$ is found in solution [170]. However, other phyllosilicates dissolve to this extent in only 1/10th of the time, and montmorillonite can give rise to up to 21ppm $SiO_2$ in solution.

Obviously, if the kaolinite is dissolved, there will be no record of it in the sedimentary sequence, but it can be preserved by flocculation or the preferential solution of other phyllosilicates. Experiments show that, under conditions of 150°C, 2kbar and excess K, kaolinite is rapidly converted to $1M_d$ mica [251]. These conditions are common during burial diagenesis, but there is disagreement as to whether or not kaolinite is stable under normal marine conditions.

### 2.2.3 Micas and Expandable Minerals

Micas and smectites both have 2:1 layer structures, and thus this is the most common phyllosilicate structure, with a basic unit 1.0nm thick. In these triphormic minerals the surface charge per formula unit varies from zero to four, but the minerals tend to group in five regions of this continuum, with little evidence for any noninterstratified minerals having surface charge densities that fall outside these groups [11,12]:

1. Charge about 0.0, no interlayer cations, no swelling - pyrophyllite, talc.
2. Charge 0.5 to 1.2, CEC of about 100mEq $100g^{-1}$, unlimited swelling - montmorillonite, saponite.
3. Charge 1.2 to 1.8, CEC of about 150mEq $100g^{-1}$, limited swelling - vermiculite.
4. Charge about 2.0, CEC up to 40mEq $100g^{-1}$, no swelling - mica, illite.
5. Charge about 4.0, no CEC, no swelling - brittle mica.

However sound this classification may be in theory, it breaks down in practice, as it is very difficult to determine the layer charge of phyllosilicates that occur in mixtures or interlayered structures, leading to difficulties in classification such as those caused by illites. The occurrence of a clear cut distinction between illite and montmorillonite has been questioned on the grounds that intermediates are very common.

The pure trioctahedral magnesian end member, talc ($Mg_6Si_8O_{20}(OH)_4$), and the pure dioctahedral aluminian end member, pyrophyllite ($Al_4Si_8O_{20}(OH)_4$), do not occur as phyllosilicate clays, but the micas have a very similar structure to these minerals, with the addition of a plane of large cations in approximately 12 fold co-ordination between each layer. These cations fit into the centres of the spaces in the ditrigonal lattice formed by the basal Os of the tetrahedral sheets, and bond adjacent layers together by electrostatic attraction. Because of the 12 fold co-ordination of the interlayer sites, the most abundant micas have K as their interlayer cation, and thus micas are the most important natural source of K for plants. The power of a soil to supply K depends not only on its mica content, but also on the species and particle size of the mica, as dioctahedral micas are more resistant to weathering than trioctahedral micas, and thus release K more slowly, whilst smaller particles generally weather more rapidly than larger grains.

Interlayer cations, such as K, are needed to balance charge deficiency in micas caused by isomorphous substitution of Al for Si in the tetrahedral sheets, and Mg or $Fe^{2+}$ for Al in the octahedral sheet. A wide range of isomorphous substitutions can take place, and most micas have at least two out of Al, Fe and Mg occurring in the octahedral sheet, whilst it is not uncommon to find Mn, V, Cr, Li or Ti.

The high layer charge in micas accounts for the interlayer cations being nonexchangeable. If weakly hydrated cations, such as K, occur in a vermiculite structure, they may be fixed permanently to give rise to a mica structure. Similarly, artificial weathering can give rise to micas with hydrated interlayer cations. Both of these structures retain their original structural charge, and thus distinction between mica and vermiculite on the grounds of structural charge can no longer be made, as it contradicts the identification made by XRD.

The name "illite" was originally coined by Grim for the "mica occurring in argillaceous sediments" [97]. However, the illite from the type locality at Fithian, Illinois, has since been shown to be an interstratified mineral, as have many other specimens to which the term has been applied. Recent work by Środoń has developed a method, based on XRD measurements, for determining the degree of interstratification in these minerals even if, in the specimen as a whole, they are present in much lower quantities than the nonexpandable minerals [243]. As originally defined, illites differ from muscovites in commonly having less $K_2O$ and more $H_2O$, $SiO_2$ and MgO in their chemical analyses [207], and the term is now commonly used to describe nonexpandable minerals with a 1.0nm basal spacing that have these chemical differences from true muscovites. It is in this sense that the term will be used throughout this study, following Brindley and Brown [40]. Many authors have used the term "hydrous mica" instead of illite for these minerals, in order to avoid the possibility of confusion over interstratification, but this is not a recommended use [11,12].

Illites are commonly found in sediments and soils, rather than in igneous or metamorphic rocks, and are predominantly dioctahedral. Where trioctahedral illites are found it is usually due to the leaching of interlayer cations from biotite. Muscovite has the unit formula $K_2Al_4Si_6Al_2O_{20}(OH)_4$, and thus a structural charge of two, but the most common illites have only half this amount of Al for Si substitution, and one eighth of their octahedral cations are divalent, giving rise to a structural negative charge of about 1.5.

The term "glauconite" is technically restricted to dioctahedral K deficient, Fe rich illites [10], but is commonly applied to many fine grained Fe rich phyllosilicates. More than 50% of the Fe is present as $Fe^{3+}$, and less Al substitutes for Si than in illites. As with illites, many glauconites include interstratified or otherwise altered material.

The major problem with the use of the terms illite and glauconite is in deciding how the minerals they correspond to are to be included in a classification system. If the calculated layer charges of as low as 1.6 [207] are correct, then they should be classified as vermiculites (see below). However, in true vermiculites, much of the structural charge originates in the octahedral sheet, which is not the case in true micas, nor does it seem to be the case in most illites [207]. The other possibility to be considered is that the calculated formulae and layer charges are wrong, due to the difficulties in determining layer charges caused by interlayering.

If mica structures are indexed on the basis of a monoclinic unit cell, the a and b dimensions are approximately the same for all micas, although the b dimension is generally slightly smaller for dioctahedral than trioctahedral structures. The c dimension depends on the polytype. Micas exhibit excellent cleavage parallel to (001), and thus usually occur as flakes which are quite flexible. On sedimentation, both in nature and in the laboratory, these flakes take up a parallel orientation.

The presence of mica in a specimen can be determined by XRD analysis. In both random and oriented mounts, micas give a diffraction peak at 1.0nm, which is unaltered by Mg saturation, K saturation, Mg saturation followed by ethanl,2diol solvation, or K saturation followed by heating at 550°C. Other diagnostic peaks occur at 0.5 and 0.33nm. The intensity of the 0.5nm peak varies with the type of octahedral cations; it is intense for aluminous micas, such as muscovite, but weak or absent for Fe rich micas like biotite.

XRD can be used to distinguish between dioctahedral and trioctahedral micas because of the smaller b dimension in the dioctahedral micas. The (060) reflection is generally used; it occurs at 0.150nm for dioctahedral micas and between 0.152 and 0.154nm for trioctahedral micas. The larger b dimension is due both to the greater number of cations present in the trioctahedral sheet, and to the fact that Mg and $Fe^{2+}$ have larger ionic radii than Al. In specimens known to contain appreciable quantities of quartz, it may be necessary to use a different (0k0) reflection, such as (020), as quartz has a reflection at 0.1541nm which could cause interference.

In the mica structure polymorphism occurs because of six possible orientations, at 60° intervals, of a second 2:1 layer when placed upon an original layer. The polymorphs are caused by differences in stacking of the octahedral sheets, as the tetrahedral sheets are restricted to fit around the interlayer cations. There are two sets of octahedral sites that can be occupied in each sheet, and three ways in which the two tetrahedral sheets in a layer can be positioned relative to each other (Figure 2.10). From combinations of these possibilities the polymorphs can be constructed.

Due to the octahedral sheet repeat distance being smaller than that of the tetrahedral sheet, the tetrahedra are rotated and tilted to give a better fit. This gives rise to ditrigonal, rather than hexagonal, co-ordination rings around the interlayer cations, which favour stacking angles of 0, 120 and 240°, especially in dioctahedral structures. When mica structures are observed in detail, it can be shown that the 60 and 300° angles and the 120 and 240° angles are mirror equivalents. It is also found that the majority of micas stack regularly with only one stacking angle, or a combination of two mirror equivalents. With this as a basis, it can be shown that only six simple polymorphs can occur (Figure 2.12), although structures of high periodicity with more complex stacking can be found [240]. Polymorphs are identified by the number of layers in the stacking repeat, followed by a symbol for the symmetry, and the simple polymorphs are 1M, $2M_1$, $2M_2$, 2O, 3T and 6H, of which 2O and 6H have not been found in nature.

$2M_1$ is formed by an alternation of 120 and 240° angles, and $2M_2$ by an alternation of 60 and 300° angles, and thus the two polymorphs have different structures, despite the same stacking repeat and symmetry. $2M_2$ has only been found to occur in nature in lepidolites [240]. $2M_1$ is the most common polymorph for dioctahedral micas, whilst 1M and 3T also occur. Glauconites usually show 1M or $1M_d$ structures, whilst illites are usually $2M_1$. Trioctahedral micas are usually of 1M polymorph.

In natural dioctahedral micas, $1M_d$ forms metastably at all temperatures, and eventually inverts to $2M_1$ at temperatures higher than 200°C and to 1M at temperatures below this [240,251,274]. Subsequent experimental re-examination of the muscovite system showed that the $2M_1$ polymorph is the only stable form, and thus 1M is metastable relative to $2M_1$ [251]. However, with Fe and Mg in the composition, the 1M and

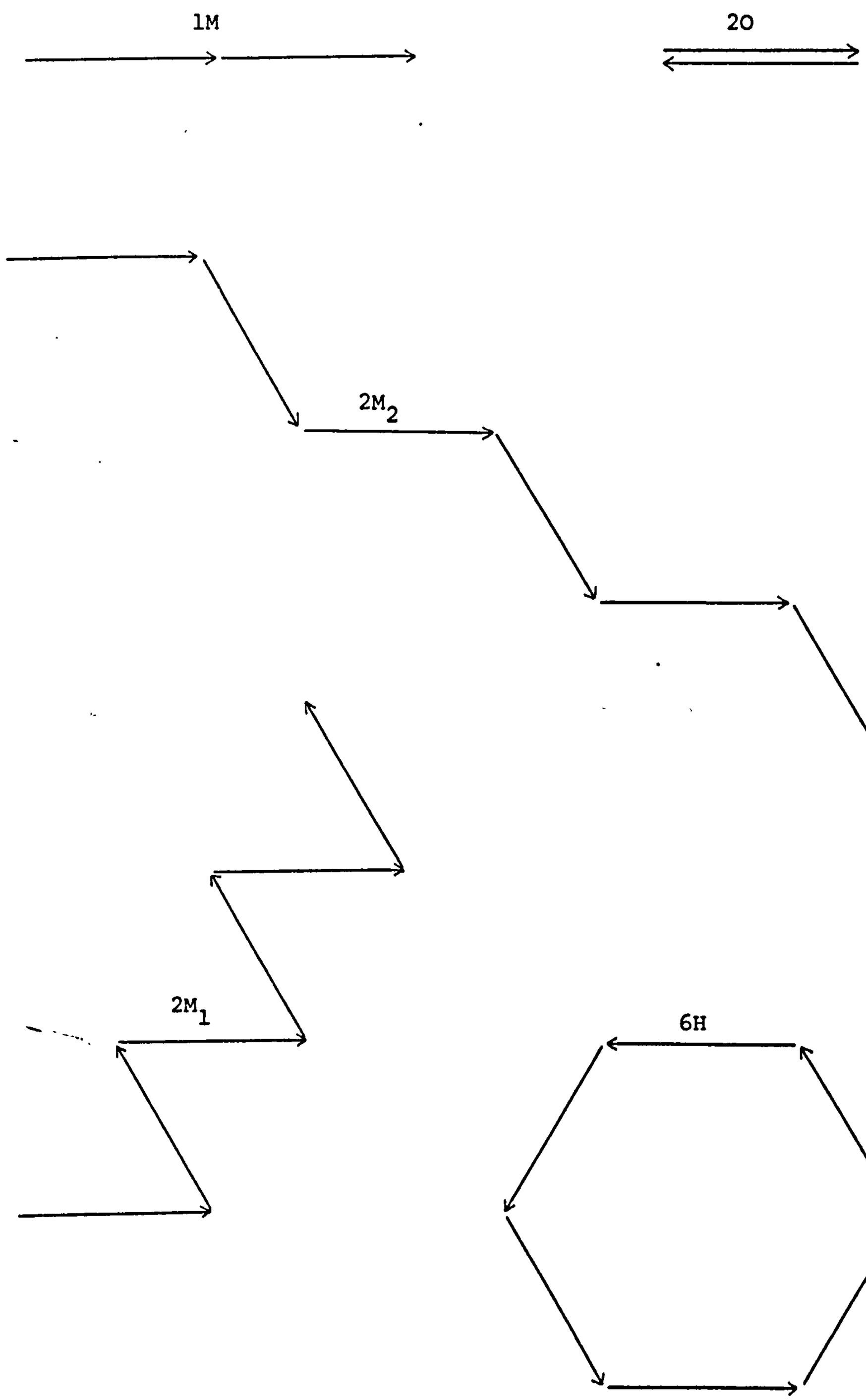


Figure 2.12 The Six Simple Ways of Stacking Mica Layers in an Ordered Manner after Smith and Yoder [240]

3T polymorphs appear to have real stability fields [128], and studies have shown that illite occurs in nature as polymorphs $1M_d$, 1M, $2M_1$ and 3T [161]. $2M_1$ mica is generally interpreted as forming in medium to high grade metamorphic rocks, igneous rocks or pegmatites. Nevertheless, the $2M_1$ polymorph has been shown to form at diagenetic temperatures, and thus its discovery is of no help in suggesting an origin for the mica [128], although in most Palaeozoic shales $1M_d$ is dominant, and $2M_1$ is only found in the coarser than 1μm fraction [252].

Polymorph determination can be carried out by XRD, using reflections in the range 0.27 to 0.43nm, which are mainly (021) and (111) reflections [56,161]. Because the three polymorphs that occur in muscovites and similar micas in nature have different numbers of layers in their stacking repeats, identification by the position of their peaks on powder diffractograms is relatively easy, and structure factors do not have to be calculated [56,240,274]. The diffraction patterns from $2M_1$ structures show more reflections than those of 1M and 3T structures, but the variation in c dimension with polymorph, i.e. the fact that c = 3.0nm for a 3T structure, is not revealed by XRD.

Differential thermal analysis (DTA) and thermogravimetry cannot positively identify mica species, but well crystallised micas show an endotherm at 800 to 1000°C due to dehydroxylation, whilst illites show endotherms in the ranges 150 to 240°C and 500 to 700°C. The actual temperatures of the endotherms increase as the dominant octahedral cation changes from Fe through Al to Mg. At higher temperatures a further endotherm, due to complete recrystallisation, occurs, whilst small exotherms at about 350°C are due to release of structural strain [97].

Infrared analysis can be used to distinguish between dioctahedral and trioctahedral micas. Trioctahedral structures have more complex OH-stretching bands, as any vacancies in the trioctahedral lattice are randomly distributed, whereas those in the dioctahedral lattice are well ordered [250]. Adsorption of polarised infrared radiation can be used to determine hydroxyl orientation [19], and it has been shown that in dioctahedral micas the interlayer cations are exposed to more negative charge, and are thus held more tightly, as the protons in the hydroxyl ions are oriented towards the vacant octahedral cation sites [19,195].

The micas occurring in igneous and metamorphic rocks are mainly macroscopic, with formulae close to the ideals for muscovite and biotite. Close to source rock areas, macroscopic mica is also common in coarse sediments, but as micas have hardnesses of only two to three, they are readily broken down, and are thus generally more common in fine grained sediments. Shales are usually rich in illitic micas, and the terrigenous fraction in limestones commonly contains much illite, often resulting in illite being the dominant phyllosilicate in the subsoil of profiles formed on shales and limestones [137]. True muscovites can occur as detrital particles in shales, and may be inherited by soils forming on shales or other micaceous rocks.

Soil micas are largely, if not entirely, inherited, and are not known to form to any significant extent in soils. Examples of apparently pedogenic mica in Hawaii have been shown to be due to aeolian input [97], and thus this possibility must be carefully eliminated before any occurrence of pedogenic mica can be accepted. However, mica crystals have formed from kaolinite during alteration of K feldspar in arkosic sandstones under earth surface conditions, whilst fixation of K to form illite by beidellites that are believed to have originally formed from illite is known from the finer than 0.2μm fraction of heavily fertilised soils [97]. Micas in soils are often partly transformed to expandable minerals, occurring as interstratified minerals or as mica cores surrounded by outer zones of expandable minerals.

As micas in soils are derived from parent materials and tend to alter to expandable minerals with time, they are most prevalent amongst the phyllosilicates of younger, less weathered, soils. In these soils they tend to occur as discrete mica particles, whereas when they do occur in more weathered soils, it is commonly in an interstratification with expandable minerals. Soil clay micas are dominantly dioctahedral, and up to 6% muscovite can persist even in the 20-200μm fraction of oxic horizons [97].

The mica content of soils developed on uniform parent materials usually increases with depth, reflecting an increase in weathering towards the surface. However, some soils may show a maximum mica content in the surface horizon, due to aeolian addition to soils otherwise low in mica. In soils where clay mica is affected by illuviation, the mica accumulates in the Bt horizon, which may thus contain more mica than either the A or C horizons.

Micas tend to occur preferentially in certain soil size fractions. In soils developed on sediments, micas tend to occur in the 0.2-2μm fraction, as coarser micas are broken down more rapidly during transport and pedogenesis than accompanying minerals such as quartz and feldspar, and finer micas are rapidly altered to 2:1 expandable minerals. In soils developed on parent materials containing macroscopic micas, the mica grain size increases down the profile, but even sand and silt size micas in deeper horizons may be altered to vermiculite.

Adequate K is necessary for the formation of illite or mica. Illite can be formed by the weathering of pre-existing igneous, hydrothermal or metamorphic micas, or by simple size reduction of sedimentary micas from an earlier generation of sediments. Illites are most commonly derived from pre-existing shales, where they have often formed at the expense of smectites or kaolinites during diagenesis. Illite can also form by the weathering of feldspar, diagenetic alteration of kaolinite, montmorillonite or degraded micas, or by authigenesis from solution. Illite can thus have widely varying precursors, yet its composition does not vary too widely. This may possibly suggest that illite composition is governed by equilibration with oceanic water [251] and, if so, this in turn suggests that seawater composition has varied little through geological time [141].

It seems that there is considerable disagreement as to whether any micas are stable phases in contact with seawater and, if so, which ones. Keller [141] believes that [K] is below the equilibrium value for mica to be stable in normal seawater, and suggests that because of this little illitisation of montmorillonite takes place under sedimentary conditions, but occurs readily under conditions of deep burial. With increasing depth, illite formed from montmorillonite is converted to $2M_1$ mica. As an example, in Montana and Idaho, the percentage of the $2M_1$ polytype in the mica assemblage increases from 0% at 1,350m to 100% at 11,400m depth. K to promote illitisation may be provided by low order plants, and while it is often adsorbed onto mineral particles before reaching the ocean, it is not fixed in the structure until diagenetic conditions prevail. However, Fanning and Keramidas [97] point out that glauconites are of marine origin, forming during or after sedimentation, and are probably a stable phase, as they believe that the composition of seawater falls within the mica stability field.

Expandable 2:1 minerals cover a wide range of composition and charge, but are characterised by loosely bound cations and planes of water between the layers. The thickness of the interlayer is variable, as water can be easily driven off and then readsorbed. If the interlayer cations of any 2:1 structure are removed, water can penetrate between the layers and form expandable minerals. Other polar organic molecules can be adsorbed instead of water. Differentiation between smectites and vermiculites is made on the basis of structural charge (see above).

Dioctahedral expandable minerals are most common, and have a charge of 0.5 to 1.8 per formula unit. Those with a charge of 0.5 to 1.2 are known as smectites or montmorillonites, and most of their charge originates in the octahedral sheet. The basal spacing of montmorillonite varies with the saturating cation and the relative humidity, but has fixed values of 1.71nm when ethanl,2diol is adsorbed, and 1.77nm when propan1,2,3triol is adsorbed. Those minerals with a high contribution of charge from the tetrahedral sheets, leading to a total charge of 1.4 to 1.6, are known as beidellites, although they are often called vermiculites when it is known that they are derived by the leaching of K from muscovite or illite.

Montmorillonites form in a range of environments, as their structures allow for great variation in charge distribution between tetrahedral and octahedral sheets, resulting in a wide compositional range and a variety of interlayer cations. They commonly form by the alteration of volcanic glass, and are also common in alkaline soils. Compared with the formation of kaolinite, metal cations except K are retained, and the ratios Si/Al and $Si/H^+$ are higher. Conditions of formation are thus alkaline, and there is no removal of Fe from the system, implying either semi-arid conditions where evaporation is greater than precipitation, or ineffective leaching caused by waterlogging, in rocks of low permeability, or where ash has been deposited in water.

Montmorillonite forms from silicates with high surface area and high reactivity, such as volcanic ash, in which silica is often retained as clay size cristobalite. A pyroclastic texture with evidence of glass shards, flow structures or pseudomorphs after igneous minerals is also often retained. Sheet deposits, known as bentonites, are almost always derived from ash, but it is not known whether alteration ensues almost immediately upon deposition, or whether it it brought about later by circulating groundwater. Much bentonite is nonmarine.

Some montmorillonite that occurs on modern ocean floors is transported by rivers, whilst the rest is formed by in situ alteration of volcanic ash, evidence for which is provided by accompanying authigenic phillipsite and pyroclastic materials. However, there is no positive criterion to signify terrestrial derivation. Montmorillonite can be lost from sediments by solution, or by conversion to illite or chlorite. It is suggested that montmorillonite formed by the alteration of tectosilicates is more stable against further alteration to mica or chlorite than the degraded illites which may readily regrade by adding K or Mg [141].

Certain trioctahedral smectite compositions are stable to high temperatures and pressures, where they may even form as primary minerals. Saponites are found in the kyanite and sillimanite zones of Dalradian metalimestones, and other trioctahedral smectites are found in andesitic lavas in Scotland. In neither case is there evidence to suggest that the minerals are retrogressive.

Trioctahedral phyllosilicates showing limited expansion and a charge of 1.2 to 1.8 are classified as vermiculites and, like smectites, have a variable basal spacing, which is up to 1.44nm when Mg saturated, and 1.45nm when propan1,2,3triol is adsorbed. Practical differentiation between smectite and vermiculite is usually based on the fact that the low charge smectites will adsorb two planes of propan1,2,3triol and expand to 1.77nm, whilst the high charge vermiculites will only expand to 1.45nm by adsorbing one plane of propan1,2,3triol. Low charge (0.5 to 1.0) trioctahedral expandable phyllosilicates are not common in sediments, but include hectorite and saponite.

### 2.2.4 Chlorite Mineralogy and Classification

The chlorites are related by isomorphous substitution within the framework of alternating 2:1 layers ($(Fe,Mg,Al)_6(Si,Al)_8O_{20}(OH)_4$) and interlayer hydroxide sheets ($(Fe,Mg,Al)_6(OH)_{12}$), giving a structural unit thickness of 1.4nm. The 2:1 layers and interlayer sheets are bound by a negative charge on the layers, caused by the substitution of Al for Si, and a corresponding positive charge on the interlayers, caused by the substitution of Al or $Fe^{3+}$ for Mg or $Fe^{2+}$ [18].

The cell parameters of chlorite were first determined in 1930, and in the same year Pauling [203] described the basic features of the atomic structure as alternating "mica like" and "brucite like" layers, with

a = 0.533nm, b = 0.923nm, $\beta$ = 97° and csin$\beta$, perpendicular to the cleavage, = 1.43nm. When taken together, the values of $\beta$ and c implied a displacement of successive cells by a/3. The layers are continuous in the a and b directions, with a basal cleavage between them. Pauling also pointed out that a pure Si tetrahedral sheet would be too small to fit on a pure Mg octahedral sheet, and that the substitution of $Al_2$ for SiMg would allow an unstrained junction. The simplest unit cell is monoclinic, with one layer unit per cell. As well as electrostatic bonding, hydrogen bonding occurs between planes of hydroxyl ions in the interlayer and adjacent planes of Os in the tetrahedral sheets (Figure 2.9).

Minerals with incomplete interlayers are able to expand in polar liquids, and are intermediates between chlorite and either smectite or vermiculite [18]. These minerals have been known as "swelling chlorite" or "pseudochlorite", especially where the dominant cation in the interlayer is Mg [171], but are better described as "hydroxy interlayered" vermiculite or smectite [18]. Distinction between chlorites and hydroxy interlayered vermiculites and smectites can be made by the fact that the interlayer in chlorite is stable, but in the hydroxy interlayered minerals is unstable, when compared with the separate occurrence of the interlayer composition [147].

An idealised formula is $(Mg,Fe,Al)_{12}(Si,Al)_8O_{20}(OH)_{16}$; most chlorites belong to the solid solution series between Fe and Mg end members, with 1.0 to 4.0 Al per 12 octahedral sites balancing the charge due to a similar number of Al per eight tetrahedral sites. The majority of chlorites have 2.0 to 2.8 Al in tetrahedral sites. The extreme range of Fe/(Fe + Mg) variation is 0.01 to 0.96. Often some of the Fe is oxidised, and this can replace octahedral Al. Chlorites are often subdivided into the $Fe^{3+}$ rich leptochlorites and the $Fe^{3+}$ poor orthochlorites. Less common substituents are Mn, Ni, V, Cu and Li. Most chlorites are trioctahedral, but dioctahedral and hybrid forms occur rarely. Cookeite is an Li,Al chlorite with a dioctahedral 2:1 layer but a trioctahedral interlayer, whilst donbassite is a totally dioctahedral aluminous chlorite [9].

The name chlorite derives from the Greek "chloros", green, which is the colour of most varieties, and it is chlorite that is responsible for the colouration of most green rocks. In thin section chlorite often shows pleochroism in shades of green, which are more intense for Fe

rich varieties. As Fe/(Fe + Mg) decreases through 0.52, the optic sign changes from negative to positive, and the anomalous interference colours, caused by the chlorite being isotropic for part of the spectrum but anisotropic for the rest [9], change from blue to brown [2], enabling rapid determination of the dominant octahedral cation. Blue anomalous interference colours reveal the Fe rich nature of the Plynlimon chlorite. However, most authigenic type I chlorites are nonpleochroic, and do not show anomalous interference colours [119]. The birefringence of 0 to 0.01 is lower than that of illite (0.03) or vermiculite (0.02 to 0.03).

There is a perfect basal cleavage parallel to (001) which dominates large, well formed crystals, but fine grained crystal aggregates are more common. The true crystal symmetry is monoclinic, despite the common hexagonal or rhombohedral morphology. The cleavage flakes are flexible but inelastic, with a variable lustre, and have a hardness of 2.5. Density varies from 2.6 to 3.3 x $10^{3}kgm^{-3}$.

As chlorite is the most important mineral in this study, it is necessary to understand how the classification of chlorites and their differentiation from other minerals has developed since the first classification by Tschermak in 1890. However, a most thorough review of that, and all subsequent classifications, exists in the literature [9], whilst the most important classifications are also reviewed by Rezk [219] and Hey [124]. It is on these sources that this review is based, and thus early classifications will only be described briefly, with more attention being paid to the two most important classifications for present use, those of Hey [124], proposed in 1954, and Foster [99], published in 1962.

Tschermak proposed that most chlorites belong to an isomorphous series between antigorite, a serpentine mineral with a formula equivalent to $Mg_{12}Si_{8}O_{20}(OH)_{16}$, and amesite, a septechlorite equivalent to $Mg_{8}Al_{8}Si_{4}O_{20}(OH)_{16}$, but with unlimited substitution of $Fe^{2+}$ for Mg. This series was known as the orthochlorites, and was divided into species at 10% molar increments of the end members. Leptochlorites, containing $Fe^{3+}$, were divided into four groups by the use of four further end members, but the classification proved to be inadequate because of a lack of subdivision on the basis of $Fe^{2+}$ for Mg substitution. Dalmer's classification of 1898 was similar, except that a different method of subdividing the leptochlorites, employing

different end members, was used. In 1939, Hallimond's classification, subdivided the leptochlorites on the bases of origin and $Fe^{2+}/Fe^{3+}$, but was otherwise based on Tschermak's work.

Winchell's classification of 1926 was the first real advance on Tschermak, and used the $Fe^{2+}$ containing equivalents of amesite and antigorite as additional end members in the orthochlorite series. Further end members were provided to allow for compositions containing $Fe^{3+}$ or Cr. However, Winchell insisted that Fe + Mg should total 12 atoms per formula unit, no matter what the octahedral Al content, and thus his formulae resulted in variable O + OH totals. The chlorites were divided into species at 20% molar increments of the end members, but arbitrary species names were employed, ignoring previous usage. Winchell recalculated leptochlorite formulae by reducing all Fe to $Fe^{2+}$, at the same altered sufficient O to OH to preserve charge balance, showed that the vast majority of analyses then fitted in the orthochlorite series, and proposed that only orthochlorites and orthochlorites which had been subsequently oxidised existed. This classification never gained widespread acceptance, because of the variable O + OH contents of the formulae.

In 1927 Orcel began from new chlorite analyses, and showed that no previous classification was suitable. He subdivided chlorites into groups on the basis of $SiO_2/M_2O_3$, and then into species by means of FeO/MgO and $Fe_2O_3/Al_2O_3$. As a result of DTA work, antigorite was rejected as a nonchlorite, but amesite, stilpnomelane and other nonchlorites were retained, amesite even after a revision in 1950 based on the chlorite crystal structure. The revised classification was subdivided on the bases of the number of Si atoms and total Fe atoms, and thus was in some ways a backwards step, as $Fe^{3+}$ containing chlorites were not distinguished from those with all Fe as $Fe^{2+}$. Divisions between species were based on the divisions apparent from analyses of natural occurrences.

Hey's classification [124] followed Winchell's idea of normal and oxidised orthochlorites, drawing the line between them at 4% $Fe_2O_3$, claimed to be in close accord with previous general practice. Amesite was excluded, and the isomorphous series were subdivided on the bases of Si content and Fe/(Fe + Mg). The classification scheme is shown in Figures 2.13 and 2.14, with species limits corrected for full unit cell formulae. The position of an analysis along the Si axis is obviously

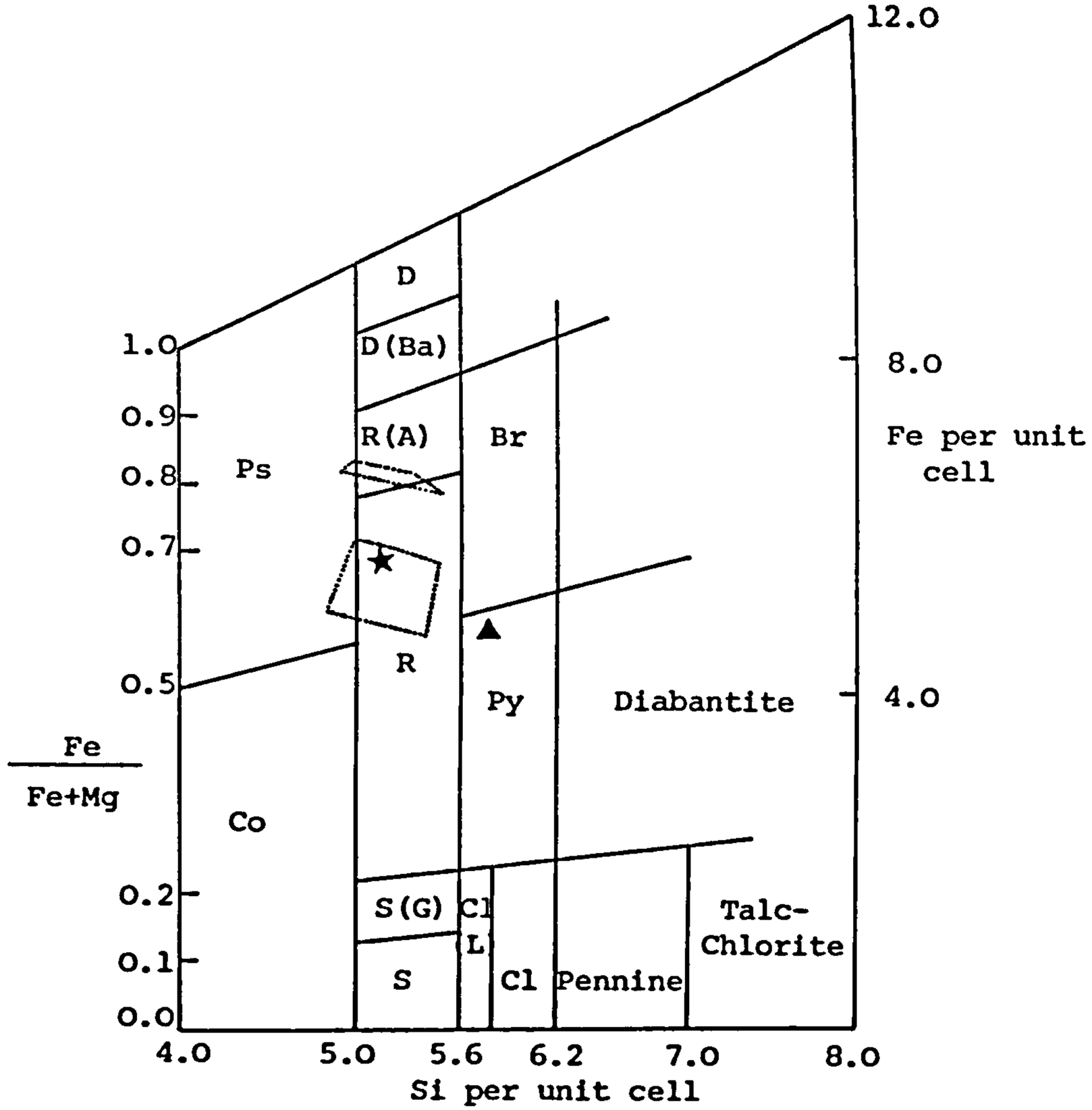


Figure 2.13 Hey's Classification of Orthochlorites [124]

A = Aphrosiderite, Ba = Bavalite, Br = Brunsvigite, Cl = Clinochlore, Co = Corundophilite, D = Daphnite, G = Grochauite, L = Leuchtenbergite, Ps = Pseudothuringite, Py = Pycnochlorite, R = Ripidolite, ____= Composition areas in which Plynlimon chlorites are determined by microprobe to fall, S = Sheridanite. Terms in brackets are varieties of the given species. ▲ = Mean compostion of Rezk's chlorite, as determined by chemical analysis [219], ✱ = Mean composition of Plynlimon chlorite, as determined by microprobe analysis (see section 5.1.1)

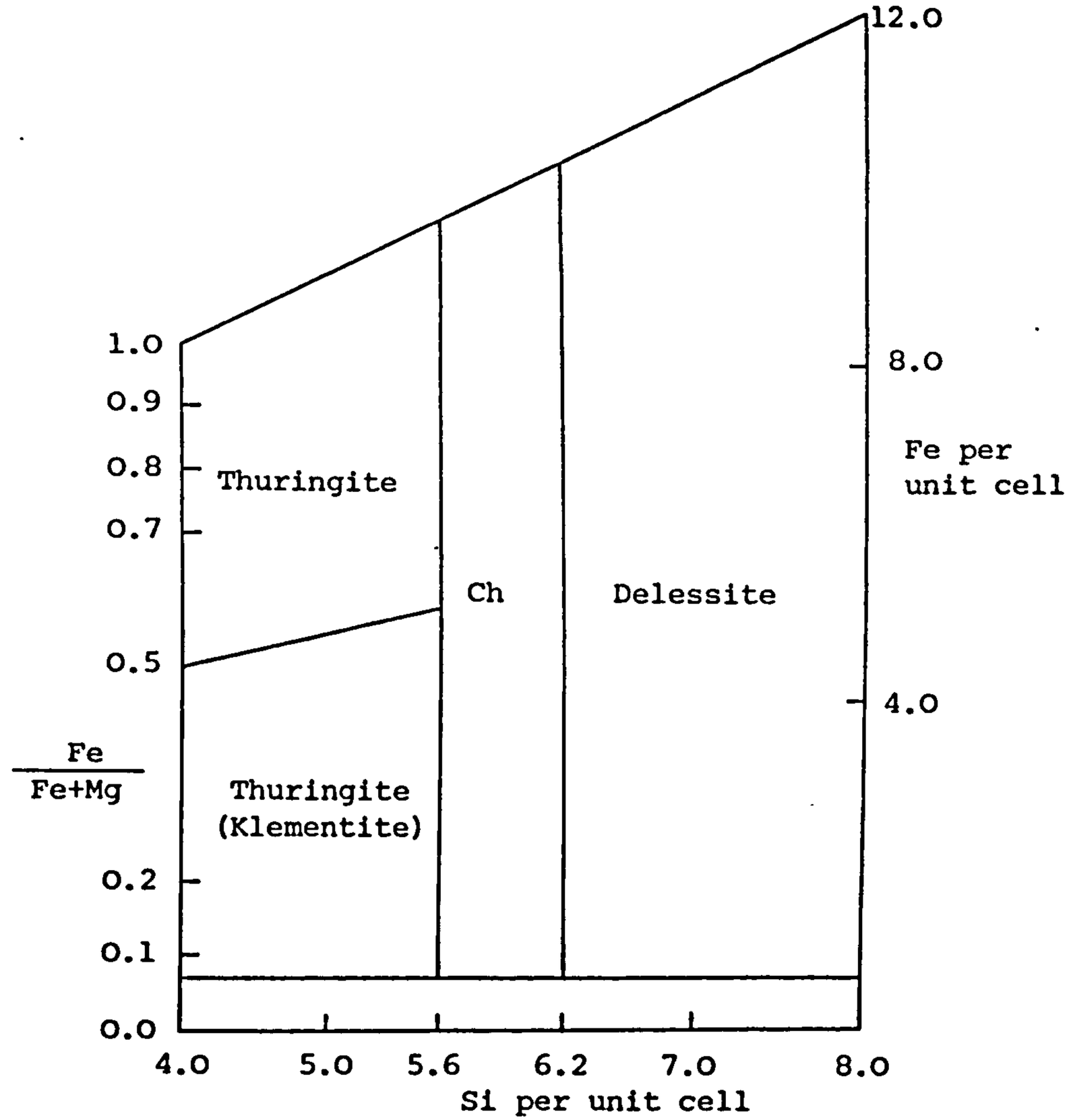


Figure 2.14 Hey's Classification of Oxidised Chlorites [124]

Ch = Chamosite. Terms in brackets are varieties of the given species.

derived, but the position perpendicular to this axis is found on a line joining the appropriate values of total Fe and (total Fe)/(Fe + Mg). This means that chlorites with the same Fe/(Fe + Mg) but different octahedral Al contents might plot in different species fields, but with most analyses the effect of this is not great, although a small change in octahedral Al could alter chlorite of approximate composition $Fe_{5.34}Mg_{4.36}Al_{2.30}Si_{5.70}Al_{2.30}O_{20}(OH)_{16}$ from pycnochlorite to brunsvigite, with no change in Fe/(Fe + Mg).

This classification has been criticised because of its assumption that $Fe^{3+}$ is not an original constituent, and only occurs because of oxidation, because of the arbitrary choice of a 4% $Fe_2O_3$ content to divide orthochlorites from oxidised chlorites, and because of the limited amount of subdivision of the oxidised chlorites, which have subsequently been shown to be more common than orthochlorites.

Foster [99] recast 150 chlorite analyses from the literature into formulae based on the equivalent of 36 O + OH. From this data she was able to show that there was no relationship between the $Fe^{3+}$ and O contents, which would have been expected if the $Fe^{3+}$ was solely due to $Fe^{2+}$ oxidation, as proposed by Winchell and Hey [124]. She found that most chlorites contained more than 4% $Fe_2O_3$, and thus produced a classification based on Si content and $Fe^{2+}/M^{2+}$, with no subdivisions based on $Fe^{3+}$ content. Three divisions on each axis were made, giving rise to nine species, although one was not named. Figure 2.15 illustrates this classification when corrected for full unit cell formulae.

Both Foster [99] and Albee [2] have shown that the $Fe^{3+}$ content of chlorites increases with increasing $Fe^{2+}$, but Albee also reviewed the geological occurrence, chemical composition and optical properties. However, his classification differed from that of Foster [99] in that chlorites were divided into two groups on the basis of Fe content, the dividing line being set at (Fe + Mn + Cr)/(Fe + Mn + Cr + Mg) = 0.1. For chlorites with values of this ratio greater than 0.1, he found that $Fe^{3+}$ constituted 14 ± 9% of total Fe + Mn + Cr, whilst in all other chlorites the $Fe^{3+}$ content was very small.

Other modern classifications are those of Lapham, for chromian chlorites, Phillips, who produced a numerical classification based on six factors, and Van der Marel, who attempted a classification on the

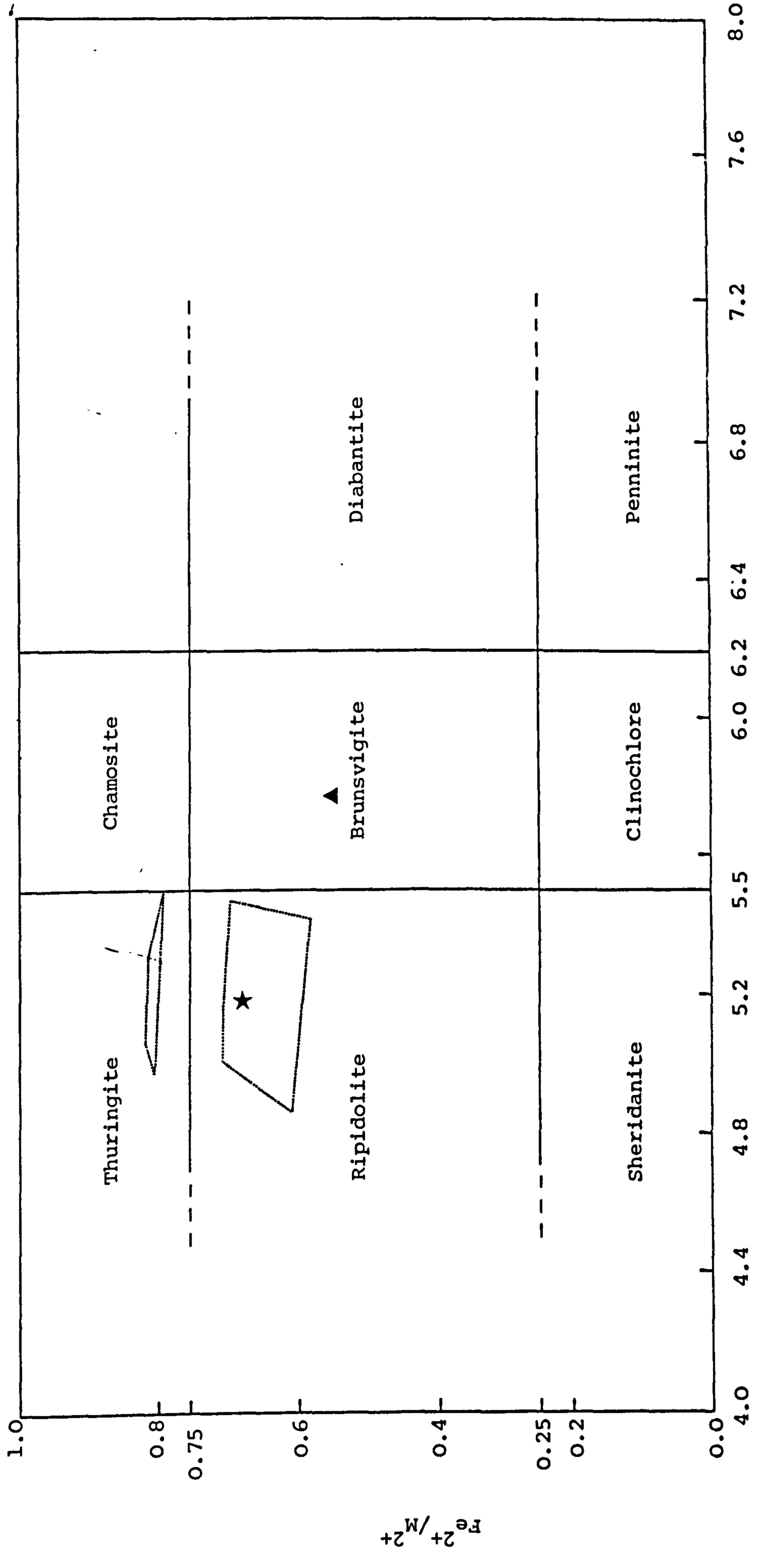


Foster's Classification of Chlorites [99]

★ = Mean composition of Plynlimon chlorite, as determined by microprobe analysis (see Section 5.1.1)

----= Composition areas in which Plynlimon chlorites are determined by microprobe analysis to fall

▲ = Mean composition of Rezk's chlorite, as determined by chemical analysis [219]

Figure 2.15 Foster's Classification of Chlorites [99]

basis of origin and particle size, but the classifications of Foster [99] and Hey [124] have by far the most importance.

Just as with mica polymorphism, polytypism occurs in chlorites because of the possibility of arranging successive layers in different stacking relationships, and also because of the additional possibility of a variable orientation of the interlayer with respect to the 2:1 layer.

The vast majority of chlorites have structures based on one layer polytypes with semirandom stacking of adjacent layers, but with a fixed relationship between the orientation of the 2:1 layer and the interlayer [9,10,43]. Given a defined position for the 2:1 layer, the interlayer can be of either type I or type II, depending on which of the two possible sets of octahedral sites are occupied. Either of these types can be placed over the 2:1 layer in position "a", where one of the interlayer cations is directly above the centre of the ring of Os in the top plane of the 2:1 layer, or position "b", where the three interlayer cations are symmetrically positioned relative to the upper plane of tetrahedral cations in the 2:1 layer (Figure 2.16). This gives four possible structures for each layer/interlayer combination, but there are then two possible groups, each of three randomly chosen ways of arranging the next 2:1 layer on the top of the previous interlayer, resulting in eight structures. However, only six are different, which are: Ia with $\beta = 97°$, Ib with $\beta = 90°$ or $97°$, IIa with $\beta = 90°$ or $97°$ and IIb with $\beta = 97°$. These can all be distinguished by X-ray powder diffractometry using (h01) reflections, and structure factors for the different polytypes are readily available [9,43].

The relative stability of the different polytypes can be predicted from the lengths of their hydrogen bonds and the degree of repulsion between the cations in the tetrahedral sheets and those in the interlayers, and only the four polytypes predicted to be most stable have so far been found to occur naturally. What is more, their relative abundance is as predicted from their theoretical stabilities; out of 303 chlorites, 243 were IIb, 37 Ib with $\beta = 90°$, 13 Ib with $\beta = 97°$ and 10 Ia, with neither of the IIa polytypes being found [9,10,43].

Although the IIb polytype is most stable, when chlorite is formed authigenically in low energy situations it generally occurs as metastable Ia and Ib polytypes [43,119]. The activation energy of the transformation to IIb requires a low grade metamorphic temperature of

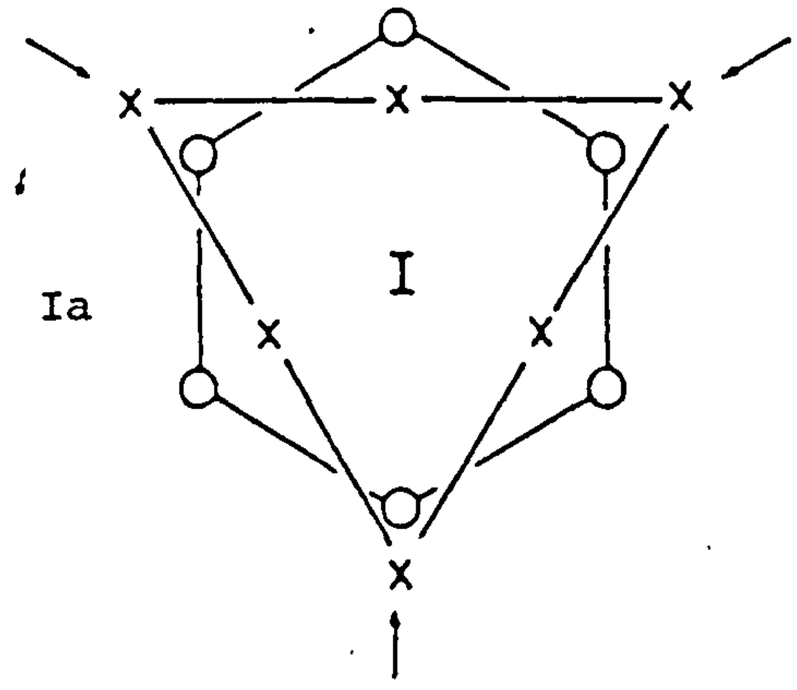


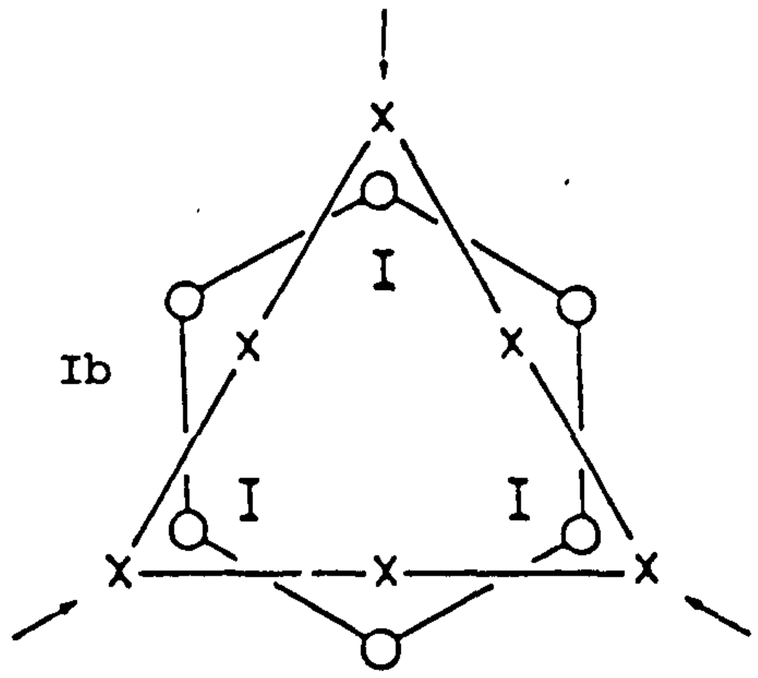


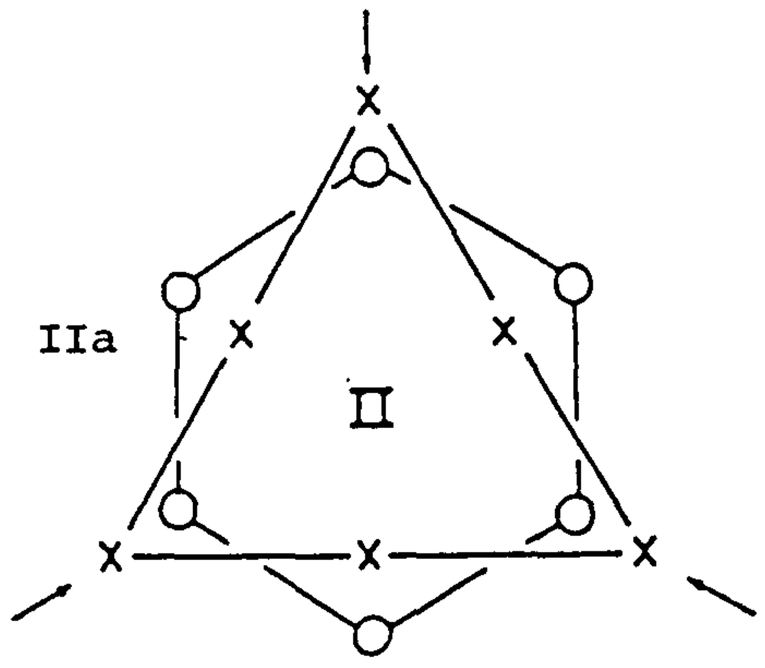


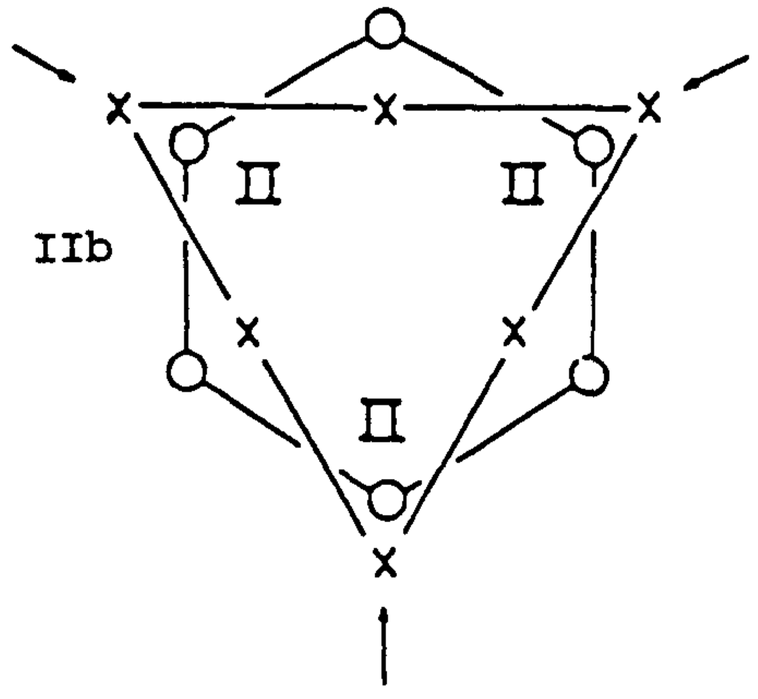


X = Hydroxyl ion in interlayer hydroxide sheet

O = Oxygen in tetrahedral sheet of 2:1 layer

I = Octahedral cation in type I interlayer hydroxide sheet

II = Octahedral cation in type II interlayer hydroxide sheet

Figure 2.16 Possible Structures of Chlorite Layer-interlayer Combinations after Brown and Bailey [43] Shifts of the interlayer hydroxide sheets by $a/3$ in any of the directions shown by the small arrows will convert a Ia structure to Ib, and IIa to IIb, or vice versa.

150 to 200°C to bring it about, occurring at a grade equivalent to the transformation of shale to slate and illite to $2M_1$ dioctahedral mica [119,125], as the IIb structure is the only one in which the interlayer is arranged antiparallel to the octahedral sheet in the 2:1 layer [119].

As well as the one layer polytypes with semirandom stacking, 12 one layer structures with regular stacking are possible [10,43]. Two of these are triclinic with $\alpha = 102°$, two have orthorhombic unit cells but monoclinic symmetry, and eight have monoclinic unit cells, one of each polytype with monoclinic symmetry and one of each polytype with triclinic symmetry. Identification of the regularly stacked monoclinic structures can only be made via the intensities of (hkl) reflections for $k \neq 3n$. These reflections are weak, and thus identification usually requires single crystal photographs, on which the $k \neq 3n$ reflections are sharp for regular structures, but streaked for semirandom polytypes [10]. This streaking indicates random selection of interlayer shifts related by ±b/3.

Of the 12 regular structures, only three have so far been found in nature, and only four chlorite structures have been refined in detail: a semirandom Ib ripidolite, a IIb-4 corundophilite, a Ia-4 Cr pennine and a IIb-2 pycnochlorite (the number after the polytype for the regular structures refers to the direction of stagger of the repeating 2:1 layer relative to the direction of stagger between the initial 2:1 layer and the interlayer) [9]. Single crystal studies often show that the regular structures have a symmetry lower than the ideal for their polytype, and this is considered to be due to the ordering of cations.

For 10 of the regular polytypes, two out of three octahedral sites are related by symmetry, but for the two remaining polytypes the sites are independent. Of the four refined structures, the pycnochlorite and corundophilite show ordering only in the interlayer, whilst the pennine shows it in both octahedral sheets. In this mineral, all trivalent octahedral cations are in the unique site, and thus are positioned exactly between the loci of excess negative charge in the tetrahedral sheets due to ordering of Al substitution for Si. This is the best way of preserving charge balance. Only one of the other chlorites shows an ordered tetrahedral distribution, but three of the structures show most of the octahedral charge to be located in the interlayer, whilst in the fourth structure it is split equally between the octahedral sheets.

There are significant differences in compositional range between the polytypes [43]. Ia and Ib with $\beta$ = 97° have much lower tetrahedral Al contents than IIb and Ib with $\beta$ = 90° structures, having average Al contents of 2.06 and 1.74 respectively, compared with 2.62 and 2.64. The Ib with $\beta$ = 97° structure also has a layer thickness greater than that of the other polytypes by an average of 0.014nm, due to weaker interlayer bonding because of lower Al for Si substitution. The compositions of Ib with $\beta$ = 97° and Ia chlorites tend to fall in the chamosite, brunsvigite and diabantite fields of Foster, whereas IIb compositions occur in parts of all the named fields except diabantite.

### 2.2.5 Chlorite Occurrence

Chlorite is now known to be found in many rocks and soils as a minor mineral, but is rarely a dominant mineral. In igneous rocks it is not a primary mineral, but a widespread product of hydrothermal alteration of biotite, pyroxene or amphibole. Often the composition is determined by that of the primary mineral, with Fe rich chlorites replacing Fe rich ferromagnesian minerals. Pseudomorphous chloritisation of biotite is particularly common in granites. Chlorite is also found infilling amygdales and in low temperature hydrothermal veins with quartz and feldspar.

Chlorite is common in regionally metamorphosed rocks, and is the most characteristic mineral of the greenschist facies, being stable up to 450°C and 10kbar. At higher metamorphic grades the chlorite content decreases, and biotite is formed by the reaction of chlorite with a K rich mineral. The chlorites from metabasic rocks are usually rich in Al, being derived from Al rich hornblende or epidote.

In sediments chlorite can be both detrital and authigenic, forming alongside glauconite in nearshore marine environments. It occurs as a cement in some porous sandstones and as ooliths in Fe formations. Authigenic chlorite is of polytype Ib, whilst detrital chlorite is usually IIb, stable in the chlorite zone of regional metamorphism. Chlorite may dominate the finer than 2μm fraction of a sediment. It can occur in interstratified structures with other phyllosilicates, such as a regular 1-1 chlorite-vermiculite interstratification. Mn containing chlorites are usually associated with Mn ores, but the Mn content of chlorites from the Cambrian Manganese Shale Group of the Harlech Dome, Gwynedd, is calculated not to be high [184].

Chlorite can form during diagenesis, especially where pore waters are Mg rich, and it is second only to illite in abundance amongst the phyllosilicates of Palaeozoic and older shales, of which it typically forms 20%. Vermiculite is converted to chlorite during diagenesis via the corrensite structure [218]. It is also possible for chloritisation of montmorillonite to occur in the sea. Chlorite formed in this way can be distinguished by its Cl content of about 1000ppm, compared to the 100ppm found in other chlorites. This high level of Cl is due to the fact that when montmorillonites are altered to chlorites by the addition of an interlayer hydroxide sheet, in the marine environment Mg hydroxychlorides are incorporated into the hydroxide sheet [141].

Berthierine, commonly known as chamosite, is an Fe rich layer silicate with a basal spacing of 0.7nm which is common in oolitic Fe ores, but it is more closely related to the serpentine minerals than to the kaolinites [10]. However, true chlorite minerals with identical chemical compositions to berthierine exist, and distinction can only be made by means of XRD analysis or DTA. Distinction is complicated by the fact that interconversion of the crystal structures can occur.

Soils can also contain both detrital chlorite and chlorite formed pedogenically from other layer silicates. Interstratified minerals may reveal this transformation in progress. Once again, chlorite is not usually a dominant mineral, but dominantly chloritic soils are known from Snowdonia, Gwynedd, where the soils form on pumice-tuff, from which the chlorite is inherited [16]. In general, the occurrence of soil chlorite is directly related to the occurrence of chlorite in the soil parent material.

### 2.2.6 Chlorite Identification

Chlorite is readily identified on XRD traces by its regular sequence of (001) peaks. These are not affected by standard treatments except that, on heating to 500 to 550°C, the intensity of the (001) peak increases two to fivefold, and the intensity of the other (001) peaks decreases. However, in the presence of kaolinite, any quantitative XRD measurements of chlorite are prevented by the fact that the (001) and (002) reflections of kaolinite respectively overlap the (002) and (004) reflections of chlorite [9,18,45]. If both minerals are well crystallised, the chlorite (004) and kaolinite (002) peaks may be partially resolved, but if the minerals are poorly crystallised, other treatments are necessary. In theory heating to 450 to 500°C should

disorder the kaolinite but leave the chlorite unaffected, but in practice many poorly crystalline chlorites are altered at temperatures below this [9,18,45]. For this reason it is generally recommended that intersalation of the kaolinite should be carried out, which increases its basal spacing from 0.72nm, and thus away from the chlorite reflections, without affecting the chlorite structure. Intersalation with potassium acetate followed by washing with ammonium nitrate increases the kaolinite basal spacing to 1.16nm [9,18], whilst alternatively treating the K saturated specimen with dimethyl sulphoxide increases the kaolinite basal spacing to 1.13nm [219].

A characteristic chlorite DTA curve has a large endotherm at 450 to 650°C due to dehydroxylation of the interlayer, a smaller endotherm at about 700°C due to the dehydroxylation of the 2:1 layer, and an exotherm between 750 and 900°C due to decomposition. However, chlorites from soils seldom show these peaks [13]; all of the peaks are weakened, and the major endotherm is split into two by the effects of Fe oxidation. In well crystallised chlorites progressive dehydroxylation of the interlayer starts with sites associated with $Fe^{3+}$ at 250°C, followed by those associated with $Fe^{2+}$ at 430°C, Al at 500°C and Mg at 640°C. A similar pattern occurs with the 2:1 layer, where sites associated with $Fe^{2+}$ dehydroxylate at 530°C, those associated with Al at 750°C and Mg at 820°C [18].

Using infrared adsorption analysis, chlorites can be distinguished from serpentines of similar composition by the fact that the latter have strong adsorption bands in the 3571 to 3704$cm^{-1}$ O-H stretching region, which are either very weak or not present in true chlorites. Similarly, true chlorites show no resolved band at 910$cm^{-1}$ [9]. Dioctahedral chlorites can be distinguished from trioctahedral by the lack of an adsorption band near 760$cm^{-1}$, which is present for Mg trioctahedral chlorites and strong for Fe trioctahedral structures [9]. Infrared analysis can also be used to estimate chlorite composition. The wave number of the strongest Si-O band in the 620 to 692$cm^{-1}$ region increases with increasing octahedral Al, but decreases with increasing Mg and Fe. The two strong OH adsorption bands in the 3400 to 3436 and 3560 to 3586$cm^{-1}$ regions also decrease in wave number with increasing Fe, and similar relationships are found in other regions of the spectrum [9].

### 2.2.7 Noncrystalline Clay Size Minerals

Besides the minerals with well defined structures considered in Sections 2.2 to 2.2.6, noncrystalline clay size minerals can play an important role in soils. The boundary between crystalline and noncrystalline materials is not sharp, and some well defined mineral species have order in only one or two dimensions. Even in materials which appear to be truly without a regular structure, there needs to be a statistical ordering of atoms to fulfil co-ordination requirements, and thus the term "noncrystalline" is preferred to "amorphous" for these minerals [11,12].

In soils, hydrated noncrystalline Al, Fe and Si oxides and Al and Fe silicates can be very important, especially in soils developed on ashes and lavas, where they may be the dominant minerals. In other soils they are common as thin surface coatings on other minerals. Allophane has the approximate composition $Al_2O_3.2SiO_2.nH_2O$, whilst imogolite is more aluminous ($Al_2O_3.SiO_2.2.5H_2O$), and may form from allophane by desilication. Imogolite has a one dimensional structure, forming tubes with an outer diameter of 2.0nm, making it possible to identify under the electron microscope [75]. Noncrystalline minerals tend to have high specific surface areas and CECs [105], and are thus very reactive. As a result of this, they tend to be short lived intermediaries formed during the formation of secondary crystalline minerals.

## 2.3 THE WEATHERING OF ROCKS AND MINERALS

Weathering is the process by which rocks and minerals are altered towards equilibrium with the environment in which they are found, that of the terrestrial surface [164]. The minerals of most rocks are not in equilibrium with the earth surface environment, because they were formed under conditions of higher temperature and pressure than are found at the earth's surface. This is obvious for igneous and metamorphic rocks, but it is also true for most sedimentary rocks, as many clastic sediments are the remnants of a previous weathering cycle that has been interrupted by lithification before reaching equilibrium.

There has been considerable discussion as to what constitute weathering and pedogenesis, but it is clear that the processes are closely related [219]. Some have held that weathering transforms the rock into a soil parent material, which is then altered into the soil by pedogenesis. In particular, pedogenesis has been distinguished from weathering by the lack of biological activity in the latter. However, other authors

have held either that weathering is the first stage in soil formation, or that pedogenesis is the final stage of weathering. Whatever view is taken, soil is the end product of weathering and pedogenesis, and because of the wide variety of rocks and the range of climatic and topographic conditions under which weathering can occur, there is great diversity in the soils that can be formed.

When presented with a soil, the degree of weathering it has experienced can be interpreted by comparing its mineralogy with that of its parent material. The relative rates of alteration of different minerals may vary slightly with changes in the environment, but in broad terms a general order of mineral stability can be produced, which suggests that soils containing considerable proportions of the less stable minerals have experienced little weathering. One of the earliest studies of weathering, by Goldich in 1938 [111], gave rise to a stability order the reverse of that found in Bowen's reaction series for the temperature of crystallisation of minerals in igneous rocks. This finding is not unreasonable; it would be expected that the minerals which are stable under conditions most different from those prevalent at the earth's surface would be the ones that react to reach equilibrium most rapidly. Thus Goldich's work showed quartz to be the most stable igneous mineral, and olivine the least stable. Goldich considered that any apparent deviation from this order of stability indicated the occurrence of abnormal weathering conditions. Other mineral stability scales have been based on energies of formation and on the proportion of the unit cell that is occupied by ions, but the conclusions have been similar.

When considering soils, hydrous minerals not found in the reaction series, such as chlorite, must be included, and work on clay size particles suggests that quartz is relatively unstable compared to most phyllosilcates, whilst Fe oxides and heavy minerals are the most stable phases [114,134]. Jackson's weathering indices were derived from observations made on mineral assemblages in soils [134].

The nature of the bonding in aluminosilicate minerals is very important in determining the degree of susceptibility to weathering. Although feldspars contain readily mobilised Na, K and Ca, they are more stable under weathering conditions than forsterite which contains the less mobile Mg. This is because the feldspar structure is a three dimensional framework, hindering cation movement, whilst olivine

contains individual $SiO_4$ tetrahedra which present little resistance to Mg loss [71], and expose more cations on the mineral surface.

There are in fact two aspects to weathering, physical and chemical, but considerably more research has been carried out into the chemical aspects. However, it is rare for either physical or chemical weathering to act alone. Physical weathering, in its action in breaking down a rock to unconsolidated particles, and in reducing the size of those particles, ensures that there is a greater free surface for chemical reactions to take place on, and a closer approach between the rock particles and the weathering agencies such as soil solutions. Similarly, chemical weathering can cause irregularities in grain surfaces, such as the fraying of mica edges, which provide openings for the activities of physical weathering [97,195,214], whilst the concentration of chemical attack along grain boundaries due to high surface free energies rapidly leads to physical disaggregation.

### 2.3.1 Physical Weathering

Amongst the agencies of physical weathering are thermal expansion and contraction, fire, plant root growth, frost action and changes in the loading experienced by the rock. Physical weathering may act along lines of weakness already present in the rock, such as grain boundaries or bedding planes, or new lines of weakness may be generated. On a large scale, physical weathering is more important than chemical weathering in its effects on a fresh rock, but as scale is reduced, the effects of chemical weathering tend to become dominant, especially when the weathering agents are acting on very fine grained material.

### 2.3.2 Chemical Weathering

Rather than only reducing particle size, which it may do by removing a cementing phase from a rock, chemical weathering also acts to alter or completely dissolve some mineral components of the rock undergoing weathering, perhaps generating new mineral phases in the process. All chemical weathering is carried out through the medium of water, but the rate of weathering is much enhanced by the solution of active materials, such as $CO_2$, organic acids derived from plants, or inorganic acids derived from the oxidative weathering of sulphides, in the water. Because of the importance of water, chemical weathering is reduced in arid areas; it is also reduced under arctic and alpine conditions where, although water may be present, the rate of reaction is slowed down because of the low temperatures, or because the water is present

as a solid phase. In humid climates, the rate of weathering increases with temperature, and reaches a maximum in the tropics. As almost all weathering environments are open systems, the rate of leaching by water is very important in determining how rapidly weathering progresses, and eventually weathering products will be removed from the reaction area, either by precipitation of stable phases, or by leaching in solution [164]. Only in areas where potential evapotranspiration exceeds precipitation can weathering products accumulate in the reaction area.

Water on its own can only be an effective weathering agent through the action of hydration and hydrolysis, but when it contains active dissolved phases it can be effective through the mechanisms of ion exchange, chelation and oxidation as well. Although mineral crystals are electrically neutral, they have broken bonds in their crystal lattices on edges and faces, which result in localised charge. The extent of the charge depends on the pH of the environment; at the isoelectric point pH, which varies with mineralogy, no surface charge is developed. Below the isoelectric point pH, minerals develop positive charges, and above it negative charges are developed. When placed in water, these charges create dipoles in adjacent water molecules, which can lead to ionisation into $H^+$ and $OH^-$. The $H^+$ ion is very small, but highly charged for its size, and readily penetrates into crystal lattices, where the high charge:radius ratio tends to cause the lattice to expand, forcing ions from the crystal into solution to replace the $H^+$ which has become part of the mineral grain [6,101]. The build up of metal and hydroxyl ions in solution will eventually make attack by $H^+$ more difficult, unless a source of $H^+$, such as dissolved $CO_2$ [111] or organic acid, is available. An alternative mode of attack is for metal ions at the surface of the crystal to attract complete water molecules, and then to be taken into solution as hydrated ions, allowing access by water to the next layer of ions in the crystal.

The effect of hydrolysis is to increase the pH of the weathering environment, especially near to the surface of the grains being weathered, although the precise effect depends on the nature of the material being attacked. It has been suggested that the higher the pH developed, the more susceptible the mineral is to weathering [131]. A high pH reduces further attack by hydrolysis, but as leaching increases the released metal ions can be removed, and the pH lowered. If the potential rate of removal due to leaching is greater than the rate of

release, the soil can become acid, as in podsols. However, in arid areas, where evaporation is greater than precipitation, alkali and alkaline earth metals are not leached, and the environment retains a high pH. pH is of considerable importance in weathering, as the relative solubilities of different elements, particularly Al and Si, vary significantly with pH. At a pH less than four, Al is more soluble than Si, but from pH five to nine Si is more soluble than Al. This behaviour is consistent with the occurrence of diphormic clays in acid environments, and triphormic clays in alkaline environments [90,262].

Ion exchange is an extension of hydrolysis, but with ions other than $H^+$ being taken up from solution. For instance, mica has a high preference for K on interlayer sites at frayed edges [97,175]. These sites will take up K from solution when it is present only in very low concentrations, and in doing so will prevent the weathered edge expanding into the crystal, by collapsing the structure to 1.0nm thickness. However, other minerals may take up readily hydrated cations if their concentration in solution is sufficiently high, allowing hydration and structural attack to occur. Exchange of ions with plant roots can take place [142], but in this case the plant usually gains essential cations from the mineral, replacing them in the mineral structure with $H^+$, which causes instability and breakdown.

For ferromagnesian minerals oxidation is one of the most important mechanisms in weathering, as it alters the charge balance, forcing other ions to leave the crystal to maintain electrical neutrality. Conditions in soils are normally oxidising above the water table and reducing below it, but large quantities of organic matter can produce locally reducing conditions above the water table. The effects of oxidation are most commonly seen in Fe containing minerals, as most Fe bearing minerals have Fe in the reduced state when formed in igneous or metamorphic rocks. For this reason oxidation can play an important role in the weathering of mica and chlorite [65,107,129].

Transition elements usually show different levels of solubility associated with different oxidation states, and thus variation in Eh can affect the mobility of an element during weathering. Eh/pH diagrams can thus provide a useful means of indicating the minerals that are stable in a given chemical system under different environmental conditions. However, their drawbacks are that they are built up from thermodynamic data derived from pure substances, that no

suitable thermodynamic data are available for the organic matter which is an important control of Eh, and that they represent equilibrium conditions, which are rarely found in the weathering environment. Eh is controlled by the access of atmospheric $O_2$ and the presence of organic matter, so well drained soils tend to be more oxidising than those that are waterlogged. If the Eh/pH stability field diagram for Fe containing species is drawn, the boundary between $Fe^{2+}$ and $Fe(OH)_3$ falls in the middle of the Eh/pH range covered by natural environments, for the normal range of Fe activity contours. For this reason, oxidation or reduction of Fe would be expected to be a common phenomenon in weathering, occurring with only slight changes in Eh or pH. The change from $Fe^{2+}$ to $Fe(OH)_3$ causes a considerable reduction in the mobility of Fe.

As well as affecting weathering by altering pH and Eh, organic matter can be even more effective in weathering because of its complexing abilities. Many relatively simple organic compounds produced by plants, such as oxalic and salicylic acids and polyphenols, are very powerful complexing agents, and readily extract metal cations from mineral surfaces [130,189]. Lichens, mosses and algae are particularly important in the release of these chemicals, and laboratory and field studies have shown that extracts from them accelerate weathering. Polyphenols washed by rain from the leaves of higher plants are also effective chelating agents. Chelation of Fe and Al is important in their eluviation from the Ae horizons of podsols [47], whereas lower in the soil profile the chelates can be destroyed by micro-organisms, leading to precipitation of Fe and Al, which can also be brought about by an increase in the cation:organic matter ratio.

Once released from its original crystal structure, the behaviour of an element could follow several possible routes. Under appropriate Eh/pH conditions, it can remain in solution and be transported from the soil into a stream and eventually to the sea. If Eh/pH conditions change, the solubility can be reduced, and the element precipitated at varying distances from its source in different chemical forms. Interaction with other minerals or noncrystalline phases through ion exchange or surface adsorption is possible, with phyllosilicate surfaces able to adsorb both anions and cations, depending on pH and mineralogy. Sorption by organic matter can also remove considerable amounts of some elements from the weathering system. Of particular importance is the sorption of Fe and Al hydroxy complexes by expandable phyllosilicates,

which can lead to their fixation and the transformation of the minerals to hydroxy interlayered structures [18]. As weathering progresses, most of the original minerals are transformed, leaving only the most resistant, such as quartz and the heavy minerals rutile, ilmenite, zircon, tourmaline and magnetite, together with hydrous aluminosilicates which may be either in the form of noncrystalline colloids or crystalline phyllosilicates [134].

Starting with the work of Goldich [111], early weathering studies were mainly descriptive, indicating differences between the mineralogy of fresh and altered material. They tended to be based on whole rocks, rather than individual minerals, but sometimes included basic chemical studies of cation release. Some theoretical interpretation of weathering relationships was also carried out [114,164]. Following on from this, more detailed studies of cation loss have been made, starting initially with well crystallised granites [109,118,181,273], being extended to a wider range of igneous and metamorphic rocks under different environmental conditions [53,54,153,235,237,272], and finally covering finer grained metamorphic rocks and sediments [36,113,120, 257]. At the same time, other studies began to investigate the surface morphology of fresh and weathered mineral grains [269].

Chemical weathering indices such as $Al_2O_3/(FeO + MgO)$ have been proposed to indicate the degree of weathering a rock has undergone [89,237]. These are generally based on the assumption that elements such as Al and Ti are not mobile during weathering, or that Zr minerals are not affected by weathering, but there is evidence to suggest that these assumptions are not valid under all conditions [100]. Although early weathering studies were mainly concerned with the interpretation of field observations, experimental weathering investigations, to accelerate the natural processes, have developed rapidly, using different methods and chemical systems [123,170,268].

One of the first studies of small scale weathering mechanisms was that of Garrels and Howard [101], who produced a theoretical explanation for the observed rates of movement of ions into solution from finely ground feldspar and micas. Feldspar weathering had been investigated since 1848, when it was first observed that finely powdered feldspars gave an alkaline reaction when placed in water [5], but since the mid 1970s a very considerable amount of work on feldspar weathering has been carried out, being an example of the more general trend in weathering

studies away from descriptions of whole rock weathering towards more detailed studies of aspects of the weathering of single species.

Early experimental work on feldspars showed that Si and Al could be taken into solution in cold water, along with the alkalis [5]. In fact, in a closed weathering system in a soxhlet apparatus, it was shown that silica was dissolved in preference to alkalis, no doubt due to the high pH of 10.5 that was reached in the system [32]. Most of the more recent work has concentrated on the elucidation of the mechanisms behind feldspar dissolution, and the kinetics of the reactions controlling these mechanisms [50,51,194,204,247]. The discussion in these papers is concerned with whether dissolution is controlled by selective reaction at the feldspar surface, or by diffusion through an altered surface layer. Detailed scanning electron microscope (SEM) comparisons of naturally weathered and laboratory altered feldspars are now seen to favour the former mechanism [21,22, 126], and similar SEM work has been extended to other mineral species [23]. As well as the studies of the kinetics of feldspar dissolution, much other recent work has developed the mathematical modelling and interpretation of mineral stability and dissolution reaction kinetics in general [20,74,146,159,216,238,265,266].

The type of work that has been carried out in detail on feldspars will no doubt be extended in future to other minerals including the phyllosilicates, which have more variable chemical compositions and mineral structures. The ultimate aim of the mathematical modelling of weathering reactions must be to be able to predict the interactions that occur between the different minerals in a rock that are all being altered at the same time. As will be seen in Sections 2.3.3 and 2.3.4, the mathematical modelling that has been applied to feldspars has yet to be related to the weathering of chlorites and micas, where the mechanisms controlling attack under different conditions are not fully agreed, and several mechanisms may be in operation at once.

When modern techniques became available, it was shown that, contrary to expectations, REEs were concentrated on weathering [165,166]. The application of REE ratios is now able to show whether marine weathering products are locally derived, or formed on land [66,67,83]. An even more sophisticated technique uses uranium isotope disequilibria between rocks, soils and river waters to calculate weathering rates [186], whilst hydrogen and oxygen isotope ratios can be used similarly [155].

Despite these very considerable advances in techniques and methods of interpretation, differentiating the effects of environmental conditions from those due to rock variability is sometimes a problem in field studies, although it can be readily overcome in laboratory studies. However, it has been suggested [78] that the study of the alteration of building stones can indicate the effects of environment, as in different manmade exposures, a single type of decorative or structural rock could be subjected to many different environments.

### 2.3.3 The Weathering of Mica

Many studies [1,14,18,47,55,63-65,72,77,80-82,91,92,107,110,119,136, 139,151,168,174,182,208,211,219,220,258] have been made of the weathering of chlorite and illite in soils developed on different parent materials, but where both illite and chlorite are present, the conclusion has always been, except in two cases [220,253], that chlorite is more susceptible to weathering. Most studies have involved the weathering of trioctahedral chlorite and dioctahedral illite, which are the most common forms. However, one study that showed illite to be more rapidly altered concerned trioctahedral illite [220], suggesting that, in general, it is trioctahedral phyllosilicates which are broken down most readily in soils. Where both chlorite and illite were dioctahedral [1], it was chlorite that was most susceptible to alteration. Artificial weathering experiments also indicate that dioctahedral minerals are more resistant to chemical attack [19,158,195]. It might be that the absolute susceptibility to weathering of illite is not substantially less than that of chlorite, but it is suggested that the earlier breakdown of chlorite can saturate the soil solution with the cations that would be produced by breakdown of illite, thus protecting the illite [81,182].

The weathering of micas can be both physical and chemical. Although little investigated, the former is quite important, as it generally consists of a reduction in particle size, to which many mica properties are related. Chemical and mineralogical alteration have been investigated in considerably more detail, particularly the common alteration of micas to 2:1 expandable minerals [195], which takes place by replacing interlayer K by hydrated cations. After alteration, much of the original mica structure remains intact, and thus the transformation process is known as simple transformation, and takes place according to the equation [97]:

K Micas + Hydrated Cations ⟶ Expandable 2:1 Minerals + K

Simple transformation can occur by both edge and layer alteration (Figure 2.17) [214]. When transformation occurs by layer weathering, the interlayer cations are completely replaced in some units, whilst remaining more or less intact in others, and thus interstratified mica-vermiculite or mica-smectite results. The intensity of weathering, the nature of the soil and the mica polytype determine whether the expandable mineral is formed directly, via interstratified intermediates, or whether the weathering does not proceed further than the interstratified minerals. This model is supported by the occurrence of such interstratified minerals in soils, although it is possible that they could form there by the preferential uptake of K by certain interlayers in expandable minerals. The same factors determine whether vermiculite or montmorillonite is the final product, and whether hydroxy interlayers are present.

In some cases of layer weathering, regular interstratification results [139]. This may be due either to less strong bonding of K in alternate interlayers in two layer polytypes, or because the loss of K from one interlayer causes a reorientation of the protons in adjacent hydroxyls towards the now expandable interlayer, thus exposing the K ions in the adjacent interlayer to a greater effective negative charge [195].

Edge weathering may occur simultaneously with layer weathering, but initially only involves a partial replacement of K in the interlayer sites, leaving unaltered mica cores with frayed edges of more or less expandable minerals. Evidence for this mechanism is provided by scanning electron micrographs [214]. Layer weathering seems to be more common in small particles and edge weathering in larger particles [195]. Wedge sites in partially altered micas show a very strong selectivity for K and other large, weakly hydrated cations, such as Ba, Rb and $NH_4$ [175]. Although basal sites only have a selectivity coefficient for K compared with Na of two, the selectivity coefficient of wedge sites for K is 500 [97], and thus K is very readily fixed into the structure again, should its concentration in the weathering environment increase even slightly.

As weathering takes place, there appears to be an accompanying reduction in the layer charge [6,158,195], but the reason for this is not well understood. The idea that oxidation of structural Fe could

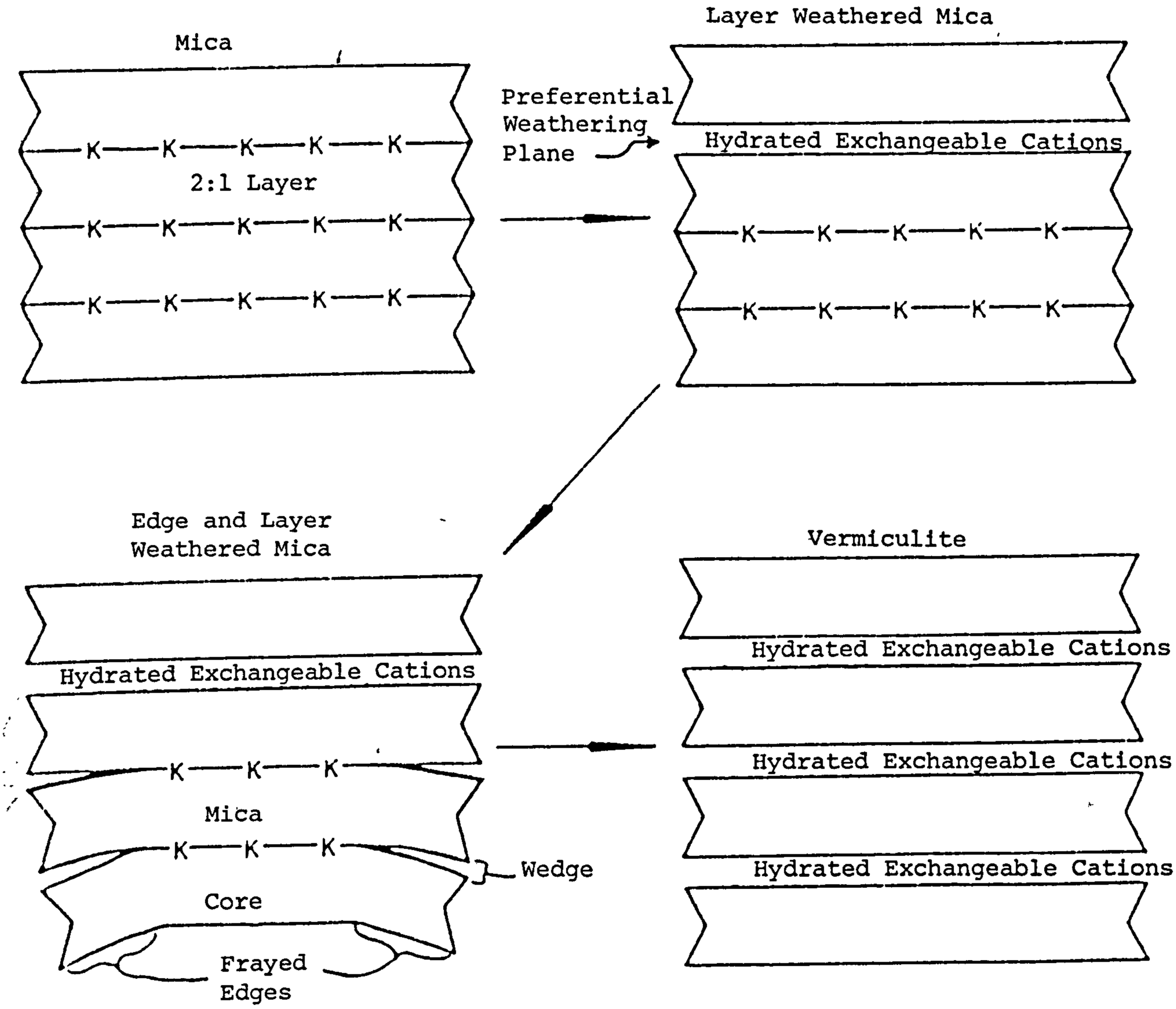


Figure 2.17 Edge and Layer Weathering of Mica by Replacement of Interlayer Potassium with Hydrated Cations after Fanning and Keramidas [97]

reduce the layer charge was once favoured [129,195], but this oxidation has also been shown to retard the loss of K [108], and thus the rate of alteration. Alteration of OH to O by proton ejection often accompanies Fe oxidation, and this would tend to maintain the structural charge. However, it is also possible for ejection of oxidised Fe to take place, forming a dioctahedral structure [98,108], which could increase the layer charge. Two possible mechanisms for the reduction of layer charge are the formation of OH from apical Os, and the replacement of Al with Si, evidence for which is provided by the fact that vermiculites and smectites have lower tetrahedral Al/Si than micas.

Evidence for simple transformation comes from both artificial weathering studies in which interlayer K is removed by chemical or biological agents [25,26,34,130,145,189,195,214,234,267], and from studies of phyllosilicate distributions in soil profiles [52,72,80-82, 91,110,139,192]. Several chemical methods have been used to bring about the transformation, and most produce vermiculite. However, a few experiments show the production of smectite from illite and glauconite.

In the field, alteration beyond simple transformation can occur, especially under acid conditions, with the structure either being completely destroyed, octahedral sheet first [34], or tending towards the formation of pedogenic chlorite, with the incorporation of an interlayer hydroxide sheet. The latter process can only occur where leaching is less intense, as it is in a sense constructive. In spodosols where illite is altered to vermiculite in the Bh horizon, the alteration product is interstratified chlorite-vermiculite in the Bir horizon [63], and in brown podsolic soils in New England, where irregularly interstratified illite-vermiculite is found in the D horizon, it alters to interstratified chlorite-illite, or chlorite-vermiculite-illite, higher in the profile [168]. Under conditions of relatively high pH, it is typical to see mica content increasing with depth in the profile, and expandable minerals increasing towards the surface, often with interstratified minerals occurring in intermediate horizons, and the implication is made that mica is being transformed into expandable 2:1 minerals. In Palaeozoic shales chlorite commonly occurs together with mica, and its simultaneous alteration to expandable 2:1 minerals would complicate the overall picture.

It is often found that the illite plus vermiculite or chlorite plus vermiculite contents are constant throughout a soil, with the

vermiculite:illite or vermiculite:chlorite ratio increasing up the profile [77]. A relationship such as this indicates the derivation of vermiculite from illite or chlorite, respectively. However, for a given horizon, it is usually found that the vermiculite content increases as the particle size decreases [77], although when weathering is sufficiently severe, the vermiculite may be at least partially converted to montmorillonite in the finest particles [258]. This shows that vermiculite is forming from illite in the upper horizons, rather than illite from vermiculite in the lower horizons, as alteration would be expected to take place most rapidly in the finer fractions with higher surface areas. Where the intensity of weathering decreases rapidly down the profile, illite may be altered to montmorillonite in the A horizon, but to vermiculite in the B horizon [63,77], whereas in soils that are more intensely weathered throughout, an irregularly interstratified illite-montmorillonite may be found in all horizons. Because a strongly leached environment is required to remove K and thus enable the illite to vermiculite reaction to proceed, illite is usually altered to montmorillonite where gleying occurs [77]. In environments similar to the one examined in this study, it has been proposed that illite alters directly to interstratified illite-montmorillonite [91, 92], although it is considered that this alteration probably took place before the onset of podsolisation.

In acid soils vermiculites invariably contain hydroxy interlayers [77], and hydroxy interlayered vermiculite is often their most abundant mineral as, under these conditions, it is more stable than kaolinite. It is generally formed from a nonhydroxy interlayered vermiculite which has, in its turn, formed from illite [77].

Where leaching and podsolisation are intense, particularly towards the soil surface, vermiculite forms at the expense of illite, via an interstratified intermediate, and often becomes the dominant mineral in podsol A horizons [14,77]. If an independent method of quantifying the degree of weathering, such as comparing the concentration of $TiO_2$ in the Ae horizon with its level in the C horizon, is available, it is possible to show that the alteration of illite increases with the intensity of weathering [151]. The same study of Canadian podsols showed that the distribution of structural units within interstratified minerals transitional between illite and expandable minerals became more irregular as weathering intensity increased [151], but the opposite effect has been observed in Scandinavian podsols [110].

The three main factors that affect the rate of simple transformation of mica are the particle size, the mineral species and the characteristics of the surrounding environment. Initial release of K is more rapid from fine particles than coarser particles [172], and an equilibrium concentration of K in solution may be reached in 10 days for 0.2-0.7μm muscovite, whereas equilibrium is only reached in 1,000 days for particles of 50-60μm [97]. About 50% of the equilibrium amount is released almost instantaneously from finer particles, but almost no K is released immediately from coarse micas. The initial very rapid release is due to layer weathering [163], and further release from all particle sizes is by edge weathering [234]. Edge weathering is diffusion controlled, and thus the larger the particle size, the longer it takes to reach equilibrium.

In spite of the very rapid initial release, fine particles usually retain a small part of their original K content in a form that is extremely difficult to remove [195]. This is considered to be in the form of stabilised mica units in regular 1-1 mica-vermiculite interstratifications, and possibly explains why not all the K content can be readily extracted from illites, which often show interstratification coupled with very small particle size.

The effect of mica type on weathering seems to be mediated through the roles of structural charge and hydroxyl orientation in affecting the strength of the bonding of interlayer K. Lepidolites contain F instead of OH, and in these micas there is no possibility of shielding the interlayer K from negative charge by the hydroxyl protons. What is more, F is very strongly electronegative and, as a result, despite the fact that they are trioctahedral, these micas bond K very strongly and are the micas least susceptible to weathering [158,195,214]. F replacing some OH in other micas also retards K release [214].

In trioctahedral micas the hydroxyl proton is oriented directly towards the interlayer K site, and is thus closer to it, resulting in a lower effective negative charge to bond K. In practice, it is over an order of magnitude more difficult to remove K from dioctahedral than trioctahedral micas [158,212]. The strength of bonding of K increases with layer charge, and charge originating in the tetrahedral sheet is more effective in preventing K loss than that originating in the octahedral sheet [97].

As far as environmental factors are concerned, the most important are pH, the activities of K and other ions in solution, temperature and Eh. When K in solution is higher than the equilibrium level, K is adsorbed from solution by the expandable minerals; when it is lower than the equilibrium value, it is lost from mica interlayers. Equilibrium levels for muscovite are less than, or equal to, 1ppm in various solutions, being only 0.19ppm in $10^{-3}$M Ca, perhaps the best approximation to an actual soil solution amongst the solutions investigated so far. For biotite, equilibrium levels are up to 35ppm, but under conditions approximating to those in actual soils, as given by $10^{-3}$M Ca, the equilibrium level is only 0.35ppm. A real micaceous soil gave an equilibrium value of 0.47ppm K with the same solution [97]. The concentration of other cations in solution can considerably affect the equilibrium K level [214,264].

Low pH increases the rate of K release, especially from trioctahedral minerals, but this may be due only to attack on the 2:1 layer [264]. Living organisms may produce complexing organic acids which can accelerate the loss of K [34], whilst leaching by solutions with a lower than equilibrium level of K will favour weathering, as does increasing temperature or plant uptake of K.

Other possible alterations of the mica structure have not been studied as extensively as simple transformation, but under acid conditions the 2:1 layer can break down just as rapidly as K is lost from interlayer sites. Mineral stability data suggest that in many acid soils kaolinite is the stable phase relative to both mica and vermiculite, mica only being stable at high pH and high [K], and vermiculite at high pH and very high [Ca]. In some soils montmorillonite may be the stable phase [262]. However, alteration of mica to kaolinite and even montmorillonite involves a complex transformation and 2:1 layer breakdown, for which the reaction rate is much slower than for the simple transformation to vermiculite. Thus vermiculite tends to form initially, although it is theoretically unstable [145], with the stable phase only forming after extensive weathering has occurred. Alteration is most effective at the top of a soil profile, as it is here that the K in percolating water is lowest, at least partly due to plant uptake.

### 2.3.4 The Weathering of Chlorite

Chlorite is rapidly weathered and, except for its occurrence in igneous and metamorphic rocks, is thus usually found only in arid or high

latitude soils, where chemical weathering is not intense, or in sediments derived from them. Under these conditions, chlorite may remain unaltered as it moves from a rock into a soil and eventually into a marine sediment. An example of this is the preservation of IIb brunsvigite in soils on Ordovician pumice-tuff in north Wales [16], where chlorite is the dominant mineral in the clay fraction of both the rock and soils. There are no consistent differences in the chlorite within or between profiles, and although weathering causes a colour change from greyish green to brown, there is no evidence of transformation of the chlorite to other phyllosilicates. However, it is possible that the soil chlorite is being rapidly released from the parent material, and equally rapidly destroyed by weathering. This soil is, in any case, almost unique. However, sediments more than 1,000 years old in Llyn Llydaw contain IIb chlorite, and thus it is likely to be discharged to the sea in this form. In modern ocean sediments the distribution of chlorite is inversely related to those of kaolinite and gibbsite. Because it is altered so rapidly, provenance is the most important factor determining the occurrence of chlorite in soils and sediments. It is considered that preservation of chlorite is favoured by high relief, good drainage, abundant year round rainfall, short distance of terrestrial transport, and the lack of afforestation, in other words by a short period over which weathering is able to act.

The importance of the latter factor is shown in a study of Fe chlorites in podsols in Scotland [14]. Under a Sitka spruce plantation, the chlorite is dissolved, decreasing more rapidly towards the surface than associated mica. However, in similar unafforested profiles, the chlorite is preserved even in the surface horizons. It is considered that the difference in behaviour is due to a 7.9% organic matter content in the B horizon of the afforested profile, extracts from which dissolve chlorite better than HCl.

A study of very low grade metamorphic Palaeozoic shales of similar mineralogy to those in this study suggests from chemical analyses of different horizons and particle size fractions that Mg rich chlorite, found in rocks where Fe is taken into siderite, is more resistant to weathering than illite, whereas Fe rich chlorite, found in adjacent carbonate free rocks, is less stable [253].

The dissolution of chlorite to leave either no solid products, or only noncrystalline silica, is one of the two most common weathering routes

proposed [1,14,25,26,47,48,63,92,151,223-225], the most common being its alteration to vermiculite [65,72,80-82,91,92,107,110,119,136,139, 169,174,182,208,226,227], which may in its turn be further altered by weathering. Although complete dissolution in an acid soil, to leave no solid residue, would seem to be an obvious possibility, little work has investigated this. Instead, the assumption has commonly been made that, if at least part of the chlorite has left a solid residue, then all of the chlorite will have behaved similarly. Both vermiculite and noncrystalline silica are, however, ultimately only intermediate stages in the total dissolution of the chlorite. For many years evidence was produced for and against both of these routes in particular situations, with the proponents of alteration to vermiculite suggesting that weathering first attacks the interlayer [65,80-82,139,182], allowing hydration of the cations and formation of vermiculite.

One method of determining which path the chlorite is following is to monitor the Mg and Fe contents of the soil horizons. Most of the Mg and Fe is in chlorite, and some is inherited by vermiculite. When chlorite breaks down to noncrystalline silica, all of its Fe and Mg is lost in solution [151].

However, an explanation can now be provided as to why some chlorites alter to vermiculite, whilst others are dissolved to leave only noncrystalline silica. Artificial weathering studies suggest that chlorites that have only been subjected to low temperatures will weather to noncrystalline silica, whereas those that have been subjected to high temperatures during metamorphism will alter to vermiculite [174,227], although one study suggests that the presence of a high $Fe^{2+}$ content is sufficient to alter the weathering product from noncrystalline silica to vermiculite or smectite [169]. The original experimental work [227] involved heating a chlorite to 610°C, after which attack with a mixture of 0.2M HCl and 0.2M NaCl converted 90% to vermiculite, whereas chlorite that had not been heated simply dissolved. Dehydroxylation of the interlayer sheet occurs at a lower temperature than that of the octahedral sheet in the 2:1 layer (Section 2.2.6), and results in disordering of the structure and oxidation of any Fe present. This mechanism can also explain why Fe rich chlorite is more easily altered on weathering [65] than Mg rich chlorite, as dehydroxylation occurs at lower temperatures in sites associated with Fe rather than Mg or Al (Section 2.2.6), and the oxidation of any Fe adds to the structural disorder caused by dehydroxylation.

Other workers have proposed that any IIb chlorite would be initially weathered to vermiculite [174], suggesting that temperatures of only 150 to 200°C would cause sufficient structural disorder to allow alteration to vermiculite [119]. Perhaps because of this, as 80% of natural chlorites are of IIb polytype [119], it is the route of alteration to vermiculite through interstratified chlorite-vermiculite that is most commonly proposed to explain the weathering of chlorite [219]. Evidence for this mode of alteration is provided by interstratified chlorite-vermiculites in soils where chlorite in the parent material is not interstratified [65,80-82,91,107,110,119,136, 139,208], as well as by artificial weathering studies [65,174]. However, some of the material identified as interstratified chlorite-vermiculite may be hydroxy interlayered vermiculite, as is suggested by the basal spacing progressively contracting as temperature is increased [208]. Even if this misidentification does occur, the case for vermiculite formation is not weakened; removal of hydroxy interlayers is simply proceeding in a less organised fashion than if interstratified chlorite-vermiculite was formed. Nevertheless, care must be taken to ensure that the vermiculite is not being derived from the weathering of mica associated with the chlorite.

It is generally postulated that, as chlorite is altered to vermiculite, attack starts in the interlayer [65,80-82,139,174,182], where $H^+$ replaces interlayer cations [139], converting hydroxyl ions to water molecules. These then envelope the remaining cations, allowing the whole of the interlayer to become hydrated. Attack on the interlayer is favoured both by metamorphic dehydroxylation [174,227] and by oxidation of Fe, which causes structural disorder [65,107]. However, some chlorites which weather to vermiculite have been shown to have more than 75% of their Fe content in the octahedral sheet of the 2:1 layer [136,174], suggesting that metamorphic dehydroxylation is more important than Fe oxidation in destabilising the interlayer. Detailed analysis of the shape, position and behaviour after various treatments of both 1.0nm and 1.4nm XRD peaks is often able to indicate the derivation of vermiculite from chlorite, even in the presence of illite which is also undergoing alteration. Heat treatment can, in particular, indicate the emptying of chlorite interlayers [80,82].

The weathering pattern in soils on chloritic metabasalts in Maryland is typical of soils in which chlorite weathers to vermiculite [65]. There is little or no vermiculite, and no mica, in the parent material, but

the trioctahedral chlorite content varies from 10% to more than 70%. The content of trioctahedral vermiculite increases up the profile, whilst no chlorite is found except as particles coarser than 2mm. Other mafic minerals survive longer than chlorite, and thus the authors conclude that the vermiculite is derived from chlorite, which is supported by the presence of interstratified chlorite-vermiculite in adjacent soils on the same parent material. Similar interstratified minerals can be generated by treating the chlorite with hot Br water. In the upper horizons, the content of vermiculite is apparently reduced, because of its inability to fix K, indicating the formation of hydroxy interlayers [64,65]. On further weathering, this hydroxy interlayered vermiculite may alter to kaolinite and Fe oxides [65]. The alteration to vermiculite occurs under acid, oxidising conditions, and it is suggested that oxidation of Fe in the interlayer leads to attack on the mineral. Oxidation of Fe is also seen in soils developed on phyllites in Australia, where the chlorite alters to vermiculite through an irregularly interstratified chlorite-vermiculite at the same time as Fe is oxidised [107]. Artificial weathering studies also reinforce the importance of Fe oxidation. When chlorite with Fe constituting 53% of its octahedral cations was held at pH2 and 100°C in a nonoxidising environment, little alteration was seen, as was also the case when a 7% octahedral Fe chlorite was held for five months in Br water of pH2 at 100°C. However, when the 53% octahedral Fe chlorite was held in the Br water at 100°C, 80% had been altered to a low charge vermiculite within three weeks. At the same time considerable cation loss and a reduction in d(060) from 0.1557 to 0.1537nm occurred [227].

However, the alteration of chlorite to vermiculite can take place without Fe oxidation [91,92]. In soils developed on postglacial scree derived from Lower Palaeozoic mudstones in mid Wales, chlorite is not found at all in the surface horizons. It is, however, found in all size fractions of the BC and Bfe horizons, and in the silt and coarser grains of the eluvial horizons. The vermiculite content reaches a maximum in the Bg horizon, the zone of contemporary weathering, and on this basis it is suggested that the chlorite, which on the evidence only of chemical analysis is believed to be ditrioctahedral, is altered by loss of the trioctahedral interlayer to dioctahedral vermiculite, which weathers further to noncrystalline silica [92]. This weathering route is supported by the fact that chlorite weathering can account for all of the Fe and Mg and almost all of the Al lost during pedogenesis, and that the Al is released after the Fe and Mg, which would be

expected in a two stage breakdown process. It would be expected that the trioctahedral sheet would be altered first, but it was postulated that at the same time sufficient Al was lost from the 2:1 layer to destabilise the resultant vermiculite and cause it to weather to noncrystalline silica.

It is generally agreed that chlorite is not found in the A horizons of podsols, although it is usually present in all the lower horizons when it is found in the parent material. It is believed that this is due to the protection of the chlorite by Fe and Al hydroxides, whilst these are usually leached from the Ae horizon [47]. In many podsols it is considered that chlorite is broken down to vermiculite [80-82,91,92, 107,110,119,139,208]. In podsols in Quebec a regularly interstratified chlorite-vermiculite is seen in the parent material and fragipan, but only vermiculite is found in the Ae horizon [72]. If similar soils in the same area are compared, it is found that as the pH increases, the mineral structure becomes more ordered and chlorite like. As a result of this study a relationship between chlorite $I_{001}/I_{002}$ and the degree of vermiculitisation was proposed. Another study of podsols in Canada showed chlorite weathering to vermiculite in the C horizon [169]. In the B horizon Al hydroxy interlayers were formed in the vermiculite, but these were lost in the Ae horizon and the vermiculite was altered to smectite. The chlorite sheets were observed to lose cations as weathering progressed, giving a dioctahedral structure. Further weathering to kaolinite was considered to be prevented by the presence of organic matter.

A more general study of weathering in podsols showed that noncrystalline silica should be expected as the final weathering product of chlorite, but that intermediate stages of dioctahedral vermiculite and montmorillonite will occur on this main alteration path for chlorite [182]. Chlorite interlayer cations are first removed, and this loss is then balanced by loss of Mg from the 2:1 layer, resulting in a dioctahedral structure that is richer in Al than the original chlorite. It is considered that lower initial Al contents in the interlayer give rise to more rapid weathering.

Weathering of chlorite to vermiculite also occurs in tills, as well as soils besides podsols. In the USA, well crystallised Fe chlorite is seen in unaltered Wisconsin and Illinoian tills [80,82]. Alteration through interstratified chlorite-vermiculite takes place in the till

itself, so that only vermiculite is seen in the top surface of the till. This alteration is explained by attack of $H^+$ in the till on the chlorite interlayer. A similar alteration process is developed further in soils in Indiana [81]. Here chlorite is altered to irregularly interstratified chlorite-vermiculite which, on further weathering, is altered to a better organised vermiculite, then interstratified vermiculite-montmorillonite, and finally montmorillonite. The formation of irregularly interstratified chlorite-vermiculite is attributed to attack on the interlayer and dissolution of octahedral cations occurring at different rates. In southern Norway, Pleistocene marine clays show alteration of chlorite to vermiculite via an irregularly interstratified intermediate, but here the chlorite is Mg rich, and the Mg is considered to be replaced in the interlayer by $H^+$ [139].

In other soils in Scandinavia, the weathering pattern is slightly different [110]. Chlorite decreases up the profile, and the chlorite that remains becomes less thermally stable. The initial stage of alteration is to interstratified chlorite-vermiculite, but this is then altered to interstratified illite-vermiculite, followed by vermiculite and finally montmorillonite. In soils developed on the lower greenschist grade Upper Jurassic Mariposa Slate in California, the 45% chlorite content rapidly alters to an irregularly interstratified chlorite-vermiculite, although this retains a 1:1 chlorite:vermiculite ratio [208]. The following weathering steps, involving alteration to vermiculite, or kaolinite if excess groundwater is present, take place much more slowly.

Where 1-1 regularly interstratified chlorite-vermiculite is formed on the weathering of chlorite, it has been suggested that the initial chlorite was a two layer polytype, with alternate interlayers bonded with different strengths [136]. This weathering pattern was seen in soils developed on a Precambrian metabasaltic greenstone, and the chlorite was shown by XRD analysis to have all its Fe concentrated in the 2:1 layer. Regular interstratifications of chlorite and vermiculite are usually found under conditions of less intense weathering [72,119,136].

A further complication in the weathering of chlorite is the possibility of polytype alteration. Most vermiculites are of polytype Ia, and when IIb chlorite weathers, it is often through a regularly interstratified chlorite-vermiculite, before irregularly interstratified chlorite-

vermiculite, and finally Ia vermiculite, are formed [119]. Ib chlorite with $\beta$ = 90° has been observed to weather to the Ia polytype in the Carboniferous Winslow Formation and Wedington Sandstone in Arkansas. The weathered material has lower $Fe^{2+}$ and tetrahedral Al contents. In the same area sediments containing Ia chlorite weather to irregularly interstratified Ia chlorite-vermiculite.

In tropical soils a IIb metamorphic chlorite with more than three quarters of its Fe content in the 2:1 layer and with a very high $Fe^{3+}$ content is seen to alter to a regularly interstratified chlorite-vermiculite, thence to a beidellite and finally to kaolinite [174]. Experimental work to decipher the mechanism behind this path showed that attack by a salt solution released 35% of the Mg, but produced an irregularly interstratified product. An oxidising treatment released 33% of the Fe content, but gave rise to the same mineral. The standard reducing treatment used to remove Fe oxides [179] only released 12.5% of the Fe, but produced a regularly interstratified chlorite-vermiculite as seen in the field. The amount of Fe removed was consistent with removal of all of the Fe in the interlayer, and the interlayer was observed to become more Mg rich. This work showed that Mg removal or Fe oxidation only leads to irregular disruption of the chlorite structure, whereas removal of oxidised Fe from the interlayer is necessary to bring about vermiculitisation. However, a different study has shown that oxidation of Fe as a result of high intensity weathering may give rise to a chlorite that is better crystallised, and thus more stable in the weathering environment [219].

As with the weathering of illite, it has been suggested that an increase in weathering intensity can result in smectite instead of vermiculite being formed from chlorite [55,81]. Very few studies have observed weathering terminating with interstratified chlorite-smectites, or vermiculite-smectites, but instead have reported weathering as far as smectite, with or without interstratified intermediates [219]. However, major differences between the weathering of illite and chlorite are that the trioctahedral vermiculite ususally formed from chlorite may itself transform to noncrystalline silica in the upper horizons [91,92], whilst chlorite often shows alteration to interstratified minerals in the C horizon, particularly in the fraction finer than 0.2μm [151].

In Ontario, interstadial clays, deposited during a pause in the advance of the ice sheet, contain Fe chlorite derived from Devonian shales by glacial erosion [211]. It is proposed that, on weathering, Fe oxidation lowers charge deficiency and enables hydration and expansion to occur to form a smectite. The smectite observed in the altered sediment is still highly charge deficient, readily collapsing to 1.0nm on K saturation. In eastern Canada, the weathering of chlorite in podsols, humic podsols and podsoregosols is seen to be different from that occurring in grey brown podsolic and grey wooded soils [47]. In the podsols the Ae horizon is sharply different to the B, and contains no chlorite, but instead smectite, smectite and vermiculite, or a complex interstratified structure in the finer than 1μm fraction. The B horizon contains chlorite and vermiculite, but not smectite, and it is considered that hydroxy Al and Fe coatings prevent uptake of $H^+$, release of Fe and Mg, and breakdown of the chlorite. Free Al and Fe hydroxides are removed from the Ae horizon, and eventually all that remains of the chlorite is noncrystalline silica, the other elements being taken into solution. In contrast, in the other soils, chlorite is found in the Ae horizons wherever it is present in the associated C, and smectite is only present in the Ae if it is also in the C. The chlorite is observed to become more disordered, and to decrease up the profile, whereas a vermiculite-smectite interstratification increases from the C to Ae. In these soils the B horizon is not distinguishable from the Ae. Chlorite has also been observed to weather to montmorillonite in poorly drained soils developed on serpentinite in Cornwall [53] and on olivine basalt near Oslo [54].

Before turning to the alteration of chlorite to noncrystalline silica, mention should be made of a study in West Germany in which it is suggested that chlorite is altered to illite by the action of stream waters [188]. These have a pH of 6.8 and a K concentration of 4ppm, and it is suggested that the interlayer Al is dissolved, followed by addition of K.

There is considerable evidence from experimental weathering studies [1,25,26,48,223-225] to support field observations that, under certain conditions, chlorite in podsols is broken down in the Ae horizon to noncrystalline silica and cations in solution [1,14,47,63,92,151]. When either granite fragments, or artificial soil profiles formed from granite and its derived soils, were weathered under both sterile and nonsterile conditions, considerable differences were seen [25,26].

Under sterile conditions little effect was seen on the chlorite in the granite fragments after 10 months leaching at a pH less than five, and little $Fe_2O_3$ was released. When Bacillus and Pseudomonas species were employed, a pH of three to four was generated and the chlorite was completely dissolved. However, in the free draining columns less than 1/15th of the amount of $Fe_2O_3$ released in the waterlogged columns was set free.

Mg clinochlore grains are readily attacked by Si saturated 2M HCl at 60°C [223]. The proportions of Al, Fe and Mg dissolved remain constant throughout the experiment, and XRD shows the residue to be noncrystalline. When only noncrystalline material is left, the whole original content of Al, Fe and Mg is found to be in solution. This suggests that preferential solution of the interlayer does not take place [224], although it is possible that interrupting the experiment at an earlier stage might have revealed preferential solution, despite this requiring the compositions of the two octahedral sheets to be identical. The kinetics of the reaction support a model of diffusion controlled attack on disc shaped chlorite grains from their peripheries, with the Si-O network acting as a diffusion barrier. Further work indicates that the dissolution rate increases with increasing $FeO + Fe_2O_3$ content [225].

This work was extended to acid concentrations more appropriate to those found in podsols [48], $10^{-2}$, $10^{-3}$ and $10^{-4}$M HCl, when XRD showed no change in the chlorite at the end of the experiment. However, the solution pH increased, and solution analyses suggested that both the 2:1 layer and the interlayer were dissolving. It was suggested that, in the $10^{-2}$M solution, $Al_2O_3$ and $Fe_2O_3$ precipitates were buffering the pH at approximately four, and were coating the chlorite grains, preventing Mg release. In stronger acids the coatings would dissolve, allowing chlorite dissolution. In podsol A horizons pH is high enough to precipitate Al and Fe hydrous oxides, but chlorite dissolution still occurs. This must be because Al and Fe are eluviated to the B horizon, where they can prevent chlorite dissolution for 10,000 years.

One study combined field observation of soils in mid Wales with experimental weathering [1]. The parent material was a mudstone, 10 to 20% of the rock consisting of what was claimed to be ditrioctahedral chlorite, with $I_{002}/I_{003}$ varying between 1.4 and 1.7. In the Aeg horizon of a humic podsol, the chlorite was totally removed,

and it was reduced in quantity in the B of a brown forest soil. No chlorite was found in the finer than 2μm fraction of any of the soils. Chlorite degradation was strongest in the podsol eluvial horizons, possibly because of a surface accumulation of organic matter. On weathering, coarse grains break down to silt and clay [244], and a correlation between silt and clay content and $Fe_2O_3$ and MgO release suggests that all $Fe_2O_3$ and MgO is released by the time grain breakdown is complete. As the majority of MgO and $Fe_2O_3$ in the rock is in chlorite, the weathering rate of the chlorite can be seen to be proportional to the rate of breakdown of coarse grains.

In the artificial weathering experiments particles finer than 20μm were either boiled for 45 minutes in 25% $HClO_4$, or kept at 60°C for 60 hours in 2M HCl. No chlorite was present in either of the residues, and only noncrystalline silica could be identified as an alteration product. Approximately 80% of the Mg and Fe was released, in the ratio of 1:3.1, but less than 1% of the K, suggesting that mica was resistant to the treatments applied. However, Al release was lower than in the field, suggesting that some mica weathering takes place in the field. It was suggested that the chlorite formed as a cement by marine diagenesis, and was more efficient as a cement where it occurred interstratified with mica. The Mg and Fe released in the weathering experiments suggested that chlorite composed 14% of the rock.

A study of spodosols in New York, where the chlorite is added to the soil as airborne dust, suggests that it is altered to noncrystalline silica in the albic horizon, and the noncrystalline material is then translocated to the spodic horizon [63]. It is generally believed that the transformation of chlorite to noncrystalline silica occurs because of rapid decompositon of both the interlayer and the octahedral sheet in the 2:1 layer. The tetrahedral sheets decompose much more slowly, losing Al to give noncrystalline silica towards the soil surface [219].

The possibility of kaolinite being formed from chlorite via intermediate crystalline phases, especially under waterlogged or tropical conditions [63,65,208], has already been mentioned. However, direct transformation of chlorite to kaolinite or the formation of kaolinite from the noncrystalline decomposition products of chlorite, have also been proposed [219]. For direct conversion to occur, one of the tetrahedral sheets from every 2:1 layer must invert the position of its apical O atoms, breaking their bonding with the octahedral sheet,

and then bonding them with the interlayer hydroxide sheet, to form two kaolinite layer units from every layer plus interlayer combination.

In alpine podsols in Perthshire chlorite decreases and kaolinite increases towards the soil surface. Mg is taken into the soil solution and Fe is translocated to the B horizon where it crystallises as Fe oxides. However, the Al in solution and noncrystalline silica recombine to form kaolinite in the A horizon [219].

In conclusion, from the literature it seems likely that the initial step in weathering, whether to vermiculite or noncrystalline silica, is determined by whether the interlayer has been destabilised by metamorphism or oxidation or not. Provided that the chlorite has not been oxidised in any abnormal manner, it thus ought to be possible either to predict the weathering route of the chlorite if the metamorphic history of its parent rock is known in some detail, or possibly to use the chlorite weathering route to map a type of isograd. However, before such work could be carried out, it would be necessary to carry out a detailed investigation of the metamorphic conditions that provide the boundary between chlorite that will weather to vermiculite, and that which alters only to noncrystalline residues.

If destabilisation causes vermiculite to form, the literature suggests that how far the weathering process proceeds depends on the intensity of weathering; it may end at vermiculite, or pass on to smectite, kaolinite or noncrystalline silica, or even form illite if the K concentration in solution is sufficient.

In some studies in the literature, total confidence cannot be placed in the reports of chlorite weathering to vermiculite. Most often the octahedrality of the vermiculite has not been determined and thus, if mica is present, it is quite possible that it is the mica weathering to vermiculite, and that the chlorite is actually being altered to produce unnoticed noncrystalline phases. Only where trioctahedral vermiculite is shown to be present, or where there is no mica in the parent material, can total confidence be placed in reports of chlorite weathering to vermiculite. A further cause for caution is that none of the field studies reported have made any attempt to separate the mineral phases, and then to subject those phases independently to the weathering processes, to confirm the hypotheses developed from observations of the weathering of the whole parent material.

# CHAPTER 3

# PLYNLIMON SHALES AS A PARENT MATERIAL

## 3.1 THE IDEAL REQUIREMENTS FOR A STUDY OF WEATHERING

As pointed out in Section 2.3.2, the study of weathering has become widely diversified, varying from the detailed electron microscopy of the surface morphology of weathered mineral grains to the measurement of cation loss in stream flow from a catchment area of several $km^2$, and including many other facets of environmental, mineralogical and chemical study. Each of these branches of study will, of necessity, have different specific requirements that need to be fulfilled by the site from which samples are obtained, or where measurements are carried out, in order that the results of the study should be meaningful, and applicable on a wider basis than just that of the study site itself. However, all of the study methods employed in the investigation of weathering have a common set of basic requirements that should be fulfilled if results are to be relevant to other situations:

1. The samples or area studied should be representative, or else the results may be of local interest only, not being applicable to other situations. Although soils developed on a rare rock type might make a fascinating weathering study in themselves, the results are not likely to be widely applicable, because very few other soils will develop from the combination of minerals found in the rare rock type. Similarly, environmental conditions should not be unique to the area of study. The study of shale weathering at Plynlimon readily fulfils these criteria. Shales constitute more than 60% of the sedimentary record, shales of similar mineralogy occur throughout the world, and shales of similar mineralogy and age outcrop over much of Wales, the Lake District and the Southern Uplands of Scotland. These shales outcrop at similar elevations and experience similar climatic conditions in all three areas, where land use is also very similar. Thus, results from shale weathering at Plynlimon should be directly applicable to weathering in all of these areas.

2. Background data should be available on a broad basis, so that the detailed study being carried out can be interpreted as part of a coherent picture, rather than as an isolated set of results. At Plynlimon, IH has monitored climate and stream flow for 16 years,

and as part of this co-operative project ITE has monitored stream flow, surface runoff and subsurface flow through the soils, together with the chemical composition of stream and soil waters. In another part of this project, the geological mapping of the area was revised by IGS, who have also analysed rocks and stream sediments for major and trace element chemistry. Soil maps of the area are available from a previous study of water movement at Plynlimon [149], and detailed profile descriptions were made by ITE. The petrology of the rocks on which the soils are developed has been studied [135], whilst a colleague has carried out considerable work on the artificial weathering and surface morphology of mineral grains from Plynlimon soils [27]. This study is thus adding to an already considerable and detailed data bank on the weathering environment at Plynlimon.

3. The study should have something new to offer. It is perfectly possible to study the weathering of a similar group of rocks under similar conditions to those in studies that have already been carried out, not surprisingly often producing similar conclusions. Such a study is of little value unless it adds to the data produced by previous workers, or questions their results. Although this study is based on materials similar to those investigated by other workers under similar climatic conditions [1,91,92,94,95,219,244,245], it is believed that the detailed analyses of particle size and quantitative mineralogy (Chapter 6) and the application of crystallinity variation to weathering (Chapter 8) will have added useful information to the data base on the weathering of shales under cool temperate conditions. The results of magnetic separation experiments (Chapter 4) also suggest that the easy separation path for pure chlorite from soils [219] cannot be followed when separating chlorite from crushed shale or boulder clay.

4. When combined with information already available, the results should add to the body of knowledge in an appropriate manner. The first study in a new field often remains in isolation for a long time, until related studies can be carried out. This could happen if the weathering of a specific mineral in a given soil type under particular climatic conditions was studied when neither the weathering of that mineral under a different climatic regime, the weathering of different minerals in the same soil type, nor the

development of different soil types under the same climate had been studied, even though the study might fulfil the three previous criteria. Work related to this study on soils developed on shales has been carried out, but differences between the shale starting materials, in terms of degree of metamorphism and the chemical compositions and mineralogical structures of the mineral phases, make the additional data presented here worthwhile.

For a study carried out in the manner of this one, when effort has been concentrated on mineralogical study of changes due to weathering occurring in one soil profile, it is also important to know details of:

1. The uniformity of the parent material over the area for which the results are considered applicable, with particular reference in this study to whether the soils are developed directly on the rock, or on rock derived glacial scree or boulder clay. If the latter is the case, the degree of mineralogical alteration brought about by the derivation of the scree or boulder clay from the rock should be known.

2. The duration of the present climatic conditions in the area under investigation, especially when compared to the time required for soil formation. If soil formation has required a period of time of the same order as that for which the climate is known to have been stable, it may be that some of the processes occurring in soil formation are no longer active, and others may have replaced them.

3. Whether any change in land use or vegetation has occurred. Ploughing in the past could obviously have had a dramatic effect on the structure of a soil profile, whilst addition of fertiliser or a change in nature of the vegetation could lead to a change in the weathering pattern of sensitive mineral species.

4. Any other geomorphological processes, particularly those involved in erosion, that could have interfered with soil development. The most relevant possibilities are the occurrence of solifluction, landslips or soil creep, or the addition of fine wind blown material to the surface horizons of the soil.

For an ideal study, the amount of parent material variability should be as low as possible, unless deliberate comparison of the effects of variability is being made, when variation in one factor at a time is desired, whilst other factors remain constant. However, such ideal conditions are not readily found in the real world, and certainly do not occur at Plynlimon, as can be seen in Sections 3.2 to 3.4.

## 3.2 THE GEOGRAPHY AND GEOLOGY OF PLYNLIMON

The samples on which this study is based were all collected within the catchment area of the River Wye (Afon Gwy) at Plynlimon, in mid Wales. The geographical location of this site is shown in Figure 3.1. The Plynlimon catchments of the Rivers Severn and Wye are approximately 26km east of the coast of Cardigan Bay, and show the gentle slopes and broad interfluves of the eastern side of the Welsh watershed. The catchment ranges from 360 to 580m above sea level.

The Wye catchment at Plynlimon covers an area of 10.55km$^2$, of which less than 2% is forested. The main channel has a length of 7.32km and a slope of 3.63%. There is a drainage density of 2.04kmkm$^{-2}$, with the main tributaries within the catchment being the Nant Gerig, Nant Iago and Afon Cyff, as shown in Figure 3.4. The mean annual rainfall is 2,532mm, and the mean annual temperature 7°C. The mean annual minimum temperature is -10°C, and the mean annual maximum 25°C, with an absolute minimum of -16°C, and an absolute maximum of 29°C.

The major elements of the landscape are caused by the outcrop of grit bands amongst the shales, or by faulting (Figure 3.2). The planar features are developed as broad interfluves mantled by blanket peat, but between them the valleys have been entrenched by glaciation. Following entrenchment, their floors have been covered by boulder clay, head and colluvium and then reincised, so that bedrock is now once again the dominant control on the river channels. The flat hill tops are characterised by extensive areas of peat and grass covered rock pavements where the peat has been eroded. The land is used for rough grazing, and the present vegetation is dominated by grasses, together with Sphagnum, Juncus, Erica and Vaccinium species.

In the last century and the earlier part of this century, small scale mining for Pb, Zn and Ag was carried out in the area. Three disused mines occur in the extreme east of the catchment area shown in Figure 3.4, and old shafts and levels are scattered across the catchment.

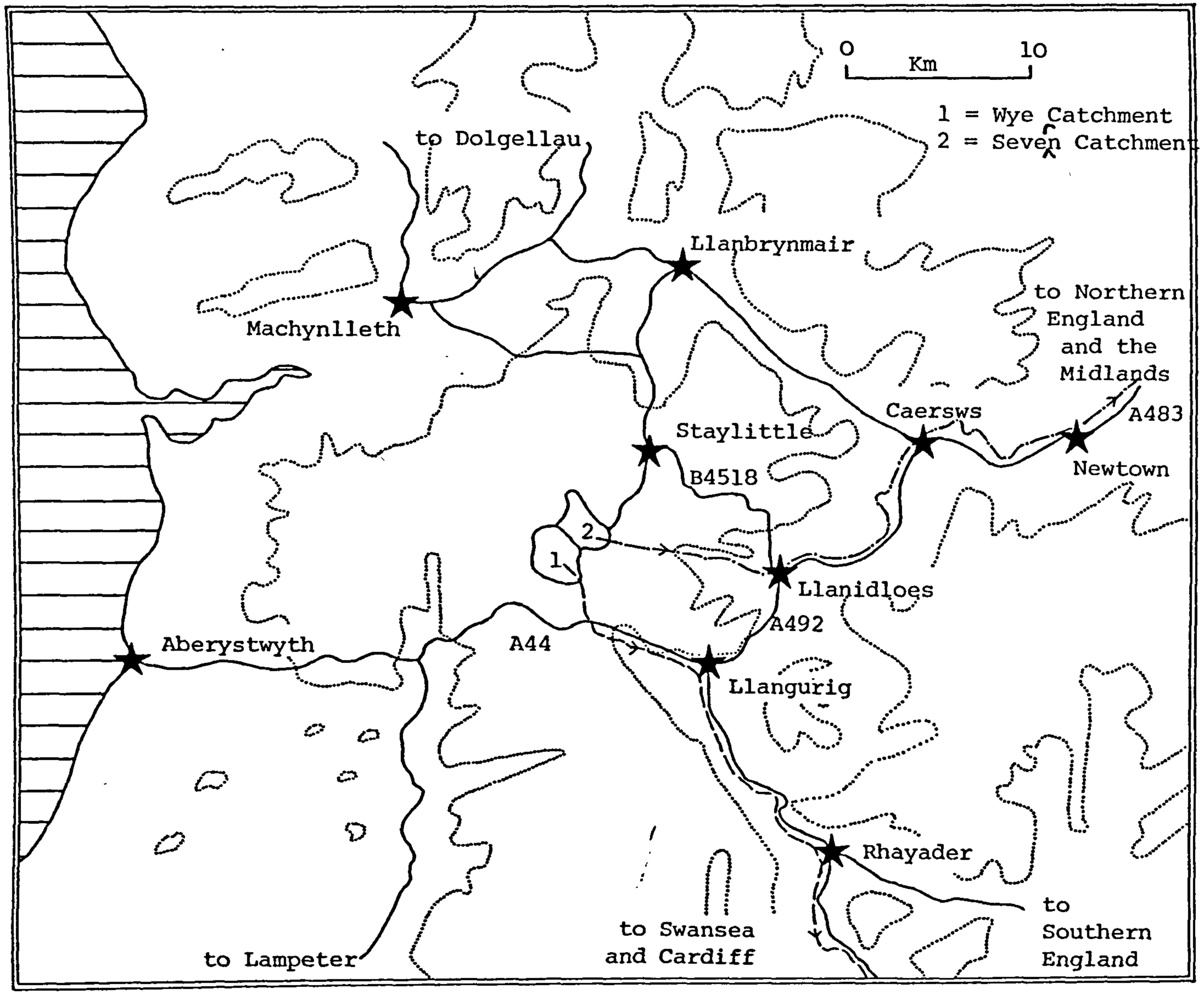


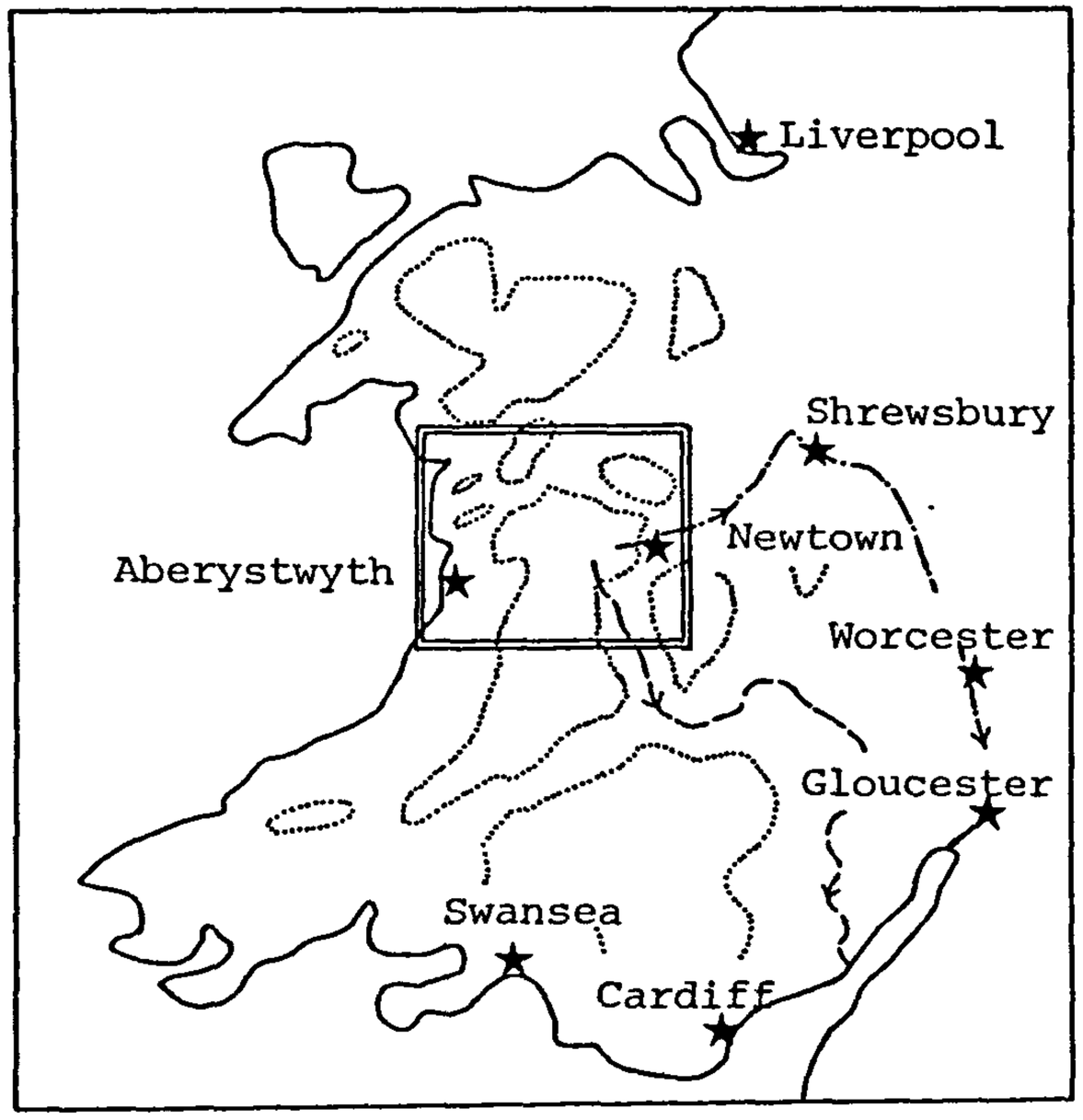


Figure 3.1 The Location of the Wye Catchment at Plynlimon

Figure 3.2 The Geology of Part of the River Wye Catchment Area at Plynlimon

This map is based on a remapping of the area by IG

Key:

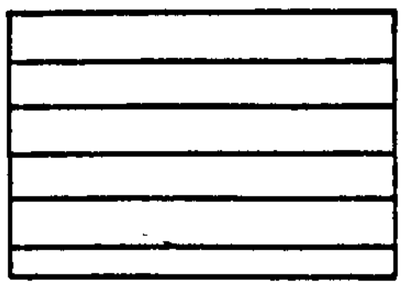

= Frongoch Mudstone Series

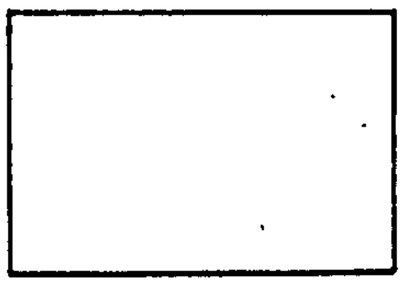

= Gwestyn Shale Group

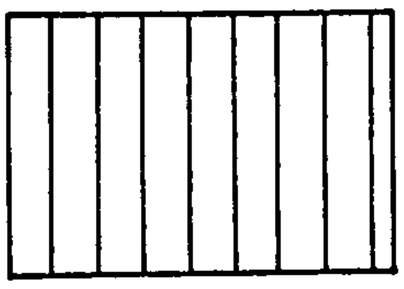

= Upper Fan Series (Fan Shales)

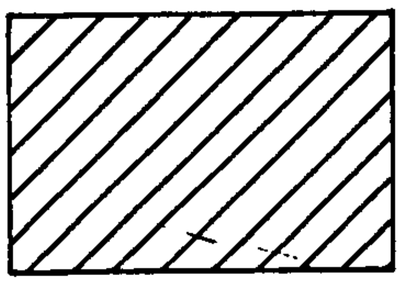

= Lower Fan Series (Fan Grits)

= Geological Boundary

= Fault

= Anticline

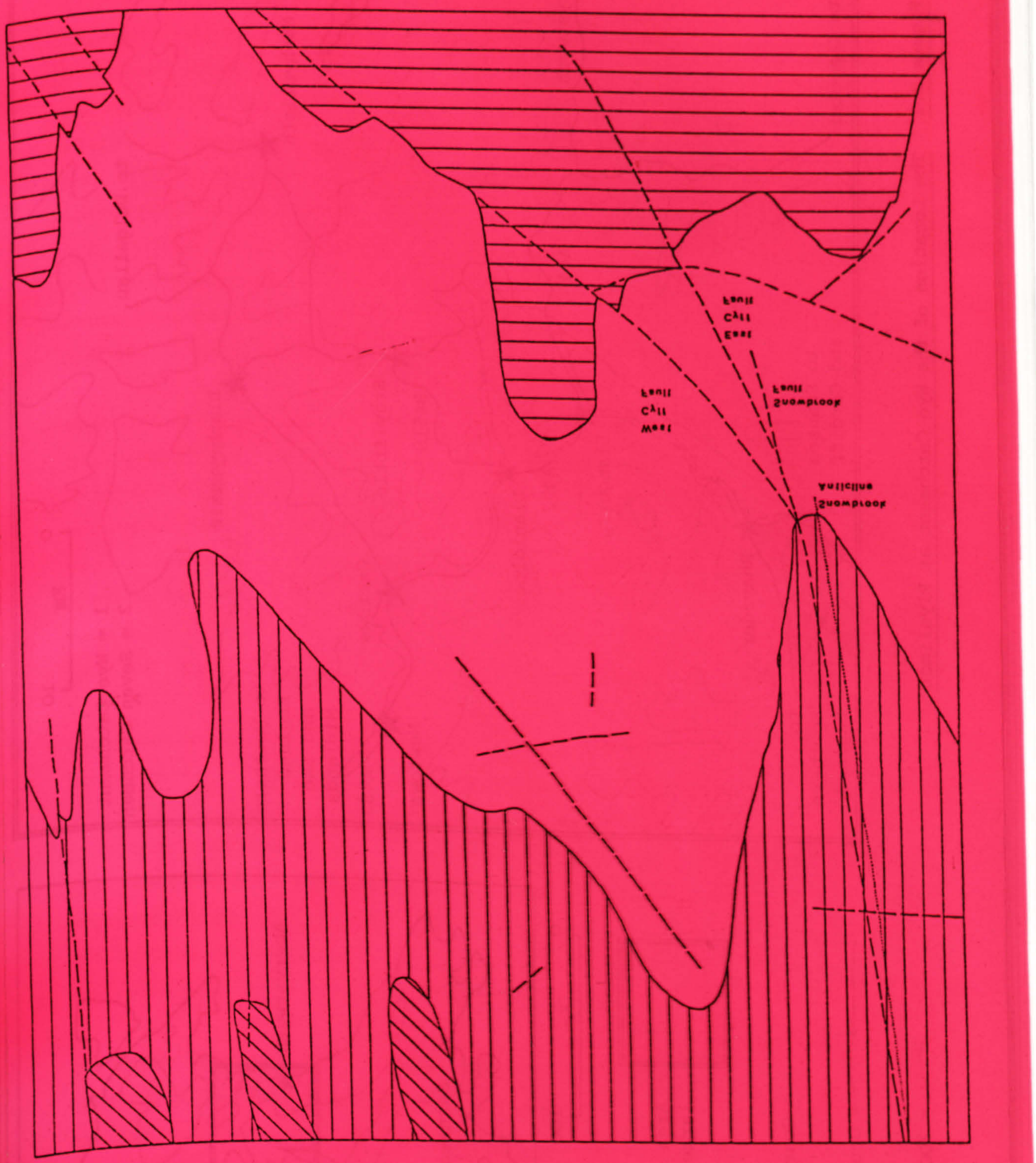
Tamil Nadu
Tamil Nadu Coastal Plain
Tamil Nadu Coastal Plain
Tamil Nadu Western Ghats

Figure 3.2 The Geology of Part of the River Wye Catchment Area at Plynlimon

This map is based on a remapping of the area by IGS

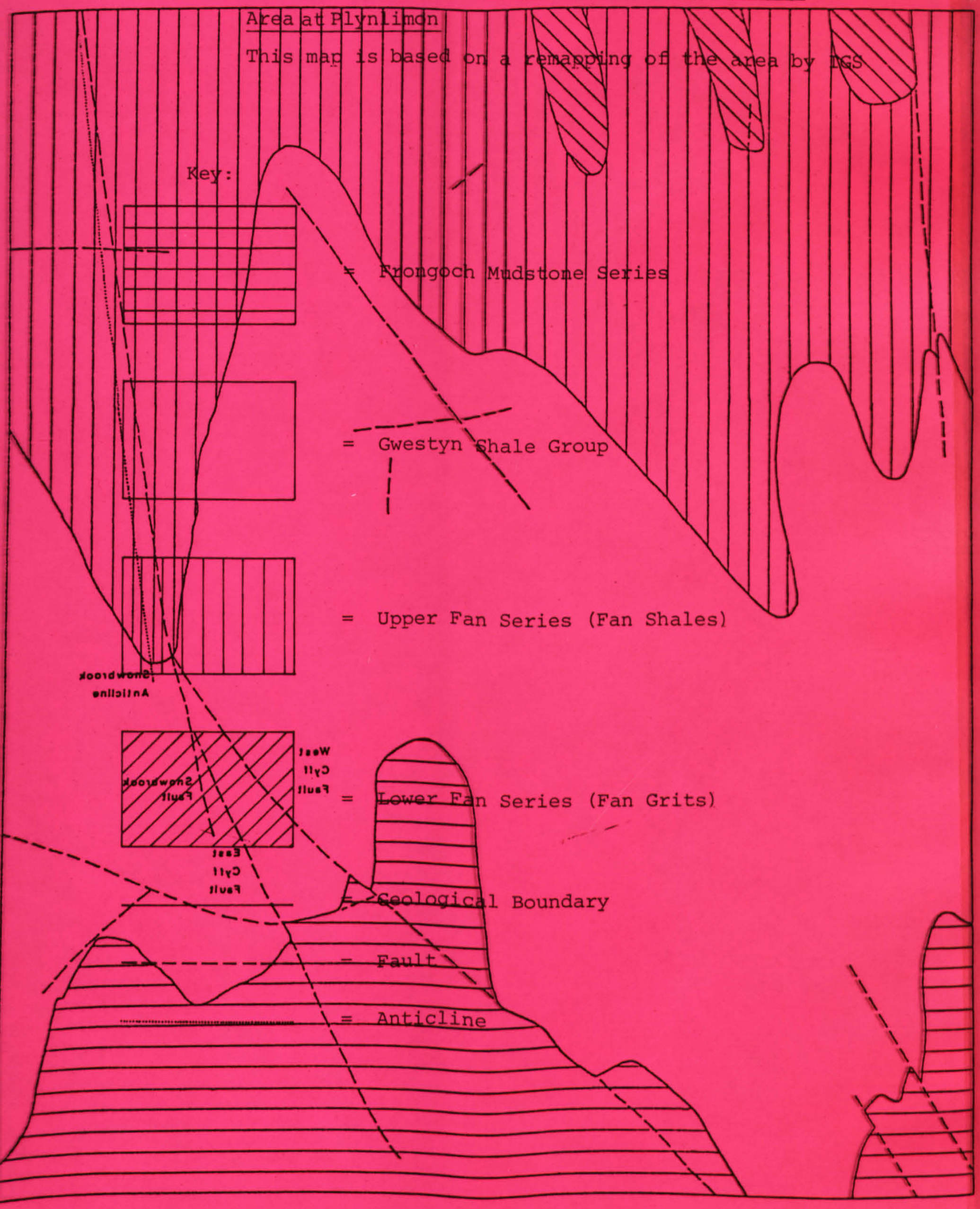

Figure 3.3 The Soils Developed on Part of the River Wye Catchment Area at Plynlimon

This map is based on that of Knapp [149], which is, in turn, based on the work of Rudeforth.

Key:

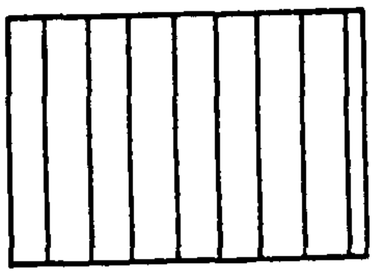

= Cyff Series

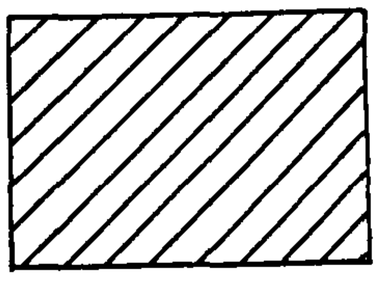

= Manod Series

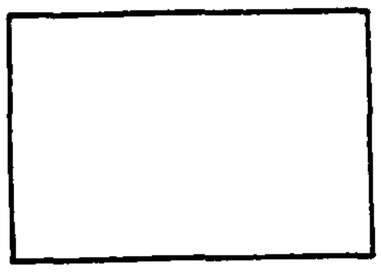

= Hiraethog Series

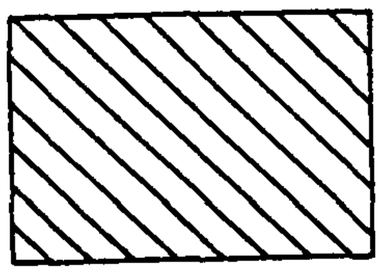

= Ynys Series

= Caron Series

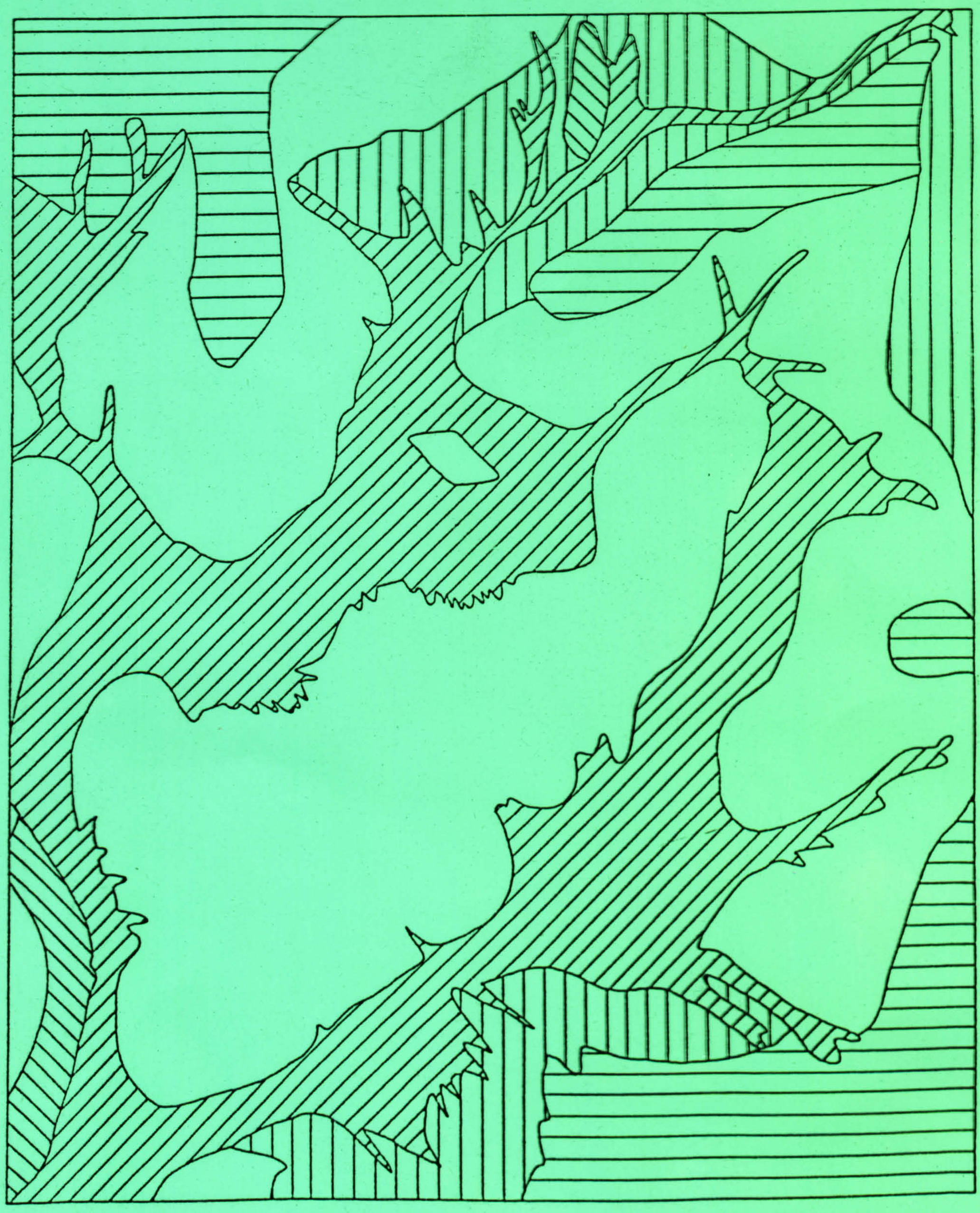

Figure 3.3 The Soils Developed on Part of the River Wye Catchment Area at Plynlimon

This map is based on that of Knapp [149], which is, in turn, based on the work of Rudeforth.

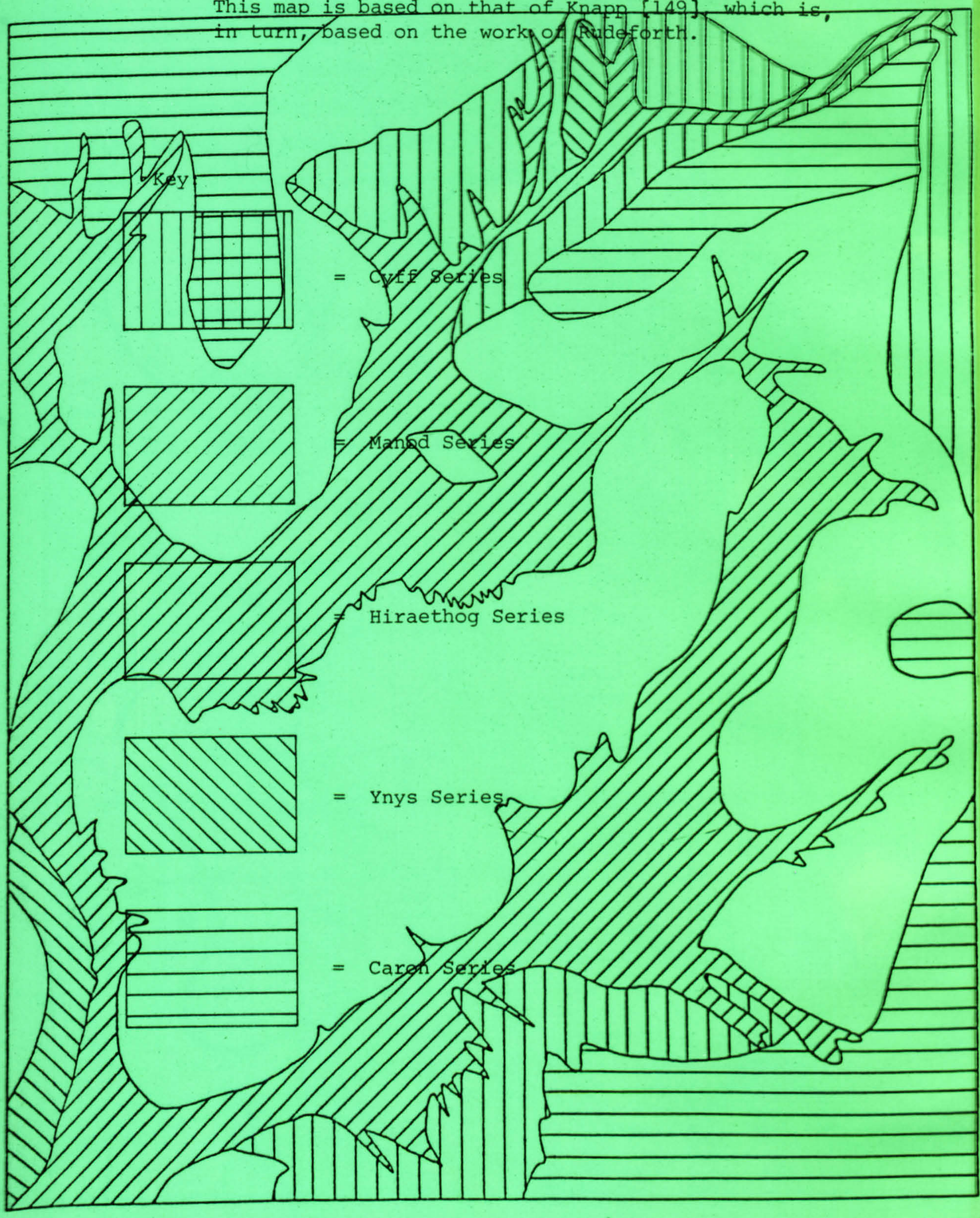

Figure 3.4 The Location of Samples Collected from Part of the River Wye Catchment Area at Plynlimon

Sample locations on the map are numbered as referred to in the text, except that the GCR series samples, numbered from 1 to 49 and collected by IGS, are shown on the map without the GCR prefix. The area of the map occurs within the National Grid 100 km square reference SN, and the 1 km square boundaries are numbered at the edges of the map.

= Natural watercourse

= Manmade watercourse

★ = Location of rock sample collected by author and colleagues

⊠ = Location of rock sample collected by IGS

▲ = Location of boulder clay sample

□ = Location of soil sample

= Pond

= Boundary of National Grid 1 km squares

= Contour line

♦ = Location of disused mine

N

0 200 400
metres

Scale: 1:7,500

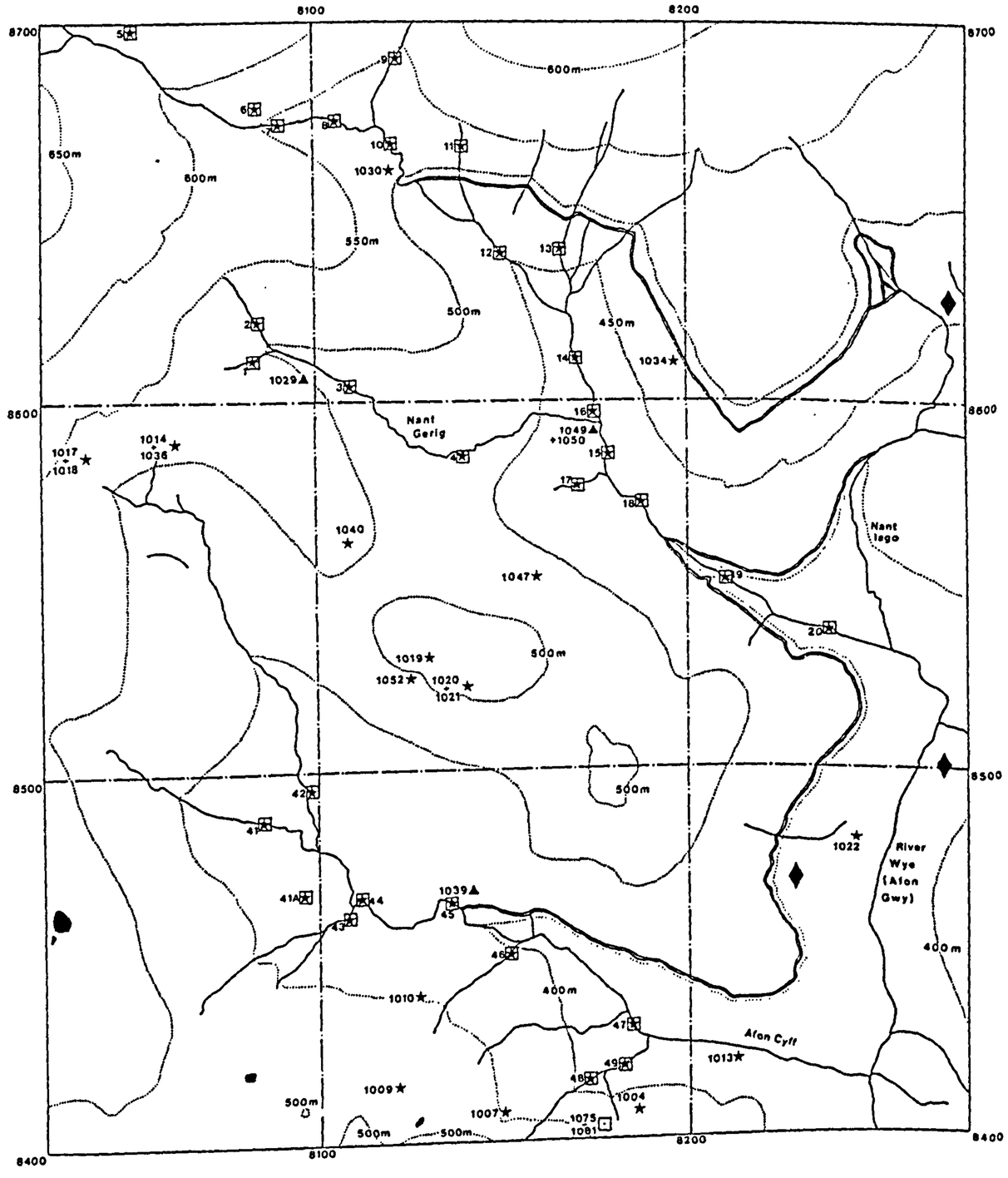

Apart from the small overgrown spoil heaps, the only evidence found for mineralisation in the area was provided by a partially submerged stone in the Nant Iago, close to the mouth of a disused adit. The stone consisted of brecciated shale fragments in a calcitic matrix, but its surface was encrusted with hydrozincite ($Zn_5(OH)_6(CO_3)_2$), a common secondary mineral associated with zinc deposits. However, several artificial watercourses were constructed to supply waterwheels, and these are still in existence. They are shown on Figure 3.4 together with the natural watercourses.

The main reason for the choice by ITE of the Wye catchment at Plynlimon for this study was the background information available from IH on the climate, stream flow and soil moisture content of the site, measurements having been taken over 16 years [241]. Other advantages include the relatively uniform parent material with a simple mineralogy, the availability of background data on the soils [149] and rocks [135], and the ease of access to the site because of the well maintained network of tracks. The major disadvantages include the lack of exposure of parent material except in stream beds and on some valley sides, the prevalence of boulder clay, head and colluvium acting as soil parent materials, and the presence of mineralised zones.

The geology of the area investigated is relatively simple, but a recent revision of the stratigraphical nomenclature has resulted in two sets of names being employed. Within the Wye catchment, the conformable boundary [135,138] between the Ordovician and Silurian systems is found, and thus the outcropping sediments are from the uppermost Ordovician and lowest Silurian. The oldest rocks, the Lower Fan Series, outcrop in the north, and the dip is generally southwards, although this is complicated by a series of approximately north to south trending folds, of which the most important is the Snowbrook Anticline (Figure 3.2). Major faulting occurs in a direction varying between north to south and northeast to southwest, the main faults being the West and East Cyff Faults and the Snowbrook Fault, which parallels the line of the Snowbrook Anticline. Less important faults occur in varying orientations, in some cases cross cutting the major faults almost at right angles (Figure 3.2). The rocks are dominantly composed of shales and mudstones, with less important occurrences of grits. Figure 3.5 is a simplified stratigraphic column of the sequence as found in the Wye catchment, and correlates the old and new stratigraphic nomenclatures.

| Top not seen | New Stratigraphic Nomenclature | Old Stratigraphic Nomenclature | Geological Stages | Graptolite Zones |
|---|---|---|---|---|
| | | | Upper Llandovery | M. sedgwicki |
| | Frongoch Mudstone Series 70 m | Derwen Group | Middle Llandovery | M. regularis |
| | | | | M. leptotheca |
| | | | | Mesograptus magnus |
| | Gwestyn Shale Group 165 m | Cwmere Group | Lower Llandovery (Silurian) | M. triangulatus |
| | | | | M. cyphus |
| | | | | M. acinaces |
| | | | | M. atavus |
| | | | | Akidograptus acuminatus |
| | | | | Glyptograptus persculptus |
| | Upper Fan Series (Fan Shales) 345 m | Brynglas Group | Ashgill (Ordovician) | |
| Base not seen | Lower Fan Series (Fan Grits) 270 m | Drosgol Group | | |

Figure 3.5 A Stratigraphic Column of the Sediments exposed in the Wye Catchment at Plynlimon, after Jones and Pugh [138] M = Monograptus

The basal rocks of the Lower Fan Series, consisting of dark blue mudstones with bands of tough grey grit, are not seen within the Wye catchment at Plynlimon, but where they are present the total thickness of the series is 270m [138]. In the Wye catchment the Lower Fan Series is represented by dominantly coarse grained alternations of dark blue mudstones, grey conglomeratic grits and gritty or pebbly mudstones. The grits show knotted weathering surfaces, which are related to the internal structure of contorted laminae [138]. Some of the mudstones contain well rounded vein quartz pebbles, which may be aggregated into discontinuous bands, but are more usually randomly scattered. However, most of the coarse quartz occurs as angular fragments. The quartz particles may be 25mm or more in diameter, and are associated with some rotted feldspar. Both the grits and the mudstones contain scattered pyrite cubes, but neither have yielded fossils.

The whole of the Lower Fan Series is considered to have been derived from the east, laterally with respect to the depositional basin [135]. The sediments are interpreted as proximal turbidites, with the conglomeratic grits being formed from fluxoturbidites and traction deposits, whilst the contorted laminar structure of the pebbly mudstones is due to an origin by mass flow redistribution of the fluxoturbidite deposits. A single major fan of proximal turbidites is considered to occur at the top of the Lower Fan Series in the Plynlimon area [135].

The Upper Fan Series is 345m thick, and consists of massive blue black mudstones and shales in which bedding planes are difficult to determine. Intersecting cleavages cause the rocks to split into lenticular fragments. The rocks are soft and weather to a grey colour, and are interpreted as suspension deposits [135]. They are not fossiliferous.

The Gwestyn Shale Group is about 165m thick in the Plynlimon area [138]. At the base is a 15 to 18m band of blue compact mudstones, which rest sharply but conformably on the underlying Upper Fan Series, and which are more resistant to weathering than the rest of the Gwestyn Shale Group. The rest of the group consists of grey to black shales and mudstones with siliceous siltstone bands from 3 to 150mm thick scattered throughout the sequence. The Gwestyn Shale Group is characterised by its locally highly pyritiferous nature, and thus it

weathers to yellows, reds and browns due to the Fe oxides developed from the pyrite. About halfway up the sequence is a group of thin pale siliceous flags. The rocks are highly cleaved, the shales fragmenting into thin pieces and the flagstones forming rhomboidal prisms. There are occasional layers of calcareous nodules. Locally the rocks are richly fossiliferous, and yield a Lower Llandovery fauna.

The Frongoch Mudstone Series includes all of the Middle Llandovery rocks, which are only 40m thick, together with the lowest 30m of the Upper Llandovery, which is 780m thick in the area. The top of the series is not seen in the Wye catchment. The rocks are mainly pale grey mudstones, with minor dark blue graptolitic shale bands, and have a strongly developed cleavage. Flagstones occur and cone-in-cone structures are locally common. The bedding in the mudstones is usually difficult to determine. In general the mudstones are not fossiliferous, but have yielded rare brachiopods and trilobites.

### 3.2.1 Drift Deposits

In many parts of the Wye catchment area at Plynlimon, bedrock does not outcrop at the surface. Instead, it is covered by glacial, periglacial or postglacial deposits, respectively boulder clay, soliflucted head and colluvium. When fresh, the boulder clay is bluish grey in colour, tough and highly impermeable, but it weathers to an ochre shade, due to the oxidation of its Fe content. It consists of a rock flour matrix containing striated and plucked mudstone and grit boulders, and smaller fragments of mudstone and shale, suggesting a local derivation. It commonly occurs in the valley bottoms, where it is up to 30m thick but, particularly on the south facing slopes, it has been partially or completely removed by erosion and slumping. However, it has been suggested [149] that the whole area of development of Ynys series soils (Figure 3.3) is underlain by boulder clay.

Periglacial conditions occurred in much of mid and north Wales during the post-Allerød interstadial climatic recession from 8,800 to 8,300BC [17]. These conditions allowed frost shattering to become an effective rock breakdown mechanism, and as a result screes developed on slopes underlain by Lower Palaeozoic shales are widespread. As well as the frost shattering, periglacial conditions brought about freeze/thaw cycles in water saturated unconsolidated deposits, such as the boulder clay. During the seasonal thawings, these deposits slowly flowed downslope, reworking and reorienting the larger fragments in the

boulder clays. Where boulder clay or soil cover was underlain by scree, this was also carried downslope by the effects of solifluction on the overlying material, giving rise to the deposit known as head. This consists mainly of reworked angular fragments, in a sparse finer matrix derived from boulder clay or soil, which may have also contributed more rounded stones [17]. Boulder clay, head and scree deposits often grade into one another, but at Plynlimon the head is mainly to be found on the upper slopes of the hills, having moved little distance from the frost shattered scree deposits from which it was derived.

The colluvium is due to present day soil creep, and consists of the products of weathering on the upper hill slopes which have been moved downslope to mantle the boulder clay deposits in the valley bottoms. It consists of weathered chunks or flakes of mudstone within a silty matrix of mudstone weathering products. It is less than 1m thick on the upper hill slopes, but it thickens downslope due to transport. Heavy mineral studies have shown that there are no loess deposits within the Wye catchment at Plynlimon.

## 3.3 THE CHEMISTRY AND MINERALOGY OF PLYNLIMON SHALES

Because of the occurrence of four different stratigraphic groups of rocks within the Wye catchment at Plynlimon (Figures 3.2 and 3.5), it was considered important to investigate the variation in mineralogy and chemistry between samples from different groups. It is possible that the soils could have been derived from any of the rocks outcropping in the area, and not just the one they overlie, due to the movement of rock fragments by glacial and periglacial processes.

The rock investigated in most detail, 1040, belongs to the Gwestyn Shale Group, whereas the humic stagnopodsol profile is developed on a periglacial deposit of angular shale fragments overlying Frongoch Mudstone Series rocks. The other soil profiles sampled, a brown podsolic, a gley, a blanket peat and a woodland podsol, were respectively developed on soliflucted head, reworked boulder clay, scree deposits and scree overlying Gwestyn Shale Group rocks.

A total of 17 rock samples were collected within the Wye catchment by the author and colleagues, from the locations shown on Figure 3.4. Further rock collections were made by IGS, and the locations of the 30 of their samples for which information is available, 20 of which were

taken as duplicates, is also given on Figure 3.4. All four rock groups are represented by samples, and Table 3.1 correlates rock groups with sample numbers, whilst Table A.1 in the Appendix provides hand specimen descriptions of the author's samples.

| Rock Group | Sample Numbers |
|---|---|
| Frongoch Mudstone Series | 1004, 1007, 1009, 1013, GCR46, GCR47, GCR48, GCR49 |
| Gwestyn Shale Group | 1010, 1014, 1017, 1018, 1019, 1020, 1021, 1022, 1036, 1040, 1047, 1052, GCR4, GCR14, GCR15, GCR16, GCR17, GCR18, GCR19, GCR41, GCR41A, GCR42, GCR43, GCR44, GCR45 |
| Upper Fan Series | GCR1, GCR2, GCR3, GCR8, GCR9, GCR10A, GCR11, GCR12, GCR13, GCR20 |
| Lower Fan Series | 1030, GCR5, GCR6, GCR7, GCR10B |

Table 3.1 The Correlation Between Samples and Rock Groups

The overall impression given by the samples is that the dominant rock type is shale, but this can be either fine grained or silty and either laminated or homogeneous. The colour is dominantly grey, but this varies from greyish white to dark bluish grey, and the effects of weathering may add brown tones to the rock surfaces. Besides shale, the only other rock type encountered is occasional coarse sandstone. From the descriptions in Table A.1, it can be seen that within the rock groups there is considerable variation in appearance, from coarse sandstone (1010) to finely laminated shale (1019) in the case of the Gwestyn Shale Group. Some samples from the different rock groups also have very similar appearances, as for instance the silty shales 1004 and 1020, respectively representatives of the Frongoch Mudstone Series and the Gwestyn Shale Group.

The hand specimen evidence alone is thus sufficient to suggest that there is considerable petrological variation in the parent material within a given rock group, as well as between the four groups that are relevant when the catchment is considered as a whole. However, it was felt worthwhile to investigate variation in the parent material in more detail, to assess the relative levels of variation both within and between the rock groups. This was carried out by calculating Zr/Sr ratios from the trace element analyses of the samples collected by IGS, which were produced by a direct reading arc spectrograph. Many other

pairs of elements could have been employed in a similar way, but the Zr/Sr ratio was chosen for comparison with the work of Evans and Adams [94]. Similar analyses were also carried out for the author's rock sample 1040, boulder clays 1029, 1039 and 1049, and weathered boulder clay 1050, and these are included for comparison purposes with the analyses of the other samples in Table 3.2. It would be expected that, in the rocks, the Zr would be found almost entirely in zircon crystals, whilst the Sr would be concentrated in feldspars [94]. Both of these phases, particularly the zircon, are resistant to weathering relative to chlorite, and thus the Zr/Sr ratio should indicate variation in the original rock compositions, even when weathering of the surfaces of the rock samples analysed has occurred.

Sample GCR10 was collected from very close to the geological boundary between the Fan Grits and the Fan Shales, and the appearance and analyses confirm the decision of IGS to group sample GCR10A with the Fan Shales, and its duplicate, GCR10B, with the Fan Grits. Mean values of Zr, Sr and Zr/Sr were calculated for each group of rocks, and four samples (1040, GCR8A, GCR8B and GCR18A) were found to be outside two standard deviation limits from the means of the appropriate groups. These sample values were thus eliminated from further calculations, together with the values for the duplicate sample GCR18B, where applicable. These aberrant analyses all occur in the finer grained rock groups, and it is likely that most correspond to samples from the coarser silt or sandstone bands in the mainly shale or mudstone groups. It is evident that the Zr/Sr ratio is higher in the sandstones than the shales. None of these sample locations occur sufficiently close to the boundary with the Lower Fan Series to suggest that the samples may be from a different rock group to those shown on Figures 3.2 and 3.4.

Statistical analysis of the modified data was carried out, using the Zr/Sr ratio, rather than the Zr or Sr values, as this showed the greatest difference in value between the groups when compared to the variation within the groups. A t test was used to determine the significance of differences between the mean values for the different rock groups. This showed that the Lower Fan Series is significantly different from the other three groups with greater than 99% confidence, and that the Frongoch Mudstone Series is different from the two remaining groups with greater than 90% confidence. The analyses of the Gwestyn Shale Group and the Upper Fan Series are not significantly different in terms of Zr/Sr, but are different in terms of Sr content

| Rock Group | Sample Number | Zr (ppm) | Sr (ppm) | Zr/Sr |
|---|---|---|---|---|
| Frongoch Mudstone Series | GCR 46 | 216 | 131 | 1.65 |
| " | GCR 47 | 171 | 111 | 1.54 |
| " | GCR 48 | 278 | 116 | 2.40 |
| " | GCR 49 | 254 | 113 | 2.25 |
| " | Mean ± Std. Deviation | 230±47 | 118 ± 9 | 1.96±0.43 |
| Gwestyn Shale Group | 1040 | (402) | 89 | (4.52) |
| " | GCR 4A | 157 | 156 | 1.01 |
| " | GCR 4B | 222 | 170 | 1.31 |
| " | GCR 14A | 215 | 157 | 1.37 |
| " | GCR 14B | 233 | 171 | 1.36 |
| " | GCR 15A | 244 | 162 | 1.51 |
| " | GCR 15B | 199 | 159 | 1.25 |
| " | GCR 16A | 329 | 168 | 1.96 |
| " | GCR 16B | 194 | 157 | 1.24 |
| " | GCR 17A | 166 | 147 | 1.13 |
| " | GCR 17B | 254 | 150 | 1.69 |
| " | GCR 18A | (383) | 77 | (4.97) |
| " | GCR 18B | (226) | 81 | (2.79) |
| " | GCR 19A | 243 | 156 | 1.56 |
| " | GCR 19B | 155 | 157 | 0.99 |
| " | GCR 41 | 218 | 214 | 1.02 |
| " | GCR 41A | 186 | 143 | 1.30 |
| " | GCR 42 | 174 | 147 | 1.18 |
| " | GCR 43 | 221 | 117 | 1.89 |
| " | GCR 44 | 244 | 129 | 1.89 |
| " | GCR 45 | 126 | 71 | 1.77 |
| " | Mean ± Std. Deviation | 228 ± 70 | 142 ± 36 | 1.80±1.07 |
| " | " Eliminating Bracketed Values | 210 ± 47 | 142 ± 36 | 1.41±0.32 |
| Boulder Clay | 1029 | 304 | 148 | 2.05 |
| " | 1039 | 282 | 145 | 1.94 |
| " | 1049 | 328 | 174 | 1.89 |
| " | Mean ± Std. Deviation | 305 ± 23 | 156 ± 16 | 1.96±0.08 |
| Upper Fan Series | GCR 1B | 237 | 160 | 1.48 |
| " | GCR 2A | 245 | 168 | 1.46 |
| " | GCR 2B | 201 | 170 | 1.18 |
| " | GCR 3A | 298 | 156 | 1.91 |
| " | GCR 3B | 174 | 173 | 1.01 |
| " | GCR 8A | (473) | (47) | (10.06) |
| " | GCR 8B | (480) | (46) | (10.43) |
| " | GCR 9A | 237 | 190 | 1.25 |
| " | GCR 9B | 248 | 203 | 1.22 |
| " | GCR 10A | 256 | 197 | 1.30 |
| " | GCR 11A | 246 | 215 | 1.14 |
| " | GCR 11B | 210 | 220 | 0.95 |
| " | GCR 12A | 282 | 170 | 1.66 |
| " | GCR 12B | 339 | 172 | 1.97 |
| " | GCR 13A | 251 | 139 | 1.81 |
| " | GCR 13B | 240 | 136 | 1.76 |
| " | GCR 20A | 219 | 125 | 1.75 |
| " | GCR 20B | 204 | 113 | 1.81 |
| " | Mean ± Std. Deviation | 269 ± 84 | 156±49 | 2.45± 2.85 |
| " | " Eliminating Bracketed Values | 243 ± 40 | 169±31 | 1.48 ± 0.34 |
| Lower Fan Series | GCR 5A | 255 | 45 | 5.67 |
| " | GCR 5B | 407 | 44 | 9.25 |
| " | GCR 6A | 329 | 101 | 3.26 |
| " | GCR 6B | 298 | 99 | 3.01 |
| " | GCR 7A | 561 | 48 | 11.69 |
| " | GCR 7B | 207 | 46 | 4.50 |
| " | GCR 10B | 500 | 57 | 8.77 |
| " | Mean ± Std. Deviation | 365 ± 130 | 63±26 | 6.59 ± 3.34 |
| Weathered Boulder Clay | 1050 | 253 | 214 | 1.18 |

TABLE 3.2 Zr/Sr Ratios of the Different Rock Groups and Boulder Clays

alone with greater than 95% confidence. Although these analyses are only of one limited detail of the chemistry of the rocks concerned, it is likely that the inhomogeneity in Zr/Sr ratio seen between the groups will be reflected in other elements of the mineralogy and chemistry of the rocks, and thus it must be concluded that the parent material in the Wye catchment at Plynlimon is not homogeneous. This finding is at variance with that of Hornung et al [127], who, from major element evidence alone, found that the Frongoch Mudstone Series and Gwestyn Shale Group are "geochemically very similar". Variation in major element chemistry, both within and between the rock groups and boulder clays, is shown in Table 3.3, where the results of betaprobe analyses, carried out by IGS, are given, together with median analyses for the Frongoch Mudstone Series and Gwestyn Shale Group [127].

As well as the quite considerable overall differences between the two samples from the Lower Fan Series, the major differences to be noted from Table 3.3 are those between the rocks and the boulder clays. The boulder clays all have lower $SiO_2$, and higher $TiO_2$ and $K_2O$ contents than any of the rocks. Incorporation of wind blown material into the boulder clays could obviously alter their compositions, but there is no evidence for loess deposits in the catchment. Similarly, the occurrence of weathering during the Tertiary, and the incorporation of the weathering products, could have a similar effect on composition, but again there is no evidence for this mechanism. The finding of higher $TiO_2$ and lower $SiO_2$ contents might possibly be expected, as in the transformation from rock to boulder clay a little chemical weathering may occur, which would concentrate the resistant $TiO_2$ containing phases, and dissolve quartz which had been ground to a very fine dust by glacial action. However, the increase in $K_2O$ content is quite anomalous, as it implies that the $K_2O$ containing minerals such as mica and feldspar are more resistant to glacial alteration than the resistant $TiO_2$ containing phases. This is most unlikely to be the case, and thus it must be postulated that pore waters rich in K were present during or after the formation of the boulder clay. If the mica present in the original rock was deficient in $K_2O$, or if any vermiculite was present in the rock, it could have taken up K from the water and fixed it into the mineral structure, giving rise to an increase in $K_2O$ on the alteration of the rock to boulder clay (see Section 7.2.1).

| Sample Group | Frongoch Mudstone Series | Gwestyn Shale Group | | | | Upper Fan Series | Lower Fan Series | | Boulder Clay | | | Weathered Boulder Clay |
|---|---|---|---|---|---|---|---|---|---|---|---|---|
| Sample Number | Median [127] | 1040 | GCR4A | GCR17A | Median [127] | GCR20A | GCR6A | GCR7A | 1029 | 1039 | 1049 | 1050 |
| % $SiO_2$ | 62.50 | 63.39 | 58.21 | 60.14 | 63.50 | 61.78 | 64.24 | 82.97 | 56.85 | 59.50 | 56.72 | 57.80 |
| % $TiO_2$ | 1.06 | 1.13 | 1.21 | 1.16 | 1.22 | 1.14 | 1.08 | 0.52 | 1.39 | 1.31 | 1.29 | 1.29 |
| % $Al_2O_3$ | 22.50 | 17.63 | 22.70 | 23.61 | 24.80 | 21.29 | 19.73 | 9.40 | 23.25 | 23.25 | 23.40 | 23.11 |
| % Fe as $Fe_2O_3$ | 8.50 | 9.26 | 10.04 | 7.65 | 8.52 | 8.16 | 8.45 | 5.38 | 10.40 | 6.71 | 10.12 | 10.35 |
| % MgO | 2.13 | 2.38 | 1.80 | 2.19 | 2.31 | 1.80 | 1.45 | 0.83 | 1.42 | 1.61 | 1.57 | 1.57 |
| % CaO | 0.04 | 0.13 | 0.08 | 0.14 | 0.01 | 0.23 | 0.14 | 0.26 | <0.05 | <0.05 | <0.05 | <0.05 |
| % $Na_2O$ | n.d. | 1.17 | 0.96 | 1.16 | n.d. | 1.21 | 0.59 | 1.06 | 1.02 | 1.12 | 0.94 | 0.95 |
| % $K_2O$ | 4.00 | 2.89 | 3.45 | 3.89 | 3.90 | 3.42 | 3.58 | 1.02 | 4.24 | 4.17 | 4.29 | 4.26 |
| % $P_2O_5$ | n.d. | 0.16 | 0.18 | 0.08 | n.d. | 0.17 | 0.18 | 0.13 | 0.20 | 0.03 | 0.16 | 0.13 |
| % F | n.d. | 0.08 | 0.13 | 0.10 | n.d. | 0.10 | 0.10 | 0.05 | 0.11 | 0.09 | 0.10 | 0.12 |

Table 3.3 Major Element Variation in Soil Parent Materials at Plynlimon

(n.d. = not determined)

Bjørlykke [28] worked on the petrology of Ordovician sediments from Wales, and found the average shale to contain only 1.4% MgO, compared to a 2.32% world average for Palaeozoic shales. He also found the shales to have high feldspar contents and high Na/K and K/Rb ratios, which he interpreted to indicate that the rocks he had investigated were immature sediments derived from acid and intermediate volcanics and Precambrian basement rocks, with little contribution from gabbroic rocks. Elsewhere, the average shale is considered to have an MgO content of 2.44% and an Na/K ratio of 0.40 [209], very close to the figures of 2.38% and 0.40 found for sample 1040 (Table 3.3). All except one of the other rock samples have Na/K ratios ranging from 0.16 to 0.35, coupled with MgO contents above 1.45%. However one grit, GCR7A, has an MgO content of 0.83% and an Na/K ratio of 1.04. These figures suggest that, although the Ordovician and Silurian sediments at Plynlimon may be derived from sources which are not rich in basic rocks, except for the grit they are chemically and mineralogically more mature than the Ordovician sediments studied by Bjørlykke.

Mineralogical variation between the rock samples from Plynlimon was investigated by semiquantitiative XRD. Diffractometer traces were obtained from random powder mounts of 17 different rocks, four belonging to the Frongoch Mudstone Series, 12 from the Gwestyn Shale Group, and one from the Lower Fan Series. Although the traces, except for that for 1040, were not obtained using appropriate diffractometer parameters for full quantitative analysis (see Section 6.4), they were interpreted by applying the quantitative method described in Section 6.4.2 to the chlorite 12.6°2$\theta$, mica 8.8°2$\theta$ and quartz 20.8°2$\theta$ peaks. The resulting analyses, and quartz/mica ratios, are given in Table 3.4 for the whole rock samples. Other investigators have used the quartz/mica ratio of the silt fraction alone to investigate mineralogical uniformity of soil parent materials [94].

The mean figures in Table 3.4 for the Gwestyn Shale Group samples used in statistical analysis were those for which values outside two standard deviations from the mean had been eliminated. Although the mean quartz/mica ratios of the Frongoch Mudstone Series and the Gwestyn Shale Group are not significantly different, the mean chlorite contents are significantly different with greater than 99% confidence, whilst the mean quartz contents are different with greater than 95% confidence. Because only one sample from the Lower Fan Series was analysed, its analysis cannot be compared statistically

| Rock Group | Sample Details | % Mica | % Chlorite | % Quartz | Quartz/ Mica |
|---|---|---|---|---|---|
| Frongoch | 1004 | 42.7 | 32.6 | 24.7 | 0.58 |
| Mudstone | 1007 | 41.6 | 26.8 | 31.6 | 0.76 |
| Series | 1009 | 41.4 | 37.4 | 21.2 | 0.51 |
| " | 1013 | 45.4 | 31.8 | 22.8 | 0.50 |
| " | Mean ± Standard Deviation | 42.8±1.8 | 32.2±4.3 | 25.1±4.6 | 0.59±0.12 |
| Gwestyn | 1010 | (8.8) | 12.0 | (79.2) | (9.00) |
| Shale | 1014 | 42.3 | 23.2 | 34.5 | 0.82 |
| Group | 1017 | 55.6 | 14.8 | 29.6 | 0.53 |
| " | 1018 | 40.7 | 32.8 | 26.5 | 0.65 |
| " | 1019 | 47.6 | 22.1 | 30.3 | 0.64 |
| " | 1020 | 48.1 | 25.1 | 26.8 | 0.56 |
| " | 1021 | 53.9 | 17.5 | 28.6 | 0.53 |
| " | 1022 | 40.5 | 25.8 | 33.7 | 0.83 |
| " | 1036 | 53.2 | 14.8 | 32.0 | 0.60 |
| " | 1040 | 28.4 | 33.1 | 38.5 | 1.36 |
| " | 1047 | 46.0 | 30.8 | 23.2 | 0.50 |
| " | 1052 | 32.8 | 25.4 | 41.8 | 1.27 |
| " | Mean ± Standard Deviation | 41.5±13.2 | 23.1±7.2 | 35.4±14.7 | 1.44±2.40 |
| " | " Eliminating Bracketed Values | 44.5± 8.6 | 23.1±7.2 | 31.4± 5.5 | 0.75±0.30 |
| Lower Fan Series | 1030 | 10.8 | 30.5 | 58.7 | 5.44 |

Table 3.4 Semiquantitative Mineralogy of Plynlimon Rock Samples

with those of the other two rock groups, but it would appear that both the quartz and mica contents, and the quartz/mica ratio, are likely to be different from those of the Gwestyn Shale Group and the Frongoch Mudstone Series. The results of this mineralogical analysis confirm the view that the parent material in the Wye catchment at Plynlimon is not homogeneous.

Little further detailed work on the Plynlimon shale parent materials was carried out, although two minor investigations can be reported. Firstly, polished blocks of typical laminated shale were prepared, with surfaces cut parallel to either the cleavage or the laminations. These were then subjected to XRD analysis, which showed high intensity phyllosilicate basal reflections from the surface parallel to the cleavage, but low intensity basal reflections and well defined (hkl) reflections from the surface parallel to the laminations. This indicates that the phyllosilicate sheets in the shale have been reoriented from their original orientation parallel to the lamination to become parallel to the cleavage.

Secondly, point count analysis was carried out on a thin section of the same rock sample cut parallel to the cleavage. A total of 3,000 points were counted, and gave rise to a mean analysis of:

| | |
|---|---|
| Unresolved matrix (finer than 5μm) | 60.7 ± 2.2% |
| Chlorite | 13.5 ± 2.5% |
| Quartz | 10.7 ± 0.9% |
| Mica | 8.8 ± 2.7% |
| Feldspar | 5.4 ± 0.8% |
| Opaque minerals | 0.6 ± 0.2% |
| Other phases | 0.3 ± 0.5% |

Having examined other thin sections, this point count analysis would appear to be typical of the Plynlimon rock samples, and Plate 1 is a photomicrograph of 1040, taken under crossed polars. The largest grains visible are chlorite, showing anomalous blue interference colours. These are typical in size of the largest grains in the rock, at about 200μm, but one grain about 600μm across was also seen in thin section. In most of both the large and small chlorite grains bands of a yellowish interference colour can be seen, which is due to mica intergrown with the chlorite. In general, the chlorite grains seem to be reasonably well rounded.

the present climatic conditions, but that instead the different horizons have been added by climatic variation over the last 8,000 years. Most probably the Hiraethog soils were originally brown earths or, if there was tree cover, podsolised brown earths. Climatic changes would have led to the loss of any trees, and an increase in rainfall to peat development. This in turn would have caused an accumulation of water in the soil, and consequential gleying. The weathering environment in the Hiraethog series soils is thus a combination of both past and present influences. This makes it difficult to interpret, but also its diversity shows that the study of a Hiraethog series profile is most appropriate to the study of the weathering of the shale parent material.


Plate 1 Photomicrograph of Rock 1040

# CHAPTER 4

# SEPARATION OF MINERAL PHASES

## 4.1 INTRODUCTION

To study the mineral components of the samples in detail, it was necessary to separate the minerals, so that the measurements on one would not be affected by the presence of others. For coarse grains in the rock it was possible to separate them in situ by targetting of investigation techniques (see Section 5.1) so that only the grains of interest were analysed. However, this would have been difficult to carry out on the unconsolidated samples, and could not have been used on particles below the resolution of the technique employed. As well as being separated from other components, these fine grains needed to be bulked together with a sufficient quantity of like material for their properties to be determined. In particular, it was necessary to obtain standards for quantitative mineralogical analysis that were not contaminated by other components because:

> "..it became obvious that one of the available techniques had actually overcome the problems of variability of composition and crystallinity of the clay minerals. An appropriate solution seemed to be the extraction of the individual clays from the samples themselves and then using these separated clays as the standards for the series of samples." [103]

Separation of chlorite was the main aim for three reasons: there were no materials available that even approximated to a suitable XRD standard for the Plynlimon chlorite, the chlorite showed the greatest susceptibility to weathering, and thus its initial composition needed to be known in greatest detail, and previous workers had shown that the separation of chlorite using magnetic separation was a viable proposition [24,76,219,233]. The difficulty in choosing any method of separation is twofold. Firstly, a decision must be made as to what is to be extracted from the bulk material, and then a method must be chosen that is capable of the desired extraction. Having decided on extraction of chlorite from a sample consisting mainly of quartz, mica and chlorite, it had to be acknowledged that no separation system, except the perfect combination of chemicals that would dissolve all other minerals and yet leave the chlorite unaffected, could extract the chlorite across the range of grain sizes present in an equally efficient way. However, chlorite is more reactive than either mica or

quartz, and is thus likely to be preferentially attacked, rather than concentrated, by chemical treatment.

Methods have been proposed for the separation of nonmagnetic components from soils, but these involve the use of techniques with considerable drawbacks. A method often used to eliminate quartz is only to deal with the finest size fractions [246]. However, particles finer than 0.2μm are very reactive, and the treatments proposed to remove the other phyllosilicates from micas of this size, including digestion in hot 0.5M NaOH followed by 0.5M HCl and then calcining at 500°C, are almost certain to affect the mica, even if no differences are observed with the analytical techniques employed [246]. Density separation methods have been proposed for the separation of phyllosilicates from the fractions of the original sample in which they are most concentrated, but these involve noxious chemicals, difficulty in dispersion, and low yields [103,219]. Small yields also occur with electrophoresis, although this is capable of separating phyllosilicates without involving any pretreatments likely to alter their nature [79, 200,201].

As a result of these drawbacks, an attempt was made to develop a method of separating mica from quartz (see Section 4.4), but initially disappointing results led to this being abandoned, and to mica and quartz from outside Plynlimon being used as standards in XRD analysis (see Section 6.4.2). However, reviewing the results suggests that, if effort had continued, it might have been possible to extract relatively pure samples of both mica and quartz, but this would have reduced the yield of chlorite it proved possible to obtain.

### 4.1.1 Magnetic Separation

The magnetic separation equipment, supplied by Chas. W. Cook and Sons Ltd., consisted of an electromagnet with two pole pieces separated by a gap 16mm wide, 254mm long and 31mm deep. It was supplied with a universal mount, but was designed to be operated as a dry separator, with grains in the range 63-630μm passing down a polished brass chute between the pole pieces [219]. However, the instrument could be modified for the separation of fine particles in aqueous suspension by replacing the chute with a vertical plastic or glass tube, through which the suspension could be passed [24,219].

Because coarse grains have a lower specific surface area, and are thus likely to react more slowly, and because it had been shown that at least the crystallinity, if not other properties of the chlorite, varied with particle size (see Table 8.10), attention was concentrated on the separation of fine chlorite. Dry separation of coarse chlorite was carried out by a colleague, to obtain grains large enough to study the surface morphology both in the natural state and after artificial weathering [27]. Table 5.3 compares the chemistry of coarse and fine separates.

Magnetic methods for the separation of minerals are suitable where the components have different magnetic susceptibilities. Magnetic properties are due to the spin of electrons about their axes, and their orbit about atomic nuclei, both of which produce magnetic moments. Many atoms and ions contain only orbitals in which all electrons are paired, with the result that their spin magnetic moments cancel out, but in atoms or ions with unpaired electrons there is a residual magnetic moment. Substances with no unpaired electrons are diamagnetic, and when an external field is applied show a very weak magnetisation (susceptibility $-2 \times 10^{-8}$ to $-1.5 \times 10^{-6} cm^3 g^{-1}$) opposite to the applied field, caused by the orbit of electrons about the nuclei. Paramagnetic substances contain unpaired electrons, of which the direction of spin is altered by an applied magnetic field, to produce a resultant magnetisation parallel to the applied field. This is much greater than the opposing magnetisation due to the electron orbits, giving rise to an overall susceptibility of $2 \times 10^{-8}$ to $10^{-3} cm^3 g^{-1}$. Ferromagnesian minerals are mostly paramagnetic, and the separation of chlorite depends on it having a very much higher Fe content, and thus a higher susceptibility, than the minerals it is being separated from. Ferromagnetism occurs in materials in which an external field does not simply alter the direction of spin of unpaired electrons, but aligns the spins parallel, giving rise to a very high induced magnetisation (susceptibility $10^{-1}$ to $10^{4} cm^3 g^{-1}$).

The intensity of induced magnetisation is proportional to both the applied field and the susceptibility. As a result of this, a mineral with a higher susceptibility than the other components of a mixture, such as chlorite when mixed with illite and quartz, will be preferentially retained within the magnetic field of a separator. However, other minerals with high Fe contents, such as Fe oxides, would be expected to be retained with the chlorite.

Industrial magnetic separators have developed from low field intensity separators, through high field intensity separators to, in the 1970s, high magnetic gradient separators [202]. These incorporate thin fibres of ferromagnetic material, typically 430/444 ferritic stainless steel, within the separating volume. Because of the very high susceptibility of the ferromagnetic material, strong induced fields are set up around the fibres, resulting in the intensity of the field experienced by particles passing through the separator varying widely over short distances. Such machines are used commercially in the extraction of less than 1% of paramagnetic impurities from essentially diamagnetic china clays, where 4-50μm diameter fibres filling 1 to 5% of the separator volume are employed in conjunction with 1 to 2 Tesla (T) fields. In these separators, where particles are a few μm in diameter, and move a few cm $s^{-1}$, the only important forces on the particles are magnetostatic attraction and hydrodynamic drag, which are finely balanced, with drag increasing in effect as particles become smaller. It can be shown that, for optimum separation, the ratio wire diameter:particle diameter should equal 2.339, but to prevent clogging of the wires, which are capable of holding approximately their own volume of material, wires of diameter up to 10 times the particle diameter are used, and give acceptable levels of separation [202].

High gradient fields have also been taken advantage of in laboratory separation of chlorites, Fe oxides and other minerals from crushed rocks and soils [76,233]. In this work either stainless steel wool, or ferromagnetic grooved plates or balls, have been placed in the separation volume to produce a field of considerable heterogeneity, considered essential for the separation of weakly paramagnetic materials, such as chlorite [76]. The fields used have had strengths of 1.15 or 1.6T. As found with commercial separation, reduction in particle size lowers the effectiveness of separation with a heterogeneous field, and it has been suggested that for particles finer than 10μm a uniform field should be used, even though this will not give rise to the purity of product obtained when a high gradient system is used with coarser particles [76].

## 4.2 THE MAGNETIC SEPARATION OF CHLORITE FROM SUSPENSION

Once the unweathered rock, 1040, had been obtained, effort was concentrated into the separation of chlorite, with the aim of obtaining as much as possible as pure as possible. For initial work the whole rock, after grinding for 10 minutes in a Tema mill, was made into a 10%

suspension in water. 500cm³ of suspension were used for the initial separation, with a peristaltic pump recirculating the suspension into a reservoir beaker with a magnetic stirrer. A plastic separating tube was used, containing a ferritic stainless steel mesh to create a polygradient field. The maximum current was employed in the separator, being 2.3A when switched on, but reducing to 2A as the coil heated up.

Before separation was started, the field produced by different currents was measured at five positions in the separating zone. Gaussmeter readings were taken at the top and bottom of the pole pieces, and at three equally spaced intermediate positions. The results are given in Table 4.1, and indicate the maximum field to be 1.75T, comparable with those used in commercial systems. The readings show that, at a given temperature and current, the field is uniform within ±6% over the lower three quarters of the pole pieces, but at the top of the pole pieces falls to 67% of the maximum value. The data also show that an identical current is not always produced by the same setting on the rheostat; a higher setting is needed to produce the same current at a higher temperature, and at a higher temperature a given current produces a lower field.

Table 4.1 Magnetic Fields Measured at Different Currents

| Rheostat Setting | Current (A) | Measured Suspension Temperature (°C) | Magnetic Field (T) Measured at Position: | | | | |
|---|---|---|---|---|---|---|---|
| | | | Top | 2 | 3 | 4 | Bottom |
| 0 | 0.0 | | 0.018 | 0.021 | 0.021 | 0.022 | 0.023 |
| 59 | 0.5 | | 0.29 | 0.40 | 0.43 | 0.43 | 0.43 |
| 68 | 0.6 | | 0.36 | 0.48 | 0.51 | 0.51 | 0.50 |
| 73 | 0.7 | | 0.42 | 0.56 | 0.62 | 0.63 | 0.62 |
| 77 | 0.8 | | 0.49 | 0.66 | 0.69 | 0.70 | 0.69 |
| 80 | 0.9 | | 0.54 | 0.74 | 0.78 | 0.78 | 0.77 |
| 84 | 1.0 | 21 | 0.65 | 0.85 | 0.90 | 0.91 | 0.91 |
| 96 | 1.5 | | 0.98 | 1.25 | 1.30 | 1.30 | 1.25 |
| 102 | 2.0 | | 1.25 | 1.55 | 1.65 | 1.65 | 1.65 |
| Maximum | 2.3 | | 1.35 | 1.65 | 1.75 | 1.75 | 1.70 |
| 102 | 2.0 | 22 (Coil 33.5) | 1.15 | 1.45 | 1.50 | 1.45 | 1.45 |
| 86 | 1.0 | 23 | 0.60 | 0.73 | 0.77 | 0.77 | 0.75 |

The suspension was passed through the separator for 30 minutes, at $10.2cm^3min^{-1}$, and then the separation tube was flushed with distilled water for five minutes before the current was turned off. The tube was then washed with a jet of distilled water, and a total of 100cm³ of washings were kept. Three further, identical, separations of the original suspension were carried out, to give a total of 400cm³ of first order separate. This magnetic fraction was then separated in a similar way to the original suspension, but only 50cm³ of washings were collected after each of the runs. Glass slides for XRD analysis were made from the original material and subsequent separates; the peak height ratios of these are given in Table 4.2.

Although both first and second order separates show an increase in chlorite content when compared to their starting material, this increase is not comparable with that shown by Rezk [219], who produced a 1.4nm/1.0nm peak height ratio of 15.0 in even his most concentrated suspension after only one separation, whereas in this study the ratio was only increased to 0.87, and to 1.74 after two separations.

On the other hand, if the results are compared with the peak intensity ratios given by Dominik and Siwiec [76] (Table 4.3), it can be seen that for five out of their six sets of peak intensity data, the degree of separation achieved in this study is similar or higher. The material investigated was a shale, as here, but the 2-120μm fraction was employed, coupled with a field of 1.15T and either ferromagnetic balls or grooved plates in the separating zone.

Although the fact that the suspension was twice as concentrated as that employed by Rezk almost certainly had a part to play, due to interactions between particles during separation, it was felt that a lower current might reduce the percentage of nonmagnetic material retained with the chlorite. Thus, both third and fourth order separations were carried out at 1A, although otherwise the procedure was as for the second order separation.

This reduction of current appeared to be effective in the third order separation, in that the improvement in chlorite concentration was greater between the second and third order separates than between the first and second order. However, a reduction in chlorite concentration was observed between the third and fourth order magnetic fractions, and it was felt that this could be due to coarser particles being

| Material | Peak Height Ratios | | | | |
|---|---|---|---|---|---|
| | Chlorite 0.70nm/ Chlorite 1.4nm | Chlorite 1.4nm/ Mica 1.0nm | Mica 1.0nm/ Chlorite 0.70nm | Quartz 0.43nm/ Chlorite 0.70nm | Mica + Quartz 0.33nm/ Chlorite 0.70nm |
| Original Suspension | 4.98 | 0.21 | 0.97 | 0.70 | 3.33 |
| 1st Order Magnetic | 3.90 | 0.87 | 0.30 | 0.12 | 0.64 |
| 2nd Order Magnetic | 4.06 | 1.74 | 0.14 | 0.07 | 0.32 |
| 3rd Order Magnetic | 3.54 | 4.10 | 0.07 | 0.02 | 0.17 |
| 4th Order Magnetic | 3.38 | 3.93 | 0.08 | 0.04 | 0.19 |
| 4th Order Magnetic >10μm | 3.84 | 1.77 | 0.15 | 0.06 | 0.31 |
| 5th Order Magnetic | 3.34 | 4.97 | 0.06 | 0.03 | 0.11 |
| 6th Order Magnetic Not Retained at 0.5A | 3.40 | 3.81 | 0.08 | 0.03 | 0.13 |
| 6th Order Magnetic Retained at 0.5A | 3.27 | 4.61 | 0.07 | 0.03 | 0.13 |
| 7th Order Magnetic | 3.15 | 4.95 | 0.06 | 0.03 | 0.12 |
| 9th Order Magnetic | 3.39 | 3.14 | 0.09 | 0.05 | 0.28 |

Table 4.2 Peak Height Ratios of Glass Slide Specimens Prepared at Different Stages of Magnetic Separation

multimineralic, and thus carrying illite and quartz into the magnetic fraction along with the chlorite.

Table 4.3 Magnetic Separation Data of Dominik and Siwiec [76]

| Separation Order | Peak Intensity Ratios | | |
|---|---|---|---|
| | Mica 1.0nm / Chlorite 0.70nm | Quartz 0.43nm / Chlorite 0.70nm | Mica + Quartz 0.33nm / Chlorite 0.70nm |
| System Including Grooved Plates | | | |
| Original | 0.57 | 0.21 | 1.28 |
| 1st | 0.20 | 0.04 | 0.31 |
| 2nd | 0.05 | 0.02 | 0.16 |
| System Including Balls | | | |
| Original | 0.94 | 0.29 | 1.77 |
| 1st | 0.37 | 0.13 | 0.86 |
| 2nd | 0.22 | 0.11 | 0.55 |
| 3rd | - | 0.08 | - |

The yield of fourth order magnetic separate was 80.9mg $g^{-1}$ of crushed rock, but before further separation this was split at 10μm by sedimentation, to investigate whether the coarser material had higher concentrations of illite and quartz. This was shown to be the case (Table 4.2), and thus the fifth order separation was carried out on the finer than 10μm material from the fourth order separate. The fifth order separation employed the same conditions as the fourth order, except that each run was extended to one hour, and resulted in a magnetic fraction with a higher chlorite concentration than any previous separate.

The sixth order separation used the same conditions, but only one run was carried out. At the end of the run, after washing, the current was lowered from 1 to 0.5A, and the material falling away was collected. Further washing was carried out with the current at 0.5A, and then the current was turned off and a second magnetic fraction collected, to see whether the material retained at the lower current had a higher chlorite content. Although this material showed a slightly better chlorite concentration, neither fraction showed an improvement over the

fifth order separate, and thus they were bulked together for the seventh order separation. For this two runs were carried out at 0.5A, to investigate whether some of the material that should have been retained on the magnet at 0.5A after the sixth order separation was pulled off by the material falling away.

The seventh order separate showed no improvement in chlorite concentration over the fifth order, and thus it was considered that further reduction in particle size would be necessary for better separation. The finer than 2μm material was separated by centrifugation, which gave rise to a very dilute suspension, and thus this was run through the separator operating in single pass mode at full current to concentrate it. This material was then run at 1A using a recirculating system. As well as giving a poor yield, the chlorite content of this ninth order separate was lower than from any order since the second, and thus it was decided that separation of the appropriate size fraction should take place before magnetic separation.

### 4.2.1 Separation from Finer than 2μm Starting Material

40g of Tema milled unweathered rock were suspended in 800cm³ distilled water and ultrasonically dispersed for 10 minutes, before being centrifuged to separate the finer than 2μm material. Additional water was added to fill the centrifuge bottles to the correct depth, and thus about 1.25l of finer than 2μm suspension was produced. 600cm³ were passed through the separator at full current for 30 minutes, using a recycling system. XRD analysis of magnetic and nonmagnetic fractions was carried out for this and subsequent separations, and the peak height ratios are given in Table 4.4. It was hoped that the time required for the separation of a given proportion of the original chlorite could be quantified, and thus semiquantitative estimates of the mineralogy of the original material and the separates were made.

The original semiquantitative estimate, on which all separation times were based, expressed the peak height of each mineral as a percentage of the summed heights of the chlorite 12.6°, mica 8.8°, quartz 26.7° and feldspar 27.5°2$\theta$ peaks. This was likely to introduce error, because the 26.7°2$\theta$ peak results from both quartz and illite, and thus recalculation was made excluding the feldspar peak and using the 20.8°2$\theta$ peak for quartz. Before being summed, the peak heights were divided by the reference intensity ratios determined for use in quantitative mineralogical analysis (see Section 6.4.2), to account for

| Material | Peak Height Ratios | | | | |
|---|---|---|---|---|---|
| | Chlorite 0.70nm/ Chlorite 1.4nm | Chlorite 1.4nm/ Mica 1.0nm | Mica 1.0nm / Chlorite 0.70nm | Quartz 0.43nm / Chlorite 0.70nm | Mica + Quartz 0.33nm/ Chlorite 0.70nm |
| Original <2μm Suspension | 2.67 | 0.44 | 0.84 | 0.19 | 0.87 |
| 349N | 2.68 | 0.32 | 1.17 | 0.16 | 0.75 |
| 349M | 3.36 | 1.55 | 0.19 | 0.06 | 0.29 |
| 349N, 349N | 1.30 | 0.10 | 7.73 | 0.54 | 3.38 |
| 349N, 349M | 2.51 | 0.48 | 0.83 | 0.10 | 0.55 |
| 30N | 2.40 | 0.29 | 1.44 | 0.15 | 0.88 |
| 30M | 3.88 | 0.91 | 0.28 | 0.13 | 0.70 |
| 30N, 349N | 2.18 | 0.12 | 3.85 | 0.44 | 1.98 |
| 30N, 349M | 3.62 | 1.05 | 0.26 | 0.07 | 0.38 |
| 30N, 349N, 349N | 1.89 | 0.14 | 3.87 | 0.34 | 2.00 |
| 30N, 349N, 349M | 2.38 | 0.28 | 1.51 | 0.23 | 1.26 |
| (30N,349M+30M),349N | 2.26 | 0.56 | 0.79 | 0.11 | 0.48 |
| (30N,349M+30M),349M | 3.16 | 1.25 | 0.25 | 0.16 | 0.83 |
| (30N,349M+30M),349N,349N | 1.99 | 0.53 | 0.95 | 0.09 | 0.50 |
| (30N,349M+30M),349N,349M | 3.29 | 0.77 | 0.40 | 0.21 | 0.94 |
| (30N,349M+30M),349N,349N,349N | 2.30 | 0.65 | 0.67 | 0.14 | 0.68 |
| (30N,349M+30M),349N,349N,349M | 3.38 | 0.67 | 0.44 | 0.16 | 0.65 |

TABLE 4.4 Peak Height Ratios of Glass Slide Specimens Prepared to Assess the Number of First Order Separations Required The separations were carried out in the order given, 'N' indicating a nonmagnetic fraction and 'M' magnetic fraction, and are preceded by the number of minutes for which separation was carried out.

the different diffracting abilities. It is these recalculated values that are given in Figure 4.1.

If X is the proportion of chlorite present in the original suspension that remains in the reservoir beaker after t minutes separation, then:

$$\frac{dX}{dt} = \frac{-fX}{V}, \quad \text{where:}$$

V = volume of suspension in the system ($cm^3$), and
f = flow rate through the separator ($cm^3 min^{-1}$).

This equation assumes perfect mixing in the reservoir, and 100% removal of the chlorite as it passes through the magnetic field. After substituting for V and f, and knowing that X = 1 when t = 0, integration gives:

$$\ln X = -0.017t,$$

suggesting that after 30 minutes separation only 60.0% of the original chlorite should be remaining in suspension. In fact, if the values given in Figure 4.1 for the chlorite contents of the original material and the nonmagnetic fraction after 30 minutes separation are compared, it will be found that 78.1% of the chlorite remains in suspension. This indicates that separation is not perfect, and a factor P, the proportion of chlorite not retained as it passes through the field, must be introduced, to give:

$$\frac{dX}{dt} = \frac{(P-1)fX}{V}.$$

From the calculated chlorite contents, P can be determined as 0.52, giving:

$$\ln X = -0.0082t.$$

It was considered reasonable to remove 90% of the chlorite present in the suspension, and thus X was set at 0.1, giving a value for t of 280 minutes. However, because a different method of estimating the chlorite content was originally used, and because an incorrect value was used for the flow rate, it was believed that a minimum time of 349

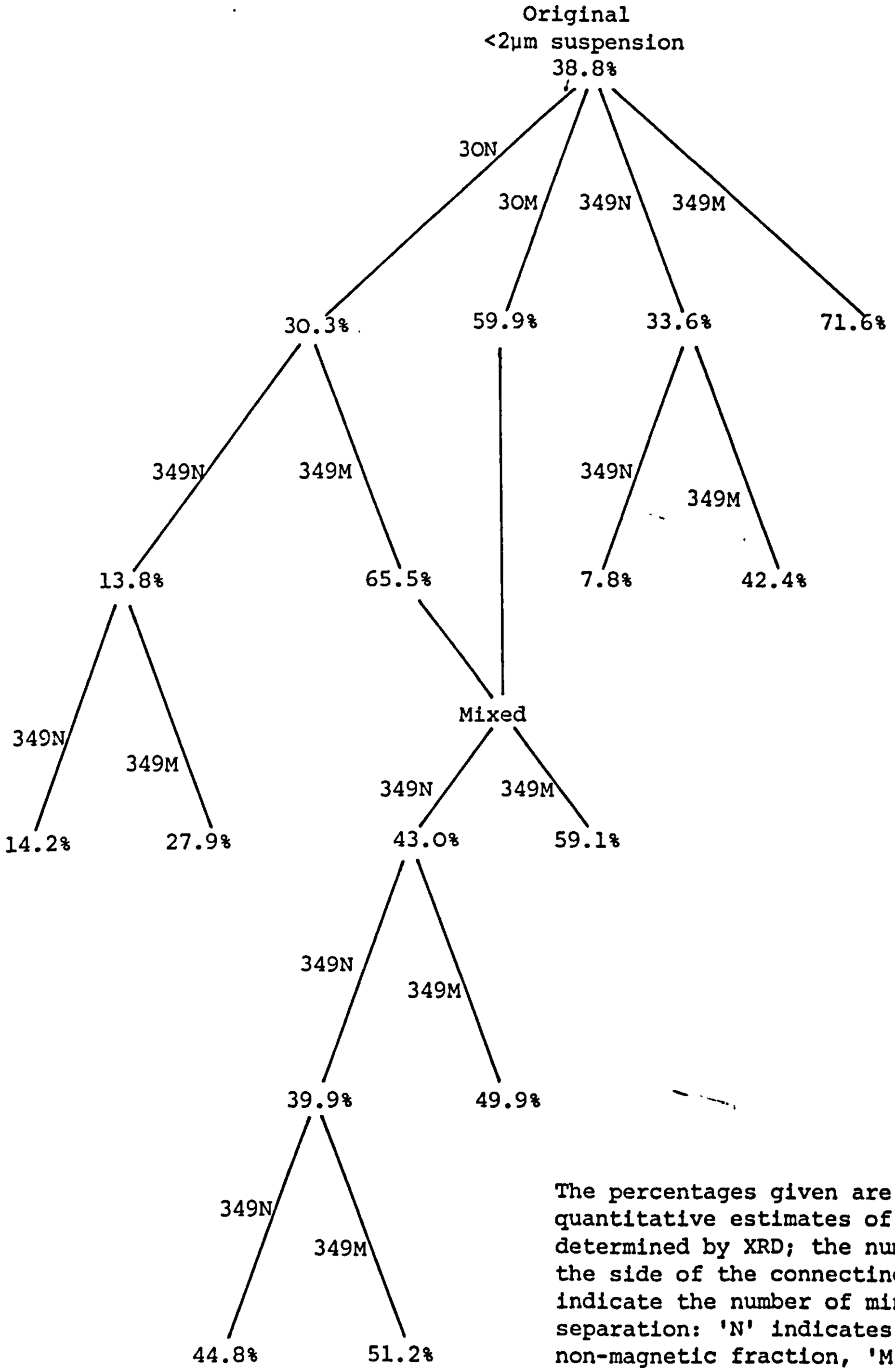


The percentages given are semi-quantitative estimates of chlorite, determined by XRD; the numbers at the side of the connecting lines indicate the number of minutes separation: 'N' indicates the non-magnetic fraction, 'M' the magnetic fraction. 349 minute separations were carried out at 1A, 30 minute separations at maximum current.

Figure 4.1 Chlorite Contents of Magnetically Separated Specimens

minutes would be required, and this was the minimum time employed, although some separations continued overnight.

The initial test of the predicted 349 minutes for 90% separation was carried out on the nonmagnetic fraction derived from the initial suspension after 30 minutes separation, and resulted in 45.5% of the chlorite originally present remaining in the nonmagnetic fraction, rather than the predicted 10%. The reasons for this lower efficiency are likely to include the fact that separation was carried out at 1A, rather than at the full current with which the equation was derived, the saturation of the stainless steel with chlorite, preventing additional grains being held and, possibly, the blocking effect of nonmagnetic components of polymineralic grains held in the field.

A second trial of the effectiveness of 349 minutes separation at 1A was carried out on the original finer than 2μm suspension. This showed 86.8% of the chlorite remaining in the nonmagnetic fraction, but a much higher chlorite content in the magnetic fraction than when 30 minutes separation at maximum current was employed (Figure 4.1). The nonmagnetic material after this 349 minute separation was again passed through the separator for 349 minutes at the same current, because of its relatively high chlorite content. After this second 349 minute period, only 23.2% of the chlorite present at the start was left in the nonmagnetic fraction, a figure much closer to the theoretical 10% than was found for any other separation indicated in Figure 4.1. This suggested that either saturation or blocking of the stainless steel was taking place in the first 349 minute separation. Further 349 minute periods of separation were carried out on different fractions, to see how profitable continued separation of originally nonmagnetic material would be. A tree of separation times used and the chlorite contents resulting is given in Figure 4.1, which shows that the semiquantitative estimates of chlorite content cannot be totally relied upon, as in some instances both magnetic and nonmagnetic fractions have chlorite contents either higher or lower than the material at the start.

The very low chlorite content of the nonmagnetic fraction after two 349 minute periods of separation suggested that the most efficient way of removing chlorite from the suspension would be to carry out two 349 minute periods of separation and bulk the two magnetic fractions before further separation. This would retain 95.6% of the chlorite, whilst increasing its abundance from 38.8 to 47.5%.

Second order separation was carried out at maximum current, when it was essential not to run the separator for more than two hours, due to overheating of the coils and consequent reduction of current and magnetic field. The equation used at the time suggested that 90% separation of 206cm³ could be achieved in two hours, but batches of 200cm³ were separated for 117 minutes, to ease measurement of the suspension. 93 minutes ought to have been sufficient to carry out this separation, if the factor P had remained constant and the correct equation had been used.

Before second order separation, 10 minutes ultrasonic dispersion was employed, as on occasions the first order magnetic fraction was left standing for more than a week, and it was felt that at least partial flocculation might have occurred. Each 200cm³ was passed through the separator for two periods of 117 minutes, and the magnetic fractions were bulked. XRD analysis of this and subsequent magnetic and nonmagnetic fractions was carried out; peak height ratios are given in Table 4.5, and the calculated chlorite contents in Figure 4.2. The bulked second order magnetic material was again ultrasonically dispersed for 10 minutes before each 200cm³ was separated for two periods of 117 minutes. The fact that the first run produced a very large yield confirmed the need for a second run, and again the two magnetic fractions were bulked.

### 4.2.2 Calgon Addition

Although the yield of third order magnetic material was high, the relative XRD peak heights and calculated composition indicate that the chlorite content has been slightly reduced. This is unlikely to be due to polymineralic grains, due to the grain size, but could be due either to the concentration of the suspension, which increases with separation order, or to flocculation causing mica to clump together with the chlorite, and thus to be held in the field. Other workers have found flocculation to be a problem when the illite:chlorite ratio drops below 0.15, with third order separates being almost entirely flocculated, and it was suggested that flocculation is caused by strongly negatively charged illite adhering to positively charged areas on the overall weakly negatively charged chlorite [24]. In this study, the illite: chlorite ratio of the second order magnetic fraction is 0.36, but flocculation seems the most likely mechanism to bring about a reduction in the chlorite content of the third order separate. Other workers have found that adding Calgon (sodium hexametaphosphate) to bring its

| Material | Peak Height Ratios | | | | |
|---|---|---|---|---|---|
| | Chlorite 0.70nm/ Chlorite 1.4nm | Chlorite 1.4nm/ Mica 1.0nm | Mica 1.0nm/ Chlorite 0.70nm | Quartz 0.43nm/ Chlorite 0.70nm | Mica+Quartz 0.33nm/ Chlorite 0.70nm |
| 2nd Order Nonmagnetic | 1.96 | 0.75 | 0.68 | 0.09 | 0.34 |
| 2nd Order Magnetic | 3.13 | 1.23 | 0.26 | 0.14 | 0.71 |
| 3rd Order Magnetic | 2.93 | 1.04 | 0.33 | 0.15 | 0.98 |
| 4th Order Nonmagnetic | 2.34 | 0.58 | 0.74 | 0.11 | 0.52 |
| 4th Order Magnetic | 3.64 | 1.30 | 0.21 | 0.06 | 0.36 |
| 5th Order Nonmagnetic | 2.22 | 0.59 | 0.76 | 0.10 | 0.52 |
| 5th Order Magnetic | 3.86 | 2.02 | 0.13 | 0.04 | 0.22 |
| 6th Order Nonmagnetic | 2.21 | 0.65 | 0.69 | 0.04 | 0.27 |
| 6th Order Magnetic | 3.35 | 3.32 | 0.09 | 0.02 | 0.07 |
| 7th Order Nonmagnetic | 2.92 | 1.76 | 0.19 | 0.02 | 0.11 |
| 7th Order Magnetic | 3.02 | 3.16 | 0.10 | 0.00 | 0.06 |
| 8th Order Magnetic | 3.04 | 4.09 | 0.08 | 0.00 | 0.06 |

TABLE 4.5 Peak Height Ratios of Glass Slide Specimens Prepared at Different Stages of Separation of Finer Than 2$\mu$m Material.

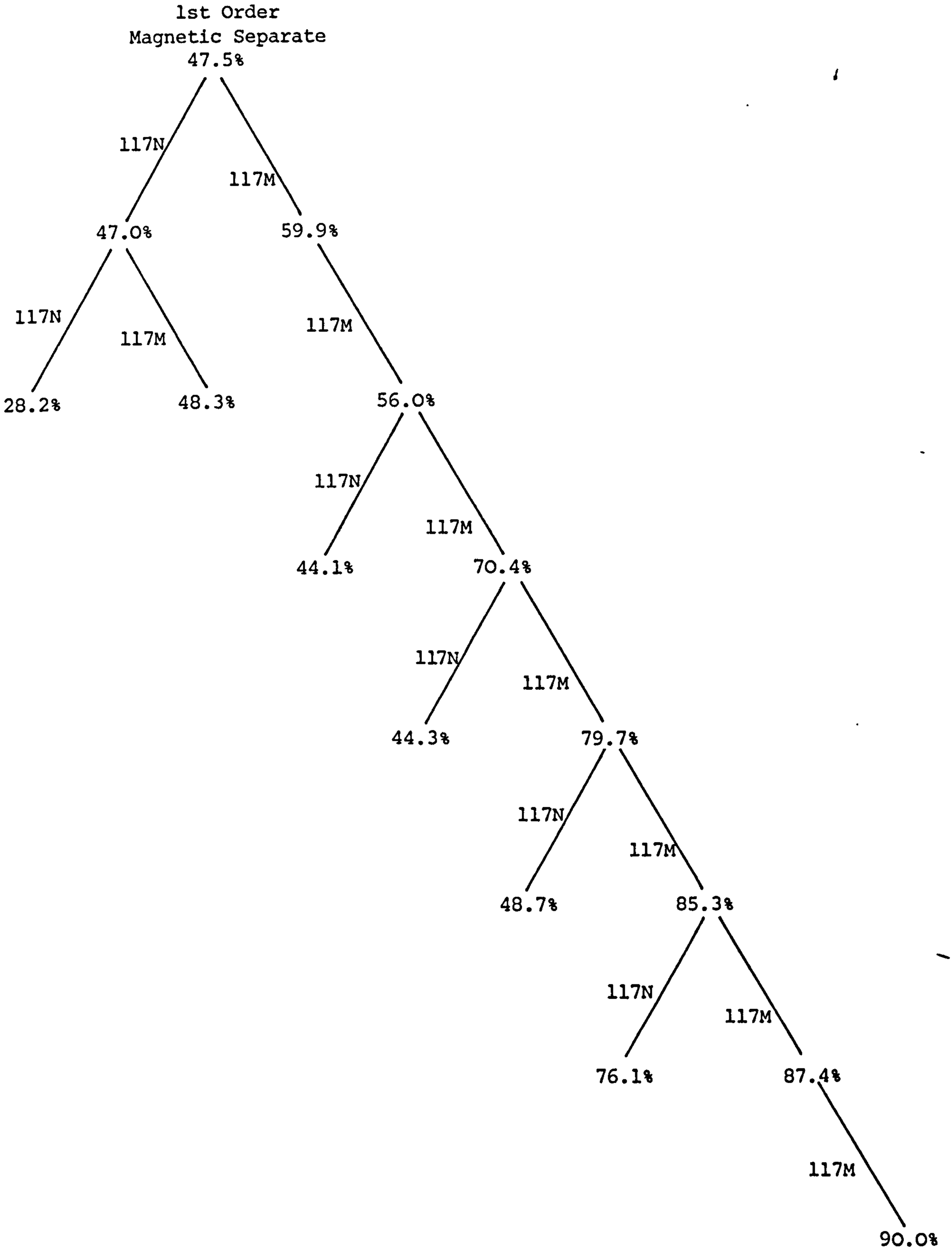


Figure 4.2 Chlorite Contents of Second and Subsequent Order Magnetically Separated Specimens

Key as for Figure 4.1. All separations carried out at maximum current.

concentration to 5 x $10^{-4}$M would reduce the flocculation of the third order separate to less than 25%, but even a concentration of 4 x $10^{-3}$M had no effect on their flocculated fourth order separate [24]. Thus, to test the effectiveness of Calgon, sufficient was added to 50cm³ of third order separate to bring its concentration to 2 x $10^{-3}$M when the suspension was diluted to 200cm³. Ultrasonic dispersion followed by two runs of 117 minutes at 1A were employed, and thorough washing of the magnetic fraction was carried out to ensure the Calgon was removed. As can be seen from Figure 4.2, this procedure resulted in a considerable increase in the chlorite concentration between the third and fourth order separates, and thus Calgon was added to all subsequent magnetic fractions before further separation. A comparison of the yields and purities of magnetic fractions obtained with and without Calgon is made in Section 4.3. Fifth to eighth order separations were carried out in the same way as the fourth order, except that 100cm³ of the previous separate was employed in making up the suspension. Also, because the suspension in the reservoir appeared to be very dilute after only one run, a second pass was not employed.

If the calculated analyses of the separates from the uncentrifuged suspensions, for which peak height ratios are given in Table 4.2, are compared with those from finer than 2μm suspensions (Figure 4.2), it is seen that none of the separates from the bulk material reach the 90.0% chlorite content of the eighth order magnetic fraction from the finer than 2μm suspension. Also, the separates from the bulk material continue to retain quartz up to the ninth order, whereas quartz is totally eliminated from the seventh and eighth order separates from the finer than 2μm material. For these reasons, effort was concentrated on separating finer than 2μm suspensions, but, because of the efficiency of Calgon in increasing the chlorite content of the separates (Figure 4.2), trials were carried out with Calgon additions to the lower order runs.

The finer than 2μm suspension was prepared as above, except that it was made up in 4 x $10^{-3}$M Calgon solution, and ultrasonic dispersion was carried out for 30 minutes. The separation procedure was to take 600cm³ of finer than 2μm suspension, and run it at 1A for 349 minutes, to obtain a first order separate. An XRD analysis was not made, but the material separated in the same way from the suspension not treated with Calgon had a chlorite content of 71.6% (Figure 4.1). The nonmagnetic material was discarded. For this and subsequent

separations, a powerful electric fan was attached to the top of the separator coils, preventing overheating by blowing air around the coils and through the gap between the pole pieces.

As a considerable amount of the first order separate with a chlorite content of 47.5% was available (Figure 4.2), this was used in the same way as the freshly prepared separate. The peak height ratios and chlorite contents in Table 4.6 refer to specimens derived at least partly from this less pure starting material, and separation of the higher purity material is likely to have produced specimens at the same separation order with higher chlorite contents. To 100cm$^3$ of the first order magnetic material sufficient Calgon was added to bring its concentration to 2 x $10^{-3}$M when the suspension was diluted to 200cm$^3$. This suspension was ultrasonically dispersed, then run for 117 minutes at full current. Again the nonmagnetic fraction was discarded. The second order separate was treated identically, except that it was passed twice through the system, the magnetic extracts being bulked to give a third order magnetic fraction. All subsequent orders were carried out in the same way, except that the current was held at 1A. At every stage the nonmagnetic material was discarded. Peak height ratios and chlorite contents are given in Table 4.6, and if these are compared with the chlorite contents when Calgon was not added to the lower separation orders (Figure 4.2), it can be seen that at every stage the chlorite content is higher when Calgon is added.

Although the calculated chlorite contents of the ninth, 10th and 11th order separates were considered to be acceptable as the nearest attainable to pure chlorite by the magnetic separation methods employed, other results suggested that more chlorite could be extracted per gram of unweathered rock if a lower concentration suspension was used [219]. Thus, a final modification to the system was made so that only 20g of Tema milled rock was dispersed to produce 800cm$^3$ of suspension, which was made at a Calgon concentration of 2 x $10^{-3}$M. This suspension was then treated identically to the methods described above, except that the first order nonmagnetic fraction was passed through the separator for two runs of 349 minutes at 1A, to see whether further runs were worthwhile for a more dilute suspension. As Table 4.7 shows, the calculated chlorite contents of the magnetic extracts from initially nonmagnetic material were lower than the 38.8% chlorite of the starting suspension, and thus the first order nonmagnetic material was subsequently discarded. During the initial 349 minute

| Material | Peak Height Ratios | | | | | Calculated Chlorite Content (%) |
|---|---|---|---|---|---|---|
| | Chlorite 0.70nm/ Chlorite 1.4 nm | Chlorite 1.4nm/ Mica 1.0nm | Mica 1.0nm/ Chlorite 0.70nm | Quartz 0.43nm/ Chlorite 0.70nm | Mica+Quartz 0.33nm/ Chlorite 0.70nm | |
| 2nd Order Magnetic | 3.02 | 1.18 | 0.28 | 0.10 | 0.52 | 62.3 |
| 3rd Order Magnetic | 2.98 | 1.83 | 0.18 | 0.07 | 0.24 | 71.7 |
| 4th Order Magnetic | 2.75 | 3.93 | 0.09 | 0.03 | 0.10 | 83.4 |
| 5th Order Magnetic | 3.32 | 4.64 | 0.06 | 0.00 | 0.04 | 91.8 |
| 6th Order Magnetic | 3.04 | 5.64 | 0.06 | 0.00 | 0.04 | 92.5 |
| 7th Order Magnetic | 3.18 | 6.23 | 0.05 | 0.00 | 0.03 | 93.5 |
| 8th Order Magnetic | 3.12 | 7.29 | 0.04 | 0.01 | 0.03 | 91.5 |
| 9th Order Magnetic | 2.86 | 9.56 | 0.04 | 0.00 | 0.02 | 95.2 |
| 10th Order Magnetic | 3.29 | 13.63 | 0.02 | 0.00 | 0.00 | 97.0 |
| 11th Order Magnetic | 2.80 | 12.93 | 0.03 | 0.00 | 0.02 | 96.3 |

TABLE 4.6 Peak Height Ratios and Calculated Chlorite Contents of Glass Slide Specimens Obtained with Calgon Addition to Low Order Separations

| Material | Peak Height Ratios | | | | | Calculated Chlorite Content (%) |
|---|---|---|---|---|---|---|
| | Chlorite 0.70nm/ Chlorite 1.4nm | Chlorite 1.4nm/ Mica 1.0nm | Mica 1.0nm/ Chlorite 0.70nm | Quartz 0.43nm/ Chlorite 0.70nm | Mica+Quartz 0.33nm/ Chlorite 0.70nm | |
| 1st Order Magnetic | 2.11 | 1.66 | 0.29 | 0.00 | 0.14 | 71.8 |
| 349N, 349M | 2.37 | 0.25 | 1.72 | 0.00 | 0.67 | 29.6 |
| 349N,349N,394M | 1.69 | 0.16 | 3.73 | 0.00 | 1.57 | 16.3 |
| 2nd Order Magnetic | 2.36 | 0.91 | 0.47 | 0.00 | 0.15 | 60.8 |
| 3rd Order Magnetic | 2.60 | 1.09 | 0.35 | 0.00 | 0.16 | 67.2 |
| 4th Order Magnetic | 2.99 | 1.81 | 0.19 | 0.00 | 0.10 | 79.6 |
| 5th Order Magnetic | 3.03 | 2.55 | 0.13 | 0.00 | 0.08 | 84.8 |
| 6th Order Magnetic | 3.10 | 4.15 | 0.08 | 0.01 | 0.05 | 89.2 |
| 7th Order Magnetic | 2.99 | 6.23 | 0.06 | 0.00 | 0.05 | 93.1 |
| 8th Order Magnetic | 3.15 | 9.65 | 0.04 | 0.00 | 0.04 | 95.7 |
| 9th Order Magnetic | 2.88 | 11.13 | 0.03 | 0.00 | 0.03 | 95.9 |
| 10th Order Magnetic+ | 4.97 | 7.00 | 0.03 | 0.00 | 0.04 | 96.2 |

TABLE 4.7 Peak Height Ratios and Calculated Chlorite Contents of Glass Slide Specimens Obtained from Diluted Original Finer Than 2$\mu$m Suspensions Key as for Table 4.4. + = Random powder specimen

separation, the suspension in the reservoir beaker was found to be at a temperature of 26°C, and to have a pH of 6.4 ± 0.05, much lower than the value of 8.0 found for a stirred 4% suspension of unseparated Tema milled unweathered rock.

A comparison of the calculated chlorite contents in Tables 4.6 and 4.7 indicates an overall similar level of chlorite at the same level of extraction, except for the first order extract from the dilute suspension, which gives an anomalously high calculated chlorite content for which no explanation can be given. All subsequent separation was carried out with the more dilute suspension, and analytical results from the chlorite extracted are given in Sections 5.2, 5.3.1 to 5.3.3, 5.3.5 and 5.4.

Considering the chlorite 0.70nm/1.4nm peak height ratios given in Tables 4.2 and 4.4 to 4.7, there is no consistent trend with order of separation. However, where the ratio is given for both magnetic and nonmagnetic fractions from the same separation, in every case the magnetic fraction has a higher value of peak height 0.70nm/peak height 1.4nm, which is equivalent to $I_{002}/I_{001}$. For chlorites, this and other (001) peak intensity ratios, or structure factors calculated from them, can be used to calculate the Fe content, which increases with increasing $I_{002}/I_{001}$. Thus, in every stage of separation for which data are available, the chlorite retained in the magnetic fraction has a higher Fe content than that which passes through the separator.

Rezk [219] does not calculate peak height ratios for nonmagnetic fractions, but if the peak height ratio data in Table 4.9 are examined, it can be seen that for the data from Rezk's Appendix 4.b.4.1, and for both 1040 separations carried out with mesh, the peak height ratio of the magnetic fractions consistently decreases in consecutive runs, showing that the chlorite with the highest Fe content is first extracted, and less Fe rich chlorite is only extracted on subsequent extractions from the same starting material. There is general agreement with this pattern for the peak height ratios from the 1029 separation, but no consistent pattern for the 1040 separation without mesh or Calgon. Table 4.9 indicates a peak height ratio for Rezk's material approximately double that of the Plynlimon chlorites, which would suggest it has a higher Fe content, but this is not confirmed by the analyses in Sections 5.1 and 5.2.

## 4.3 A CRITIQUE OF THE MAGNETIC SEPARATION DATA OF REZK

As seen in the previous section, at least eight passes through the separating system had to be used to produce chlorite of more than 95% purity, and three further passes did not increase the purity beyond 97%. This difficulty in separation and inability to obtain 100% pure chlorite was surprising, as Rezk had claimed yields of up to 132.2mg of 100% pure chlorite from each gram of starting material after only one pass [219, Appendix 4.b.1]. In fact higher yields of higher purity chlorite than found by Rezk would have been expected, because of the higher Fe content, and thus higher magnetic susceptibility, of the chlorite in this study (see Sections 5.1 and 5.2).

Because the separation procedures were not the same as those used by Rezk, it was felt worthwhile to replicate his procedures as closely as possible to see whether his yields could be reproduced using the material from Plynlimon. It was possible that using a crushed rock as starting material might have led to polymineralic grains, and thus less efficient separation, even in the finer than 2μm fraction, and thus separation was also carried out on the finer than 2μm fraction of the boulder clay 1029, for which the naturally generated particle size distribution would have approximated much more closely to those of Rezk's materials than that of an artificially crushed rock.

To investigate the effects of ferritic stainless steel mesh and Calgon, neither of which were employed by Rezk, three sets of separations based on the crushed rock 1040 were used. The first set used neither mesh nor Calgon; the second set used mesh but not Calgon, and the third set used both Calgon, at a concentration of $1.4 \times 10^{-3}$M, and mesh. The separations of the boulder clay, 1029, employed both Calgon and mesh.

It was assumed that Rezk's optimum experimental procedure for separation in aqueous suspension [219, Sections 3.4.3.6 and 3.4.5.1] was followed where no other details were given, and these conditions were replicated, with the following modifications:

1. A cooling fan was installed on top of the coils, which restricted the maximum temperature of the suspension to 27.5°C, rather than the 34.1°C found by Rezk. After the requisite 30 minute ultrasonic dispersion, the suspension temperature was between 38 and 44°C, and thus all suspensions were cooled to 23°C before separation. From this temperature 27.5°C could be reached in 90

minutes, but although the temperature of the coils was measured at 33.5°C during separation, the suspension temperature never exceeded 27.5°C.

2. The suspension was continuously recirculated through the field, rather than operating a single pass system. Recirculation would not have been possible for Rezk without increasing unacceptably the temperature of the suspension. Rezk used a flow rate of $9cm^3min^{-1}$ and 90 minute runs, indicating that 810cm³ would pass through the separator per run. In replicating the experiments, a flow rate of $10.2cm^3min^{-1}$ was employed (the nearest to Rezk's rate possible with the equipment available), and the volume of suspension was calculated so that 90% of the suspension would pass through the coils in 90 minutes. This calculation suggested that 352cm³ of suspension should be used, and this volume was employed, but, because at the time of calculation the flow rate was believed to be $9cm^3min^{-1}$, 92.6% of the suspension passed through the coils. The calculated yield is adjusted to allow for the 7.4% of starting material that does not pass between the coils.

Table 4.8 compares the yields, in absolute terms and per gram of starting material, for the data of Rezk's Appendix 4.b.4.1 with the four replicate separations carried out with material from Plynlimon, and Table 4.9 compares the purity of the separates. From Table 4.8 it can be seen that the yield is reduced as the number of separations from the suspension increases. This is as expected, as magnetic material is removed with each separation, leaving a lower concentration for further separation to act upon. Secondly, the table shows that the use of steel mesh increases the yield 4.05 times, and a combination of mesh and Calgon increases the yield 4.64 times. As the starting suspensions for the separations of 1040 without Calgon were identical, these results suggest that the field alone is incapable of holding 250mg of magnetic material, and that it is only the mesh that enables such yields to be held. The high yields found by Rezk do, however, apparently contradict this conclusion. The action of Calgon in increasing the yields more than with the mesh alone is best explained by reference to both the yield (Table 4.8) and purity (Table 4.9).

With Calgon addition the yield is increased, but purity is reduced. Calgon acts as a deflocculant, and thus, if it deflocculated the suspension totally, the purity of the magnetic fraction would be

| Run | Yield (mg $g^{-1}$) | | | | | Absolute Yield (mg) | | | | |
|---|---|---|---|---|---|---|---|---|---|---|
| | Rezk 4.b.4.1. | 1040 No wire, no Calgon | 1040 Wire, no Calgon | 1040 Wire and Calgon | 1029 Wire and Calgon | Rezk 4.b.4.1 | 1040 No wire, no Calgon | 1040 Wire, no Calgon | 1040 Wire and Calgon | 1029 Wire and Calgon |
| 1 | 32.7 | 14.6 | 84.5 | 104.0 | 58.8 | 264.9 | 47.6 | 275.5 | 339.1 | 191.7 |
| 2 | 28.9 | 12.5 | 50.8 | 57.1 | 30.8 | 234.1 | 40.8 | 165.7 | 186.2 | 100.4 |
| 3 | 18.1 | 9.4 | 30.9 | 35.4 | 23.9 | 146.6 | 30.6 | 100.8 | 115.4 | 77.9 |
| 4 | 12.0 | 8.2 | 25.6 | 25.5 | 16.7 | 97.2 | 26.7 | 83.5 | 83.2 | 54.5 |
| 5 | 9.8 | 7.2 | 18.5 | 18.7 | 15.6 | 79.4 | 23.5 | 60.3 | 61.0 | 50.9 |
| Total | 101.5 | 51.9 | 210.3 | 240.7 | 145.8 | 822.2 | 169.2 | 685.8 | 784.9 | 475.4 |

TABLE 4.8 Yields of Magnetic Fractions Under Different Separation Conditions

| Run | Calculated Chlorite Content (%) | | | | | Peak Height Ratio $\frac{\text{Chlorite 0.70nm}}{\text{Chlorite 1.4nm}}$ | | | | |
|---|---|---|---|---|---|---|---|---|---|---|
| | Rezk 4.b.4.1 | 1040 No wire, no Calgon | 1040 Wire, no Calgon | 1040 Wire and Calgon | 1029 Wire and Calgon | Rezk 4.b.4.1 | 1040 No wire, no Calgon | 1040 Wire no Calgon | 1040 Wire and Calgon | 1029 Wire and Calgon |
| 1 | 100.0 | 84.6 | 72.6 | 65.3 | 85.7 | 5.70 | 2.15 | 3.09 | 2.73 | 2.90 |
| 2 | 100.0 | 84.2 | 49.1 | 37.9 | 69.7 | 5.00 | 2.05 | 2.40 | 2.47 | 2.42 |
| 3 | 100.0 | 73.8 | 33.6 | 31.7 | 51.6 | 5.00 | 2.02 | 2.12 | 2.36 | 2.41 |
| 4 | 100.0 | 69.0 | 20.0 | 23.7 | 43.7 | 4.86 | 2.30 | 2.03 | 1.84 | 1.79 |
| 5 | 100.0 | 65.8 | 15.6 | 19.9 | 27.1 | 4.71 | 2.32 | 1.62 | 1.82 | 2.03 |
| Mean | 100.0 | 77.5 | 49.8 | 45.9 | 65.6 | 5.18 | 2.15 | 2.52 | 2.45 | 2.50 |

TABLE 4.9 Peak Height Ratios and Calculated Chlorite Contents of Fractions Obtained Under Different Separation Conditions

expected to be increased, as the only nonmagnetic grains that would be retained would be those physically trapped between magnetic grains, or onto the mesh. Without Calgon, the suspension is partially flocculated, forming clumps of chlorite and mica grains [24]. If the chlorite content of the clump is low, the clump is likely to pass through the field. However, if the chlorite content is higher, both the chlorite and mica in the floccule will be retained, because they are bound together by their flocculated state. As Calgon decreases the degree of flocculation, it can be postulated that the outer micaceous layers of the floccules will be released, effectively increasing the chlorite content of the clumps of grains. These smaller floccules are likely to have higher mica contents than the grains retained when the system was more fully flocculated, and yet will be retained by the field. This mechanism can thus explain both an increase in yield and a decrease in purity when Calgon is added.

Relative to the unweathered rock, the yield from the boulder clay is both smaller and of higher chlorite content. As the finer than 2μm fractions of the materials have almost identical chlorite contents, it is difficult to see how the yield can differ so widely unless the chlorite in 1029 is less magnetic, but the analytical data in Sections 5.3.2 and 5.3.3 are insufficient to draw such a conclusion. If this were the case, the larger chlorite containing floccules in 1029 might not be held in the separation zone, leading to only the smaller floccules with higher chlorite contents remaining in the magnetic fraction, reducing the yield, but increasing its purity.

As the yield in mg $g^{-1}$ increases, so does the difference in yield between first and fifth runs of the suspension. This is because a higher yield in the first run reduces the amount of magnetic material in suspension for the second and subsequent runs. An explanation has already been put forward for the reduction in purity observed on Calgon addition, but it can be seen from Table 4.9 that a reduction in purity also occurs with the introduction of the mesh. The reason for this is likely to be twofold. Firstly, the mesh will generate very steep magnetic gradients, which may be sufficient to retain some floccules containing low chlorite contents. Secondly, the mesh will act as a physical barrier to the passage of particles through the separating zone, leading to nonmagnetic material being retained, particularly when the yield is high, as then the pores in the mesh are often completely covered by adhering grains.

Perhaps the most important difference between Rezk's results and those from the Plynlimon materials is in the purity of the magnetic fractions. Rezk did not obtain a lower than 100% purity until after nine runs from the same suspension, whereas even on the first run of the Plynlimon materials, the highest calculated chlorite content was 85.7%. This is itself likely to be an overestimate, as the standards used for calculation were determined from random powder mounts, whereas the magnetic separates were measured as glass slide specimens, which preferentially increase the height of phyllosilicate peaks relative to those of quartz.

The only straightforward explanation for the retention of other minerals with chlorite in the magnetic fraction would be if these minerals were themselves magnetic, and also more magnetic than the equivalent minerals in Rezk's material. The major contaminant of the magnetic fractions is mica, and Rezk does not give analyses for the mica from his soils. However, it is unlikely to contain significantly less Fe than that from Plynlimon, as microprobe analyses of chlorite and mica in the unweathered rock show that, in atomic percent terms, the chlorite contains more than 25 times as much Fe than the mica, and thus would be expected to have at least 25 times the magnetic susceptibility (see Section 5.1). It is thus unlikely that a difference in susceptibility between Rezk's mica and that from Plynlimon leads to the former passing through the separator whilst the latter is retained. However, examination of Rezk's appendices concerned with magnetic separation leads to the conclusion that correct experimental details have not been supplied, or else that yields have been incorrectly measured or calculated, and thus it is possible that the 100% purity quoted for most of the magnetic fractions is not correct.

## 4.4 THE SEPARATION OF ILLITE

As well as separating chlorite from the unweathered rock, it was hoped that mica could be separated from quartz. The first attempt to separate these minerals was based on the fact that, because of its low Fe content, mica is likely to be more paramagnetic than quartz. The material with the least amount of chlorite produced by previous magnetic separations, a mixture of the specimens identified as 349N,349N and 30N,349N,349N in Table 4.4, respectively containing 7.8% and 14.2% chlorite, was used for further separation. 20g were resuspended in water, ultrasonically dispersed, and then centrifuged to

remove any particles that had agglomerated to become coarser than 2μm. 600cm³ of suspension were produced, and this was run eight times for 349 minutes, at 1A. After each run, the magnetic fraction was removed, and a specimen of the remaining material prepared as a glass slide for XRD analysis. After the first run, which showed a reduction in chlorite to 4.6%, no consistent changes in either chlorite content or mica:quartz ratio occurred, as can be seen from Table 4.10. These results suggest that a small proportion of the chlorite cannot be effectively removed from the mica by magnetic separation, possibly because mica and chlorite occur as physical intergrowths (see Section 5.1). However, this is relatively unimportant, as the chlorite content has been reduced to less than 5%. More important is that neither quartz nor mica is consistently concentrated into the nonmagnetic fraction, indicating that the susceptibility of the mica is not sufficient to enable it to be separated from quartz.

It is known that finer than 2μm clinochlore can be dissolved by 2M HCl at 60°C for 45 hours [224], and also that, the higher the Fe content of the chlorite, the more rapidly it is dissolved [225]. As, in atomic percent terms, the chlorite from Plynlimon rock samples contains from 4.6 to 7.0 times as much Fe as the clinochlore (see Section 5.1), it was felt that Plynlimon chlorite would be dissolved after 72 hours in 2M HCl at 60°C, a treatment which does not affect quartz or mica, except for altering the exchangeable cations. An experiment was thus carried out to see whether, after the dissolution of chlorite, the susceptibility of the mica could be increased by replacing its exchange cations by highly paramagnetic ones, so that it could then be separated from quartz.

Of the readily available cations, $Co^{2+}$ has the highest susceptibility, and thus experiments used this ion. The finer than 2μm fraction of the boulder clay 1029 was employed, with a composition of 74.8% mica, 19.5% chlorite and 5.7% quartz, and 0.5g aliquots were stirred continuously in 250cm³ 2M HCl at 60°C for 72 hours. The resulting suspension was centrifuged, and the sediment carefully washed, followed by saturation with 1M Mg. It was considered that simple saturation with Co might not totally replace the K, both because of the difficulty in cation exchange with transition metal ions [210], and because of the tenacity with which K is held by the mica structure [97,158,195,214]. Sodium tetraphenyl boron has been used to remove K from micas [158], as a precipitate of potassium tetraphenyl boron is formed in the presence of

| Passes of Nonmagnetic Material Through Separator | Calculated Mineralogy | | |
|---|---|---|---|
| | % Mica | % Chlorite | % Quartz |
| 1 | 81.7 | 4.6 | 13.7 |
| 3 | 71.1 | 3.5 | 25.4 |
| 4 | 78.8 | 4.1 | 17.1 |
| 5 | 71.3 | 3.5 | 25.2 |
| 6 | 72.0 | 4.4 | 23.6 |
| 7 | 73.2 | 0.0 | 26.8 |
| 8 | 75.3 | 5.3 | 19.4 |

Table 4.10 The Attempted Magnetic Separation of Mica from Quartz

K. However, sodium tetraphenyl boron is reactive, and if present in excess may destroy the phyllosilicate structure. Triethanolamine forms an insoluble complex with sodium tetraphenyl boron, and can be used to remove the excess, whilst allowing the preferential formation of potassium tetraphenyl boron with available K. Normally K removed from the mica structure is replaced by Na from the sodium tetraphenyl boron, but in this experiment the medium was made sufficiently concentrated in Co to ensure that Co would replace any K removed.

As the likely effects of the reagents on the phyllosilicate structure were not known, the 2g of acid treated material, with a composition expected to be 92.9% mica and 7.1% quartz, was divided into thirds, to which were added different reagents. To the first portion 80cm³ 1M Co and 20cm³ $H_2O$ were added. To the second portion, 80cm³ 1M Co, 10cm³ 0.1M sodium tetraphenyl boron dissolved in 0.1M acetic acid and 10cm³ $H_2O$ were added, and to the final portion 80cm³ 1M Co, 10cm³ 1M triethanolamine and 10cm³ 0.1M sodium tetraphenyl boron dissolved in 0.1M acetic acid. Reagents were added in the order given, and the mixtures were shaken in plastic bottles for 60 hours at room temperature. The suspensions were then centrifuged and the sediment washed with water, twice with acetone to remove any triethanolamine/ sodium tetraphenyl boron complex, and then twice more with water.

XRD analysis of the resulting specimens, mounted on glass slides, showed little difference between the Mg saturated material, the specimen shaken with Co alone, and that shaken with Co and sodium tetraphenyl boron. However, the specimen shaken with the mix including triethanolamine showed a severely degraded phyllosilicate structure, with the 1.0nm mica peak height being reduced by a factor of six, accompanied by considerable broadening of the peaks. This material was thus discarded, and magnetic separation of the fractions treated with Co alone, and with Co and sodium tetraphenyl boron, was carried out. XRD analysis of the magnetic fractions showed that, after treatment with Co alone, all traces of the quartz 20.8°2$\theta$ peak had been removed, but that the 26.7°2$\theta$ peak retained a broad tail in the up $\theta$ direction. No significant chlorite peak was seen. On the other hand, the magnetic fraction treated with both Co and sodium tetraphenyl boron showed different effects. A peak at 12.6°2$\theta$ was reintroduced, and slight evidence for a quartz peak at 20.8°2$\theta$ was present. However, the broad up $\theta$ tail to the 26.7°2$\theta$ peak had been completely removed, leaving a clean peak at 26.8°2$\theta$, and distinct peaks at 27.5 and 27.9°2$\theta$.

These results suggest that, even after a complex series of treatments, single stage magnetic separation could not provide a pure mica, and thus analysis of micas was confined to large grains in rock sections (see Section 5.1) and the fine fractions of some samples which XRD analysis indicated to be 100% mica (see Section 5.5). However, assuming that the 12.6°2$\theta$ peak on the XRD traces of the magnetic fraction treated with both Co and sodium tetraphenyl boron was due to chlorite not dissolved, and not to a phase formed by the action of sodium tetraphenyl boron on mica, it appears that this treatment, preceded by more severe acid treatment, and followed by more passes through the separator, might have yielded a very nearly pure mica.

## 4.5 CONCLUSIONS

As a result of the work in this chapter, the following conclusions can be drawn:

1. Magnetic separation can give chlorite of more than 95% purity, but to achieve this needs at least eight passes through the separator.

2. It is not possible to produce 100% pure chlorite with less than 12 passes, if at all.

3. Addition of Calgon to the suspension, and ferritic stainless steel mesh to the separation volume, both increase the yield of magnetic fraction, but decrease its purity.

4. The chlorite retained in the magnetic fraction has a higher Fe content than that which remains in the nonmagnetic fraction.

5. As the number of separations from the suspension increases, the yield and chlorite content of the magnetic fraction, and the Fe content of the chlorite, all decrease.

6. Separation is most effective with finer than 2μm material.

7. Dilution of the suspension does not appreciably change the purity of the magnetic fraction.

8. It may be possible to magnetically separate mica from quartz if all chlorite is first removed, and the mica is effectively saturated with Co.

# CHAPTER 5

# CHARACTERISATION OF MINERAL PHASES

## 5.1 THE ELECTRON PROBE MICROANALYSIS OF MINERAL GRAINS

Although relatively pure chlorite was successfully separated from the unweathered rock, 1040 (Section 4.2), this material could only provide analytical data for 0.063-2μm chlorite from one particular rock exposure at Plynlimon. Because of the time involved in separation, neither other grain sizes nor chlorites from other rocks could be separated for analysis in this way, and Section 4.4 has shown that successful separation of mica for analysis was not achieved at all. For this reason, a rapid, but accurate, method of analysis of both chlorite and mica was needed to support the analyses of the chlorite separated magnetically and of the fine grained soil fractions that consisted only of mica. It was felt that electron probe microanalysis provided a suitable method of analysis, as specimen preparation only involved conductively coating a rock slab or uncovered thin section that had been polished to the required finish. During analysis the electron beam could be focussed to 1μm diameter to ensure that the analysis was being generated by only one grain, and the grain could be observed optically to ensure that it was of identifiable mineralogy. Polished sections were made of the unweathered rock, 1040, together with six other rock samples, of which the origins are shown in Figure 3.4 and descriptions, where available, are given in Table A.1 in the Appendix.

Initial analysis trials were carried out on the JEOL JXA3A microprobe in the Department of Electronic Engineering at UCNW, Bangor. This machine had not been used previously for the quantitative analysis of silicates, and thus much time was spent analysing standard minerals supplied by Mrs. Jennifer Bevan of the British Museum (Natural History), and implementing a ZAF computer programme provided by Dr. Norman Charnley of the Department of Geology and Mineralogy, University of Oxford. This type of programme corrects the observed X-ray intensities for the atomic number - Z, adsorption - A, and fluorescence - F of the specimen matrix. Unfortunately, the only result of this work was to show that the microprobe at Bangor could not provide conditions that were stable enough for quantitative analysis, coupled with the fact that K could not be analysed successfully because of its vaporisation from the specimen.

Further microprobe work was thus carried out at IGS, Gray's Inn Road, London, where a microprobe dedicated to the quantitative analysis of silicates and other naturally occurring minerals was made available for a week by Dr. J. Bowles. The major part of the work carried out was the spot analysis of chlorite and mica grains. A total of 35 chlorite analyses from different grains were obtained, together with four analyses of micas that were optically observed to be intergrown with chlorite, and a further analysis of a discrete mica grain.

### 5.1.1 Analytical Results

For both chlorite and mica the elements analysed were Si, Al, Ti, Fe, Mg and K, which gave totals ranging between 81.3 and 88.3% with a mean of 86.0 ± 1.6% for chlorite, and between 89.0 and 95.4% with a mean of 93.7 ± 2.7% for mica. These values compare well with total chemical analyses [71], for which the average $H_2O$ content is 11.9% for chlorites and 6.2% for illites and muscovites, and with the chemical analyses of the separated chlorite grains (see Section 5.2) which total 91.45 and 91.72% when Fe is calculated as $Fe_2O_3$, rather than the FeO which is used here.

The analyses from the microprobe were run through a computer programme specifically written to recalculate them into the same format as the theoretical formulae of $(Mg,Al,Fe)_{12}(Si,Al)_8O_{20}(OH)_{16}$ for chlorite, and $K_yAl_4(Si_{8-y}Al_y)O_{20}(OH)_4$ for illite. In chlorite the analysed K and Ti contents were substituted for (Mg,Al,Fe) in the octahedral sites, and in illite the analysed Ti, Fe and Mg were substituted for Al in the octahedral sites. Mean compositions from all the analyses were calculated as:

$$(Mg_{2.61}Al_{3.53}Fe_{5.47}Ti_{0.01}K_{0.08})(Si_{5.16}Al_{2.84})O_{20}(OH)_{16}$$

for the chlorite, and:

$$K_{1.47}(Al_{3.47}Mg_{0.40}Fe_{0.65}Ti_{0.03})(Si_{5.93}Al_{2.07})O_{20}(OH)_4$$

for the illite. Other chlorite and illite analyses from Wales include those of Rezk [219], who found a mean chlorite composition of:

$$(Mg_{3.56}Al_{2.92}Fe^{3+}_{0.52}Fe^{2+}_{4.30}Mn_{0.06}Ti_{0.02})(Si_{5.76}Al_{2.24})O_{20}(OH)_{16}$$

by chemical analysis, Ball [16], who gave formulae for chlorite of:

$$(Mg_{6.50}Al_{1.90}Fe^{3+}_{0.68}Fe^{2+}_{2.54}Mn_{0.04})(Si_{5.92}Al_{2.08})O_{19.88}(OH)_{16.12}$$

by chemical analysis and:

$$(Mg_{6.58}Al_{2.42}Fe_{3.00})(Si_{5.58}Al_{2.42})O_{20}(OH)_{16}$$

by XRD methods, and Evans [92], who found a mean composition of:

$$(Mg_{1.60}Al_{5.04}Fe^{3+}_{0.50}Fe^{2+}_{3.10})(Si_{6.02}Al_{1.98})O_{20}(OH)_{16}$$

for chlorite and:

$$K_{1.72}Na_{0.64}(Al_{3.68}Mg_{0.22}Fe_{0.10}Mn_{0.02})(Si_{5.86}Al_{2.14})O_{20}(OH)_{4}$$

for illite, using a combination of chemical and XRD techniques.

### 5.1.2 Discussion of the Mean Chlorite Analysis

The analyses from this study immediately present problems, as they both fall outside the normally expected ranges of composition [2,128]. Considering the chlorite first, the octahedral Al content is very much greater than would be expected. In a typical chlorite analysis, the number of tetrahedral Al ions is equal to the total number of octahedral Al and $Fe^{3+}$ ions, to preserve charge balance. In the calculated mean analysis, there is an excess of at least 0.69 octahedral Al ions, and possibly more, depending on what proportion of total Fe is $Fe^{3+}$. To maintain structural neutrality with this excess of trivalent octahedral ions, there has to be a considerable number of vacancies in the octahedral sites; only 11.7 out of 12 are occupied, indicating that the structure is 92.5% trioctahedral, 7.5% dioctahedral. However, Rezk [219] found an occupancy from chemical analysis of only 11.38 sites, yet concluded his chlorite was trioctahedral, whilst Evans [92] suggested that his chlorite was ditrioctahedral.

The second anomalous feature of the chlorite is the relatively high level of K in the analysis. The most obvious explanation for high levels of both Al and K and low values for octahedral site occupation

would be if the chlorite analyses were contaminated by the collection of X-rays generated by small amounts of mica intergrowths. These are seen to occur on a visible scale down to a few microns, and are just as likely to occur on a submicron scale that it is not possible to resolve optically. In order to investigate this possibility, the correlation coefficients between K and both octahedral Al and (octahedral Al - tetrahedral Al) were determined for the chlorite analyses. The correlation coefficients were respectively 0.333 and 0.593 which, although low, are respectively significant at the 90 and 99% levels because of the large number of analyses. This implies that part of the excess Al and K is due to micaceous intergrowths that cannot be distinguished optically. However, because of the low correlation coefficients, it must also be concluded that the rest of the excess Al is a constituent part of the chlorite structure, and this in turn implies that the chlorite is not typical.

Phyllosilicate mineralogical analysis also suggests that the chlorite is not typical (see Section 7.1), with XRD analysis implying that the material in the fresh rock initially identified as chlorite is at least partially composed of hydroxy interlayered vermiculite (see Section 7.1.1). The partial replacement of the trioctahedral interlayer hydroxide sheet of the chlorite structure with an Al hydroxy interlayer would be expected to affect the analyses in the way that is observed. Working from the mean chlorite analysis, the 2:1 layer can be made totally trioctahedral by equalling the substitution of Al for Si in the tetrahedral sheets by substitution of Al for (Fe,Mg) in the octahedral sheet. If the remaining Al is assigned to the interlayer hydroxide sheet, 5.7 out of 6 octahedral sites are occupied, indicating a 15% dioctahedral character, or a replacement of 15% of the chlorite by vermiculite with Al hydroxy interlayers.

According to the classification schemes of both Foster [99] and Hey [124] (Figures 2.13 to 2.15), the mean Plynlimon chlorite analysis is that of a ripidolite. Rezk [219] claims that his mean analysis falls into the brunsvigite field in both classifications, whereas it appears that, according to Hey's classification, it should correctly be termed a pycnochlorite. As can be seen from Figures 2.13 and 2.15, although the mean Plynlimon chlorite analysis is that of a ripidolite, some of the individual analyses fall into different species fields. The chlorites from rock 1030 form a composition area separate from the main area in the classifications of both Foster [99] and Hey [124]. In

Foster's classification it is only the chlorites from 1030 that are not ripidolites, and these are all thuringites. However, in Hey's classification, part of the main compositional area falls into the pseudothuringite field, whilst the 1030 analyses fall into either the aphrosiderite, pseudothuringite or ripidolite composition areas.

5.1.3 Discussion of the Mean Mica Analysis

With the mica, there are two major deviations from the analysis typical of an illite group mineral. Firstly, the content of tetrahedral Si is very low, falling below the value of 75% of the tetrahedral sites which would be expected for a pure muscovite, which is itself lower than the 81 to 88% typical of an illite. Secondly, there is a large degree of substitution of Fe and Mg for octahedral Al, leading to 4.55 octahedral sites being occupied, corresponding to a 27.5% trioctahedral, 72.5% dioctahedral, mineral. As considered with regard to the chlorite analyses, it is possible that the mica analyses could be contaminated by X-rays collected from the intergrown chlorite, which would account for the high degree of Fe and Mg substitution for Al and the low levels of tetrahedral Si. To check this possibility, correlation coefficients between both tetrahedral Si and (tetrahedral Si/tetrahedral Al) against octahedral Fe plus Mg and total octahedral occupancy were calculated. These range from -0.974 to -0.993, indicating very close association between the variables investigated. This suggests that the two major anomalies in the illite analyses could well be due to contamination of the analyses with chlorite, which would increase octahedral Fe and Mg and total octahedral site occupancy, and decrease tetrahedral Si. Confirmation of this contamination is provided by a correlation coefficient of -0.972 between K content and total octahedral site occupancy, as K would not be expected in chlorite, which would be expected to have a higher octahedral site occupancy than illite.

From the analyses, it appears that the two micas from sample 1034 are the most contaminated; a mean of the other three analyses gives the formula:

$$K_{1.71}(Al_{3.69}Mg_{0.19}Fe_{0.27}Ti_{0.04})(Si_{6.16}Al_{1.84})O_{20}(OH)_4.$$

This formula is far more typical of a mica, and suggests that the mica being analysed is half way between a muscovite and an illite. It is noticeable that the micas that are less contaminated have higher Ti contents, and all of the micas show higher Ti contents than the

chlorites. The Ti could be included in the mica structure, or might occur as inclusions of rutile, sphene or FeTi oxides. A summary of the analyses of the grains examined is given in Tables 5.1 and 5.2, whilst the full analyses are given in Table A.8 in the Appendix.

### 5.1.4 Statistical Analysis of Microprobe Data

A brief comparison of the analyses of the four intergrown chlorite and mica pairs was made, to see whether there was any correlation between the analyses of the minerals co-existing in a single grain. Of the 11 features in the analyses, only two showed a correlation coefficient that was significant at a level of 90% or more. These were the Ti content, with a correlation coefficient of 0.911, significant at the 90% level, and the Fe/Mg ratio, with a correlation coefficient of 0.950, significant at the 95% level. As the large grains that were analysed were detritally derived, it is likely that the correlation in the Ti content and the Fe/Mg ratio reflects the values of these features in the original rocks from which the grains were derived. Why these particular features should be well correlated, and not the others is, however, not apparent.

### 5.1.5 Differences Between Chlorite Analyses

Further statistical investigation was carried out on the analytical results to see whether there were any significant differences between the analyses obtained from different rocks. For the chlorite, t tests on all the possible pairs from the means of the analysed values for each rock for all of the analysed variables were carried out by computer. These showed that, except for the Ti contents, at least one pair of means was significantly different in every analysed variable. More than half of the pairs showed differences that were significant with more than 95% confidence for the Fe and Mg contents and the Fe/Mg and octahedral Al/Mg ratios, with the Fe/Mg ratio showing the greatest differences. The mean values that showed significant differences when compared with at least one other mean value from a different rock were then compared with the mean value for all of the other analyses taken together. Fewer significant differences were found, but it was shown that, with more than 99% confidence, when compared with the chlorites in the other rocks:

1. The chlorite in rock 1018 has a lower Si content, a lower K content and a lower tetrahedral Si/Al ratio.

| Sample | Octahedral Sites | | | | | Tetrahedral Sites | | Total Octahedral Occupancy | Octahedral | | Tetrahedral Si/Al |
|---|---|---|---|---|---|---|---|---|---|---|---|
| | Mg | Al | Fe | Ti | K | Si | Al | | Fe/Mg | Al/Mg | |
| 1018 Mean | 2.51 | 3.48 | 5.73 | 0.01 | 0.02 | 5.04 | 2.96 | 11.75 | 2.28 | 1.39 | 1.70 |
| 1018 S.D. | 0.06 | 0.07 | 0.12 | 0.01 | 0.03 | 0.04 | 0.04 | 0.04 | 0.07 | 0.05 | 0.03 |
| 1022 Mean | 2.93 | 3.57 | 5.05 | 0.01 | 0.10 | 5.23 | 2.77 | 11.65 | 1.73 | 1.22 | 1.89 |
| 1022 S.D. | 0.12 | 0.12 | 0.26 | 0.01 | 0.08 | 0.10 | 0.10 | 0.10 | 0.14 | 0.04 | 0.10 |
| 1030 Mean | 1.62 | 3.42 | 6.57 | 0.01 | 0.14 | 5.20 | 2.80 | 11.75 | 4.05 | 2.12 | 1.87 |
| 1030 S.D. | 0.06 | 0.15 | 0.36 | 0.01 | 0.15 | 0.24 | 0.24 | 0.12 | 0.14 | 0.16 | 0.25 |
| 1034 Mean | 2.74 | 3.50 | 5.43 | 0.00 | 0.04 | 5.10 | 2.90 | 11.72 | 1.99 | 1.28 | 1.76 |
| 1034 S.D. | 0.12 | 0.03 | 0.13 | 0.01 | 0.06 | 0.05 | 0.05 | 0.02 | 0.13 | 0.06 | 0.05 |
| 1036 Mean | 3.22 | 3.57 | 4.75 | 0.01 | 0.15 | 5.20 | 2.80 | 11.69 | 1.47 | 1.11 | 1.87 |
| 1036 S.D. | 0.09 | 0.11 | 0.25 | 0.01 | 0.06 | 0.24 | 0.24 | 0.15 | 0.07 | 0.06 | 0.23 |
| 1040 Mean | 2.59 | 3.58 | 5.41 | 0.01 | 0.05 | 5.19 | 2.81 | 11.63 | 2.10 | 1.39 | 1.85 |
| 1040 S.D. | 0.15 | 0.09 | 0.18 | 0.01 | 0.03 | 0.16 | 0.16 | 0.11 | 0.15 | 0.10 | 0.17 |
| 1047 Mean | 2.43 | 3.55 | 5.62 | 0.01 | 0.08 | 5.11 | 2.89 | 11.70 | 2.31 | 1.46 | 1.76 |
| 1047 S.D. | 0.09 | 0.07 | 0.08 | 0.00 | 0.06 | 0.04 | 0.04 | 0.02 | 0.07 | 0.08 | 0.04 |

Table 5.1 Mean Microprobe Analyses of Chlorites in Rock Samples

| Sample | K | Octahedral Sites | | | | Tetrahedral Sites | | Total Octahedral Occupancy | Octahedral | | Tetrahedral Si/Al |
|---|---|---|---|---|---|---|---|---|---|---|---|
| | | Al | Mg | Fe | Ti | Si | Al | | Fe/Mg | Al/Mg | |
| 1018 | 1.65 | 3.68 | 0.16 | 0.38 | 0.04 | 6.09 | 1.91 | 4.26 | 2.41 | 23.00 | 3.19 |
| 1022 | 1.65 | 3.71 | 0.21 | 0.23 | 0.03 | 6.23 | 1.77 | 4.18 | 1.12 | 17.67 | 3.53 |
| 1034 Mean | 1.11 | 3.14 | 0.71 | 1.22 | 0.02 | 5.57 | 2.43 | 5.08 | 1.75 | 4.77 | 2.30 |
| 1034 S.D. | 0.04 | 0.31 | 0.24 | 0.34 | 0.01 | 0.16 | 0.16 | 0.26 | 0.12 | 2.05 | 0.22 |
| 1040 | 1.82 | 3.67 | 0.19 | 0.20 | 0.06 | 6.17 | 1.83 | 4.11 | 1.04 | 19.32 | 3.36 |

Table 5.2 Microprobe Analyses of Micas in Rock Samples

2. The chlorites in rocks 1022 and 1036 have higher Mg contents, lower Fe contents and lower Fe/Mg and octahedral Al/Mg ratios.

3. The chlorite in rock 1030 has a lower Mg content, a higher Fe content and higher Fe/Mg and octahedral Al/Mg ratios.

And, with more than 95% confidence:

4. The chlorite in rock 1018 has a higher Fe content and a higher total octahedral site occupancy.

5. The chlorite in rock 1034 has a lower octahedral Al/Mg ratio.

6. The chlorite in rock 1036 has a higher K content.

These results are helpful, in that they show that the chlorite in 1040, the rock chosen as the standard material, does not differ significantly in any way from the mean chlorite composition of the seven rocks analysed, a condition that is only satisfied by the chlorite in one other rock, 1047. This suggests that 1040 is indeed a suitable material upon which to base a study of weathering at Plynlimon. If the range of values of each of the variables about their means is considered, it can be seen that there is 123% variability about the mean for Fe/Mg and 75% for octahedral Al/Mg, yet only 10% variability for tetrahedral Si/Al. The variability in Mg content is 61%, and 33% for the Fe content, yet less than 10% for the Si and octahedral and tetrahedral Al contents. This degree of variability accounts for the greater number of significantly different mean values for Fe and Mg contents and Fe/Mg and octahedral Al/Mg ratios than for any of the other measured variables.

There are two possible explanations for this variability; either the rock samples are from horizons which were initially deposited with significantly different chlorite mineralogies, or else initially similar chlorites have been altered by diagenesis and metamorphism. A relationship between the Fe/(Fe + Mg) ratio of the chlorite and the pyrite/chlorite ratio of the rock as a whole has been found for mid Devonian shales in New York [116]. It was found that the higher the pyrite/chlorite ratio, the lower the Fe/(Fe + Mg) ratio of the chlorite, and it was proposed that initially Fe rich chlorite is altered by the reaction of the Fe with $SO_4$ in marine pore water to form

pyrite, with the Fe being replaced by Mg from the pore water. In the shale studied, the present day pore water was found to be depleted in Mg relative to sea water, thus supporting the proposed mechanism. In the example given, when pyrite/chlorite = 0.0, Fe/(Fe + Mg) in the chlorite = 0.7, whereas when pyrite/chlorite = 4.5, Fe/(Fe + Mg) in the chlorite = 0.3. The chlorites from Plynlimon range in Fe/(Fe + Mg) from 0.6 for 1036 to 0.8 for 1030, and as at least some pyrite is present in 1030, the relationship cannot be precisely as found in the original study. However, it would seem worthwhile for a future worker to investigate whether the variation in Fe/(Fe + Mg) ratio in Plynlimon chlorites is related to the variation in pyrite content of the rocks in which the chlorite occurs.

### 5.1.6 Differences Between Mica Analyses

Because only one of the rocks provided more than one mica analysis, it was not possible to compare the analyses from different rocks one with another, as was done for the chlorite, but the mean values for the micas from rock 1034 were compared with the mean analysis of the other three micas. This showed that, with more than 99% confidence:

1. The mica in rock 1034 has a lower K content and a lower octahedral Al/Mg ratio.

And, with more than 95% confidence:

2. The mica in rock 1034 has a higher Fe content and a higher total octahedral occupancy, but a lower Si content and a lower tetrahedral Si/Al ratio.

These findings are all compatible with the mica analyses from rock 1034 being more contaminated by chlorite that those from the other rocks.

## 5.2 THE CHEMICAL ANALYSIS OF CHLORITE

As well as the in situ electron probe microanalysis of coarse chlorite grains in rock sections, chemical analyses of three separated chlorite specimens from the unweathered rock, 1040, were carried out. All analyses were carried out at IGS, Gray's Inn Road, London, using either a betaprobe analyser or inductively coupled plasma atomic emission spectrometry (ICPAES). The analyses given in Table 5.3 were from the finer than 2μm 11th order magnetic separate reported in Table 4.6 to consist of 96.3% chlorite and 3.7% mica, the finer than 2μm 10th order

| Specimen | <2μm 11th Order Magnetic Separate | <2μm 10th Order Magnetic Separate | 63-200μm Magnetic Separate |
|---|---|---|---|
| Analysis Method | Betaprobe | ICPAES | ICPAES |
| % $SiO_2$ | 29.00 | 24.80 | 25.92 |
| % $Al_2O_3$ | 21.48 | 23.52 | 24.28 |
| % Total Fe as FeO | 30.77 | 30.45 | 29.14 |
| % MgO | 8.00 | 8.43 | 8.18 |
| % CaO | 0.13 | 0.00 | 0.02 |
| % $Na_2O$ | 0.01 | 0.20 | 0.21 |
| % $K_2O$ | 0.56 | 0.53 | 0.60 |
| % $TiO_2$ | 0.28 | 0.13 | 0.13 |
| % F | 0.19 | - | - |
| % $P_2O_5$ | 0.09 | - | - |

Table 5.3 Chemical Analyses of Chlorite Separated from the Unweathered Rock 1040

magnetic fraction reported in Table 4.7 to cónsist of 96.2% chlorite and 3.8% mica, and a 63-200μm chlorite magnetic separate obtained by a colleague [27].

In order to provide a direct comparison with the microprobe analyses, the values for $SiO_2$, $Al_2O_3$, FeO, MgO, $K_2O$ and $TiO_2$ from Table 5.3 were recalculated to a chlorite formula in the same way as the microprobe analyses. The resulting formulae are given in Table 5.4, together with the mean formula for the microprobe analyses of chlorite grains in 1040. The table shows that the chemical and microprobe analyses are encouragingly similar, and statistical analysis indicates that, with 95% or more confidence, the only differences are that the chemically analysed chlorites have higher K and Ti contents. As these are minor, or possibly even contaminant, components, it can be concluded that agreement between microprobe and chemical analyses of the chlorite in the unweathered rock is very good.

## 5.3 STRUCTURAL FORMULA DETERMINATION OF CHLORITE

Besides the use of chemical and microprobe analyses to estimate chlorite and mica compositions, XRD data can be used to achieve the same purpose [2,8,41,44,92,143,205,219,230]. XRD data also provide the only simple method of estimating the distribution of different atoms between the octahedral sheet in the 2:1 layer and the interlayer octahedral hydroxide sheet in chlorites [8,41,44,205,219,230]. In theory similar methods can be applied to the determination of mica compositions, but the XRD peak positions and intensities are complicated by the presence of variable amounts of K in the structure, and until 1980 [45] little attention had been given to determining mica compositions in this way, although information on the structure factor contributions of the different elements of the mica structure was available [44]. Because of the presence of quartz in all of the specimens in this study that were finer than 0.2μm yet contained no chlorite, and because of the broad mica reflections from the finer than 0.2μm specimens, no investigation into the relationship between XRD data and mica chemical composition was made. However, comprehensive reviews of methods for determining the composition of chlorite from XRD data are available [8,45,219], one of which also gives the errors found when comparing the formulae calculated by different methods from XRD data with the chemical analyses of the same specimens, and suggests reasons why the errors are often unacceptably large [8].

| Specimen | Octahedral Sites | | | | | Tetrahedral Sites | | Total Octahedral Occupancy | Octahedral | | Tetrahedral Si/Al |
|---|---|---|---|---|---|---|---|---|---|---|---|
| | Mg | Al | Fe | Ti | K | Si | Al | | Fe/Mg | Al/Mg | |
| <2μm 11th Order Magnetic Separate | 2.48 | 3.31 | 5.36 | 0.04 | 0.15 | 6.04 | 1.96 | 11.34 | 2.16 | 1.33 | 3.08 |
| <2μm 10th Order Magnetic Separate | 2.71 | 3.33 | 5.50 | 0.02 | 0.15 | 5.35 | 2.65 | 11.71 | 2.03 | 1.23 | 2.02 |
| 63-200μm Magnetic Separate | 2.59 | 3.57 | 5.17 | 0.02 | 0.16 | 5.50 | 2.50 | 11.51 | 2.00 | 1.38 | 2.20 |
| Mean Chemical Analysis | 2.59 | 3.40 | 5.34 | 0.03 | 0.15 | 5.63 | 2.37 | 11.52 | 2.06 | 1.31 | 2.43 |
| Mean Microprobe Analysis | 2.59 | 3.58 | 5.41 | 0.01 | 0.05 | 5.19 | 2.81 | 11.63 | 2.10 | 1.39 | 1.85 |

Table 5.4 A Comparison of Chlorite Formulae Calculated from Chemical and Microprobe Analyses

There are three major types of method to relate XRD data to chemical and structural compositions, involving the use of either the c axis spacing, the b axis spacing or the relative diffracted intensities of the (001) peaks. It is only the latter group of methods that can indicate the distribution of atoms between the two octahedral sheets in the chlorite structure.

### 5.3.1 c Axis Spacing Methods

Methods based on the use of the c axis, or d(001), spacing are mainly used to indicate tetrahedral Al content. The relationships employed are based on the fact that, as the Si content of the tetrahedral sheets increases, the charges on the 2:1 layer and the interlayer hydroxide sheet are both reduced. For charge balance to be maintained, any reduction in the negative charge on the tetrahedral sheets by substitution of Si for Al must be compensated for by an equal reduction in positive charge on the octahedral sheets by substitution of either $M^{2+}$, or $2/3M^{3+}$ plus 1/3 vacancy, for $M^{3+}$. As the charges on all sheets are reduced, the intersheet bonding is reduced, and thus the d(001) spacing is increased. As the tetrahedral sheets are almost entirely composed of Si and Al, a decrease in d(001) can be directly related to an increase in $Al^{[4]}$ [2,8,41,124,143].

Depending on the chlorites employed and the method of correlating chemically analysed Al with d(001), five different equations relating these factors have been produced. As reproduced here, all have been updated to give d(001) in nm, and some have also been simplified. The earliest, produced in 1954 by Hey [124] was:

$$d(001) = 1.4385 - 0.0115x, \quad (1)$$

with x being the number of Al per 8 [4] sites. In 1956 Brindley and Gillery [41] produced:

$$d(001) = 1.45 - 0.0155x \quad (2)$$

This equation was revised by Brindley to include data from other workers [219], and to allow for Hey's correction for $Fe^{3+}$, although this correction is now considered to operate in the wrong direction [8]. This gave:

$$d(001) = 1.455 - 0.0145x - 0.0025Fe^{3+}, \quad (3)$$

with $Fe^{3+}$ being quoted per 20 [4] and [6] sites.

In 1962 Albee [2] presented an equation relating d(001) to the total Al and Cr content, putting forward the view that an increase in Al in [6] sites would have an equal effect on d(001) to the same increase taking place in [4] sites. This equation can be stated as:

$$d(001) = 1.452 - 0.007y, \quad \ldots\ldots(4)$$

where y is $Al^{[4]} + Al^{[6]} + Cr$ per 20 sites.

Kepezhinskas [143], after multiple regression analysis of data from 47 chlorites, presented a simple equation relating d(001) to $Al^{[4]}$, as well as a more complex multiple regression formula. Bailey states that he derived the equation:

$$d(001) = 1.4648 - 0.0189x \quad \ldots\ldots(5)$$

from Kepezhinskas's complex multiple regression formula [8,143], but this equation is totally consistent with direct derivation from the more simple equation.

Although Bailey gave the average errors he found for the original forms of equations (3), (4) and (5) when applied to four chlorites with well refined structures [8], it was felt worthwhile to compare the results obtained from all four equations with specimens from this study. Suitable X-ray traces from random powder specimens were available from all of the whole rocks analysed by microprobe (Table 5.1). For 1040, the most important material in this study, three different additional traces were employed, using a random powder specimen of a magnetic fraction extracted from the whole rock, and glass slides of magnetic fractions extracted from both the whole rock and the finer than 2μm fraction. In addition to these specimens, two specimens of the boulder clay 1029 were analysed, both being magnetic extracts from K saturated finer than 2μm material, one prepared as a random powder, the other as a glass slide.

On almost all traces the (001) peaks were asymmetrical, and thus the peak position was taken as the mean of the position at the top of the peak and the midpoint at 50% peak height. This position was chosen because the precise position of the peak was often obscured by noise,

yet the midpoint at 50% height alone could not give an accurate value because of the asymmetry. It is estimated that any error in measurement of the peak position would give rise to a maximum error of 2% in calculated Al contents. For all except the random powder trace from the boulder clay, peaks up to (005) were available for measurement, with the (005) peak missing in that one case. It was found that the d(001) spacing differed considerably, depending on whether the value from the (001) peak alone was used, or a mean of the values appropriate to all the available peaks was taken. For this reason, calculations were carried out using both sets of values, with the mean position being calculated from the peak positions expressed in nm, rather than °2$\theta$. Table 5.5 compares the calculated Al contents with those obtained by microprobe analysis.

Comparing the mean errors from the values calculated from the position of the (001) peak alone with those from the values calculated from the mean position of the (001) peaks, it can be seen that, for each of the five calculation methods, the error is lower when the mean position value for d(001) is used. This is likely to be at least partially due to the fact that any error in measuring peak positions on a °2$\theta$ scale will result in a greater error in terms of nm at low 2$\theta$ values. As the peaks other than (001) would be expected to occur at precise subdivisions of the d(001) spacing in nm, the mean value taken from all available (001) peaks should thus be more accurate than that derived from the (001) peak position alone.

Bailey [8] found the mean errors to be very similar for the methods he tested, ranging from 7.5% for Albee's method to 9.9% for Brindley's method, contradicting Rezk's statement that Bailey found Brindley's method to give the best estimate for tetrahedral Al [219], and that this gave a mean error of 21%. The mean errors presented in Table 5.5 for the calculations based on the mean d(001) spacing of all (001) peaks range from 6.3% for Kepezhinskas's method [143] to 12.8% for Brindley's method, with Albee's method giving the lowest mean bias, at 3.6% [2]. However, although these errors are similar to those found by Bailey [8], no significant correlation can be found between the microprobe determined Al contents and the values calculated from d(001) spacings by any of the methods.

The tetrahedral Al contents of the microprobe analysed specimens only vary from 2.77 to 2.96 atoms, and the total Al contents from 6.22 to

| Sample | Specimen | d(001) (nm) | | Al Content per 8 [4] Sites | | | | | | | | | Al Content per 20 [4] + [6] Sites | | |
|---|---|---|---|---|---|---|---|---|---|---|---|---|---|---|---|
| | | | | | Calculated on the Basis of (001) Peak Using: | | | | Calculated on the Basis of All (001) Peaks Using: | | | | | Calculated Using Albee on the Basis of: | |
| | | Based on (001) Peak | Based on All (001) Peaks | Measured by Microprobe | Hey | Brindley & Gillery | Brindley | Kepezhinskas | Hey | Brindley & Gillery | Brindley | Kepezhinskas | Measured by Microprobe | (001) Peak | All (001) Peaks |
| 1018 | Random Powder Whole Sample | 1.4051 | 1.4094 | 2.96 | 2.90 | 2.90 | 3.44 | 3.16 | 2.53 | 2.62 | 3.14 | 2.93 | 6.44 | 6.70 | 6.09 |
| 1022 | Random Powder Whole Sample | 1.4062 | 1.4103 | 2.77 | 2.81 | 2.83 | 3.37 | 3.10 | 2.45 | 2.56 | 3.08 | 2.88 | 6.34 | 6.54 | 5.96 |
| 1029 | Random Powder Magnetic Extract from K Saturated Whole Sample | 1.4096 | 1.4105 | - | 2.51 | 2.61 | 3.13 | 2.92 | 2.43 | 2.55 | 3.07 | 2.87 | - | 6.06 | 5.93 |
| 1029 | Glass Slide Magnetic Extract from K Saturated Whole Sample | 1.4243 | 1.4166 | - | 1.23 | 1.66 | 2.12 | 2.14 | 1.90 | 2.15 | 2.65 | 2.55 | - | 3.96 | 5.06 |
| 1030 | Random Powder Whole Sample | 1.4029 | 1.4089 | 2.80 | 3.10 | 3.04 | 3.59 | 3.28 | 2.57 | 2.65 | 3.18 | 2.96 | 6.22 | 7.01 | 6.16 |
| 1034 | Random Powder Whole Sample | 1.3973 | 1.4071 | 2.90 | 3.58 | 3.40 | 3.98 | 3.57 | 2.73 | 2.77 | 3.30 | 3.05 | 6.40 | 7.81 | 6.41 |
| 1036 | Random Powder Whole Sample | 1.4029 | 1.4096 | 2.80 | 3.10 | 3.04 | 3.59 | 3.28 | 2.51 | 2.61 | 3.13 | 2.92 | 6.37 | 7.01 | 6.06 |
| 1040 | Random Powder Whole Sample | 1.3908 | 1.4031 | 2.81 | 4.15 | 3.82 | 4.43 | 3.92 | 3.08 | 3.03 | 3.58 | 3.26 | 6.39 | 8.74 | 6.99 |

Table 5.5 A Comparison of Methods to Calculate Chlorite Al Contents from d(001) Spacings

| Sample | Specimen | d(001)(nm) | | Al Content per 8 [4] Sites | | | | | | | | | Al Content per 20 [4] + [6] Sites | | |
|---|---|---|---|---|---|---|---|---|---|---|---|---|---|---|---|
| | | | | | Calculated on the Basis of (001) Peak Using: | | | | Calculated on the Basis of All (001) Peaks Using: | | | | | Calculated Using Albee on the Basis of: | |
| | | Based on (001) Peak | Based on All (001) Peaks | Measured by Microprobe | Hey | Brindley & Gillery | Brindley | Kepezhinskas | Hey | Brindley & Gillery | Brindley | Kepezhinskas | Measured by Microprobe | (001) Peak | All (001) Peaks |
| 1040 | Glass Slide 3rd Order Magnetic Extract from Whole Sample (Table 4.2) | 1.4255 | 1.4161 | 2.81 | 1.13 | 1.58 | 2.03 | 2.08 | 1.95 | 2.19 | 2.68 | 2.58 | 6.39 | 3.79 | 5.13 |
| 1040 | Random Powder 11th Order Magnetic Extract from <2μm Fraction (Table 4.6) | 1.3962 | 1.4049 | 2.81 | 3.68 | 3.47 | 4.06 | 3.63 | 2.92 | 2.91 | 3.46 | 3.17 | 6.39 | 7.97 | 6.73 |
| 1040 | Glass Slide 11th Order Magnetic Extract from <2μm Fraction (Table 4.6) | 1.4062 | 1.4094 | 2.81 | 2.81 | 2.83 | 3.37 | 3.10 | 2.53 | 2.62 | 3.14 | 2.93 | 6.39 | 6.54 | 6.09 |
| 1047 | Random Powder Whole Sample | 1.4085 | 1.4112 | 2.89 | 2.61 | 2.68 | 3.21 | 2.98 | 2.37 | 2.50 | 3.02 | 2.84 | 6.44 | 6.21 | 5.83 |
| | Mean % Error | - | - | - | 19.6 | 15.0 | 29.3 | 18.4 | 12.3 | 9.0 | 12.8 | 6.3 | - | 16.0 | 6.6 |
| | Mean % Bias | - | - | - | 5.3 | 4.4 | 23.7 | 13.2 | -9.6 | -6.7 | 11.9 | 4.1 | - | 7.1 | -3.6 |
| Range in Individual Errors (%) | | - | - | - | -59.8 → 47.7 | -43.8 → 35.9 | -27.8 → 57.7 | 26.0 → 39.5 | -30.6 → 9.6 | -22.1 → 7.8 | -4.6 → 27.4 | -8.2 → 16.0 | - | -40.7 → 36.8 | -19.7 → 9.4 |

Table 5.5 (continued)

6.44 atoms. These very restricted ranges may not provide an adequate test of the calculation methods, and thus it must be concluded that the accuracy of the different calculation techniques cannot be distinguished on the basis of the specimens employed in this study. In fact the straightforward assumption that all of the analysed chlorites contain 2.85 tetrahedral Al atoms leads to a mean error of 1.9%, and the assumption that all of the chlorites have a total Al content of 6.37 atoms gives an error of only 0.7%, both of which are much lower than the errors produced by any of the proposed methods of calculation. Rezk [219] claimed an average error of only 2.7% for Bailey's equation derived from Kepezhinskas's work, but it appears that he used a mean value for d(001) in all of his calculations, rather than the d(001) value appropriate to each chemically analysed specimen.

### 5.3.2 b Axis Spacing Methods

Methods based on the use of the b axis spacing rely on the measurement of the position of the chlorite (060) peak, the only significant (0k0) peak, which occurs at about 60°2$\theta$. The position of the peak primarily depends on whether the mineral is trioctahedral, when it occurs at about 0.154nm, or dioctahedral, when it occurs at about 0.150nm, due to the smaller dimensions required of the structure when one third of the octahedral sites are vacant [87]. However, within each group, the precise peak position depends on the substitution of ions of different sizes in both the tetrahedral and octahedral sheets, and it would be expected that the actual spacing would be a compromise between that required by the substitutions in the tetrahedral sheets, and that required by the substitutions in the octahedral sheets. Thus, $AlO_4$ substituting for $SiO_4$ would increase the size of the tetrahedral sheets, whilst Al substituting for Mg would reduce the size of the octahedral sheet. However, it has been suggested that, where at least some ions intermediate in radius between Al (0.057nm) and $Fe^{2+}$ (0.083nm), such as Mg (0.078nm), are present, the structure is buffered against variations in b axis spacing, except expansion caused by ions the size of $Fe^{2+}$ or larger substituting in the octahedral sheets [219]. As $Fe^{2+}$ is by far the most common of these ions, most equations based on the b axis spacing directly relate the spacing to $Fe^{2+}$, or $Fe^{2+}$ + Mn, contents.

One difficulty in measuring the position of the (060) peak is that other phyllosilicate minerals also have their (060) peaks in approximately the same position as those of chlorite, whilst the (211)

quartz peak occurs at 0.1542nm. For this reason, the chlorite (060) spacings were only measured on magnetic extracts from samples 1029 and 1040. In fact a specimen from a nonmagnetic fraction from finer than 2μm 1040 showed the mica to be dioctahedral, with d(060) = 0.1496nm. At least six different equations have been used to relate b spacing to Fe content, and the results of using these equations with the specimens for which (060) peak positions were measured, two from 1040 and four from 1029, are given in Table 5.6.

Von Engelhardt produced the earliest relationship in 1942, in the form of a graph relating b to $Fe^{2+}$ content [8,9,219]. If the erroneously included high Fe cronstedtite is removed from the graph, the plot becomes linear, and can be expressed by the equation:

$$b = 0.922 + 0.0014Fe^{2+}, \quad (6)$$

with b in nm and $Fe^{2+}$ expressed per 12 [6] sites. Hey [124] followed in 1954 with an equation relating total Fe and Mn to b, which can be simplified to give:

$$b = 0.9202 + 0.0014Fe \quad (7)$$

As no distinction between $Fe^{2+}$ and $Fe^{3+}$ could be made in the microprobe analyses, all Fe was calculated as $Fe^{2+}$, and thus the results using Hey's equation would be expected to be closest of all the equations to the microprobe results, but, as Table 5.6 shows, this is not the case. Shirozu produced the equation:

$$b = 0.921 + 0.00195Fe^{2+}, \quad (8)$$

whereas Brindley plotted a different line, equivalent to:

$$b = 0.921 + 0.00185Fe^{2+}, \quad (9)$$

through Shirozu's points [8,9,219].

Radoslovich produced an equation with an error factor included:

$$b = 0.923 + 0.0015Fe^{2+} \pm 0.0029, \quad (10)$$

| Sample | Specimen | b (nm) Calculated from (060) Peak | Fe Content Measured by Microprobe | Fe Content per 12 [6] Sites Calculated by the Method of: | | | | | | | |
|---|---|---|---|---|---|---|---|---|---|---|---|
| | | | | Von Engelhardt | Hey | Shirozu | Brindley | Radoslovich | Kepezhinskas Equation (11) | Kepezhinskas Equation (12) | Kepezhinskas Equation (13) |
| 1029 | Random Powder Magnetic Extract from K Saturated Whole Sample | 0.9306 | - | 6.14 | 7.43 | 4.92 | 5.19 | 5.07 | 6.29 | 6.64 | - |
| 1029 | Random Powder Magnetic Extract from K Saturated Whole Sample | 0.9307 | - | 6.21 | 7.50 | 4.97 | 5.24 | 5.13 | 6.36 | 6.70 | - |
| 1029 | Random Powder Magnetic Extract from K Saturated Whole Sample | 0.9317 | - | 6.93 | 8.21 | 5.49 | 5.78 | 5.80 | 7.03 | 7.33 | - |
| 1029 | Glass Slide Magnetic Extract from K Saturated Whole Sample | 0.9318 | - | 7.00 | 8.29 | 5.54 | 5.84 | 5.87 | 7.10 | 7.11 | - |
| 1040 | Random Powder 11th Order Magnetic Extract from <2μm Fraction (Table 4.6) | 0.9294 | 5.41 | 5.29 | 6.57 | 4.31 | 4.54 | 4.27 | 5.48 | 6.15 | 4.15 |
| 1040 | Random Powder 10th Order Magnetic Extract from <2μm Fraction (Table 4.7) | 0.9305 | 5.41 | 6.07 | 7.36 | 4.87 | 5.14 | 5.00 | 6.22 | 6.84 | 5.06 |

Table 5.6 A Comparison of Methods to Calculate Chlorite Fe Contents from b Spacings

but this factor is more than 10% of the expected difference between dioctahedral and trioctahedral structures [8,9,87,219], which may give some indication of how accurate these methods are.

Kepezhinskas [143] in fact produced three equations of different degrees of complexity to relate b to Fe content:

$$b = 0.921234 + 0.0014889Fe \pm 0.0013 \quad (11)$$

$$b = 0.81447 + 0.074875d(001) + 0.0015844Fe^{2+} \pm 0.0013 \quad (12)$$

$$b = 0.9346241 + 0.0012074Fe^{2+} - 0.0004709Mg - 0.0009769Si - 0.0011022Al^{[6]} \pm 0.023 \quad (13)$$

Of these equations, (11) is the simplest, in that it does not require any analytical information other than the b spacing to calculate a value for Fe. Rezk [219] wrongly states that Kepezhinskas's equation (11) was recalculated by Bailey [8] from Kepezhinskas's equation (13). Equation (12) requires the substitution of d(001) values, as well as b spacings, and the results in Table 5.6 have been calculated using the most appropriate values for d(001) from Table 5.5: 1.4105nm for the random powder specimen of 1029, 1.4166nm for the glass slide specimen of 1029 and 1.4049nm for the specimens of 1040.

It is likely that Kepezhinskas's equation (13) was intended for the determination of the b parameter when a full chemical analysis had been carried out. However, it can be used to determine Fe contents if values for b and microprobe analyses for Mg, $Al^{[6]}$ and Si are inserted as appropriate. For this reason, calculations could only be carried out for the two specimens of 1040 for which b had been determined. The mean values of the microprobe analyses for 1040, given in Table 5.1, were used in the calculations.

In all of equations (1) to (13), the same number of significant figures have been quoted as were given in the original papers. However, an estimate of the true accuracy of these methods can be obtained by considering equation (11). The error in estimating the position of the (060) peak is ±0.01°2$\theta$, and this can be translated into an error of ±0.1 Fe atoms. However the error in equation (11) as quoted by Kepezhinskas [143], of ±0.0013, actually results in an error of ±0.9 Fe atoms.

Bailey [8,9] used the same four well refined chlorites as he used with the d(001) equations in order to test the errors in the Fe contents calculated with equations (6) to (12), when compared to a microprobe measurement of total heavy atom content. The mean errors ranged from 8.4% for equation (6) to 71.2% for equation (7) [124], with equations (8), (9) and (12) [143] also producing mean errors of less than 13%. The mean bias from equation (12) is only -0.4%, and that from equation (8) 2.7%. Mean errors were calculated for the Fe contents determined for the two specimens of 1040 that have a corresponding microprobe analysis. Although it would be unwise to rely on these values, equation (6) again gives the lowest mean error, of 7.2%, and the highest error, of 28.7%, comes from equation (7). Equations (9) and (11) also give mean errors below 13%. Rezk [219] only estimated the error involved in calculations using equation (9), but did not clearly state whether he found the mean error to be 4.9 or 5.4%, when it can be calculated from his results to be 6.6%. It would thus seem that the earliest equation produced to relate b spacing to Fe content, that of Von Engelhardt [8,9,219], is at least as accurate as any of the later modifications and refinements.

### 5.3.3 Peak Intensity Methods

The third type of method relating chemical composition to XRD analysis does not depend on the measurement of peak positions, but instead on the intensities of the chlorite (00l) peaks [8,9,41,44,45,205,219,230]. Knowing the form and geometry of the specimen and diffractometer, these intensities can be converted to structure factors, which can also be calculated theoretically for different chlorite compositions from the sum of the X-ray scattering factors for the elements making up the mineral. The integrated peak intensity, I, is related to the structure factor, F, by the equation:

$$I = K(j)\frac{1}{V^2}(A\theta)F^2(L.P.), \text{ where:}$$

K = system geometry constant

j = multiplicity factor

V = unit cell volume

$A\theta$ = adsorption factor

L.P. = Lorentz-polarisation factor [230].

In practice, however, many of the factors relating to the specimen and diffractometer system, such as the system geometry constant and the adsorption factor, are difficult to determine, and thus ratios of the determined structure factors are usually compared with the ratios of the theoretical structure factors for the same peaks, as in this way the factors that are most difficult to determine are eliminated. The Lorentz-polarisation factor takes the form:

$$\frac{1 + \cos^2 2\theta}{\sin^2\theta\cos\theta}$$

for random powder specimens, and:

$$\frac{1 + \cos^2 2\theta}{\sin 2\theta}$$

for glass slides, and thus measurement of peak positions and a not insignificant amount of calculation is required even if ratios of structure factors, instead of absolute values, are used in calculating chemical compositions. For this reason Petruk [205] uses a graphical method and Brown and Brindley [45] use tables to relate intensity ratios directly to composition, without the need for conversion to structure factors.

Structure factors can be related to chemical composition because different atoms have different X-ray scattering factors. However, the scattering factors for $Cu_{K\alpha}$ radiation for Mg, Al and Si are very similar to one another, as are those for Fe, Mn and Cr, whilst the values for the two groups are quite different, and thus a distinction can be made between total heavy atoms, usually taken as the Fe content, and the other components of the structure. The chlorite structure has two octahedral sheets passing through each unit cell, and these are repeated uniformly in the c direction from cell to cell, so that each sheet is separated from the next by d(001)/2. For (001) reflections where l is even, the scattering from the octahedral sheets is in phase, and thus the scattered intensity varies as a direct function of the heavy atom content, no matter whether the heavy atoms are uniformly distributed between the octahedral sheet in the 2:1 layer and the octahedral interlayer hydroxide sheet or not. Where l is odd, the scattering from the octahedral sheets is out of phase, and if the composition of the two sheets is identical, there will be no resultant

scattered X-rays contributed by the octahedral sheets, the reflections being solely due to contributions from the tetrahedral sheets. If, however, the heavy atoms are distributed asymmetrically between the octahedral sheets, there will be a resultant from the octahedral sheets that is due to the difference in scattering power between the two sheets to be added to the contribution from the tetrahedral sheets. Short of full structural analysis, this is the only method that can be employed to determine the degree of asymmetry in heavy atom content between the two octahedral sheets in chlorites [9,219].

The methods of Brown [44], Brindley and Gillery [41], Schoen [230], Petruk [205] and Brown and Brindley [45] were all evaluated using the same specimens as were used for evaluating the equations relating Al content to d(001). Peak intensities were measured by means of a Digiplan image analyser (see Section 6.4.2), and peak positions were taken as the mean of the position at the top of the peak and the midpoint at half peak height. The measurements on which all further calculations are based are given in Table A.9 in the Appendix, together with the length factors employed with the (001) and (002) peaks.

Length factors are necessary because, at low $2\theta$ angles, part of the X-ray beam does not fall on the specimen. The intensity of the reflection is thus reduced relative to the intensity that would be produced if the specimen were longer, and intercepted the whole of the incident X-ray beam. The length of specimen required to intersect the whole of the incident beam is given by:

$$L\ (mm) = \frac{\gamma R}{57.3 \sin\theta}, \text{ where:}$$

$\gamma$ = divergence slit aperture (°), and
R = goniometer radius (mm) [230],

in this case $\gamma$ and R taking the values 1 and 173 respectively. The length factor is the factor by which the actual length of the specimen, in this study 20mm for a random powder in a purpose built Al window, and 38mm for a glass slide, must be multiplied to equal the length required to just intersect the whole incident beam. The length factor is required to make the intensities of the low angle peaks comparable with those for which the whole of the incident beam falls on the specimen. When the specimen is longer than necessary to intersect the

whole beam, no multiplying factor is required. The use of length factors has, however, been criticised on the grounds that the X-ray intensity may not be uniformly distributed across the incident beam [45]. Table A.10 in the Appendix gives the structure factors calculated from the data in Table A.9.

The calculated Fe contents given in Table 5.7 have been produced from the data in Tables A.9 and A.10 in the Appendix exactly as described by the authors of the relevant methods [41,44,45,205,230], except that all resultant Fe or Mg contents have been converted to Fe per 12 [6] sites, in order to carry out comparisons with the microprobe analyses. However, using Schoen's method [230], a value for Fe content based on $F_{004}$, as well as the one based on $F_{002}$ described by Schoen, has been derived. Schoen's method involves the calculation of the asymmetry by means of the $F_{003}/F_{001}$ ratio and, knowing the asymmetry, the theoretical $F_{003}$ and $F_{001}$ values can be determined, and thus a ratio between theoretical and determined structure factors can be produced. Schoen recommends that, by multiplying the determined $F_{002}$ by this ratio, the theoretical $F_{002}$ can be found, and thus the heavy atom content.

However, Schoen also provides a table of theoretical $F_{004}$ values for different compositions, and theoretical $F_{004}$ values can be equally well estimated in the same way as theoretical $F_{002}$, if the calculated $F_{004}$ is multiplied by the appropriate ratio. Nevertheless, if Table 5.7 is examined, it can be seen that the Fe contents calculated from $F_{004}$ for the specimens from this study are in every case higher than those calculated on the basis of $F_{002}$, and the mean error is increased from 27.2 to 68.6%. There is no theoretical reason why this should be so; in fact, based on the $F_{002}$ and $F_{004}$ values given by Schoen, and the assumption that the chlorite specimens do not have a homogeneous composition [112], there should be a tendency for the Fe content derived from $F_{002}$ to be slightly higher than that derived from $F_{004}$. It thus seems likely that Schoen also found that the values derived from $F_{002}$ produced better agreement with chemical analyses, and only mentioned this possibility in his paper [230].

Like Schoen, Petruk [205] first derives a value for asymmetry, in this case from the $I_{003}/I_{005}$ ratio, and uses it to produce a theoretical symmetrical value for $I_{003}$. The Fe content is then determined from the ratio $(I_{002} + I_{004})/I_{003sym}$. Petruk uses a graphical method of

| Sample | Specimen | Fe Content per 12 [6] Sites by Microprobe or Chemical Analysis | Calculated Fe Content (Atoms per 12 [6] Sites by the Method of: | | | | | | | | | | | | | |
|---|---|---|---|---|---|---|---|---|---|---|---|---|---|---|---|---|
| | | | Brown | Brindley and Gillery | | | | | | Schoen | | | Petruk | Brown and Brindley | | |
| | | | $F_{004}/F_{002}$ | $F_{002}/F_{001}$ | $F_{002}/F_{003}$ | $F_{004}/F_{002}$ | $F_{004}/F_{003}$ | $F_{004}/F_{005}$ | Mean | $F_{002}$ | $F_{004}$ | Mean | $\frac{I_{002}+I_{004}}{I_{003}}$ | $\frac{I_{002}+I_{004}}{I_{001}+I_{003}}$ | $\frac{I_{002}+I_{004}}{I_{003}}$ | Mean |
| 1018 | Random Powder Whole Sample | 5.73 | 3.87 | 4.41 | 9.13 | 9.37 | 9.00 | 8.24 | 8.03 | 6.54 | 8.05 | 7.30 | 5.87 | 1.00 | 5.90 | 3.45 |
| 1022 | Random Powder Whole Sample | 5.05 | 0.75 | 4.87 | 8.56 | 5.04 | 11.52 | 7.42 | 7.48 | 6.37 | 10.53 | 8.45 | 4.11 | 0.89 | 5.65 | 3.27 |
| 1029 | Random Powder Magnetic Extract from K Saturated Whole Sample | - | 4.03 | 5.37 | 7.83 | 9.57 | 6.43 | - | 7.30 | 6.06 | 7.24 | 6.65 | - | 2.15 | 5.05 | 3.60 |
| 1029 | Glass Slide Magnetic Extract from K Saturated Whole Sample | - | 2.14 | 4.17 | 9.12 | 6.97 | 10.77 | 9.09 | 8.02 | 6.44 | 9.24 | 7.84 | 5.64 | 0.58 | 6.01 | 3.30 |
| 1030 | Random Powder Whole Sample | 6.57 | 0.08 | 3.00 | 7.05 | 3.98 | 10.00 | 5.00 | 5.81 | 4.91 | 8.84 | 6.88 | 2.73 | <0 | 4.38 | 2.19 |
| 1034 | Random Powder Whole Sample | 5.43 | 2.60 | 5.10 | 9.20 | 7.63 | 10.45 | 5.01 | 7.48 | 6.85 | 9.51 | 8.18 | 3.59 | 0.37 | 5.59 | 2.98 |
| 1036 | Random Powder Whole Sample | 4.75 | 5.50 | 7.02 | 10.14 | 11.64 | 9.34 | 6.60 | 8.95 | 8.01 | 9.19 | 8.60 | 5.49 | 2.50 | 6.55 | 4.53 |
| 1040 | Random Powder Whole Sample | 5.41 | 2.88 | 6.86 | 9.17 | 8.03 | 10.12 | 7.63 | 8.36 | 7.35 | 10.08 | 8.72 | 5.08 | 2.90 | 6.20 | 4.55 |

Table 5.7 A Comparison of the Calculated and Measured Chlorite Fe Contents

| Sample | Specimen | Fe Content per 12 [6] Sites by Microprobe or Chemical Analysis | Calculated Fe Content (Atoms per 12 [6] Sites by the Method of: | | | | | | | | | | | | | |
|---|---|---|---|---|---|---|---|---|---|---|---|---|---|---|---|---|
| | | | Brown | Brindley and Gillery | | | | | | Schoen | | | Petruk | Brown and Brindley | | |
| | | | $F_{004}/F_{002}$ | $F_{002}/F_{001}$ | $F_{002}/F_{003}$ | $F_{004}/F_{002}$ | $F_{004}/F_{003}$ | $F_{004}/F_{005}$ | Mean | $F_{002}$ | $F_{004}$ | Mean | $\frac{I_{002}+I_{004}}{I_{003}}$ | $\frac{I_{002}+I_{004}}{I_{001}+I_{003}}$ | $\frac{I_{002}+I_{004}}{I_{003}}$ | Mean |
| 1040 | Glass Slide 3rd Order Magnetic Extract from Whole Sample (Table 4.2) | 5.41 | 2.28 | 4.26 | 7.11 | 7.17 | 7.05 | 3.20 | 5.76 | 5.37 | 7.41 | 6.39 | 2.73 | 0.14 | 4.20 | 2.17 |
| 1040 | Random Powder 11th Order Magnetic Extract from <2μm Fraction (Table 4.6) | 5.41 | 4.48 | 6.02 | 9.60 | 10.12 | 9.29 | 10.95 | 9.20 | 7.40 | 8.93 | 8.17 | 7.52 | 3.08 | 6.69 | 4.89 |
| 1040 | Glass Slide 11th Order Magnetic Extract from <2μm Fraction (Table 4.6) | 5.41 | 2.80 | 4.15 | 8.91 | 7.91 | 9.70 | 9.29 | 7.99 | 6.30 | 8.51 | 7.41 | 6.11 | 0.96 | 5.90 | 3.43 |
| 1047 | Random Powder Whole Sample | 5.62 | 1.45 | 5.25 | 9.11 | 5.91 | 11.57 | 6.32 | 7.63 | 6.85 | 10.54 | 8.70 | 3.92 | 0.69 | 5.82 | 3.26 |
| | Mean % Error | | 52.9 | 22.4 | 62.4 | 50.8 | 80.1 | 43.0 | 44.1 | 27.2 | 68.6 | 45.3 | 26.7 | 76.2 | 16.3 | 35.5 |
| | Mean % Bias | | -49.7 | -5.2 | 62.4 | 42.9 | 80.1 | 28.5 | 41.8 | 22.0 | 68.6 | 45.3 | -12.7 | -76.2 | 5.1 | -35.5 |
| Range in Individual Errors (%) | | | -98.8→ 15.8 | -54.3→ 47.8 | 7.3→ 113.5 | -39.4→ 145.1 | 30.3→ 128.1 | -40.9→ 102.4 | -11.6→ 88.4 | -25.3→ 68.6 | 34.6→ 108.5 | 4.7→ 81.1 | -58.4→ 39.0 | -100.0→ -43.1 | -33.3→ 37.9 | -66.7→ -4.6 |

Table 5.7 (continued)

| Sample | Specimen | Fe Content per 12 [6] Sites by Microprobe or Chemical Analysis | Calculated Fe Content (Atoms per 12 [6] Sites by the Method of: | | | | | | | | | | | | | |
|---|---|---|---|---|---|---|---|---|---|---|---|---|---|---|---|---|
| | | | Brown | Brindley and Gillery | | | | | | Schoen | | | Petruk | Brown and Brindley | | |
| | | | $F_{004}/F_{002}$ | $F_{002}/F_{001}$ | $F_{002}/F_{003}$ | $F_{004}/F_{002}$ | $F_{004}/F_{003}$ | $F_{004}/F_{005}$ | Mean | $F_{002}$ | $F_{004}$ | Mean | $\frac{I_{002}+I_{004}}{I_{003}}$ | $\frac{I_{002}+I_{004}}{I_{001}+I_{003}}$ | $\frac{I_{002}+I_{004}}{I_{003}}$ | Mean |
| Rezk p-28 as Given | Glass Slide Magnetic Extract from <2µm Fraction | 5.16 | 5.95 | 5.90 | 8.40 | 4.30 | 6.20 | - | 6.20 | 6.60 | - | 6.60 | 4.40 | - | - | - |
| Rezk p-28 Recalculated | Glass Slide Magnetic Extract from <2µm Fraction | 5.13 | 5.74 | 5.94 | 8.53 | 11.96 | 6.25 | 9.33 | 8.40 | 6.69 | 7.10 | 6.90 | 2.33 | 6.69 | 4.80 | 5.75 |
| Rezk p-29 as Given | Glass Slide Magnetic Extract from <2µm Fraction | 4.82 | 10.00 | 6.40 | 8.38 | 3.90 | 3.90 | - | 5.65 | 6.50 | - | 6.50 | 4.70 | - | - | - |
| Rezk p-29 Recalculated | Glass Slide Magnetic Extract from <2µm Fraction | 4.78 | 9.95 | 6.51 | 8.24 | >12 | 3.71 | 8.73 | 7.84 | 6.64 | 5.42 | 6.03 | 2.87 | 7.12 | 4.53 | 5.83 |
| Rezk p-30 as Given | Glass Slide Magnetic Extract from <2µm Fraction | 4.72 | 8.00 | 6.00 | 8.50 | 3.92 | 4.80 | - | 5.81 | 6.95 | - | 6.95 | 4.76 | - | - | - |
| Rezk p-30 Recalculated | Glass Slide Magnetic Extract from <2µm Fraction | 4.71 | 8.85→ 9.24 | 6.05 | 8.59→ 8.85 | >12 | 4.56→ 5.16 | 8.63→ 8.84 | 8.07 | 6.76→ 6.94 | 5.83→ 6.21 | 6.44 | 2.48→ 2.95 | 6.61→ 6.73 | 4.64→ 4.79 | 5.69 |
| Rezk p-31 as Given | Glass Slide Magnetic Extract from <2µm Fraction | 4.84 | 10.40 | 4.20 | 8.80 | 3.76 | 4.00 | - | 5.19 | 6.10 | - | 6.10 | 5.72 | - | - | - |
| Rezk p-31 Recalculated | Glass Slide Magnetic Extract from <2µm Fraction | 4.73 | >12 | 4.27 | 9.18 | >12 | 3.88 | 10.52 | 7.97 | 6.52 | 4.32 | 5.42 | 4.09 | 5.73 | 4.81 | 5.27 |

Table 5.7 (continued)

calculating both asymmetry and Fe content. His curves involving intensity, rather than structure factor, ratios are, however, based on theoretical values derived from atomic scattering factors [205]. Brown and Brindley [45] re-examined the assumptions behind Petruk's graphs, and concluded that he had used inappropriate values for the atomic scattering factors. Their method is based on the more recently determined appropriate values, and is also extended to employ $I_{003}/I_{001}$ in the assessment of asymmetry and $(I_{002} + I_{004})/(I_{001sym} + I_{003sym})$ in the calculation of Fe content, because $I_{001}$ is less affected than $I_{005}$ by variation in atomic z co-ordinates. Their method for correcting $I_{001}$ and $I_{003}$ for the effects of asymmetry is also more detailed than that provided by Petruk [205]. Neither Brown [44] nor Brindley and Gillery [41] use intensity ratios corrected for asymmetry to derive Fe contents. With the information given by Brown it is likely that only the ratio $F_{004}/F_{002}$ will be used to calculate Fe content, and this is not affected by the degree of asymmetry. However, Brindley and Gillery give a table relating Fe content to the ratios $F_{002}/F_{001}$, $F_{002}/F_{003}$, $F_{004}/F_{003}$ and $F_{004}/F_{005}$, as well as to $F_{004}/F_{002}$. All of these other ratios will be affected by the degree of asymmetry, as they involve structure factors for (001) peaks where l is odd. It would thus be expected that the value for Fe content provided by the $F_{004}/F_{002}$ ratio would be more accurate than that provided by any of the other ratios, where chlorites with any significant degree of asymmetry are concerned. In fact the data in Table 5.7 from specimens in this study show that the $F_{002}/F_{001}$ ratio provides the most accurate estimate of chemical composition, with a mean error of 22.4%, whilst $F_{004}/F_{002}$ gives rise to a mean error of 50.8%.

From the results in Table 5.7 for the specimens in this study, it would appear that the most accurate method for estimating Fe contents from chlorite (001) peak intensities or structure factors is that of Brown and Brindley [45], based on $(I_{002} + I_{004})/I_{003}$, with a mean error of 16.3% and a mean bias of 5.1%, followed by the $F_{002}/F_{001}$ ratio method of Brindley and Gillery [41], with a mean error of 22.4% and a mean bias of -5.2%, the method of Petruk [205] with a mean error of 26.7% and a mean bias of -12.7%, and that of Schoen based on $F_{002}$ [230], with a mean error of 27.2% and a mean bias of 22.0%. The mean errors found for Schoen's method based on $F_{002}$ and for Brindley's and Gillery's method based on $F_{004}/F_{002}$ are both very similar to the mean errors found by Bailey [9], working with four well refined chlorites, which were respectively 26.9 and 48.6%, but the mean error found in this

study for Petruk's method is considerably higher than the 19.3% found by Bailey.

Rezk [219], using four chlorites, quotes mean errors of 0.8, 34, 34.8 and 74% respectively for the methods of Petruk [205], Schoen using $F_{002}$ [230], Brindley and Gillery using a mean of $F_{002}/F_{001}$, $F_{002}/F_{003}$ and $F_{004}/F_{003}$ [41] and Brown [44]. Even using his own calculated compositions, the mean error for Petruk's method should be 9.1%. However, as can be seen from Table 5.7, Rezk has miscalculated many of his estimates of Fe contents from (001) intensities and structure factors.

To ensure that his mineralogical compositions were correctly based on his chemical analyses, the analyses in his Table 8 were recalculated on the same basis as the microprobe analyses used in this study. Despite the fact that Rezk separated FeO from $Fe_2O_3$, and also analysed Mn, neither of which were carried out in this study, the maximum difference between the mineralogical analyses produced was less than 3% in any given element. It must thus be concluded that Rezk's recalculated mineralogical compositions are correctly derived from his chemical analyses.

However, errors both major and minor occur in Rezk's calculations of asymmetry and Fe content from (001) intensities. It is impossible to say whether the true peak heights for the p-30 (003) and (004) reflections are 1,500 and 3,600 counts per second (cps), as given in Rezk's Appendix 6.b.1 and used in some calculations, or 1,550 and 3,650cps, as used in other calculations. For this reason, both values have been employed in recalculation. Minor errors creep into Rezk's calculation of $F_{004}$ and $F_{005}$ for p-29, and a major error, due to a misprint, occurs in $F_{005}$ for p-30, which is given as 31.410, and is correctly 14.037. In assessing Brindley's and Gillery's $F_{004}/F_{002}$ ratio, Rezk's calculations can be seen to be totally wrong, as is his use of Petruk's graphs, whereas relatively smaller errors occur in his use of Brown's and Schoen's methods, and the others of Brindley's and Gillery's ratios. In fact, had his calculations been carried out correctly, Rezk would have found mean errors, when compared to his own chemical composition, of 38.3% (instead of 0.8%) for Petruk's method, 36.8% (instead of 34%) for Schoen's method, 29.9% (instead of 34.8%) for Brindley's and Gillery's method, and 89.3% (instead of 74%) for Brown's method, assuming that Fe contents calculated as being outside

the possible range, i.e. more than 12 atoms per 12 [6] sites, are taken as the limit of the range, i.e. 12 atoms per 12 [6] sites.

5.3.4 Investigation of Errors

Despite the fact that the mean errors determined in this study are of the same order of magnitude as those found by Bailey [9], it is disconcerting that, no matter which method of recalculation is used, the correlation coefficient between the data from microprobe analysis of Fe and the Fe contents calculated from (001) intensities is negative. In fact the correlation coefficient varies from -0.09 for Brindley's and Gillery's [41] $F_{004}/F_{003}$ ratio to -0.92 for the mean values from Brown's and Brindley's [45] ratios, if no analyses from 1040 are included. If an analysis of 1040 is included, depending on which one, the correlation coefficient in no case improves significantly, and actually reaches 0.00 for Brindley's and Gillery's $F_{004}/F_{003}$ ratio. This is in marked contrast to Bailey's findings [9], where the correlation coefficients for all four methods he tested are either 0.98 or 0.99.

It was felt that the lack of correlation found in this study might be due wrong assumptions made in the course of the calculations and thus, in order to check this possibility, the data were recalculated in three further ways, using Schoen's method [230]:

1. A single crystal Lorentz-polarisation correction was employed, replacing the random powder factor used in previous calculations. Schoen [230] states that a random powder factor is appropriate for glass slide specimens, as well as random powders, and thus it was initially used in this study. However, Brindley and Gillery [41] suggest that the single crystal factor should be employed for glass slides, and this advice was followed by Rezk [219].

2. Peak heights, instead of integrated peak intensities, were employed. Schoen [230] states that peak heights are directly proportional to peak intensity for (001) peaks from the same mineral, but results from this study suggest that this is not in fact the case.

3. The length factor, criticised on the grounds of nonuniform intensity across the X-ray beam [45], was omitted from the calculation.

The results of these calculations are given in Tables 5.8 and A.11 in the Appendix and, although lower mean errors occur in five of the calculation methods when compared to the standard methods, these differences are not significant at the 90% level for paired data. What is more, correlation coefficients remain negative except for the calculation based on $F_{004}$ when peak heights are used, when it reaches 0.30. It can also be noted that the asymmetry values are very considerably altered when the single crystal Lorentz-polarisation correction is used, or when the length factor is omitted. It must thus be concluded that the errors are inherent in the totality of the methods employed and, as Bailey [9] found good correlation for his results, if not good overall agreement for every method, the errors are likely to be found in either instrumental variability in the diffractometer, specimen preparation [230], the measurement of peak intensities from the diffractometer trace, the microprobe analyses of the chlorites or, perhaps most likely, significant differences in composition between the coarse chlorites analysed by microprobe and the overall compositions assessed by (001) intensities, which are a function of all the chlorite grain sizes present in the specimen.

It also seems likely that length factors in some way significantly contribute to the errors, even though their omission leads to considerable changes in calculated asymmetry (Table 5.8). If the results of the two methods of calculating the Fe content proposed by Brown and Brindley [45] are compared, there is seen to be very much more error in the calculation when $(I_{002} + I_{004})/(I_{001} + I_{003})$ is used instead of $(I_{002} + I_{004})/I_{003}$. When calculating Fe from $(I_{002} + I_{004})/(I_{001} + I_{003})$, any error in the length factor associated with $I_{001}$ is included four times; firstly in calculating the asymmetry from $I_{003}/I_{001}$, then in using this asymmetry value to correct $I_{001}$ and $I_{003}$ to symmetrical values, and finally in multiplying the corrected $I_{001}$ value before it is used in further calculation. The length factor associated with $I_{002}$ is much smaller than with $I_{001}$, and the error associated with the $I_{001}$ length factor only occurs twice, in calculating the asymmetry and in correcting $I_{003}$ for asymmetry, when Fe is calculated from $(I_{002} + I_{004})/I_{003}$. Further evidence is provided by results recalculated from Rezk's [219] data, where length factors are not employed. The error when his analyses are calculated using Brown's and Brindley's $(I_{002} + I_{004})/(I_{001} + I_{003})$ [45] method is only 34.3%, and when the $(I_{002} + I_{004})/I_{003}$ method is employed, the mean error is reduced to 3.4%.

| Sample | Specimen | Fe Content as Analysed by Microprobe | Standard Method as in Tables 5.7 and 5.9 | | | | Using Single Crystal Lorentz-Polarisation Correction | | | | Using Peak Heights | | | | Eliminating Length Factors | | | |
|---|---|---|---|---|---|---|---|---|---|---|---|---|---|---|---|---|---|---|
| | | | Asymmetry | Fe from $F_{002}$ | Fe from $F_{004}$ | Mean Fe | Asymmetry | Fe from $F_{002}$ | Fe from $F_{004}$ | Mean Fe | Asymmetry | Fe from $F_{002}$ | Fe from $F_{004}$ | Mean Fe | Asymmetry | Fe from $F_{002}$ | Fe from $F_{004}$ | Mean Fe |
| 1018 | Random Powder Whole Sample | 5.73 | 0.84 | 6.54 | 8.05 | 7.30 | 2.70 | 6.28 | 1.50 | 3.89 | 0.85 | 7.22 | 8.39 | 7.81 | -0.54 | 6.28 | 11.41 | 8.85 |
| 1022 | Random Powder Whole Sample | 5.05 | 0.65 | 6.37 | 10.53 | 8.45 | 2.45 | 6.26 | 3.29 | 4.78 | 0.64 | 6.97 | 9.23 | 8.10 | -0.73 | 5.97 | >12 | 8.99 |
| 1029 | Random Powder Magnetic Extract from K Saturated Whole Sample | - | 0.41 | 6.06 | 7.24 | 6.65 | 2.14 | 6.13 | 1.26 | 3.70 | 0.58 | 7.44 | 10.45 | 8.95 | -0.98 | 5.55 | 9.99 | 7.77 |
| 1029 | Glass Slide Magnetic Extract from K Saturated Whole Sample | - | 0.88 | 6.44 | 9.24 | 7.84 | 2.78 | 6.18 | 2.27 | 4.23 | 0.51 | 6.59 | 10.65 | 8.62 | 0.35 | 7.33 | 10.68 | 9.01 |
| 1030 | Random Powder Whole Sample | 6.57 | 0.82 | 4.91 | 8.84 | 6.88 | 2.67 | 4.76 | 2.09 | 3.43 | 0.95 | 5.40 | 9.05 | 7.23 | -0.56 | 4.67 | >12 | 8.34 |
| 1034 | Random Powder Whole Sample | 5.43 | 0.71 | 6.85 | 9.51 | 8.18 | 2.52 | 6.71 | 2.62 | 4.67 | 0.59 | 7.15 | 10.10 | 8.63 | -0.66 | 6.50 | >12 | 9.25 |
| 1036 | Random Powder Whole Sample | 4.75 | 0.50 | 8.01 | 9.19 | 8.60 | 2.25 | 8.02 | 2.53 | 5.28 | 0.56 | 6.50 | 7.61 | 7.06 | -0.88 | 7.49 | >12 | 9.75 |
| 1040 | Random Powder Whole Sample | 5.41 | 0.36 | 7.35 | 10.08 | 8.72 | 2.05 | 7.46 | 3.25 | 5.36 | 0.79 | 7.03 | 8.93 | 7.98 | -1.01 | 6.77 | >12 | 9.39 |

Table 5.8 A Comparison of the Asymmetries and Fe Contents of Chlorites Calculated Using Schoen's Method with Different Assumptions

| Sample | Specimen | Fe Content as Analysed by Microprobe | Standard Method as in Tables 5.7 and 5.9 | | | | Using Single Crystal Lorentz-Polarisation Correction | | | | Using Peak Heights | | | | Eliminating Length Factors | | | |
|---|---|---|---|---|---|---|---|---|---|---|---|---|---|---|---|---|---|---|
| | | | Asymmetry | Fe from $F_{002}$ | Fe from $F_{004}$ | Mean Fe | Asymmetry | Fe from $F_{002}$ | Fe from $F_{004}$ | Mean Fe | Asymmetry | Fe from $F_{002}$ | Fe from $F_{004}$ | Mean Fe | Asymmetry | Fe from $F_{002}$ | Fe from $F_{004}$ | Mean Fe |
| 1040 | Glass Slide 3rd Order Magnetic Extract from Whole Sample (Table 4.2) | 5.41 | 0.54 | 5.37 | 7.41 | 6.39 | 2.33 | 5.33 | 1.25 | 3.29 | 0.27 | 5.91 | 10.35 | 8.13 | -0.05 | 6.01 | 8.48 | 7.25 |
| 1040 | Random Powder 11th Order Magnetic Extract from <2μm Fraction (Table 4.6) | 5.41 | 0.59 | 7.40 | 8.93 | 8.17 | 2.37 | 7.39 | 2.36 | 4.88 | 0.68 | 7.66 | 9.79 | 8.73 | -0.78 | 7.00 | >12 | 9.50 |
| 1040 | Glass Slide 11th Order Magnetic Extract from <2μm Fraction (Table 4.6) | 5.41 | 0.85 | 6.30 | 8.51 | 7.41 | 2.72 | 6.08 | 1.84 | 3.96 | 0.62 | 6.03 | 9.15 | 7.59 | 0.33 | 7.15 | 9.83 | 8.49 |
| 1047 | Random Powder Whole Sample | 5.62 | 0.66 | 6.85 | 10.54 | 8.70 | 2.47 | 6.74 | 3.30 | 5.02 | 0.63 | 7.56 | 9.16 | 8.36 | -0.72 | 6.46 | >12 | 9.23 |
| | Mean % Error | | - | 27.2 | 68.6 | 45.3 | - | 26.2 | 55.6 | 19.8 | - | 27.7 | 68.3 | 46.3 | - | 24.7 | 108.8 | 64.0 |
| | Mean % Bias | | - | 22.0 | 68.6 | 45.3 | - | 20.4 | -55.6 | -17.6 | - | 24.2 | 68.3 | 46.3 | - | 18.9 | 108.8 | 64.0 |
| Range in Individual Errors (%) | | | - | -25.3 → 68.6 | 34.6 → 108.5 | 4.7 → 81.1 | - | -27.5 → 68.8 | -76.9 → -34.9 | -47.8 → 11.2 | - | -17.8 → 38.0 | 37.7 → 91.3 | 10.0 → 61.4 | - | -28.9 → 57.7 | 56.7 → 152.6 | 26.9 → 105.3 |

Table 5.8 (continued)

However, the reasons Bailey put forward for the errors he found obviously also hold true in this study:

> "1. The calculated F and I values are based on ideal z parameters of the atoms. The actual z parameters differ from the ideal as a result of compositional and structural variations in sheet thicknesses.
>
> 2. The values for asymmetry and heavy atom content are very sensitive to small changes in F or I. Experimental errors of ±5% must be expected in individual F or I values." [9]

If Brindley's and Gillery's [41] table for $F_{004}/F_{002}$ is used, and 5% errors in $F_{004}$ and $F_{002}$ act together in the worst way, it is possible to generate an error of approximately ±4 atoms of Fe per 12 octahedral sites! For example, $F_{004}/F_{002}$ has a theoretical value of 1.46 when the Fe content is 6 atoms per 12 sites. If an error in $F_{004}$ decreases its value by 5%, and a simultaneous error in $F_{002}$ increases its value by 5%, $F_{004}/F_{002}$ becomes 1.32, which is the theoretical value for an Fe content of 10 atoms per 12 sites.

The conclusion must be drawn that, although the assumptions used for the calculations in Table 5.7 do not produce acceptable correlation coefficients, neither do any of the possible alternative assumptions. It may be that the range of Fe contents in the specimens analysed is insufficient to provide an effective test of the validity of any of the calculation methods employed, or else that the errors described above are so large as to render the results of any calculations invalid.

### 5.3.5 Asymmetry Assessment

Despite the errors pointed out above, comparison of (001) peak intensity ratios or structure factors is the only way, short of full structural analysis, to assess asymmetry in the Fe distribution in chlorite between the octahedral interlayer hydroxide sheet and the octahedral sheet in the 2:1 layer [9], and thus asymmetries calculated by the methods of Brown [44], Brindley and Gillery [41], Schoen [230], Petruk [205] and Brown and Brindley [45] are given in Table 5.9. These results have all been converted to (the number of Fe atoms in the 2:1 octahedral sheet - the number of Fe atoms in the octahedral interlayer hydroxide sheet) per 12 octahedral sites. The calculation methods of Brown [44] and Schoen [230] are identical, and thus the results using their methods should also be identical, although this is not the case for all of Rezk's data [219].

| Sample | Specimen | Calculated Asymmetry (Fe in 2:1 [6] Sheet - Fe in Interlayer [6] Sheet per 12 [6] Sites) by the Method of: | | | | | | | | | |
|---|---|---|---|---|---|---|---|---|---|---|---|
| | | Brown | Brindley and Gillery | | | | Schoen | Petruk | Brown and Brindley | | |
| | | $F_{003}/F_{001}$ | $F_{001}/F_{003}$ | $F_{001}/F_{005}$ | $F_{003}/F_{005}$ | Mean | $F_{003}/F_{001}$ | $I_{003}/I_{005}$ | $I_{003}/I_{001}$ | $I_{003}/I_{005}$ | Mean |
| 1018 | Random Powder Whole Sample | 0.84 | 0.90 | 1.71 | 0.19 | 0.93 | 0.84 | 0.79 | 0.99 | 0.78 | 0.89 |
| 1022 | Random Powder Whole Sample | 0.65 | 0.67 | 0.53 | 0.91 | 0.70 | 0.65 | 1.81 | 0.85 | 1.32 | 1.09 |
| 1029 | Random Powder Magnetic Extract from K Saturated Whole Sample | 0.41 | 0.42 | - | - | 0.42 | 0.41 | - | 0.67 | - | 0.67 |
| 1029 | Glass Slide Magnetic Extract from K Saturated Whole Sample | 0.88 | 0.96 | 1.61 | 0.39 | 0.99 | 0.88 | 1.05 | 1.10 | 0.90 | 1.00 |
| 1030 | Random Powder Whole Sample | 0.82 | 0.88 | 0.69 | 1.13 | 0.90 | 0.82 | 2.12 | 0.98 | 1.49 | 1.24 |
| 1034 | Random Powder Whole Sample | 0.71 | 0.74 | 0.38 | 1.23 | 0.78 | 0.71 | 2.25 | 0.89 | 1.56 | 1.23 |
| 1036 | Random Powder Whole Sample | 0.50 | 0.51 | 0.49 | 0.63 | 0.54 | 0.50 | 1.44 | 0.73 | 1.08 | 0.91 |
| 1040 | Random Powder Whole Sample | 0.36 | 0.37 | 0.28 | 0.57 | 0.41 | 0.36 | 1.33 | 0.60 | 1.03 | 0.82 |
| 1040 | Glass Slide 3rd Order Magnetic Extract from Whole Sample (Table 4.2) | 0.54 | 0.55 | 0.26 | 0.98 | 0.60 | 0.54 | 1.90 | 0.79 | 1.36 | 1.08 |
| 1040 | Random Powder 11th Order Magnetic Extract from <2μm Fraction (Table 4.6) | 0.59 | 0.61 | 1.64 | -0.32 | 0.64 | 0.59 | -0.02 | 0.80 | 0.40 | 0.60 |
| 1040 | Glass Slide 11th Order Magnetic Extract from <2μm Fraction (Table 4.6) | 0.85 | 0.92 | 1.86 | 0.10 | 0.96 | 0.85 | 0.66 | 1.02 | 0.73 | 0.88 |
| 1047 | Random Powder Whole Sample | 0.66 | 0.69 | 0.34 | 1.16 | 0.73 | 0.66 | 2.16 | 0.87 | 1.51 | 1.19 |

Table 5.9 A Comparison of the Calculated Chlorite Structural Asymmetries

| Sample | Specimen | Calculated Asymmetry (Fe in 2:1 [6] Sheet - Fe in Interlayer [6] Sheet per 12 [6] Sites) by the Method of: | | | | | | | | | |
|---|---|---|---|---|---|---|---|---|---|---|---|
| | | Brown | Brindley and Gillery | | | | Schoen | Petruk | Brown and Brindley | | |
| | | $F_{003}/F_{001}$ | $F_{001}/F_{003}$ | $F_{001}/F_{005}$ | $F_{003}/F_{005}$ | Mean | $F_{003}/F_{001}$ | $I_{003}/I_{005}$ | $I_{003}/I_{001}$ | $I_{003}/I_{005}$ | Mean |
| Rezk p-28 as Given | Glass Slide Magnetic Extract from <2μm Fraction | 0.35 | 0.50 | - | - | 0.50 | 0.40 | 1.60 | - | - | - |
| Rezk p-28 Recalculated | Glass Slide Magnetic Extract from <2μm Fraction | 0.41 | 0.43 | 1.54 | -0.61 | 0.45 | 0.41 | 1.94 | -0.67 | 1.39 | 0.36 |
| Rezk p-29 as Given | Glass Slide Magnetic Extract from <2μm Fraction | 0.20 | 0.36 | - | - | 0.36 | 0.20 | 1.00 | - | - | - |
| Rezk p-29 Recalculated | Glass Slide Magnetic Extract from <2μm Fraction | 0.24 | 0.27 | 1.73 | -1.13 | 0.29 | 0.24 | 1.21 | -0.83 | 0.97 | 0.07 |
| Rezk p-30 as Given | Glass Slide Magnetic Extract from <2μm Fraction | 0.38 | 0.50 | - | - | 0.50 | 0.32 | 1.20 | - | - | - |
| Rezk p-30 Recalculated | Glass Slide Magnetic Extract from <2μm Fraction | 0.40-0.45 | 0.41-0.46 | 1.83 | -0.75 ⟶ -0.86 | 0.49 | 0.40-0.45 | 1.57-1.74 | -0.63 ⟶ -0.68 | 1.18-1.27 | 0.29 |
| Rezk p-31 as Given | Glass Slide Magnetic Extract from <2μm Fraction | 0.80 | 0.90 | - | - | 0.90 | 0.60 | 0.40 | - | - | - |
| Rezk p-31 Recalculated | Glass Slide Magnetic Extract from <2μm Fraction | 0.87 | 0.95 | 4.45 | -1.55 | 1.28 | 0.87 | 0.71 | -0.28 | 0.75 | 0.24 |

Table 5.9 (continued)

Mean errors cannot be calculated for the different methods, as the true asymmetry values are not known, but it is perhaps not surprising that the results using the $F_{003}/F_{001}$ method common to Brown [44] and Schoen [230] have a correlation coefficient of 1.00 with, and are very close in numerical value to, the results derived from the $F_{001}/F_{003}$ method of Brindley and Gillery [41]. The results from Petruk's method [205], based on $I_{003}/I_{005}$, also have a correlation coefficient of 1.00 with those from Brindley's and Gillery's [41] $F_{003}/F_{005}$ method, but their numerical values are quite different, the regression equation being:

Petruk = 1.45(Brindley and Gillery) + 0.49.

This equation does not, however, give even an approximate fit to the values recalculated from Rezk's data [219]. As there are no correct values of asymmetry to compare the calculated values to, the safest course of action must be to assume that, because the errors found for the different total Fe content determinations used in this study were in general agreement with the errors found by Bailey for the same methods [9], it is likely that Bailey's findings on the accuracy of the different methods for determining asymmetry would be the best to apply here. Bailey found the results from Petruk's curve [205] to be most accurate, followed by the method of Brindley and Gillery [41], and then that of Schoen [230]. However, the results above have shown that, although very well correlated, the values for asymmetry derived from Petruk's curve [205], and Brindley's and Gillery's [41] table, for $F_{003}/F_{005}$ are very different. When the means of Brindley's and Gillery's methods are employed, the values are not only very different, but correlate negatively with those from Petruk's method [205]. On the other hand, the correlation coefficient between Brindley's and Gillery's mean values [41] and Schoen's results [230] is 1.00, and the actual values are relatively close to each other.

This indicates that Bailey's findings [9] cannot be assumed to be correct for the results of this study, and there is thus no absolute way of telling which of the methods of calculating asymmetry actually gives the values which are closest to the true values. However, there is no reason to expect that asymmetry would correlate either positively or negatively with total Fe content, and thus the highly significant correlation coefficient of -0.93 between the total Fe content and the asymmetry calculated using Petruk's curves [205] might suggest that the methods with much lower negative correlations (-0.40 for Brown's method

[44], -0.35 for Schoen's method [230] and particularly -0.14 for Brindley's and Gillery's method [41]) are likely to produce better estimates of asymmetry. Rezk [219] found, and his data when recalculated still also show, a higher asymmetry from Petruk's method of calculation than from any other method. However, his statement that this is not consistent with the trioctahedral nature of his chlorite is erroneous, as is the statement that the asymmetry of his specimens was best determined by either Brown's [44] or Schoen's [230] method.

## 5.4 POLYTYPE DETERMINATION OF CHLORITE

Four diffractometer traces of chlorite separated magnetically were available for the polytype determination of the material investigated in this study: two traces prepared from finer than 2mm chlorite extracted from the boulder clay 1029, one trace (A) of the finer than 2μm 11th order magnetic separate from 1040, reported in Table 4.6, and one trace (B) of the finer than 2μm 10th order magnetic separate from 1040, reported in Table 4.7. All were prepared as random powders and scanned at $1/8°2\theta min^{-1}$, with a time constant of 16 seconds, to reduce the background, as a full scale deflection (fsd) of only 200cps had to be employed. The areas of the peaks on the diffractometer trace were measured with a Digiplan image analyser, and structure factors were calculated. Comparing the positions of the peaks with those of the theoretical polytypes, it was obvious that all of the traces were derived from structures with $\beta = 97°$. The structure factors calculated for the (h01) peaks on the traces were thus correlated with the structure factors for the four $\beta = 97°$ theoretical polytypes [9,43], to see which structure provided the best agreement. The results are given in Table 5.10, and all of the traces show a very much better correlation with the theoretical IIb polytype than with any other theoretical polytype. None of the other correlation coefficients are significant at the 90% level, but all of the correlation coefficients with the theoretical IIb polytype are significant at a level very much greater than 99%. As the theoretical structure factors were calculated for an Fe free composition, the agreement between observed and theoretical values is considered to be very good [43].

Although it is likely that the coarse chlorite grains in the Plynlimon shales are detrital, it is possible that the chlorite in the matrix could have formed diagenetically, when it would have been expected to have had either Ia or Ib polytype. However, the low greenschist grade metamorphism that the shales have experienced (see Section 8.3) would

| Peak | Theoretical \|F\| Values for Polytype: | | | | Calculated \|F\| Values for: | | | | | |
|---|---|---|---|---|---|---|---|---|---|---|
| | Ia | Ib | IIa | IIb | 1029A | 1029B | 1029 Standardised Mean | 1040A | 1040B | 1040 Standardised Mean |
| $20\bar{1}$ | 44 | 41 | 60 | 7 | 10.4 | 13.1 | 12.2 | 6.6 | 9.2 | 7.3 |
| 200 | 86 | 52 | 52 | 15 | | | | 7.8 | | 8.6 |
| $20\bar{2}$ | 68 | 91 | 6 | 96 | 23.9 | 23.1 | 24.2 | 18.4 | 25.2 | 22.7 |
| 201 | 58 | 58 | 134 | 117 | 22.4 | 23.1 | 23.5 | 18.2 | 21.9 | 21.0 |
| $20\bar{3}$ | 1 | 192 | 96 | 151 | 20.5 | 22.2 | 22.0 | 19.0 | 21.4 | 21.2 |
| 202 | 218 | 20 | 117 | 98 | 25.6 | 22.8 | 24.9 | 20.7 | 22.2 | 22.5 |
| $20\bar{4}$ | 44 | 99 | 151 | 89 | 26.0 | 24.8 | 26.2 | 21.6 | 22.0 | 22.9 |
| 203 | 26 | 61 | 80 | 39 | 5.4 | 8.9 | 7.4 | 5.5 | 6.4 | 6.2 |
| $20\bar{5}$ | 53 | 135 | 46 | 38 | 11.6 | 9.0 | 10.6 | 6.0 | 8.0 | 7.3 |
| 204 | 147 | 41 | 55 | 153 | 47.0 | 46.0 | 47.9 | 35.0 | 38.3 | 38.4 |
| $20\bar{6}$ | 38 | 89 | 112 | 87 | 31.3 | 30.0 | 31.6 | 23.8 | 25.1 | 25.6 |
| 205 | 19 | 32 | 44 | 104 | 25.9 | 16.4 | 21.7 | 15.0 | 13.4 | 15.0 |
| $20\bar{7}$ | 60 | 182 | 100 | 73 | 9.3 | 10.9 | 10.4 | 10.9 | 8.5 | 10.2 |
| 206 | 217 | 54 | 189 | 84 | 28.5 | 21.0 | 25.4 | 21.5 | 21.9 | 22.8 |
| $20\bar{8}$ | 120 | 111 | 124 | 194 | 50.7 | 45.0 | 49.2 | 36.5 | 39.6 | 39.9 |
| 207 | 46 | 136 | 39 | 27 | 32.0 | 32.8 | 33.4 | 21.6 | 26.5 | 25.1 |
| $20\bar{9}$ | 65 | 78 | 91 | 32 | 9.2 | 8.6 | 9.2 | 10.9 | 8.2 | 10.1 |
| 208 | 47 | 131 | 82 | 192 | - | 45.2 | 48.0 | 30.8 | 38.6 | 36.3 |
| $40\bar{1}$ | 81 | 36 | 91 | 4 | - | 25.3 | 26.9 | - | - | - |
| $40\bar{2}$ | 94 | 93 | 76 | 57 | - | | | - | - | - |
| Correlation Coefficient with Theoretical Ia | | | | | 0.33 | 0.17 | 0.21 | 0.36 | 0.23 | 0.33 |
| Correlation Coefficient with Theoretical Ib | | | | | -0.22 | -0.01 | -0.06 | 0.05 | -0.04 | 0.07 |
| Correlation Coefficient with Theoretical IIa | | | | | 0.06 | 0.01 | 0.03 | 0.27 | 0.03 | 0.21 |
| Correlation Coefficient with Theoretical IIb | | | | | 0.73 | 0.75 | 0.77 | 0.83 | 0.80 | 0.83 |

Table 5.10 A Comparison of Theoretical and Measured Chlorite Polytype (h0l) Structure Factors

have been quite sufficient to bring about the inversion of any Ia or Ib chlorite to a IIb polytype, and thus finding that IIb chlorite occurs in finer than 2μm material cannot be used to confirm or deny an authigenic origin for the chlorite in the shale matrix.

If magnetic separation from a more weathered sample had been carried out, it might have shown a change in chlorite polytype as the chlorite weathered to vermiculite, but evidence in the literature suggests that IIb chlorite alters to an interstratified mineral and thence to Ia vermiculite, rather than from IIb to Ia chlorite and thence to Ia vermiculite, even though Ib chlorite has been observed to transform to Ia before altering to Ia vermiculite [119].

## 5.5 POLYMORPH DETERMINATION OF ILLITE

As micas were not separated from the Plynlimon samples, a specimen for mica polymorph determination was chosen which was shown by quantitative XRD analysis to consist of 100% mica, the 0.063-0.2μm fraction of the soil Bsgd/1078D horizon (see Section 6.5). The observed (hkl) peaks were found to correspond in position to those of the $2M_1$ polymorph, the only differences being that some of the reflections at very similar d spacings could not be distinguished. To confirm the identification, peak intensities were measured using a Digiplan image analyser, and were correlated with literature values for $2M_1$ muscovite [274]. The comparison is made in Table 5.11, and the correlation coefficient found between the two sets of intensities was 0.82, which is significant at a level of very much more than 99% confidence. Although other diffractometer traces were not examined in such detail, a wide range of traces from both coarse and fine grain sizes from all of the samples analysed were examined, and the positions of the (hkl) peaks were found to be identical in every case. It can thus be concluded that the mica in the Plynlimon shale is of a $2M_1$ polymorph, and that weathering has no significant effect in altering this polymorph.

A method for determining the percentage of $2M_1$ illite in a mixture of $1M_d$ and $2M_1$ has been proposed [252], and is based on the ratio of the intensities of the 0.374nm peak and the peak complex at approximately 0.258nm. From Table 5.11, this ratio for the specimen examined would be 0.100 which, according to the authors of the method, would be expected to be due to a $2M_1$ content in the mixture of about 27%, with the remaining 73% being $1M_d$ mica. This is, however, totally contradictory with the absence on the diffractometer trace of any peaks

| Peak | Peak Position (nm) | Peak Intensity in Literature ($I/I_1$) | Observed Peak Intensity (counts) |
|---|---|---|---|
| 002 | 1.001 | >100 | 137,302 |
| 004 | 0.502 | 55 | 26,367 |
| 110 | 0.448 | 55 | 17,338 |
| $11\bar{1}$ | 0.446 | 65 | |
| 021 | 0.439 | 14 | |
| 111 | 0.430 | 21 | 689 |
| 022 | 0.411 | 14 | 3,683 |
| 112 | 0.397 | 12 | 4,316 |
| $11\bar{3}$ | 0.389 | 37 | |
| 023 | 0.374 | 32 | 3,034 |
| $11\bar{4}$ | 0.350 | 44 | 2,214 |
| 006 | 0.335 | >100 | 68,989 |
| 024 | | | |
| 114 | 0.321 | 47 | 2,419 |
| 025 | 0.300 | 47 | 6,215 |
| 115 | 0.287 | 35 | 4,316 |
| $11\bar{6}$ | 0.280 | 22 | 1,864 |
| $13\bar{1}$ | 0.259 | 50 | 30,296 |
| 116 | 0.258 | 45 | |
| $20\bar{2}$ | 0.256 | 90 | |
| 008 | 0.251 | 20 | |
| $13\bar{3}$ | 0.246 | 19 | 3,767 |
| 202 | 0.245 | 12 | |
| $20\bar{4}$ | 0.240 | 10 | 5,656 |
| 133 | 0.238 | 24 | |
| $22\bar{1}$ | 0.225 | 12 | 1,640 |
| 040 | | | |
| 041 | 0.224 | 5 | |
| 221 | 0.220 | 5 | 2,106 |
| $22\bar{3}$ | 0.218 | 7 | |
| 222 | 0.215 | 10 | 5,960 |
| 043 | 0.213 | 23 | |
| 135 | | | |

Table 5.11 A Comparison of Observed Mica Peak Intensities with the $2M_1$ Intensity Values of Yoder and Eugster [274]

which cannot be identified as belonging to a $2M_1$ polymorph, and the presence of all of the expected $2M_1$ peaks. It must thus be concluded that the method employed is not applicable to the mica compositions in the specimens examined in this study.

From the observations made here, and evidence from the literature, it is likely that at least the fine grained mica in the shale was originally authigenic in origin, with a probable $1M_d$ polymorph. However, the low greenschist grade metamorphism that the shales have undergone has resulted in transformation of all the mica to a $2M_1$ polymorph [125], and no subsequent change has occurred on weathering. This is consistent with the results of Rezk [219], and the presence of only IIb chlorite in this study, although Evans [92] claimed to have found a type I chlorite in similar shales close by which, if substantiated, might suggest that they had not experienced such high temperatures as those at Plynlimon.

The illite is dioctahedral, with a d(060) spacing of 0.1496nm, as mentioned in Section 5.3.2.

## 5.6 CONCLUSIONS

As a result of the work in this chapter, the following conclusions can be drawn:

1. The mean chlorite composition is:

$$(Mg_{2.61}Al_{3.53}Fe_{5.47}Ti_{0.01}K_{0.08})(Si_{5.16}Al_{2.84})O_{20}(OH)_{16}$$

which is that of a ripidolite. This compares with Rezk's mean composition of:

$$(Mg_{3.56}Al_{2.92}Fe^{3+}_{0.52}Fe^{2+}_{4.30}Mn_{0.06}Ti_{0.02})(Si_{5.76}Al_{2.24})O_{20}(OH)_{16}$$

[219], which is a brunvigite by Foster's classification [99], but a pycnochlorite by Hey's classification [124].

2. The chlorite K and octahedral Al contents are very high. This can be partly explained by submicron scale mica intergrowths, and partly by some of the chlorite actually being Al hydroxy interlayered vermiculite.

3. The chlorite is trioctahedral, with 11.7 sites per unit cell occupied, and is a IIb polytype. Rezk's chlorite is also trioctahedral [219], but only has an occupancy of 11.38 octahedral sites out of every 12.

4. The chlorite from different rocks varies in chemical composition, particularly in Fe/Mg ratio, which ranges from 1.47 to 4.05.

5. The mean mica composition is:

$$K_{1.47}(Al_{3.47}Mg_{0.40}Fe_{0.65}Ti_{0.03})(Si_{5.93}Al_{2.07})O_{20}(OH)_4.$$

6. The mica Fe and Mg contents are very high, and the Si content very low, which can be explained by submicron scale chlorite intergrowths. A better mean composition may be obtained from the analyses of the three least contaminated micas, which give:

$$K_{1.71}(Al_{3.69}Mg_{0.19}Fe_{0.27}Ti_{0.04})(Si_{6.16}Al_{1.84})O_{20}(OH)_4.$$

This formula suggests the mica is intermediate in composition between illite and muscovite.

7. The mica is dioctahedral, and is a $2M_1$ polymorph.

8. The Fe/Mg ratios in intergrown chlorites and micas correlate with more than 95% confidence.

9. Errors in estimating the chlorite Al content by c axis spacing methods are similar to those found by Bailey [8]. Kepezhinskas's method [143] gives the lowest mean error, of 6.3%, but the range of chlorite compositions may be too low to effectively compare the accuracy of different methods.

10. With the limited amount of data available, it appears that the best method to estimate the Fe content of chlorite using the b axis spacing is that of Von Engelhardt [8,9], the same conclusion as found by Bailey [8]. The mean error is 7.2%.

11. Using peak intensity methods to estimate chlorite Fe content, the lowest mean error, of 16.3%, is found for Brown's and Brindley's $(I_{002} + I_{004})/I_{003}$ method [45]. For some peak intensity methods

errors are similar to those found by Bailey [8]; for others they are quite different. However, the negative correlation coefficients between the Fe contents calculated by these methods and those determined by microprobe analysis do not inspire confidence in the peak intensity methods.

12. All of the peak intensity methods used to investigate chlorite asymmetry suggest that there is more Fe in the 2:1 sheet than the interlayer sheet, which is consistent with the view that part of the chlorite is actually Al hydroxy interlayered vermiculite. It is not possible to determine which method of asymmetry estimation is most accurate.

# CHAPTER 6

# QUANTITATIVE MINERALOGICAL ANALYSIS

## 6.1 INTRODUCTION

If the analysis of a complex system is to be of any value, a great deal must be known about the interrelationships between the components before any useful interpretations of the influence of an external agency upon the system as a whole can be drawn. In the case of the weathering of a rock, the relationships between the different mineral components must be understood before the response of the rock to the environment can be interpreted as a product of the responses of its components. It is not enough to know the overall mineralogy of the rock; the mineralogy is likely to vary with particle size and, because of this, the surface area of each mineral available for weathering cannot be derived from the product of the specific surface area of the rock with the percentage of the mineral of interest. The chemistry of each mineral phase may vary with particle size because, as weathering proceeds, the minerals are chemically altered to approach equilibrium with their environment, and are also reduced in size. It is even possible that the same mineral, when found in two size fractions, may be derived from different sources, and thus have two different chemical compositions. The breakdown products of one mineral may influence the breakdown mechanisms of another component, and many other possible interactions could be listed.

For this reason it was obvious that a quantitative analysis of each of the samples was necessary, both in terms of the grain size distribution in the soil or rock as a whole, and of the mineralogy of each of the size fractions from every sample. An analysis of this sort is bound to be time consuming, no matter what methods are used, but to follow the scheme of Adams et al [1], who investigated the weathering of Silurian mudstone in an environment similar to the one under consideration here, would have been out of the question because of the number of specimens involved. It was felt that no short cuts in the separation of the size fractions could be employed, but that, because of the essentially three component mineralogy of the samples, the use of a quantitative XRD method could rapidly provide an accurate mineralogical analysis for each of the size fraction specimens, upon which an interpretation of the effects of the weathering environment could reliably be based. This was therefore the course pursued.

## 6.2 PARTICLE SIZE FRACTIONATION

The limits to the particle size fractions were provided by two mechanisms. At the coarse end an ultimate limit is reached, above which there are no further particles. For materials containing coarse particles, this limit can be dependent on the sample size, but was found to be 25mm for the 25kg sample of boulder clay 1029. However, above a certain size smaller than this, the particles show properties that do not vary with size, as they are polymineralic particles of relatively unweathered rock with a low surface area to volume ratio. For most of the samples, the mineralogy remains approximately constant in all of the fractions coarser than 63μm[(1)], but for the soil Ea1d/1076D, Ea2d/1077D and Bsgd/1078D horizons, there is a considerable difference in mineralogy between the 63-200μm fraction and the relatively constant coarser fractions. For this reason, particle size fractions finer than 200μm were examined in detail for each of the samples, together with coarser fractions for those samples from which they could readily be extracted. The lower particle size limit is empirical, and is provided by the requirement for a centrifuge to sediment out an adequate quantity of particles in a reasonable period of time. Even after saturation with 1M KCl was used to bring about flocculation, sufficient particles finer than 0.063μm could not be recovered, and thus this provided a lower limit.

The choice of particle size ranges between the limits, into which the samples should be separated, was decided by a number of factors. A very large number of fractions could not be processed in the time available, and separation of fractions showing little difference in size would in any case be likely to be incomplete, leading to contamination of one fraction with particles that truly belonged in another. On the other hand, if too few fractions were chosen, the critical differences in the behaviour of different particle sizes during weathering might not be observed.

The difference in particle size between the finest particles, at 0.063μm, and the coarsest, at 25mm, is nearly 400,000 times, and thus a linear division of the range of particle sizes could not be of use. It

---

(1) Separation was carried out at 61μm, the nearest available size of nylon mesh to the 63μm required by BSI [42], but because of the similarity of the two sizes, results are quoted as if the separation had taken place at 63μm.

was thus decided to use a logarithmic division of the particle size range, separating two fractions for each order of magnitude increase in particle size, as specified by BSI [42]. The apparatus available allowed this scheme to be followed from 0.063μm to 6.35mm, and a final division was made at 12.7mm for those samples which contained particles as coarse as this.

### 6.2.1 Experimental Separation Procedure

The methods used for separating the samples into the different size fractions are shown in detail in Figure 6.1, but in essence they consist of dry sieving for cutoff points coarser than 200μm, wet sieving for the divisions at 63μm and 200μm, sedimentation for the cutoff points at 6.3μm and 20μm and centrifugation for cutoff points finer than 6.3μm. Nylon meshes were used for all except the two coarsest sieve divisions. Even if these methods had not been used, a combination of at least two methods would have been needed, as no single method could cover the very large particle size range. However, when two or more methods are used, it must be acknowledged that different methods classify particles by means of different criteria, and misinterpretation of data may occur at the methodological junction [256].

Sieving is not affected by the density of the particles, instead classifying them on the basis of whether the particle's median dimension is smaller than the mesh, and thus allowing through into the finer fraction particles of which the largest dimension may be considerably larger than the nominal cutoff size. On the other hand, the cutoff size in sedimentation and centrifugation is affected both by the density and the shape of the particle. The behaviour of particles unaffected by either Brownian motion or turbulent flow, i.e. in the range 0.2-200μm, can be described by Stokes' Law.

The denser a particle is, the more rapidly it will be sedimented, and thus a size fraction will contain coarser light minerals than denser minerals. In fact, if the time for centrifugation is chosen to sediment a 2.00μm particle of quartz of density 2.65gcm$^{-3}$, particles of illite of density 2.75gcm$^{-3}$ and size 1.94μm, and of chlorite of density 2.95gcm$^{-3}$ and size 1.84μm will also be sedimented.

The size of a particle undergoing sedimentation is expressed in terms of the esd and, for a sphere, which is the shape which experiences

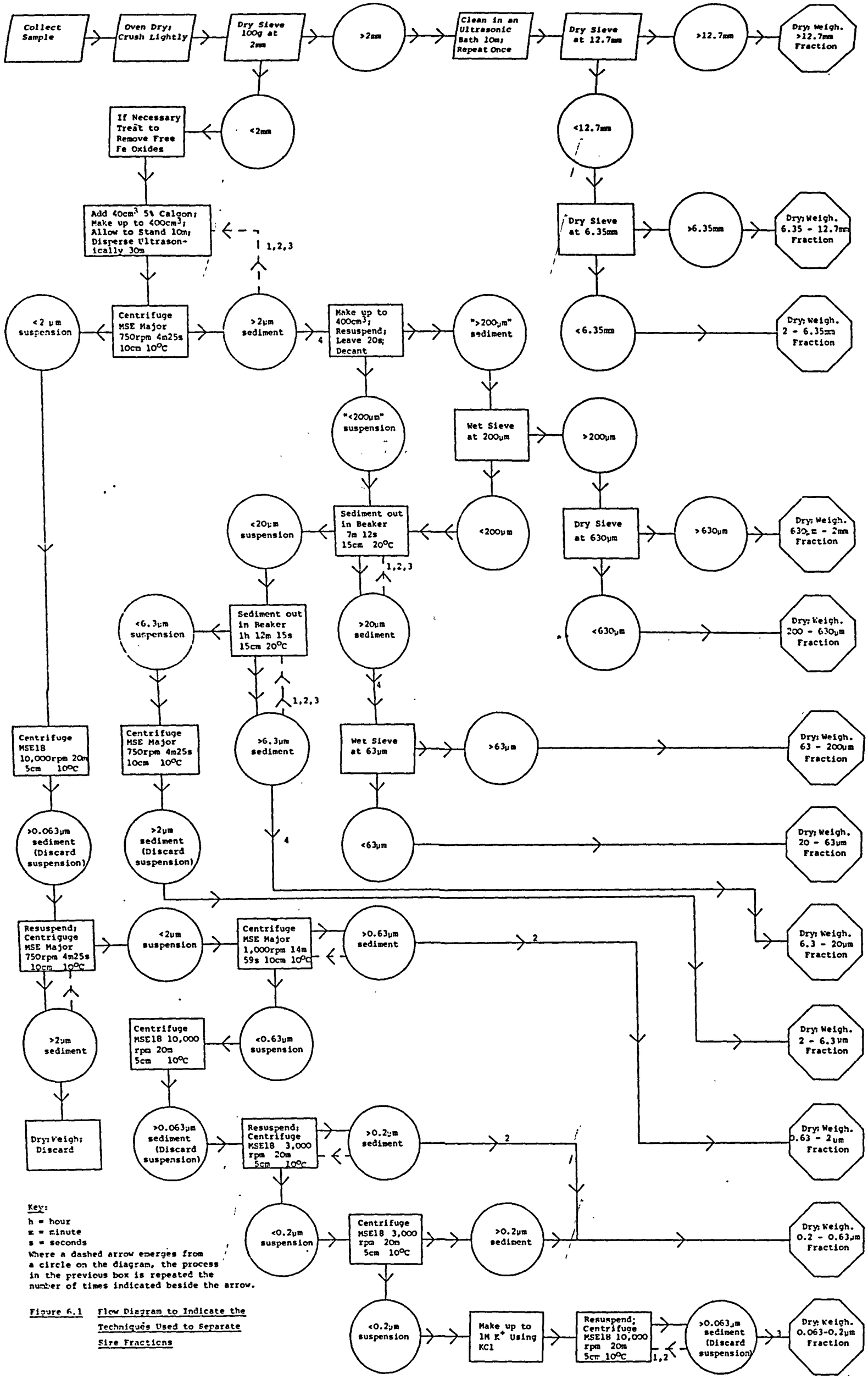


Key:

h = hour
m = minute
s = seconds
Where a dashed arrow emerges from a circle on the diagram, the process in the previous box is repeated the number of times indicated beside the arrow.

Figure 6.1 Flow Diagram to Indicate the Techniques Used to Separate Size Fractions

least drag when falling through a fluid, the diameter is the same as the esd. Other shapes of particle, such as the flat sheets to which chlorite and illite particles approximate, experience a greater drag than a sphere of the same maximum dimension. The drag that they experience is the same as that experienced by a sphere of larger size, and thus they will be sedimented into the fraction which contains spherical particles of that larger size, which is defined as the esd. However, because of the very small size of the particles considered here, and their low settling velocity, the Reynolds number is so low that the difference in drag between differently shaped particles of the same maximum dimension is negligible [178]. It is thus the case that variation in density between the minerals has a much greater effect in altering the cutoff point for a mineral away from the nominal cutoff point than does any difference in shape between the particles, but there is no obvious way of overcoming this effect on the separation procedure.

From Figure 6.1 it can be seen that some sedimentation and centrifugation steps had to be repeated. This was because particles finer than the expected cutoff size that started near the base of the column of suspension were sedimented along with the particles coarser than the cutoff size. Sufficient repetitions of each stage were carried out to ensure that the material smaller than the cutoff size was included in the finer fraction. At two points in the separation procedure, material coarser than the expected cutoff size was found to be remaining in suspension. This was due to the concentration of the suspension increasing the density of the suspending medium, and was countered by further centrifugation of the suspension under the same conditions, after the removal of the sedimented material.

### 6.2.2 Sample Preparation

Where necessary, samples were treated with buffered sodium dithionite solution, to remove free Fe oxides [179]. 100g of dry, finer than 2mm, material from the initial sample were placed in a large conical flask, to which was added 50cm³ of 1M $NaHCO_3$ and 400cm³ of 0.3M trisodium citrate. The flask was placed in an oven at 80°C and, when the temperature of the suspension reached 70°C, 10g of sodium dithionite were added whilst stirring. After an hour, the suspension was stirred again, and then left overnight. After cooling, the suspension was centrifuged for 10 minutes in an MSE Major centrifuge at 2,500rpm. Because of the high ionic concentration of the solution, decanting the

liquid without the loss of any suspended solid was a simple process, and the rest of the separation was continued as shown in Figure 6.1. Samples treated with sodium dithionite solution are identified by the letter "D" suffixed to their identification numbers, or "d" suffixed to their horizon notation.

In order to determine the total amount of material solubilised by sodium dithionite, duplicate treatments, each using one 10th of the quantities used in preparing the material for particle size analysis, were carried out. After cooling, the suspensions were transferred to MSE18 centrifuge bottles and centrifuged for 20 minutes at 10,000rpm. The supernatant was discarded, and the solid was twice resuspended in distilled water and centrifuged as before. The solids were then dried and weighed. After this treatment, the colour of some of the samples suggested that free Fe oxides remained, and thus the treatment was repeated to determine whether any further weight loss occurred. The results are given in Table 6.1.

Table 6.1 Solution of Soil Material by Buffered Sodium Dithionite

| Sample | % Weight Loss During 1st Dithionite Treatment | % Weight Loss During 2nd Dithionite Treatment | Total % Weight Loss During Dithionite Treatment |
|---|---|---|---|
| 1080D | 12.66 ± 1.36 | 1.68 | 15.07 |
| 1079D | 12.22 ± 0.12 | 3.30 ± 0.08 | 15.11 ± 0.05 |
| 1078D | 11.91 ± 0.25 | 2.94 | 14.66 |
| 1077D | 7.38 ± 0.04 | 1.10 ± 0.26 | 8.39 ± 0.28 |
| 1076D | 6.60 ± 1.10 | 1.38 ± 0.67 | 7.88 ± 0.45 |

For every sample, at least 81% of the extractable material was removed during the first treatment, and thus the treated samples used for particle size determination contained at most 19% of their original free Fe oxide contents. As some loss of material must be expected during repeated centrifugation and decantation, it is possible that only the results for 1078D and 1079D indicate an extraction of material by the second treatment. The figures for the amount of material lost during dithionite treatment given in Table 6.2 only include the amount lost during the first extraction, as this was the only treatment received by the material used for particle size analysis.

Before particle size analysis could be carried out for the unweathered rock, 1040, it was desired to break down the rock in a way that would

| Sample | 1040 | 1029 | 1039 | 1049 | 1080D | 1079D | 1078D | 1077D | 1076D | 1079 | 1077 | 1087 |
|---|---|---|---|---|---|---|---|---|---|---|---|---|
| % of whole sample >12.7mm | - | 10.87 | 2.11 | 22.73 | 7.96 | n.d. | n.d. | n.d. | n.d. | n.d. | n.d. | 9.60 |
| % of whole sample 6.35-12.7mm | - | 8.57 | 4.22 | 7.19 | 13.07 | n.d. | n.d. | n.d. | n.d. | n.d. | n.d. | 8.12 |
| % of whole sample 2-6.35mm | - | 20.33 | 14.30 | 14.31 | 62.45 | n.d. | n.d. | n.d. | n.d. | n.d. | n.d. | 12.02 |
| Total % of whole sample >2mm | - | 39.77 | 20.63 | 44.23 | 83.48 | 15.09 | 0.43 | 0.41 | 0.11 | 15.09 | 0.41 | 29.74 |
| % of <2mm material >630µm | - | 23.41 | 16.40 | 16.13 | 26.90 | 1.45 | 0.26 | 0.10 | 0.06 | 8.59 | 0.96 | 13.38 |
| % of <2mm material 200-630µm | 0.05 | 9.66 | 6.18 | 9.97 | 4.09 | 1.29 | 1.04 | 0.45 | 0.18 | 3.96 | 1.05 | 4.48 |
| % of <2mm material 63-200µm | 1.91 | 10.38 | 4.19 | 7.42 | 1.95 | 0.80 | 0.75 | 1.06 | 0.57 | 2.63 | 2.34 | 6.80 |
| % of <2mm material 20-63µm | 26.15 | 8.41 | 8.54 | 6.71 | 3.78 | 6.67 | 5.46 | 6.56 | 4.99 | 9.17 | 8.51 | 11.25 |
| % of <2mm material 6.3-20µm | 21.76 | 8.87 | 8.87 | 10.74 | 9.34 | 19.00 | 19.46 | 21.02 | 20.65 | 17.46 | 21.52 | 13.48 |
| % of <2mm material 2-6.3µm | 32.95 | 13.90 | 6.31 | 17.67 | 14.96 | 28.42 | 29.30 | 32.25 | 34.38 | 26.96 | 31.11 | 19.14 |
| % of <2mm material undivided but >2µm | 1.01 | 5.14 | 5.05 | 5.09 | 6.61 | 2.12 | 2.28 | 3.62 | 2.75 | 1.20 | 2.61 | 5.14 |
| % of <2mm material 0.63-2µm | 4.92 | 5.18 | 5.46 | 5.20 | 5.28 | 8.98 | 9.97 | 5.41 | 5.55 | 5.96 | 5.86 | 6.18 |
| % of <2mm material 0.2-0.63µm | 4.78 | 6.05 | 7.16 | 9.01 | 3.04 | 2.54 | 2.79 | 1.57 | 1.67 | 3.13 | 6.63 | 7.02 |
| % of <2mm material 0.063-0.2µm | 0.84 | 3.59 | 4.20 | 4.45 | 6.00 | 10.62 | 11.83 | 12.42 | 14.03 | 8.06 | 5.18 | 3.66 |
| % of <2mm material lost during dithionite treatment | - | - | - | - | 12.66 | 12.22 | 11.91 | 7.38 | 6.60 | - | - | - |
| Total % of <2mm material accounted for | 94.37 | 94.59 | 72.36 | 92.39 | 94.61 | 94.11 | 95.05 | 91.84 | 91.43 | 87.12 | 85.77 | 90.53 |

TABLE 6.2 Raw Data from Quantitative Particle Size Analysis

n.d. = not determined

retain its original particle size distribution, rather than reflecting the mechanics of a crushing process. It is known that the particle size distribution of a crushed hard rock can be fitted by the Weibull/ Rosin-Rammler equation, no matter what its original particle size distribution [159], and thus crushing would be very unlikely to give rise to information about the particle size distribution within the rock. For this reason, ultrasonic dispersion is favoured for dissaggregating shales [76,256], and an attempt was thus made to ultrasonically disperse the unweathered rock.

The rock was crushed into particles finer than 10mm in maximum size, which were placed in a 5% Calgon solution to act as a dispersing agent. The particles were then subjected to ultrasonic dispersion for increasing periods of time, until the experiment had to be stopped because the input of ultrasonic energy had caused the solution to reach boiling point. However, even the combination of ultrasonic vibration, dispersing agent and raised temperature had no apparent disaggregating effect on the well consolidated shale, and thus crushing had to be resorted to, despite its undesirable effect on the particle size distribution.

Preliminary experiments using particles of approximately 10mm maximum dimension extracted from the boulder clay, 1029, showed that, using a Tema vibrating sample mill, the greatest proportion of finer than 2μm particles could be obtained if a grinding time of four minutes, rather than either two or 16 minutes, the other times tested, was used. The rock was thus broken into pieces of approximately 10mm maximum dimension, and about 10g were placed into each silicon carbide lined chamber of the mill, which was run for four minutes, using a silicon carbide coated cylindrical weight inside each chamber to bring about the crushing. The first 10g of material in each run were used to clean the chamber, and then discarded, before collecting subsequent material. Unweathered rock crushed in this way was used for particle size analysis and all other experiments.

### 6.2.3 Recalculation of Results

The data presented in Table 6.2 show a mean recovery during particle size analysis of 92%, if the data for sample 1039 are excluded. Sample 1039 was the first to be fractionated, and it is considered that the low recovery, of only 72%, was due to some of the desired material being lost along with supernatants, as well as to losses during wet

sieving. After an improvement of experimental technique, losses during fractionation were kept below 15% for the remaining samples.

Once the raw data had been obtained, a method for recalculating it into an accurate particle size distribution was required, taking into account the loss during dithionite treatment, the unseparated material coarser than 2μm which remained in suspension with the finer than 2μm material, and the material unaccounted for. Obviously, the greater the proportion of a size fraction present, the greater the likelihood of material of that size being lost during separation, and thus the correction employed must take into account the amount of material in each fraction that was recovered.

Although it is most likely that:

1. Finer particles would be preferentially dissolved by dithionite treatment,

2. Coarser than 2μm material remaining in suspension with the finer material would not be much coarser than 2μm, and

3. Fine particles would be preferentially lost during the separation procedure,

no way of quantifying how rapidly the proportion of material lost to each of these causes decreased with increasing grain size was available. Because no case could be made for any particular nonlinear size distribution of particles dissolved, remaining in suspension or lost, a distribution of the losses proportional to the amount recovered in each fraction was used. The first calculation performed was to allocate the dithionite loss, where present, amongst all of the finer than 2mm fractions, including the undivided coarser than 2μm material. Next, the undivided coarser than 2μm material was allocated to all of the coarser than 2μm but finer than 2mm fractions. Finally, the unaccountable loss was allocated to all fractions finer than ~~2μm~~ 2 mm, to give a 100% total. The recalculated particle size data is given in Table 6.3 and shown diagrammatically in Figures 6.2 to 6.13.

### 6.2.4 Interpretation of Particle Size Distributions

Looking at the particle size distribution data in Table 6.3, several conclusions can be drawn about the relationships between the samples.

| Sample | 1040 | 1029 | 1039 | 1049 | 1080D | 1079D | 1078D | 1077D | 1076D | 1079 | 1077 | 1087 |
|---|---|---|---|---|---|---|---|---|---|---|---|---|
| % >630µm | - | 26.45 | 24.93 | 18.75 | 36.37 | 1.84 | 0.33 | 0.13 | 0.08 | 10.03 | 1.17 | 15.88 |
| % 200 - 630µm | 0.05 | 10.92 | 9.40 | 11.59 | 5.54 | 1.64 | 1.30 | 0.56 | 0.23 | 4.63 | 1.27 | 5.32 |
| % 63 - 200µm | 2.05 | 11.72 | 6.37 | 8.63 | 2.64 | 1.01 | 0.94 | 1.32 | 0.70 | 3.08 | 2.83 | 8.08 |
| % 20 - 63µm | 28.05 | 9.50 | 12.98 | 7.80 | 5.11 | 8.44 | 6.83 | 8.22 | 6.15 | 10.71 | 10.32 | 13.36 |
| % 6.3 - 20µm | 23.34 | 10.02 | 13.49 | 12.49 | 12.64 | 24.05 | 24.35 | 26.36 | 25.44 | 20.39 | 26.09 | 16.01 |
| % 2 - 6.3µm | 35.34 | 15.71 | 9.59 | 20.54 | 20.23 | 35.98 | 36.67 | 40.44 | 42.36 | 31.48 | 37.72 | 22.73 |
| % 0.63 - 2µm | 5.21 | 5.48 | 7.55 | 5.63 | 6.44 | 10.97 | 11.99 | 6.41 | 6.55 | 6.84 | 6.83 | 6.83 |
| % 0.2 - 0.63µm | 5.07 | 6.40 | 9.89 | 9.75 | 3.71 | 3.10 | 3.36 | 1.86 | 1.96 | 3.59 | 7.73 | 7.75 |
| % 0.063 - 0.2µm | 0.89 | 3.80 | 5.80 | 4.82 | 7.32 | 12.97 | 14.23 | 14.70 | 16.53 | 9.25 | 6.04 | 4.04 |

TABLE 6.3 Particle Size Distribution of <2mm Material Recalculated to Total 100%

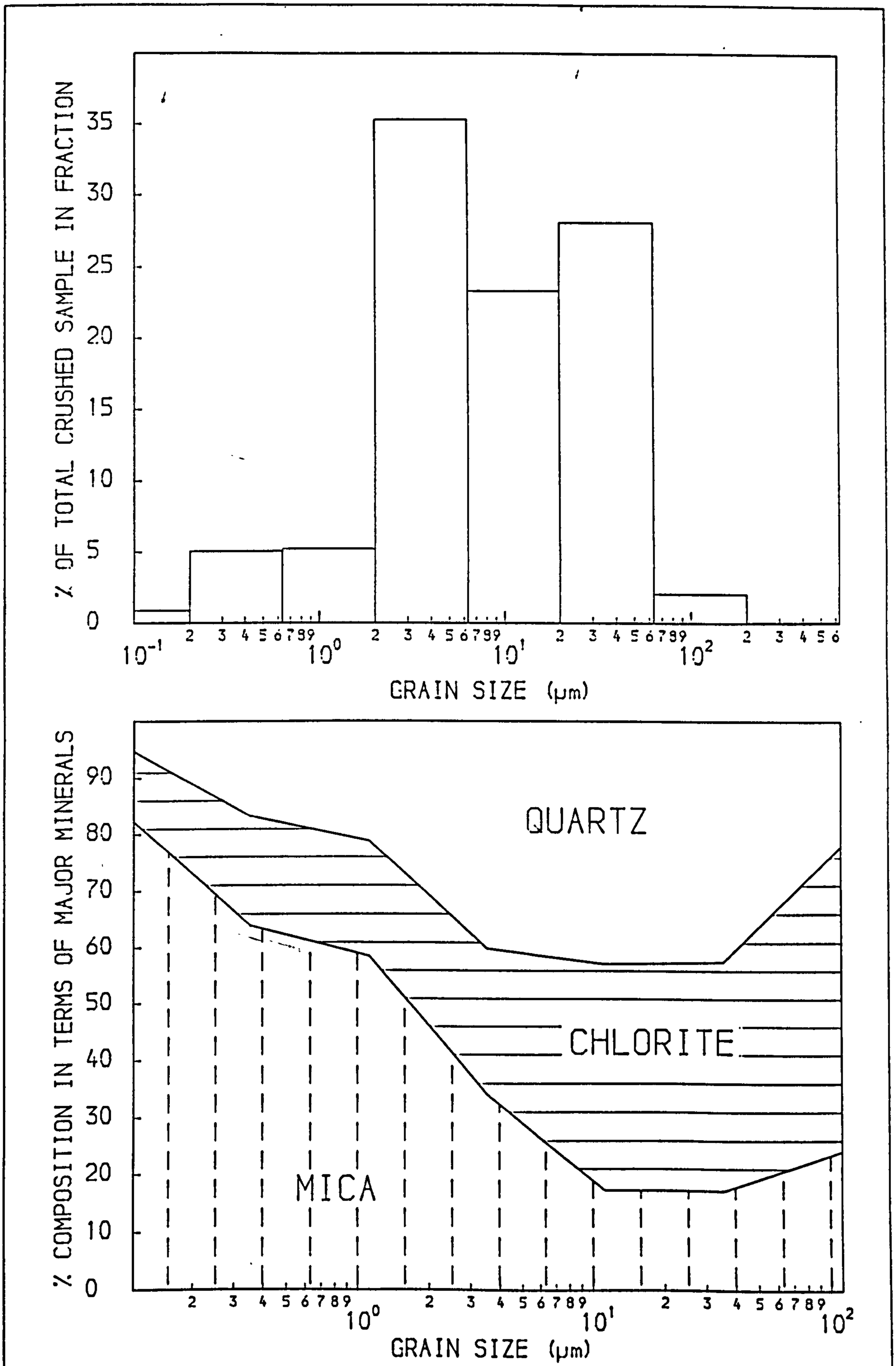


FIGURE 6.2. QUANTITATIVE MINERALOGICAL COMPOSITION AND PARTICLE SIZE DISTRIBUTION OF SAMPLE 1040, AFTER CRUSHING IN A VIBRATING SAMPLE MILL.

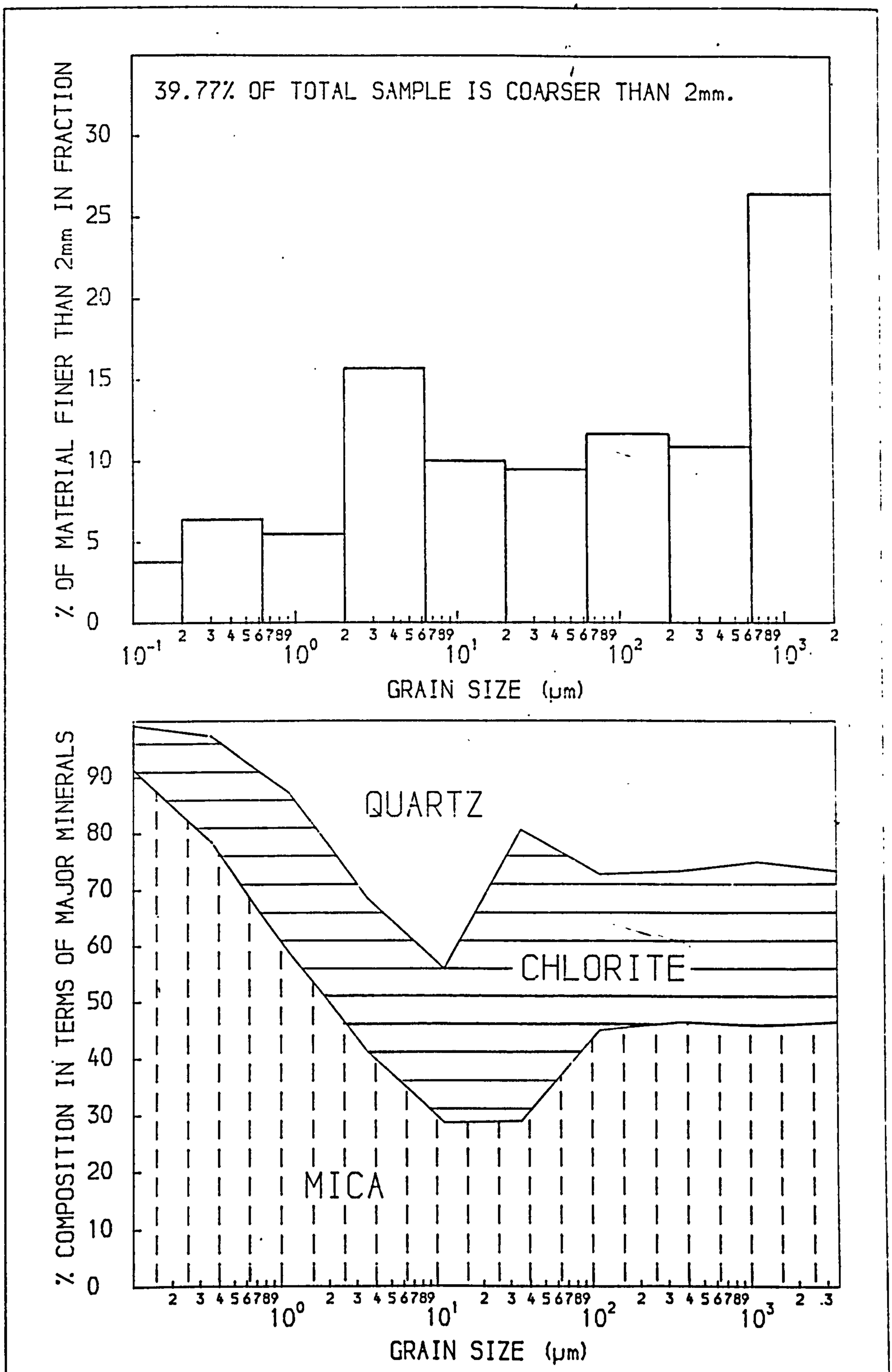


FIGURE 6.3. QUANTITATIVE MINERALOGICAL COMPOSITION AND PARTICLE SIZE DISTRIBUTION OF SAMPLE 1029.

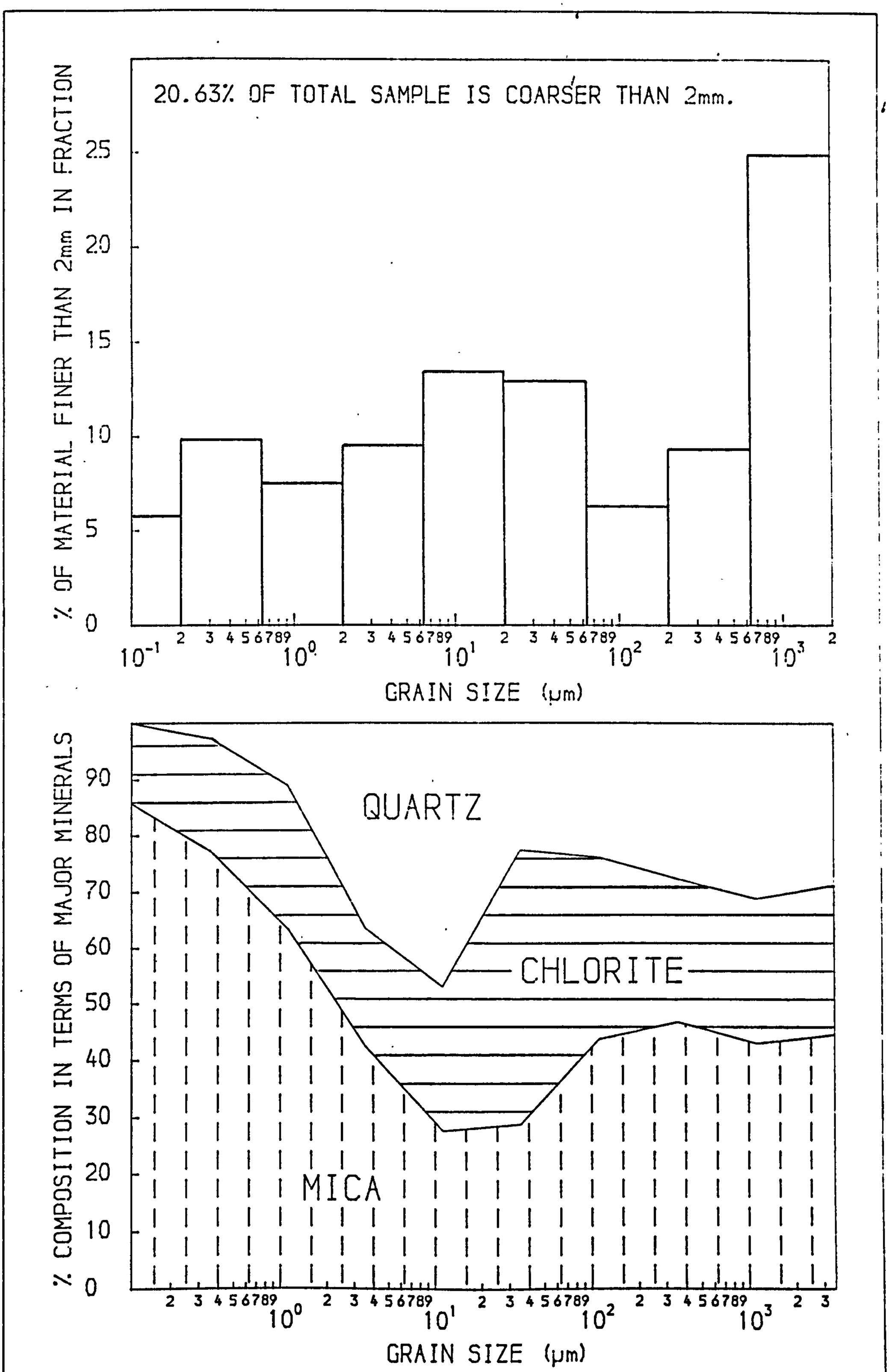


FIGURE 6.4. QUANTITATIVE MINERALOGICAL COMPOSITION AND PARTICLE SIZE DISTRIBUTION OF SAMPLE 1039.

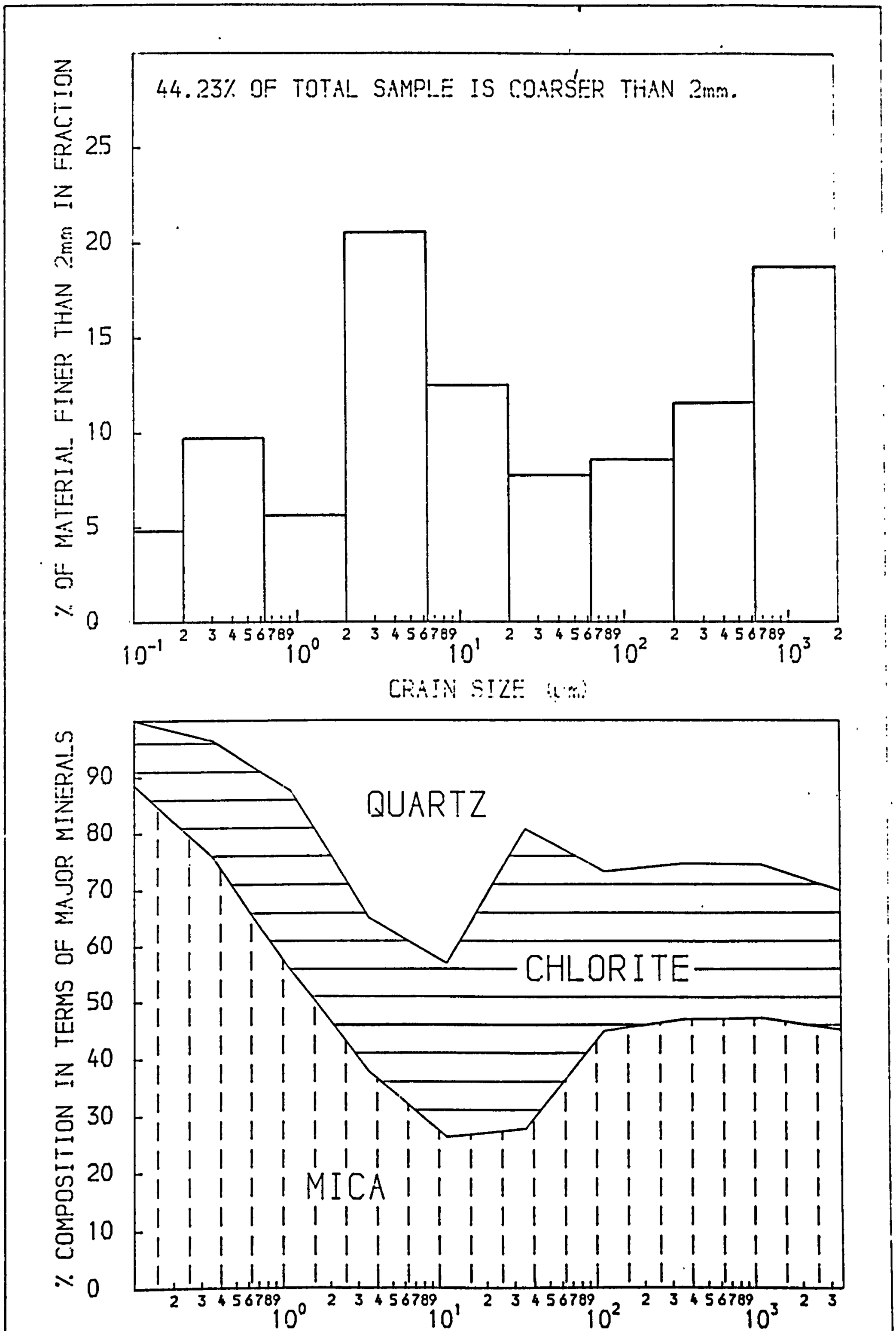


FIGURE 6.5. QUANTITATIVE MINERALOGICAL COMPOSITION AND PARTICLE SIZE DISTRIBUTION OF SAMPLE 1049.

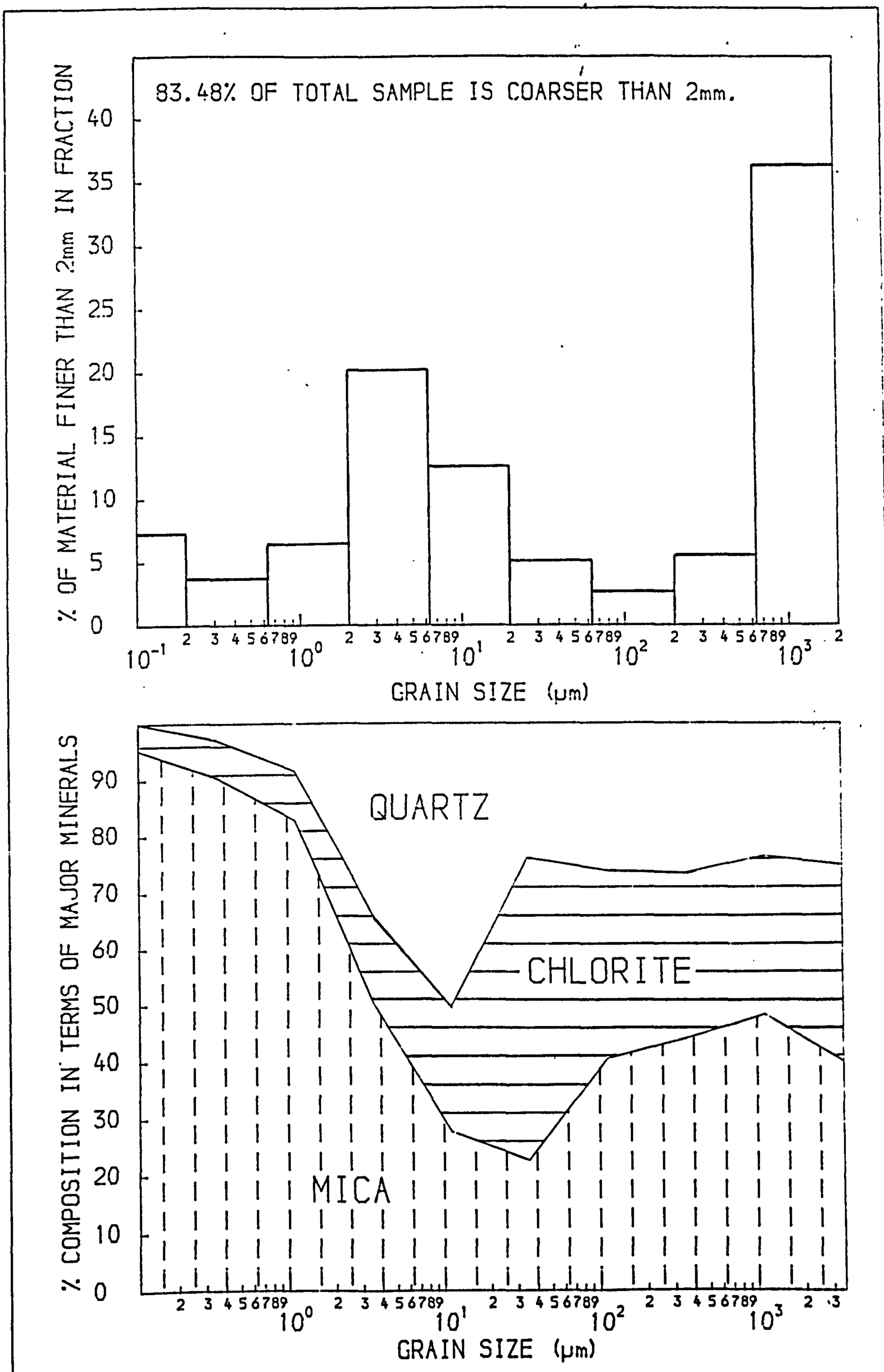


FIGURE 6.6. QUANTITATIVE MINERALOGICAL COMPOSITION AND PARTICLE SIZE DISTRIBUTION OF SAMPLE 1080, FOLLOWING TREATMENT WITH SODIUM DITHIONITE

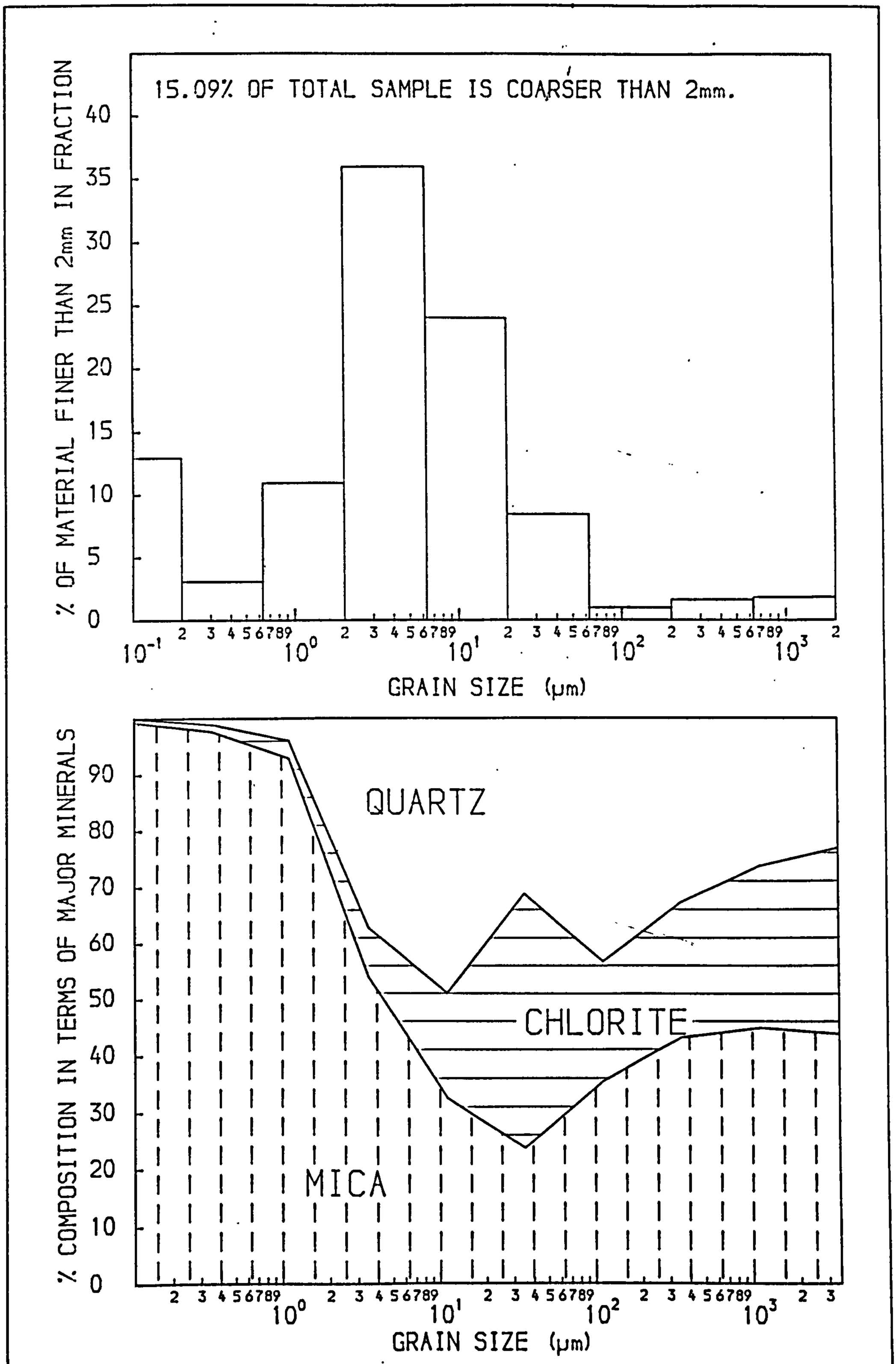


FIGURE 6.7. QUANTITATIVE MINERALOGICAL COMPOSITION AND PARTICLE SIZE DISTRIBUTION OF SAMPLE 1079, FOLLOWING TREATMENT WITH SODIUM DITHIONITE

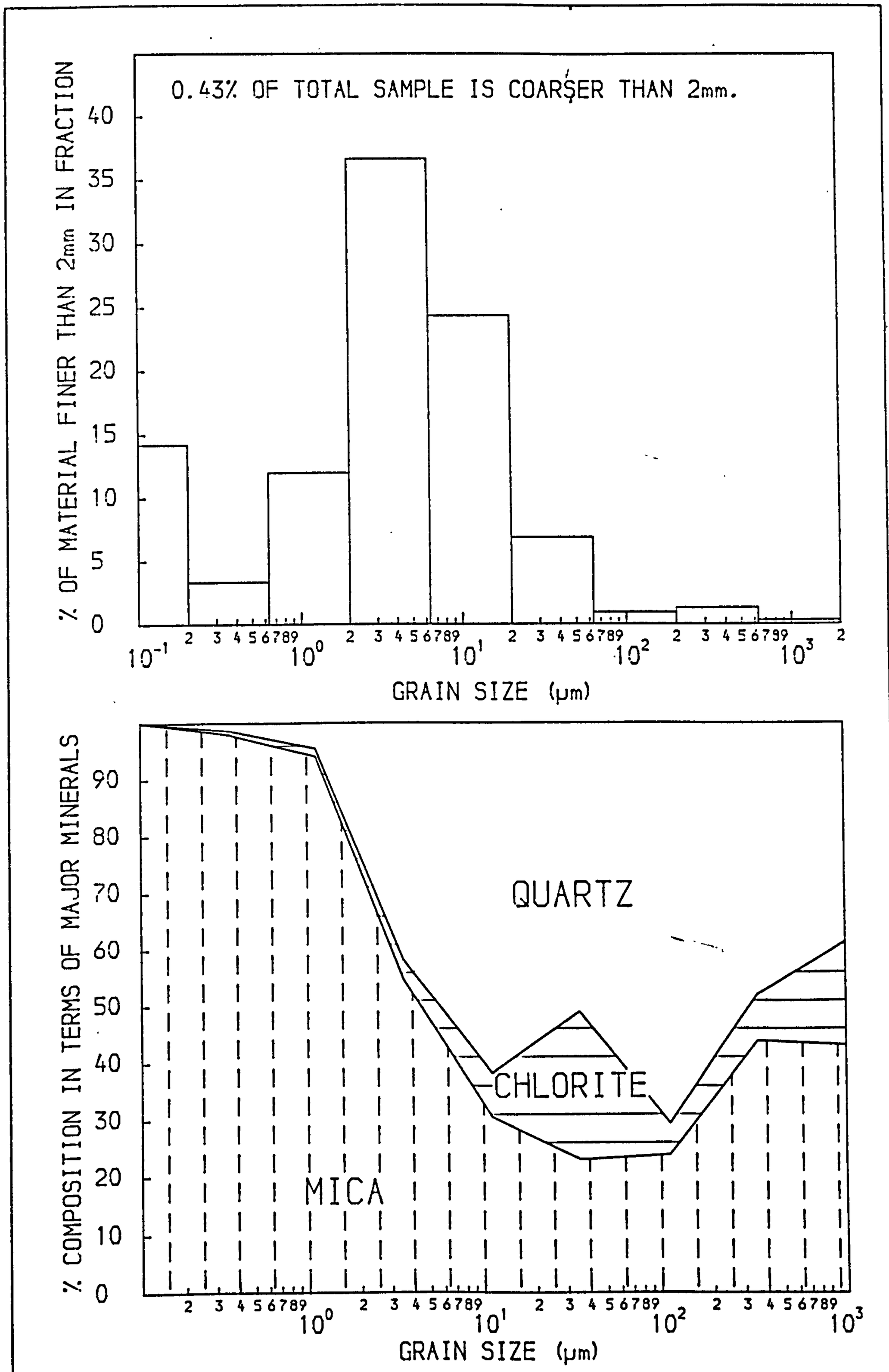


FIGURE 6.8. QUANTITATIVE MINERALOGICAL COMPOSITION AND PARTICLE SIZE DISTRIBUTION OF SAMPLE 1078, FOLLOWING TREATMENT WITH SODIUM DITHIONITE

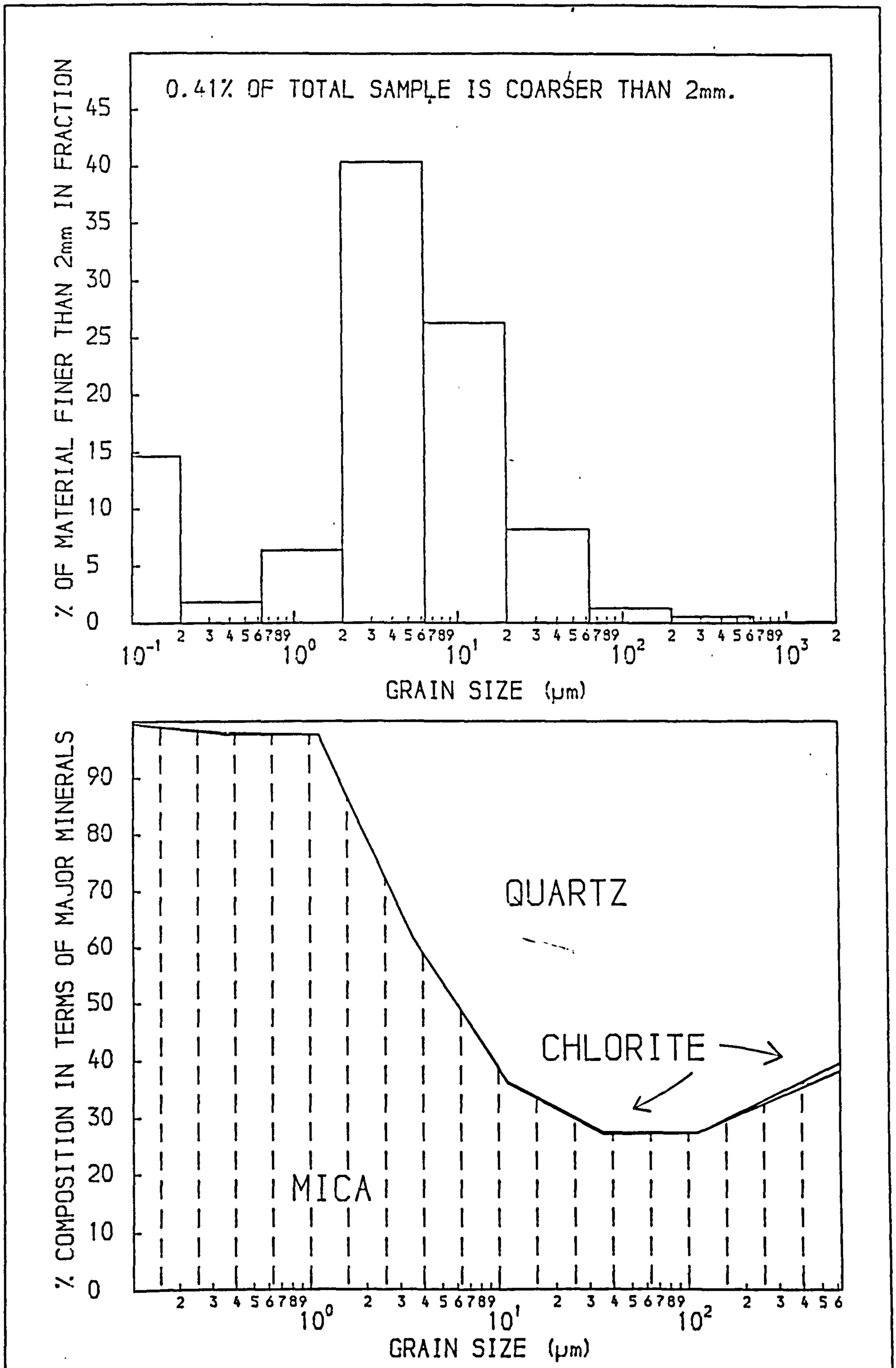


FIGURE 6.9. QUANTITATIVE MINERALOGICAL COMPOSITION AND PARTICLE SIZE DISTRIBUTION OF SAMPLE 1077, FOLLOWING TREATMENT WITH SODIUM DITHIONITE

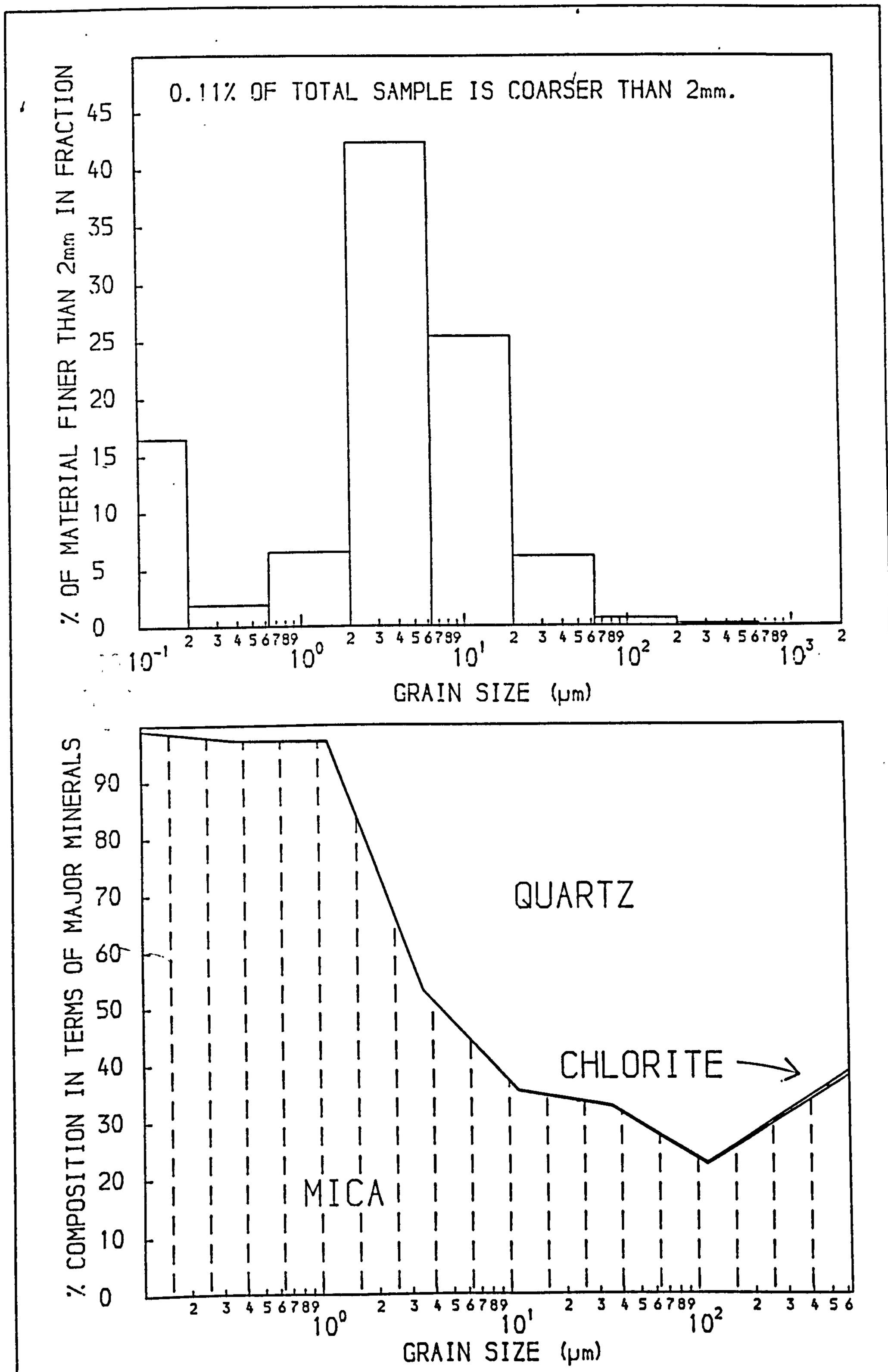


FIGURE 6.10. QUANTITATIVE MINERALOGICAL COMPOSITION AND PARTICLE SIZE DISTRIBUTION OF SAMPLE 1076, FOLLOWING TREATMENT WITH SODIUM DITHIONITE

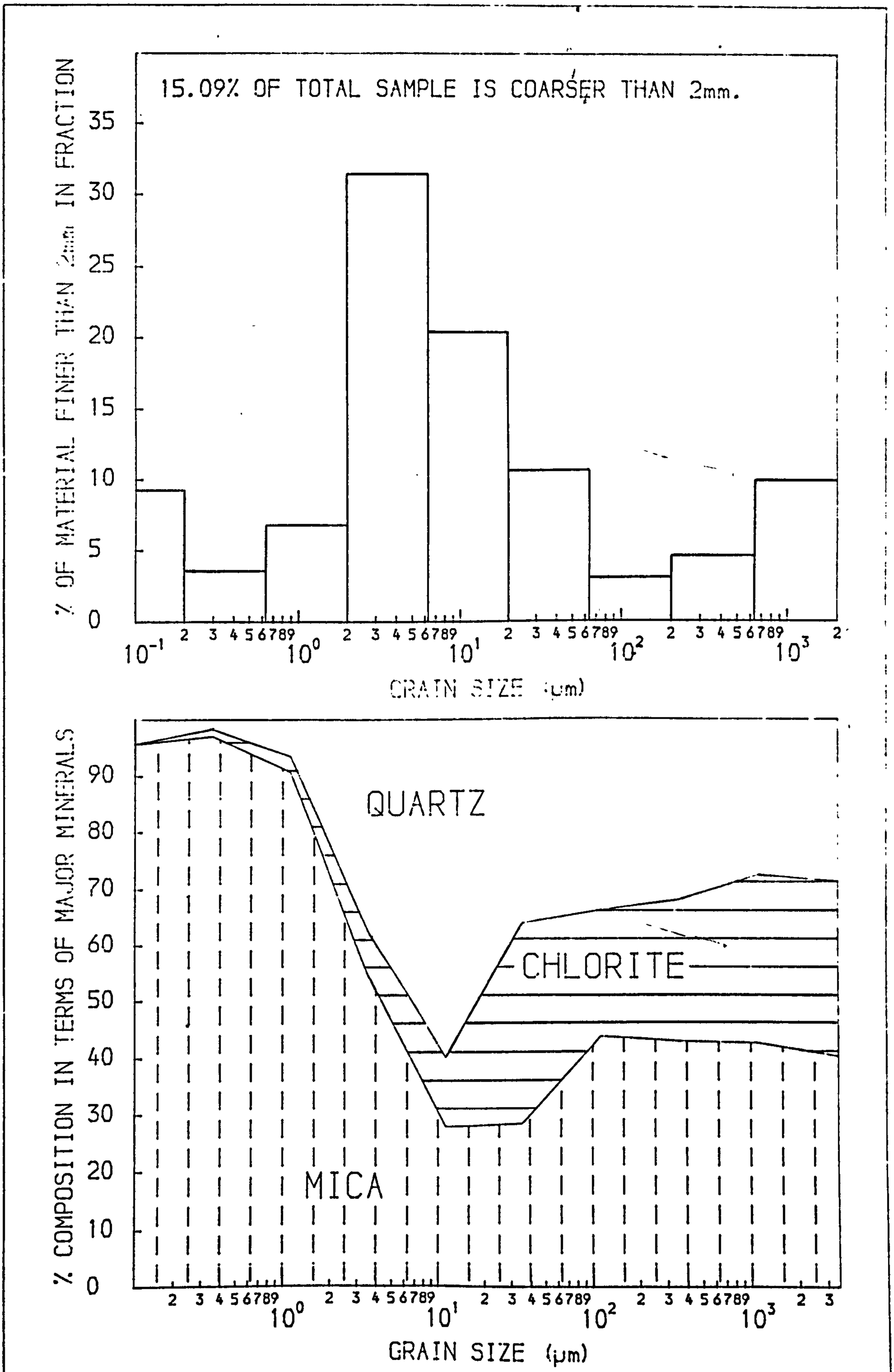


FIGURE 6.11 QUANTITATIVE MINERALOGICAL COMPOSITION AND PARTICLE SIZE DISTRIBUTION OF SAMPLE 1079.

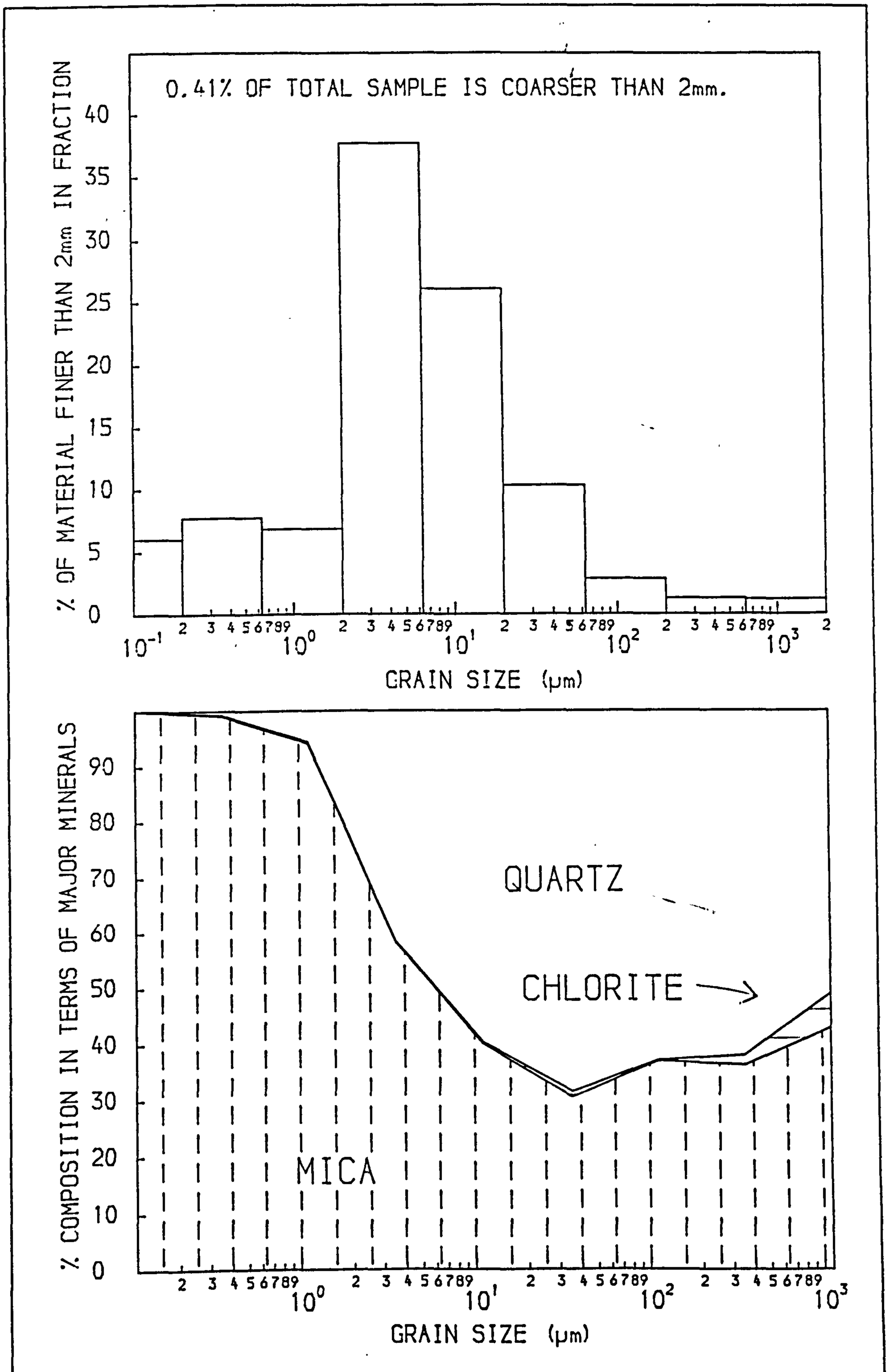


FIGURE 6.12. QUANTITATIVE MINERALOGICAL COMPOSITION AND PARTICLE SIZE DISTRIBUTION OF SAMPLE 1077.

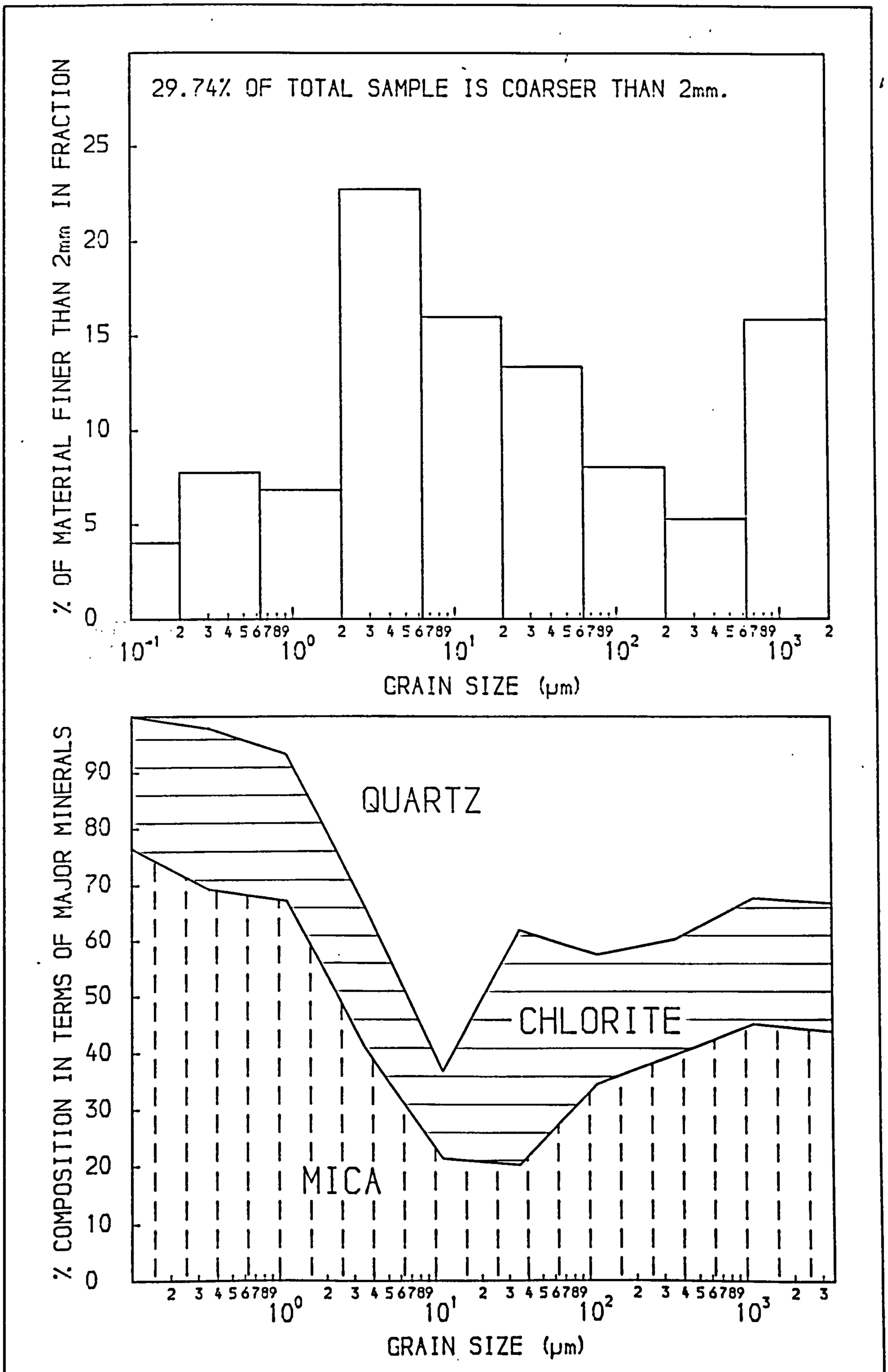


FIGURE 6.13. QUANTITATIVE MINERALOGICAL COMPOSITION AND PARTICLE SIZE DISTRIBUTION OF SAMPLE 1087.

Firstly, dithionite treatment can be seen to reduce the average particle size. If the data for 1079 and 1077 are compared with the results for 1079D and 1077D, it can be seen that the proportions of all the fractions coarser than 20μm are reduced after dithionite treatment, the greatest reduction being seen in the coarsest size fraction. As a result of this relative decrease in coarser material, the fractions finer than 20μm make up a larger proportion of the sample after treatment. This behaviour is most simply explained by the hypothesis that some of the coarse particles in the untreated samples consist of finer grains cemented together by Fe and Al oxyhydroxides. These multiple grains are not broken down by the separation procedure, but the oxyhydroxides are dissolved by the dithionite treatment, breaking up the coarse multiple grains into individual finer grains, and thus affecting the particle size distribution. If this is the true explanation, then the distribution given by the dithionite treated samples is closer to the ultimate particle size distribution than that provided by the untreated samples, but it is difficult to predict which distribution most closely reflects the distribution seen by the weathering agents acting in the soil. This would depend on both the physical properties of the oxyhydroxide cement, such as porosity and permeability, and on the chemical properties of the soil which, if a complexing agent were present, could lead to dissolution of the oxyhydroxide and breakdown of the multiple grains.

Although most of the fractions finer than 20μm are relatively increased after dithionite treatment, both 1079D and 1077D show a reduction in the 0.2-0.63μm fraction, and 1077D, which shows the largest reduction, also shows a reduction in the 0.63-2μm fraction. This cannot be explained by the hypothesis used for the coarser than 20μm fractions, nor by preferential dissolution of chlorite by dithionite, as there is negligible chlorite in the finer than 2μm fractions of these samples, even before dithionite treatment. The only likely explanation is that dithionite treatment is causing the breakup of fine grained single crystal illites, which already have frayed edges due to weathering [214]. This hypothesis is supported by the fact that illite is the dominant mineral in the 0.2-0.63μm fraction, and that the illites in this fraction in 1077 are more weathered and less well crystallised than those in the same fraction of 1079 (see Section 8.3), and are thus more likely to have frayed edges for the dithionite to act upon. Evidence for this action is given in Section 7.1.2.

A second conclusion that can be drawn is that particle size decreases upwards in the profile, suggesting that weathering reduces particle size. It is the two coarsest fractions of the dithionite treated material, as well as the coarser than 2mm particles, that show the most dramatic and consistent reduction from the BC horizon through to the Ea1 horizon, whilst the 0.063-0.2μm and the 2-6.3μm fractions show a complementary increase. Contrary to expectations, the 0.2-0.63μm and 0.63-2μm fractions do not show a consistent increase towards the top of the profile, although two explanations are possible for the maximum content of the 0.63-2μm fraction in the Bsg horizon. It may be that 0.2-2μm illite is being translocated down the profile from the Ea1 and Ea2 horizons to the Bsg horizon, or else it is possible that the more intensive weathering experienced in the two upper horizons is causing the breakup of fine grained single crystal illites.

The first of these possibilities has never before been suggested to occur in a podsol profile, and thus, if it were proved to be the correct explanation, it would be a striking conclusion, requiring revision of pedogenetic theories to allow the translocation of phyllosilicates between different horizons to take place during podsol genesis. However, other evidence in this study, such as the illite crystallinity values of the finer than 2μm fractions (see Section 8.3) and the relationship between the contents of silt, fine clay and coarse clay described in the next section, favours this explanation. Conclusive proof or disproof of the translocation of phyllosilicates in this soil profile could only be provided by a detailed micromorphological study, which would be expected to show the development of argillans if clay translocation had taken place, whereas it is normally believed that the only translocation taking place in podsols is that of Fe and Al complexed by organic matter.

6.2.5 Breakdown of Shale Particles

Following Stewart et al [244], linear regression equations were calculated for silt and clay on coarse material, and clay on silt, for the data from the dithionite treated samples (Table 6.4). These indicate that both silt and fine clay increase up the profile, whilst the coarse and total clay reach maxima in the Bsg horizon. Whereas Stewart et al found that the coarse material broke down to produce 59% silt and 41% clay, the data from this profile show 72% silt and 28% clay to be produced, indicating that the parent material is coarser than at Cwmcadian. The regression equations are:

Silt = -0.722(Coarse Material) + 71.3, R = -0.995,
Clay = -0.278(Coarse Material) + 28.7, R = -0.969, and
Clay = 0.373(Silt) + 1.9, R = 0.941,

showing higher correlation coefficients than the data of Stewart et al, and also a lower intercept value for the regression of clay on silt. This would suggest that the profile has suffered negligible contamination by foreign material, and that on weathering the shale releases silt and clay in a fixed ratio, with little weathering of silt to clay or translocation of clay. The correlation coefficient for the regression of clay on silt is significant with more than 95% confidence, whilst the other two correlation coefficients are significant with more than 99% confidence.

Table 6.4 Particle Size Distributions of Dithionite Treated Samples

| Sample | 1080D | 1079D | 1078D | 1077D | 1076D |
|---|---|---|---|---|---|
| Horizon | BCd | Bsd | Bsgd | Ea2d | Ea1d |
| % Coarse Material (>20μm) | 91.68 | 26.07 | 9.79 | 10.60 | 7.26 |
| % Silt (2-20μm) | 5.43 | 50.97 | 60.76 | 66.53 | 67.73 |
| % Clay (0.063-2μm) | 2.89 | 22.96 | 29.45 | 22.88 | 25.01 |
| % Coarse Clay (0.2-2μm) | 1.68 | 11.95 | 15.28 | 8.24 | 8.50 |
| % Fine Clay (0.063-0.2μm) | 1.21 | 11.01 | 14.17 | 14.64 | 16.51 |

However, if the data are considered in more detail, a different picture emerges. If the clay is subdivided into coarse and fine fractions, and these are regressed on silt, the correlation coefficient for the regression of fine clay on silt is seen to be higher, and significant with more than 99% confidence, and the intercept lower, than for total clay on silt. On the other hand, only a low correlation coefficient is seen for the regression of coarse clay on silt, and this is not significant:

Fine Clay = 0.233(Silt) - 0.2, R = 0.994, and
Coarse Clay = 0.139(Silt) + 2.1, R = 0.714.

In view of the fact that the fine clay correlates very well with silt, but the coarse clay does not, and also that, relative to silt and fine clay, the coarse clay is reduced in the Ea1 and Ea2 horizons but

increased in the Bsg horizon, it would appear that the data are only consistent with the translocation of 0.2-2μm particles from the Ea1 and Ea2 horizons to the Bsg horizon. If the reduction in coarse clay particles in the Ea1 and Ea2 horizons was due to breakdown of these particles into finer material, without translocation, as was suggested as an alternative possibility in the previous section, an excess of fine clay relative to silt would be expected in the Ea1 and Ea2 horizons, which is not found, whilst the excess of coarse clay found in the Bsg horizon would not be expected.

Table 6.5 Mean Particle Size of Material Finer than 2mm

| Sample | Mean Particle Size (μm) |
|---|---|
| 1040 | 8.3 |
| 1029 | 58.9 |
| 1039 | 32.2 |
| 1049 | 16.5 |
| 1080D | 19.6 |
| 1079D | 4.7 |
| 1078D | 4.4 |
| 1077D | 4.9 |
| 1076D | 4.5 |
| 1079 | 6.1 |
| 1077 | 5.4 |
| 1087 | 13.7 |

Assuming a uniform distribution of weight with grain size within each fraction, a mean particle size can be calculated for the finer than 2mm materials. These figures are given in Table 6.5, and clearly show the particle size reduction caused by dithionite treatment. The mean particle sizes the dithionite treated soil horizo except BCd/1080D, are very similar. figures in Table 6.5 show more clearly than those in Table 6.3 the differences in particle size between the boulder clays, indicating that 1049 is finer than the soil BCd/1080D horizon. Cg/1087 has a mean particle size most similar to that of 1049. If a correlation is carried out between the proportion in each size fraction and the proportion in the same size fraction for each of the Plynlimon samples, the best correlation coefficient, of 0.82, is also found with 1049. This suggests that the parent material of the Hiraethog comparison profile is most likely to be a boulder clay with properties similar to those of 1049.

Both the particle size distribution and the mean particle size of the crushed rock, 1040, indicate that it is qualitatively different from any of the other samples, and this is presumably due to the effects of grinding. Almost all of the particles coarser than 63μm have been broken down, yet there is less material finer than 2μm than in any of the other samples, which suggests that mechanical action is not

sufficient to bring about complete disaggregation, and that the chemical activity seen in weathering is needed to produce the finest particles in significant quantity.

### 6.2.6 Particle Size Distribution by the Bouyoucos Method

In an attempt to confirm the particle size distributions obtained by the method described above, determinations using the Bouyoucos hydrometer were carried out on the samples that were not treated with dithionite. The Bouyoucos method covers the range from 2 to 50μm, besides giving figures for the total material coarser than 50μm or finer than 2μm. The results are given in Table 6.6, where comparison is made with the results from Table 6.3, recalculated into the fractions obtained from the Bouyoucos data. The assumption that there is a uniform distribution of weight with grain size within each fraction is again used.

Table 6.6 Comparison of Two Methods of Particle Size Analysis

| Sample | Analysis | % >50μm | % 20-50μm | % 6.3-20μm | % 2-6.3μm | % <2μm |
|---|---|---|---|---|---|---|
| 1040 | Bouyoucos | 11.98 | 19.07 | 20.07 | 13.05 | 35.83 |
| 1040 | Table 6.3 | 9.63 | 20.52 | 23.34 | 35.34 | 11.17 |
| 1029 | Bouyoucos | 45.10 | 6.02 | 10.04 | 8.03 | 30.81 |
| 1029 | Table 6.3 | 51.64 | 6.95 | 10.02 | 15.71 | 15.68 |
| 1039 | Bouyoucos | 34.86 | 7.05 | 13.09 | 11.07 | 33.93 |
| 1039 | Table 6.3 | 44.18 | 9.50 | 13.49 | 9.59 | 23.24 |
| 1049 | Bouyoucos | 34.46 | 6.05 | 12.10 | 10.08 | 37.31 |
| 1049 | Table 6.3 | 41.06 | 5.71 | 12.49 | 20.54 | 20.20 |
| 1079 | Bouyoucos | 16.09 | 12.28 | 16.37 | 12.28 | 42.98 |
| 1079 | Table 6.3 | 20.61 | 7.84 | 20.39 | 31.48 | 19.68 |
| 1077 | Bouyoucos | 15.15 | 9.20 | 17.38 | 15.33 | 42.94 |
| 1077 | Table 6.3 | 8.04 | 7.55 | 26.09 | 37.72 | 20.60 |
| 1087 | Bouyoucos | 31.57 | 10.06 | 14.09 | 8.05 | 36.23 |
| 1087 | Table 6.3 | 32.86 | 9.78 | 16.01 | 22.73 | 18.62 |

This table shows considerable discordance between the methods with, in every case, the Bouyoucos determination giving a much higher content of the finer than 2μm material, in all but one sample accompanied by a lower content of the 2-6.3μm fraction. On the other hand, the 6.3-20μm

and 20-50μm fractions are in general agreement between the two methods; the mean differences, calculated from the Bouyoucos results, are only 16% for the 6.3-20μm fractions and 17% for the 20-50μm fractions, whereas the mean difference for the 2-6.3μm fractions is 124%. These differences are not explicable, unless the cup dispersing machine used as a part of the Bouyoucos method has a disintegrating effect on the 2-6.3μm fractions which is not brought about by the ultrasonic dispersion used in the main analytical scheme.

## 6.3 QUANTITATIVE MINERALOGICAL ANALYSIS BY X-RAY DIFFRACTION

The intensity of a particular XRD peak is obviously related to the proportion of the component causing that peak, and thus the development of quantitative methods for analysis of mixtures using XRD began as early as 1936. These methods have been continuously refined, but the derivation of quantitative data from XRD of mixtures is still not usually simple as, in general, the relationship between the proportion of a component in a mixture and the intensity of its XRD peaks in the diffraction pattern generated by that mixture is not linear.

This nonlinearity is caused by the fact that minerals have different mass attenuation coefficients for X-rays, resulting in each component of a mixture having a different mass attenuation coefficient, unless two components have the same chemical composition. This would occur if, for example, anatase and rutile, polymorphs of $TiO_2$, were both present. The relationship between the intensity, $I_i^\circ$, of an (hkl) peak of a pure mineral and the intensity, $I_i$, of the same peak when that mineral occurs as a weight fraction, $X_i$, of a mixture is:

$$X_i = \frac{I_i \, \mu_m}{I_i^\circ \, \mu_i}, \text{ where} \qquad (14)$$

$\mu_m$ = mass attenuation coefficient of the mixture, and
$\mu_i$ = mass attenuation coefficient of pure component i [148].

The nonlinearity is introduced because $\mu_m$ is dependent on $X_i$.

It is thus possible to determine the percentage of a component in a mixture by measuring the mass attenuation coefficients of both the pure mineral and the mixture [160,196], which can be carried out by inserting the specimens in turn into the X-ray beam and measuring the reduction in intensity of the beam after its passage through the

specimen. However, this measurement requires a monochromatic X-ray beam, as although filtering greatly reduces the intensity of Kβ radiation relative to Kα, a considerable amount of background radiation is transmitted by the β filter [39]. As no crystal monochromator was available, this method could not be employed.

Most other methods of determining the proportion of a component which gives rise to a particular diffracted intensity involve the use of standards, with which peak intensities can be compared. These may either be composed of known mixtures of the components that are present in the unknown mixture [191,232], or else may consist of the unknown mixture to which a known quantity of standard has been added [3,103, 121,148,150,183,199]. One of the components of the unknown mixture may be added as the standard.

No matter what other components are present, the ratio of the diffracted intensities of two components is proportional to the ratio of the concentrations of those components [58-60,69,185]. This ratio can be determined for mixtures of one component separately with each of the other components, by making up a series of two component mixtures of known composition. The composition of the unknown mixture can then be determined by using the ratios of diffracted intensities from the unknown mixture and the constants of proportionality determined from the mixtures of pairs of components. This method is effective as long as the components of the unknown mixture can be separated to make the known two component mixtures, and there are no noncrystalline or indeterminate minerals present, provisos that apply to many other methods.

Applying this result to the use of an internal standard, a known weight of standard can be added to a given weight of an unknown mixture. If two component mixtures of the standard with each of the components of interest from the unknown mixture are then analysed, the amounts of the minerals of interest can be determined, whether or not noncrystalline or unanalysed components are present, because the amount of the standard added is known.

It is possible to analyse a mixture without the use of standards, if it can be divided in such a way that its parts each have different ratios of the minerals of the original mixture. It is also necessary for a sufficient number of subdivisions to be made to enable the solution of

the series of simultaneous equations generated from the intensities of the diffraction peaks of the minerals in each of the parts taken together with the weights of those parts [228]. Division of the mixture is commonly carried out by size or density fractionation.

### 6.3.1 Chung's Method for Quantitative X-ray Diffraction Analysis

The method of XRD analysis chosen for use had to be one that did not require the addition of standards to the specimens for analysis, some of which were required for further study, due to the small amounts of particular size fractions obtained after particle size separation. As it was impossible to measure the mass attenuation coefficients, it might have seemed that a method based on subdividing the initial specimen and analysing both the original material and the subdivided fractions [228] would be ideal for use in this study, where the samples were quantitatively divided into different size fractions, to investigate the mineralogical variations between those fractions.

However, where mass attenuation coefficients were not measured, this method gave 50% errors in the estimated concentration of a component present at a level of 25% in an artificial three component mixture, even when the concentrations of the components in the subdivided fractions changed by 20% to 30% of their levels in the initial mixture [228]. In this study it was known that fractionation of the samples would be unlikely to bring about mineral concentration changes of this magnitude, particularly amongst the coarser fractions, and additional density separation was not practical because of the large number of specimens. In any case, chlorite and quartz were likely to be present at concentrations much below 25% in some specimens, and thus the combination of these factors would be likely to lead to unacceptably high levels of error in the estimation of component concentrations. For these reasons, the method of Chung [58,59] was chosen, a method using external standards which required only one standard to be made for each mineral of interest, no matter what the composition of the unknown specimen.

In general, equation (14) presents the problem that the mass attenuation coefficients of both the pure components of interest and the unknown mixture have to be determined to carry out quantitative analysis. The usual procedure to avoid these determinations has been to add internal standards to each unknown mixture, and to construct calibration curves from mixtures of the standard separately with each

of the phases of interest [3]. However, if the mass attenuation coefficients could be eliminated from equation (14), the procedure for quantitative X-ray analysis of mixtures would become much simpler, and this was the approach taken by Chung [58].

It was initially shown that, by adding a known quantity of a flushing agent, not present in the sample, and determining the intensities of the flushing agent and the components of interest both in the sample and in 1:1 reference intensity mixtures with corundum, the concentrations of the unknowns could be determined without the need for a calibration curve. Once the reference intensity of the flushing agent has been determined, only one reference intensity standard is required for each component of interest. In fact, if all the crystalline components are determined by this method, it is possible to quantify the noncrystalline material. It can be shown that equation (15) holds for the relationship between any two components of the mixture, not just between the flushing agent and one of the unknown components, thus:

$$X_i = \frac{X_f I_i k_f}{I_f k_i}, \text{ where} \quad \ldots\ldots(15)$$

$X_f$ = weight fraction of the flushing agent,
$k_f$ = reference intensity ratio of the flushing agent,
$I_f$ = intensity of X-rays diffracted by the (hkl) plane of the flushing agent in the mixture, and
$k_i$ = reference intensity ratio of component i.

The only distinction between the flushing agent and the other components is that its concentration is known.

Unless the concentration of one of the components is known, equation (15) can only be solved in terms of a ratio of the concentrations of two components, rather than in absolute terms. However, if the mixture is of two components, the equation can be solved in absolute terms, as the sum of the weight fractions must equal one. In fact:

$$X = \frac{1}{1 + \frac{k_i I_j}{I_i k_j}}, \quad \ldots\ldots(16)$$

where the variables with j subscripts have the same meaning for the second component as those with i subscripts have for the first. Thus, for the analysis of a binary mixture, no flushing agent is required; only the reference intensities and the intensities in the mixture of the two components need to be known for complete solution.

In a subsequent paper [59], Chung extends this analysis to n component mixtures, showing that there are n-1 independent equations of a form similar to that of equation (15), each relating the concentration of the first component of the mixture to that of one of the other components. If no components of the mixture are noncrystalline or remain unanalysed, a normalisation equation of the form:

$$\sum_{i=1}^{n} X_i = 1 \qquad (17)$$

will allow simultanteous solution of the equations, to give a result corresponding to equation (16) for binary mixtures:

$$X_i = \frac{1}{1 + \sum_{j=1}^{n} \frac{k_i I_j}{I_i k_j}} \qquad (18)$$

As a result, no flushing agent is required to be added to an n component mixture to obtain a quantitative analysis. Instead, besides the intensities of the components as present in the mixture, all that is required is the determination of the reference intensity ratio for each component, which Chung shows in a further paper [60] needs only one combined standard, although separate standards were used in this study.

As the derivation of this quantitative solution for the analysis of mixtures does not rely on the use of particular diffraction lines, any line that is free from interference can be chosen for intensity measurement, provided only that it is the intensity of this line that is used in the derivation of the reference intensity ratio. Opportunity has been taken in this study to use the (100) quartz line at 20.8°2$\theta$ instead of the stronger (101) line at 26.7°2$\theta$, as the latter is rarely distinguishable from the intense mica (006) and (024) lines

at 26.6°2$\theta$. Similarly, in the determination of all the reference intensity ratios, the corundum (113) line at 43.4°2$\theta$ has been used in preference to the (102) and (104) lines at 25.5 and 35.1°2$\theta$, as these respectively suffer from interference from the strong chlorite (004) line at 25.3°2$\theta$ and strong mica ($13\bar{1}$), (116), ($20\bar{2}$) and (008) lines between 34.7 and 35.7°2$\theta$.

The other advantages claimed for this method, besides those of freedom from the need for internal standards and calibration curves, are:

1. No information is required about the approximate concentration of the components of interest, and

2. All the intensity information is obtained from a single diffractometer scan, greatly reducing errors due to instrumental drift and sample preparation.

It is pointed out that, in order to attain high precision and accuracy in the analysis, the reference materials must have the same levels of crystallinity as the relevant components of the mixture, and that the sample must be both thoroughly ground to ensure optimum particle size and homogeneity, and loaded as a powder to avoid any preferred orientation [58].

## 6.4 EXPERIMENTAL TECHNIQUES

Although results of previous work had indicated that specimens sedimented onto glass slides were unsuitable for quantitative XRD analysis, because of the effects of preferred orientation and differential settling on phyllosilicate diffraction intensities [15,68, 102,104], it was felt that an investigation should be carried out to determine whether glass slide mounts could be used in this study, as their use would enable analysis to be carried out with much smaller specimens than would be necessary for random powder mounts. Specimens sedimented onto glass slides had to be prepared to investigate qualitative variations in mineralogy (Section 7.1), and thus specimen preparation would have been considerably reduced if the same slides could have been used for quantitative analysis. If the reference intensities were also determined from specimens sedimented onto glass slides, there was no obvious reason why preferred orientation should be a disadvantage to the analytical accuracy, provided that the degree of preferred orientation remained constant for each mineral.

In order to investigate the analytical accuracy of specimens sedimented onto glass slides, two component mixtures of mica, collected either from Trefriw or Parys Mountain, and vein quartz, collected from Penrhyn Quarry, Bethesda, were prepared, and 96.4 ± 1.4mg of each mixture were dispersed in a minimum quantity of water and sedimented onto a 48 x 27mm glass slide, giving a specimen thickness of about 29μm. A technique was devised to obtain an XRD analysis from the base of the sedimented specimen, as well as from its top surface, to investigate the effects of differential settling (Figure 6.14). Once the specimen had dried, X-ray analysis of the top surface was carried out. After this, the specimen was inverted onto a second glass slide, which had been covered with double-sided Sellotape. Slight pressure, to ensure adhesion of the mineral film to the tape, followed by a shearing movement of the slides away from one another led, in every case, to a clean transfer of the entire mineral film from one slide to the other, with the surface finally exposed being originally at the base. It was thus possible to obtain an XRD analysis from the base of the specimen as originally sedimented.

Semiquantitative analysis of both surfaces of these specimens was carried out, using the random powder standards made up for quantitative analysis. For the specimens containing Trefriw mica, the results indicated that the surface of the mineral film was enriched in quartz, whereas the base showed an enrichment in mica. The average error in the determination of the quartz content was 7% if the means of the two determinations were employed. However, for the specimens containing Parys Mountain mica, differential settling was much more noticeable, and was complicated by the increase in intensity of the mica peak relative to quartz in the glass slides, when compared with the random powder standards. This resulted in the data from both surface and basal analyses indicating an enrichment of mica above that known to occur, with the surface enrichment appearing to be much greater than at the base. This led to an average error of 54% in the determination of the quartz content if the means of the two determinations were used.

It appears that the Trefriw mica particles sediment more rapidly than the powdered vein quartz, whereas the Parys Mountain mica particles sediment less rapidly. This difference is likely to be due to a combination of both particle size and shape and compositional effects, and as both of these were likely to vary between the specimens on which quantitative analysis was being carried out, it was concluded that

**Figure 6.14** A Procedure to Enable X-ray Diffraction Analyses to be Carried Out on Both the Surface and the Base of Specimens Sedimented on to Glass Slides

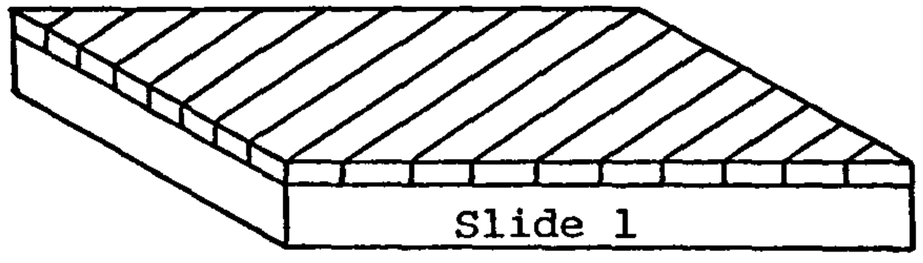


A) Specimen prepared in usual manner. XRD analysis carried out.

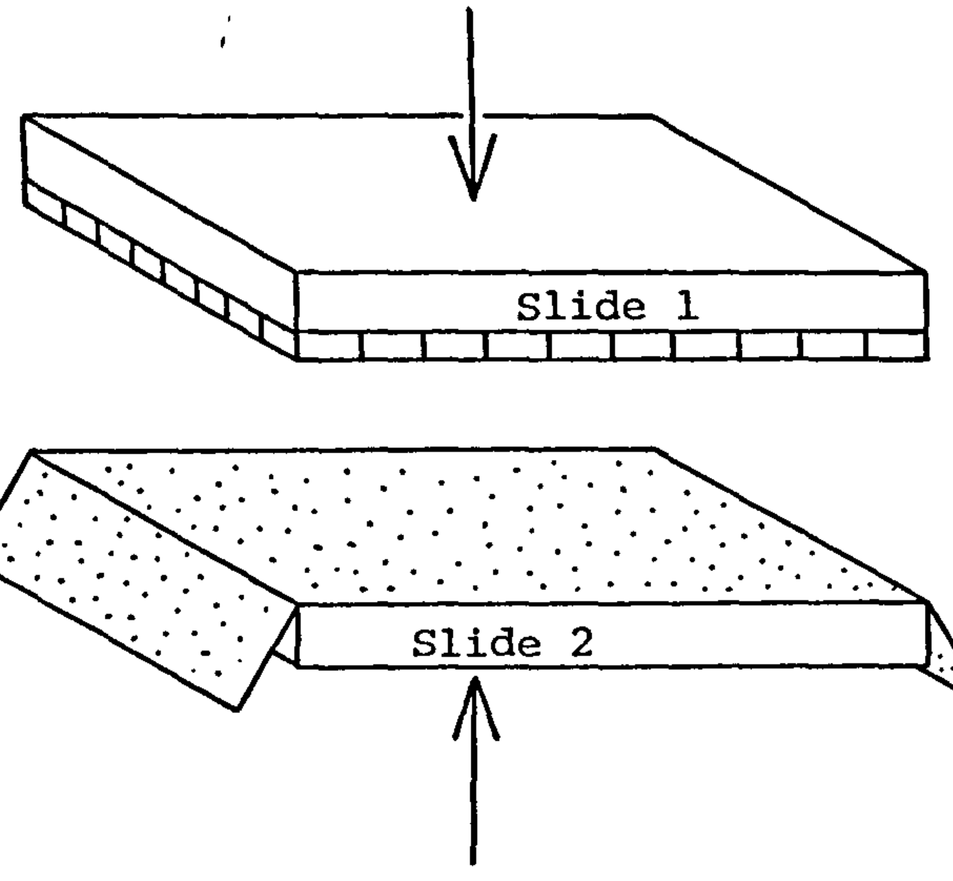


B) Slide holding specimen inverted on to 2nd slide, previously covered with double sided Sellotape. Pressure applied to ensure adhesion.

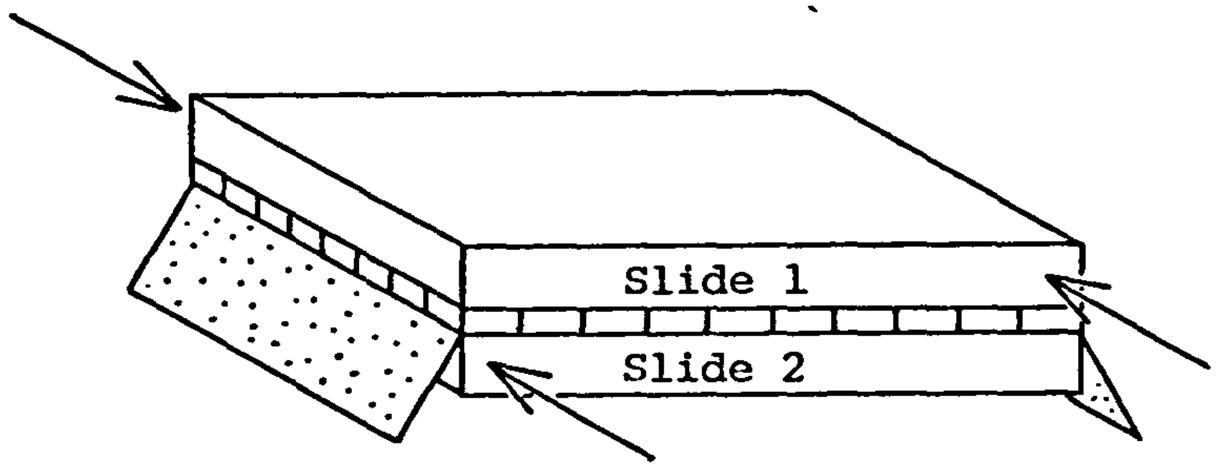


C) Shearing apart of slides.

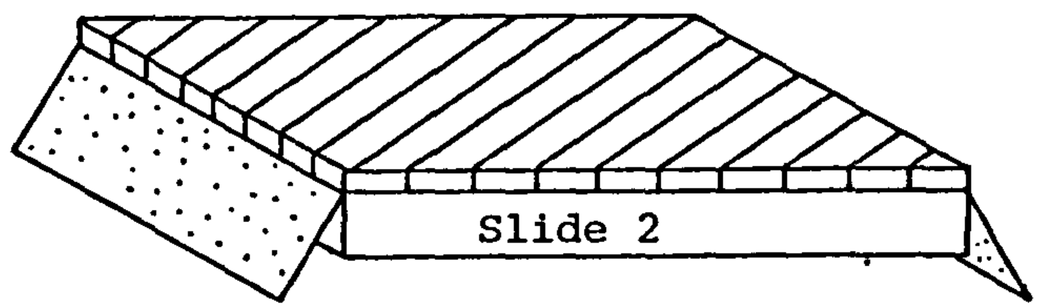


D) Adhesion of clay film to tape exposes original base of specimen. XRD analysis carried out.

glass slide specimens could not be used. Little success was achieved in preparing specimens by the use of pressure onto ceramic tiles [15], and thus it was decided that random powder mounts should be used for all quantitative analyses.

It is clear from the literature [58,103,191,199] that in the ideal case it is essential to use a standard that has the same crystallinity, as well as the same composition, as the mineral in the specimen being analysed. If peak height is used as a measure of diffracted intensity, the consequences of peak broadening and loss of peak height due to reduced crystallinity will result in minerals that are better crystallised than the standard being overestimated [191]. This problem can be at least partly overcome if peak areas are measured, but because of the difficulty in obtaining standards that are crystallographically identical to the unknown minerals, it is often recommended that the standards should be extracted from the samples to be analysed [103]. In any event, this is a difficult process to carry out, and as the effect of different size fractions giving rise to different diffracted intensities, even if they have the same crystallinity [39,103,191] is not eliminated, it would be necessary to extract standards from every size fraction.

For substances that crystallise with high structural perfection, such as quartz, diffracted intensity decreases when crystallite size exceeds 15μm, due to primary extinction, whilst line broadening and peak height reduction begin to occur for particles finer than 0.1μm [39,148]. It has been found that, even for random powder samples, the degree of preferred orientation of mica increases with size, resulting in a recommendation that, for quantitative analysis, particle size should be less than 4μm [180]. On the other hand, it is recommended that quartz particles should not be finer than 5μm, as for such particles a reduction in diffracted intensity is caused by the development of a disordered or noncrystalline surface layer [39,148]. Diffracted intensity can only be restored by solution of the surface layers in HF. Other coatings, particularly of noncrystalline Fe oxyhydroxides, can have very considerable effects on diffracted intensity, as they have linear attenuation coefficients for X-rays up to 20 times those of phyllosilicates. As different types and thicknesses of coating can occur on the surfaces of different minerals in the same specimen, it is considered essential that these coatings are removed by treatment with dithionite before any quantitative XRD analysis is carried out [103].

Once the choice of random powder mounts had been made, only the experimental conditions and standard minerals remained to be decided before quantitative analysis could be carried out. The specimens were prepared from material that had been lightly crushed by means of a small agate pestle and mortar, and were pressed into an Al sample holder held firmly in position against a glass sheet, in order to produce a flat surface on the powder sample. The particle size of the specimens was not determined, but differences in the appearance of 6.3-20μm material before and after crushing suggested that no particles in the specimens were coarser than 6.3μm.

To reduce the effect of background variability on the diffractometer trace, it would have been ideal to use the slowest scan rate, $0.125°2\theta\,min^{-1}$, with the appropriate time constant of 16 seconds. However, paper speeds on the chart recorder were not compatible with this scan rate in such a way as to provide a chart on which $1°2\theta$ was represented by 10mm. As a result, a scan rate of $0.25°2\theta min^{-1}$ and a time constant of eight seconds were used, with a chart speed of 150mm $hr^{-1}$. Ni filtered $Cu_{K\alpha}$ radiation was used at a tube voltage of 40kV and current of 20mA; the divergence and scatter slits were set at 1°, and the receiving slit at 0.1mm. These conditions were used for all XRD analyses except where stated otherwise. A chart fsd between 400 and 4000cps was chosen as appropriate. Each specimen was scanned between 4 and $23°2\theta$.

Using a 1° divergence slit causes part of the incident X-ray beam to fall beyond the ends of the 20mm long specimens for angles lower than $17.1°2\theta$ [230], but the 0.5° slit required to ensure that the whole beam falls on the specimen down to an angle of $8.8°2\theta$, the smallest angle at which quantitative measurement was carried out, would have considerably reduced peak intensities. For absolute intensity measurements, correction factors have been suggested to allow for the proportion of the beam falling off the specimen [230], but these have been criticised on the grounds that the distribution of intensity across the beam is not uniform [45]. However, in studies where concentrations are determined by measurement of intensities relative to known standards [103], as is the case here, provided that the specimens and standards are of equal size and are mounted in identical positions relative to the beam, no error is introduced into the calculated concentrations, as the determined reference intensities are appropriate for use with the proportion of the incident beam that actually falls on the specimen.

### 6.4.1 Mineralogical Assumptions Made

When the analyses were carried out on the samples listed in Table 6.7, the assumption was made that the specimens consisted only of mica, chlorite and quartz, with no noncrystalline material or other crystalline phases. Provided that any material with a basal spacing between 1.0 and 1.4nm was included with the mica, from which it could not be distinguished in a quantitative manner by XRD, the diffractometer traces suggested that this was a reasonable assumption, with only one type of exception. (The qualitative differentiation of mica from minerals with a basal spacing between 1.0 and 1.4nm by XRD is outlined in Section 7.1, and the quantitative estimation of these minerals by chemical methods is described in Section 7.2).

Table 6.7 Samples Investigated

| Sample Identification | Sample Description |
|---|---|
| 1040 | Unweathered Plynlimon shale |
| 1029 | Plynlimon boulder clay from Nant Gerig catchment |
| 1039 | Plynlimon boulder clay from Afon Cyff catchment |
| 1049 | Plynlimon boulder clay from River Wye catchment |
| BCd/1080D | Dithionite treated BC horizon from Plynlimon humic stagnopodsol profile |
| Bsd/1079D | Dithionite treated Bs horizon from Plynlimon humic stagnopodsol profile |
| Bsgd/1078D | Dithionite treated Bsg horizon from Plynlimon humic stagnopodsol profile |
| Ea2d/1077D | Dithionite treated Ea2 horizon from Plynlimon humic stagnopodsol profile |
| Ea1d/1076D | Dithionite treated Ea1 horizon from Plynlimon humic stagnopodsol profile |
| Bs/1079 | Bs horizon from Plynlimon humic stagnopodsol profile |
| Ea2/1077 | Ea2 horizon from Plynlimon humic stagnopodsol profile |
| Cg/1087 | Cg horizon from Hiraethog humic stagnogley profile, studied by Rezk [219] |

The exception was that, on the diffractometer traces of all size fractions from sample Bs/1079, of the coarser than 200μm fractions from Ea2/1077 and Bsgd/1078D, and of the finer than 2μm fractions from

Cg/1087 and Bsd/1079D, a peak of significant size was seen at 14.2°2θ, and could be identified as produced by lepidocrocite. Lepidocrocite (γFeO.OH) typically occurs under oxidising conditions as a weathering product of Fe bearing minerals [71], and thus is likely to be due to the weathering of the chlorite. In the coarse fractions it is likely to occur as a cement, causing an aggregate of small particles to behave as a single larger particle, whilst in the finer fractions it could be expected as a coating on mineral surfaces. If these are the true modes of occurrence, it would appear that the dithionite treatment is effective in removing the cement, but not the coatings, as after treatment only the finer fractions of 1079D show lepidocrocite, whereas before treatment it was present in all fractions.

Because of the modes of occurrence of lepidocrocite, it would have been impossible to remove without altering the proportions of the other minerals, and there was no way of quantifying its crystallinity in order to produce a standard and allow for its presence in the analyses. Although the lepidocrocite peak intensity is in some specimens greater than that for chlorite, this only occurs in specimens with a maximum chlorite content of 2.8%, and thus it is believed that, because of its higher linear attenuation coefficient for X-rays than any of the minerals being analysed, in no specimen did the lepidocrocite constitute more than 10% of the total mass. Although without knowing its precise distribution between the surfaces of quartz, mica and chlorite and as an intergranular cement it would be impossible to estimate its effect on the quantitative determination of mineralogy, it is most likely that, if the effect is significant, the proportion of chlorite in specimens containing lepidocrocite will be underestimated.

The diffractometer traces were examined for goethite at 21.2°2θ, the position corresponding to its (110) reflection, but no evidence could be found for its presence. Similarly, the preliminary traces, scanned as far as 35°2θ, showed no evidence of rutile at the 26.0°2θ position characteristic of its (110) peak. However, these traces show evidence for feldspar in every specimen except one. In the majority, both plagioclase and K feldspar are indicated by peaks at 28.0 and 27.5°2θ, respectively, with the intensity of the plagioclase peak almost always greater than that due to K feldspar. The peaks are weak relative to those of the major minerals, indicating that the feldspar contents are not significant, and thus a quantitative assessment of the feldspars was not carried out.

6.4.2 Interpretation of Diffractometer Traces

Once the diffractomer traces had been obtained, intensities were determined by measurement of peak areas. Initial measurements were carried out by tracing the peaks onto Daler Gateway 60g $m^{-2}$ paper, cutting out the peak shapes and weighing them to ±0.05mg. As the study progressed, a Digiplan image analyser became available, and all peak areas were remeasured. The image analyser was capable of reading to ±0.05$mm^2$, thus increasing the possible accuracy 17 fold. Each peak was measured five times using the Digiplan, and the complete set of measurements was rejected, and remeasurement carried out, if the coefficient of variation was more than 10%. The mean of the measurements was used in the calculation of quantitative mineralogy, which was carried out by a small computer programme based on equation (18), and allowed the choice of an appropriate standard for the mica, depending on the crystallinity value determined in the specimen being analysed (see Section 8.3).

The standards were made up of 50.00% AA crystal corundum and 50.00% of the mineral for which it was required to measure the reference intensity. Once the minerals had been mixed, the standards were treated in the same way as the specimens made from the sample fractions, except that the diffractometer scan was extended to 50°2$\theta$, to include the corundum (113) line at 43.4°2$\theta$, used as the reference peak. The reference intensities were calculated as:

$$k_i = \frac{\text{Peak area of standard mineral peak}}{\text{Peak area of corundum (113) peak}},$$

and are given in Table 6.8, along with the crystallinity ranges for which the mica standards were used (see Section 8.3). The peaks used for measuring the reference intensities, and thus for all other peak intensity measurements for quantitative analysis, were the quartz (100) line at 20.8°2$\theta$, the mica (002) line at 8.8°2$\theta$ (using the $2M_1$ nomenclature), and the chlorite (002) line at 12.6°2$\theta$, as these were the strongest lines free from interference from other minerals.

Only one standard each was used for quartz and chlorite. For quartz, coarsely crystalline white vein quartz from Penrhyn Quarry, Bethesda, was crushed finer than 6.3µm, as it had not proved possible to separate quartz from the samples. The chlorite was extracted magnetically (Section 4.2) from the finer than 2µm fraction of 1040, and its

chemistry and crystal structure are described in Sections 5.2 and 5.3, respectively. As it proved impossible to separate mica from the samples (Section 4.4), micas from elsewhere had to be used as standards. The reference intensities were determined for five micas, and the mica nearest in crystallinity value to the mica in the specimen being analysed was used as the standard. Where the crystallinity value was midway between those of two standard micas, the calculations were carried out using both micas, and the mean value was used.

Table 6.8 Reference Intensities of Standard Minerals

| Standard Mineral | Reference Intensity | Crystallinity Value (see Section 8.3) | Crystallinity Range Over Which Used as Standard |
|---|---|---|---|
| Vein Quartz | 1.333 | - | - |
| Plynlimon Chlorite | 2.456 | - | - |
| Trefriw Mica | 0.932 | 0.21 | <0.30 |
| Parys Mountain Mica | 1.779 | 0.39 | 0.30 - 0.46 |
| Llanddulas Mica | 1.383 | 0.53 | 0.46 - 0.885 |
| Conwy Town Ditch Illite | 0.599 | 1.24 | 0.885 - 1.25 |
| Fithian Illite | 1.174 | 1.26 | >1.25 |

Although diffracted intensity is affected by crystallinity, it is also affected by the composition and particle size of the mica [39,103,191], and thus choosing a standard solely on the basis of its crystallinity is not ideal. However, no data were available for either the chemical compositions or the particle size distributions of the illites that were pure enough to use as standards, and thus the choice had to be made on the basis of crystallinity. All the available information concerning the illites used is given in Sections 8.3 and 8.4.

If any of the coarser than 2μm fractions extracted from the samples had consisted of 95% or more mica, it might have proved better to have used these impure materials, with correct crystallinity and composition, as standards, rather than pure micas of unknown composition. However, no size fraction coarser than 2μm contained more than 62% mica, and thus nonPlynlimon standards were used.

## 6.5 CALCULATED MINERALOGICAL ANALYSES

The calculated compositions are given in Tables 6.9 to 6.11, and are presented graphically in Figures 6.2 to 6.13. It can be seen that, in all samples, there is considerable variation in mineralogy between the size fractions. The greatest mica content consistently occurs in the 0.063-0.2μm fraction, and that of chlorite in the 20-63μm fraction. These differences are related to the modes of occurrence in the parent rock: mica occurs in the fine grained matrix, whereas chlorite is often found as matrix supported clasts (Section 3.3). Quartz most often has its greatest percentage in the 6.3-20μm fraction, although in the more weathered samples the greatest percentage occurs in the 63-200μm fraction. The prevalence of silt size quartz in the parent rock accounts for its peak in the 6.3-20μm fractions, whilst mica and chlorite are reduced by weathering in the 63-200μm fraction, causing a relative increase in quartz. As the transition to weathered material occurs in the soil, the intermediate samples, Bsd/1079D and Bsgd/1078D, show bimodal distributions, with maxima in the 6.3-20μm and 63-200μm fractions. This bimodal distribution is seen to a lesser extent in the Hiraethog sample Cg/1087.

When whole samples are considered, mica content ranges between 28 and 60%, chlorite between 0 and 33%, and quartz between 25 and 42%, the highest chlorite and lowest mica contents occurring in the unweathered rock, the lowest chlorite and highest mica and quartz levels occurring in the upper soil horizons, and the lowest quartz level being found in the soil BC horizon. When the size fractions are considered separately, the range of values is much increased: from 17 to 100% for mica, from 0 to 54% for chlorite and from 0 to 77% for quartz. These values occur in the appropriate fractions of the samples which show the extremes of the ranges for whole samples, except for the 0% occurrences of quartz, which are in the finest fractions of several samples.

An interesting pattern emerges if the coefficients of variation are calculated for each mineral in each sample over the whole range of size fractions (Table 6.12). The sums of the coefficients of variation for the boulder clays and the comparison material from Hiraethog are very similar, but are lower than for the rock, which is in turn lower than for the soil horizons. When these are considered, the values increase up the profile, reaching a maximum in the Ea2 horizon, then decreasing in the Ea1 horizon. Dithionite treatment appears to have little effect on the sums of the coefficients of variation for 1077 and 1079.

| Size Fraction (μm) \ Sample | 1040 Unweathered Shale | | | 1029 Boulder Clay-Nant Gerig | | | 1039 Boulder Clay-Afon Cyff | | | 1049 Boulder Clay-River Wye | | |
|---|---|---|---|---|---|---|---|---|---|---|---|---|
| | % Mica | % Chlorite | % Quartz | % Mica | % Chlorite | % Quartz | % Mica | % Chlorite | % Quartz | % Mica | % Chlorite | % Quartz |
| 0.063 - 0.2 | 82.3 | 12.4 | 5.4 | 91.4 | 7.8 | 0.8 | 85.8 | 14.2 | 0.0 | 88.5 | 11.5 | 0.0 |
| 0.2 - 0.63 | 63.9 | 19.4 | 16.6 | 78.5 | 18.8 | 2.7 | 77.3 | 20.0 | 2.7 | 75.7 | 20.7 | 3.6 |
| 0.63 - 2 | 58.5 | 20.3 | 21.3 | 58.9 | 28.4 | 12.7 | 63.5 | 25.5 | 11.1 | 55.7 | 31.9 | 12.5 |
| 2 - 6.3 | 33.9 | 26.0 | 40.0 | 41.1 | 27.4 | 31.6 | 42.5 | 21.1 | 36.4 | 37.7 | 27.4 | 34.9 |
| 6.3 - 20 | 17.3 | 39.9 | 42.8 | 28.6 | 27.3 | 44.1 | 27.7 | 25.4 | 46.9 | 26.3 | 30.6 | 43.1 |
| 20 - 63 | 17.2 | 40.4 | 42.4 | 28.9 | 51.8 | 19.3 | 28.8 | 48.7 | 22.5 | 27.8 | 53.0 | 19.2 |
| 63 - 200 | 24.1 | 53.9 | 22.0 | 44.9 | 27.8 | 27.2 | 43.8 | 32.4 | 23.8 | 44.9 | 28.3 | 26.8 |
| 200 - 630 | - | - | - | 46.4 | 26.9 | 26.7 | 46.8 | 25.5 | 27.7 | 47.0 | 27.6 | 25.4 |
| 630 - 2000 | - | - | - | 45.7 | 29.2 | 25.1 | 43.0 | 25.8 | 31.2 | 47.2 | 27.2 | 25.7 |
| >2000 | - | - | - | 46.4 | 26.8 | 26.7 | 44.6 | 26.6 | 28.8 | 45.1 | 24.7 | 30.2 |
| Whole Sample | 28.4 | 33.1 | 38.5 | 46.3 | 28.1 | 25.6 | 46.4 | 27.2 | 26.4 | 45.7 | 26.9 | 27.4 |

TABLE 6.9 Calculated Mineralogy of Plynlimon Rock and Boulder Clays

| Size Fraction (μm) \ Sample | 1080D Humic stagnopodsol BC horizon | | | 1079D Humic stagnopodsol Bs horizon | | | 1078D Humic stagnopodsol Bsg horizon | | | 1077D Humic stagnopodsol Ea2 horizon | | | 1076D Humic stagnopodsol Eal horizon | | |
|---|---|---|---|---|---|---|---|---|---|---|---|---|---|---|---|
| | % Mica | % Chlorite | % Quartz | % Mica | % Chlorite | % Quartz | % Mica | % Chlorite | % Quartz | % Mica | % Chlorite | % Quartz | % Mica | % Chlorite | % Quartz |
| 0.063-0.2 | 95.3 | 4.7 | 0.0 | 99.3 | 0.7 | 0.0 | 100.0 | 0.0 | 0.0 | 99.5 | 0.0 | 0.5 | 99.1 | 0.0 | 0.9 |
| 0.2 - 0.63 | 90.5 | 6.6 | 2.9 | 97.6 | 1.3 | 1.1 | 98.0 | 0.7 | 1.2 | 97.6 | 0.4 | 2.1 | 97.3 | 0.0 | 2.7 |
| 0.63 - 2 | 82.9 | 8.7 | 8.4 | 92.9 | 3.1 | 4.1 | 94.1 | 1.4 | 4.5 | 97.6 | 0.0 | 2.4 | 97.0 | 0.2 | 2.8 |
| 2 - 6.3 | 50.4 | 15.7 | 33.9 | 53.8 | 8.9 | 37.3 | 54.7 | 3.5 | 41.8 | 61.6 | 0.0 | 38.4 | 53.0 | 0.0 | 47.1 |
| 6.3 - 20 | 27.7 | 21.9 | 50.4 | 32.5 | 18.5 | 49.0 | 30.5 | 7.7 | 61.8 | 36.0 | 0.3 | 63.7 | 35.3 | 0.2 | 64.4 |
| 20 - 63 | 22.6 | 53.5 | 23.9 | 23.7 | 45.1 | 31.2 | 23.0 | 25.9 | 51.1 | 27.1 | 0.4 | 72.5 | 32.5 | 0.2 | 67.4 |
| 63 - 200 | 40.5 | 33.3 | 26.1 | 35.5 | 21.2 | 43.3 | 23.9 | 5.5 | 70.6 | 27.4 | 0.0 | 72.6 | 22.3 | 0.4 | 77.3 |
| 200 - 630 | 44.0 | 29.4 | 26.6 | 43.1 | 24.2 | 32.7 | 43.8 | 8.3 | 47.8 | 38.1 | 1.4 | 60.5 | 37.9 | 0.8 | 61.3 |
| 630 - 2000 | 48.3 | 28.2 | 23.5 | 44.8 | 28.8 | 26.3 | 43.0 | 18.4 | 38.6 | | | | | | |
| >2000 | 39.9 | 34.8 | 25.2 | 43.7 | 33.2 | 23.2 | - | - | - | - | - | - | - | - | - |
| Whole Sample | 41.8 | 32.8 | 25.3 | 55.1 | 16.1 | 28.8 | 58.8 | 5.3 | 35.9 | 60.0 | 0.1 | 39.9 | 58.3 | 0.1 | 41.6 |

TABLE 6.10 Calculated Mineralogy of Dithionite Treated Plynlimon Soil Horizons

TABLE 6.11 Calculated Mineralogy of Other Samples

| Sample / Size Fraction (μm) | 1079 Plynlimon humic stagnopodsol Bs horizon | | | 1077 Plynlimon humic stagnopodsol Ea2 horizon | | | 1087 Hiraethog humic stagnogley Cg horizon | | |
|---|---|---|---|---|---|---|---|---|---|
| | % Mica | % Chlorite | % Quartz | % Mica | % Chlorite | % Quartz | % Mica | % Chlorite | % Quartz |
| 0.063-0.2 | 95.7 | 0.0 | 4.3 | 100.0 | 0.0 | 0.0 | 76.5 | 23.5 | 0.0 |
| 0.2-0.63 | 97.1 | 1.2 | 1.7 | 99.1 | 0.3 | 0.6 | 69.3 | 28.6 | 2.1 |
| 0.63-2 | 90.7 | 2.8 | 6.6 | 94.1 | 0.4 | 5.6 | 67.2 | 26.1 | 6.7 |
| 2-6.3 | 54.5 | 8.0 | 37.5 | 58.2 | 0.2 | 41.6 | 41.0 | 25.3 | 33.7 |
| 6.3-20 | 27.8 | 12.2 | 60.0 | 40.0 | 0.4 | 59.6 | 21.3 | 15.5 | 63.2 |
| 20-63 | 28.3 | 35.5 | 36.2 | 30.6 | 1.0 | 68.4 | 20.2 | 41.8 | 38.0 |
| 63-200 | 43.6 | 22.5 | 34.0 | 37.0 | 0.2 | 62.8 | 34.7 | 22.9 | 42.3 |
| 200-630 | 42.7 | 25.2 | 32.1 | 36.2 | 1.8 | 62.0 | 39.9 | 20.5 | 39.6 |
| 630-2000 | 42.4 | 29.8 | 27.7 | 42.8 | 6.1 | 51.1 | 45.2 | 22.5 | 32.4 |
| >2000 | 40.1 | 30.9 | 29.0 | - | - | - | 43.8 | 22.9 | 33.3 |
| Whole sample | 50.2 | 16.5 | 33.4 | 57.7 | 0.4 | 41.9 | 41.5 | 24.6 | 33.9 |

Table 6.12 Coefficients of Variation of Mineral Distribution

| Sample | Coefficients of Variation of Abundance Over All Size Fractions | | | Sum of Coefficients of Variation |
|---|---|---|---|---|
| | Mica (%) | Chlorite (%) | Quartz (%) | |
| 1040 | 61 | 49 | 54 | 163 |
| 1029 | 39 | 40 | 61 | 140 |
| 1039 | 38 | 35 | 64 | 137 |
| 1049 | 40 | 37 | 61 | 138 |
| BCd/1080D | 48 | 65 | 68 | 181 |
| Bsd/1079D | 51 | 81 | 71 | 203 |
| Bsgd/1078D | 56 | 111 | 76 | 243 |
| Ea2d/1077D | 54 | 153 | 84 | 291 |
| Ea1d/1076D | 56 | 121 | 81 | 257 |
| Bs/1079 | 49 | 80 | 67 | 196 |
| Ea2/1077 | 49 | 167 | 74 | 290 |
| Cg/1087 | 42 | 28 | 69 | 139 |

From these data, it would appear that a sum of coefficients of variation of about 160 corresponds to the variation of mineralogy with grain size seen in the fresh rock, due to the preferential occurrence of the minerals in particular grain sizes. The lower sums of coefficients of variation of the boulder clays and the Hiraethog comparison material can be explained in terms of their formation. Boulder clay is formed by the physical breakdown of rock and mineral grains, and thus would be expected to even out the size distributions of different minerals with similar physical properties, such as mica and chlorite. On the other hand, the soil horizons are derived by chemical weathering, which emphasises differences in mineralogy with grain size, by bringing about the breakdown of different minerals in different fractions. As weathering becomes more intense, differences in mineralogy between grain sizes within a soil horizon become more pronounced. Thus the sum of coefficients of variation increases until, in the Ea1 horizon, the amount of chlorite present becomes negligible, and the sum of the coefficients of variation decreases. It is the coefficient of variation of the chlorite content that increases most markedly as weathering progresses, and chlorite is the mineral most affected by weathering.

Although the profile studied is developed on weathered periglacial scree, many of the soils of Plynlimon are formed on boulder clays, and would thus show evidence of two phases of mineral particle size alteration; the first due to the physical processes producing the boulder clay, and the second to the chemical processes of soil formation. In fact, evidence from the phyllosilicate composition of the boulder clays (see Section 7.3) suggests that they have undergone chemical alteration at some stage, possibly in a preDevensian interstadial, and were further modified by Devensian periglacial activity to produce the compositions and mineral distributions seen today.

Because $TiO_2$ normally occurs in phases which are resistant to weathering, it can be used to indicate that weathering has taken place, even if other evidence is obscured by subsequent alteration. As other elements are removed by weathering, so the relative concentrations of $TiO_2$ increase from the parent material to the weathered product. $TiO_2$ contents were determined for the finer than 2mm material from the boulder clays and crushed rock by means of both betaprobe and DC arc direct reading emission spectrometric analysis. The results are given in Table 6.13, from which it is evident that some chemical weathering has taken place during the development of the boulder clays.

Table 6.13 $TiO_2$ Contents of Plynlimon Rock and Boulder Clays

| Sample | % $TiO_2$ When Total Analysis After Loss on Ignition is Normalised to 100% | |
|---|---|---|
| | Betaprobe | DC Arc Direct Reading Emission Spectrometer |
| 1040 | 1.15 | 1.05 |
| 1029 | 1.41 | 1.46 |
| 1039 | 1.34 | 1.27 |
| 1049 | 1.31 | 1.22 |
| Mean of 30 IGS Rock Samples (described in Section 3.3) | - | 1.08 |
| Mean of 5 IGS Rock Samples Included in Above (GCR4A, GCR6A, GCR7A, GCR17A, GCR20A) | 1.02 | 0.99 |

6.5.1 Mineralogy and Chemistry of Weathered Rock Surfaces

As well as calculating the mineralogy of the size fractions present in the soil horizons showing the effects of different degrees of weathering, a similar procedure was employed for those of the rock samples described in Section 3.3 from which it was possible to separate both fresh rock and weathered surface material. The analytical results for these samples are given in Table 6.14. It would be expected that the chlorite content would be reduced towards the surface of a weathered rock, and this is found to be the case for all the samples except 1036, in which the chlorite content increases towards the surface. Both mica and quartz are more resistant to weathering than chlorite, but the change in the quartz:mica ratio towards the weathered surface of the rock samples does not follow a consistent pattern, although overall there appears to be a slight increase in quartz relative to mica as the rock surface is approached.

Table 6.14 Semiquantitative Mineralogy of Fresh and Weathered Rocks

| Rock Group | Sample | Degree of Alteration | % Mica | % Chlorite | % Quartz | Quartz / Mica |
|---|---|---|---|---|---|---|
| Gwestyn Shale Group | 1018 | Fresh Interior | 40.7 | 32.8 | 26.5 | 0.65 |
| " | 1018 | Intermediate | 37.6 | 24.8 | 37.6 | 1.00 |
| " | 1018 | Weathered Surface | 49.3 | 17.5 | 33.2 | 0.67 |
| " | 1036 | Fresh Interior | 53.2 | 14.8 | 32.0 | 0.60 |
| " | 1036 | Weathered Surface | 50.8 | 19.6 | 29.6 | 0.58 |
| " | 1040 | Fresh Interior | 28.4 | 33.1 | 38.5 | 1.36 |
| " | 1040 | Weathered Surface | 22.6 | 6.8 | 70.6 | 3.12 |
| " | 1047 | Fresh Interior | 46.0 | 30.8 | 23.2 | 0.50 |
| " | 1047 | Weathered Surface | 59.5 | 9.1 | 31.4 | 0.53 |
| " | 1052 | Fresh Interior | 32.8 | 25.4 | 41.8 | 1.27 |
| " | 1052 | Intermediate | 38.6 | 2.3 | 59.1 | 1.53 |
| " | 1052 | Weathered Surface | 35.1 | 0.8 | 64.1 | 1.83 |
| Lower Fan Series | 1030 | Fresh Interior | 10.8 | 30.5 | 58.7 | 5.44 |
| " | 1030 | Intermediate | 14.3 | 20.5 | 65.2 | 4.56 |
| " | 1030 | Weathered Surface | 14.5 | 0.0 | 85.5 | 5.90 |

Attempts were made to investigate further the changes occurring in the weathered surfaces of rock particles by employing the electron probe microanalyser at IGS. This was used in a scanning mode to traverse across thin sections of rock samples that had been cut perpendicular to the weathering surface, in order to follow changes in elemental analyses as the surface was approached. In general, little success was achieved, although in samples 1036 and 1047 changes in the Fe content could be detected. In 1036 a zone of Fe enrichment about 360μm wide was found 240μm in from the surface, whilst in 1047 it was possible to show that the outer 990μm had an average Fe as FeO content of 6.4% which, after a peak of 10.4% FeO 1050μm from the surface of the rock, settled to a level of 7.8% further into the body of the rock. These findings are consistent with both the hand specimen and thin section appearances of the samples. In future work it would undoubtedly be useful to carry out further microprobe investigation of weathering surfaces, to see if chemical and mineralogical changes taking place at the surface of large, polymineralic rock particles are the same as, or different from, the changes taking place in clay size particles.

## 6.6 THE EFFECTS OF WEATHERING ON MINERAL DISTRIBUTION PATTERNS

The effects of weathering on mineralogy can be seen most clearly in the dithionite treated soil horizons, for which the mineralogy of a size fraction can be compared throughout the profile, and changes in composition can be related to the intensity of the weathering process in the horizons. The most obvious effect is a reduction in chlorite content as weathering progresses. In Ea1d/1076D and Ea2d/1077D, the chlorite content has been effectively reduced to zero, and no useful comparisons can be made. However, if the chlorite contents of the finer than 63μm fractions of the other dithionite treated samples are compared, it can be seen that the amount of chlorite is consistently reduced up the profile, and that the reduction is most marked in the finest fractions (Table 6.15). This indicates that, as expected, chlorite is the most readily broken down of the major minerals, and that breakdown of the finest grains takes place most rapidly.

When quartz is considered, the picture becomes more complex. In the clay fractions, the percentage of quartz present in all of the higher horizons is reduced relative to the BC horizon, whilst in the coarser fractions the percentage of quartz is increased, and increases further as weathering becomes more severe, particularly in the 20-2000μm fractions. The combined effect is that, in the sample as a whole, the

percentage of quartz is lowest in the BC horizon, and increases towards the surface.

Table 6.15 The Effect of Weathering on the Chlorite Content of Dithionite Treated Soil Horizons

| Size Fraction (μm) | % Chlorite in 1079D / % Chlorite in 1080D | % Chlorite in 1078D / % Chlorite in 1080D |
|---|---|---|
| 0.063 - 0.2 | .15 | .00 |
| 0.2 - 0.63 | .20 | .11 |
| 0.63 - 2 | .36 | .16 |
| 2 - 6.3 | .57 | .22 |
| 6.3 - 20 | .84 | .35 |
| 20 - 63 | .84 | .48 |

There are two explanations for this behaviour of quartz. The first is that the quartz is not being reduced in the finer than 2μm fractions, but that it is only its diffracted X-ray intensity that is being reduced, by the development of a noncrystalline surface on the fine grains [39,148]. If, because of the effects of weathering, the noncrystalline layer developed to a greater extent in the upper soil horizons, the pattern of quartz distribution could be explained.

On the other hand, it might be that quartz is the most resistant of the major minerals as long as the particle size is greater than 2μm, but that it breaks down rapidly once its size has been reduced to less than this. Evidence provided by detailed scanning electron microscopy of quartz surfaces suggests that under similar weathering conditions an altered surface layer does not form on quartz grains [152], and thus it seems that quartz becomes more susceptible to the effects of weathering once its size is reduced below 2μm.

When mica is considered, the picture is different again. Taking all fractions together, the percentage of mica increases up the profile, reaching a maximum in the Ea2 horizon, with a fall off in the Ea1 horizon. When the fractions are considered separately, the mica is increased in all the upper horizons, when compared to the BC horizon, in the fractions finer than 63μm, but reduced in the coarser than 63μm fractions, with the relative reduction increasing with particle size. In all horizons, mica dominates the mineralogy of the clay fractions,

and this may explain the distribution pattern seen. The coarser fractions, in which the mica is reduced as weathering takes place, contain a significant proportion of polymineralic grains. If the weathering process breaks these grains down then, as weathering proceeds, a greater proportion of the grains remaining in the coarser fractions will be monomineralic. Because quartz occurs as coarser grains than mica in the fresh rock, the mica contents of the coarse fractions will decrease as weathering proceeds.

A further explanation for the reduction in the mica content of the coarser fractions may be provided by the weathering of chlorite/mica intergrowths. These occur as large, matrix supported grains, similar to the chlorite grains, but have variable proportions of intergrown chlorite and mica, as observed by electron probe microanalysis [219] (Section 5.1). As the chlorite is weathered, so the mica will remain as grains finer than the original intergrown particles.

Dithionite treatment appears to have little effect on the relationship of mineralogy to grain size, but differences can be seen between the materials from Hiraethog and Plynlimon. In mineral distribution, the Hiraethog sample is most similar to the boulder clays, but has a higher quartz content and a lower and more uniformly distributed chlorite content. The uniform distribution of chlorite suggests that it has experienced little chemical weathering, whilst the lower overall chlorite content suggests that it is derived from a parent rock with a mineralogy different to that of the Plynlimon rock. This may at least partially explain the differences between the conclusions drawn by Rezk [219], and those of this study.

# CHAPTER 7

# COMPOSITIONAL VARIATION WITHIN MINERAL PHASES

## 7.1 THE X-RAY DIFFRACTION ANALYSIS OF CLAY SEPARATES

The results of the quantitive XRD analysis given in Section 6.5 show that the proportions of the major minerals change from sample to sample, and differ between the fractions extracted from the same sample. However, this analysis is unable to indicate changes taking place in the structure and composition of each mineral phase. Nevertheless, the variations in illite crystallinity values and peak symmetry ratios, which will be described in Sections 8.3 and 8.4, show that changes other than simple dissolution are taking place. This would be expected from the results of other workers, who have observed the formation of interstratified minerals during the weathering in soils of both illite and chlorite [14,47,63,65,72,80-82,91,92,107,110, 136,139,208].

The most effective way of studying these changes by means of XRD is to prepare specimens by sedimentation onto glass slides. Although this brings about differential settling of the minerals (Section 6.4), this is not detrimental to qualitative analysis, and the preferred orientation, which enhances the intensity of phyllosilicate basal reflections relative to other reflections, is advantageous. By examination of the d spacings of the (001) reflections after standard treatments, the mineral phases can be identified, and irregularly and regularly interstratified minerals can be differentiated [45,168,218, 229]. After appropriate treatments, vermiculite can be distinguished from illite, and pedogenic chlorite, with incomplete hydroxy interlayers, from metamorphic chlorite, which has a completely filled interlayer structure.

Even using this technique, information cannot be gained about which of the possible modes of quartz alteration are taking place. The quartz could be taken directly into solution, and lost from the sample, or transformed into noncrystalline or opaline silica which could not be directly determined by XRD. Although not carried out, the most obvious method to clarify which of these possibilities was occurring would be to add to the specimen for quantitative analysis a known weight of quartz of the same crystallographic character as that already present. Comparison of the XRD analyses before and after addition would indicate

if any noncrystalline or opaline silica was present. This method could only work if there was no other noncrystalline material present, and if the only method of formation of noncrystalline or opaline silica was by the breakdown of quartz, which is not likely to be the case.

Theoretical consideration of the surface areas of different fractions suggests that structural changes are likely to be most pronounced in the finest, and this is confirmed by the evidence from quantitative mineralogical analysis that the finest fractions have a mineralogy most distinct from the least weathered material, represented by the coarser than 2mm material from the same sample (Section 6.5). Even for the specimens prepared as random powders for quantitative analysis, the diffractometer traces show the phyllosilicate peaks developing tails and shoulders in some of the finer than 6.3μm fractions, particularly those finer than 2μm. As this part of the study could only provide qualitative results, and there was no reason to suggest that the alterations occurring in the coarser fractions were any different to those taking place in the finer than 2μm fractions of the same samples, except in terms of intensity of alteration, only the finer than 2μm fractions were investigated.

Although the argument used to justify investigation of only the three finest fractions also suggests that the fraction likely to show the greatest alteration would be the finest, the results from the next finest, 0.2-0.63μm, will be described in more detail, although comparison will also be made with the 0.063-0.2 and 0.63-2μm fractions when any differences occur. The most important reason for not using the 0.063-0.2μm fractions is that these were saturated with K during separation (Figure 6.1). K is readily fixed into interlayer exchange sites in vermiculites, contracting the basal spacing to 1.04nm, and is not easily removed by saturation with other ions [77,255]. This means that any vermiculite previously saturated by K could appear to behave as a mica. The coarser fractions were not saturated with K during separation, and thus do not suffer from this problem. A second reason for the use of the 0.2-0.63μm fractions is that it is evident from the quantitative XRD data given in Tables 6.10 and 6.11 that four of the samples show no chlorite in their 0.063-0.2μm fractions, but contain small amounts of chlorite in their 0.2-0.63μm fractions. This suggests that, in these samples, chlorite has broken down totally in the finest fractions, but that its breakdown processes might be observed in their final stages in the 0.2-0.63μm fractions.

For each sample, two specimens were prepared for each fraction finer than 2μm. One was prepared from clay saturated with K by twice shaking in an excess of 1M KCl, followed by centrifugation. The supernatants were discarded, and the clay twice washed in an excess of distilled water, followed by further centrifugation to remove any residual KCl. The other was prepared from clay saturated with Mg using the same procedure, but substituting $(CH_3COO)_2Mg$ for KCl. Approximately 25mg of clay were dispersed in 0.5cm³ of distilled water, and pipetted onto a 48 x 27mm glass slide. Drying was carried out under a tungsten filament lamp.

XRD of these specimens was carried out, and then they were subjected to a series of treatments, with a further diffractometer trace being recorded after each. The Mg saturated specimens were all treated with ethan1,2diol vapour by placing them for two hours in a sealed desiccator containing liquid ethan1,2diol, held at a temperature of 60°C. After diffraction, the specimens prepared from the 0.063-0.2μm fractions were left in an oven at 60°C overnight to drive off the adsorbed vapour, and were then treated with propan1,2,3triol vapour in a manner similar to the treatment with ethan1,2diol. The K saturated specimens were all heated at 250°C for one hour and, after diffraction, the specimens made from the 0.063-0.2μm fractions were heated in turn to 350°C for one hour and 450°C for one hour. All the K saturated specimens were then heated to 550°C for two hours. Some K saturated specimens were treated with dimethyl sulphoxide in order to determine whether kaolinite was making any contribution to the 0.7nm peaks. No peaks were seen at 1.12nm after treatment, and thus the remaining specimens were not treated, and kaolinite was assumed not to be present in any of the samples.

The most important information about phyllosilicate structures is revealed by the K saturated, Mg saturated, K saturated and heated to 550°C, and Mg saturated and treated with ethan1,2diol material, and thus the diffractometer traces for these treatments for the 0.2-0.63μm fractions are reproduced in Figures 7.1 to 7.4. The corresponding traces for the 0.063-0.2 and 0.63-2μm fractions are given in Figures A.1 to A.12 in the Appendix. Standard instrumental conditions were employed for XRD (Section 6.4), and scanning was carried out between 2 and 15°2$\theta$. A chart fsd between 1,000 and 10,000cps was chosen as appropriate.

For reasons of typographical clarity, abbreviations have been used in some figures and tables when referring to the different pretreatments given to specimens for XRD analysis. The figures and tables affected are Figures 7.1 to 7.4, 8.1 and A.1 to A.12, and Tables 7.4, 8.2, 8.6 and 8.10, and the abbreviations used are as follows:

| | |
|---|---|
| /K | = K saturated. |
| /Mg | = Mg saturated. |
| /K550 | = K saturated and then heated to 550°C. |
| /MgED | = Mg saturated and then treated with ethan1,2diol vapour. |

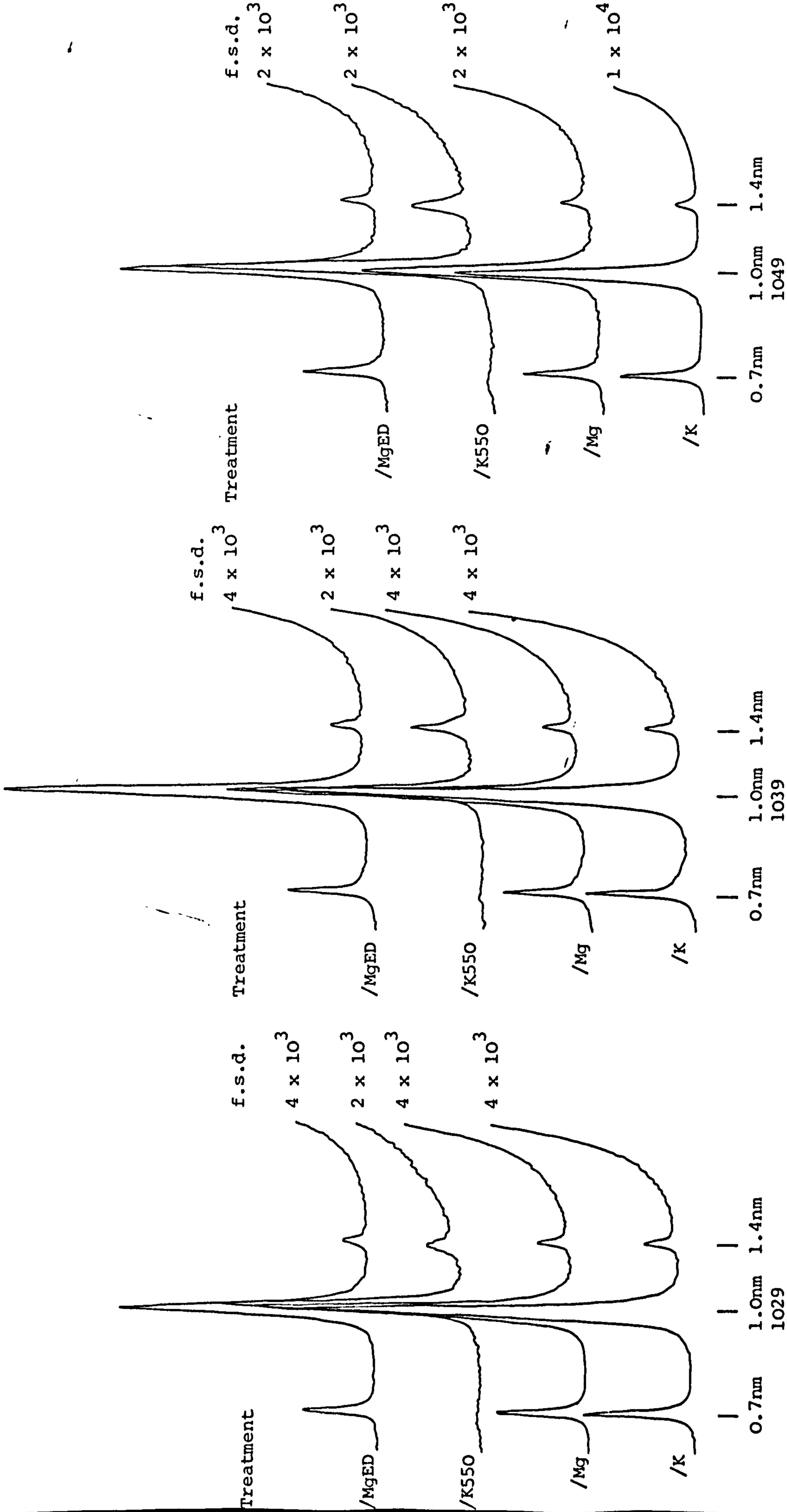


Figure 7.1 X-ray Diffractometer Traces of 0.2-0.63 µm Fractions of Plynlimon Boulder Clays

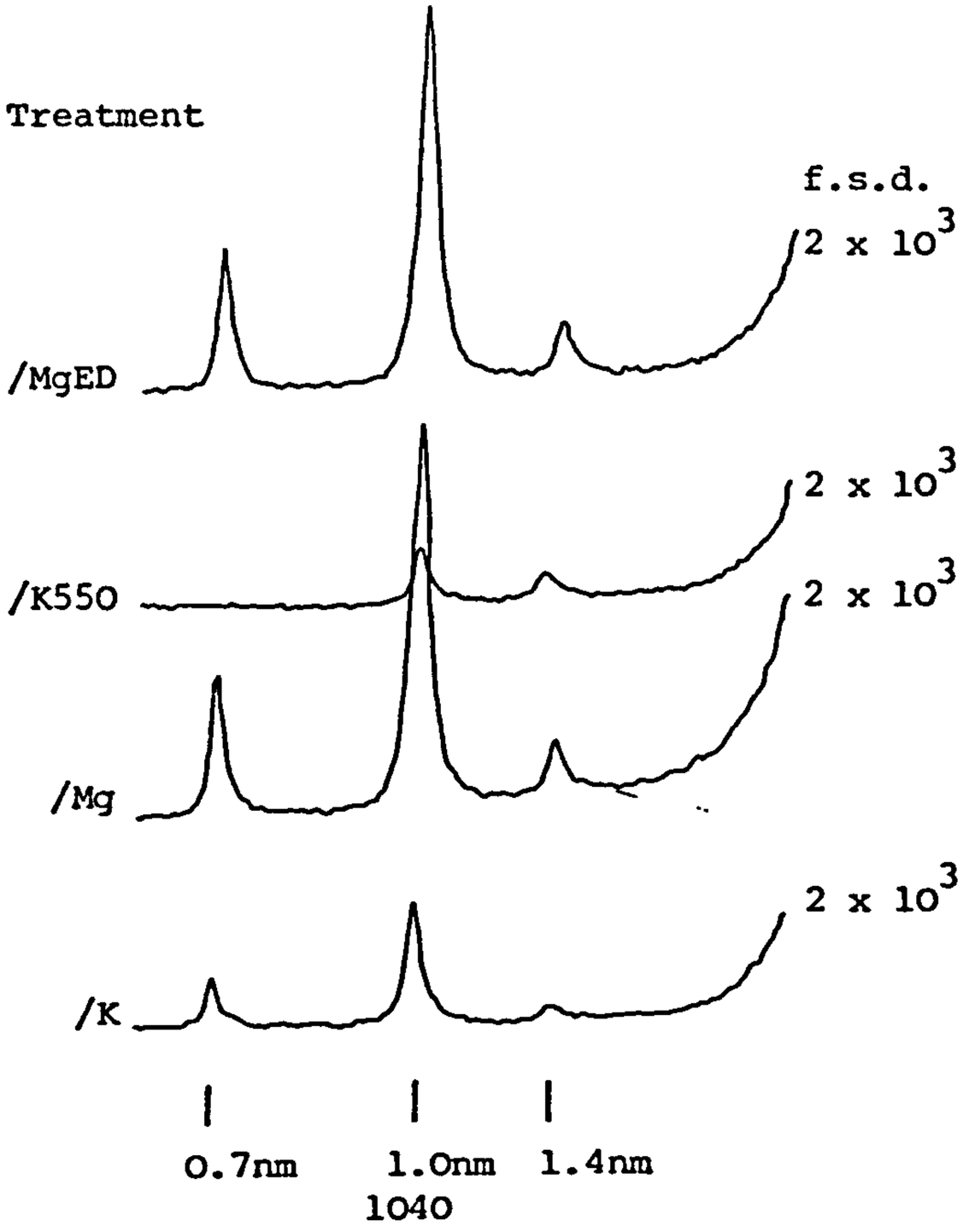


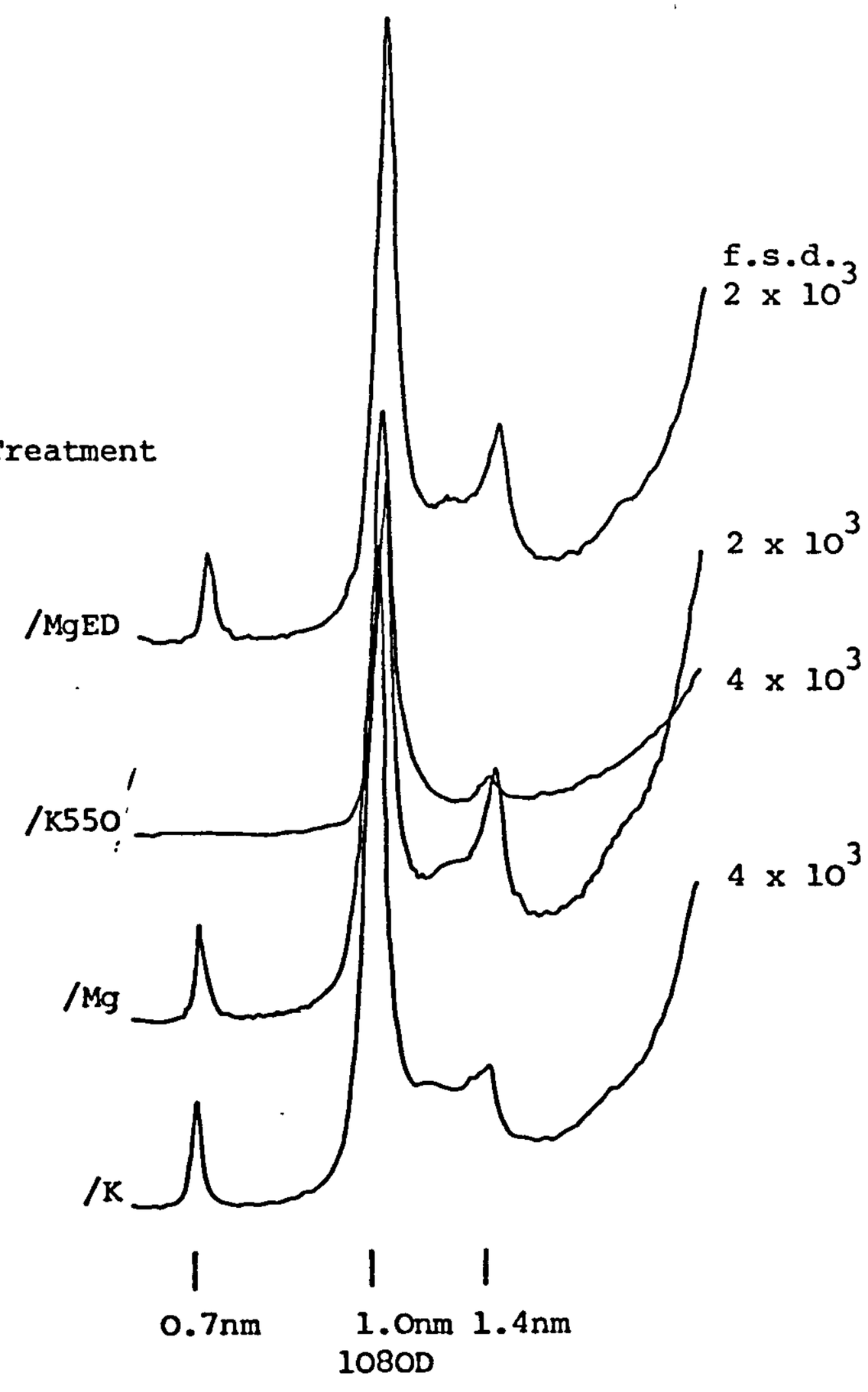


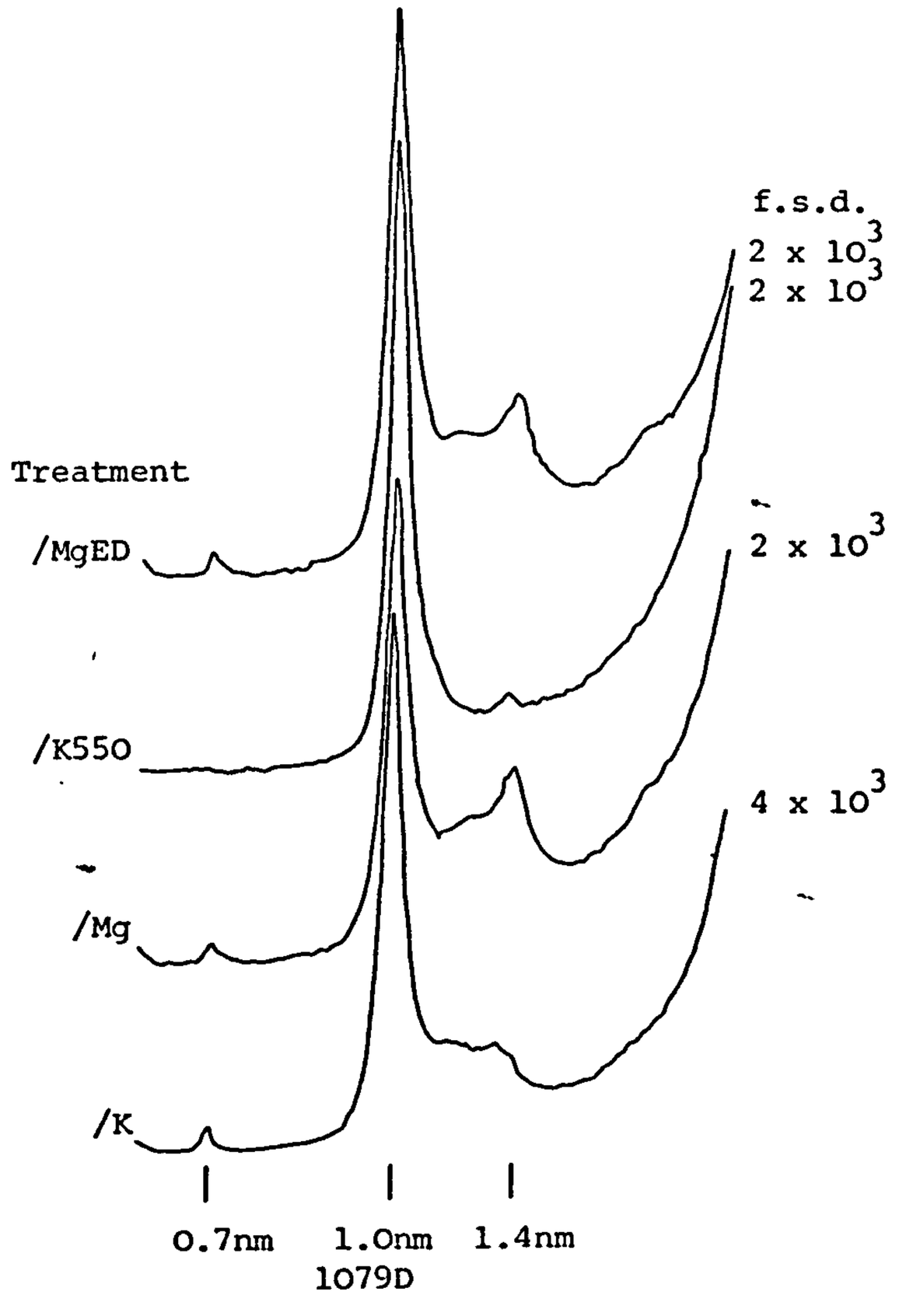


Figure 7.2 X-ray Diffractometer Traces of 0.2-0.63μm Fractions of Plynlimon Unweathered Rock and Dithionite Treated Lower Soil Horizons

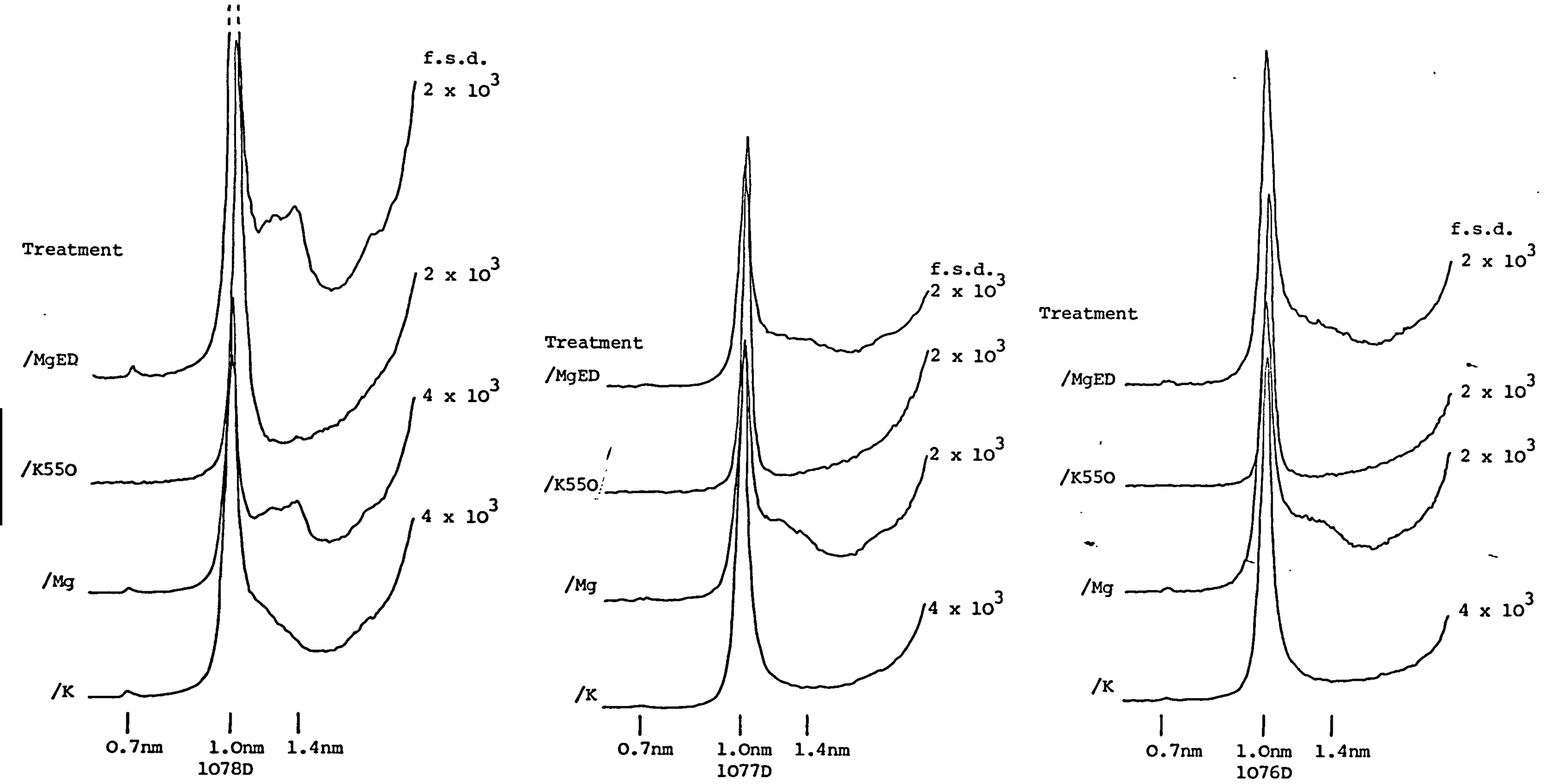


Figure 7.3 X-ray Diffractometer Traces of 0.2-0.63 μm Fractions of Dithionite Treated Plynlimon Upper Soil Horizons

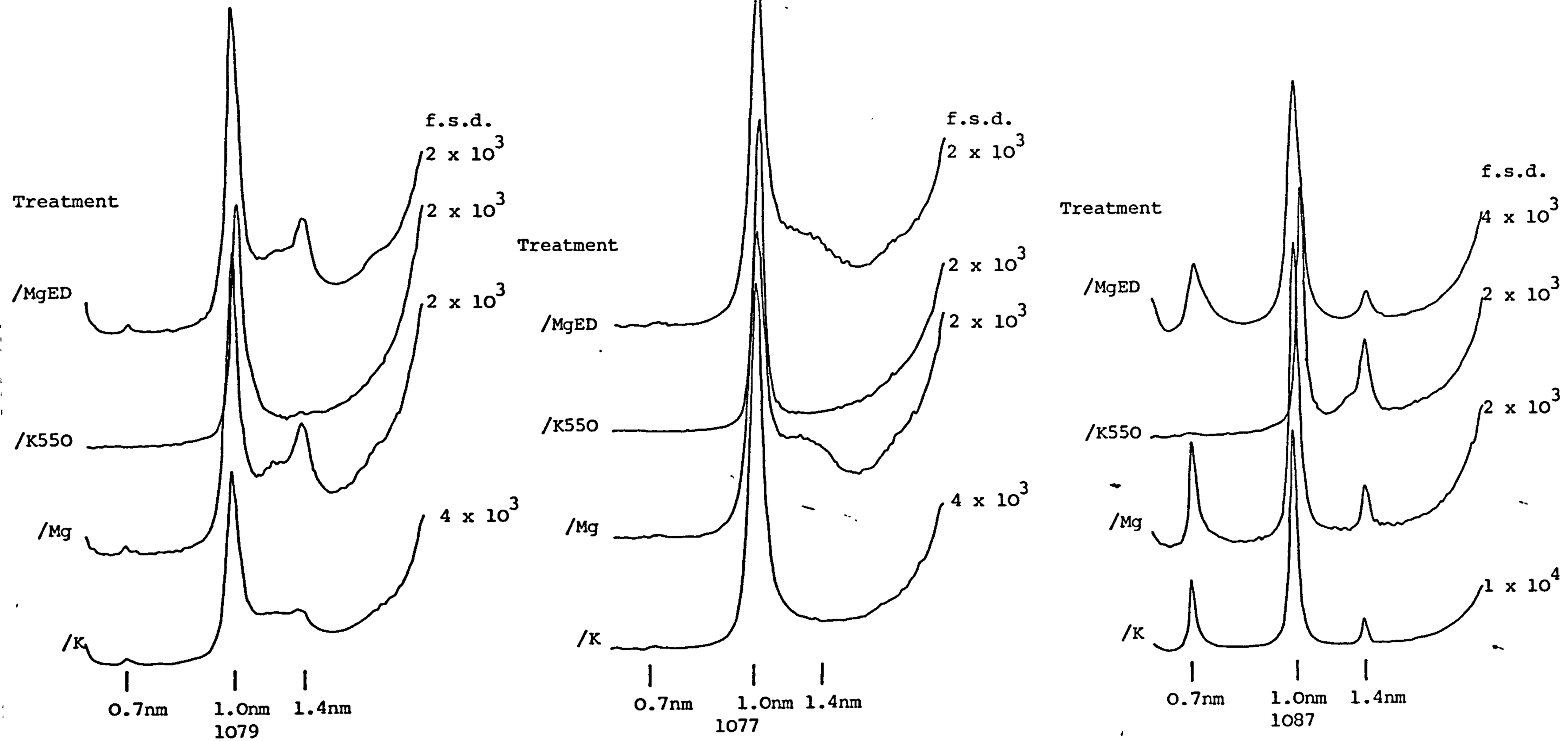


Figure 7.4 X-ray Diffractometer Traces of 0.2-0.63μm Fractions of Untreated Plynlimon Soil Horizons and Hiraethog Comparison Material

### 7.1.1 Hydroxy Interlayered Vermiculite

In the interpretation of the diffractometer traces, reference is made to hydroxy interlayered vermiculite. Hydroxy interlayered minerals can be considered as solid solution series, with chlorite at one end and vermiculite or smectite at the other. The chemical composition depends on the degree of filling of the interlayers with Al or Fe hydroxy complexes, and this is a dynamic parameter, related to the environment [18]. Hydroxy interlayered minerals occur in soils as weathering products, where they result from precipitation of hydroxy polymers in the interlayer spaces of expandable minerals, particularly in acid soils [18,133], or the degradation of chlorite. Such minerals have been known as swelling chlorite [229]. Hydroxy interlayering is observed most frequently in surface horizons, but is widespread in soils and has been reported in sediments [18]. It is difficult to find soil vermiculites that are wholly free from hydroxy interlayers [168].

Hydroxy interlayered minerals show XRD properties typical of chlorite at room temperature, but incomplete filling of the interlayers leads to a lack of stability of the 1.4nm K saturated peak on heating, bringing about collapse towards 1.0nm. Both the temperature required to bring about partial collapse, and the extent of collapse on heating to 550°C, can be used to indicate the degree of filling. The higher the temperature required to bring about a peak shift, and the smaller the amount of shift, the more completely are the interlayers filled. However, where only a small degree of interlayering is present, it is difficult to distinguish the mineral from pure smectite or vermiculite, and when the infilling approaches completeness, the mineral becomes difficult to distinguish from chlorite [18]. Some confusion exists between interstratified chlorite-vermiculite and hydroxy interlayered vermiculite, but distinction can be made by the fact that the interstratified mineral will partially collapse at room temperature on K saturation, and then maintain a constant spacing on heating at least as far as 400°C, whereas the hydroxy interlayered vermiculite will not collapse on K saturation, but will show a gradual collapse on heating. It is possible for interstratified chlorite- or vermiculite-hydroxy interlayered vermiculite to exist, confusing matters further [229]. It is also considered that interstratified chlorite-vermiculites can form in the same ways as hydroxy interlayered vermiculites [168].

Investigations of the solubilities of the interlayer sheets in both chlorite and hydroxy interlayered minerals relative to their separate

phase counterparts of brucite and gibbsite suggest the interlayers in chlorite are stable, whilst those in hydroxy interlayered minerals are unstable [147]. This study also suggests that authigenic chlorite will only form at pH values greater than 7, whereas hydroxy interlayered minerals form at about pH5. This confirms observations that hydroxy interlayering occurs in acid clays when expandable minerals are present [133,168]. XRD evidence cannot distinguish hydroxy interlayered vermiculites with completely filled interlayers from true chlorites, but the evidence is that pedogenic chlorites are unlikely to form from illites via vermiculites and hydroxy interlayered vermiculites, because of the different pH values required to form chlorite and hydroxy interlayered vermiculite. The low pH of the soils at Plynlimon would favour the formation of hydroxy interlayered vermiculite. If the interlayers were chemically removed [18], analysis of the resulting solution could indicate whether the minerals with partly filled interlayers were degraded chlorites with Fe and Mg rich interlayers, or hydroxy interlayered vermiculites, formed by the weathering of illites, with aluminous interlayers.

### 7.1.2 Interpretation of Diffractometer Traces

1029 The traces from all clay fractions of this boulder clay appear to be very similar. Neither mica nor chlorite peaks show any changes in d spacing or development of tails or shoulders on K or Mg saturation or treatment with ethan1,2diol or propan1,2,3triol. The only differences between the fractions are the gradual broadening of peaks as the size is reduced, and the changes of relative intensity of the mica and chlorite peaks, both of which are seen in the other samples investigated. However, on heating, a change in the d spacing of the chlorite (001) peak is seen, which is most pronounced in the 0.063-0.2μm fraction.

After K saturation, the (001) spacings are 1.40, 1.40 and 1.41nm for the 0.063-0.2, 0.2-0.63 and 0.63-2μm fractions, respectively. After heating to 250°C, the mean spacing remains the same, but the scatter increases, with the individual values being 1.41, 1.39 and 1.41nm, respectively. On heating to 350, 450 and 550°C, the (001) spacing of the chlorite in the 0.063-0.2μm fraction is reduced to 1.40, 1.39 and then 1.36nm, whilst after heating to 550°C, the (001) spacings of the chlorite from the 0.2-0.63 and 0.63-2μm fractions are reduced only as far as 1.38nm.

In a preliminary experiment, finer than 2μm material from 1029 was K saturated, and then heated in steps of about 20°C to investigate the breakdown of the chlorite. Some of the specimens had been treated with dithionite and $H_2O_2$ before K saturation, but the results of the experiment suggest that this treatment had no effect on the behaviour of the chlorite. In none of the specimens were any changes in the mica observed.

At temperatures up to 350°C, no significant differences were seen between the traces given by specimens heated to different temperatures, either in the relative peak heights of the chlorite (001) peaks, or in the peak positions. The mean peak positions and peak height ratios from all specimens not heated beyond 350°C are given in Table 7.1. After heating to 355°C overnight, both the (004) and (005) peaks split into two. A more intense peak at 0.353nm with another peak at 0.349nm correspond to the (004) position, and a peak at 0.282nm with a slightly weaker peak at 0.280nm correspond to the (005) position. All three traces made from specimens heated to 400°C show two peaks at the (004) position, with their relative intensity varying from trace to trace, whilst only one of the traces shows two peaks at the (005) position, the other two showing a very broad peak centred at 0.283nm. This broad (005) peak remains in the same position, becoming less intense as temperature increases, until it is no longer seen at 485°C and above. The (003) peak remains single, sharp and at the same position on all traces, but loses intensity until it is no longer seen at 480°C and above.

Once 420°C has been reached, the (001) spacing begins to decrease, reaching a minimum of 1.37nm at 550°C, after which it begins to increase rapidly, attaining 1.43nm at 600°C. This peak does not split, but at temperatures up to 560°C a shoulder is seen at a higher d spacing, whilst at 580°C there is a very broad peak centred on 1.39nm, and at 600°C there is a shoulder at a lower d spacing, suggesting that a transformation is occurring between a low temperature structure with d(001) about 1.38nm, and a high temperature structure with d(001) about 1.43nm.

The (002) spacing does not change significantly until 485°C, but at 480°C the (002) peak is very broad. Between 485 and 560°C, there are two peaks corresponding to the (002) position, the one

| Peak | d Spacing (nm) | Peak Height / Peak Height of (002) |
|---|---|---|
| (001) | 1.41 | 0.13 |
| (002) | 0.705 | 1.00 |
| (003) | 0.470 | 0.23 |
| (004) | 0.353 | 0.83 |
| (005) | 0.282 | 0.13 |

Table 7.1 Positions and Relative Heights of Chlorite (001) Peaks from the 0.063-0.2μm Fraction of 1029, at Temperatures up to 350°C

| Treatment | Reflection Positions (nm) | | |
|---|---|---|---|
| | 0.063-0.2μm Fraction | 0.2-0.63μm Fraction | 0.63-2μm Fraction |
| Mg Saturation | 2.30 | 2.45 | 2.40 |
| Ethan1,2diol | - | 2.40 | 2.20 |

Table 7.2 High d Spacing Discontinuities Observed on Diffractometer Traces of 1079D

| Treatment | Reflection Positions (nm) | | |
|---|---|---|---|
| | 0.063-0.2μm Fraction | 0.2μm-63μm Fraction | 0.63-2μm Fraction |
| K Saturation | - | - | 2.15 |
| Mg Saturation | - | 2.30 | 2.25 |
| Ethan1,2diol | 2.40 | 2.20 | 2.30 |
| Propan1,2,3triol | 2.30 | not investigated | not investigated |

Table 7.3 High d Spacing Discontinuities Observed on Diffractometer Traces of 1078D

with the lower d spacing varying from 0.685 to 0.705nm, whilst the other peak varies between 0.730 and 0.755nm. Below 500°C the low d spacing peak is most intense, but above 500°C the high d spacing peak becomes relatively more intense, until at 580°C it is the only (002) peak remaining, although it is very weak.

The (004) peak behaves in a very similar way to the (002) peak above 480°C. The two (004) peaks seen from 355 to 400°C amalgamate to form one broad peak centred at 0.352nm at temperatures of 420 and 440°C. This peak splits again at 460°C, giving a low d spacing peak varying in position from 0.343 to 0.355nm, and a high d spacing peak which is found between 0.354 and 0.374nm. Two peaks remain up to 550°C, above which either no (004) peak is seen, or a very weak peak is found at 0.359nm. The change from the low to the high d spacing peak being stronger occurs at 500°C, the same temperature as the similar change occurs in the (002) peak.

These results suggest that four phases of structural alteration are taking place as temperature is increased, and these are illustrated in Figure 7.5:

1. Between 355 and 400°C a slight splitting of (004) and (005) peaks occurs. This may also affect the other peaks, but if it does, its effects are not discernible on the diffractometer traces.

2. The intensity of the (003) and (005) peaks is reduced to zero between 460 and 485°C, and in this temperature range the (002)/(001) intensity ratio begins to decrease from its mean value of 7.7 at lower temperatures, eventually reaching 0.2 at 580°C.

3. At about 500°C, a structural change occurs which increases the d spacings of the (002) and (004) peaks.

4. A further change occurs at 580°C, increasing the d spacing of the (001) peak.

In comparison, the changes seen in the K saturated finer than 2μm material from a comparison Ynys profile are much simpler. Up to

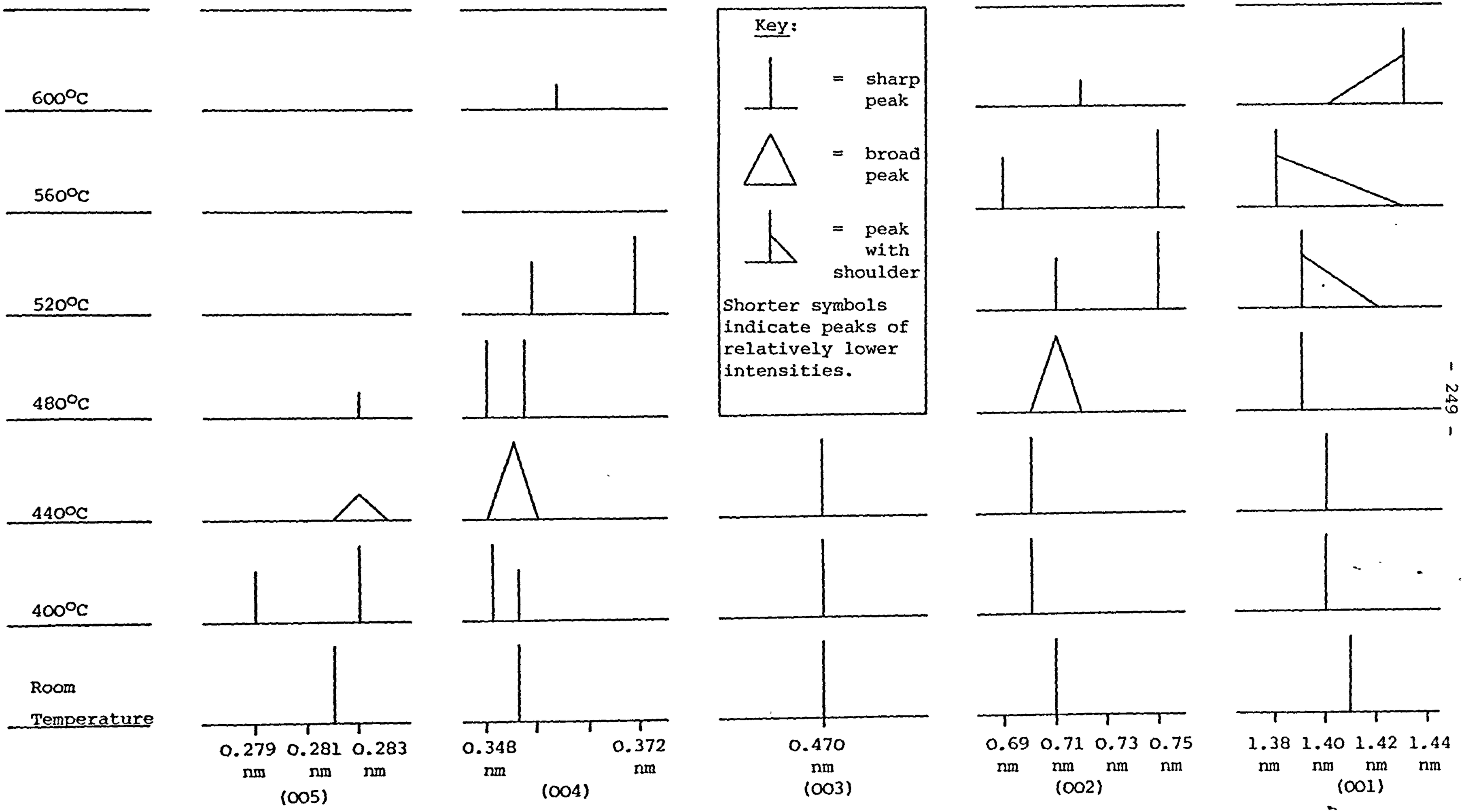


Figure 7.5 A Diagrammatic Interpretation of the Effect of Heating on the d Spacing and Intensity of the (00ℓ) Peaks of Finer than 2μm "Chlorite" from Sample 1029

400°C, no significant changes in the basal spacings are seen, but by 485°C a very slight increase in the d spacings of all the recorded (001) peaks has occurred, changing the (001) spacing from 1.41 to 1.42nm, the (004) spacing from 0.353 to 0.354nm and the (005) spacing from 0.282 to 0.284nm. At 550°C and above, the intensity of the (001) peak is very much increased relative to that of the other (001) peaks, whilst the weak (003), (004) and (005) peaks have their d spacings reduced to 0.450nm, from an original value of 0.470, 0.347 and 0.278nm, respectively.

The behaviour of the chlorite from the Ynys material is what would be expected of a typical chlorite, suggesting that some of the material in the clay fractions of 1029 that appears to be chlorite from examination of room temperature diffractometer traces, is not chlorite. The Plynlimon material does not show the typical increase of (001) peak intensity relative to that of the other (001) peaks on heating to 550°C, and heating appears to show two separate crystal structures, which undergo alteration at different temperatures.

The most simple interpretation of this is that the "chlorite" in the clay fractions of 1029 actually consists of both true chlorite and hydroxy interlayered vermiculite, with the latter being found particularly in the finest fraction. On progressive heating, K saturated hydroxy interlayered vermiculites collapse from a 1.4nm (001) spacing towards 1.0nm, with the degree of collapse increasing as the hydroxy interlayers are emptied, and the similarity of the material to true chlorite is decreased [18]. In the finer than 2μm material investigated in the preliminary experiment, collapse only went as far as 1.37nm, but when the fractions were investigated separately, the 0.063-0.2μm fraction showed collapse to 1.36nm, whilst the 0.2-0.63 and 0.63-2μm fractions only showed collapse to 1.38nm. This suggests that, although the hydroxy interlayers are almost completely full in all clay fractions, the finest fraction contains the mineral with the least full interlayers. From 355°C, when differences begin to emerge between the behaviour of chlorite and hydroxy interlayered vermiculite, to 500°C, it is the partially collapsed hydroxy interlayered vermiculite structure that dominates the diffractometer traces but, due to its greater thermal stability,

the true chlorite structure with larger basal spacings is seen more clearly at higher temperatures.

Although the progressive heating experiments necessary to provide confirmation of the presence of hydroxy interlayered vermiculite were not carried out for any of the other samples, interpretation of their mineralogical compositions will be made in the light of the evidence described above.

1039 The diffractometer traces produced by this sample are essentially similar to those of 1029, being dominated by sharp mica and chlorite peaks, but there are differences in detail. All of the specimens except those K saturated and heated to 550°C show tails from 0.7 to 0.85nm on the chlorite (002) peak, which are most pronounced in the 0.063-0.2μm fraction. These would seem most likely to be due to irregularly interstratified chlorite-mica, being caused by a combination of the chlorite (002) reflection and the 1.0nm peak of the mica [168,229], as lack of peak movement on treatment with ethan1,2diol shows that chlorite interstratified with an expandable mineral must be ruled out.

On heating, loss of intensity of the K saturated (002) chlorite peaks does not occur until about 450°C, compared with a similar intensity loss in 1029 at about 350°C. This may be related to the fact that the d spacing of the K saturated (001) chlorite peak is increased from 1.41nm at room temperature to 1.42nm at 450°C, and only collapses to 1.38nm in the 0.063-0.2μm fraction at 550°C. This suggests that most of this chlorite has more completely filled hydroxy interlayers than in 1029, and is thus more thermally stable. However, although the chlorite peak in the K saturated 0.063-0.2μm material heated to 550°C is found at 1.38nm, there appears also to be material present between the mica and chlorite peaks, with a d spacing of 1.16 to 1.26nm. No evidence of this is seen in any of the other fractions, at different temperatures, or after different treatments, which suggests that it is hydroxy interlayered vermiculite, with very much less well filled interlayers than are found in 1029.

1049 This appears to show a combination of the features observed in the other boulder clays. The diffraction pattern is dominated by well defined mica and chlorite peaks without tails or shoulders,

and on K saturation and heating to 550°C, an increase in the intensity of the chlorite (001) peak is seen. At room temperature and 250°C, the (001) spacing of the K saturated 0.063-0.2μm chlorite is 1.41nm. On further heating, collapse takes place, to 1.39nm at 350°C and 1.38nm at 450°C, and this is accompanied by a reduction in the intensity of the chlorite (002) peak, starting at temperatures as low as 350°C, as in 1029. At 550°C, material is seen in this fraction with a d spacing between 1.16 and 1.26nm, suggesting the presence of poorly filled hydroxy interlayered vermiculite, although less than in 1039.

1040 The diffractometer traces from this unweathered rock indicate that it has the most simple phyllosilicate mineralogy of the samples. There is no evidence of vermiculite, and the behaviour of the K saturated chlorite when heated shows that it consists of hydroxy interlayered vermiculite, with very nearly completely filled hydroxy interlayers, even in the coarser clay fractions. No significant reduction in the intensity of the K saturated chlorite (002) peak is seen until 450°C, whilst the mean chlorite (001) spacing of the coarser clay fractions is reduced from 1.41nm at 20°C to 1.40nm at 250°C and 1.38nm at 550°C. The relative intensity of the (001) peak is increased at 550°C.

1080D As can be seen in the diffractometer traces in Figure 7.2, the mineralogy of this dithionite treated soil horizon is more complex than those of the samples so far considered. The most obvious difference is the presence of a considerable amount of material with a d spacing between 1.11 and 1.26nm, after K saturation, Mg saturation or treatment with ethan1,2diol. This spacing indicates the presence of irregularly interstratified mica-chlorite or mica-hydroxy interlayered vermiculite. Although the variation in the (001) spacings of the K saturated chlorite after heat treatment does not follow a regular pattern, and it is thus impossible to determine whether the chlorite is a true chlorite or a very nearly completely filled hydroxy interlayered vermiculite, it would seem that the mineral irregularly interstratified with the mica is not chlorite, but hydroxy interlayered vermiculite. The evidence for this is provided by the behaviour on heating of the K saturated material. At temperatures as low as 250°C, the amount of material with a basal spacing in the range 1.11 to 1.26nm has been considerably

reduced, and by 550°C has been reduced to a negligible amount, whereas irregularly interstratified mica-chlorite would be expected to retain its original d spacing on heating to 550°C.

Besides this irregularly interstratified mineral, there is a considerable amount of vermiculite present in all fractions investigated. This is identified by comparing the 1.4nm peak after K saturation and Mg saturation, when it is seen that the peak after Mg saturation is considerably more intense. Vermiculite has an (001) spacing of 1.0nm after K saturation, and 1.4nm after Mg saturation. The diffractometer traces indicate that most vermiculite is found in the 0.2-0.63μm fraction, but it may be that some of the vermiculite present in the 0.063-0.2μm fraction has been permanently collapsed to 1.0nm by the K saturation used in the fractionation procedure.

Close examination of the diffractometer traces indicates the presence of a very small amount of a mineral with a 2.45nm d spacing. This is seen in the coarser clay fractions, and appears after K saturation, Mg saturation, and after treatment with ethan1,2diol. The 2.45nm d spacing and its invariability after different treatments indicates regularly interstratified mica-chlorite or possibly mica-hydroxy interlayered vermiculite.

The final difference between the mineralogy of this sample and those of the boulder clays and rock is the presence of a small amount of lepidocrocite, identified by a peak at 0.625nm, which is entirely removed by heating to as low as 250°C.

1079D The diffractometer traces from 1079D are similar to those from 1080D, except that there is a reduction in the amount of chlorite, or hydroxy interlayered vermiculite. When K saturated, no individual 1.4nm peak can be distinguished, indicating that the chlorite, or hydroxy interlayered vermiculite, is imperceptibly merged with its irregular interstratification with mica, which is still present in considerable quantities, as is evidenced by the material with 1.11 to 1.43nm d spacing. The loss of most of this material on heating favours the presence of hydroxy interlayered vermiculite rather than true chlorite. When Mg saturated, the coarser clay fractions show separate 1.4nm peaks, indicating the presence of vermiculite, and the change in

shape of the diffraction profile of the 0.063-0.2μm fraction in the 1.4nm region also indicates the presence of a smaller amount of vermiculite. In the unheated specimens, there is evidence of more lepidocrocite than in 1080D.

The very small shoulders and slight discontinuities in the slope of the diffractometer trace that correspond to regularly interstratified minerals are only seen after Mg saturation or treatment with ethan1,2diol. This indicates that the (001) spacing of both components of the interstratification must be identical after K saturation, suggesting that the mineral is mica-vermiculite, which would give reflections at 2.4nm after Mg saturation or ethan1,2diol treatment and 1.0nm after K saturation or heating to 550°C. The observed spacings are listed in Table 7.2, and these are all reasonably consistent with the presence of regularly interstratified mica-vermiculite.

1078D The K saturated specimens of this sample show no separate 1.4nm peaks, even when heated to 550°C, and the 0.7nm peak has been eliminated by 450°C. Instead, the 1.0nm mica peaks show very broad tails from 1.11 to 1.43nm, which are considerably reduced in intensity by heating. This shows that no significant amount of chlorite, or hydroxy interlayered vermiculite, remains in the sample.

On Mg saturation, peaks are seen at both 1.39 and 1.21nm in the coarser clay fractions, with a band from 1.11 to 1.21nm in the 0.063-0.2μm fraction. Neither treatment with ethan1,2diol or propan1,2,3triol appears to affect these positions, indicating that the mineral responsible for the 1.39nm peak is vermiculite, whilst that responsible for the 1.21nm peak and the 1.11 to 1.21nm band is irregularly interstratified mica-vermiculite.

Less lepidocrocite is seen than on the traces of 1079D, but the discontinuities due to regularly interstratified minerals are better defined, and are detailed in Table 7.3. All of the reflections for the coarsest clay fraction can be explained by regularly interstratified mica-chlorite or mica-hydroxy interlayered vermiculite, but the interpretation of the reflections from the finer clay fractions depends on whether the absence of a high d spacing reflection after K saturation is real

or due to insufficient resolution from the background. If the absence is real, then the remaining reflections from the finer fractions must be due to regularly interstratified mica-vermiculite, whereas if the absence is apparent, the reflections will be due to regularly interstratified mica-chlorite or mica-hydroxy interlayered vermiculite, as in the coarsest fraction.

1077D In this sample, all chlorite, hydroxy interlayered vermiculite and lepidocrocite have been eliminated, leaving only mica, vermiculite and interstratifications of the two. None of the K saturated specimens, whether heated or not, show any reflections except a sharp peak at approximately 1.0nm. Although rather broader than the K saturated peak, even when Mg saturated or treated with ethan1,2diol or propan1,2,3triol, the 0.063-0.2µm fraction only shows this reflection, indicating its phyllosilicate mineralogy to be almost entirely mica, with possibly a little irregularly interstratified mica-vermiculite. The coarser fractions show evidence of irregularly and regularly interstratified mica-vermiculite, with a higher proportion regularly interstratified than in 1078D, and with larger amounts of both interstratified phases in the 0.63-2µm fraction. This fraction shows a clear peak at about 2.45nm when Mg saturated or treated with ethan1,2diol, whereas the 0.2-0.63µm fraction shows a broad band of interstratified material from 1.95 to 2.70nm after both treatments. For the 0.2-0.63µm fraction, the irregularly interstratified material appears as a tail to the 1.0nm mica peak, whereas in the 0.63-2µm fraction it occurs in a well defined band from 1.23 to 1.41nm. A very weak 0.7nm reflection occurs in the Mg saturated specimens, indicating the presence of a little vermiculite in a noninterstratified form.

1076D The traces produced by this sample are very similar to those given by 1077D, except that it is only in the 0.63-2µm fraction that both regularly and irregularly interstratified mica-vermiculite are seen. In the 0.2-0.63µm fraction, the irregularly interstratified mica-vermiculite is represented by a broad tail to the 1.0nm peak, whereas in the 0.63-2µm fraction a distinct peak is seen at 1.21nm, with a shoulder to 1.40nm. The regularly interstratified mica-vermiculite peak seen in the coarsest fraction is at 2.40nm, and a very weak vermiculite (002) peak is seen at 0.7nm in the coarser clay fractions.

1079 Except in two details, the diffractometer traces produced by this sample do not differ from those of the dithionite treated sample of the same horizon. The most obvious difference, which would be expected, is that there is far more lepidocrocite in the untreated specimens than in the treated ones. The second difference, which is not readily explicable, is that the 0.7nm peaks are invariably stronger in dithionite treated specimens, no matter whether the clay has been Mg or K saturated, yet the 1.4nm peaks are not consistently stronger in either treated or untreated specimens. Figure 7.6 shows that there is no evidence that dithionite treatment of this sample produces regularly interstratified chlorite-vermiculite, as has been suggested to occur [174], but this may be due to the starting material not being true chlorite, but hydroxy interlayered vermiculite, or because of its interstratification with mica.

1077 When compared to the similarity between diffractometer traces from 1079D and 1079, the difference between the traces from 1077D and 1077, as seen in Figure 7.6, is obvious. No differences at all can be discerned between the untreated and dithionite treated specimens when K saturated, or when Mg saturated specimens of the 0.063-0.2μm fractions are considered. However, the well defined peaks due to both irregularly and regularly interstratified mica-vermiculite seen in the 0.63-2μm fraction of 1077D when Mg saturated or treated with ethan1,2diol are represented in the same fraction of 1077 only by a broad tail to the 1.0nm mica peak of irregularly interstratified mica-vermiculite. In the 0.2-0.63μm fraction, tails to this peak occur in both treated and untreated specimens, with the tails in the untreated specimens being larger.

Only one plausible mechanism can be invoked to explain these observations. In order to produce the significant amounts of interstratified mica-vermiculite seen in 1077D but not in 1077, the dithionite must be breaking down the mica structure. If this is the case, then the mica in 1077 must be different to that in 1079, as no similar production of interstratified material occurs after treatment of 1079. This difference can only have been brought about by the effects of weathering, and the most likely mechanism of alteration is the oxidation of $Fe^{2+}$ to $Fe^{3+}$. This will reduce the structural negative charge which holds the

**Figure 7.6** The Effect of Dithionite Treatment on the Phyllosilicate Mineralogy of the O.63-2μm Fractions of Two Plynlimon Soil Horizons. All Traces are of Mg Saturated Specimens Recorded at a Full Scale Deflection of $2 \times 10^3$ cps

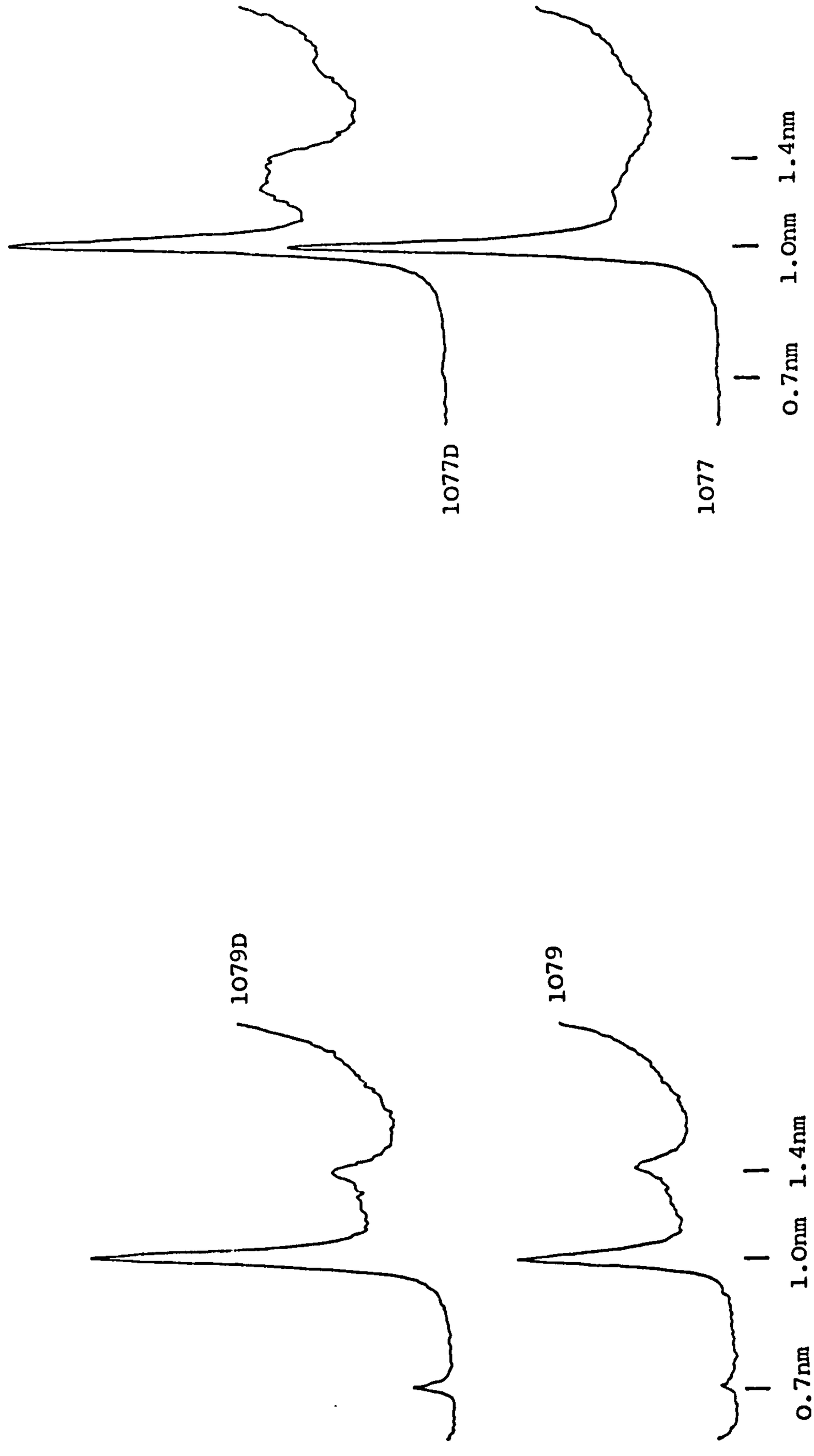

interlayer cations in place, enabling removal of K and alteration to vermiculite to take place more easily [98,195]. It has been shown that dithionite treatment can alter phyllosilicates, causing an increase in the CEC of up to six times, particularly when interstratified chlorite-vermiculites are present [220].

Although the 0.2-0.63μm fraction of 1077 apparently contains more irregularly interstratified mica-vermiculite than the 0.63-2μm fraction, after dithionite treatment the diffractometer trace of this finer fraction is almost identical, whereas in the 0.63-2μm fraction the amount of irregularly interstratified mineral is increased, and regularly interstratified mica-vermiculite is revealed by dithionite treatment. If weathering had altered the mica structure to make it more susceptible to attack, the effects would be expected to be seen more clearly in the finer size fraction. Even though alteration may have taken place as expected, it has been shown that K removal from micas to form vermiculites becomes more difficult as particle size decreases from about 1μm [195]. No adequate theory has been proposed to explain the tenacity with which K is held by very small mica particles, but this phenomenon would appear to explain the differences between the effects of dithionite treatment on the coarser clay fractions from 1077.

1087 Examination of the traces produced by this sample show that its phyllosilicate mineralogy, although similar in outline, is different in detail to the mineralogy of the Plynlimon samples. When the traces from K saturated specimens are compared with those from Mg saturated specimens, the similarity of the clean, sharp 1.4 and 1.0nm peaks on both sets of traces indicates that the phyllosilicates are dominated by mica and chlorite. The amount of lepidocrocite increases with decreasing particle size. A similarity between this sample and 1039 is that after all of the treatments except K saturation coupled with heating to more than 350°C, or treatment with ethan1,2diol, the 0.7nm chlorite (002) peak shows a tail to 0.85nm in the 0.063-0.2μm fraction. A similar, but less well developed, tail is seen in the 0.2-0.63μm fraction after Mg saturation or ethan1,2diol treatment.

After heating to 550°C, the chlorite (002) peak, together with its tail, is almost completely removed, but the chlorite (001)

peak, at a mean position of 1.40nm, is much intensified, and develops a tail between 1.2 and 1.3nm. This could be due to either irregularly interstratified chlorite-vermiculite or chlorite-mica, but the presence of the tail on the (002) peak after both Mg and K saturation favours irregularly interstratified chlorite-mica, as is seen in 1039. However, the behaviour of the interstratified minerals in the two samples on heating to 550°C is different, and thus there must be some structural difference between them.

### 7.1.3 Estimation of Vermiculite Content by X-ray Diffraction

Although the XRD analysis used to identify the phyllosilicate mineralogy cannot be used in a strictly quantitative way, the fact that the vermiculite structure collapses from 1.4nm when Mg saturated to 1.0nm on K saturation opens up the possibility of estimating the relative vermiculite contents of different specimens. Because there are interstratified minerals in many of the specimens, peak areas on the diffractometer traces cannot be assigned with any certainty to the 1.4 or 1.0nm peaks, and thus peak heights have been used in the calculations. These were measured for the 1.4, 1.0 and 0.7nm peaks of both the Mg saturated and K saturated specimens, and the ratios:

$$\frac{\text{Height at 1.0nm K Saturated}}{\text{Height at 1.4nm K Saturated}} : \frac{\text{Height at 1.0nm Mg Saturated}}{\text{Height at 1.4nm Mg Saturated}}, \text{ and}$$

$$\frac{\text{Height at 1.0nm K Saturated}}{\text{Height at 0.7nm K Saturated}} : \frac{\text{Height at 1.0nm Mg Saturated}}{\text{Height at 0.7nm Mg Saturated}}$$

were calculated for the clay fractions of each sample. Both 1.4 and 0.7nm peaks were used, as in general the 0.7nm peak is larger for the rock, boulder clays and Hiraethog comparison material, whilst the 1.4nm peak is larger for the soil horizons.

When Mg saturated, any vermiculite should be expanded to 1.4nm, and thus contribute to the denominator of the peak height ratio, whilst when K saturated the vermiculite will collapse to 1.0nm and be counted into the numerator. This leads to values for the overall ratios given above which increase with the vermiculite content, varying from one for a specimen free of vermiculite to infinity for a specimen in which both chlorite and mica have been entirely replaced by vermiculite. In effect, the overall ratios are quantifying the same features, as the 0.7nm peak is due to the (002) reflection of the phases with a 1.4nm

(001) reflection. For this reason, the mean of the overall ratios is given in Table 7.4, as well as the values for the expressions separately.

A theoretical approach suggests that the minimum value for the overall ratios should be 1.0, but in practice values lower than this occur 7 out of 36 times for the ratio based on the 0.7nm peak, and 3 out of 36 times for the ratio based on the 1.4nm peak. The lowest value recorded is 0.84, and the mean of the values lower than 1.0 is 0.95, which suggest that the value of 1.0 is the true minimum, with lower values being caused by experimental inaccuracies. The maximum value of the ratio based on the 0.7nm peak is 4.48, whilst that for the ratio based on the 1.4nm peak is 29.87. The correlation coefficient between the natural logarithms of the two sets of values is 0.654, a logarithmic scale being used because a variation of vermiculite content from 0 to 100% results in a variation in overall ratio from one to infinity.

If the mean values for each fraction of the mean of the overall ratios are compared, it can be seen that, on average, the amount of vermiculite increases with size from a value of 1.46 in the 0.063-0.2μm fraction through 3.09 in the 0.2-0.63μm fraction to 3.49 in the 0.63-2μm fraction. This suggests that the finest fraction has a lower vermiculite content than the coarser fractions, which is borne out by the individual overall means of the dithionite treated soil horizons. However, in the Plynlimon rock and boulder clays, and the comparison material from Hiraethog, none of which have been subjected to as much weathering as the soil, the vermiculite contents are similar in all clay fractions, and are very much lower than in the soil samples. This could either be explained by the K saturation of the 0.063-0.2μm fraction during separation causing the majority of the vermiculite present in that fraction to contract permanently to a basal spacing of 1.0nm, or by vermiculite in the finest fraction being broken down very much more rapidly than either the chlorite or mica in the same fraction, or the vermiculite in the coarser fractions.

If the mean for each sample of the mean of the overall ratios are examined, the observations made by visual examination of the diffractometer traces are seen to be confirmed by this semiquantitative analysis. As an overall ratio as low as 0.84 was measured, it is reasonable to assume that values as high as 1/0.84, 1.19, could possibly be due to experimental error rather than to the presence of

TABLE 7.4 Estimation of Relative Vermiculite Contents by Measurement of Peak Heights After Different Saturation Treatments

| Sample | Size Fraction (μm) | Peak Height at 1.0nm / Peak Height at 0.7nm | | | Peak Height at 1.0nm / Peak Height at 1.4nm | | | Mean of /K / /Mg Values |
|---|---|---|---|---|---|---|---|---|
| | | /K | /Mg | /K / /Mg | /K | /Mg | /K / /Mg | |
| 1040 | 0.063-0.2 | 5.6 | 4.1 | 1.35 | 12 | 9.7 | 1.26 | 1.31 |
| 1040 | 0.2 - 0.63 | 2.5 | 2.7 | 0.92 | 7.8 | 7.3 | 1.07 | 0.99 |
| 1040 | 0.63 - 2 | 2.0 | 2.0 | 1.00 | 5.8 | 6.5 | 0.89 | 0.95 |
| 1029 | 0.063-0.2 | 7.1 | 5.1 | 1.38 | 18 | 15 | 1.22 | 1.30 |
| 1029 | 0.2 - 0.63 | 3.4 | 3.5 | 0.97 | 12 | 10 | 1.15 | 1.06 |
| 1029 | 0.63 - 2 | 1.7 | 1.1 | 1.51 | 8.3 | 7.1 | 1.16 | 1.34 |
| 1039 | 0.063-0.2 | 5.9 | 5.0 | 1.18 | 21 | 19 | 1.11 | 1.15 |
| 1039 | 0.2 - 0.63 | 4.1 | 4.1 | 0.98 | 14 | 11 | 1.23 | 1.11 |
| 1039 | 0.63 - 2 | 1.7 | 1.5 | 1.15 | 7.9 | 8.1 | 0.97 | 1.06 |
| 1049 | 0.063-0.2 | 5.4 | 5.1 | 1.05 | 17 | 14 | 1.18 | 1.12 |
| 1049 | 0.2 - 0.63 | 2.9 | 3.0 | 0.99 | 11 | 8.4 | 1.34 | 1.17 |
| 1049 | 0.63 - 2 | 1.3 | 1.1 | 1.18 | 7.2 | 6.2 | 1.16 | 1.17 |
| 1080D | 0.063-0.2 | 6.7 | 5.8 | 1.16 | 4.9 | 3.4 | 1.43 | 1.30 |
| 1080D | 0.2 - 0.63 | 6.1 | 6.0 | 1.02 | 7.0 | 3.4 | 2.06 | 1.54 |
| 1080D | 0.63 - 2 | 3.0 | 2.9 | 1.05 | 5.7 | 3.4 | 1.67 | 1.36 |
| 1079D | 0.063-0.2 | 36 | 27 | 1.33 | 7.5 | 4.9 | 1.52 | 1.43 |
| 1079D | 0.2 - 0.63 | 21 | 20 | 1.04 | 8.8 | 3.7 | 2.36 | 1.70 |
| 1079D | 0.63 - 2 | 9.6 | 8.3 | 1.16 | 8.6 | 4.5 | 1.92 | 1.54 |
| 1078D | 0.063-0.2 | 70 | 61 | 1.15 | 16 | 7.6 | 2.12 | 1.63 |
| 1078D | 0.2 - 0.63 | 52 | 37 | 1.41 | 19 | 4.5 | 4.25 | 2.83 |
| 1078D | 0.63 - 2 | 30 | 21 | 1.40 | 19 | 3.8 | 4.95 | 3.18 |
| 1077D | 0.063-0.2 | 150 | 120 | 1.27 | 77 | 20 | 3.82 | 2.55 |
| 1077D | 0.2 - 0.63 | 270 | 61 | 4.48 | 91 | 8.5 | 10.70 | 7.59 |
| 1077D | 0.62 - 2 | 160 | 120 | 1.38 | 110 | 3.6 | 29.87 | 15.62 |
| 1076D | 0.063-0.2 | 190 | 140 | 1.40 | 64 | 26 | 2.49 | 1.95 |
| 1076D | 0.2 - 0.63 | 130 | 60 | 2.13 | 130 | 8.9 | 14.30 | 8.21 |
| 1076D | 0.63 - 2 | 210 | 92 | 2.30 | 71 | 6.2 | 11.49 | 6.89 |
| 1079 | 0.063-0.2 | 31 | 18 | 1.75 | 4.6 | 3.7 | 1.26 | 1.51 |
| 1079 | 0.2 - 0.63 | 24 | 29 | 0.84 | 5.7 | 3.3 | 1.74 | 1.29 |
| 1079 | 0.63 - 2 | 15 | 12 | 1.30 | 5.7 | 3.1 | 1.82 | 1.56 |
| 1077 | 0.063-0.2 | 73 | 77 | 0.95 | 44 | 33 | 1.33 | 1.14 |
| 1077 | 0.2 - 0.63 | 180 | 84 | 2.09 | 110 | 7.2 | 14.56 | 8.32 |
| 1077 | 0.63 -2 | 130 | 94 | 1.34 | 130 | 11 | 11.22 | 6.28 |
| 1087 | 0.063-0.2 | 4.0 | 3.7 | 1.08 | 12 | 10 | 1.16 | 1.12 |
| 1087 | 0.2 - 0.63 | 3.1 | 2.8 | 1.11 | 9.0 | 6.6 | 1.36 | 1.23 |
| 1087 | 0.63 - 2 | 1.6 | 1.6 | 0.95 | 5.4 | 5.5 | 0.97 | 0.96 |

small quantities of vermiculite. The unweathered rock gives a value of 1.08, suggesting that it contains little or no vermiculite. The boulder clays and Hiraethog comparison material have the next lower values, varying between 1.10 and 1.23, with only the value for 1029 exceeding 1.19. Although the similarity between the Hiraethog material and 1039 is maintained, these are shown to have lower values than 1029 and 1049, although the opposite might have been expected. The vermiculite in the Hiraethog material has been shown to be dioctahedral [219]. All of the dithionite treated soil horizons have higher levels of vermiculite, which increase up the profile as far as the Ea2 horizon, falling off again in the Ea1 horizon. Both of the untreated soil samples show lower levels of vermiculite than the equivalent dithionite treated samples, indicating that the dithionite treatment is altering mica, and possibly chlorite, to vermiculite.

## 7.2 THE CHEMICAL DETERMINATION OF VERMICULITE AND SMECTITE

The determination of vermiculite by XRD can be at best only semiquantitative, because vermiculite commonly occurs interstratified with mica or chlorite. For this reason, a chemical method was developed to estimate the vermiculite content of soil samples in a quantitative manner [4]. Slight modifications to this method have been proposed in order to reduce the time for analysis [64], but the method used in this study is more similar to the original method than the modified scheme.

The method uses the fact that vermiculites fix K in their interlayer sites, particularly if dried at a high temperature after K saturation. The CEC can be determined by saturating with one ion, displacing this with a second, and determining the amount of the ion displaced, whilst the CEC excluding the vermiculite interlayer sites can be determined by K saturation, drying, and then displacing the unfixed K with another ion. The CEC due to the vermiculite interlayer sites can then be determined from the difference between the two CEC values and, if the interlayer charge of the vermiculite is known, the vermiculite content can be calculated.

As the interlayer charge of the vermiculites investigated in this study was not known, the value of 154mEq $100g^{-1}$ [4] was used, being the mean value from the samples with which the method was developed. An interlayer charge of 105mEq $100g^{-1}$ for montmorillonite and an external surface charge of 5mEq $100g^{-1}$ for all phyllosilicates were assumed,

which allowed the montmorillonite content to be calculated from the amount of displaced K, although no allowance was made for the CEC of noncrystalline materials. However, allowance was made for the quartz content as determined by quantitative XRD (Section 6.5), which was not included in the original method. The equations used to calculate the vermiculite and montmorillonite contents, and the vermiculite interlayer fraction (VIF) - the proportion of the total CEC that is produced by the vermiculite interlayer sites [64] - are as follows:

$$\% \text{ Vermiculite} = \frac{CEC(Ca/Mg) - CEC(K/NH_4)}{1.54},$$

$$\% \text{ Montmorillonite} = \frac{CEC(K/NH_4) - 5\left(1 - \frac{\% \text{ Quartz}}{100}\right)}{1.05}, \text{ and}$$

$$VIF = \frac{CEC(Ca/Mg) - CEC(K/NH_4)}{CEC(Ca/Mg)}.$$

This method is thus based on the four major assumptions that:

1. Vermiculite has an interlayer exchange capacity of 154mEq $100g^{-1}$.
2. This exchange capacity is entirely blocked by K fixation.
3. Vermiculite is the only mineral present able to fix K.
4. All of the vermiculite interlayer sites are fully accessible, and full displacement will occur, except after K fixation [64].

With regard to the specimens investigated, 4. is likely to be correct, as the only evidence that cation exchange does not take place freely is provided by large flakes of mica derived vermiculite [64]. 1. cannot be totally correct, but is the best assumption to use when there is no evidence for other interlayer exchange capacities. 2. and 3. may be true, but cannot be proved to be so. However, it is certainly possible that the montmorillonite shown to be present in some specimens may be beidellitic, and could thus fix a certain amount of K [64,258], whilst it is very likely that some of the vermiculite is hydroxy interlayered, and may thus be unable to fix K because the exchange sites are kept open by the interlayers. It must thus be accepted that the vermiculite that is determined by this method is based on a practical definition, possibly including beidellites and excluding hydroxy interlayered vermiculites, rather than on the strict mineralogical definition of vermiculite.

Approximately 100mg of each specimen were accurately weighed into a 20cm³ centrifuge tube, and then shaken in sequence five times with 15cm³ of 0.5M $CaCl_2$ solution, once with distilled water and then five times with 99% methanol. Each period of shaking lasted five minutes, and was followed by centrifugation to sediment the specimen. The supernatant was discarded. After this saturation with Ca, replacement of the Ca by Mg followed. Five aliquots of 10cm³ of 0.5M $MgCl_2$ solution were added in turn to the specimen, which was then shaken for five minutes. After shaking, but before centrifugation, 5cm³ of distilled water were added to the tube. After each centrifugation the supernatant was collected, and these washings were bulked together and diluted to 100cm³ with distilled water. The displaced Ca was determined in this solution by atomic absorption spectrometry.

The specimen was then K saturated, by shaking five times with 1M KCl solution, once with distilled water, once with 99% methanol, twice with a 50:50 methanol:acetone mix and once with pure acetone. After each five minute period of shaking, centrifugation was carried out and the supernatant discarded. After the final washing, the specimen was placed in an oven at 110°C overnight, in order to fix the K onto the vermiculite interlayer exchange sites. After drying, five washings, each of 8cm³ 1M $NH_4Cl$ solution, were carried out to displace the unfixed K. The supernatants obtained after each centrifugation were bulked together and diluted to 200cm³ with distilled water. The displaced K was determined in this solution by flame emission spectrometry.

Duplicate analyses were carried out; the means and standard deviations are given in Table 7.5. Because of the restricted time available, only a limited number of specimens could be analysed, and thus no investigation was made of the 0.063-0.2μm fractions, because of the likelihood of K fixation during the separation procedure. Only the coarser clay fractions were analysed for the dithionite treated soil horizons, the unweathered rock, the most representative boulder clay and the comparison material from Hiraethog. Unfortunately, neither of the untreated soil samples were analysed, although these data would have been useful to indicate the possible extent of vermiculite formation from mica during dithionite treatment (Section 7.1.2).

However, soils that have had vermiculite contents determined both before and after dithionite treatment have shown only a mean increase

TABLE 7.5 The Vermiculite and Montmorillonite Contents of Clay Fractions, as Determined by CEC Methods

| Sample | Size Fraction (μm) | CEC by $Ca^{2+}$ Displacement (mEq $100g^{-1}$) | CEC by $K^{+}$ Displacement (mEq $100g^{-1}$) | Interlayer Charge Fixed by $K^{+}$ (mEq $100g^{-1}$) | Vermiculite as a % of the Total Specimen | Montmorillonite as a % of the Total Specimen | %Vermiculite Interlayer Fraction | Expandable Minerals as a % of Total Phyllosilicates |
|---|---|---|---|---|---|---|---|---|
| 1040 | 0.2 - 0.63 | 9.9 ± 0.9 | 9.6 ± 0.4 | 0.3 ± 1.0 | 0.2 ± 0.6 | 5.2 ± 0.4 | 3 ± 9 | 6.4 ± 0.9 |
| 1040 | 0.63 - 2 | 5.8 ± 0.5 | 6.9 ± 1.4 | -1.1 ± 1.4 | -0.7 ± 0.9 | 2.8 ± 1.3 | -20 ± 30 | 3 ± 2 |
| 1049 | 0.2 - 0.63 | 7.88 ± 0.13 | 5.20 ± 0.01 | 2.68 ± 0.13 | 1.74 ± 0.08 | 0.36 ± 0.01 | 34.0 ± 1.1 | 2.18 ± 0.08 |
| 1049 | 0.63 - 2 | 4 ± 2 | 3.1 ± 1.6 | 1 ± 3 | 0.6 ± 1.9 | -1.2 ± 1.5 | 20 ± 60 | -1 ± 3 |
| 1080D | 0.2 - 0.63 | 10.39 ± 0.07 | 7.97 ± 0.08 | 2.42 ± 0.11 | 1.57 ± 0.07 | 2.96 ± 0.08 | 23.3 ± 0.9 | 4.67 ± 0.11 |
| 1080D | 0.63 - 2 | 9.6 ± 0.3 | 8.66 ± 0.04 | 1.0 ± 0.3 | 0.63 ± 0.19 | 3.89 ± 0.04 | 10 ± 3 | 4.9 ± 0.2 |
| 1079D | 0.2 - 0.63 | 13.4 ± 0.4 | 11.28 ± 0.04 | 2.2 ± 0.4 | 1.4 ± 0.2 | 6.04 ± 0.04 | 16 ± 2 | 7.5 ± 0.2 |
| 1079D | 0.63 - 2 | 11.88 ± 0.09 | 10.5 ± 1.5 | 1.4 ± 1.5 | 0.9 ± 1.0 | 5.4 ± 1.4 | 12 ± 13 | 6.6 ± 1.8 |
| 1078D | 0.2 - 0.63 | 17.25 ± 0.08 | 11.3 ± 1.0 | 6.0 ± 1.0 | 3.9 ± 0.7 | 6.0 ± 1.0 | 35 ± 6 | 10.1 ± 1.2 |
| 1078D | 0.63 - 2 | 16.69 ± 0.09 | 8.95 ± 0.08 | 7.74 ± 0.12 | 5.02 ± 0.08 | 3.97 ± 0.08 | 46.4 ± 0.6 | 9.42 ± 0.12 |
| 1077D | 0.2 - 0.63 | 20.8 ± 0.6 | 7.9 ± 0.4 | 12.9 ± 0.7 | 8.4 ± 0.4 | 2.8 ± 0.3 | 62 ± 2 | 11.5 ± 0.6 |
| 1077D | 0.63 - 2 | 26.3 ± 0.7 | 7.5 ± 0.2 | 18.7 ± 0.8 | 12.2 ± 0.5 | 2.5 ± 0.2 | 71.3 ± 1.2 | 15.1 ± 0.5 |
| 1076D | 0.2 - 0.63 | 17 ± 2 | 7.3 ± 0.2 | 10 ± 2 | 6.3 ± 1.4 | 2.3 ± 0.2 | 57 ± 6 | 8.8 ± 1.4 |
| 1076D | 0.63 - 2 | 19.6 ± 0.5 | 6.50 ± 0.10 | 13.1 ± 0.5 | 8.5 ± 0.3 | 1.56 ± 0.10 | 66.8 ± 0.9 | 10.3 ± 0.3 |
| 1087 | 0.2 - 0.63 | 7.8 ± 0.7 | 5.5 ± 0.3 | 2.3 ± 0.7 | 1.5 ± 0.5 | 0.6 ± 0.3 | 29 ± 7 | 2.2 ± 0.6 |
| 1087 | 0.63 - 2 | 4.0 ± 0.4 | 5.6 ± 1.3 | -1.7 ± 1.4 | -1.1 ± 0.9 | 0.9 ± 1.3 | -40 ± 40 | -0.8 ± 1.7 |

of 3% in their vermiculite contents, coupled with a mean decrease of 15% in their VIF, indicating that dithionite treatment tends to preferentially open up exchange sites that do not fix K [64]. For all the specimens except the 0.63-2μm fraction from 1080D, and both specimens from 1079D, all of the analysis was carried out on the same material. However, for these specimens the original material was lost after the CEC based on Ca displacement (CaEC) had been determined, and thus further material from the same specimen was used to determine the CEC based on K displacement (KEC).

### 7.2.1 Interpretation of Results

The results in Table 7.5 are interesting in many ways. Besides confirming the presence of vermiculite, as observed in the qualitative XRD analysis, this chemical analysis appears to indicate the presence of substantial quantities of montmorillonite, which constitutes more than 6% of the 0.2-0.63μm fractions of the dithionite treated soil Bsg and Bs horizons. Although there is no evidence from XRD for the existence of montmorillonite as an independent mineral, because of the lack of a peak at 1.7 to 1.8nm after treatment with ethan1,2diol, it is possible that at least some of the mineral identified as irregularly interstratified mica-hydroxy interlayered vermiculite is in fact irregularly interstratified mica-montmorillonite. However, it would seem likely that the mineral determined as montmorillonite by CEC methods is not montmorillonite, but another mineral that is unable to fix K, yet has a high CEC. The most obvious mineral that has these properties is hydroxy interlayered vermiculite, as there is evidence that, if the interlayers are held open by partially complete hydroxy interlayer sheets, the remaining interlayer exchange sites will be unable to fix K [18,64]. The evidence from qualitative XRD analysis does not contradict this, and a hypothesis can be put forward to explain the distribution of the different phyllosilicate minerals throughout the profile, based on this interpretation (see Section 7.3).

Because the determined montmorillonite contents are based on calculations using the interlayer exchange capacity of true montmorillonite, it is likely that the figures given in Table 7.5 are not quantitative representations of the amounts of hydroxy interlayered vermiculite. As weathering of chlorite progressed, it would be expected that the amount of hydroxy interlayering would be reduced [133], and thus the interlayer exchange capacity increased. If the weathering eventually transformed chlorite into nonhydroxy interlayered

vermiculite, it would be expected that the figures given for montmorillonite in Table 7.5 would be underestimates of the hydroxy interlayered vermiculite when the interlayers were nearly complete, and the interlayer CEC was less than the 105mEq $100g^{-1}$ assumed. On the other hand, these figures would be overestimates where the weathering process had progressed, and the amount of hydroxy interlayers had been reduced so that the interlayer CEC was greater than 105mEq $100g^{-1}$.

A quantitative determination of the hydroxy interlayered vermiculite could only be carried out by first determining the nonhydroxy interlayered vermiculite, treating to remove hydroxy interlayers [18], and then again determining the vermiculite content by cation exchange methods. The difference between the measurements would correspond to the vermiculite that was originally hydroxy interlayered. It thus appears that, as well as having to accept a pragmatic definition of vermiculite, a similar approach must be used with the definition of montmorillonite as determined by CEC methods.

Considering the results in detail, the tabulated variables form two groups, except for the total expandable mineral content, which combines the attributes of both. The first group includes the CaEC, the interlayer charge fixed by K, the % vermiculite and the VIF, whilst the second includes the KEC and the % montmorillonite. The first group shows increasing values up the profile as far as the Ea2 horizon, and then a fall off in the Ea1 horizon. The only exception to this pattern is that the VIF is higher in the BC than the Bs horizon. Both the unweathered rock and the comparison material from Hiraethog show lower values for these variables than the soil horizons, whilst the boulder clay shows a lower value for CaEC, but values that are very similar to the Bs horizon for the interlayer charge fixed by K and the % vermiculite, and a value for the VIF that is intermediate between the values for the Bs and Bsg horizons. The unweathered rock, boulder clay and comparison material all show higher values of these variables in the finer of the fractions analysed, and this is also seen in the least weathered soil horizons. However, as weathering progresses, the higher values are found in the 0.63-2μm fractions.

This indicates that, as weathering proceeds, the CEC, as expressed by CaEC, is increased, showing that the original phyllosilicate minerals, illite and chlorite, are being transformed into expandable minerals with higher CECs, such as vermiculite and montmorillonite. The

parallel increase in the VIF reveals that vermiculite is the most important of the minerals being formed, except possibly in the BC horizon. This is confirmed by the observed increase in the vermiculite content. The fact that the Eal horizon shows lower values for these variables must indicate that, under the most intense conditions of weathering, the vermiculite is also being broken down, either into a noncrystalline phase or by direct dissolution, as there is no evidence for the formation of other phyllosilicates. The relative values of these variables in the fractions considered also support this hypothesis; in the least weathered materials, the larger proportion of vermiculite is found in the finer of the fractions, where weathering is most effective, whereas in the most intensely weathered Eal and Ea2 horizons, the greater proportion of vermiculite is found in the coarser fraction, where it can survive longest before being transformed.

Perhaps the most unexpected result is that the unweathered rock has a higher CaEC than either the boulder clay or the Hiraethog comparison material. Because both the vermiculite content and the VIF are calculated as negative, this cannot be due to the presence of vermiculite, and thus must be due to a smectite or hydroxy interlayered vermiculite. Although this mineral is stable in the unweathered rock, it appears that it is either immediately broken down, fixes K to form a mica, or completes its hydroxy interlayer to form a chlorite, once the rock is disaggregated sufficiently to allow water percolation.

When the second group of variables is considered, a different picture is seen. Both the KEC and the % montmorillonite show maxima in the Bs horizon, being lower in the BC horizon, and decreasing consistently towards the surface. The boulder clay and the Hiraethog comparison material give values that are lower than those from the soil horizons, whilst the values given by the unweathered rock are only exceeded by those for the Bs and Bsg horizons and, in the case of the KEC, the BC horizon. For both variables, the higher value is found in the finer of the fractions investigated, except for the Hiraethog material and the BC horizon, in which it is found in the 0.63-2μm fraction.

Following the discussion of the nature of the mineral represented by the montmorillonite, it would seem that, for the soil horizons, the figures are at least a good qualitative representation of hydroxy interlayered vermiculite, as it is in the upper horizons, which have

the lowest calculated montmorillonite, that the figures are relatively overestimated, and vice versa for the lower horizons.

It appears that, on weathering of the rock, a small increase in hydroxy interlayered vermiculite is produced, presumably by breakdown of chlorite [133]. This is in turn broken down, by further removal of hydroxy interlayers, until a nonhydroxy interlayered vermiculite is formed which, in the Eal horizon, itself begins to break down. As has been pointed out, it appears that, as soon as water is able to percolate through the unweathered rock, hydroxy interlayered vermiculite is converted to chlorite. This would occur most rapidly in the finest fraction, and might leave a little material unconverted in the coarser clay. Once true weathering began, this mineral with partially filled interlayers would begin to break down more readily than the fully chloritised finer material, leading to the higher level of hydroxy interlayered vermiculite in the coarser of the fractions from the BC horizon. However, with weathering intensified in the upper horizons, the finer grains would be altered more rapidly than the already partially altered coarser grains, and thus the pattern of hydroxy interlayered vermiculite distribution between the fractions that is observed could be developed.

In the final column of Table 7.5, the totals of the determined expandable minerals are given as percentages of the total phyllosilicate contents. This calculation thus indicates the percentage of the phyllosilicates that have been, or are in the process of being, altered to expandable minerals. The quartz content is excluded, as quartz is not known to play a part in the weathering reactions assessed by these determinations.

A feature that gives confidence in these results is the high degree of correlation between them and both the relative amounts of vermiculite estimated by analysis of peak height ratios from diffractometer traces (Section 7.1.3), and the peak widths of Mg saturated 1.0nm illite peaks (see Section 8.3). The regression equations are:

$$\ln(\text{Mean Overall Peak Height Ratio}) = 0.0871 + 0.2305(\text{Vermiculite as \% Total Specimen}),$$

with a correlation coefficient of 0.975, and:

Mg Saturated Illite Peak Width (°2θ) = 0.3576 + 0.0182( Expandable Minerals as % Total Specimen),

with a correlation coefficient of 0.829. Both of these correlation coefficients are significant with very much more than 99% confidence. The first of these equations indicates that the methods used to measure the vermiculite content are very closely correlated; the natural logarithm of the mean overall peak height ratio is used in the regression equation as the peak height ratio could range from one to infinity, whilst the vermiculite content altered from 0 to 100%.

Although the second correlation coefficient is not as high, this equation is perhaps the more important, as it indicates that the majority of the variation in crystallinity value is caused by variation in the proportion of the phyllosilicates that have been altered to expandable phases, rather than by a reduction in the crystallinity of illite whilst maintaining a constant chemical and mineralogical nature.

## 7.3 THE EFFECTS OF WEATHERING ON PHYLLOSILICATE COMPOSITION

From the results presented in Sections 7.1.2, 7.1.3 and 7.2.1, a hypothesis can be put forward to explain the differences in phyllosilicate distributions between the samples. This is not contradicted by the evidence provided by results from other methods of examination, and thus it must be compared with explanations provided by other workers to account for the mineral distributions associated with the weathering of rocks containing chlorite and illite. As far as comparing the results with observations at Plynlimon are concerned, allowances must be made for the effect of dithionite treatment, as this has been shown to alter the observed mineralogy (Section 7.1.2).

As observed in the field, the stages of weathering begin with a fresh rock, such as 1040. At the present day, this alters into a more weathered rock in its surface exposures, but also behaves as a parent material for the development of soil profiles, such as that from which 1080D to 1076D were extracted. However, during the last glaciation, a different weathering regime was acting upon the rock, leading to the development of boulder clays such as 1029, 1039 and 1049, which contain unaltered rock in a modified matrix. This boulder clay also acts as the parent material for soil development, indicating that the minerals found in the profiles developed on boulder clay may have experienced two different weathering environments.

The rock taken as starting material is dominantly composed of quartz, IIb Fe rich chlorite and $2M_1$ illite, but also contains hydroxy interlayered vermiculite, at least in its clay fractions, although no noninterlayered vermiculite can be identified. The hydroxy interlayered vermiculite has almost completely full interlayers, and is thus likely to be due to alteration of the chlorite on a microscopic scale that does not affect the fabric of the rock on a macroscopic level.

When the mineralogy of the boulder clays is examined, it can be seen that chemical and mineralogical alteration of the rock, as well as physical comminution, have taken place in their production. Both chemical and XRD methods show that the boulder clays contain a small amount of noninterlayered vermiculite, but the chemical analysis shows much lower contents of hydroxy interlayered vermiculite than are present in the fresh rock. The X-ray analysis shows variation between the boulder clays, but suggests that the hydroxy interlayered vermiculite has less full interlayers than in the fresh rock. Because the chlorite in the boulder clays has been little affected by weathering under present conditions, it appears that the vermiculite found in these samples must have been produced under glacial conditions, along with the small amount of hydroxy interlayered vermiculite with poorly filled hydroxy interlayers. It is possible that the rest of the hydroxy interlayered vermiculite seen in the fresh rock has had its interlayers removed to form the vermiculite observed in the boulder clays, or it may have experienced conditions such that the hydroxy interlayers were completed, the mineral reverting to chlorite. Although this would require at least two different weathering environments, these could have been provided by the conditions prevalent during periglacial, glacial or interglacial periods. The material from Hiraethog, 1087, shows a very similar mineralogy to the boulder clays, but also contains small amounts of both regularly and irregularly interstratified chlorite-mica, which is likely to have formed during a phase of low intensity weathering.

In the soil, alteration is considerable, even in the BC horizon. The chlorite is broken down by removal of its hydroxy interlayers, to give hydroxy interlayered vermiculite and then vermiculite. As weathering is taking place in an acid environment, it might be expected that, even in the upper horizons, any vermiculite formed would retain hydroxy interlayers [147]. However, it is believed that in soil surface

horizons organic Al complexes form in preference to Al hydroxy interlayers [253]. Towards the base of the profile, K levels are such that the illite is not noticeably broken down, and some K appears to be fixed into the interlayer sites of the vermiculite derived from the chlorite, to give the irregularly interstratified illite-hydroxy interlayered vermiculite that is observed in the BC and Bs horizons. Little hydroxy interlayered vermiculite is left in the Bsg horizon, the hydroxy interlayers being removed, and the mineral converted to a true vermiculite. However, alteration of illite to vermiculite begins to take place to a significant extent in the Bsg horizon, reaching a maximum in the Ea2 horizon, with most being irregularly interstratified, although there may be a little free vermiculite. In the Ea1 horizon, the CEC is reduced, as is the amount of vermiculite, showing that even this is broken down. Throughout the profile, except in the BC horizon, small amounts of regularly interstratified minerals are found, almost certainly originating because of selective alteration of alternate (001) planes in illite and chlorite, both of which have two layer structures.

An alternative explanation of the mineral distributions would involve chlorite breaking down to noncrystalline materials, or directly into solution, whilst alteration of illite brought about the observed distribution of vermiculite and hydroxy interlayered vermiculite. The difficulty with this is that, to form hydroxy interlayered vermiculite from illite, vermiculite would have to be formed first, followed by the deposition of hydroxy interlayers. In the profile studied, maximum alteration of illite to vermiculite occurs in the Ea2 horizon, which has the second lowest content of hydroxy interlayered vermiculite. As, in environments where hydroxy interlayered minerals are stable, they are most commonly found in the surface horizons [18], it is unlikely that illite is being altered to hydroxy interlayered vermiculite even under these most favourable conditions. It is thus most unlikely that illite is altered to hydroxy interlayered vermiculite in the lower horizons, where hydroxy interlayered vermiculite is more common than vermiculite, and yet illite shows no sign of alteration.

On the evidence available, the formation of hydroxy interlayered vermiculite from chlorite in the lower horizons, followed by alteration of this mineral and illite to vermiculite in the upper horizons, is the favoured mechanism to explain the mineral distributions. However, evidence to prove the correct mechanism could be provided by analysis

of the hydroxy interlayered vermiculite. If it was derived from chlorite, it would be expected to have a trioctahedral structure with Fe and Mg rich hydroxy interlayers, whilst if derived from illite it should have a dioctahedral structure with aluminous hydroxy interlayers [219].

The overall conclusion is that chlorite shows signs of alteration deeper in the profile than illite, and passes through hydroxy interlayered vermiculite until a true vermiculite is formed, which in turn must be converted to noncrystalline silica and cations in solution. Towards the base of the profile some of the hydroxy interlayered vermiculite formed from chlorite appears to fix K to form irregularly interstratified illite-hydroxy interlayered vermiculite, which in turn weathers through irregularly interstratified illite-vermiculite to vermiculite. The illite shows little sign of alteration until the Bsg horizon, where irregularly interstratified illite-vermiculite begins to develop, eventually being completely broken down after a period as vermiculite. A diagrammatic representation of the mineral changes taking place within the profile is given in Figure 7.7.

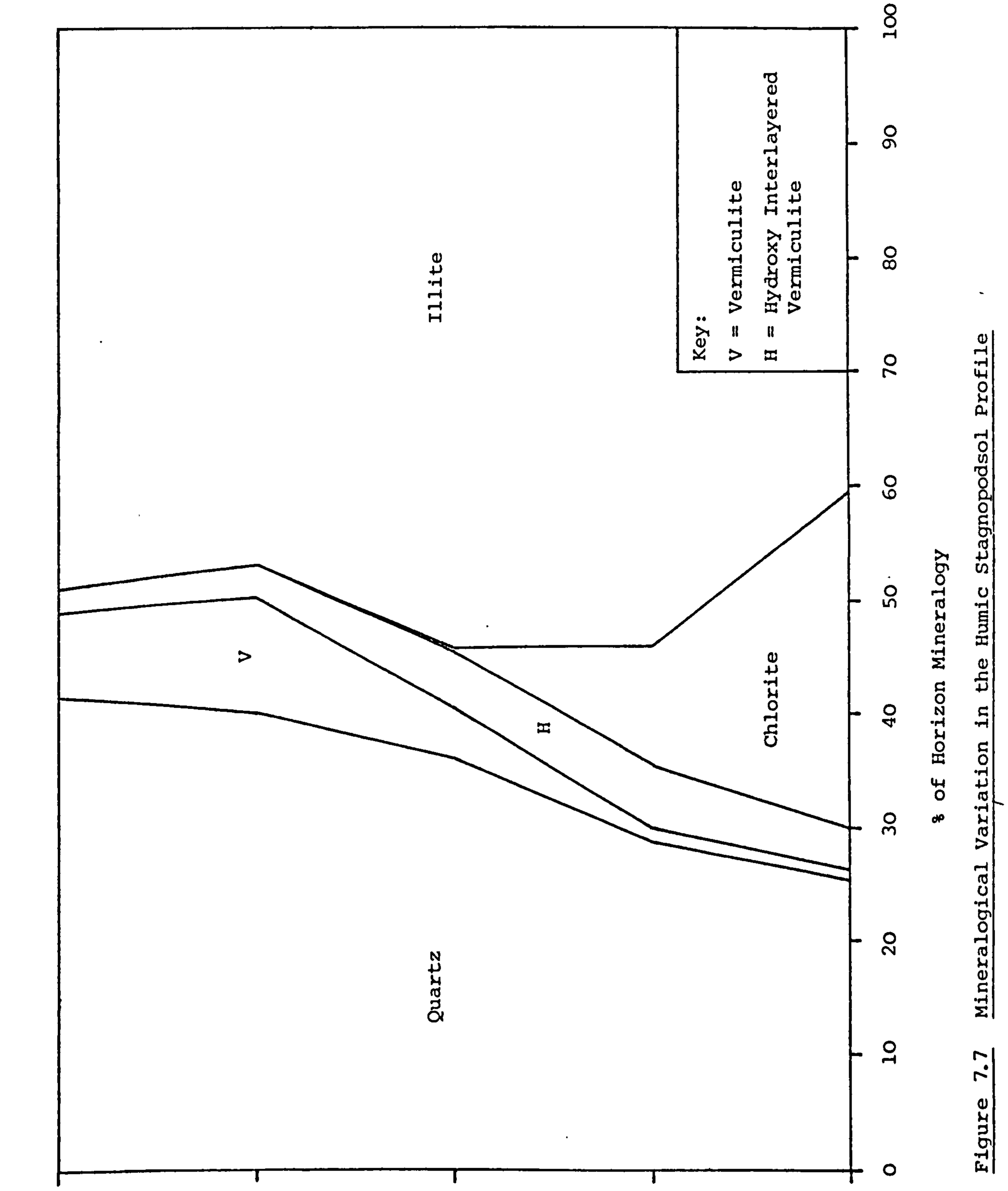


Figure 7.7 Mineralogical Variation in the Humic Stagnopodsol Profile

# CHAPTER 8

# CRYSTALLINITY DETERMINATION BY X-RAY DIFFRACTION

## 8.1 INTRODUCTION

The use of illite crystallinity in determining the intensity of low grade metamorphism was proposed by Weaver, whose interest was to obtain a quantitative measure of incipient metamorphism to assist in the search for oil [259,260]. As the degree of diagenesis and incipient metamorphism increases, the crystallite size of illite increases, and the amount of interstratified minerals is reduced. Both the reduction of interstratification and the increase in crystallite size tend towards an increase in XRD peak sharpness, and thus a decrease in width of the illite peaks [182]. Both Weaver and Kubler [154] divided the range of crystallinity variation they found into the equivalent of metamorphic zones, with the division between unmetamorphosed rocks and those in the anchimetamorphic zone being set at the position most appropriate to their interests: the value corresponding to the upper limit of metamorphic conditions for the accumulation of oil.

Just as in the search for oil, the particle size and degree of interstratification are of importance in weathering studies, and there is no reason why the methods developed to investigate the degree of metamorphism should not be used to investigate the degree of weathering, provided that two conditions are satisfied. The material under investigation must have undergone at least low grade metamorphism, or else the unweathered material would be indistinguishable from its weathered product in terms of illite crystallinity. Where metamorphism, even if only low grade, has occurred, illite crystallinity will have been increased sufficiently to allow weathering to bring about a reduction in particle size and an increase in interstratification, with a consequent reduction in crystallinity to a level similar to that before metamorphism.

If metamorphism has taken place, it is essential that all specimens have been subjected to the same degree of metamorphism, and would have provided an identical illite crystallinity value if measured before weathering. If this were not the case, and crystallinity determinations were compared for specimens that had undergone different degrees of metamorphism, it might be found that a specimen that had been highly metamorphosed, but then more intensively altered, could

give an identical crystallinity value to specimens that had experienced lower grade metamorphism, followed by less intense weathering.

The advantage of studying a single profile is that it can usually be assumed that the horizons have a common parent material, and thus their crystallinity values are derived from the effect of weathering on one metamorphic crystallinity value. The unweathered rock used as a standard parent material is from a position both geologically and geographically as near as possible to the soil profile, but was actually collected 1.72km away, as exposures closer to the profile lacked the fresh appearance of 1040. It belongs to the Gwestyn Shale Group, rather than the Frongoch Mudstone Series on which the profile is developed, although it is almost certain that this rock has had the same metamorphic history as the parent material of the soil. However, the metamorphic history of the parent materials of the boulder clays cannot with certainty be declared to be identical to that of the parent material of the soil. Even though the boulder clays were collected from within 2.2km of the profile, and the enclosed rock fragments are negligibly different, they may have undergone a slightly different metamorphic history. When the material from the Hiraethog Moors, Clwyd, is considered, it is unlikely that the parent material has undergone the same metamorphic history as material from Plynlimon, and this is at least part of the reason why, in almost every case, the crystallinity values are outside the ranges of values for materials from Plynlimon pretreated in the same way.

## 8.2 EXPERIMENTAL TECHNIQUES

Although many methods have been proposed for the determination of illite crystallinity [84,144,154,259,263], they are all based on either Weaver [259], who quantified the ratio of the peak height at 1.00nm to the peak height at 1.05nm, or Kubler [154], who quantified the peak width of the 1.0nm peak at half the peak height. Differences in techniques are rooted mainly in specimen preparation, the setting of the X-ray machine constants, and whether, for methods based on Kubler, peak widths are quoted in °2$\theta$ or mm. However, it has been suggested [263] that peak width should be standardised by reference to the mean of five determinations of the 20.8°2$\theta$ (100) peak width for vein quartz, measured alternately with five determinations of the specimen, in order to remove instrumental error. If $Hb_{rel}$ is defined as:

$$Hb_{rel} = \frac{100(\text{Illite 1.0nm Peak Width})}{\text{Quartz (100) Peak Width}},$$

and the grain size is greater than 0.2μm, it is found that when $Hb_{rel}$ is less than 130, the grain size does not affect the value of $Hb_{rel}$, and polished rock slabs cut parallel to the cleavage give the same value as oriented slides, but when $Hb_{rel}$ is greater than 130, the coarser grain sizes give lower values of $Hb_{rel}$, and polished rock slabs give values intermediate between fine and coarse oriented slides.

In recent years modifications of Kubler's method have found most favour, possibly due to Weaver's method producing errors up to three times as high for crystallised materials as those found with Kubler's method [84,154]. The peak height does not affect the crystallinity value determined by Kubler's method, provided that it is greater than 20mm, but ideally a chemical analysis is needed, as the Si:Al ratio of the specimen can affect the crystallinity value. Kubler estimated the experimental error in his method to be ±6 to 8%. Figure 8.1 shows the derivation of both measurements for a specimen from this study.

It was felt that both methods should be compared using specimens of high and low crystallinity, and then the method seen to be most appropriate and accurate should be used in the crystallinity determination of materials subsequently investigated. The initial trials were carried out using standard XRD instrumental conditions (Section 6.4). The chart speed used was the maximum possible, 20mm $min^{-1}$, to increase the accuracy of measurement of the peak positions and widths. Goniometer scan rates from 0.125 to 1°2θ$min^{-1}$ were used in order to identify any affects on crystallinity value caused by scan rate, and in each the time constant was such that:

Time Constant (Seconds) x Scan Rate (°2θ$min^{-1}$) = 2.

As well as comparing the effects of different scan rates, the specimens chosen for the initial trials (the well crystallised 6.3-20μm fraction from 1039, and the less crystallised 0.063-0.2μm fraction from 1077) were examined as both random powders and oriented specimens on glass slides. Table 8.1 shows the results of this initial experiment.

The first point to note is that none of the illite XRD peaks fall precisely at 1.00nm, the nearest being at 0.9955nm. The peaks for 1039

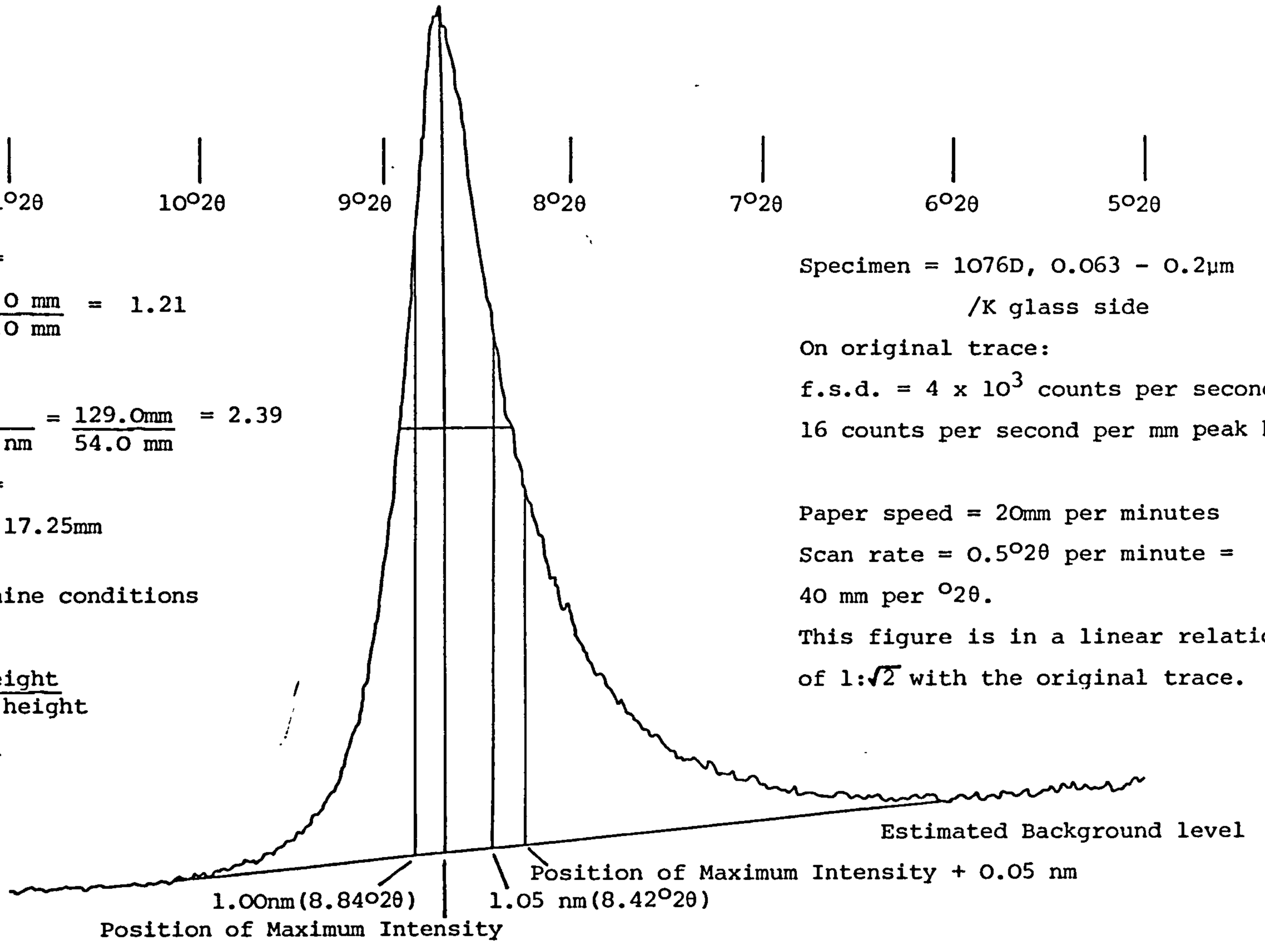


Weaver Crystallinity Value =

$$\frac{\text{Height at 1.00 nm}}{\text{Height at 1.05 nm}} = \frac{94.0 \text{ mm}}{78.0 \text{ mm}} = 1.21$$

Modified Weaver Value =

$$\frac{\text{Height at maximum}}{\text{Height at maximum + 0.05 nm}} = \frac{129.0\text{mm}}{54.0 \text{ mm}} = 2.39$$

Kulber Crystallinity Value =

width of half peak height = 17.25mm

= 0.61°2θ

= 8.1 mm using Kulber's machine conditions

Peak Symmetry Ratio =

$$\frac{\text{Width up } \theta \text{ of peak at half height}}{\text{Width down } \theta \text{ of peak at half height}}$$

$$= \frac{6.5\text{mm}}{10.75\text{mm}} = \frac{0.23°2\theta}{0.38°2\theta} = 0.61$$

Specimen = 1076D, 0.063 - 0.2μm

/K glass side

On original trace:

f.s.d. = 4 x $10^3$ counts per second =

16 counts per second per mm peak height

Paper speed = 20mm per minutes

Scan rate = 0.5°2θ per minute =

40 mm per °2θ.

This figure is in a linear relationship of 1:$\sqrt{2}$ with the original trace.

Figure 8.1 The Derivation of Illite Crystallinity Values

| Specimen | Preparation Method | Goniometer Scan Rate ($^{o}2\theta$ $min^{-1}$) | Peak Position (nm) | Peak Height (1.00nm) / Peak Height (0.5nm) | Peak Height (max) / Peak Height (max+0.05nm) | Observed Peak Width ($^{o}2\theta$) |
|---|---|---|---|---|---|---|
| 1039 6.3 - 20μm | Random Powder | 0.125 | 0.9955 | 13.91 | 12.67 | 0.21 |
| 1039 6.3 - 20μm | Random Powder | 0.25 | 0.995 | 17.36 | 11.37 | 0.23 |
| 1039 6.3 - 20μm | Random Powder | 0.5 | 0.995 | 15.13 | 14.38 | 0.22 |
| 1039 6.3 - 20μm | Random Powder | 1.0 | 0.995 | 14.46 | 11.61 | 0.21 |
| Mean | — | — | 0.995 | 15.2 | 12.5 | 0.218 |
| Standard Deviation | | | 0.000 | 1.5 | 1.4 | 0.010 |
| 1039 6.3 - 20μm | Oriented Slide | 0.125 | 0.9940 | 12.69 | 11.99 | 0.22 |
| 1039 6.3 - 20μm | Oriented Slide | 0.25 | 0.994 | 10.52 | 10.26 | 0.22 |
| 1039 6.3 - 20μm | Oriented Slide | 0.5 | 0.995 | 10.52 | 11.63 | 0.23 |
| 1039 6.3 - 20μm | Oriented Slide | 1.0 | 0.995 | 16.37 | 12.72 | 0.20 |
| Mean | — | — | 0.995 | 13 | 11.7 | 0.218 |
| Standard Deviation | | | 0.001 | 3 | 1.0 | 0.013 |
| 1077 0.063-0.2μm | Random Powder | 0.125 | 1.0200 | 1.11 | 1.83 | 0.78 |
| 1077 0.063-0.2μm | Random Powder | 0.25 | 1.017 | 1.20 | 1.76 | 0.79 |
| 1077 0.063-0.2μm | Random Powder | 0.5 | 1.020 | 1.15 | 1.88 | 0.77 |
| 1077 0.063-0.2μm | Random Powder | 1.0 | 1.020 | 1.17 | 1.90 | 0.78 |
| Mean | — | — | 1.019 | 1.16 | 1.84 | 0.780 |
| Standard Deviation | | | 0.002 | 0.04 | 0.06 | 0.008 |
| 1077 0.063-0.2μm | Oriented Slide | 0.125 | 1.0250 | 0.94 | 1.80 | 0.81 |
| 1077 0.063-0.2μm | Oriented Slide | 0.25 | 1.026 | 0.90 | 1.75 | 0.78 |
| 1077 0.063-0.2μm | Oriented Slide | 0.5 | 1.030 | 0.91 | 1.91 | 0.84 |
| 1077 0.063-0.2μm | Oriented Slide | 1.0 | 1.035 | 0.98 | 1.89 | 0.83 |
| Mean | — | — | 1.029 | 0.93 | 1.84 | 0.82 |
| Standard Deviation | | | 0.005 | 0.04 | 0.08 | 0.03 |

Table 8.1 Results of Initial Crystallinity Determination Experiments

occur nearer to 1.00nm than those for 1077 and, whereas those for 1039 are at values less than 1.00nm, those for 1077 are at values greater than 1.00nm, extending in one case to a deviation of 3.5%. This variation in peak position, which is to be expected with variation in chemical composition, does not affect the crystallinity value determined by the Kubler method, but does affect the value determined by Weaver's method, which is based on illites having their diffraction maxima at precisely 1.00nm, thus revealing a defect in Weaver's method. In some of the specimens, the peak is nearer 1.05 than 1.00nm, and for this reason the value of (maximum peak height)/(height at maximum position + 0.05nm) has been calculated as well as Weaver's value.

There appears to be no correlation between the goniometer scan rate and either the peak position or the crystallinity value determined by either method. When the crystallinity values are examined, considering all scans of each specimen together, it is seen that the difference between crystallinity values derived from glass slide and random powder specimens of the same material is relatively greater when determined by Weaver's method, than when determined by Kubler's method. These differences are, however, reduced when the proposed modification of Weaver's method is used to take into account the fact that the peaks do not occur at 1.00nm. The Weaver crystallinity values given by glass slides are also significantly lower than the values derived from random powder specimens, at least partly because, for glass slides, the peak positions are further away from the optimum 1.00nm. A further apparent advantage of Kubler's method is that it produces lower coefficients of variation for the groups of scans of each specimen than either the original Weaver method or the Weaver method modified to use the maximum peak height in the ratio calculation.

For these reasons, it was felt that a method based on Kubler would give more reproducible crystallinity values, and thus a modification of Kubler's method [144] was used for all subsequent determinations. This particular modification was chosen because it could be implemented precisely as described on the XRD equipment used in this study. The instrumental conditions used were as for the initial investigations, except that the scan rate was maintained at $0.5°2\theta min^{-1}$, a time constant of four seconds was used where the chart fsd was less than 1,000cps, otherwise one of two seconds was used, and a receiving slit of 0.2mm was employed. The crystallinity value was expressed in $°2\theta$, rather than in mm as originally proposed by Kubler [154]. Perhaps the

main disadvantage of this method, and of all methods based on Kubler, is that, as the crystallinity of the illite increases, the crystallinity value decreases, and vice versa [144].

## 8.3 ILLITE CRYSTALLINITY STUDIES

For each of the samples investigated in detail, illite crystallinity values were determined for four different pretreated specimens (K saturated, K saturated and heated to 550°C, Mg saturated, and Mg saturated followed by treatment with ethan1,2diol) for each of the clay fractions (0.063-0.2, 0.2-0.63 and 0.63-2μm), prepared as oriented slides. Crystallinity values were also determined for four coarser, unpretreated fractions (2-6.3, 6.3-20, 20-63 and 63-200μm) for each of the samples and, where material was available, for fractions coarser than 200μm, all as random powders. Illite crystallinity was also determined for five standard illites and the finer than 2μm fraction from a Sailbeck alluvial deposit (1053) in the form of oriented slides, to act as comparisons. The results of these determinations are given in Tables 8.2 to 8.5. None of the specimens were prepared in duplicate, or run twice, so estimates of errors due to specimen preparation and machine variability cannot be made. However, errors in measurement of the peak width are estimated to be ±0.01°2$\theta$. The shape of the majority of peaks is such that the background can be estimated easily, giving an accurate position for the half height. The width at this position can be measured to ±0.25mm, which is more than 0.005°2$\theta$ but less than 0.01°2$\theta$.

The range of crystallinity values varies from Fithian illite, the least crystallised, with a value of 1.26°2$\theta$, to the 200-630μm fraction of the Bsgd/1078D horizon, and the 63-200μm fraction of the Ea1d/1076D horizon, both most crystallised with values of 0.16°2$\theta$. The least crystallised illite from Plynlimon is found in the Mg saturated 0.063-0.2μm fraction of the Ea2/1077 horizon, and has a value of 0.84°2$\theta$.

The data for the finer than 2μm fractions were analysed as a three way analysis of variance problem, using sample, size and pretreatment as the sources of variation, and treating the triple product as a residual. Significant differences in crystallinity values were determined by the use of the Studentised Range Statistic [270].

| Specimen | Pretreatment /K | /Mg | /K550 | /MgED | Specimen | Pretreatment /K | /Mg | /K550 | /MgED |
|---|---|---|---|---|---|---|---|---|---|
| 1040 0.063-0.2μm | 0.54 | 0.62 | 0.53 | 0.61 | 1078D 0.063-0.2μm | 0.71 | 0.77 | 0.59 | 0.72 |
| 1040 0.2-0.63μm | 0.35 | 0.39 | 0.31 | 0.39 | 1078D 0.2-0.63μm | 0.46 | 0.54 | 0.46 | 0.51 |
| 1040 0.63-2μm | 0.26 | 0.34 | 0.33 | 0.31 | 1078D 0.63-2μm | 0.49 | 0.51 | 0.45 | 0.46 |
| 1029 0.063-0.2μm | 0.61 | 0.72 | 0.56 | 0.70 | 1077D 0.063-0.2μm | 0.64 | 0.76 | 0.46 | 0.68 |
| 1029 0.2-0.63μm | 0.41 | 0.45 | 0.41 | 0.44 | 1077D 0.2-0.63μm | 0.46 | 0.61 | 0.35 | 0.53 |
| 1029 0.63-2μm | 0.36 | 0.41 | 0.28 | 0.39 | 1077D 0.63-2μm | 0.41 | 0.52 | 0.35 | 0.49 |
| 1039 0.063-0.2μm | 0.61 | 0.67 | 0.60 | 0.66 | 1076D 0.063-0.2μm | 0.61 | 0.73 | 0.46 | 0.66 |
| 1039 0.2-0.63μm | 0.39 | 0.39 | 0.34 | 0.39 | 1076D 0.2-0.63μm | 0.46 | 0.57 | 0.32 | 0.53 |
| 1039 0.63-2μm | 0.33 | 0.36 | 0.31 | 0.37 | 1076D 0.63-2μm | 0.43 | 0.53 | 0.38 | 0.48 |
| 1049 0.063-0.2μm | 0.57 | 0.67 | 0.55 | 0.62 | 1079 0.063-0.2μm | 0.73 | 0.77 | 0.67 | 0.76 |
| 1049 0.2-0.63μm | 0.36 | 0.42 | 0.34 | 0.41 | 1079 0.2-0.63μm | 0.51 | 0.50 | 0.48 | 0.49 |
| 1049 0.63-2μm | 0.31 | 0.33 | 0.33 | 0.31 | 1079 0.63-2μm | 0.43 | 0.48 | 0.46 | 0.47 |
| 1080D 0.063-0.2μm | 0.69 | 0.78 | 0.66 | 0.71 | 1077 0.063-0.2μm | 0.79 | 0.84 | 0.54 | 0.77 |
| 1080D 0.2-0.63μm | 0.45 | 0.53 | 0.42 | 0.48 | 1077 0.2-0.63μm | 0.52 | 0.69 | 0.37 | 0.63 |
| 1080D 0.63-2μm | 0.47 | 0.49 | 0.44 | 0.48 | 1077 0.63-2μm | 0.41 | 0.48 | 0.33 | 0.43 |
| 1079D 0.063-0.2μm | 0.66 | 0.69 | 0.57 | 0.61 | 1087 0.063-0.2μm | 0.49 | 0.52 | 0.54 | 0.51 |
| 1079D 0.2-0.63μm | 0.46 | 0.54 | 0.43 | 0.53 | 1087 0.2-0.63μm | 0.30 | 0.35 | 0.31 | 0.32 |
| 1079D 0.63-2μm | 0.44 | 0.51 | 0.44 | 0.47 | 1087 0.63-2μm | 0.29 | 0.31 | 0.34 | 0.28 |

Table 8.2 Observed Illite Crystallinity Values of Finer Than 2μm Fractions in $^{o}2\theta$

Table 8.3 Observed Illite Crystallinity Values of 2-200μm Fractions in $^{o}2\theta$

| Sample | 2-6.3μm | 6.3-20μm | 20-63μm | 63-200μm |
|---|---|---|---|---|
| 1040 | 0.22 | 0.24 | 0.19 | 0.19 |
| 1029* | 0.26 | 0.22 | 0.19 | 0.22 |
| 1039* | 0.23 | 0.21 | 0.19 | 0.21 |
| 1049* | 0.23 | 0.21 | 0.19 | 0.21 |
| 1080D* | 0.26 | 0.21 | 0.19 | 0.24 |
| 1079D* | 0.23 | 0.20 | 0.17 | 0.19 |
| 1078D | 0.24 | 0.23 | 0.17 | 0.19 |
| 1077D | 0.27 | 0.21 | 0.19 | 0.18 |
| 1076D | 0.30 | 0.21 | 0.19 | 0.16 |
| 1079* | 0.24 | 0.21 | 0.20 | 0.26 |
| 1077 | 0.26 | 0.18 | 0.19 | 0.18 |
| 1087* | 0.21 | 0.23 | 0.21 | 0.20 |
| Mean All | 0.25 | 0.213 | 0.189 | 0.20 |
| S.D. Data | 0.03 | 0.016 | 0.011 | 0.03 |
| Mean Only | 0.24 | 0.215 | 0.190 | 0.22 |
| S.D. *Data | 0.02 | 0.010 | 0.010 | 0.02 |

Table 8.4 Observed Illite Crystallinity Values of Coarser than 200μm Fractions in $^{o}2\theta$

| Sample | 200-630μm | 200-2000μm | 630-2000μm | >2000μm |
|---|---|---|---|---|
| 1029* | 0.24 | - | 0.24 | 0.24 |
| 1039* | 0.23 | - | 0.23 | 0.24 |
| 1049* | 0.23 | - | 0.23 | 0.24 |
| 1080D* | 0.28 | - | 0.26 | 0.25 |
| 1079D* | 0.23 | - | 0.24 | 0.23 |
| 1078D | 0.16 | 0.18 | - | - |
| 1077D | - | 0.18 | - | - |
| 1079* | 0.23 | - | 0.27 | 0.25 |
| 1077 | 0.21 | - | 0.27 | - |
| 1087* | 0.21 | - | 0.23 | 0.23 |
| Mean All | 0.22 | 0.180 | 0.25 | 0.240 |
| S.D. Data | 0.03 | 0.000 | 0.02 | 0.010 |
| Mean Only | 0.24 | - | 0.245 | 0.240 |
| S.D. *Data | 0.02 | - | 0.015 | 0.010 |

| Sample | Observed Crystallinity Value (°2θ) |
|---|---|
| Conwy | 1.24 |
| Fithian | 1.26 |
| Llanddulas | 0.53 |
| Parys Mountain | 0.39 |
| Sailbeck <2μm | 0.44 |
| Trefriw | 0.21 |

Table 8.5 Observed Illite Crystallinity Values for Comparison Materials

This analysis shows that the mean crystallinity value for each set of specimens, when grouped according to pretreatment, is significantly different, with more than 99% confidence, from the means of the other groups. The lowest mean, of 0.436°2$\theta$, and thus the most crystallised specimens, comes from the group heated to 550°C. This is followed by the mean of 0.484°2$\theta$ for the K saturated group, a mean of 0.517°2$\theta$ for the group treated with ethan1,2diol and, least crystalline, a mean of 0.550°2$\theta$ for the Mg saturated group. In so far as small amounts of expandable minerals are interstratified with the illite, it would be expected that the peak width determined on Mg saturated specimens would be higher than that determined on K saturated specimens. Mg saturation allows the adsorption of up to two layers of water and expansion to 1.55nm, whereas K saturation will collapse the vermiculite structure to 1.00nm, and allow the adsorption of only one layer of water by smectites, with expansion only up to 1.25nm. As long as there is only a small proportion of irregularly interstratified expandable layers, their expansion will be seen as a slight broadening of the illite peak in the down $\theta$ direction.

The effect of increasing apparent crystallinity on heating K saturated specimens to 550°C, or on treating Mg saturated specimens with ethan1,2diol, has been observed previously [144], when two explanations were put forward. When the peak sharpening was much less upon saturation with ethan1,2diol than on heating, the interstratified layers were assumed to be predominantly vermiculitic, whereas when the sharpening upon saturation with ethan1,2diol was 65% or more of the sharpening on heating, and was associated with increased symmetry of the illite (001) peak, it was attributed to the superposition of the (002) peak of a small amount of interstratified smectite, expanded to 1.70nm, upon the up $\theta$ side of the illite (001) peak. 17 of the 36 specimens showed marked peak sharpening (by 0.04°2$\theta$ or more [144]) on heating the K saturated specimen, but of these only three showed 65% or more of the same amount of sharpening, together with an increase in peak symmetry, when the Mg saturated specimen was treated with ethan1,2diol. These specimens (the 0.63-2μm fraction of the Bsgd/1078D horizon, the 0.2-0.63μm fraction of the Ea2d/1077D horizon, and the 0.63-2μm fraction from the Ea1d/1076D horizon) seem unlikely to have their peak sharpening explained by superposition of the (002) peak of a 1.70nm expanded phase, as although they rank fifth, second and third out of 16 specimens in terms of the illite chemically determined to be expandable, they only rank 9th, 12th and 15th respectively in terms of

the proportion of that expandable mineral chemically determined as smectite. In any case, this mineral is considered to be a hydroxy interlayered vermiculite, rather than a true smectite (Section 7.2.1).

However, the possibility that the peak sharpening occurring upon heating these K saturated specimens is due to the collapse of poorly crystalline chlorite interstratified with the illite also appears unlikely, as they only show chlorite contents of 1.4, 0.4 and 0.2%, respectively. The conclusion must be that the peak sharpening upon heat treatment is due to collapse of poorly filled hydroxy interlayered vermiculite to 1.00nm, whilst peak sharpening on saturation with ethan1,2diol can only be explained by expansion of interstratified vermiculite or smectite (001) peaks away from the illite 1.0nm peak. For the rest of the specimens, which generally show much greater peak sharpening upon heat treatment than on ethan1,2diol saturation, the sharpening can be explained by the behaviour of interstratified vermiculite.

When the specimens are grouped according to size, each of the groups is significantly different, with more than 99% confidence. As might be expected, it is the finest fraction that is least crystalline, with crystallinity increasing with particle size. The lower crystallinity of the 0.063-0.2μm fractions is brought about by the larger surface area to volume ratio (see Section 9.3.1) allowing weathering reactions to proceed more rapidly, breaking down the crystal structure in the process. Although no quartz standards were used, even the most crystallised samples did not show a constant crystallinity value across the different size fractions, suggesting that all the materials investigated would give $Hb_{rel}$ values greater than 130 [263].

If the specimens are grouped according to both pretreatment and size, it becomes clear that as size decreases, the effects of pretreatment on crystallinity become more noticeable. For the 0.063-0.2μm group, the mean values of the Mg saturated, and K saturated and heated to 550°C, subgroups differ by 0.151°2$\theta$, whereas for the 0.2-0.63μm group this is reduced to 0.120°2$\theta$, and for the 0.63-2μm group to 0.069°2$\theta$. As the difference between the subgroup means is reduced, so is the significance level of the difference.

If the specimens are grouped according to their origin, the statistical picture becomes more complex, and is most easily described at the 95%

confidence level, although a diagram of the similarities at both 95 and 99% confidence levels is given in Figure 8.2, in which samples which cannot be distinguished at the 99% confidence level are joined by a red line, and those which cannot be distinguished at the 95% confidence level are joined by a green line. With 95% confidence, the material from Hiraethog, 1087, is more crystallised than any of the Plynlimon samples, having a mean value of 0.380°2$\theta$. Less crystallised, and not totally distinguishable, is a group of four samples from Plynlimon, including the boulder clays 1029, 1039 and 1049, and the rock, 1040, with mean values varying from 0.415 to 0.478°2$\theta$. Least crystallised is the group containing the soil horizons, with mean values varying from 0.513 to 0.567°2$\theta$. The effect of dithionite treatment on crystallinity is clearly seen when the values for 1079 and 1077 are compared with those of 1079D and 1077D. The untreated samples are the least crystalline of the samples investigated, and have values higher than their treated counterparts by 0.033 and 0.045°2$\theta$, respectively. This increase in crystallinity upon dithionite treatment is caused by the dissolution of the least crystalline illite during the treatment process. If the crystallinity values for only the 0.063-0.2μm fractions are considered, the difference between untreated and treated specimens increases to 0.100°2$\theta$ for both 1079/1079D and 1077/1077D, showing that the least crystalline material is concentrated in the finest fraction of the horizons.

If the samples from the dithionite treated horizons are considered, an interesting pattern emerges. Although not different at the 99% confidence level, the crystallinity values indicate that it is illite from the Ea1d/1076D horizon that is most crystallised, followed in order by that from the Ea2d/1077D horizon, the Bsd/1079D horizon, the BCd/1080D horizon and, least crystalline, the Bsgd/1078D horizon. This pattern may be explained as follows: the top two mineral horizons (Ea1 and Ea2) are undergoing the most intensive weathering, and it is under these conditions that the less crystalline material is preferentially altered and removed. If the weathering intensity simply decreased down the profile, the crystallinity would be expected to become less down the profile. This is the case, except for the anomalous position of the Bsg horizon, which shows the least crystalline illite. This must be explained by part of the less crystallised illite from the horizons above being translocated down the profile, rather than being completely removed into solution (Sections 6.2.4 and 6.2.5).

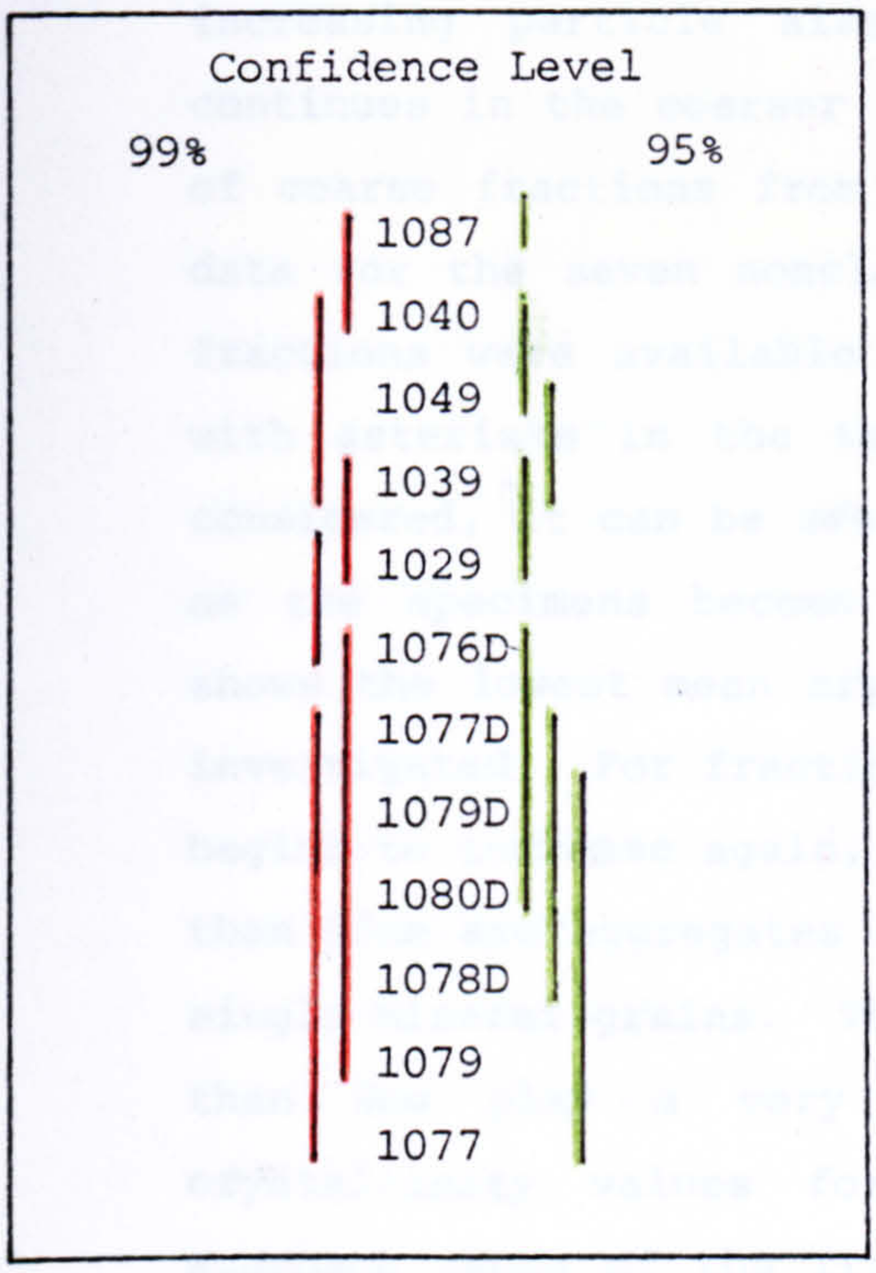


Figure 8.2 Similarities of Observed Crystallinity Values

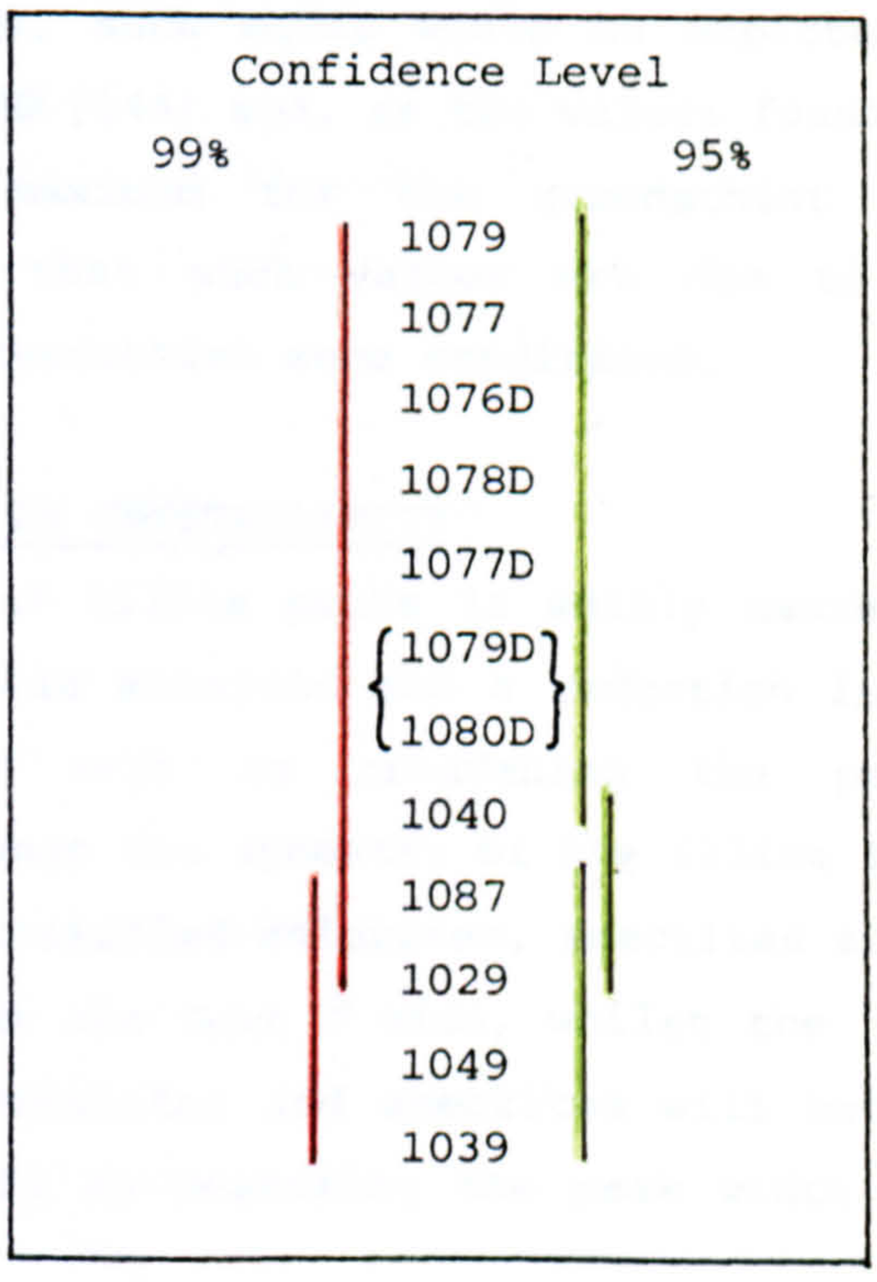


Figure 8.4 Similarities of Peak Symmetry Ratios

The crystallinity data from fractions coarser than 2μm, given in Tables 8.3 and 8.4, suggest that the trend to more crystallised illite with increasing particle size, seen in the finer than 2μm fractions, continues in the coarser fractions. Because of the very small amounts of coarse fractions from some samples, it was not possible to obtain data for the seven nonclay fractions. However, data for all nonclay fractions were available for seven samples, and these are identified with asterisks in the tables. When the data for these samples are considered, it can be seen that the mean crystallinity value decreases as the specimens become coarser, until the 20-63μm fraction, which shows the lowest mean crystallinity value, 0.190°2$\theta$, of the fractions investigated. For fractions coarser than 63μm, the crystallinity value begins to increase again, suggesting that some of the particles coarser than 63μm are aggregates of both fine and coarse material, rather than single mineral grains. The data do, however, suggest that grains finer than 2μm play a very minor role in these aggregates, as the crystallinity values for the fractions coarser than 63μm do not approach those of the fractions finer than 2μm. It is possible that the low crystallinity values given by the coarse fractions indicate the presence of unweathered micas of igneous or metamorphic origin, incorporated into the soil parent material during deposition. However, using the techniques employed here, such micas would be expected to give crystallinity values of 0.11°2$\theta$ [144] and, as the values found are only slightly lower than the maximum for the greenschist zone (0.21°2$\theta$), it seems more likely that such values are due to the metamorphism of illite under low greenschist zone conditions.

## 8.4 THE EFFECTS OF INTERSTRATIFICATION ON CRYSTALLINITY

As has been seen, the broadening of illite peaks is mainly caused by the interstratification of expandable minerals and a reduction in the perfection of the lattice. As well as broadening the peaks, interstratified minerals should change the symmetry of the illite 1.0nm peak, as the (001) peaks of interstratified chlorites, smectites and Mg saturated vermiculites will broaden the down $\theta$ side, whilst the (002) peaks of ethan1,2diol treated vermiculites and smectites will broaden the up $\theta$ side [144]. Thus, as well as measuring the peak width, the ratio of:

$$\frac{\text{Width at Half Height Up } \theta \text{ of Maximum}}{\text{Width at Half Height Down } \theta \text{ of Maximum}}$$

was determined, and is given in Tables 8.6 to 8.9. It has been suggested [187] that the peak position should be taken as the midpoint of the peak at 80% of its height. This may give a more accurate peak position by eliminating irregularities in the trace near the maximum, but is not suitable for use in calculating the peak symmetry ratio. Figure 8.3 indicates that calculating the peak symmetry ratio from the midpoint at 80% peak height will bias symmetry ratios towards unity because, if the peak is uniformly asymmetric, the midpoint at 80% height will be moved from the maximum position towards the side of the peak which slopes most shallowly, tending to make the distances from the edges of the peak to the chosen central position more similar. The data for the fractions finer than 2μm were processed by the same statistical package as the crystallinity data. Because of very much larger standard errors, this analysis does not produce results that are as clear cut as those from the crystallinity values, but it is still possible to identify trends.

There are no significant differences between the mean peak symmetry ratios when the specimens are grouped together according to size, despite the fact that size is the cause of 60% of the variation in the crystallinity values. This suggests that, although the illite may be less crystallised in finer fractions, it does not contain any higher proportion of interstratified minerals. When the data are grouped according to pretreatment, significant differences do become apparent. The specimens heated to 550°C give rise to the least symmetrical peaks, with a mean ratio of 0.705, which is indistinguishable at the 95% confidence level from the mean of 0.725 for the Mg saturated specimens. These groups are different, however, with more than 95% confidence, from the mean ratios of 0.793 for the ethan1,2diol treated specimens and 0.849 for the K saturated specimens, which are themselves indistinguishable at the 95% confidence level.

The K saturated specimens would be expected to give the most symmetrical peaks, as after K saturation only smectite could be expanded away from 1.00nm. Similarly, the peaks of the Mg saturated specimens would be expected to be more asymmetrical, as both smectite and vermiculite would be expanded away from 1.00nm. Following the reasoning of Kisch [144], the ethan1,2diol treated specimens should hold an intermediate position, as vermiculite (001) peaks will be expanded away from 1.00nm, whilst the smectite will be expanded as far as 1.70nm, resulting in no contribution to the down $\theta$ side of the

| Specimen | Pretreatment /K | /Mg | /K550 | /MgED | Specimen | Pretreatment /K | /Mg | /K550 | /MgED |
|---|---|---|---|---|---|---|---|---|---|
| 1040 0.063-0.2µm | 0.86 | 0.88 | 0.71 | 0.74 | 1078D 0.063-0.2µm | 0.69 | 0.67 | 0.74 | 0.67 |
| 1040 0.2-0.63µm | 0.84 | 0.77 | 0.48 | 0.77 | 1078D 0.2-0.63µm | 0.84 | 0.74 | 0.59 | 0.65 |
| 1040 0.63-2µm | 0.53 | 0.89 | 0.65 | 0.94 | 1078D 0.63-2µm | 0.81 | 0.55 | 0.55 | 0.77 |
| 1029 0.063-0.2µm | 1.18 | 0.67 | 0.93 | 0.79 | 1077D 0.063-0.2µm | 0.83 | 0.55 | 0.70 | 0.66 |
| 1029 0.2-0.63µm | 0.95 | 1.05 | 0.78 | 1.00 | 1077D 0.63-2µm | 0.64 | 0.56 | 0.75 | 0.77 |
| 1029 0.63-2µm | 0.89 | 0.78 | 0.56 | 0.86 | 1077D 0.63-2µm | 0.71 | 0.68 | 0.67 | 0.81 |
| 1039 0.063-0.2µm | 1.03 | 0.97 | 0.88 | 1.06 | 1076D 0.063-0.2µm | 0.61 | 0.49 | 0.59 | 0.69 |
| 1039 0.2-0.63µm | 1.17 | 0.95 | 0.89 | 1.17 | 1076D 0.2-0.63µm | 0.77 | 0.50 | 0.68 | 0.83 |
| 1039 0.63-2µm | 1.06 | 0.89 | 0.82 | 0.85 | 1076D 0.63-2µm | 0.79 | 0.71 | 0.65 | 0.92 |
| 1049 0.063-0.2µm | 1.19 | 0.86 | 1.39 | 1.07 | 1079 0.063-0.2µm | 0.52 | 0.45 | 0.49 | 0.62 |
| 1049 0.2-0.63µm | 1.00 | 0.75 | 1.00 | 0.78 | 1079 0.2-0.63µm | 0.76 | 0.67 | 0.60 | 0.75 |
| 1049 0.63-2µm | 0.94 | 0.74 | 0.74 | 0.94 | 1079 0.63-2µm | 0.72 | 0.78 | 0.59 | 0.96 |
| 1080D 0.063-0.2µm | 0.73 | 0.70 | 0.57 | 0.61 | 1077 0.063-0.2µm | 0.68 | 0.56 | 0.50 | 0.51 |
| 1080D 0.2-0.63µm | 0.96 | 0.89 | 0.62 | 0.78 | 1077 0.2-0.63µm | 0.93 | 0.64 | 0.76 | 0.62 |
| 1080D 0.63-2µm | 0.81 | 0.53 | 0.52 | 0.66 | 1077 0.63-2µm | 0.71 | 0.66 | 0.74 | 0.79 |
| 1079D 0.063-0.2µm | 0.78 | 0.82 | 0.58 | 0.65 | 1087 0.063-0.2µm | 1.04 | 0.86 | 0.86 | 0.89 |
| 1079D 0.2-0.63µm | 0.84 | 0.64 | 0.59 | 0.66 | 1087 0.2-0.63µm | 1.14 | 0.84 | 0.72 | 1.00 |
| 1079D 0.63-2µm | 0.69 | 0.70 | 0.69 | 0.74 | 1087 0.63-2µm | 0.93 | 0.72 | 0.79 | 0.56 |

Table 8.6 Illite Peak Symmetry Ratios for Finer than 2µm Fractions

Table 8.7 Illite Peak Symmetry Ratios of 2-200μm Fractions

| Sample | Size Fraction | | | | Mean ± Standard Deviation |
|---|---|---|---|---|---|
| | 2-6.3μm | 6.3-20μm | 20-63μm | 63-200μm | |
| 1040 | 1.00 | 0.85 | 0.73 | 1.11 | 0.92±0.17 |
| 1029* | 0.73 | 0.69 | 0.90 | 0.69 | 0.75±0.10 |
| 1039* | 0.77 | 0.91 | 0.90 | 0.75 | 0.83±0.08 |
| 1049* | 0.92 | 0.91 | 0.90 | 0.75 | 0.87±0.08 |
| 1080D* | 0.63 | 0.75 | 0.90 | 1.00 | 0.82±0.16 |
| 1079D* | 0.92 | 0.82 | 0.70 | 1.11 | 0.89±0.17 |
| 1078D | 1.18 | 0.77 | 0.89 | 0.90 | 0.94±0.17 |
| 1077D | 0.59 | 0.91 | 0.90 | 0.80 | 0.80±0.15 |
| 1076D | 0.58 | 0.75 | 0.73 | 1.00 | 0.77±0.17 |
| 1079* | 0.71 | 1.10 | 1.00 | 0.73 | 0.9 ±0.2 |
| 1077 | 0.73 | 1.00 | 0.90 | 1.25 | 1.0 ±0.2 |
| 1087* | 0.91 | 0.64 | 1.10 | 0.82 | 0.87±0.19 |
| Mean } All | 0.81 | 0.84 | 0.88 | 0.91 | - |
| S.D. } Data | 0.18 | 0.13 | 0.11 | 0.18 | - |
| Mean } Only | 0.80 | 0.83 | 0.91 | 0.84 | - |
| S.D. } *Data | 0.12 | 0.16 | 0.12 | 0.16 | - |

Table 8.8 Illite Peak Symmetry Ratios of Coarser than 200μm Fractions

| Sample | Size Fraction | | | >2000μm |
|---|---|---|---|---|
| | 200-630μm | 200-2000μm | 630-2000μm | |
| 1029* | 0.60 | - | 0.71 | 0.71 |
| 1039* | 0.92 | - | 0.92 | 0.71 |
| 1049* | 0.92 | - | 0.64 | 0.85 |
| 1080D* | 0.87 | - | 0.73 | 0.56 |
| 1079D* | 0.77 | - | 0.60 | 0.77 |
| 1078D | 1.00 | 0.80 | - | - |
| 1077D | - | 0.64 | - | - |
| 1079* | 0.77 | - | 0.80 | 0.56 |
| 1077 | 0.62 | - | 0.93 | - |
| 1087* | 0.91 | - | 0.77 | 0.64 |
| Mean } All | 0.82 | 0.72 | 0.76 | 0.69 |
| S.D. } Data | 0.14 | 0.11 | 0.12 | 0.11 |
| Mean } Only | 0.82 | - | 0.74 | 0.69 |
| S.D. } *Data | 0.12 | - | 0.11 | 0.11 |

| Sample | Peak Symmetry Ratio |
|---|---|
| Conwy | 1.25 |
| Fithian | 0.30 |
| Llanddulas | 0.51 |
| Parys Mountain | 0.86 |
| Sailbeck <2μm | 0.22 |
| Trefriw | 0.75 |

Table 8.9 Illite Peak Symmetry Ratios for Comparison Materials

| Observed Crystallinity Value (°2θ) | Peak Width Caused by Instrumental Effects (°2θ) | Corrected Crystallinity Value (°2θ) |
|---|---|---|
| 0.16 | 0.08 | 0.08 |
| 0.17 | 0.07 | 0.10 |
| 0.18-0.19 | 0.06 | 0.12-0.13 |
| 0.20-0.23 | 0.05 | 0.15-0.18 |
| 0.24-0.28 | 0.04 | 0.20-0.24 |
| 0.29-0.39 | 0.03 | 0.26-0.36 |
| 0.40-0.63 | 0.02 | 0.38-0.61 |
| 0.64-1.89 | 0.01 | 0.63-1.88 |

Table 8.11 Corrections to Peak Widths to Allow for Instrumental Effects

| Particle Size (μm) | Broadening of Peak Caused by Particle Size (°2θ) |
|---|---|
| 0.063 | 0.13 |
| 0.2 | 0.04 |
| 0.63 | 0.01 |
| ⩾2 | 0.00 |

Table 8.12 The Effect of Particle Size on Peak Width

Peak symmetry ratio calculated from position of peak maximum $= \frac{15mm}{60mm} = 0.25$

Peak symmetry ratio calculated from position of mid point at 80% peak height $= \frac{24mm}{51mm} = 0.47$

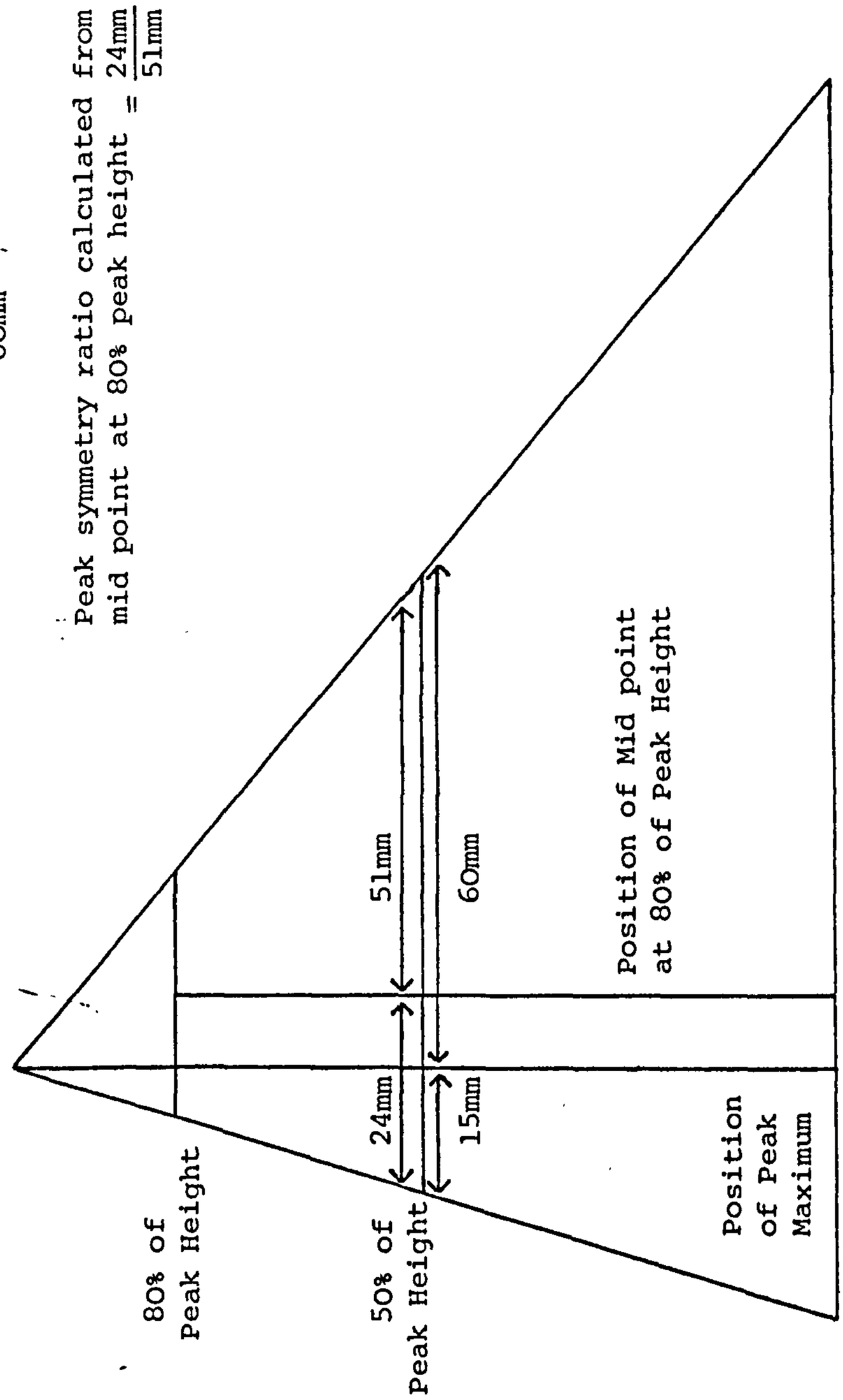


Diagrammatic Representation of the Effect of Using Different Peak Positions on the Peak Symmetry Ratio

Figure 8.3

illite peak, but giving a contribution from the smectite (002) peak on the up $\theta$ side. Explanations of the marked asymmetry of the specimens heated to 550°C cannot depend on interstratifications of illite, vermiculite and smectite, as after heating to 550°C they should all give a 1.00nm basal spacing. However, hydroxy interlayered vermiculite, found in many specimens (Section 7.1.2), is prevented from collapsing to 1.00nm by partly filled interlayers. This material, which may attain a basal spacing of 1.1 to 1.2nm after heating to 550°C, would, in interstratifications with illite, effectively reduce the symmetry of the 1.0nm peak by contributing to its down $\theta$ side. This is thus the most likely explanation for the reduced peak symmetry ratios of the specimens heated to 550°C.

A diagram of the similarities between samples at 95 and 99% confidence levels is given in Figure 8.4 for the data grouped according to specimen origin. The key is as for Figure 8.2. Although the samples cannot be divided with statistical confidence into more than two groups, one containing the soil and rock samples with mean ratios from 0.659 to 0.755, and the other the boulder clays and Hiraethog sample with mean ratios from 0.863 to 0.978, the actual mean values are useful. They show that the degree of interstratification apparently differs very little between the horizons that have been dithionite treated, and even the untreated soil samples are very little more asymmetrical, suggesting that the interstratified expandable minerals are not particularly susceptible to dithionite attack. The rock has a lower degree of interstratification of illite than any of the horizons, as might be expected, but for the boulder clays to show considerably less interstratification of expandable minerals than the unweathered rock is contrary to expectations. This possibly suggests that the phyllosilicates in the boulder clays have experienced an environment, not experienced by the rock or soil samples, which encouraged the conversion of interstratified expandable minerals to illite or chlorite, but it must be borne in mind that the boulder clays could be derived from rocks with originally lower contents of interstratified expandable minerals than 1040.

When the peak symmetry data for the fractions coarser than 2μm are considered, the picture is very similar to that for the crystallinity data, with the most crystallised fraction, 20-63μm, also showing the most symmetrical illite peaks, and thus the lowest degree of interstratification of expandable minerals. There is a correlation

coefficient of -0.845 between the mean peak symmetry ratios and the mean crystallinity values for the data from the samples for which all the coarse fractions are available. The values are connected by the equation:

Peak Symmetry Ratio = 1.544 - 3.281(Crystallinity Value (°2θ)),

which suggests that a specimen with a perfectly symmetrical peak would have a crystallinity value of 0.166°2θ. The specimens with crystallinity values of 0.16°2θ do have perfectly symmetrical illite peaks. This correlation is not continued into the clay fractions, where size has a profound effect on crystallinity value, yet the degree of interstratification, as expressed by the peak symmetry ratio, is little affected by size.

## 8.5 CHLORITE CRYSTALLINITY

Although previous work investigating mineral crystallinity as an indicator of the degree of metamorphism has been confined to illites, there is no reason why this should not be extended to other minerals, provided that they are subject to processes similar to those which bring about variation in the crystallinity of illite. Chlorite is subject to interstratification by expandable minerals, leading to peak broadening and reduction in symmetry, to breakdown of the crystal structure during weathering, leading to peak broadening, and to recrystallisation during low grade metamorphism, leading to sharpening of the peaks. For this reason, crystallinity values and peak symmetry ratios for chlorite were measured on specimens of the rock, 1040, and the soil BCd/1080D horizon, using an identical method to that used for illite, in order to investigate whether, during weathering, chlorite crystallinity and peak symmetry follow the same pattern as the illite values. The results are given in Table 8.10.

The most obvious similarity between the chlorite and illite data is that, for both minerals, the coarser the size, the better crystallised is the mineral. However, the chlorite from the BCd/1080D horizon appears to be more crystallised than that from the rock, 1040, whereas for illite this is reversed. This apparent inconsistency can be explained in terms of a greater attack on chlorite than illite by the dithionite pretreatment. Dithionite has been shown to alter chlorite containing $Fe^{3+}$ [174] and, if the least crystallised chlorite is preferentially attacked, then, after treatment, the improvement in

TABLE 8.10 Observed Chlorite Peak Widths and Peak Symmetry Ratios

| Sample | Observed Crystallinity Value (°2θ) | | | | | Peak Symmetry Ratio | | | | |
|---|---|---|---|---|---|---|---|---|---|---|
| | Pretreatment | | | | Mean S.D. | Pretreatment | | | | Mean S.D. |
| | /K | /Mg | /K550 | /MgED | | /K | /Mg | /K550 | /MgED | |
| 1040 | | | | | 0.52 | | | | | 1.0 |
| 0.063-0.2μm | 0.54 | 0.46 | 0.58 | 0.48 | 0.06 | 0.80 | 0.59 | 1.42 | 1.00 | 0.4 |
| 1040 | | | | | 0.29 | | | | | 0.8 |
| 0.2-0.63μm | 0.28 | 0.26 | 0.36 | 0.27 | 0.05 | 0.75 | 0.63 | 1.12 | 0.80 | 0.2 |
| 1040 | | | | | 0.29 | | | | | 0.80 |
| 0.63-2μm | 0.27 | 0.32 | 0.33 | 0.22 | 0.05 | 0.80 | 0.78 | 0.94 | 0.69 | 0.10 |
| Mean | 0.36 | 0.35 | 0.42 | 0.32 | 0.36 | 0.78 | 0.67 | 1.2 | 0.83 | 0.9 |
| S.D. | 0.15 | 0.10 | 0.14 | 0.14 | 0.12 | 0.03 | 0.10 | 0.2 | 0.16 | 0.2 |
| 1080D | | | | | 0.380 | | | | | 0.8 |
| 0.063-0.2μm | 0.38 | 0.38 | 0.39 | 0.36 | 0.015 | 0.81 | 0.46 | 1.17 | 0.80 | 0.3 |
| 1080D | | | | | 0.29 | | | | | 0.91 |
| 0.2-0.63μm | 0.24 | 0.25 | 0.42 | 0.26 | 0.08 | 0.85 | 0.79 | 0.83 | 1.17 | 0.18 |
| 1080D | | | | | 0.25 | | | | | 1.0 |
| 0.63-2μm | 0.19 | 0.23 | 0.39 | 0.20 | 0.09 | 0.73 | 0.64 | 2.00 | 0.82 | 0.6 |
| Mean | 0.27 | 0.29 | 0.400 | 0.27 | 0.31 | 0.80 | 0.63 | 1.3 | 0.9 | 0.9 |
| S.D. | 0.10 | 0.08 | 0.015 | 0.08 | 0.09 | 0.06 | 0.17 | 0.6 | 0.2 | 0.4 |

crystallinity would be greater for the chlorite than for the illite in the same specimen, giving rise to the crystallinity values observed.

When chlorite crystallinity values are measured, a complication that is not found with illite occurs: the breakdown of the chlorite structure on heat treatment. Although the K saturated, Mg saturated, and Mg saturated and ethan1,2diol treated, crystallinity values and peak symmetry ratios were measured on the (001) peak, the (002) peak had to be used for the specimens heated to 550°C, as the (001) peak had collapsed to an insignificant size by this temperature. Because of this, a direct comparison of the crystallinity values and peak symmetry ratios after heating to 550°C with the data from specimens pretreated in other ways cannot be made.

There are insufficient data available to come to a conclusion on the effect of pretreatment on the chlorite crystallinity value, although it does appear that Mg saturation gives rise to the least symmetrical chlorite (001) peak, whereas treatment with ethan1,2diol gives the most symmetrical peak, with K saturation giving intermediate results. This pattern can be explained by smectite interstratification with the chlorite. When Mg saturated, smectite has a basal spacing of 1.4 to 1.5nm, and broadens the down $\theta$ side of the chlorite (001) peak. On treatment with ethan1,2diol, the smectite is expanded to 1.7 to 1.8nm, and does not contribute to the asymmetry of the chlorite peak.

If the data from specimens heated to 550°C are excluded, good correlations can be drawn between the chlorite and illite crystallinity values derived from the same specimen. For the specimens from the rock, 1040, the correlation coefficient is 0.88, and the regression equation is:

Chlorite Crystallinity Value ($°2\theta$) = 0.77(Illite Crystallinity Value ($°2\theta$)) + 0.02,

whilst for specimens from the BCd/1080D horizon, the correlation coefficient is 0.94, and the regression equation is:

Chlorite Crystallinity Value ($°2\theta$) = 0.57(Illite Crystallinity Value ($°2\theta$)) - 0.04.

If the data from both samples are combined, the correlation coefficient is much reduced; the difference between the equations for the samples is considered to be due to the effect of the dithionite treatment in improving the apparent chlorite crystallinity, and thus reducing the chlorite crystallinity value relative to that of illite from the same specimen, for the BCd/1080D horizon specimens. If the data from the specimens heated to 550°C are included, the correlation coefficients are again reduced, suggesting that the crystallinity value given by the (002) peak is indeed different to that given by the (001) peak with the same pretreatment.

## 8.6 THE EFFECTS OF OTHER FACTORS ON CRYSTALLINITY

The results in Sections 8.3 and 8.5 have been presented with the assumption that it is only crystallinity that affects the width of the XRD peak. In fact at least two other causes contribute; these are instrumental effects caused by diffractometer parameters; and the scattering of diffracted X-rays over an extended angular range by very small crystals.

Instrumental effects should be constant for all specimens, as none of the diffractometer parameters except for fsd and, for a very few specimens, time constant, were altered between specimens. The true peak width is related to the observed peak width by the equation:

$B = \sqrt{B^2_{obs} - b^2}$, where:

B = true peak width,

$B_{obs}$ = experimentally measured peak width, and

b = peak width due to instrumental effects [38].

The value of b can be determined by measurement of the peak width of a well crystallised material, such as quartz powder, with a particle size very much greater than 1μm. This should theoretically give a peak with no width, and thus any width that is observed is due to instrumental effects, and will give a value for b. The material used to determine b was the 20-63μm fraction of crushed vein quartz from Penrhyn quarry, Bethesda, mounted as a random powder on double sided Sellotape. Instrumental conditions used were identical to those for making the crystallinity measurements (Section 8.2).

The peak width measured for this specimen was 0.14°2$\theta$, slightly lower than the minimum crystallinity value of 0.16°2$\theta$ measured for the illites from the 200-630μm fraction of the Bsgd/1078D horizon and the 63-200μm fraction of the Eald/1076D horizon. Using the same machine conditions on an identical diffractometer, minimum peak widths of 0.11°2$\theta$ were found for well crystallised muscovites [144], suggesting that either the machine used in this study was not adjusted for optimum peak resolution, or that the quartz was not sufficiently crystallised to act as a standard. A coarse, well crystallised muscovite should produce a peak width determined solely by instrumental effects, as should coarse quartz [38]. It is likely that poor machine adjustment was the cause of the high value for width due to instrumental effects, as the coarse mica in the specimens that gave crystallinity values of 0.16°2$\theta$ would also be likely to produce a peak width controlled only by instrumental effects. However, other investigators have found minimum peak widths for coarse micas as high as 0.23°2$\theta$ [144].

Table 8.11 tabulates the increase in crystallinity values observed due to instrumental effects, and shows that the correction that needs to be applied is only reduced to less than 10% for values greater than 0.30. In the literature, illite crystallinity values are published without corrections for instrumental effects [84,144,154,221], and this may be the cause of some of the disagreement between published values for the boundaries between diagenetic, anchimetamorphic and metamorphic zones [144].

As long as values are determined using the same diffractometer and instrumental conditions, there is no difficulty in comparing the uncorrected values for different specimens, as has been done in this study. However, if crystallinity values determined on different diffractometers are to be compared, or crystallinity values are to be compared with the results of other techniques, corrections for instrumental effects need to be applied.

Even if not explicitly stated, it is generally assumed that as particles of a mineral become smaller, they also become less crystallised. This is likely to be valid when a mineral is reacting with its environment, and small particles become disordered more rapidly than larger ones as they are dissolved or altered to a different composition. However, it is possible to envisage a grinding process that would produce fine particles that retained the

crystallinity of the coarse grains that produced them. Because the absolute size of a particle has a direct effect on the diffracted peak width, besides any contribution from variation in crystallinity, it is essential that the contributions to peak broadening due to particle size are separated from those due to crystallinity variation, or else all fine particles will be assumed to be less crystallised than coarse ones, simply because a reduction in particle size causes peak broadening.

The increase in peak width caused by a decrease in particle size is given by the Scherrer equation [38]:

$B = \frac{57.3k\lambda}{L\cos\theta}$, where:

B = peak broadening caused by particle size ($°2\theta$),
k = a constant related to the shape of the XRD line profile, with a value of 0.91,
$\lambda$ = wavelength of the X-rays (nm),
L = particle size (nm), and
$\theta$ = angle of the XRD peak maximum.

When values appropriate to the sizes at the boundaries between the fractions are inserted into the equation, it is found that for particles coarser than 2μm no measurable effect on the peak width can be found. For particles smaller than this, the calculated values of peak broadening, equally valid for the chlorite 1.4nm and the illite 1.0nm peaks, are given in Table 8.12, although one author has suggested that peak width is not affected by particle size until particles are finer than 0.2μm [263]. Values of broadening for particles intermediate in size between the boundaries will be intermediate between the values for the boundaries, and thus values of 0.09, 0.03 and $0.01°2\theta$ have been taken as the mean broadening caused by particle size in the 0.063-0.2, 0.2-0.63 and 0.63-2μm fractions, respectively. This shows that, particularly in the finest fraction, crystallinity values are significantly increased by the small crystallite size.

## 8.7 THE EFFECTS OF WEATHERING ON MINERAL CRYSTALLINITY

Before the effects of weathering on crystallinity can be investigated, the crystallinity of the parent material must be defined in terms of its metamorphic history. The mean illite crystallinity value of the

clay fractions from 1040 is 0.425°2$\theta$; when this is corrected for particle size it is reduced to 0.372°2$\theta$, and when instrumental effects are also allowed for to 0.328°2$\theta$. However, in the fractions coarser than 20μm, crystallinity values are found as low as 0.19°2$\theta$, which can be corrected to 0.07°2$\theta$. This pattern could have two origins. It is possible that the coarse particles are detritus from pre-existing rocks which have been elevated to higher temperatures than the finer particles, which are authigenic and have experienced only anchimetamorphism. On the other hand, the fine particles could have had the same origin as the coarser ones, but have experienced weathering not undergone by the coarse particles. Because of the fabric of the rock when collected it is unlikely that weathering has taken place since deposition of the rock, but it is possible that the finer detrital grains were weathered before the rock was deposited, and have since only been subject to anchimetamorphism.

If the measured crystallinity values are compared with those proposed as the boundaries between the diagenetic, anchimetamorphic and greenschist zones by the author of the method used, the mean value of 0.372°2$\theta$ for the clay fractions, when corrected for particle size, is very close to the boundary between diagenesis and anchimetamorphism at 0.38°2$\theta$, whilst the value of 0.19°2$\theta$ for the most crystallised fractions is in the lowest part of the greenschist zone, as the boundary is set at 0.21°2$\theta$ [144]. However, values between 0.25 and 0.64, and 0.17 and 0.41°2$\theta$ have been suggested respectively for the low and high temperature boundaries of the anchizone [144]. Estimates between 165 and 200°C have been made for the temperature of the anchizone, but evidence of pyrophyllite in rocks with crystallinity corresponding to the anchizone indicates that the upper end of this range is most likely. Once greenschist zone conditions are reached, crystallinity values do not depend as much upon metamorphic grade as upon chemistry. If the mineral composition does not correspond to an actual mica formula, two similar minerals will co-exist, leading to line broadening and an apparent lowering of crystallinity [144,154, 263].

Where differences between K saturated and Mg saturated crystallinity values are 0.05°2$\theta$ or more, it has been found that the illite $I_{002}/I_{001}$ ratio is low, at about 0.25 to 0.27 [144]. Previous work has claimed that only illites with high $I_{002}/I_{001}$ ratios should be used to investigate metamorphic grade, as $I_{002}/I_{001}$ was believed to correlate

with Al/(Mg + Fe) in illites, which increases with metamorphic grade. However, more recent studies have cast doubt on the relationship between $I_{002}/I_{001}$ and Al/(Mg + Fe). The specimens in this study have an $I_{002}/I_{001}$ range from 0.23 to 0.52, with a mean of 0.36 ± 0.07, but there is no correlation between $I_{002}/I_{001}$ and the difference between K saturated and Mg saturated crystallinity values.

Figure 8.2 is useful to illustrate the effects of weathering on crystallinity, although care has to be taken that the effects of dithionite treatment are not confused with those due to weathering. Considering only the clay fractions, none of the other Plynlimon samples is as crystallised as 1040, indicating that weathering, whether dominantly physical, to form a boulder clay, or dominantly chemical, to form a soil horizon, tends to reduce crystallinity. The fact that the boulder clays have crystallinity values most similar to that of 1040 indicates that physical weathering has less effect on crystallinity than chemical weathering.

When the crystallinity of the soil horizons is compared, it can be seen that, except for the anomalous position of the Bsgd/1078D horizon, which is least crystalline of the dithionite treated samples, crystallinity increases up the profile. At first sight this is unexpected, as it would seem most likely that increased chemical weathering would alter the crystal structure more, and thus cause a reduction in crystallinity. However, when the data are considered in detail, evidence for an explanation can be seen. Comparison of the crystallinity values of untreated and dithionite treated samples of the same horizon shows that dithionite treatment improves crystallinity. This cannot be caused by grains becoming more crystalline, and thus must be due to the dithionite dissolving the least crystalline grains, leaving only the most crystalline to give a lower crystallinity value. Of the samples analysed both before and after treatment, it is the one that is less crystalline before treatment that is more crystalline after, suggesting that the less crystalline the original sample, the more will be dissolved by dithionite, giving rise to a more crystalline product. The observed order of the crystallinity values of the treated samples thus suggests that the effect of weathering is to reduce crystallinity up the profile, allowing dithionite treatment to dissolve the weathered material more readily. The anomalous position of the Bsgd/1078D horizon is likely to be due to the translocation of illite from the Ea1 and Ea2 horizons (Sections 6.2.4 and 6.2.5).

When data for the coarser fractions are considered, the crystallinity values for the samples are very similar, and the dominant factor affecting crystallinity is grain size. It is only in the 2-6.3μm fraction that 1040 is most crystalline of the Plynlimon samples, although in this fraction it does appear that crystallinity decreases up the profile, suggesting that although these particles are small enough to be altered by weathering, they are not small enough to be dissolved by dithionite treatment. In coarser fractions no trends relating crystallinity to weathering are seen.

# CHAPTER 9

# SURFACE AREA ESTIMATION

## 9.1 INTRODUCTION

In order that the relative susceptibilities to weathering of the major minerals studied might be estimated independently of the effects of surface area, it was considered to be essential to quantify the surface areas of these mineral phases. This could have been carried out by making assumptions about the particle shapes of the different mineral phases and their size distribution within each separated fraction, and then calculating surface areas from the particle size distribution and quantitative mineralogical analysis data (Sections 6.2.3, 6.2.4 and 6.5). However, it was felt that the actual estimation of surface areas would provide data more relevant to the weathering environment, as it could include the internal surface areas of expandable minerals, and indicate whether the minerals had smooth or irregular external surfaces, as the latter give rise to surface areas up to twice those of the former. The internal surfaces of expandable minerals are open to chemical attack by polar molecules and ions just as much as the external surfaces, yet data based on particle size distribution could only indicate the latter.

Even with this analysis, it was impossible to assign the surface areas accurately between the mineral phases present within a size fraction as, for instance, the chlorite within a given fraction might be concentrated towards the coarser end, with the mica being found at the finer end. This detailed assignation could only have been carried out accurately if it had proved possible to separate the fractions into their component mineral phases.

In general, phyllosilicates have large reactive surface areas, the values of which are highly correlated with properties such as water retention and CEC. Assuming that quartz forms spherical particles, whilst phyllosilicates occur as discs with a diameter:thickness ratio of 10 [212], a phyllosilicate grain of the same volume as a quartz particle will have 2.1 times the latter's surface area. It is possible to estimate these surface areas by several different techniques [31], the majority of which depend on the measurement of surface adsorption [31,46,57,88,106,122,156,173,198,215,248]. Colloid chemists commonly measure surface area by the adsorption of $N_2$ gas at -195°C, using an

approach based on the BET multilayer adsorption equation, developed by Brunauer, Emmett and Teller [31,46]. Multilayer adsorption is characteristic of Van der Waals' attraction, and merges into capillary condensation as the vapour phase approaches saturation. If the adsorption isotherm is measured, the BET equation can be used to predict the surface area of a solid from the volume of gas required to form a monolayer. The use of BET $N_2$ adsorption to determine the surface areas of expandable phyllosilicates is unreliable, as the nonpolar $N_2$ molecule is unable to penetrate the interlayers, where up to 90% of the surface area is located [31]. It is possible to use the BET equation with a polar molecule, such as water, which will penetrate the interlayers, but this technique has not proved popular.

The BET equation can be applied to adsorption from solution, if an isotherm is measured [31,106], but it is more common to find that methods based on adsorption from solution require only one measurement, under conditions designed to bring about monolayer adsorption [106,156]. Two types of method for adsorption from solution are theoretically possible; the adsorption of polar molecules from a nonpolar solvent, and the adsorption of large organic cations from a polar solvent. No satisfactory method has been based on the first of these, as no adequate way of accounting for the simultaneous adsorption of solvent molecules by the adsorbent has been found. However, this problem is overcome in the second type of method, as the adsorption of the organic cation is so strongly preferred that adsorption of the solvent can be neglected [248]. If the adsorbate is chosen to be a dye [106], or a molecule that will react to produce a coloured product [156], it is easy to determine the concentrations before and after equilibration with the adsorbent.

However, the adsorption of dyes and similar molecules from solution can fail to give consistent results. Some molecules may show specific bonding to the solid surface, as well as the nonspecific bonds which are relied upon to produce monolayer coverage [106]. With phyllosilicates, adsorption of cationic dyes is dominated by exchange adsorption, and thus the equilibrium level of adsorption can be more dependent on the surface charge density and exchange capacity than the surface area, as described in detail by Van Olphen in a comprehensive evaluation of the methods available for determining phyllosilicate surface areas [248].

Dyes commonly show aggregation into micelles, both in solution and when adsorbed onto a solid, which means that adsorption does not produce a true monolayer. Some dyes may show a different degree of aggregation when adsorbed on the phyllosilicate surface to that shown in solution [248]. The possibility of chemical reaction between the dye and either the solid itself, or ions released into solution from it, must be avoided, and a final disadvantage is that adsorption may be related to the electrolyte concentration in solution [248]. Despite these disadvantages, adsorption from solution offers the advantages of simplicity and rapidity, and thus trials were made of a method that was specifically designed to measure the surface areas of phyllosilicates [156]. Details of the experimental procedure and results are given in Section 9.2.

Besides the most common methods of surface area determination, several other means of investigating the surface areas of phyllosilicates have been used. Some investigators have found good agreement between surface areas determined from heats of immersion and results from other methods, but in general it has been shown that the heats of immersion vary widely with charge density and exchangeable ion species, and are mainly governed by the heats of ionic hydration [248].

According to the Gouy-Chapman theory describing the electric fields around charged particles in suspension, anions will be repelled from negatively charged phyllosilicate surfaces, just as cations are attracted, and this negative adsorption can be used to determine the surface areas of phyllosilicates [167,231]. The small angle scattering of X-rays can be utilised to give a complete particle size distribution, and subsequently the surface area of a material, by means of the mathematical transformation of data obtained from step counting over the range from 0 to 8°2$\theta$. The results obtained from this method are generally in good agreement with those produced by BET adsorption measurements [96,217], but internal surfaces with spacings greater than 0.2nm are also taken into account by small angle X-ray scattering. However, a special X-ray goniometer attachment is required.

An attempt has been made to estimate soil surface areas by making assumptions about the surface areas of each of the mineral phases in the soils being studied, and summing these to produce a surface area for the whole soil [73]. The soils considered were a group of gleysols from Quebec; total surface area was measured by 2-ethoxyethanol

adsorption [57], and external surface area by BET $N_2$ adsorption. The surface area values assumed are given in Table 9.1. When the areas calculated from the assumed values were compared with those measured, the correlation was found to be significant with more than 99% confidence, and a similar level of significance was found for the correlation between the calculated smectite area and the measured internal surface area. The same degree of significance, with an approximately zero intercept, was obtained if the mineralogical analyses were recalculated to exclude quartz and feldspar. Similar results were found using assumed values for mineral CECs, the analyses being carried out because it was felt that:

> "In particular, surface area and exchange capacity have a dominant influence on the physical and chemical processes occurring in the soils." [73]

This type of approach is useful and effective when applied to a group of soils in which the mineral components have the same morphology in each of the soils analysed. However, because of differences in mineral morphology, composition and structure between different soil types, the assumed values for one soil group will not necessarily be valid for another group. If the values from Table 9.1 are applied to the mineralogical compositions presented in Sections 6.5 and 7.2, surface areas very different to those determined experimentally (see Sections 9.3 and 9.3.1) are produced. Thus, to have employed this type of method in this study, it would have been necessary to assume surface area values for each of the mineral components of the soils under investigation, and there were no data on which such assumptions could be based.

### 9.1.1 Surface Area Determination Methods Using Adsorption of Alcohols

The most commonly used methods for measuring the surface areas of phyllosilicates involve the adsorption of propan1,2,3triol, ethan1,2diol or 2-ethoxyethanol [73,88,122,156,173,198,213,215]. These are all polar molecules which are capable of expanding the basal spacings of smectites and vermiculites. Methods involving vapour phase adsorption [215], or adsorption from solution in water [173], have been proposed, but usually measurements are made as an excess of the liquid is desorbed under conditions that are considered to give rise to a stable monolayer [33,57,88,122,176]. The isotherms for the adsorption of polar molecules onto expandable phyllosilicates show considerable

| Mineral | Surface Area Assumed ($m^2g^{-1}$) |
|---|---|
| Smectite | 810 |
| Vermiculite | 350 |
| Noncrystalline Material | 200 |
| Illite | 100-125 |
| Chlorite | 100-125 |
| Quartz | <2 |
| Feldspar | <2 |

Table 9.1 Surface Areas Assumed for Different Mineral Phases

| Trial Specimen Number | Surface Area Determined by Phenanthroline Adsorption ($m^2g^{-1}$) | Surface Area Determined by Ethan1,2diol Adsorption ($m^2g^{-1}$) |
|---|---|---|
| 1 | 2.4 | 15.1 |
| 2 | 2.0 | 17.7 |
| 3 | 1.6 | 30.4 |
| 4 | 5.0 | 36.8 |

Table 9.2 Comparison of Surface Area Determinations from Preliminary Trials

| API Specimen Number | Mineralogy | Measured Surface Area ($m^2g^{-1}$) | Quoted Surface Area Values ($m^2g^{-1}$) | References |
|---|---|---|---|---|
| 5 | Kaolinite | 30.9 | 48.3, 55.4 | [57] |
| 21 | Bentonite | 641.5 | 810.0, 806.7 | [57] |
| 35 | Illite | 103.5 | 105.0, 258.1 | [7,176] |
| 42 | Metabentonite | 253.2 | 322.6 | [176] |

Table 9.3 A Comparison of Surface Area Measurements

hysteresis, due to the elastic stresses which occur at the edges of the particles when the interlayer spacings are altered. These stresses are less important during desorption, and thus desorption methods are likely to provide more accurate data [248].

Dyal and Hendricks [85] were the first to investigate the adsorption of polyalcohols as the basis of an analytical method for montmorillonite. They determined the amount of ethan1,2diol required to form the stable two layer complex with a basal spacing of 1.71nm by desorbing excess ethan1,2diol over anhydrous $CaCl_2$ in a vacuum. The rate of weight loss was measured, and desorption was found to become very slow when 0.255 ± 0.015 grams of ethan1,2diol per gram of montmorillonite remained adsorbed. At this point the montmorillonite was analysed by XRD, and was found to have the characteristic 1.71nm basal spacing. The total theoretical basal face surface area was calculated for a montmorillonite of ideal composition and known unit cell dimensions as $810m^2g^{-1}$, giving rise to an equilibrium value of 315 ± 19µg $m^{-2}$ of ethan1,2diol.

A kaolinite and a halloysite of known external surface areas were treated in a similar manner, but no useful conclusions could be drawn as to the number of layers of ethan1,2diol adsorbed onto their external surfaces. Despite this uncertainty, it was suggested that the external surface area of an expandable phyllosilicate could best be determined by ethan1,2diol adsorption after heating the phyllosilicate to 600°C to permanently collapse the interlayer structure.

The calculation used by Dyal and Hendricks gives a coverage of 0.332nm² for each molecule of ethan1,2diol adsorbed, but other methods of calculation give rise to different coverage figures, and thus to different weights adsorbed per square metre of surface [37]. To start with, the unit cell parameters used by Dyal and Hendricks were larger than those for most montmorillonites, and more representative values give a theoretical montmorillonite surface area of $760m^2g^{-1}$ and a coverage of 0.313nm² per ethan1,2diol molecule. A different approach to the problem involves the total chemical analysis of the two layer montmorillonite/ethan1,2diol complex in order to determine the number of molecules of ethan1,2diol per layer unit cell. When this value of 1.65 is combined with a theoretical surface area of $760m^2g^{-1}$, the area covered by a single molecule can be calculated as 0.281nm². The number of ethan1,2diol molecules per layer unit cell in this complex

can also be estimated from the Fourier transformation of XRD data, but this has given rise to a range of values between 1.5 and 2.0. If it is assumed that the density of the adsorbed ethan1,2diol is the same as that found in its normal liquid form at the same temperature, another method of calculating the coverage of each molecule can be derived from a value for the monolayer thickness, given by half the difference in basal spacing between the dry montmorillonite and its two layer complex with ethan1,2diol. This method gives rise to a coverage of 0.245nm$^2$ per molecule.

As well as having to take into account the variation caused by different values for the coverage of the adsorbate molecules, different conditions have been proposed to bring about equilibration. The first modification to the Dyal and Hendricks method was the inclusion of a free ethan1,2diol surface adjacent to the specimens during evacuation, and at the same time the maintenance of a constant temperature [176]. Once an equilibrium vapour pressure had been reached, the free surface ensured that it was maintained, rather than exposing the specimens to a continually decreasing vapour pressure. True equilibrium was shown tc exist by the fact that specimens reaching equilibrium from both directions had adsorbed the same amount of ethan1,2diol at equilibrium. For all specimens investigated, equilibrium was reached in 10 hours, whereas the equilibrium point was often difficult to ascertain with the Dyal and Hendricks method.

With both free ethan1,2diol and anhydrous $CaCl_2$ present in the system, it was found that a $CaCl_2$/ethan1,2diol solvate was forming and exerting control over the vapour pressure. Several proposals have taken advantage of this, controlling the vapour pressure by a mixture of anhydrous $CaCl_2$ and the solvate, rather than through the presence of a free liquid surface [33,57].

It is not certain that the different equilibration procedures achieve exactly the same densities of adsorbate molecules on both the internal and external surfaces of the phyllosilicate minerals. However, when the results from different methods for ethan1,2diol adsorption were compared, it appeared that the results were acceptably concordant, and that the differences were just as likely to be due to differences between the specimens used as to the methods employed [37]. On the other hand, when 2-ethoxyethanol is used, significant differences occur between different methods.

A method using 2-ethoxyethanol was originally introduced to reduce the time required to reach equilibrium with ethan1,2diol. 2-ethoxyethanol is much more volatile than ethan1,2diol, and it was claimed that, using a similar procedure, an equilibrium monolayer which would take 22 days to form using ethan1,2diol could be reached in two hours with 2-ethoxyethanol [57]. This initial method for 2-ethoxyethanol involved the use of a $CaCl_2$ solvate, but it was soon modified to exclude the solvate, as the determined surface area and the variation between replicates were found to be the same for both methods [122]. However, other investigators found that, although the amount of 2-ethoxyethanol retained was the same whether or not a solvate was included, a considerable difference in retention occurred between these values and the value given by a system including a free 2-ethoxyethanol surface, although it was claimed that all systems reached equilibrium in two hours [88].

The experiments were conducted on finer than 2μm Ca saturated Wyoming bentonite, and it was found that only the adsorption value obtained from the method including the free liquid surface agreed with the value calculated from the known surface area and a normal liquid density determination of the coverage of 2-ethoxyethanol. The values given by the other methods were approximately one third smaller. It was suggested that partial monolayers were stabilised under conditions with no free surface, with the full monolayer only being developed in the presence of the free surface. The partial monolayer was correlated with the 2-ethoxyethanol associated with the exchangeable cation sites, with the remainder of the monolayer only being weakly held by hydrogen bonding, and thus easily lost from the phyllosilicate surface unless a free liquid surface was also present [88].

There is considerable evidence to support the hypothesis that at least part of the adsorbate monolayer is associated with exchangeable cations of high electrostatic field strength. Using a method involving the BET adsorption of water, it was shown that more than twice as much water was adsorbed onto a Ca saturated kaolinite as on to the same material when Li saturated. The results with other cations occupied intermediate positions [248]. Similar differences were observed between the amounts of ethan1,2diol adsorbed onto Ca saturated and Na saturated montmorillonites and vermiculites. For every specimen except one, the difference between the amount of ethan 1,2diol adsorbed onto the Ca saturated phyllosilicate and that adsorbed onto the Na saturated

phyllosilicate was approximately equivalent to two molecules of ethan1,2diol for each Ca ion present on the exchange sites. Further work indicated that other simple alcohols and ketones were adsorbed to an extent of three molecules per Ca ion more when Ca saturated, as compared to Na saturated, phyllosilicates were used. These additional molecules were retained after storage under vacuum for periods of several months, whereas all of the molecules adsorbed by the Na saturated phyllosilicates were lost [37].

A further alteration in the amount of ethan1,2diol adsorbed by the specimen at equilibrium can be caused by the amount of water already present on the specimen surface. Two investigations have found that the amount of ethan1,2diol adsorbed is reduced by approximately 1mg for every 1mg of water already present [176,213]. Thus, if the moisture content of the specimen can be determined on a replicate, the uncertainties involved in drying over a desiccant and the possibility of specimen alteration caused by high temperature drying can be avoided, and an air dry specimen used for surface area determination.

Despite the claims made for the rapid equilibration of systems using 2-ethoxyethanol [57,88,122], other workers have found that true equilibrium may not be reached for 40 days [198]. For this reason, the apparent advantages claimed for 2-ethoxyethanol were not considered to be valid, unless the equilibration times reported for ethan1,2diol were also underestimates. Both propan1,2,3triol and 2-ethoxyethanol suffer from the disadvantage that, under the equilibrium conditions, they only form a one layer intercalation complex with vermiculites, but a two layer complex with smectites [37,88]. On the other hand, ethan1,2diol forms a two layer complex with both smectites and vermiculites, and thus, in order to reduce the number of measurements, the surface area of the specimens was investigated in most detail by an ethan1,2diol method [33]. Full experimental details are given in Section 9.2.

## 9.2 EXPERIMENTAL TECHNIQUES

Two surface area methods that did not involve isotherm measurement were used in initial experimental trials [33,156], and four specimens considered likely to have different surface areas were measured by each method. The aim was to see whether the results from the methods were comparable, and then to carry out replicate measurements to determine which method gave better reproducibility. For adsorption from solution, Lawrie's phenanthroline method was initially followed [156].

This procedure gave optical density values for the solutions that were equilibrated with the specimens that were not significantly different to the value given by the blank, and thus it was found necessary to increase the ratio of specimen surface area to phenanthroline available for adsorption by a factor of 100. After this modification, differences in optical densities between the specimens and the blank were measured, but the optical density of the blank was reduced much below that expected, and the surface areas calculated were found to be much lower than from the ethan1,2diol adsorption results (Table 9.2), whereas Lawrie found that results determined by phenanthroline adsorption were higher than those determined by ethan1,2diol adsorption [156]. It was considered that these problems were brought about by the dilution of the phenanthroline, the low optical density value for the blank being caused by the adsorption of the phenanthroline on the container becoming significant, and the reduced levels of phenanthroline adsorption by the specimens being due to the reduction of the phenanthroline concentration to well below saturation. Because of these problems, ethan1,2diol adsorption was used for all further surface area measurements.

The ethan1,2diol adsorption method was followed exactly as proposed by its authors [33]. A mixture of a $CaCl_2$/ethan1,2diol solvate with excess anhydrous $CaCl_2$ was prepared by adding 100g of $CaCl_2$ dried at 210°C for an hour to 20g of ethan1,2diol. After thorough stirring, the mixture was cooled in a $P_2O_5$ containing desiccator, then spread over the base of a deep sided glass dish which was just small enough to be fitted in the desiccator. Surface area determinations could be carried out on four specimens at once, approximately 1g of each being accurately weighed into a shallow flat dish which was supported above the solvate mixture by an aluminium mesh, the specimens being enclosed in the glass dish by covering it with a sheet of plain glass.

Before being placed above the solvate, the specimens were first dried to constant weight in an evacuated $P_2O_5$ containing desiccator, after which $1cm^3$ of ethan1,2diol, warmed to 60°C, was used to wet each specimen. Once in position, a rotary vacuum pump was applied for one hour to reduce the pressure to 0.025mmHg, and the desiccator was then sealed and left for 24 hours, after which the vacuum pump was applied for a further 30 minutes, followed by a further 24 hour period of being sealed. After this, the specimens were weighed, returned to the glass dish, and again evacuated for 30 minutes, but only sealed for eight

hours. The weighing and evacuation procedure was then repeated twice daily until the weights of all specimens varied by less than 1mg from their previous weights, usually requiring eight to 12 weighings. The amount of ethan1,2diol retained was calculated from the mean value of all weights agreeing better than ±1mg. The authors suggested that the equation:

$$A = \frac{Wg}{0.00031Ws}, \text{ where:}$$

A = surface area of specimen ($m^2g^{-1}$),
Wg = weight of ethan1,2diol retained (g), and
Ws = weight of specimen dried over $P_2O_5$ (g)

should be used, but instead the equation:

$$A = \frac{3000Wg}{Ws}$$

has been used, as a review of all proposed relationships between ethan1,2diol retention and surface area concludes that this is "as good a value as can be suggested from available data" [37].

Four further determinations were made of trial specimen 2, giving a mean for five values of 16.7 ± 1.5$m^2g^{-1}$, which was considered to be an acceptable level of reproducibility. In order to determine the absolute accuracy of the method, surface area measurements were carried out on four American Petroleum Institute (API) standard phyllosilicates, for which values for the surface areas were available in the literature. The results given in Table 9.3 show that all of the determined values are less than those quoted, varying from 40 to 99% of the quoted values. These differences could be due to experimental inaccuracies, or to differences in the saturating cations between the specimens measured and those for which values are quoted. It has been shown that up to 43% of the total ethan1,2diol adsorbed onto a Ca saturated phyllosilicate surface is specifically associated with the Ca ions [70] and, as no attempt was made to replace the naturally occurring saturating cations on the API phyllosilicates used in this study, it would be expected that the values determined would be less than the values measured on Ca saturated phyllosilicates. For this reason, the measured values were considered to be acceptable.

## 9.3 ETHAN1,2DIOL ADSORPTION MEASUREMENTS

Thirty surface area determination runs, each containing four specimen dishes, could be carried out in the time available. In one of these runs all four specimens were lost, in another two specimens were lost, and in two runs a single specimen was lost from each run, but all of the other runs allowed surface areas to be calculated for all of the specimens. The initial plan was to measure surface areas on duplicate specimens of the finer than 2mm material from each of the 12 samples, together with all of the finer than 6.3μm fractions from the rock, a boulder clay, two dithionite treated soil horizons and the two untreated horizons, to be followed by the coarser fractions from these samples, and fractions from other samples. However, it rapidly became clear that experimental error was very high, and up to four determinations were made for each specimen, in an attempt to eliminate spurious values from the data.

Because the specimens were assigned randomly to the runs, it was possible to determine that all specimens in certain runs gave rise to surface area measurements consistently higher, or lower, than the mean values for all replicates of these specimens. As a result of this, the data from three of the runs could be eliminated on the grounds that they gave rise to values outside ±25% limits from the mean values. In two of the runs eliminated, where the surface area measurements were consistently higher than the mean values, it is likely that equilibrium had not truly been reached when the specimen weights gave the appearance of stabilisation. For the run where the surface areas were consistently lower than the appropriate mean values, it is likely that the ethan1,2diol had been lost from the solvate, allowing ethan1,2diol to be removed from the specimens to below the level of monolayer coverage.

These three runs represent the extremes of error, and it is possible that other runs had not quite reached equilibrium, or had progressed to slightly below the level of monolayer coverage, when measurements were taken. For each specimen in a run, it is possible to calculate a factor relating the value determined in that run to the mean of all the replicates of that specimen in different runs. If a mean of these factors for the four specimens in a run is taken, a figure is obtained which can be applied to each measured surface area to correct it to the value that is likely to have been obtained if measurements had been made precisely at equilibrium. In this way, three sets of data are

generated: the uncorrected data including all measurements, the uncorrected data eliminating the data from extreme runs, and the data corrected as described. As no one of these sets of data is obviously more correct than the others, all are included in Tables 9.4 to 9.6 and 9.8.

Table 9.4 gives the values determined for the surface areas of the finer than 2mm material from the samples and, no matter which set of data is studied, several points are immediately obvious. Firstly, the unweathered rock has a very much lower surface area than any of the other specimens. Secondly, the surface area of the soil horizon specimens increases up the profile, the value in the Ea1 horizon being more than double that found in the BC horizon, which is turn approximately double that found in the unweathered rock. The biggest increase in surface area is between the Ea2 and Ea1 horizons. Neither the particle size analyses given in Table 6.3, nor the mineralogy as summarised in Figure 7.7, would suggest that this ought to be the case, as only a small increase in the finest particles occurs between the Ea2 and Ea1 horizons, together with a decrease in the content of expandable minerals with large internal surface areas. It would thus seem likely that this increase in surface area is due to a factor not considered in detail, most probably the formation of noncrystalline material. If the data in Table 9.1 are examined, it can be seen that, if noncrystalline material is formed in a soil consisting mainly of illite and quartz, the surface area will be increased, and thus this is likely to be the reason for the increase in surface area between the Ea2 and Ea1 horizons.

Support for this argument is provided by the surface area data for the specimens that have not been dithionite treated: the surface area is more than double that measured for the same horizons after treatment. As dithionite treatment is designed to remove noncrystalline oxyhydroxides of Fe and Al [179], it is likely that there is a significant amount of noncrystalline material, with a large surface area, present in all of the soil horizons before dithionite treatment. This noncrystalline material is likely to be at least partly in the form of coatings on grains and cement between grains, which could affect how the mineral grains respond to the weathering agencies in their environment. The only other possible explanations for a reduction in surface area on dithionite treatment would be if expandable minerals were preferentially dissolved by dithionite

| Sample | Surface Area of <2mm Material ($m^2 g^{-1}$) | | |
|---|---|---|---|
| | Uncorrected Data | Data from Extreme Runs Eliminated | Corrected Data |
| Unweathered Rock 1040 | 11.6 ± 1.8 | 11.6 ± 1.8 | 12.8 ± 0.3 |
| Boulder Clay 1029 | 33.3 ± 5.5 | 33.3 ± 5.5 | 33.2 ± 1.3 |
| Boulder Clay 1039 | 28.5 ± 9.2 | 28.5 ± 9.2 | 30.7 ± 5.3 |
| Boulder Clay 1049 | 29.6 ± 9.6 | 29.6 ± 9.6 | 30.5 ± 4.6 |
| Dithionite Treated BC Horizon 1080D | 23.3 ± 10.0 | 27.7 ± 6.2 | 24.2 ± 4.5 |
| Dithionite Treated Bs Horizon 1079D | 38.4 ± 5.9 | 38.4 ± 5.9 | 30.9 ± 5.5 |
| Dithionite Treated Bsg Horizon 1078D | 35.5 ± 13.5 | 40.6 ± 11.0 | 37.1 ± 4.3 |
| Dithionite Treated Ea2 Horizon 1077D | 41.4 ± 15.1 | 47.2 ± 12.0 | 44.0 ± 4.0 |
| Dithionite Treated Ea1 Horizon 1076D | 59.6 ± 0.3 | 59.6 ± 0.3 | 56.9 ± 3.2 |
| Bs Horizon 1079 | 91.7 ± 31.2 | 78.0 ± 18.1 | 84.7 ± 14.3 |
| Ea2 Horizon 1077 | 90.8 ± 24.7 | 98.9 ± 22.8 | 105.1 ± 11.7 |
| Hiraethog Comparison Material 1087 | 38.8 ± 6.4 | 38.8 ± 6.4 | 38.4 ± 2.0 |

Table 9.4 Surface Areas Determined for Material Finer than 2mm from Different Samples

treatment, or if very finely crystalline particles, perhaps attached to larger particles, were dissolved by the dithionite treatment. The data for the relative vermiculite contents of different specimens, given in Table 7.4, suggest that in fact dithionite treatment may increase the expandable mineral content, and in practice it is likely to be be very difficult to distinguish between the finest crystalline particles and noncrystalline materials, any difference being based mainly on an arbitrary definition.

The surface area for the Hiraethog comparison material, 1087, is higher than that of the boulder clays, to which it is otherwise similar, again emphasising the fact that it has a different origin to that of the Plynlimon materials.

### 9.3.1 Variation of Surface Area with Particle Size

When the data in Table 9.5 are examined, it is more difficult to come to conclusions concerning the relationship between surface area and particle size in the different samples. On theoretical grounds it would be expected that the measured surface area would be inversely proportional to the particle size. In fact specific surface area does increase as particle size decreases, but not as rapidly as predicted by theory, as can be seen by comparing the measured and theoretical surface area distributions given in Figure 9.1. This figure is based on the uncorrected surface area data with extreme runs eliminated, whilst theoretical quartz particles are assumed to be perfect spheres with a density of $2.65gcm^{-3}$, and theoretical phyllosilicates to occur as discs with a diameter:thickness ratio of 10 and a density of $2.85gcm^{-3}$. This discrepancy is due to the coarser fractions giving rise to larger surface areas than expected, as the finer fractions could not have much larger areas than those measured, unless they contained very significant amounts of expandable minerals or noncrystalline phases. Experimental error cannot be ruled out as the cause of these large areas for coarse fractions, but one possible mechanism, the change of mineralogy with particle size, can be ruled out, as the observed changes in mineralogy suggest that smaller quantities of the high surface area expandable minerals are present in the coarser fractions than the finer fractions. It is thus likely that the higher than expected surface areas measured for the coarser fractions are due to very small particles with high surface areas attached to the surfaces of the coarse particles. Evidence for this is provided by the surface areas measured for the 6.3-20 and 20-63μm

| Particle Size (μm) | Sample | Surface Area of <2mm Material ($m^2g^{-1}$) | | |
|---|---|---|---|---|
| | | Uncorrected Data | Data from Extreme Runs Eliminated | Corrected Data |
| 0.063 - 0.2 | 1040 | 82.6 ± 40.2 | 62.9 ± 10.5 | 81.4 ± 19.1 |
| 0.063 - 0.2 | 1039 | 176.7 ± 9.8 | 183.6 ± 0.0 | 149.0 ± 26.4 |
| 0.063 - 0.2 | 1079D | 75.4 ± 1.0 | 75.4 ± 1.0 | 75.8 ± 3.2 |
| 0.063 - 0.2 | 1076D | 120.8 ± 0.7 | 120.8 ± 0.7 | 120.8 ± 1.9 |
| 0.063 - 0.2 | 1079 | 235.5 ± 13.8 | 225.7 ± 0.0 | 189.2 ± 5.3 |
| 0.063 - 0.2 | 1077 | 228.4 ± 12.0 | 228.4 ± 12.0 | 198.2 ± 10.4 |
| 0.2 - 0.63 | 1040 | 78.7 ± 7.8 | 78.7 ± 7.8 | 68.3 ± 0.6 |
| 0.2 - 0.63 | 1039 | 66.4 ± 11.0 | 66.4 ± 11.0 | 71.8 ± 2.9 |
| 0.2 - 0.63 | 1079D | 59.1 ± 2.8 | 59.1 ± 2.8 | 60.6 ± 2.8 |
| 0.2 - 0.63 | 1076D | 29.3 ± 3.7 | 29.3 ± 3.7 | 29.3 ± 3.7 |
| 0.2 - 0.63 | 1079 | 78.3 ± 36.3 | 62.3 ± 15.5 | 82.7 ± 16.2 |
| 0.2 - 0.63 | 1077 | 101.9 ± 13.0 | 92.7 ± 0.0 | 88.2 ± 6.0 |
| 0.63 - 2 | 1040 | 45.1 ± 9.0 | 45.1 ± 9.0 | 42.9 ± 8.4 |
| 0.63 - 2 | 1039 | 37.7 ± 9.1 | 37.7 ± 9.1 | 40.5 ± 4.6 |
| 0.63 - 2 | 1079D | 57.1 ± 11.1 | 50.8 ± 0.2 | 55.7 ± 6.4 |
| 0.63 - 2 | 1076D | 66.2 ± 5.2 | 66.2 ± 5.2 | 66.2 ± 3.8 |
| 0.63 - 2 | 1079 | 114.7 ± 31.3 | 99.6 ± 9.8 | 112.8 ± 8.6 |
| 0.63 - 2 | 1077 | 73.4 ± 24.6 | 73.4 ± 24.6 | 80.9 ± 10.3 |
| 2 - 6.3 | 1040 | 10.7 ± 2.0 | 10.7 ± 2.0 | 11.0 ± 0.5 |
| 2 - 6.3 | 1039 | 10.9 ± 0.6 | 10.9 ± 0.6 | 10.1 ± 0.5 |
| 2 - 6.3 | 1079D | 17.8 ± 2.1 | 17.8 ± 2.1 | 17.6 ± 2.2 |
| 2 - 6.3 | 1076D | 27.7 ± 5.4 | 27.7 ± 5.4 | 27.2 ± 5.4 |
| 2 - 6.3 | 1079 | 32.8 ± 6.3 | 32.8 ± 6.3 | 34.1 ± 2.5 |
| 2 - 6.3 | 1077 | 31.4 ± 6.0 | 31.4 ± 6.0 | 27.6 ± 4.0 |
| 6.3 - 20 | 1076D | 7.5 ± 0.8 | 7.5 ± 0.8 | 7.6 ± 0.9 |
| 6.3 - 20 | 1077 | 25.8 ± 0.4 | 25.8 ± 0.4 | 25.8 ± 0.4 |
| 20 - 63 | 1076D | 1.3 ± 0.0 | 1.3 ± 0.0 | 1.3 ± 0.0 |
| 20 - 63 | 1077 | 43.3 ± 3.3 | 43.3 ± 3.3 | 43.3 ± 3.3 |

Table 9.5 Surface Areas Determined for Different Size Fractions

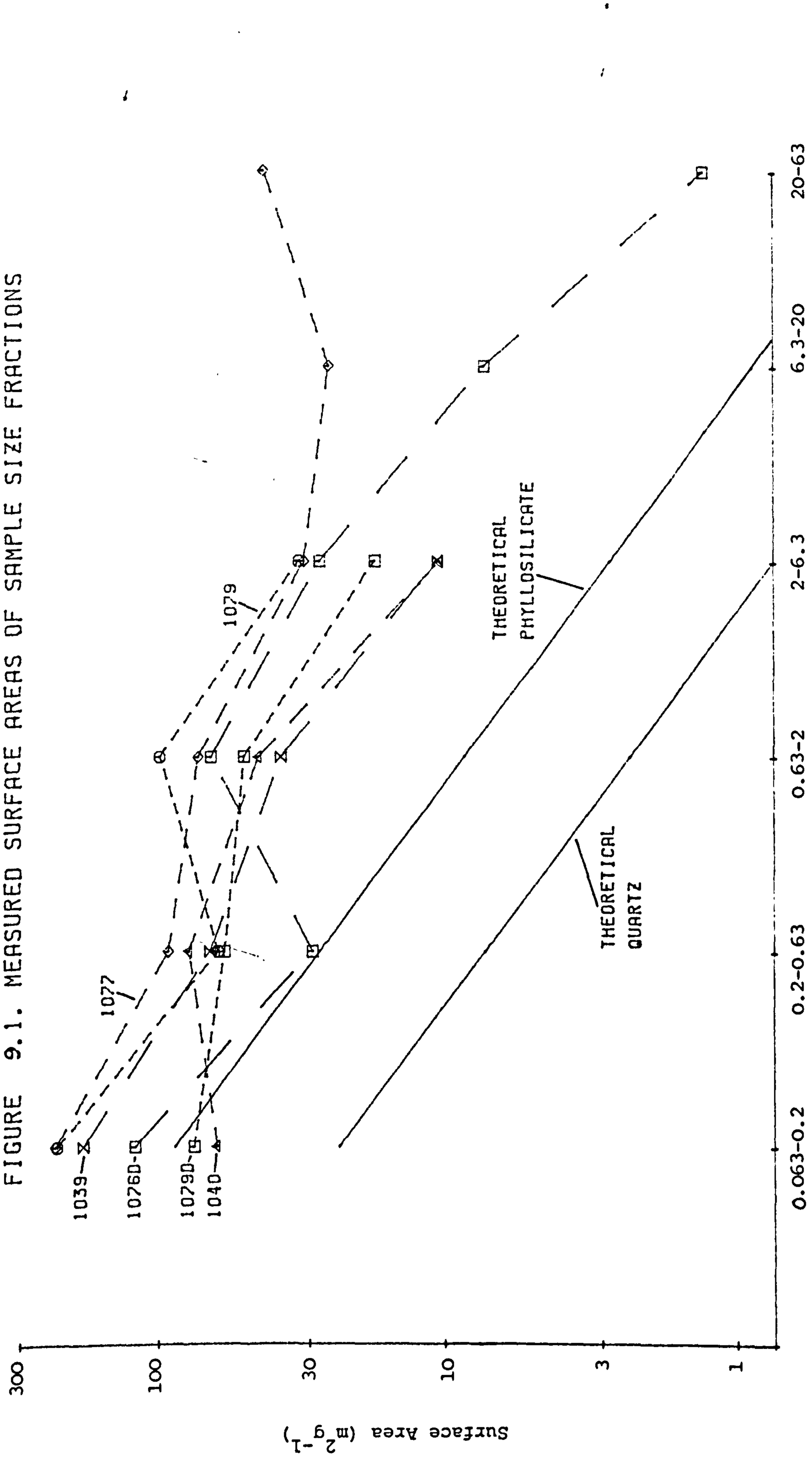


FIGURE 9.1. MEASURED SURFACE AREAS OF SAMPLE SIZE FRACTIONS

fractions. For the dithionite treated 1076D, the surface area decreases as would be expected, from the 6.3-20 to the 20-63μm fraction. However, for the untreated 1077, not only is the surface area in the 6.3-20μm fraction substantially higher than that for 1076D, both samples having similar surface areas in their 2-6.3μm fractions, but it actually increases further in the 20-63μm fraction, suggesting that, in their natural state, these larger particles are associated with considerable amounts of very fine particles.

Throughout the size fractions, it is the soil horizons that have not been dithionite treated that show the largest surface areas, suggesting that dithionite treatment is significantly altering the surface of the grains, as well as the mineralogy (Section 7.1.2). Direct comparison can be made between the surface areas measured for 1079 and 1079D.

For all samples investigated, there is a more significant difference in surface area between the 2-6.3 and 0.63-2μm fractions than between the 0.63-2 and 0.2-0.63μm fractions with, at least in the case of 1079, the 0.63-2μm fraction having a higher specific surface area than the 0.2-0.63μm fraction. This is also the case with the data for 1076D, but for this sample the very low surface area for the 0.2-0.63μm fraction is likely to be due to experimental error. However, the more significant reduction in measured surface area at 2μm is almost certainly related to the significant increase in the quartz content of fractions coarser than 2μm (Section 6.5), as quartz particles of the same esd as phyllosilicates will have specific surface areas that are about 3.7 times lower, assuming that phyllosilicate discs have a diameter:thickness ratio of 10, and that quartz particles are spherical. Unfortunately, the data are not good enough to be able to draw conclusions as to how the surface area in particular fractions alters throughout the profile, or to compare the data for the rock and boulder clay with those for the soil samples.

### 9.3.2 Comparison of Surface Area and Particle Size Data

In order to discover how consistent the surface area data were, the data presented in Tables 9.4 and 9.5 were combined with the particle size distribution data from Table 6.3, in order to calculate surface areas for the fractions finer than 2mm that had not had their surface areas measured separately. The results of these calculations are presented in Table 9.6, and give values varying between excessively large, for 1077 and 1076D, through considerably larger than would be

| Particle Size (μm) | Sample | Surface Area ($m^2 g^{-1}$) | | |
|---|---|---|---|---|
| | | Uncorrected Data | Data from Extreme Runs Eliminated | Corrected Data |
| 6.3 - 2,000 | 1040 | 1.4 | 1.7 | 4.7 |
| 6.3 - 2,000 | 1039 | 12 | 11 | 16 |
| 6.3 - 2,000 | 1079D | 38 | 40 | 18 |
| 6.3 - 2,000 | 1079 | 100 | 77 | 94 |
| 63 - 2,000 | 1076D | 2,100 | 2,100 | 1,800 |
| 63 - 2,000 | 1077 | 780 | 950 | 1,100 |

Table 9.6 Surface Areas Calculated on the Basis of Summing the Areas of the Fractions to Equal the Overall Surface Area

| Material | Surface Area ($m^2 g^{-1}$) | | |
|---|---|---|---|
| | Uncorrected Data | Data from Extreme Runs Eliminated | Corrected Data |
| Whole Fraction | 63.3 | 61.8 | 57.5 |
| Chlorite Calculated | 62.4 | 61.4 | 56.5 |
| Chlorite Measured | 27.3 ± 1.7 | 27.3 ± 1.7 | 27.2 ± 1.7 |

Table 9.8 Surface Areas for the 0.063-2μm Fraction from 1040

expected, for 1039, 1079D and 1079, to approximately what would be expected, in the case of 1040. The results for 1077 and 1076D must be dismissed as being totally due to the summation of errors from the measured surface areas, and whilst the results for 1039, 1079D and 1079 may also be due to this cause, it is possible that, particularly for 1039, the value determined is approximately the correct one, and is a result of very fine particles attached to the surfaces of the larger grains. The measured values for the finer fractions of 1040 suggest that the result for this sample is a reasonable estimate of the surface area of the 6.3-2000μm fraction, but this may be due to coincidence, rather than implying that both the measured and calculated surface area values for the size fractions of 1040 can be relied upon.

The data from these three tables were also combined in a different way, to indicate the percentage of the total finer than 2mm surface area contributed by the different size fractions, and to compare this with the weight percentage of the same fractions. The uncorrected surface area data with extreme runs eliminated were employed, and results are given in Table 9.7. This shows that, in all except one case, the dominant contribution to surface area is from the 0.063-0.2μm fraction with, again except in one case, the second most important contribution coming from the 2-6.3μm fraction. The dominance of these fractions is apparently caused by the very high specific surface areas measured for the 0.063-0.2μm fractions, and the high weight percentage of the 2-6.3μm fractions. The two exceptions are provided by the rock, where the dominant contribution comes from the 0.2-0.63μm fraction, and the boulder clay, where the second most important contribution is provided by this fraction.

Attempts were made to correlate the measured surface areas in the different fractions with the amount of vermiculite estimated by XRD methods (Table 7.4), the total expandable minerals as determined by CEC methods (Table 7.5), the quantitative mineralogy (Section 6.5), and crystallinity (Table 8.2) and peak symmetry (Table 8.6) data. No significant correlations could be found with any of these factors, suggesting that either the error in the surface area measurements is too great, or else that the surface area is dominated by noncrystalline material, which would not affect these other factors.

One further surface area determination was carried out, on the chlorite magnetically separated from the 0.063-2μm fraction of 1040 (Section

| Sample | Particle Size (μm) | % By Weight of <2mm Material | % By Surface Area of <2mm Material |
|---|---|---|---|
| 1040 | 0.063 - 0.2 | 0.89 | 4.8 |
| 1040 | 0.2 - 0.63 | 5.07 | 34.4 |
| 1040 | 0.63 - 2 | 5.21 | 20.3 |
| 1040 | 2 - 6.3 | 35.34 | 32.6 |
| 1040 | 0.063 - 6.3 | 46.51 | 92.1 |
| 1039 | 0.063 - 0.2 | 5.80 | 37.4 |
| 1039 | 0.2 - 0.63 | 9.89 | 23.0 |
| 1039 | 0.63 - 2 | 7.55 | 10.0 |
| 1039 | 2 - 6.3 | 9.59 | 3.7 |
| 1039 | 0.063 - 6.3 | 32.83 | 74.1 |
| 1079D | 0.063 - 0.2 | 12.97 | 25.5 |
| 1079D | 0.2 - 0.63 | 3.10 | 4.8 |
| 1079D | 0.63 - 2 | 10.97 | 14.5 |
| 1079D | 2 - 6.3 | 35.98 | 16.7 |
| 1079D | 0.063 - 6.3 | 63.02 | 61.5 |
| 1076D | 0.063 - 0.2 | 16.53 | 33.5 |
| 1076D | 0.2 - 0.63 | 1.96 | 1.0 |
| 1076D | 0.63 - 2 | 6.55 | 7.3 |
| 1076D | 2 - 6.3 | 42.36 | 19.7 |
| 1076D | 6.3 - 20 | 25.44 | 3.2 |
| 1076D | 20 - 63 | 6.15 | 0.1 |
| 1076D | 0.063 - 63 | 98.99 | 64.8 |
| 1079 | 0.063 - 0.2 | 9.25 | 26.8 |
| 1079 | 0.2 - 0.63 | 3.59 | 2.9 |
| 1079 | 0.63 - 2 | 6.84 | 8.7 |
| 1079 | 2 - 6.3 | 31.48 | 13.2 |
| 1079 | 0.063 - 6.3 | 51.16 | 51.6 |
| 1077 | 0.063 - 0.2 | 6.04 | 13.9 |
| 1077 | 0.2 - 0.63 | 7.73 | 7.2 |
| 1077 | 0.63 - 2 | 6.83 | 5.1 |
| 1077 | 2 - 6.3 | 37.72 | 12.0 |
| 1077 | 6.3 - 20 | 26.09 | 6.8 |
| 1077 | 20 - 63 | 10.32 | 4.5 |
| 1077 | 0.063 - 63 | 94.73 | 49.5 |

Table 9.7 Contributions of Different Size Fractions to Total Surface Area

4.2.2). Table 9.8 compares this measured surface area with the value calculated for the 0.063-2μm material before fractionation, and the value for the chlorite in that material, of which it comprises 19.5%, assuming all the minerals to have the same specific surface area. The value for chlorite is different from that for the whole fraction, as the mineralogy and surface area vary between the measured size fractions forming part of this fraction. These data suggest that the specific surface area of the chlorite is lower than the mean value for all of the minerals in this fraction. This could be due to the presence of any of noncrystalline material, vermiculite or hydroxy interlayered vermiculite (Table 7.5), all of which would be expected to have higher specific surface areas than chlorite.

## 9.4 THE EFFECTS OF WEATHERING ON MINERAL SURFACE AREA

Although the data presented in the previous section are limited by experimental inaccuracies, it is possible to draw some tentative conclusions about the effects of weathering on surface area. It is most instructive to consider the surface areas measured for the finer than 2mm material for the different samples, from which it can clearly be seen that the unweathered rock has the lowest surface area, and any form of alteration, whether to boulder clay or soil, considerably increases the surface area. The boulder clays all have very similar surface areas, suggesting formation by a similar process from originally similar materials. Both of these facts suggest that the measured values have relative, if not absolute, validity.

In the soil profile, the dithionite treated samples show an increase in surface area up the profile, in other words an increase in surface area with the intensity of weathering. The BCd/1080D horizon would be expected to have a lower surface area because of its very much larger mean particle size than those measured for the other horizons (Table 6.5). However, for the other horizons some other factor must be causing the surface area to increase with intensity of weathering. This may be partially explained by the increase in expandable minerals up the profile as far as the Ea2 horizon (Table 7.5), but the drop in the expandable mineral content in the Ea1 horizon must mean that a further factor is coming into play. The very much higher surface areas found for the soil samples not treated with dithionite suggest that this is noncrystalline material, most of which is removed by dithionite treatment, increasing up the profile with intensity of weathering.

Similar features to those observed for the finer than 2mm material are seen in the separated size fractions coarser than 0.63μm.

Perhaps the most important effect of weathering to be revealed by the surface area measurements is therefore the role that is likely to be played by noncrystalline material, which was not investigated in this study. Although the data presented are not accurate enough to quantify the mineral surface areas available for weathering, more accurate data, obtained by a similar method, should be able to help in relating available surface area to the level of mineral alteration seen throughout the profile, and might also be able to provide evidence for the amount of noncrystalline material present in the different horizons.

Even though the surface area data are not considered to be suitable to provide a quantitative estimate of relative rates of mineral alteration in the soil profile, Table 9.9 shows how calculations could be carried out if appropriate data were available. Total mineral surface areas of mica, chlorite and quartz for each soil horizon could be calculated by summing the products of the surface area, the content of the size fraction in the total sample, and the content of the mineral in the size fraction, for each size fraction. To be useful in further calculation, this would require accurate surface area data for all of the size fractions, but the available data for the four finest fractions are used in Table 9.9 as an example.

The total mineral surface areas for each horizon could then be compared, and it would be expected that, as weathering increased, total mineral surface area would decrease. The relative rates of decrease of the different minerals between two adjacent horizons would be proportional to the relative rates of weathering of the minerals between those horizons. From Table 9.9, it appears that chlorite does indeed show a considerable total surface area decrease from the Bs to the Ea2 horizon, but both mica and quartz apparently show surface area increases, which are due to either the incompleteness of, or inaccuracies in, the surface area data.

| Mineral | Size Fraction (μm) | Sample 1079 Surface Area of Size Fraction from Table 9.5 ($m^2g^{-1}$) | 1079 % Size Fraction in Total Sample from Tables 6.2 and 6.3 | 1079 % Mineral in Size Fraction from Table 6.11 | 1079 $m^2$ of Mineral Surface Area per g of Total Sample | 1077 Surface Area of Size Fraction from Table 9.5 ($m^2g^{-1}$) | 1077 % Size Fraction in Total Sample from Tables 6.2 and 6.3 | 1077 % Mineral in Size Fraction from Table 6.11 | 1077 $m^2$ of Mineral Surface Area per g of Total Sample |
|---|---|---|---|---|---|---|---|---|---|
| Mica | 0.063 - 0.2 | 189.2 | 7.85 | 95.7 | 14.21 | 198.2 | 6.02 | 100.0 | 11.93 |
| | 0.2 - 0.63 | 82.7 | 3.05 | 97.1 | 2.45 | 88.2 | 7.70 | 99.1 | 6.73 |
| | 0.63 - 2 | 112.8 | 5.81 | 90.7 | 5.94 | 80.9 | 6.80 | 94.1 | 5.18 |
| | 2 - 6.3 | 34.1 | 26.73 | 54.5 | 4.97 | 27.6 | 37.57 | 58.2 | 6.03 |
| | Total | | | | 27.57 | | | | 29.87 |
| Chlorite | 0.063 - 0.2 | 189.2 | 7.85 | 0.0 | 0.00 | 198.2 | 6.02 | 0.0 | 0.00 |
| | 0.2 - 0.63 | 82.7 | 3.05 | 1.2 | 0.03 | 88.2 | 7.70 | 0.3 | 0.02 |
| | 0.63 - 2 | 112.8 | 5.81 | 2.8 | 0.18 | 80.9 | 6.80 | 0.4 | 0.02 |
| | 2 - 6.3 | 34.1 | 26.73 | 8.0 | 0.73 | 27.6 | 37.57 | 0.2 | 0.02 |
| | Total | | | | 0.94 | | | | 0.06 |
| Quartz | 0.063 - 0.2 | 189.2 | 7.85 | 4.3 | 0.64 | 198.2 | 6.02 | 0.0 | 0.00 |
| | 0.2 - 0.63 | 82.7 | 3.05 | 1.7 | 0.04 | 88.2 | 7.70 | 0.6 | 0.04 |
| | 0.63 - 2 | 112.8 | 5.81 | 6.6 | 0.43 | 80.9 | 6.80 | 5.6 | 0.31 |
| | 2 - 6.3 | 34.1 | 26.73 | 37.5 | 3.42 | 27.6 | 37.57 | 41.6 | 4.31 |
| | Total | | | | 4.53 | | | | 4.66 |

Table 9.9 A Method for Calculating Relative Rates of Mineral Alteration

# CHAPTER 10

# CONCLUSIONS AND DISCUSSION

## 10.1 SHALE WEATHERING AT PLYNLIMON

As a result of the experimental work presented in the preceding seven chapters, a number of important conclusions can be drawn with regard to the weathering of shales at Plynlimon, as well as others relating to the techniques employed in the investigation. In general it is encouraging to see that the major conclusions are independently supported by evidence from more than one investigative technique, which suggests that these conclusions do reflect the natural weathering scheme of shale to soil parent material to humic stagnopodsol, as it occurs in the Plynlimon environment.

Considering first of all the parent material at Plynlimon, Section 3.3 shows that it varies across the catchment. The rocks are visually different in hand specimen, differences occurring even within the rock groups, and comparison of Zr/Sr ratios and semiquantitative mineralogy determined by XRD show significant differences between the groups in both chemistry and mineralogy, indicating that each rock group has a unique identity. On a more detailed level of investigation, the electron probe microanalysis of chlorite grains in thin sections of different rocks, reported in Section 5.1.5, shows that not only does the chlorite content vary from rock to rock, but also that the chlorite chemistry changes between the rocks. The most significant differences are seen in the Fe/Mg ratio, but other aspects of the chlorite chemistry, such as the tetrahedral Si/Al ratio, also show significant differences between the rocks.

The nature of the soil parent material is further complicated by the fact that the overwhelming majority of the soils are not developed directly on solid rock, but instead boulder clay, head and colluvium are more common as parent materials. Because of this, it must be accepted that some alteration of the rock has occurred before soil formation begins. Sections 3.3 and 6.5 show that the boulder clays have higher $TiO_2$ and $K_2O$, and lower $SiO_2$, contents than the rocks. The chemical and XRD analyses for expandable minerals, detailed in Sections 7.1.3, 7.2 and 7.2.1, and the illite peak symmetry studies in Section 8.4, indicate that some of the hydroxy interlayered vermiculite present in the fresh rock is converted either to chlorite, by filling

of the interlayer with Fe or Mg, or to mica, by fixation of K, or might possibly be selectively destroyed, on alteration of the rock to boulder clay.

Despite this variability in the parent material, the results presented in this thesis can be considered as representative of weathering throughout the Wye catchment at Plynlimon. The soil profile studied most intensively is from the Hiraethog series, which Figure 3.3 and Section 3.4 show to be the most widespread of the soil series in the catchment that are not developed on boulder clay. The chlorite used as a standard, that extracted from shale 1040 (Section 4.2.2), is also shown by the microprobe analyses presented in Section 5.1.5 to not differ significantly in any of its analytical parameters from the means for all of the grains analysed by microprobe.

10.1.1 Magnetic Separation

Turning to the magnetic method used to separate chlorite from the crushed rock, several conclusions can be drawn, as reported in Section 4.5. Firstly, it is obvious that the separating system used is far from perfect at removing chlorite from crushed rock. Separation is most effective on fractions finer than 2μm, but even so it requires at least eight passes through the separator to produce chlorite of more than 95% purity, and even 12 passes do not produce 100% pure chlorite. Addition of Calgon to the suspension being separated, and the insertion of a ferritic stainless steel mesh into the separating volume, both increase the yield, but decrease the purity, of the magnetic fraction. This is likely to be due to the increased effectiveness of the magnetic field allowing more of the chlorite grains that are less magnetic, because of illite intergrowths, to be retained in the magnetic field. However, dilution of the suspension being separated does not change the purity of the magnetic fraction. At each stage of separation some chlorite remains in the nonmagnetic fraction, and Section 4.2.2 shows that this material has a lower Fe content than the chlorite which is extracted into the magnetic fraction. The work on the magnetic separation of illite from quartz did not reach a positive conclusion, but there is evidence in Section 4.4 to suggest that, if the chlorite was first removed and the illite were then to be effectively saturated with $Co^{2+}$, it might be possible to magnetically separate illite from quartz.

10.1.2 Mineralogical Investigation

Having carried out the separation of the chlorite, its mineralogical nature was investigated in detail, whilst electron probe microanalysis was also employed in the analysis of illite grains in rock sections. The mean chlorite analysis from the electron probe data presented in Section 5.1.1 was recalculated to give a structural formula of:

$$(Mg_{2.61}Al_{3.53}Fe_{5.47}Ti_{0.01}K_{0.08})(Si_{5.16}Al_{2.84})O_{20}(OH)_{16},$$

with the extreme range of composition being:

$$(\ Mg_{1.55-3.31}Al_{3.29-3.72}Fe_{4.52-6.88}Ti_{0.00-0.01}K_{0.01-0.29}\ )(\ Si_{4.86-5.49}Al_{2.51-3.14}\ )O_{20}(OH)_{16}.$$

The mean composition is that of a ripidolite by both Hey's and Foster's classifications, but some analyses fall into the thuringite field of Foster's classification or the pseudothuringite or aphrosiderite fields of Hey. Similarly, the electron probe data give a mean mica analysis of:

$$K_{1.47}(Al_{3.47}Mg_{0.40}Fe_{0.65}Ti_{0.03})(Si_{5.93}Al_{2.07})O_{20}(OH)_{4},$$

with an extreme compositional range of:

$$K_{1.08-1.82}(\ Al_{2.92-3.71}Mg_{0.16-0.88}Fe_{0.20-1.46}Ti_{0.01-0.06}\ )(\ Si_{5.46-6.23}Al_{1.77-2.54}\ )O_{20}(OH)_{4}.$$

In Section 5.4, the chlorite polytype is shown conclusively to be IIb, whilst in Section 5.5 a similarly conclusive determination of the illite $2M_1$ polymorph is made. The chlorite was shown to be trioctahedral, and the mica to have a dioctahedral structure.

However, the microprobe analyses given in Section 5.1 suggest that the spot analyses obtained from large grains of chlorite or illite are not actually derived from pure mineral compositions. Instead, analyses of grains that optically appear to be either pure illite or pure chlorite indicate that the illite and chlorite grains are contaminated respectively with chlorite or illite on a scale that is too fine for optical or electron probe resolution. Nevertheless, even when this contamination of the chlorite is allowed for, the chlorite is still found to have considerable excess Al in its octahedral sites, the

amount of excess being compatible with the suggestion made in Section 5.1.2 that the chlorite on average contains 15% Al hydroxy interlayered vermiculite. This finding is supported by the results of the detailed phyllosilicate mineralogy presented in Section 7.3 where, particularly in the finest fractions, the chlorite is seen to consist of a mixture of chlorite and hydroxy interlayered vermiculite.

Section 5.2 shows that the chemical analyses obtained for both finer than 2μm and sand size chlorite separates, by two different analytical methods, agree very well with the findings of the microprobe spot analyses of large chlorite grains. However, XRD based methods for estimating chlorite compositions do not agree anywhere near as well with the microprobe analyses. The c axis methods for estimating both total and tetrahedral chlorite Al contents, described in Section 5.3.1, give values that do not correlate significantly with the microprobe determined Al contents. What is more, the error in estimating the microprobe determined Al content is much reduced if a fixed Al content, rather than that derived from any of the c axis spacing methods, is employed. Nevertheless, the errors generated by these c axis methods are similar to those found by other workers. Using XRD based methods, chlorite Fe content can be estimated by the use of either b axis spacings, as in Section 5.3.2, or peak intensity ratios, as in Section 5.3.3. The best method was found to be the b axis spacing method of Von Engelhardt, whilst the best peak intensity method gave a mean error more than twice as large. However, correlation coefficients between microprobe determined Fe, and the Fe content estimated by XRD methods, were found in Section 5.3.4 to be negative, and thus these methods were not considered to be a good way of estimating chlorite composition, although, short of full structural analysis, they are the only way of estimating the degree of asymmetry in the distribution of Fe between the octahedral sheets.

### 10.1.3 Dithionite Pretreatment

Before considering the effects of weathering on the minerals studied, mention should be made of the effects of the dithionite pretreatment that was employed on the soil horizon samples. By comparing the properties of treated and untreated samples it was possible to show that the dithionite treatment reduced the mean particle size (Section 6.2.5), but at the same time reduced the specific surface area (Section 9.3). Treatment was also found to increase the illite crystallinity (Section 8.3), whilst causing the breakdown of illite to

interstratified illite-vermiculite (Section 7.1.2). Although these findings appear to be incompatible, this is not in fact the case. Dithionite preferentially attacks the least crystallised material which, because of its partially interstratified nature, has the highest specific surface area. Dissolution of this material thus increases the average crystallinity of the remaining illite, whilst reducing its specific surface area. Crystallinity is also improved because the interstratified illite-vermiculite peak is moved away from the illite peak, as seen in Figure 7.6, and thus the interstratified material no longer contributes a broadening effect to the illite peak. The mean particle size is reduced simply because of the effect of dithionite in dissolving the Fe oxyhydroxides which act as cements between grains.

### 10.1.4 Mineral Weathering

As might be expected, the action of weathering is seen in the breakdown of mineral grains, and thus Section 6.2.5 shows that there is an overall decrease in the mean particle size of the finer than 2mm fractions of the soil horizons up the profile. Closely related to this decrease in particle size is the increase in specific surface area up the profile (Section 9.3); the specific surface area more than doubles from the BC horizon to the Ea1 horizon. The lowest mean particle size is, however, found in the Bsg horizon sample, 1078D. In particular, Sections 6.2.4 and 6.2.5 show that the 0.63-2μm fraction is most concentrated in the Bsg horizon, and the suggested explanation for this is the translocation of 0.2-2μm illite down the profile from the Ea1 and Ea2 horizons to the Bsg horizon. This movement of illite is also suppported by the crystallinity data presented in Section 8.3, which show that the least crystallised illite is found in the Bsg horizon. The least crystallised material would be expected to be produced in the Ea1 horizon, where weathering is most intense and thus, when taken together, the particle size and crystallinity data imply that fine grained, poorly crystallised illite is being illuviated from the Ea1 and Ea2 horizons into the Bsg horizon.

Although the results of this study support no other simple explanation, it must be emphasised that the suggestion of illuviation in a podsolic soil is contrary to the accepted view of pedogenesis, and contrary to the findings of Rezk working on a similar profile at Hiraethog. To provide positive proof of illuviation, it would be necessary to carry out a detailed micromorphological study of the soil horizons, looking for evidence of argillans in the Bsg horizon.

An analysis of the overall particle size distributions for the soil horizons, presented in Section 6.2.5, suggests that the shale parent material of the profile consists of 72% silt and 28% clay particles. When mineralogical analysis is combined with the determined particle size distributions, the preferred grain size of each of the mineral species can be found. Section 6.5 shows that the greatest concentration of mica is always found in the 0.063-0.2μm fraction, and the greatest concentration of chlorite in the 20-63μm fraction, due to their respective occurrences in the rock matrix and as matrix supported clasts. For quartz, the greatest concentration in samples that have been little altered is in the 6.3-20μm fraction, whilst in the samples that have been most affected by weathering, the highest quartz concentration is found in the 63-200μm fraction. This pattern occurs because silt size quartz is prevalent in the parent rock, but the rapid weathering of chlorite and illite in the 63-200μm fraction leads to the dominance of quartz in this fraction once weathering has taken hold.

The effect of weathering on the relationship between mineralogy and grain size is clearly demonstrated in Section 6.5 by the use of coefficients of variation of mineral abundance. These indicate that physical weathering, such as occurs in the formation of boulder clays, evens out the mineral distribution pattern between different size fractions, whilst the chemical weathering occurring in the soil emphasises the differences in mineralogy with grain size between the different size fractions of the same soil horizon. This line of evidence shows that the comparison material from Hiraethog has suffered little chemical weathering relative to the Plynlimon soil horizons.

The most noticeable mineralogical consequence of weathering is the rapid decrease of chlorite as weathering progresses. This is seen both in the mineralogical analyses of rock hand specimens, presented in Section 6.5.1, where chlorite is observed to decrease towards the surface, and in the soils, where the chlorite content decreases up the profile from the BC horizon to the Ea1 and Ea2 horizons (Section 6.5). In contrast, Section 7.3 shows that, relative to quartz, the mica content increases up the profile as far as the Bs horizon, but in the more intensely weathered Ea2 and Ea1 horizons the effects of illite being altered to interstratified vermiculite-illite, and then vermiculite, are most evident. The detailed pattern of chlorite alteration as the rock material transforms into a soil is also described in Section 7.3. The chlorite is seen to alter to hydroxy interlayered vermiculite, and

then trioctahedral vermiculite towards the top of the profile. However, in the Eal horizon, the vermiculite produced by alteration of both chlorite and mica is itself broken down, to form a noncrystalline phase (Section 7.1.3).

Although the quantitative mineralogical evidence provided in Sections 6.5 and 7.2.1 and Figure 7.7 is only able to prove that a very small percentage of the original chlorite and illite has passed through a stage as vermiculite during the weathering process, it is likely that much higher proportions of these minerals actually follow this route. The vermiculite formed from chlorite is particularly likely to be less stable than its parent mineral, thus weathering more rapidly and leaving evidence of only a small percentage present in the soil profile, even though all of the original chlorite and mica may pass through a stage as vermiculite.

Looking in more detail at the formation of vermiculite, the XRD method of estimating vermiculite content, described in Section 7.1.3, suggests that, in the soil horizons, the vermiculite content of the two coarser clay fractions is in every case higher than that of the 0.063-0.2μm fraction, whereas in the rock and boulder clay samples the levels of vermiculite are approximately equal in all three clay fractions. This cannot be accounted for by the K saturation of 0.063-0.2μm fractions during separation, as the finest fractions of the rock and boulder clay samples were treated similarly to those of the soil samples, and thus this vermiculite distribution must be due to chemical weathering causing a very rapid breakdown of 0.063-0.2μm vermiculite, even though vermiculite is forming from chlorite and illite at the same time. This supports this hypothesis that a large proportion of the phyllosilicates weather via vermiculite.

As well as the vermiculite content increasing up the profile as far as the Ea2 horizon, and then falling off in the Eal horizon, a very similar pattern is seen for the soil CEC. Considering the 0.63-2μm fraction of each of the horizons, Table 7.5 shows that the CEC increases from the BC horizon to a maximum in the Ea2 horizon, falling in the Eal horizon. The vermiculite content can itself also be estimated using such CEC data, as is described in Sections 7.2 and 7.2.1, and it is found that there is a high correlation coefficient between the vermiculite contents estimated by the two methods. The weathering of chlorite and particularly illite to form vermiculite can

thus be seen to be responsible for the change in CEC of the soil horizons. However, the CEC of the 0.63-2μm fraction of the fresh rock is much lower than that of the BC horizon (Table 7.5), and thus a considerable increase in CEC, that is not due to vermiculite formation, has taken place between the rock and the BC horizon. Section 7.2.1 shows that this is due to the alteration prior to subaerial weathering of chlorite to hydroxy interlayered vermiculite.

10.1.5 Crystallinity

Perhaps the most significant contribution of this work to the study of weathering involves the variation of illite crystallinity throughout the soil profile, as discussed in Chapter 8. Section 8.7 shows that the fresh rock has the best crystallised illite, with both chemical weathering to soil and, to a lesser extent, physical weathering to boulder clay, reducing the crystallinity. Section 8.3 shows that, as particle size decreases, so does the crystallinity of the illite, whilst in the soil there is also a general pattern of increasing crystallinity with increasing intensity of weathering. This is considered to be due to the effect of dithionite treatment preferentially dissolving the least crystallised material, resulting in an apparent inversion of the crystallinity values between treated and untreated specimens. The anomalously poor crystallinity of the dithionite treated Bsg horizon illite in Figure 8.2 is considered to be due to the effects of translocation of illite from the Ea1 and Ea2 horizons (Section 6.2.4).

Comparing the illite crystallinity values with the chemically determined expandable mineral contents from Section 7.2.1 shows, by a highly significant correlation coefficient between the two sets of data, that the majority of variation in illite crystallinity is due, not to an inherent increase in the crystal imperfection of the illite structure itself, but to the formation of illite irregularly interstratified with expandable minerals. These interstratified structures broaden the illite diffraction peak, and thus give the appearance of reducing crystallinity. Changes in illite peak symmetry after different treatments can indicate the expandable minerals likely to be involved in these interstratifications.

In an attempt to extend the use of crystallinity studies in weathering, the crystallinity of the chlorite in some specimens was presented in Section 8.5. The high correlation coefficients found between the

chlorite and illite crystallinity data suggest that there is a potential for using minerals besides illite in crystallinity studies.

### 10.1.6 Other Investigations

Unfortunately, the work on surface area measurement, presented in Chapter 9, was able to produce few conclusive results, except to show that the fresh rock had the lowest specific surface area, whilst the surface area increased up the soil profile with increasing weathering. Although it was hoped to produce some quantitative data on the surface areas of the major minerals available for weathering in the different soil horizons and in the different size fractions, the errors in the surface area determinations presented in Section 9.3 are such that any quantitative data based on these results would not be justified. What is more, the work presented in this thesis has not involved the investigation of noncrystalline material, which could considerably affect the validity of any such data. However, Table 9.9 does indicate how relative rates of weathering could be calculated, if the data available were sufficient to justify such calculations.

Finally, the results in Sections 5.4 and 5.5 show that weathering has no significant effect on the chlorite polytype or the mica polymorph.

## 10.2 PLYNLIMON - REPRESENTATIVE OR ANOMALOUS?

As presented in Section 10.1, and throughout the experimental chapters of this thesis, the evidence of the work carried out is that, during the weathering of shale at Plynlimon, the chlorite is altered to vermiculite before this is in turn dissolved or altered to a noncrystalline phase. In detail, even in the fresh rock, and thus apparently stable under conditions of low grade metamorphism, some of the chlorite is actually hydroxy interlayered vermiculite with very well filled interlayers, and even in the BC horizon more chlorite is altered to hydroxy interlayered vermiculite. However, further up the soil profile, this loses its hydroxy interlayers to form a true vermiculite. Little effect of weathering on mica is seen until the Bsg horizon, where the mica also begins to alter to vermiculite, via interstratified illite-vermiculite. In the Eal horizon, the weathering action is so intense that the vermiculite is itself either totally dissolved, or broken down to leave only a noncrystalline phase.

Comparing this scenario with the findings of other workers, as presented in Sections 2.3.3 and 2.3.4, there is general agreement that

the chlorite would be expected to show signs of alteration before the mica. Similarly, when mica does begin to alter, it is commonly observed to transform to vermiculite through an interstratified structure, whilst where weathering is most intense it is usual for phyllosilicates, including vermiculite, to be completely dissolved, or broken down to leave only a noncrystalline phase.

Section 2.3.4 showed that there were two main views as to the possible weathering route of chlorite, either via vermiculite, or directly to a noncrystalline material or total dissolution. The best crystallised illite in the samples studied indicates that the Plynlimon shales have been subjected to lower greenschist grade metamorphism, and thus the fact that this study supports the chlorite weathering path via vermiculite is consistent with the finding in the literature that chlorite which has suffered metamorphism weathers via vermiculite, whilst that which has not been significantly elevated in temperature weathers directly to a noncrystalline phase. As these details of chlorite weathering have not been widely investigated, it is possible that, where the chlorite has suffered an intermediate range of temperatures, both weathering routes may be operating simultaneously. In any situation where this was the case, it would be impossible to determine the relative importance of the two routes without both a detailed knowledge of the relative weathering rates of the different minerals, and a thorough investigation of soil solution chemistry and the occurrence of noncrystalline material.

The findings of this study concerning chlorite weathering in soils developed on shales are different to those of some similar studies in Wales, whilst in agreement with the findings of other studies. It is likely that the results of all the studies are correct, with the findings depending on the precise grade of metamorphism to which the shales have been subjected. It would thus seem likely that the shale parent material of the Hiraethog soils studied by Rezk has not been subjected to as high metamorphic temperatures as the shales at Plynlimon.

Although this study alone cannot provide enough evidence for proof, it may be that all chlorite that weathers via vermiculite has been at least partially altered to hydroxy interlayered vermiculite, possibly by the low grade metamorphic conditions which it has experienced. Correspondingly, chlorite which weathers directly to a noncrystalline

material would be expected to have a true chlorite structure. If this conjecture were proved to be true, it would be relatively simple to determine the weathering route of a chlorite by a study of the behaviour of its XRD reflections after a series of heat treatments.

Because of the two possible chlorite weathering routes, some of the details of this study are bound to be different to those of similar studies in areas with different metamorphic histories, but there is no reason to believe that the results in this thesis are atypical of what would be found in any study of the weathering of a shale with similar composition and metamorphic history in any similar set of environmental conditions. For this reason, the findings in this study which have not been reported by other workers, such as the variation in mica crystallinity on weathering, would seem to be applicable far more widely than just to the area covered in this study.

## 10.3 BUILDING ON PLYNLIMON

As stated in Chapter 1, this thesis presents the results of a part of a very much larger study. Because of this, many of the findings of this study were employed as they were developed, so that information on mineral weathering routes could be input into the parts of the larger study dealing with laboratory weathering and the in situ measurement of both soil and stream water chemistry, which were being carried out by colleagues.

However, some areas investigated in this study would appear to be well worth developing beyond the study of weathering at Plynlimon. Of these, the use of mica, and possibly chlorite, crystallinity in monitoring weathering would seem to be of particular importance. Similarly, as suggested in Section 10.2, it would be well worth investigating the detailed mineralogy of chlorites known to weather by different routes, to determine whether or not it is only chlorites that are actually at least partially hydroxy interlayered vermiculite that weather via vermiculite. If this hypothesis were found to be true, it would then be necessary to determine how low grade metamorphic conditions, or their consequences, bring about this change in the chlorite structure.

The biggest disappointment in this study was the poor quality of the results obtained from the surface area investigations. If a similar study were to be carried out in future, it would thus be well worth

while to be certain that the surface area measurement technique employed was both accurate and reproducible. If accurate surface area determinations had been available for all of the size fractions, and had been combined with the quantitative mineralogical results presented in this study and the determinations of soil and stream water chemistry from the larger study, accurate estimates of the rates of weathering of the minerals in the different soil horizons could have been produced.

A method of separating mica from quartz would also have been invaluable, and thus further work on the separation of very poorly magnetic minerals would undoubtedly be worthwhile, as good separation is essential before individual minerals can be studied in detail.

Finally, an obvious and valuable extension of the work presented in this thesis would be to look in similar detail at weathering in the other soil series developed on the same parent material in the Wye catchment at Plynlimon.

# APPENDIX

## TABLES, PROFILE DESCRIPTIONS AND FIGURES

### Table A.1 Hand Specimen Descriptions of Rock Samples

| Sample Number | Rock Group | Description |
|---|---|---|
| 1004 | Frongoch Mudstone Series | Mid grey silty shale, broken into irregular fragments of about 10mm thickness. It contains a few dark grains finer than 0.5mm, which are probably Fe oxides, possibly pseudomorphing pyrite. The rock weathers to a distinctive chocolate brown colour. |
| 1007 | Frongoch Mudstone Series | A mainly dark grey fine shale, but showing paler laminations with spacings greater than 10mm, some of which are highly contorted. The rock shows irregular fissility at intervals greater than 10mm, approximately at right angles to the lamination. The weathered surfaces do not develop a distinctive appearance. |
| 1009 | Frongoch Mudstone Series | Dark bluish grey fine grained shale, with indistinct 1mm thick darker laminae about 10mm apart. Fissility develops irregularly with a spacing greater than 15mm, whilst the rock develops an intense weathering crust of a pale greenish grey colour. |
| 1013 | Frongoch Mudstone Series | Pale grey shale with no evidence of lamination. It occurs shattered into fragments with maximum dimensions of 30x15x 5mm. The weathered surfaces are irregularly coloured. |
| 1010 | Gwestyn Shale Group | A very well cemented coarse sandstone, reminiscent of Millstone Grit, with a grain size of about 1mm. Mid grey in colour, with creamy specks of feldspar. The rock has two weathering zones, both about 1.5mm thick. The outer zone is pale, whilst the inner one is apparently a zone of Fe enrichment. |
| 1014 | Gwestyn Shale Group | Massive homogeneous dark bluish grey very silty shale, showing irregular weathering surfaces. |
| 1017 | Gwestyn Shale Group | Mid to dark neutral grey shale, laminated on a 2mm scale, weathering to a pale greyish brown. It is broken on irregular subparallel surfaces, about 5mm apart, approximately at right angles to the laminations. |

Table A.1 Hand Specimen Descriptions of Rock Samples (continued)

| Sample Number | Rock Group | Description |
|---|---|---|
| 1018 | Gwestyn Shale Group | Massive, homogeneous neutral grey shale, weathering to a mid brown colour. The rock contains paler patches, up to 50mm in diameter, which may be due to secondary alteration. |
| 1019 | Gwestyn Shale Group | Shale showing laminations on a 1mm scale, with colours including pale to dark grey, blue grey and brown shades. The rock breaks into irregularly parallelipipedal blocks with very distinctive chestnut weathering surfaces. |
| 1020 | Gwestyn Shale Group | Silty dark grey shale containing reddish flecks, possibly of Fe oxides pseudomorphing pyrite. The rock breaks into irregular fragments about 10mm thick, and weathers to a reddish brown colour. |
| 1021 | Gwestyn Shale Group | Highly fragmented rotten greyish shale flakes showing very little strength or cohesion. |
| 1022 | Gwestyn Shale Group | Massive, irregularly laminated shale varying in colour from dark grey to greyish white, with the paler bands apparently being more coarse. The rock weathers to the yellowish brown colour typical of limonite. |
| 1036 | Gwestyn Shale Group | Shale showing iridescent colours due to thin film interference on its weathering surfaces. |
| 1040 | Gwestyn Shale Group | Homogeneous dark blue shale. |
| 1047 | Gwestyn Shale Group | Grey shale, fissile on a 10mm scale. The rock has a 1mm thick weathering skin with a very distinctive white to pale buff outer layer. |
| 1052 | Gwestyn Shale Group | Dark grey micaceous shale with a rusty coloured weathering skin. Generally massive, with irregular cleavage planes on a 50mm scale. |

Table A.2 Profile Description of Hiraethog Series Soil

Profile Number: UCNW 1075-1081

Soil Series: Hiraethog without Fe pan (Stagnopodsol)

Location: Afon Cyff

Grid Reference: SN81768404

Slope: 15°

Land Use: Unimproved rough grazing

Parent Material: Very angular Silurian shale fragments up to 50mm in maximum dimension

Vegetation: Grass, Vaccinium, Moss, Erica

Drainage: Imperfect above, good below

| Horizon | Depth (cm) | Description |
|---|---|---|
| Of | 6 - 0 | Dark brown stratified stoneless litter with big woody roots. Abrupt boundary into: |
| Oh<br>92% $H_2O$ | 0 - 7<br>94% LOI | Black (5YR2.5/1) amorphous stoneless moist peat with a lot of fine roots. Nematodes present. Gradual transition into: |
| Ea1<br>47% $H_2O$ | 7 - 10<br>13% LOI | Compact chocolate brown (10YR3/2) structure with very few stones. Fine woody roots are common, and there are a few dark organic root traces. The clay texture smears easily. This horizon is transitional to: |
| Ea2<br>42% $H_2O$ | 10 - 13<br>11% LOI | This has a similar structure, but is light brown (2.5Y5/2) in colour and shows a diffuse boundary into: |
| Bsg<br>41% $H_2O$ | 13 - 16<br>9% LOI | Contains many angular stone fragments, varying in condition from completely unaltered to totally changed to Fe oxides, up to 20mm in maximum dimension. Grey (7.5YR6/2), with discontinuous orange red (7.5YR6/8) speckles, except where the orange red becomes dominant around stone surfaces. Roots present, but no Fe pan. Contains less clay than the Ea2 horizon, and has a blocky structure which is more open, but is gleyed except for the oxidised patches around the roots and black organic structures, which may be up to several mm thick. Diffuse boundary into: |

Table A.2 Profile Description of Hiraethog Series Soil (continued)

| Horizon | Depth (cm) | Description |
|---|---|---|
| Bs<br>42% $H_2O$ | 16 - 29<br>7% LOI | Clay rich but open texture, which does not smear easily. Yellow brown (10YR5/6). Contains small rounded rock fragments which are relatively unweathered, with a few coarse roots. The stones become larger towards the base of the horizon. Clear but uneven boundary into: |
| BC<br>14% $H_2O$ | 29 - 49<br>4% LOI | Very stony horizon in clay rich matrix, containing a few large coarse roots. The stones are up to 50mm in maximum dimension, the larger ones appearing to have a preferred horizontal orientation. Some smaller stones are rounded. The stones are not weathered or Fe stained on their surfaces, but the overall horizon colour is orange brown (10YR5/8). |
| C<br>8% $H_2O$ | 49+<br>4% LOI | Parent material. |

Table A.3 Profile Description of Manod Series Soil

Profile Number: UCNW 1064-1065

Soil Series: Manod (Brown Podsolic)

Location: River Wye

Slope: 10°

Land Use: Unimproved rough grazing

Parent Material: Broken dark blue grey Ordovician mudstone

Vegetation: Grass, moss, fern

Drainage: Free

| Horizon | Depth (cm) | Description |
|---|---|---|
| L | 6 - 2 | Shoots. |
| O | 2 - 0 | Root mat, consisting of a mixture of both decomposed and relatively undecomposed material. Tightly compacted but springy and porous. Dark brown (7.5YR4/2). Clear boundary along which this horizon can easily be pulled off from: |
| Ah | 0 - 2 | Roots, shoots and general debris. This is a wet organomineral horizon, with the mineral matter being dominantly clay size. Dark brown (7.5YR4/2). Indistinct boundary into: |
| B<br>41% $H_2O$ | 2 - 22<br>13% LOI | Highly compacted horizon, yet with granular structure. Roots extend to the bottom of the horizon. Moist, not very porous, with a clay loam texture. Contains many angular shale fragments up to 20mm, grey brown to dark brown (10YR4/3) in colour, with no preferred orientation, and no sign of weathering. Some rounded grey shale fragments appear to be breaking up. Contains occasional knotted nematodes up to 30cm long. Brown to dark brown (10YR4/3). Indistinct boundary into: |
| B/C<br>28% $H_2O$ | 22 - 42<br>6% LOI | Highly compacted horizon with a closed structure and no trace of a blocky structure. It is a loam, and contains 30% of very small, relatively unweathered fragments of mudstone and shale. There are a few large roots. The stones are angular and unoriented. Yellowish brown (10YR5/8). Transitional into: |
| C | 42+ | Parent material. |

Table A.4 Profile Description of Ynys Series Soil

Profile Number: UCNW 1066-1071

Soil Series: Ynys (Peaty Gley)

Location: Afon Cyff

Slope: 7°

Land Use: Unimproved rough grazing

Parent Material: Boulder clay with apparently horizontally oriented mudstone clasts, both angular and rounded, up to 15cm in largest dimensions

Vegetation: Grass, moss, rushes

Drainage: Impeded

| Horizon | Depth (cm) | Description |
|---|---|---|
| L<br>76% $H_2O$ | 9 - 4<br>33% LOI | Dark reddish brown (5YR3/2) root mat. Lots of litter. Diffuse boundary into: |
| O<br>70% $H_2O$ | 4 - 0<br>25% LOI | Porous, spongy horizon, full of roots. The texture is that of a sandy silt. Nematodes present. Very dark grey (5YR3/1). Distinct boundary to: |
| Eb1<br>57% $H_2O$ | 0 - 8<br>15% LOI | Copious roots with many oxidised root channels. Contains small, fragile black concretions. There is a more open, crumbly structure than in lower horizons. The texture is that of a sandy clay, with no stones. The apparent colour is brown (7.5YR5/2), but this is probably only due to mixing, the true colour being grey with orange oxidation speckles along the root channels. |
| Eb2<br>54% $H_2O$ | 8 - 16<br>13% LOI | The texture is that of a sandy clay, with a few small, angular, unweathered stones. It is compact, with no fauna, but contains roots with oxidised areas around them, and small, fragile black organic concretions. Dark greyish brown (10YR4/2). |
| Bhg<br>75% $H_2O$ | 16 - 26<br>32% LOI | Contains many roots and vegetation debris. It is compact, plastic, structureless and water saturated. There is no fauna. The texture is that of a few sand grains in a dominantly organic matrix. Dark brown (10YR3/2). Distinct boundary into: |

Table A.4 Profile Description of Ynys Series Soil (continued)

| Horizon | Depth (cm) | Description |
|---|---|---|
| BC<br>38% $H_2O$ | 26 - 56<br>6% LOI | Light yellowish grey clay with many small pieces of angular, apparently unweathered, mudstone. Many coarse roots with oxidation around them. Trace of $H_2S$. Highly compact, with unoriented stones. Fills with water. Sudden transition into: |
| C | 56+ | Parent material. |

Table A.5 Profile Description of Caron Series Soil

Profile Number: UCNW 1072-1074

Soil Series: Caron (Blanket Peat)

Location: Afon Cyff

Slope: 0°

Land Use: Unimproved rough grazing

Parent Material: Large fragments of blue grey Silurian mudstone with clean brown surfaces

Vegetation: Sphagnum, Juncus, Erica, grass

Drainage: Very poor

| Horizon | Depth (cm) | Description |
|---|---|---|
| L | 60 - 50 | Sphagnum moss. Wet, but much more open structure and better drainage than lower horizons. Pale reddish brown. Distinct boundary into: |
| Of<br>74% $H_2O$ | 50 - 40<br>70% LOI | Root mat, black (5YR2.5/1) at bottom, lighter at top. Distinct boundary into: |
| Om<br>85% $H_2O$ | 40 - 0<br>84% LOI | Very dark black compact moist peat with root and shoot debris. |
| Bs<br>44% $H_2O$ | 0 - 15<br>17% LOI | Clay texture. Structure dominated by roots which make it friable. Much root and shoot debris. This horizon does not appear to have water flow through it. Dark reddish brown (5YR2.5/2) with small pale brown (10YR6/3) to grey (N5) angular mudstone fragments which are very soft and fragile, and quartz pebbles. |
| C | 15+ | Parent material. |

Table A.6 Profile Description of Hiraethog Series Soil with Iron Pan

Profile Number: UCNW 1082-1086

Soil Series: Hiraethog with Fe pan (Stagnopodsol)

Location: River Wye

Slope: 2°

Land Use: Afforested

Parent Material: Fresh blue grey Silurian shale fragments

Vegetation: Pine

Drainage: Imperfect

| Horizon | Depth (cm) | Description |
|---|---|---|
| F<br>75% $H_2O$ | 11 - 6<br>70% LOI | Dark reddish brown (5YR2.5/2) pine needle litter in all stages of decomposition in an organic matrix. Springy texture. Open well drained structure with no stones. Little biota. Very clear boundary with easy parting to: |
| Oh<br>63% $H_2O$ | 6 - 0<br>53% LOI | Black (5Y2.5/1) organic layer containing all manner of tree roots and some shoot debris. Moist, with a springy but cohesive texture. Lots of worms, nematodes and insect larvae, but no stones. Distinct boundary to: |
| Ea<br>42% $H_2O$ | 0 - 5<br>14% LOI | Very friable horizon, with good compacted granular crumb structure. Well drained, with very small shale fragments and quartz pebbles. It has a silty loam texture, and an open, well drained, fairly dry structure. Contains roots. Dark brown to brown (7.5YR4/2), becoming paler downwards. Worms present. Distinct but undulating boundary to: |
| Bf<br>36% $H_2O$ | 5 - 7<br>12% LOI | Iron pan broken up by worm activity. Brown to dark brown (7.5YR4/4) with reddish yellow (5YR6/8) and black (5YR2.5/1) mottles. Broken shale fragments up to 2mm in maximum dimension. |

Table A.6 Profile Description of Hiraethog Series Soil with Iron Pan (continued)

| Horizon | Depth (cm) | Description |
|---|---|---|
| Bh<br>25% $H_2O$ | 7 - 20<br>8% LOI | Horizon with 30% stones at top increasing to 100% at base. No worms. The only roots are large. The stones are grey (N5) and fresh at the base, becoming redder and softer at the top. Red and black mottles, in a dominantly brown to dark brown (7.5YR4/4) matrix, seem to occur as a skin around the stones. Reddening is more distinct at the top of the horizon. The matrix is clay dominated, whilst the black staining at the top of the horizon may be due to manganese or organic matter. The stones are variable in shape, but become larger towards the base. |
| C | 20+ | Parent material. |

Table A.7 Profile Description of Cyff Series Soil

Soil Series: Cyff (Ranker)

Location: River Wye

Slope: Occurs in areas of steep slopes (more than 13°) as a dark brown profile of silty clay with an A/C horizon clearly showing the effects of current slope instability. There is a high percentage of shale fragments throughout the profile, and slight gleying of the surface occurs if the organic horizon is deep.

Land Use: Unimproved rough grazing

Drainage: Free

| Horizon | Depth (cm) | Description |
|---|---|---|
| O | 5 - 0 | Dark red organic matter with sharp junction to: |
| Ah | 0 - 18 | Brown loamy clay with small shale fragments and a weak crumb structure, merging to: |
| A/C | 18 - 48 | Yellow brown clay with larger shale fragments. |
| C | 48+ | Clayey shale. |

Table A.8 Microprobe Analyses of Individual Chlorite and Mica Grains in Rock Samples

| Chlorite Sample | Octahedral Sites | | | | | Tetrahedral Sites | | Total Octahedral Occupancy | Octahedral | | Tetrahedral Si/Al |
|---|---|---|---|---|---|---|---|---|---|---|---|
| | Mg | Al | Fe | Ti | K | Si | Al | | Fe/Mg | Al/Mg | |
| 1018A | 2.50 | 3.40 | 5.87 | 0.01 | 0.01 | 5.01 | 2.99 | 11.79 | 2.35 | 1.36 | 1.68 |
| 1018B | 2.60 | 3.50 | 5.62 | 0.01 | 0.01 | 5.04 | 2.96 | 11.73 | 2.16 | 1.35 | 1.70 |
| 1018C | 2.44 | 3.53 | 5.67 | 0.01 | 0.07 | 5.08 | 2.92 | 11.72 | 2.32 | 1.45 | 1.74 |
| 1018D | 2.48 | 3.55 | 5.64 | 0.00 | 0.02 | 5.07 | 2.93 | 11.70 | 2.28 | 1.43 | 1.73 |
| 1018E | 2.54 | 3.40 | 5.84 | 0.00 | 0.01 | 5.00 | 3.00 | 11.80 | 2.30 | 1.34 | 1.67 |
| 1022A | 2.78 | 3.57 | 5.05 | 0.00 | 0.24 | 5.38 | 2.62 | 11.64 | 1.82 | 1.28 | 2.05 |
| 1022B | 2.89 | 3.44 | 5.28 | 0.01 | 0.10 | 5.21 | 2.79 | 11.72 | 1.83 | 1.19 | 1.87 |
| 1022C | 2.83 | 3.45 | 5.36 | 0.01 | 0.13 | 5.11 | 2.89 | 11.78 | 1.90 | 1.22 | 1.77 |
| 1022D | 3.08 | 3.72 | 4.72 | 0.01 | 0.03 | 5.19 | 2.81 | 11.56 | 1.53 | 1.21 | 1.85 |
| 1022E | 3.03 | 3.52 | 5.09 | 0.00 | 0.01 | 5.17 | 2.83 | 11.66 | 1.68 | 1.16 | 1.82 |
| 1022F | 2.97 | 3.70 | 4.79 | 0.01 | 0.06 | 5.29 | 2.71 | 11.52 | 1.61 | 1.25 | 1.95 |
| 1030A | 1.65 | 3.30 | 6.84 | 0.01 | 0.00 | 5.06 | 2.94 | 11.81 | 4.14 | 2.00 | 1.72 |
| 1030B | 1.55 | 3.50 | 6.42 | 0.01 | 0.24 | 5.29 | 2.71 | 11.72 | 4.14 | 2.26 | 1.96 |
| 1030C | 1.59 | 3.58 | 6.13 | 0.01 | 0.29 | 5.49 | 2.51 | 11.60 | 3.84 | 2.25 | 2.18 |
| 1030D | 1.68 | 3.29 | 6.88 | 0.00 | 0.01 | 4.96 | 3.04 | 11.87 | 4.09 | 1.96 | 1.63 |
| 1034A | 2.94 | 3.51 | 5.23 | 0.01 | 0.04 | 5.06 | 2.94 | 11.73 | 1.78 | 1.19 | 1.73 |
| 1034B | 2.77 | 3.48 | 5.44 | 0.01 | 0.01 | 5.12 | 2.88 | 11.70 | 1.96 | 1.26 | 1.78 |
| 1034C | 2.69 | 3.47 | 5.57 | 0.00 | 0.02 | 5.05 | 2.95 | 11.75 | 2.07 | 1.29 | 1.71 |
| 1034D | 2.65 | 3.54 | 5.38 | 0.00 | 0.14 | 5.18 | 2.82 | 11.71 | 2.03 | 1.34 | 1.84 |
| 1034E | 2.65 | 3.51 | 5.52 | 0.00 | 0.01 | 5.10 | 2.90 | 11.70 | 2.09 | 1.32 | 1.76 |

Table A.8 (continued)

| Chlorite Sample | Octahedral Sites | | | | | Tetrahedral Sites | | Total Octahedral Occupancy | Octahedral | | Tetrahedral Si/Al |
|---|---|---|---|---|---|---|---|---|---|---|---|
| | Mg | Al | Fe | Ti | K | Si | Al | | Fe/Mg | Al/Mg | |
| 1036A | 3.25 | 3.60 | 4.52 | 0.01 | 0.23 | 5.41 | 2.59 | 11.60 | 1.39 | 1.11 | 2.09 |
| 1036B | 3.10 | 3.66 | 4.72 | 0.01 | 0.15 | 5.20 | 2.80 | 11.64 | 1.52 | 1.18 | 1.85 |
| 1036C | 3.31 | 3.41 | 5.10 | 0.01 | 0.09 | 4.86 | 3.14 | 11.91 | 1.54 | 1.03 | 1.55 |
| 1036D | 3.21 | 3.61 | 4.64 | 0.00 | 0.14 | 5.32 | 2.68 | 11.60 | 1.44 | 1.12 | 1.98 |
| 1040A | 2.59 | 3.58 | 5.42 | 0.01 | 0.05 | 5.16 | 2.84 | 11.65 | 2.09 | 1.38 | 1.82 |
| 1040B | 2.83 | 3.41 | 5.55 | 0.01 | 0.01 | 4.99 | 3.01 | 11.80 | 1.97 | 1.20 | 1.66 |
| 1040C | 2.63 | 3.69 | 5.10 | 0.01 | 0.08 | 5.36 | 2.64 | 11.51 | 1.94 | 1.40 | 2.03 |
| 1040D | 2.46 | 3.62 | 5.50 | 0.00 | 0.06 | 5.15 | 2.85 | 11.64 | 2.23 | 1.47 | 1.80 |
| 1040E | 2.38 | 3.64 | 5.37 | 0.01 | 0.08 | 5.46 | 2.54 | 11.48 | 2.26 | 1.53 | 2.15 |
| 1040F | 2.44 | 3.57 | 5.61 | 0.00 | 0.01 | 5.17 | 2.83 | 11.63 | 2.29 | 1.46 | 1.83 |
| 1040G | 2.71 | 3.52 | 5.51 | 0.00 | 0.01 | 4.98 | 3.02 | 11.75 | 2.03 | 1.30 | 1.65 |
| 1040H | 2.67 | 3.64 | 5.20 | 0.01 | 0.07 | 5.23 | 2.77 | 11.59 | 1.95 | 1.36 | 1.88 |
| 1047A | 2.50 | 3.52 | 5.62 | 0.01 | 0.06 | 5.11 | 2.89 | 11.71 | 2.25 | 1.41 | 1.76 |
| 1047B | 2.47 | 3.50 | 5.70 | 0.01 | 0.03 | 5.07 | 2.93 | 11.72 | 2.31 | 1.42 | 1.73 |
| 1047C | 2.33 | 3.63 | 5.55 | 0.01 | 0.15 | 5.14 | 2.86 | 11.68 | 2.38 | 1.56 | 1.80 |

| Mica Sample | K | Octahedral Sites | | | | " | " | " | " | " | " |
|---|---|---|---|---|---|---|---|---|---|---|---|
| | | Al | Mg | Fe | Ti | | | | | | |
| 1034A | 1.08 | 2.92 | 0.88 | 1.46 | 0.01 | 5.46 | 2.54 | 5.26 | 1.66 | 3.32 | 2.14 |
| 1034B | 1.14 | 3.36 | 0.54 | 0.98 | 0.02 | 5.68 | 2.32 | 4.89 | 1.83 | 6.22 | 2.45 |

| Sample | Specimen | Peak Position (°2θ) | | | | | Peak Intensity (Counts) | | | | | Length Factor for: | |
|---|---|---|---|---|---|---|---|---|---|---|---|---|---|
| | | (001) | (002) | (003) | (004) | (005) | (001) | (002) | (003) | (004) | (005) | (001) | (002) |
| 1018 | Random Powder Whole Sample | 6.290 | 12.555 | 18.885 | 25.250 | 31.705 | 11,620 | 47,155 | 11,662 | 27,844 | 4,132 | 2.75158 | 1.38060 |
| 1022 | Random Powder Whole Sample | 6.285 | 12.530 | 18.875 | 25.245 | 31.715 | 8,152 | 35,524 | 9,420 | 26,588 | 4,163 | 2.75377 | 1.38334 |
| 1029 | Random Powder Magnetic Extract from K Saturated Whole Sample | 6.270 | 12.545 | 18.875 | 25.245 | - | 22,003 | 102,950 | 29,952 | 60,134 | - | 2.76035 | 1.38169 |
| 1029 | Glass Slide Magnetic Extract from K Saturated Whole Sample | 6.205 | 12.485 | 18.820 | 25.200 | 31.675 | 80,870 | 228,442 | 40,819 | 109,402 | 15,302 | 1.46416 | - |
| 1030 | Random Powder Whole Sample | 6.300 | 12.530 | 18.895 | 25.270 | 31.730 | 14,208 | 45,696 | 14,481 | 36,876 | 6,854 | 2.74722 | 1.38334 |
| 1034 | Random Powder Whole Sample | 6.325 | 12.580 | 18.880 | 25.250 | 31.715 | 10,836 | 49,027 | 12,058 | 31,703 | 5,883 | 2.73637 | 1.37786 |
| 1036 | Random Powder Whole Sample | 6.300 | 12.535 | 18.885 | 25.235 | 31.705 | 3,677 | 21,529 | 4,719 | 11,537 | 1,908 | 2.74722 | 1.38279 |
| 1040 | Random Powder Whole Sample | 6.355 | 12.600 | 18.945 | 25.315 | 31.790 | 11,405 | 65,741 | 16,128 | 41,510 | 6,413 | 2.72346 | 1.37569 |
| 1040 | Glass Slide 3rd Order Magnetic Extract from Whole Sample (Table 4.2) | 6.200 | 12.495 | 18.825 | 25.215 | 31.680 | 8,578 | 24,504 | 5,578 | 11,640 | 2,506 | 1.46534 | - |
| 1040 | Random Powder 11th Order Magnetic Extract from <2μm Fraction (Table 4.6) | 6.330 | 12.605 | 18.935 | 25.295 | 31.750 | 16,762 | 86,496 | 20,179 | 49,171 | 6,086 | 2.73421 | 1.37514 |
| 1040 | Glass Slide 11th Order Magnetic Extract from <2μm Fraction (Table 4.6) | 6.285 | 12.545 | 18.905 | 25.250 | 31.720 | 4,862 | 13,757 | 2,525 | 6,326 | 874 | 1.44554 | - |
| 1047 | Random Powder Whole Sample | 6.275 | 12.535 | 18.865 | 25.230 | 31.690 | 8,659 | 39,888 | 9,900 | 28,055 | 4,727 | 2.75815 | 1.38279 |

Table A.9 Positions and Intensities of Chlorite (001) Peaks

| Sample | Specimen | Structure Factor (\|F\|) for | | | | |
|---|---|---|---|---|---|---|
| | | (001) | (002) | (003) | (004) | (005) |
| 1018 | Random Powder Whole Sample | 6.952 | 19.905 | 12.782 | 26.720 | 13.117 |
| 1022 | Random Powder Whole Sample | 5.821 | 17.259 | 11.481 | 26.105 | 13.171 |
| 1029 | Random Powder Magnetic Extract from K Saturated Whole Sample | 9.552 | 29.399 | 20.473 | 39.259 | - |
| 1029 | Glass Slide Magnetic Extract from K Saturated Whole Sample | 13.198 | 37.076 | 23.828 | 52.854 | 25.217 |
| 1030 | Random Powder Whole Sample | 7.694 | 19.575 | 14.251 | 30.776 | 16.908 |
| 1034 | Random Powder Whole Sample | 6.733 | 20.317 | 12.993 | 28.512 | 15.657 |
| 1036 | Random Powder Whole Sample | 3.914 | 13.439 | 8.131 | 17.189 | 8.913 |
| 1040 | Random Powder Whole Sample | 6.924 | 23.546 | 15.080 | 32.713 | 16.389 |
| 1040 | Glass Slide 3rd Order Magnetic Extract from Whole Sample (Table 4.2) | 4.297 | 12.153 | 8.811 | 17.251 | 10.207 |
| 1040 | Random Powder 11th Order Magnetic Extract from <2μm Fraction (Table 4.6) | 8.377 | 27.014 | 16.859 | 35.575 | 15.944 |
| 1040 | Glass Slide 11th Order Magnetic Extract from <2μm Fraction (Table 4.6) | 3.257 | 9.143 | 5.954 | 12.736 | 6.036 |
| 1047 | Random Powder Whole Sample | 5.994 | 18.292 | 11.764 | 26.799 | 14.023 |

Table A.10 Structure Factors for Chlorite (001) Peaks

| Sample | Specimen | Structure Factor Calculated Using Single Crystal Lorentz-Polarisation Correction for: | | | | Peak Height (cps) | | | | Structure Factor Calculated Using Peak Height for: | | | | Structure Factor Calculated Without Length Factor for: | |
|---|---|---|---|---|---|---|---|---|---|---|---|---|---|---|---|
| | | (001) | (002) | (003) | (004) | (001) | (002) | (003) | (004) | (001) | (002) | (003) | (004) | (001) | (002) |
| 1018 | Random Powder Whole Sample | 41.977 | 85.130 | 44.628 | 80.827 | 100 | 441 | 99 | 245 | 0.64496 | 1.9249 | 1.1777 | 2.5064 | 4.191 | 16.941 |
| 1022 | Random Powder Whole Sample | 35.159 | 73.886 | 40.098 | 78.975 | 74 | 351 | 86 | 217 | 0.55460 | 1.7156 | 1.0970 | 2.3584 | 3.508 | 14.674 |
| 1029 | Random Powder Magnetic Extract from K Saturated Whole Sample | 57.762 | 125.783 | 71.500 | 118.769 | 156 | 808 | 188 | 520 | 0.80427 | 2.6045 | 1.6220 | 3.6508 | 5.749 | 25.011 |
| 1029 | Glass Slide Magnetic Extract from K Saturated Whole Sample | 80.229 | 159.008 | 83.339 | 160.038 | 522 | 1,810 | 346 | 956 | 1.06034 | 3.3002 | 2.1938 | 4.9408 | 10.907 | 37.076 |
| 1030 | Random Powder Whole Sample | 46.417 | 83.799 | 49.744 | 93.059 | 146 | 475 | 134 | 361 | 0.77994 | 1.9957 | 1.3709 | 3.0450 | 4.642 | 16.643 |
| 1034 | Random Powder Whole Sample | 40.537 | 86.806 | 45.373 | 86.247 | 90 | 449 | 109 | 269 | 0.61358 | 1.9443 | 1.2354 | 2.6263 | 4.070 | 17.308 |
| 1036 | Random Powder Whole Sample | 23.614 | 57.520 | 28.389 | 52.011 | 39 | 181 | 48 | 103 | 0.40310 | 1.2322 | 0.82002 | 1.6241 | 2.361 | 11.428 |
| 1040 | Random Powder Whole Sample | 41.589 | 100.523 | 52.571 | 98.832 | 138 | 616 | 144 | 368 | 0.76160 | 2.2792 | 1.4250 | 3.0801 | 4.196 | 20.075 |
| 1040 | Glass Slide 3rd Order Magnetic Extract from Whole Sample (Table 4.2) | 26.129 | 52.099 | 30.812 | 52.219 | 412 | 1,454 | 320 | 824 | 0.94163 | 2.9603 | 2.1103 | 4.5899 | 3.550 | 12.153 |
| 1040 | Random Powder 11th Order Magnetic Extract from <2μm Fraction (Table 4.6) | 50.418 | 115.304 | 58.787 | 107.518 | 154 | 788 | 174 | 466 | 0.80294 | 2.5784 | 1.5655 | 3.4632 | 5.066 | 23.036 |
| 1040 | Glass Slide 11th Order Magnetic Extract from <2μm Fraction (Table 4.6) | 19.673 | 39.117 | 20.778 | 38.526 | 356 | 1,088 | 220 | 550 | 0.88133 | 2.5712 | 1.7575 | 3.7554 | 2.709 | 9.143 |
| 1047 | Random Powder Whole Sample | 36.236 | 78.293 | 41.095 | 81.097 | 78 | 402 | 91 | 228 | 0.56893 | 1.8363 | 1.1278 | 2.4159 | 3.609 | 15.555 |

Table A.11 Peak Heights and Alternative Structure Factors for Chlorite (001) Peaks

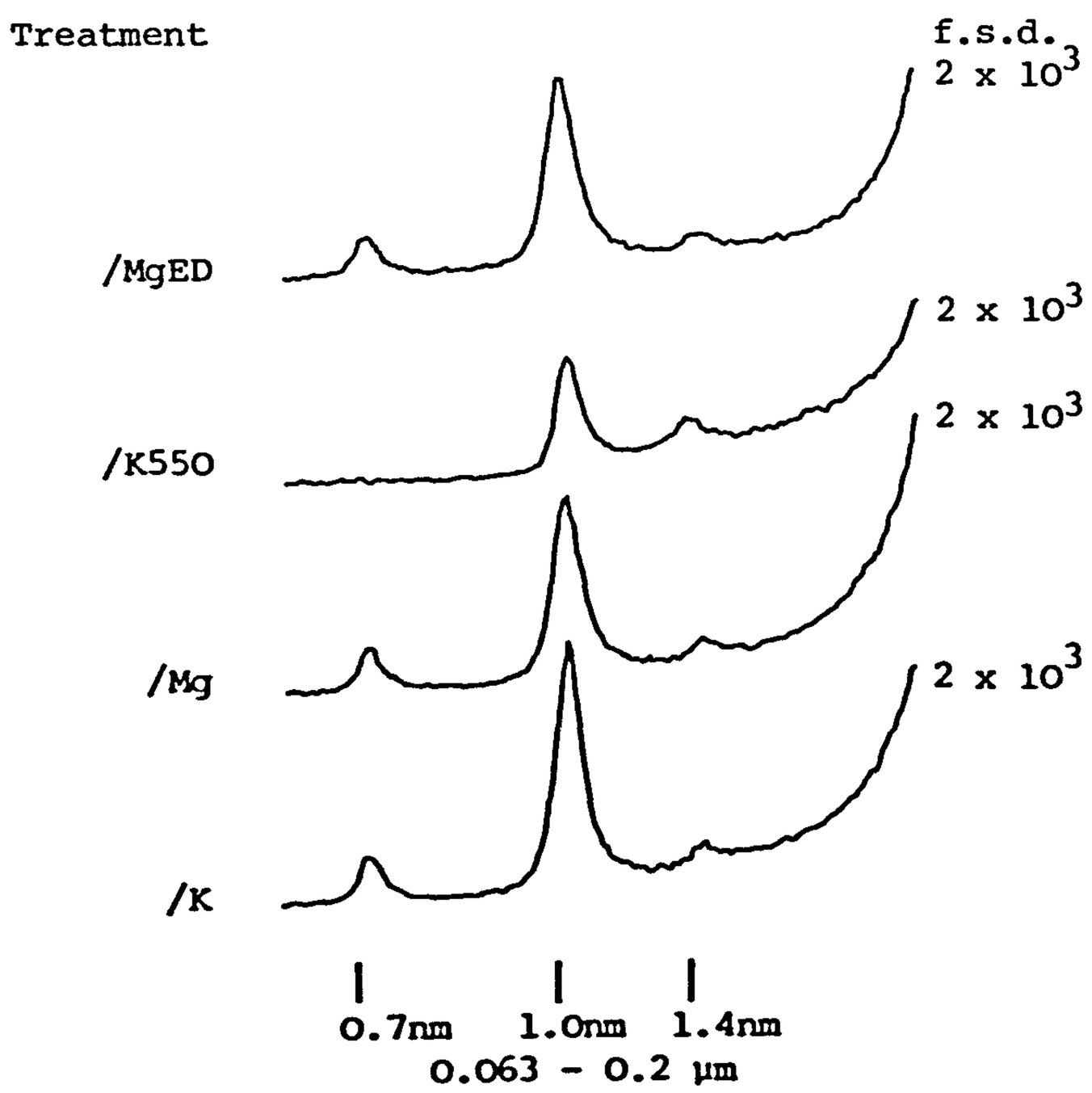


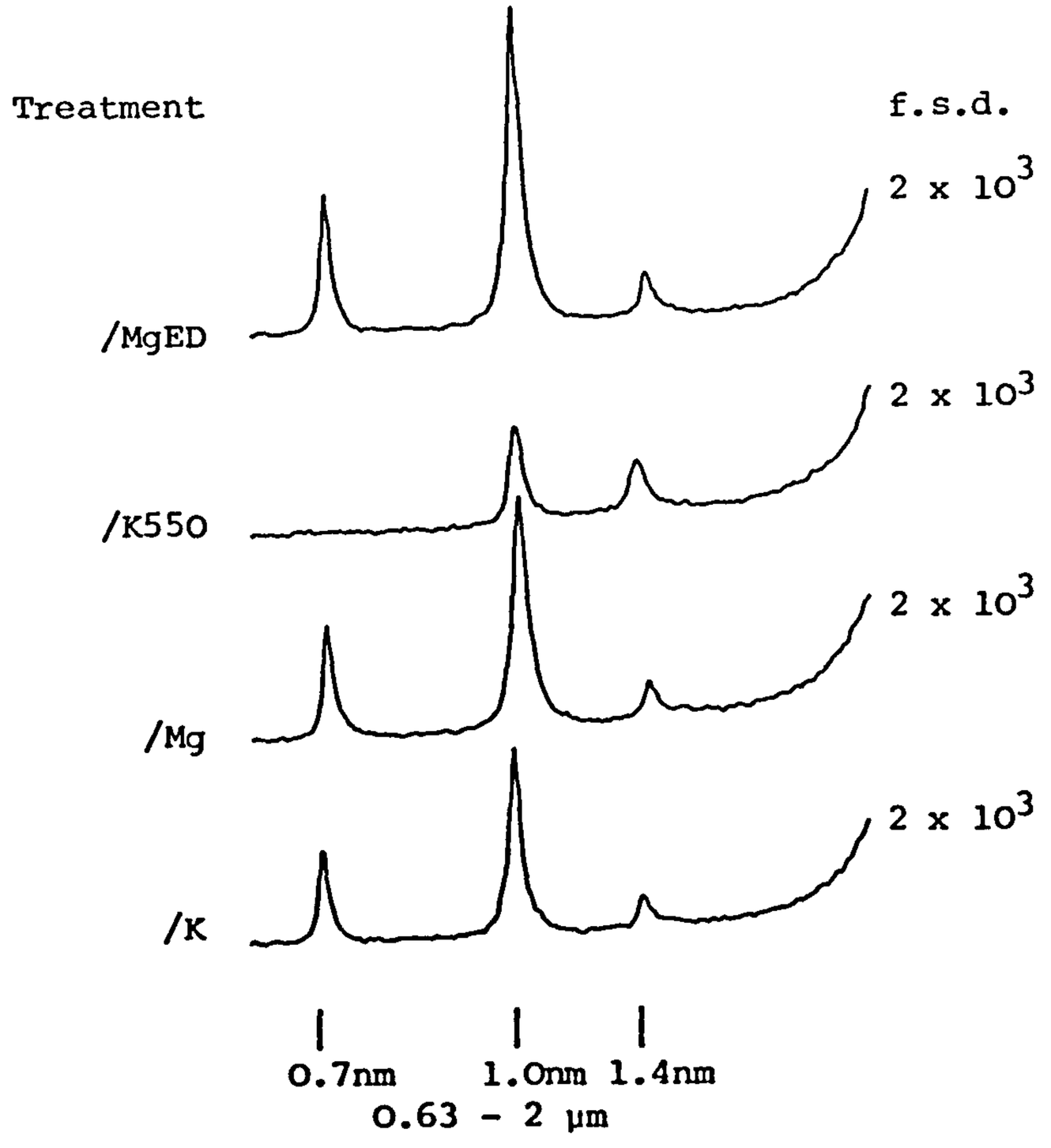


Figure A.1 X-ray Diffractometer Traces of 1040

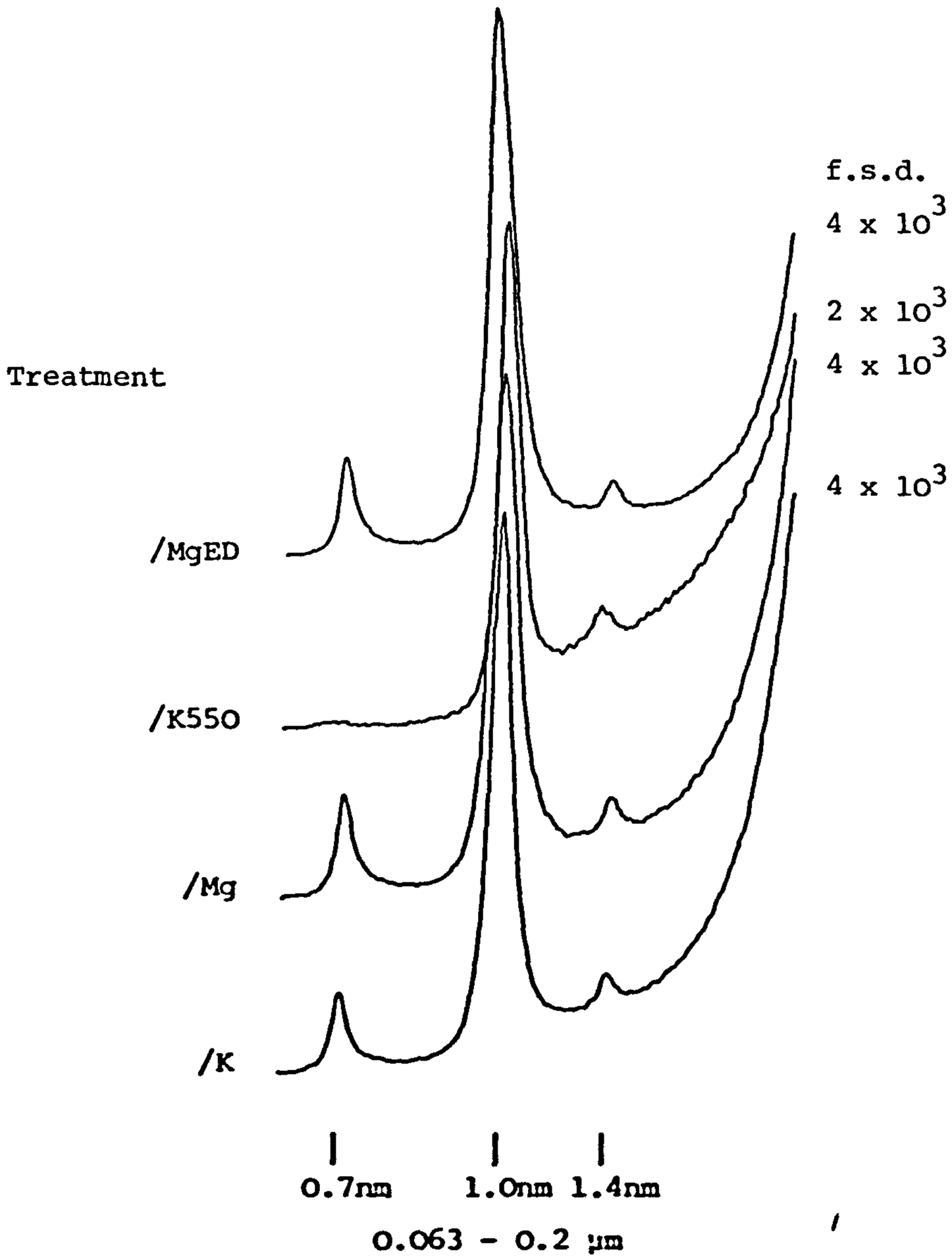


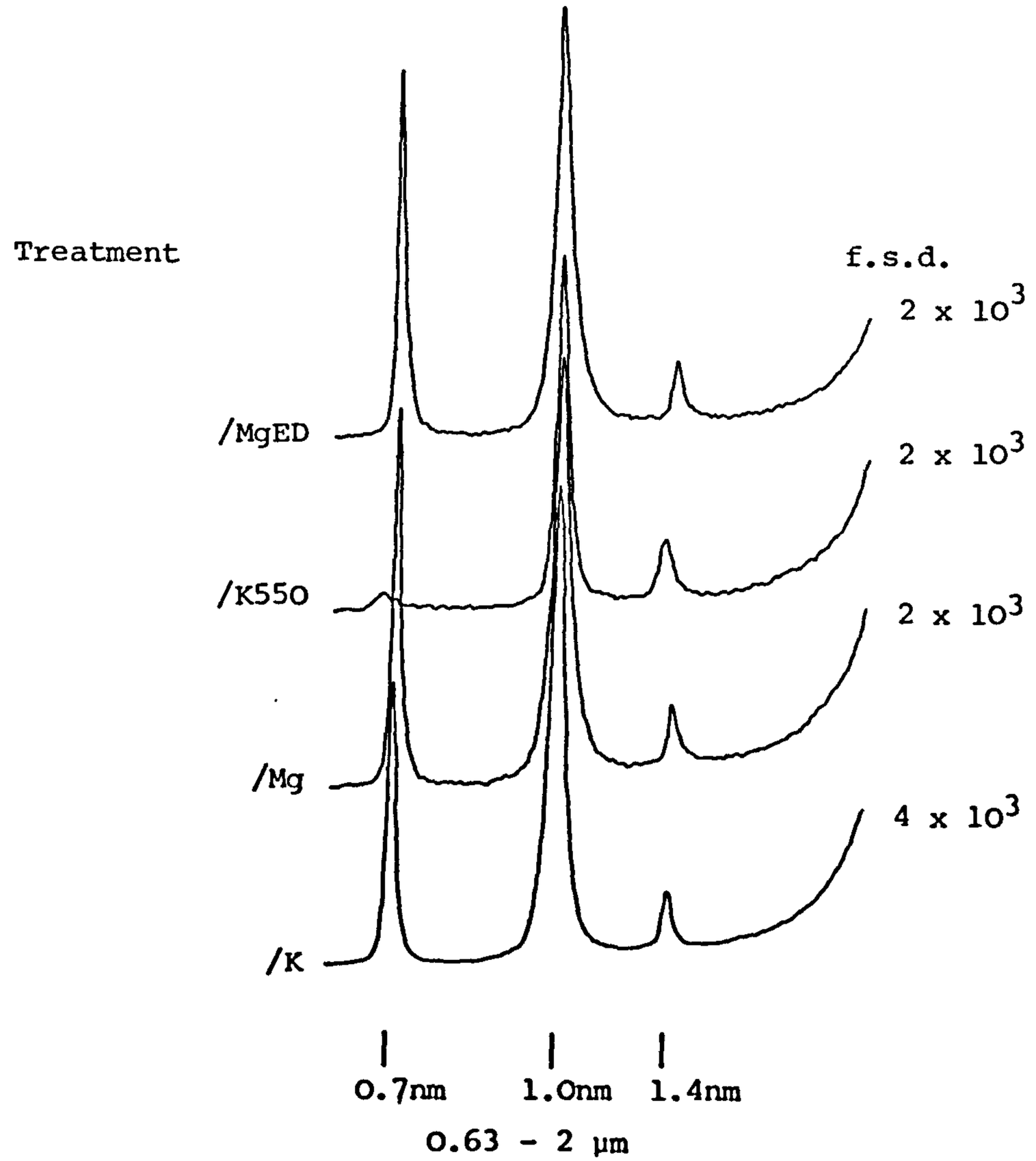


Figure A.2 X-ray Diffractometer Traces of 1029

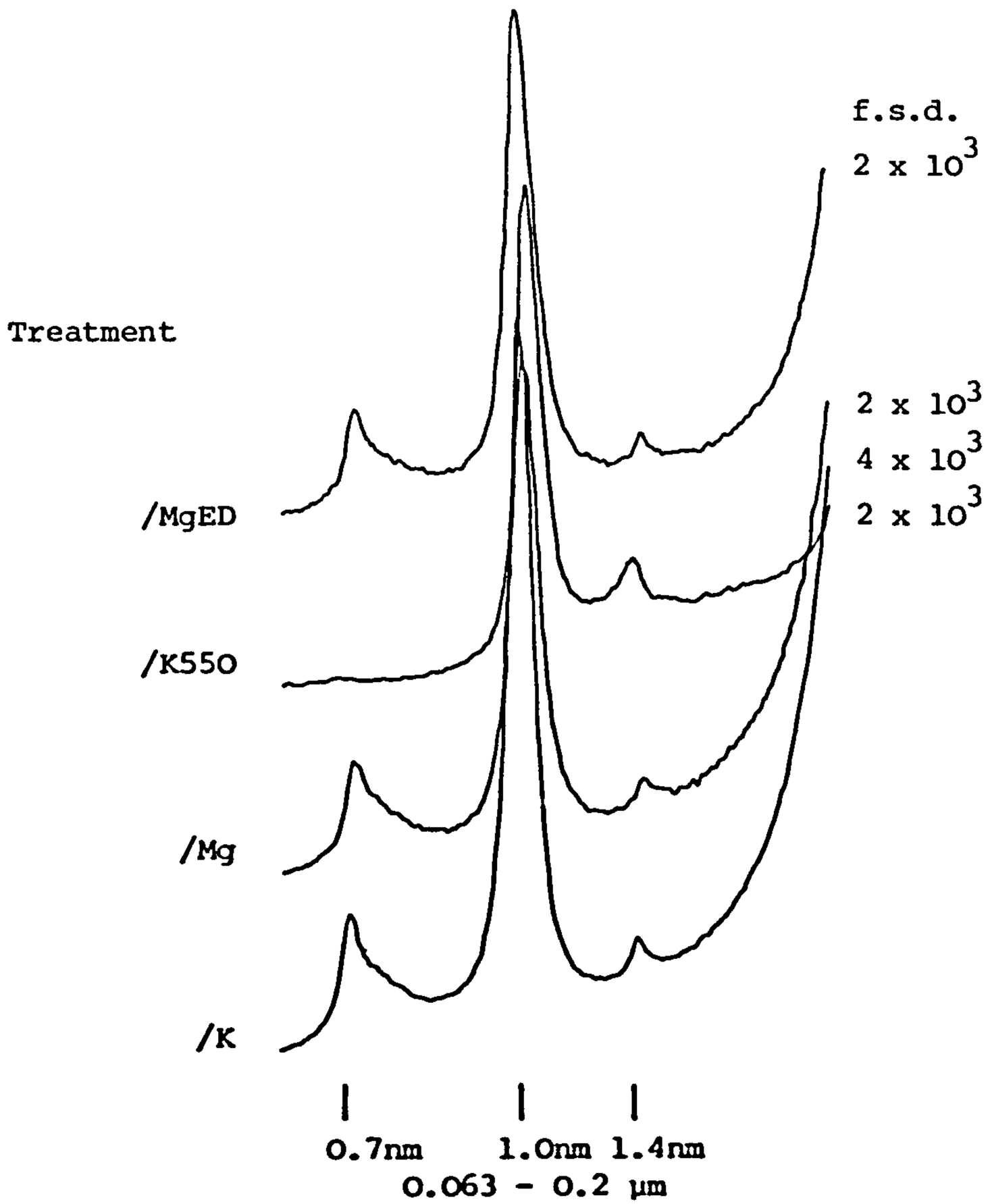


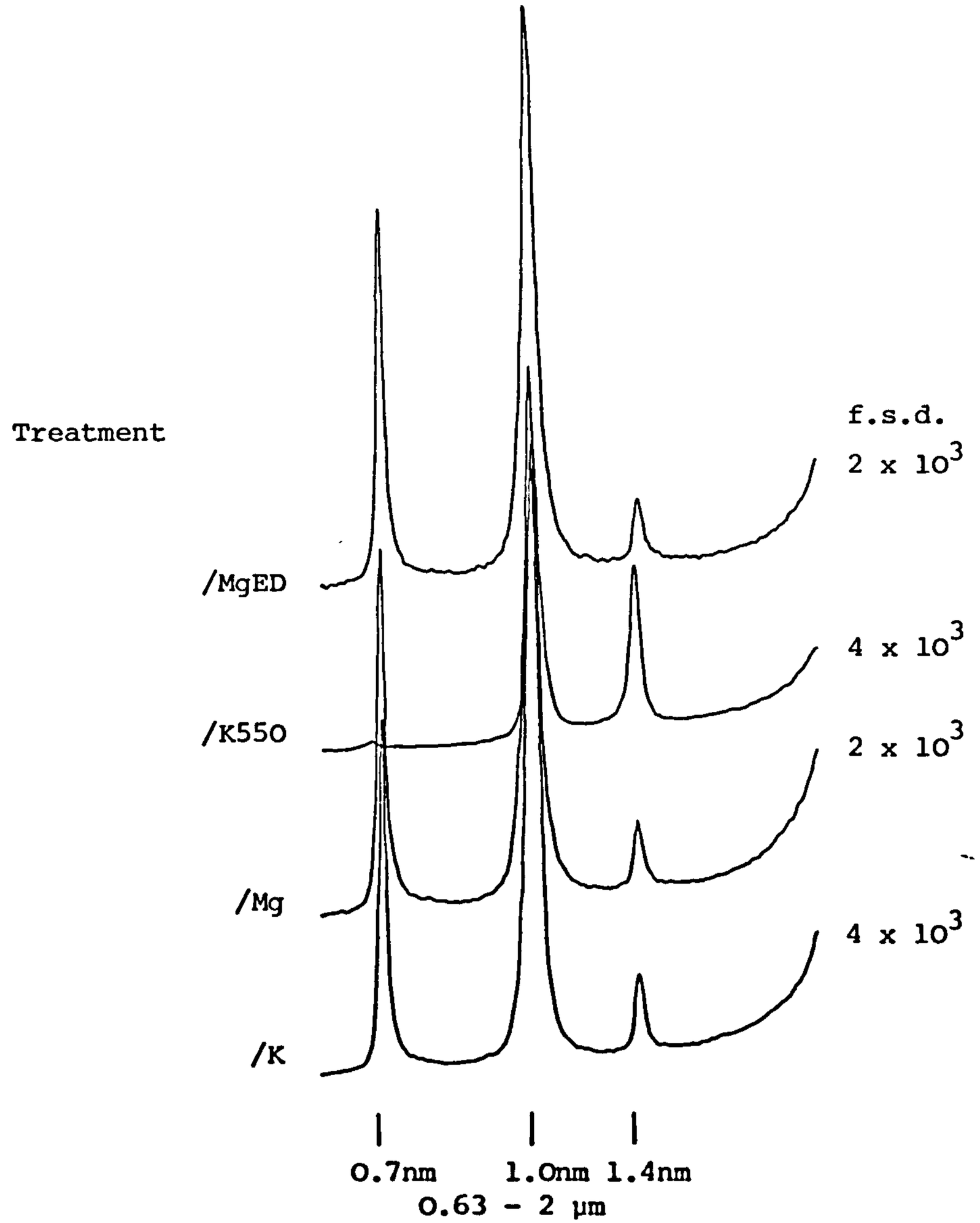


Figure A.3 X-ray Diffractometer Traces of 1039

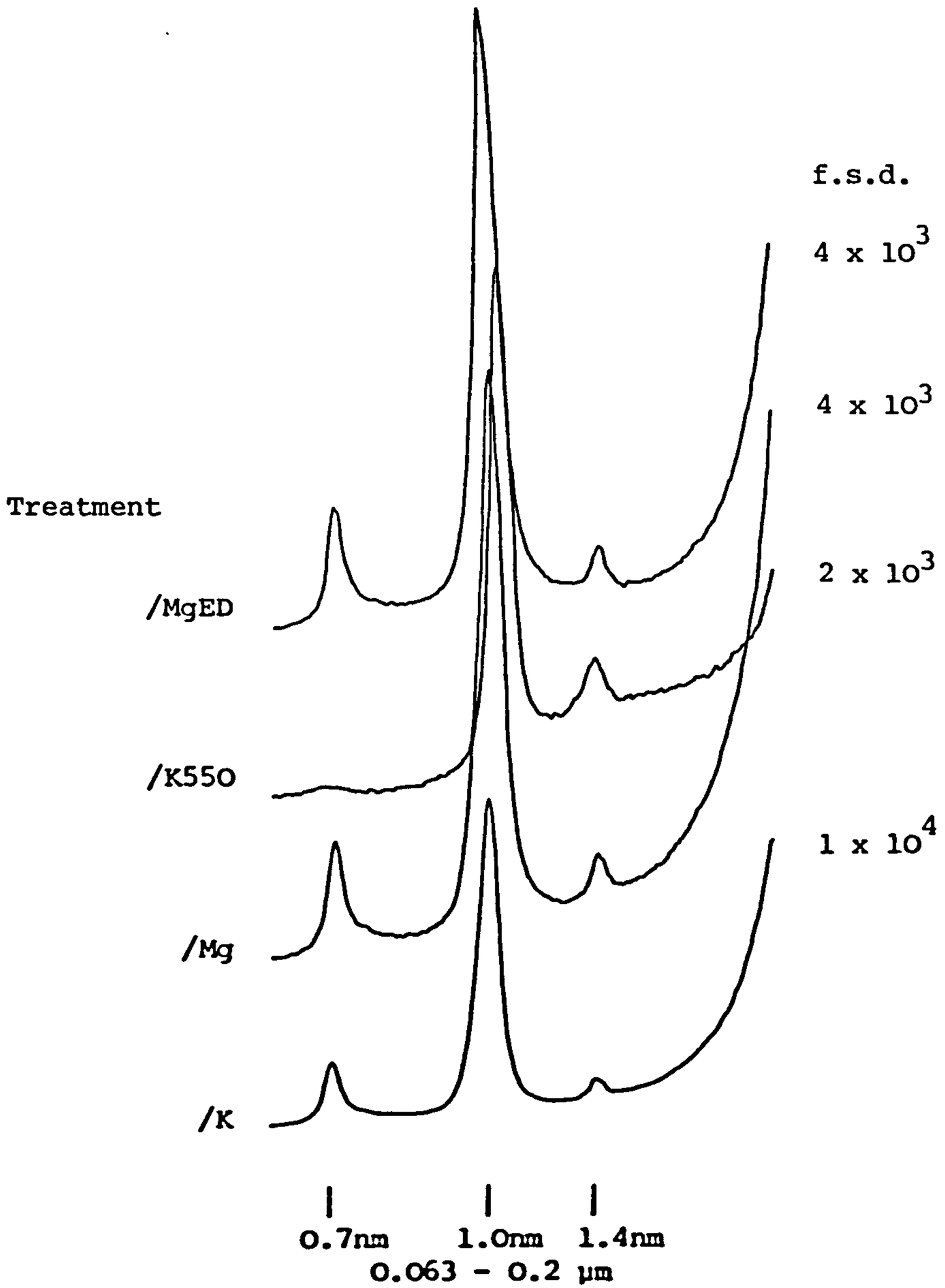


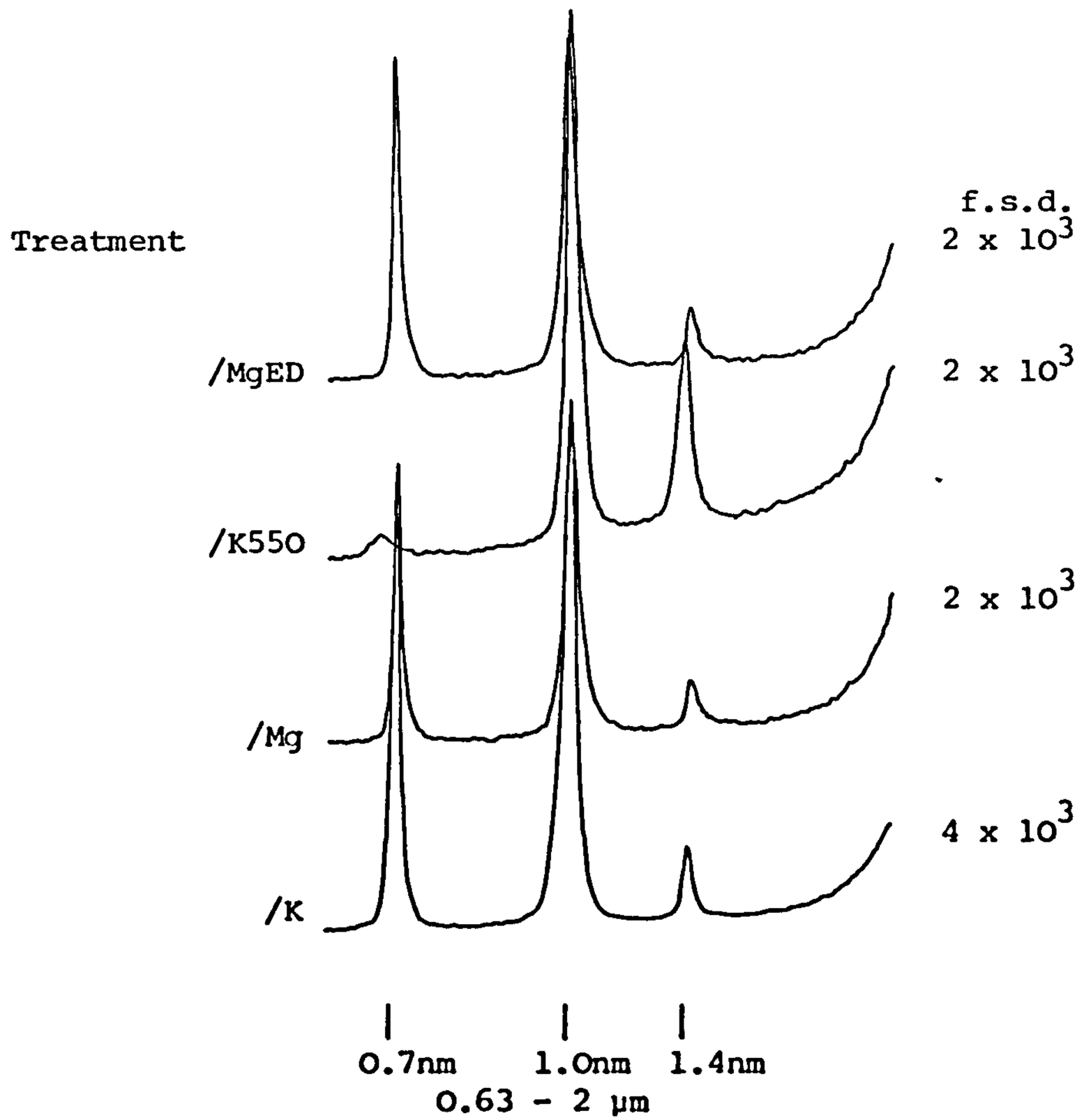


**Figure A.4** **X-ray Diffractometer Traces of 1049**

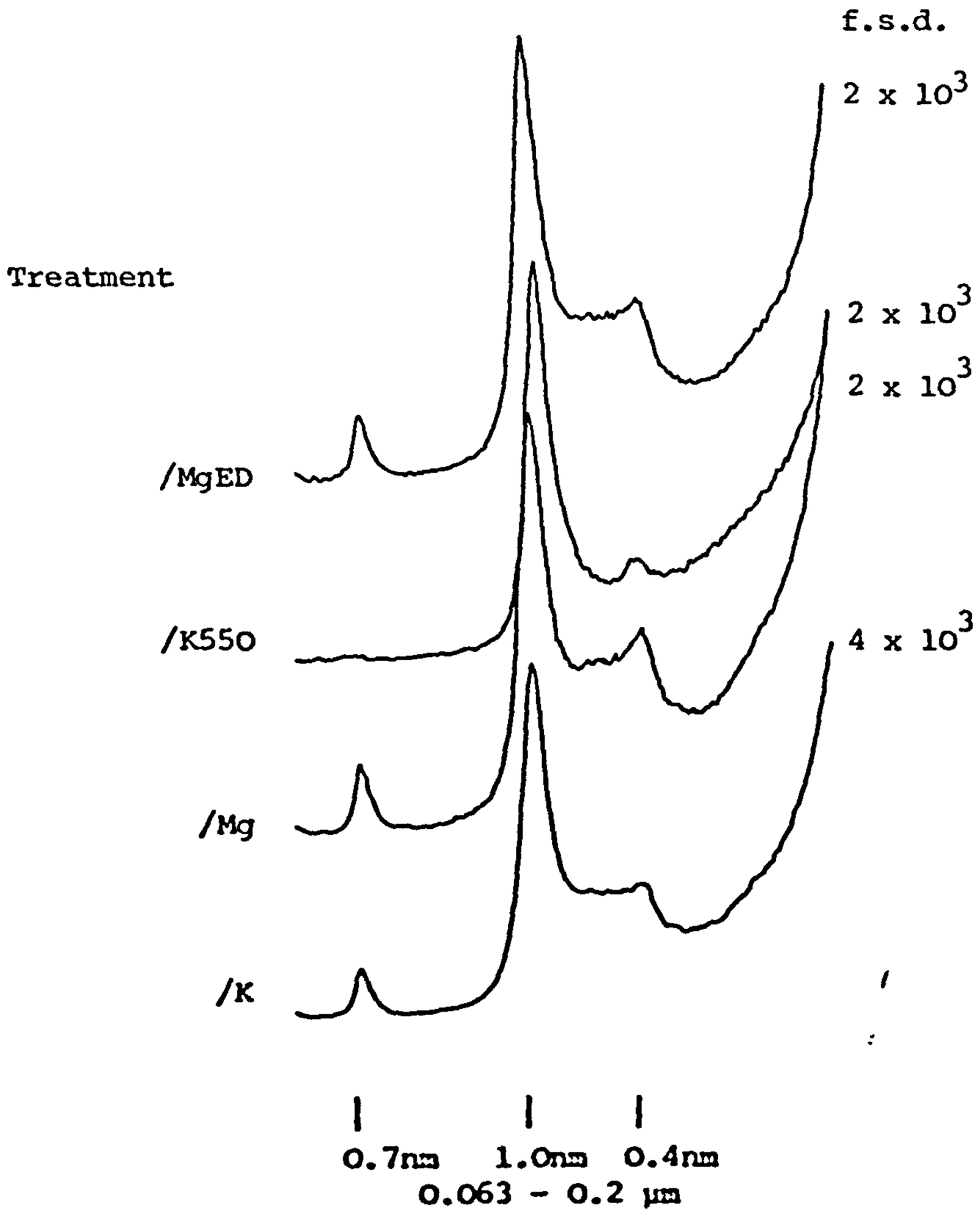


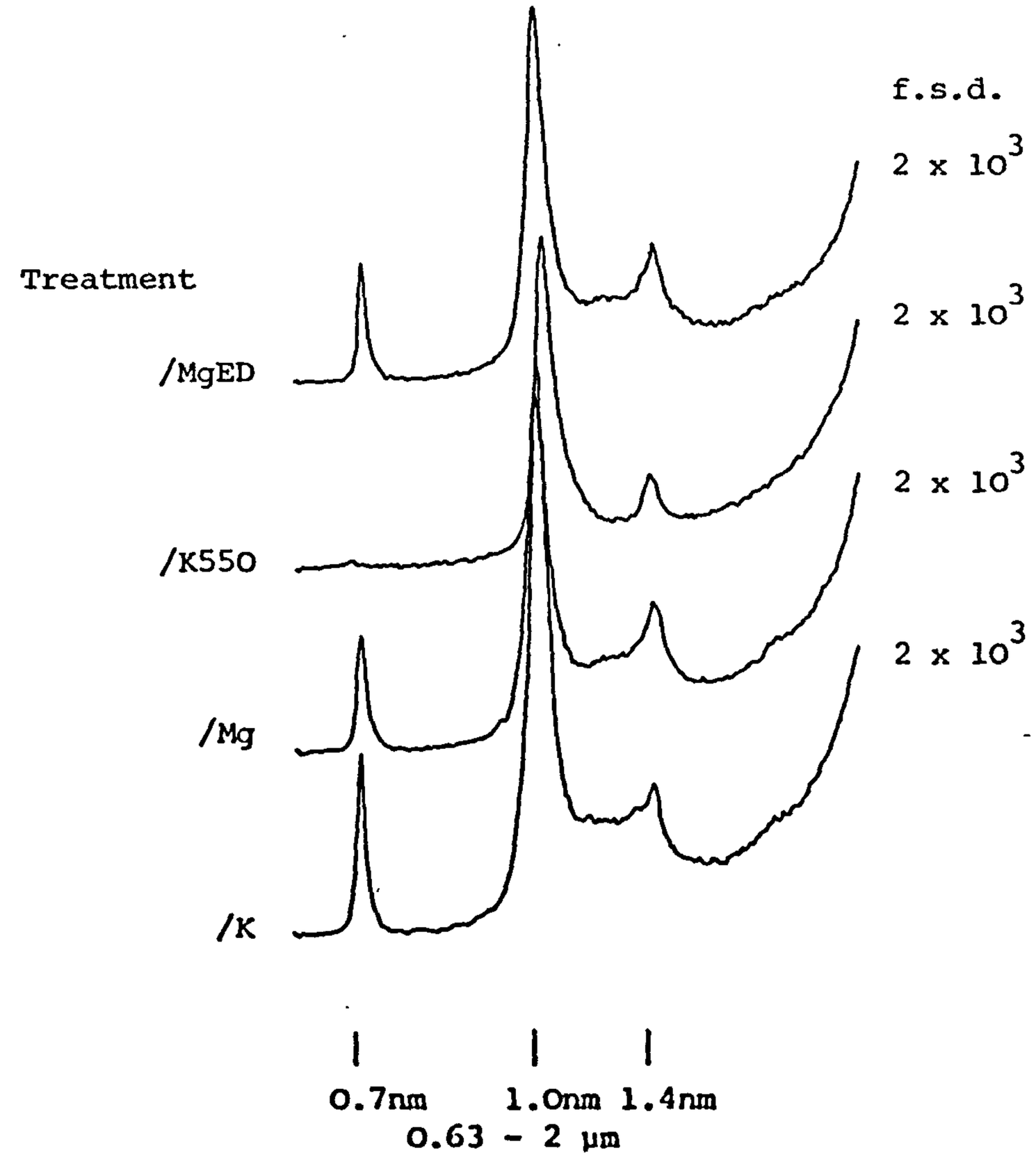


**Figure A.5** **X-ray Diffractometer Traces of 1080D**

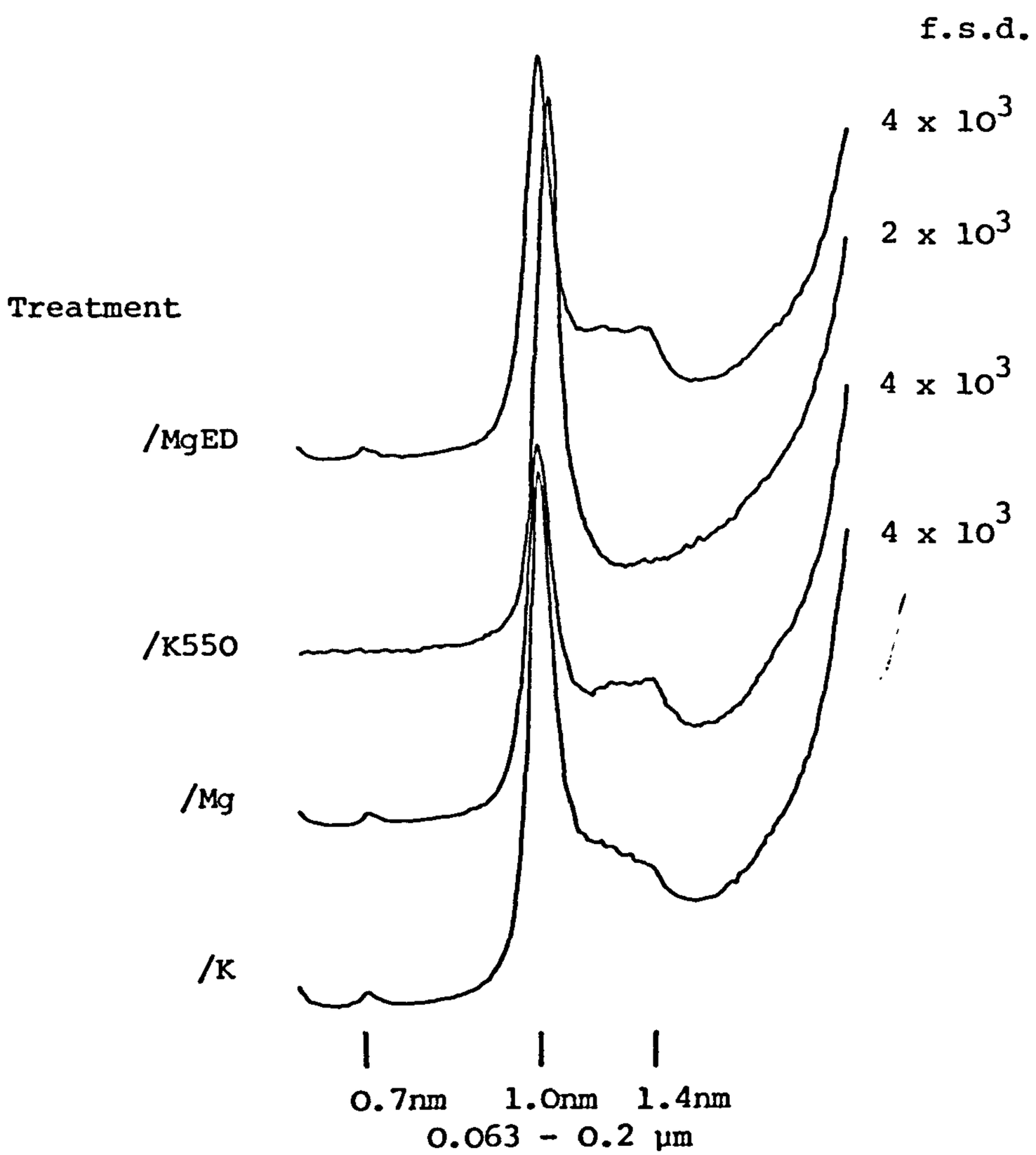


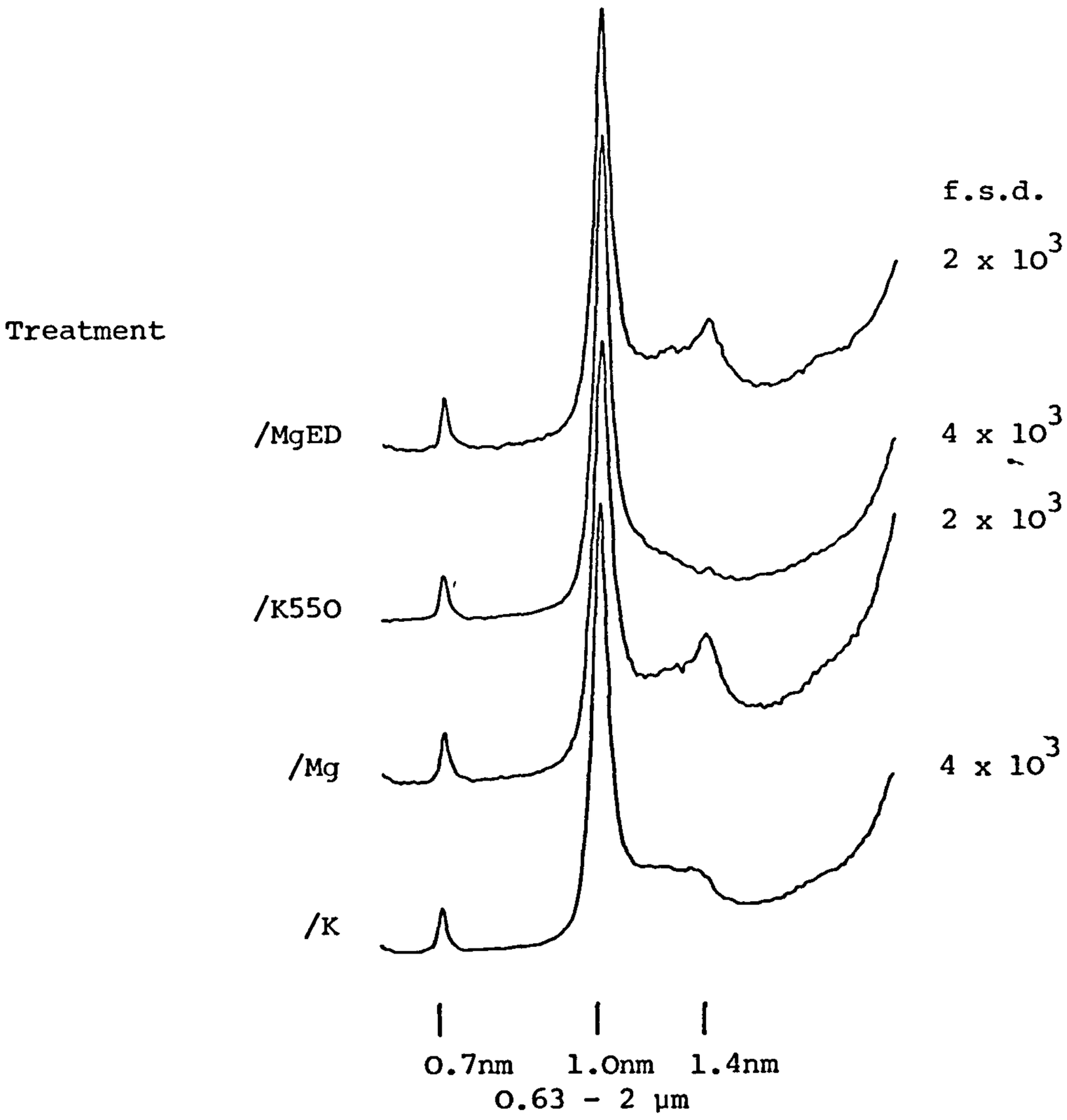


Figure A.6 X-ray Diffractometer Traces of 1079D

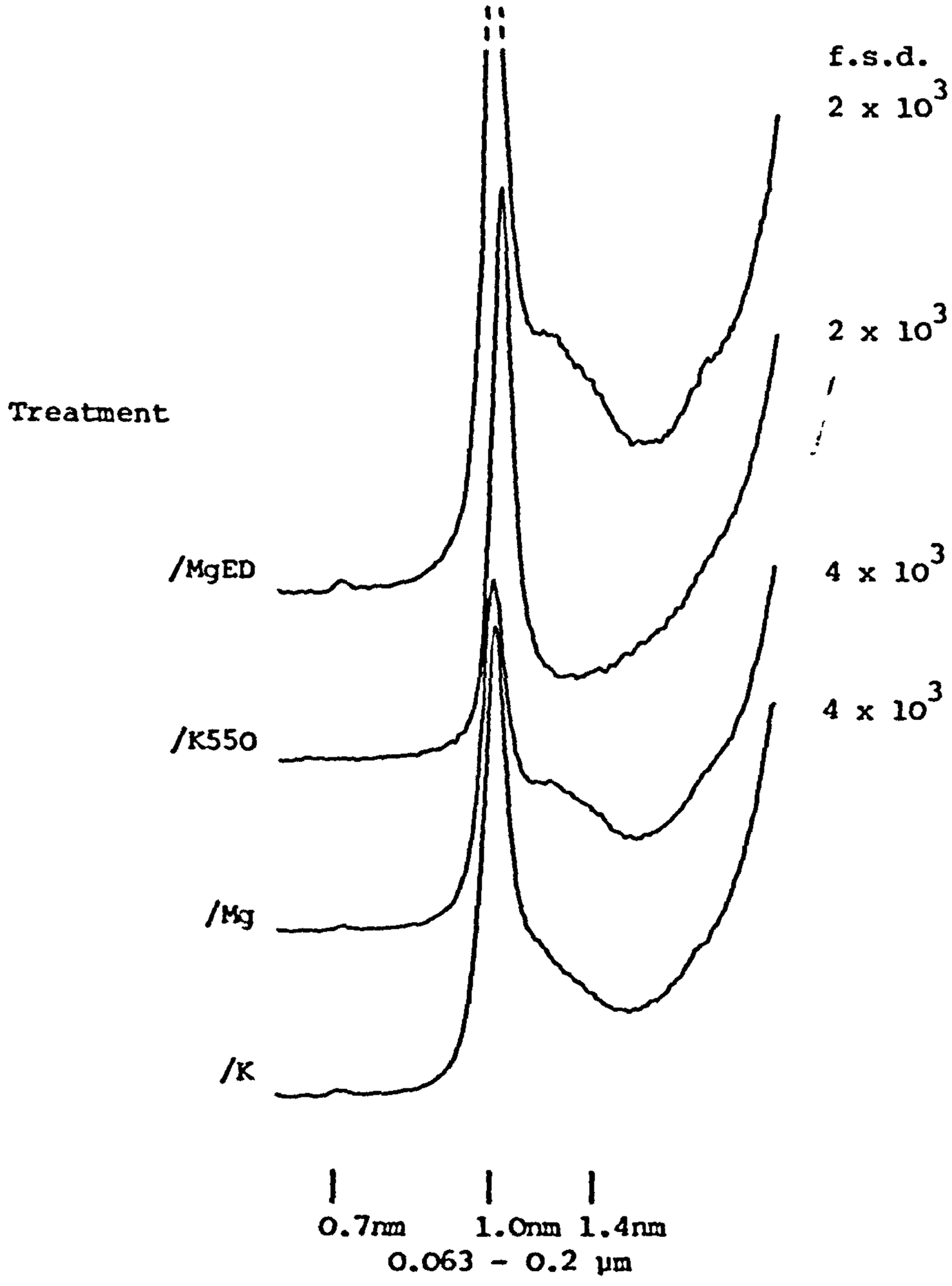


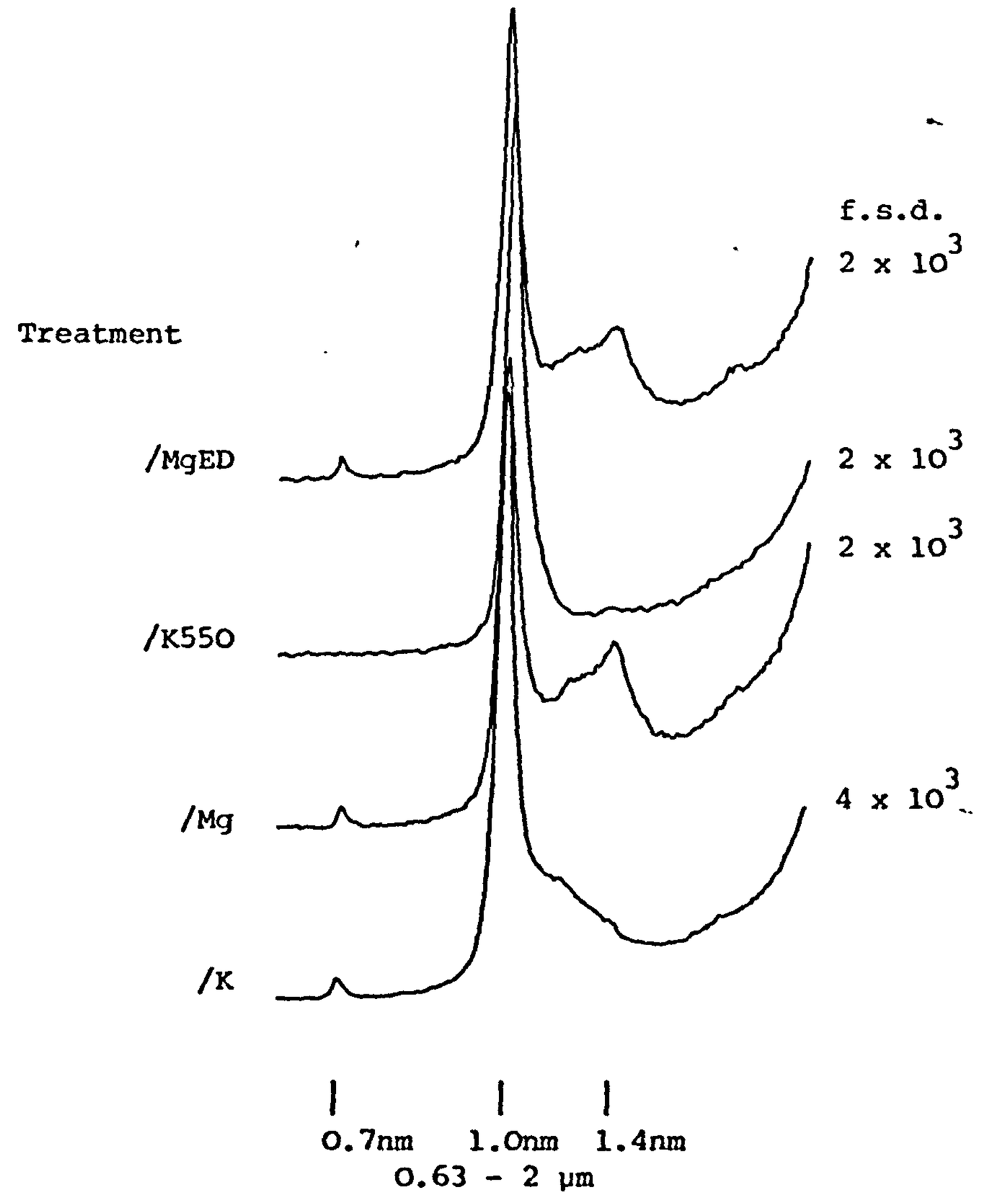


Figure A.7 X-ray Diffractometer Traces of 1078D

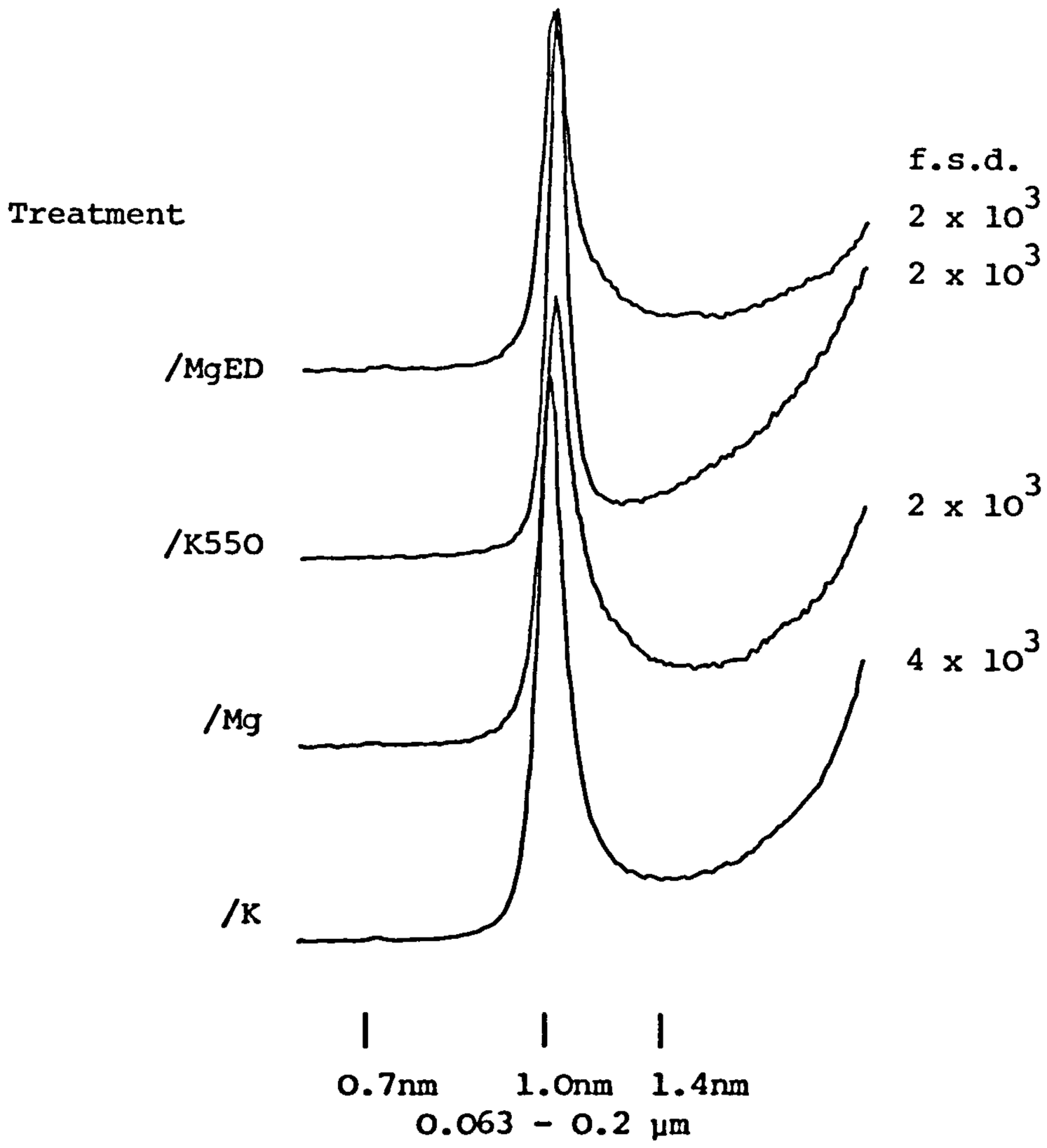


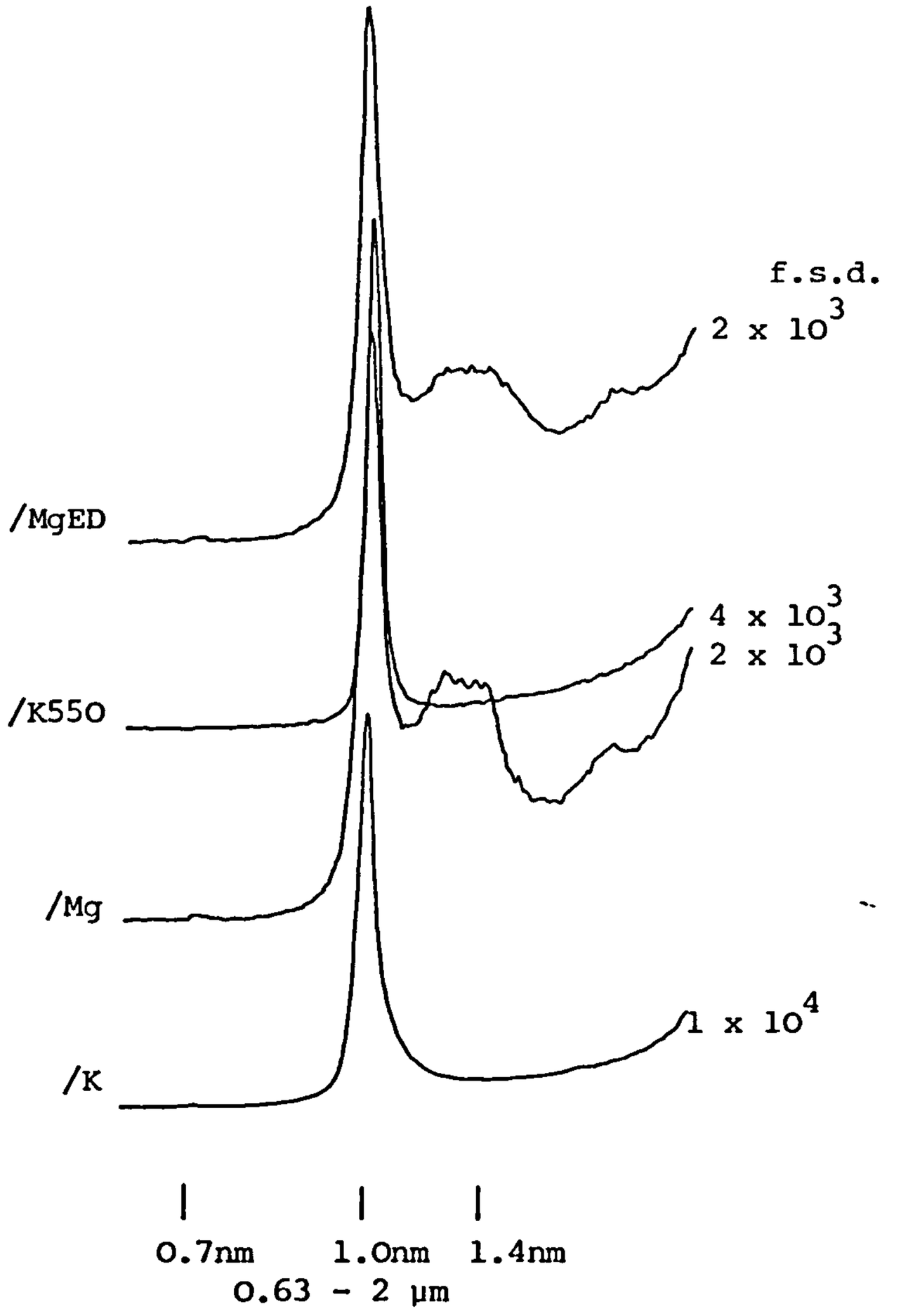


Figure A.8 X-ray Diffractometer Traces of 1077D

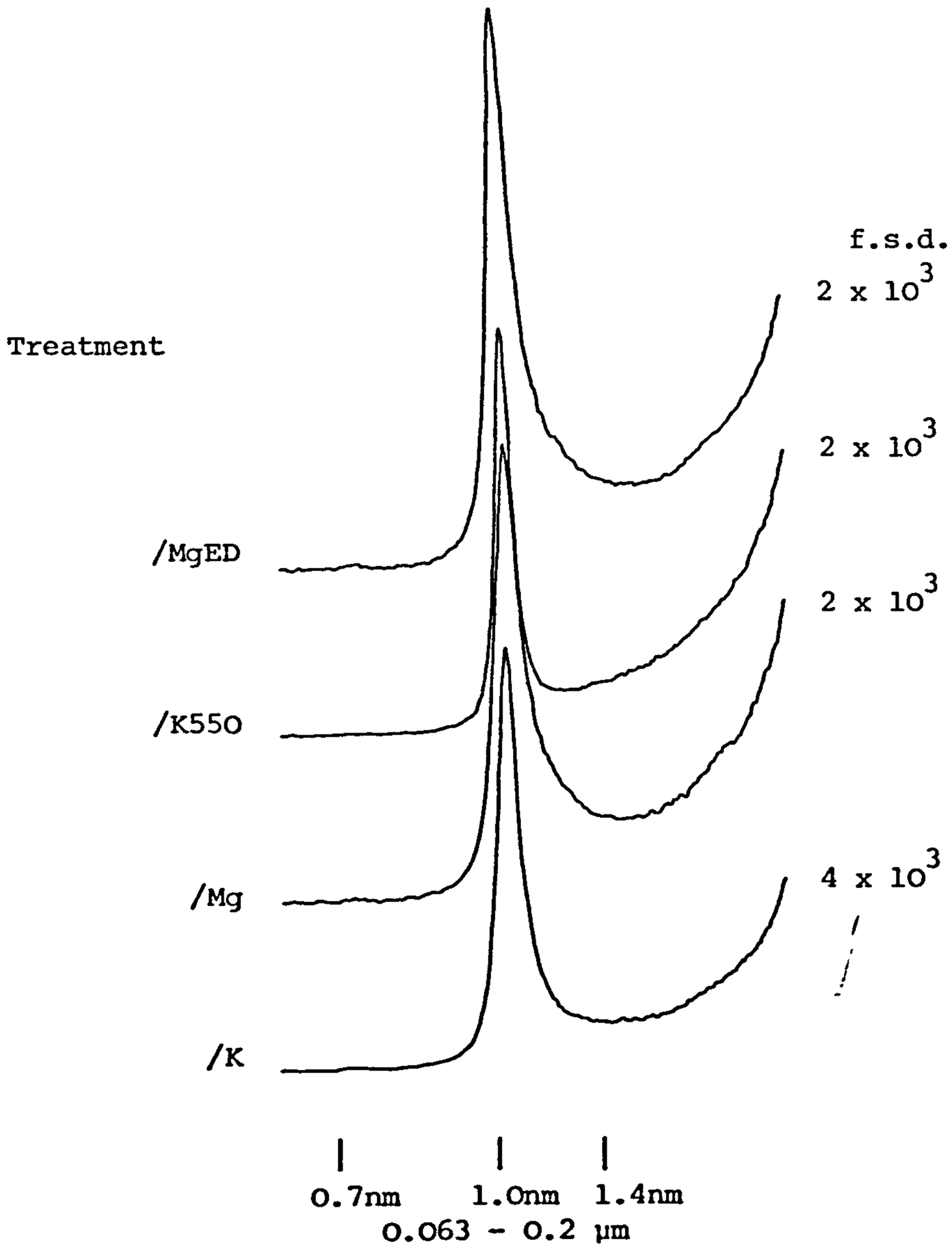


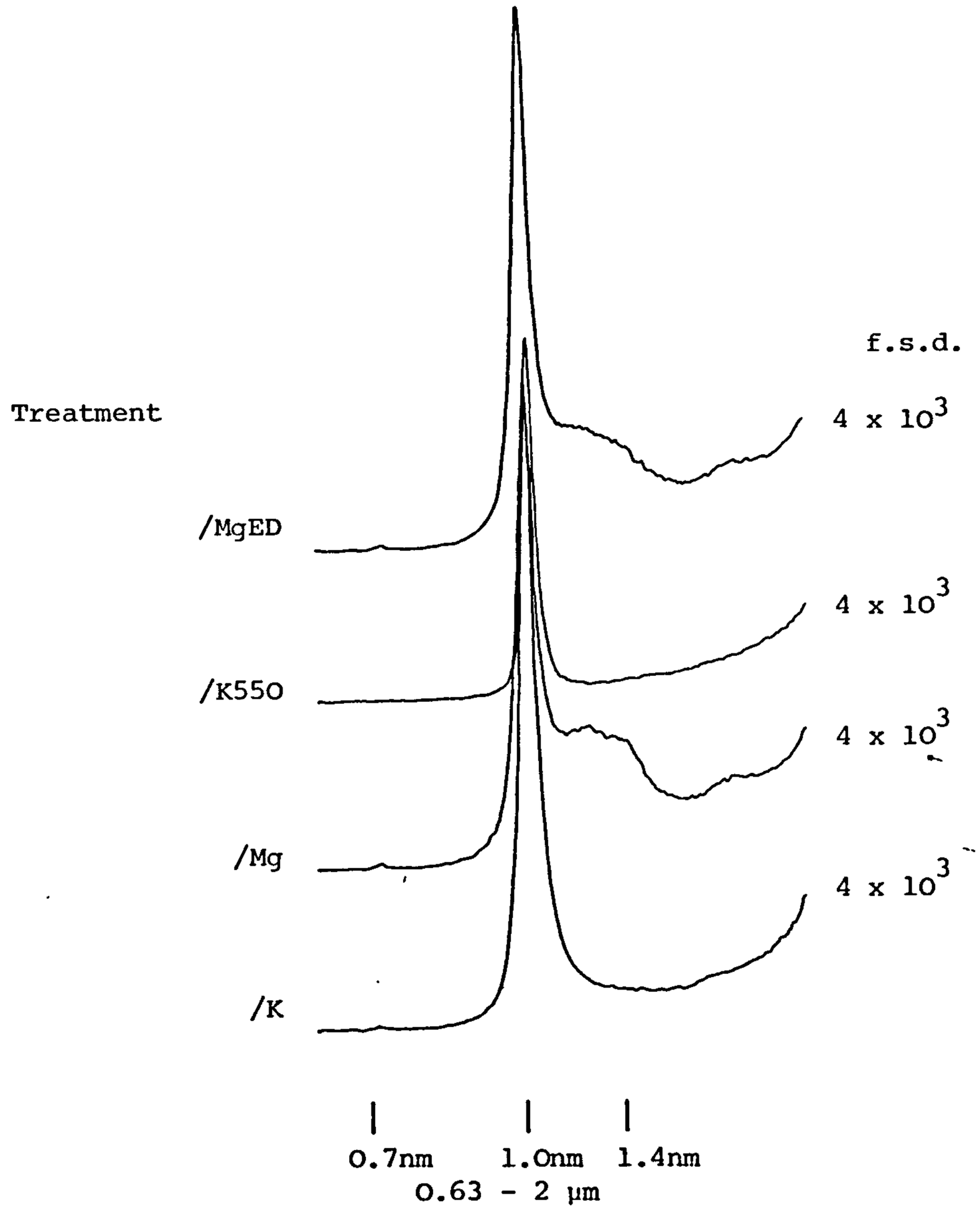


Figure A.9 X-ray Diffractometer Traces of 1076D

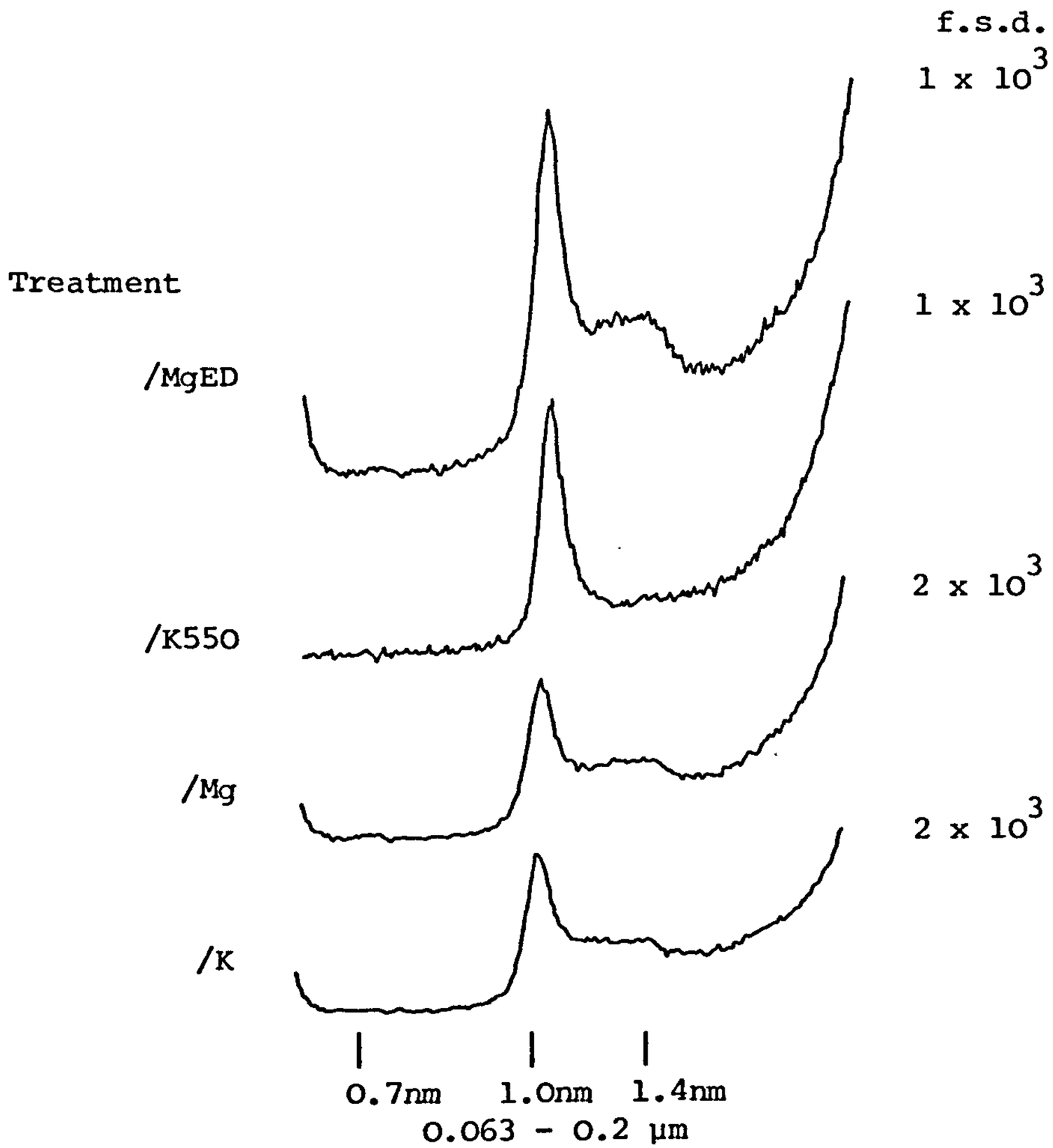


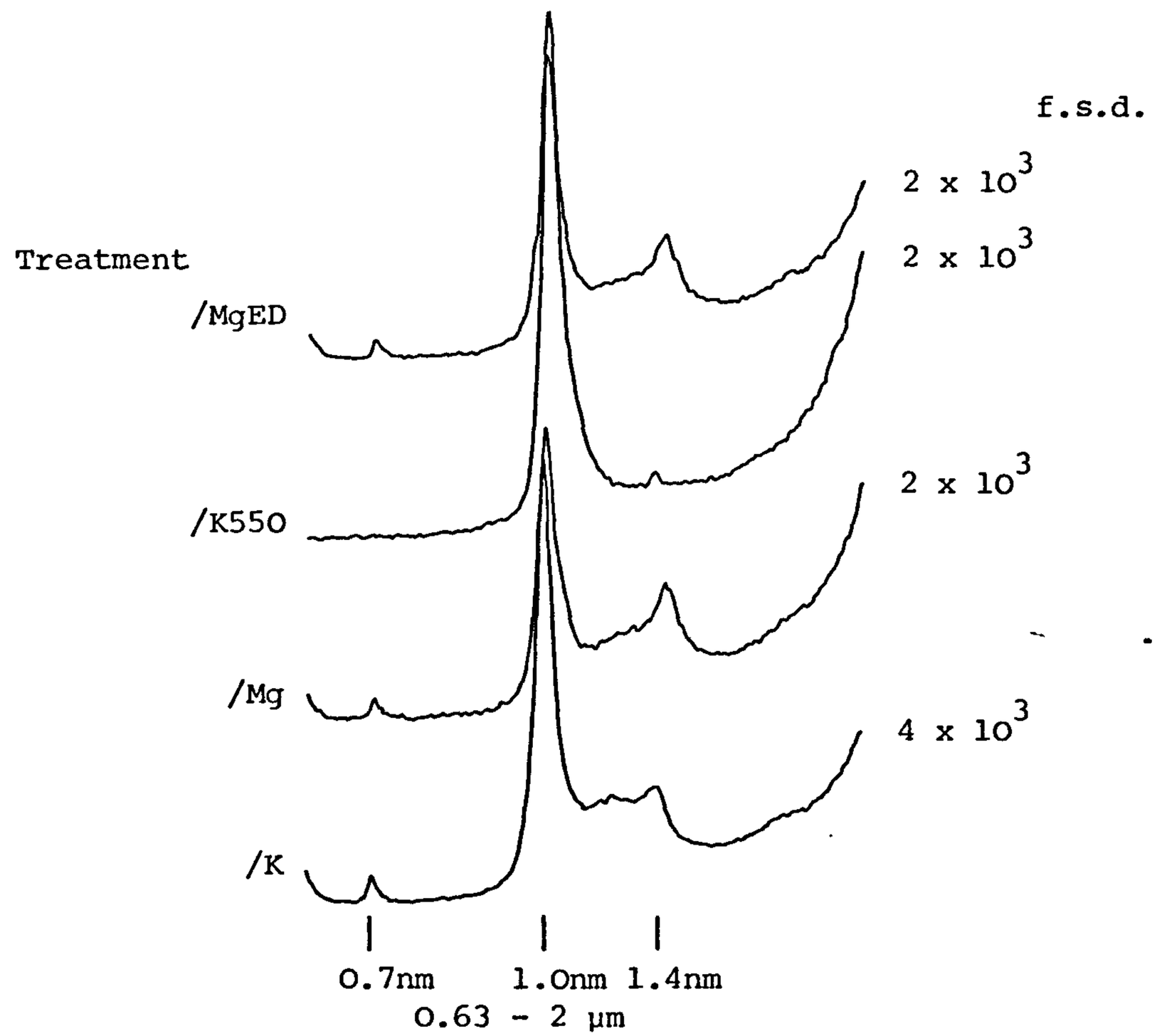


Figure A.10 X-ray Diffractometer Traces of 1079

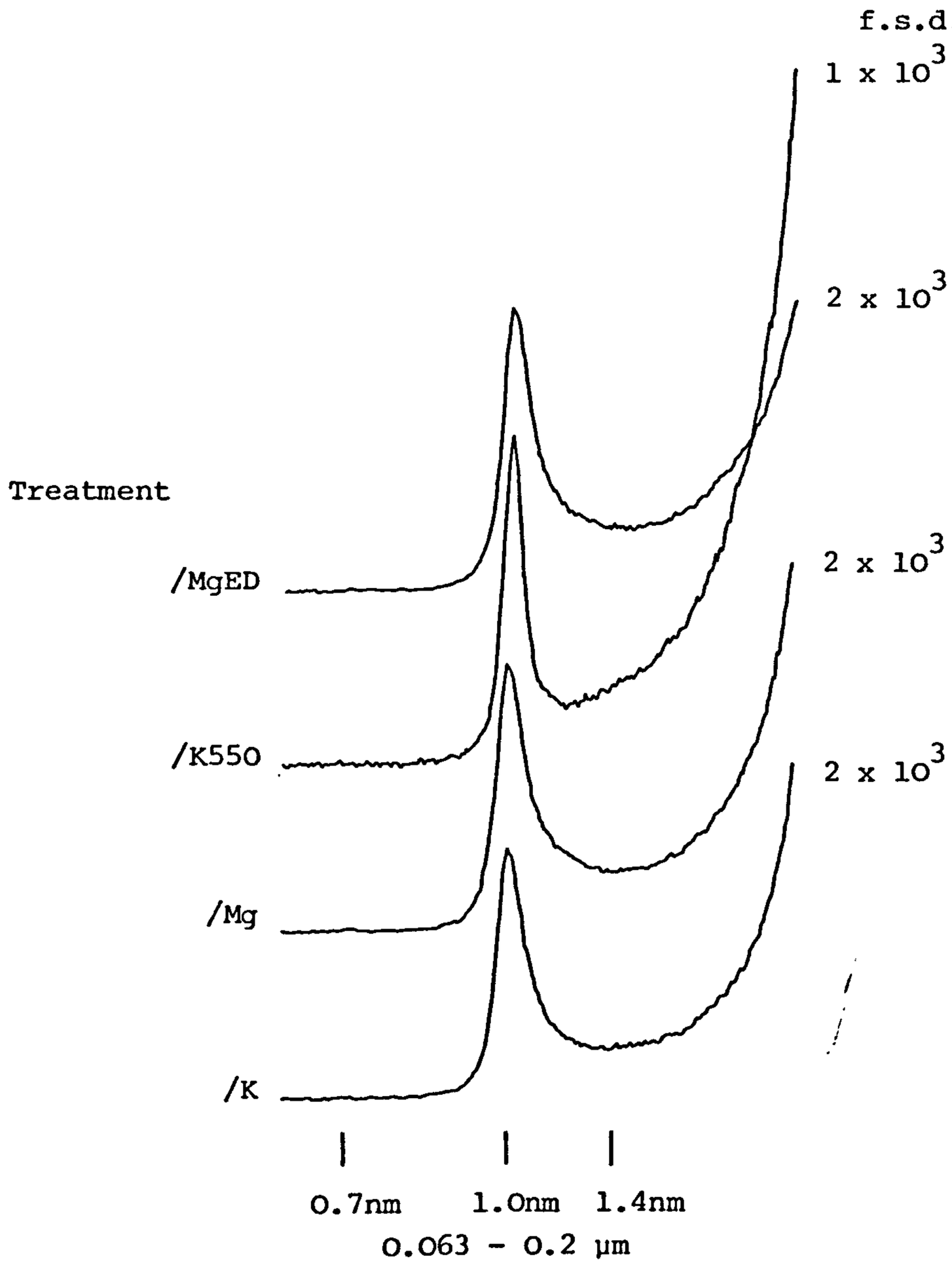


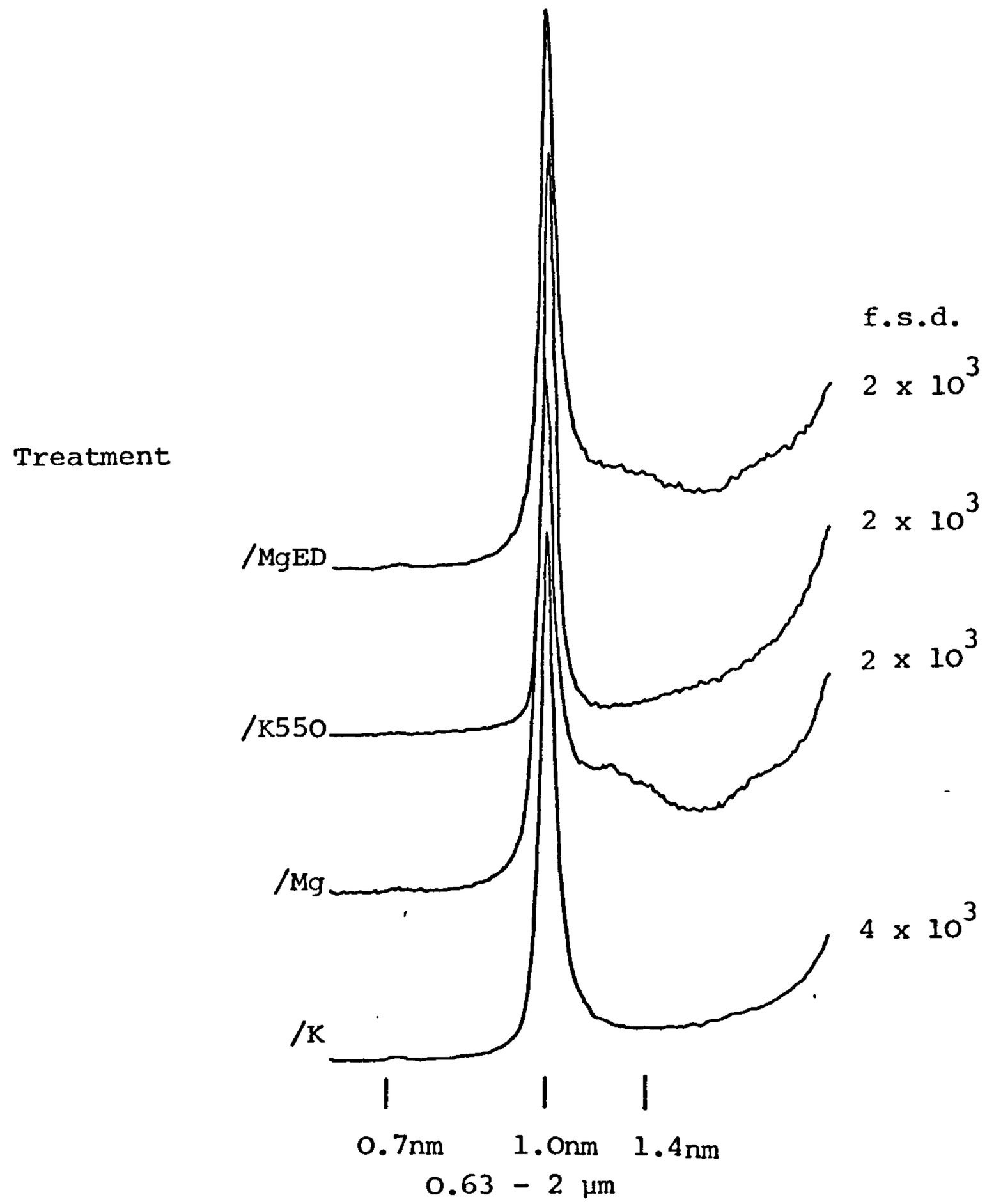


Figure A.11 X-ray Diffractometer Traces of 1077

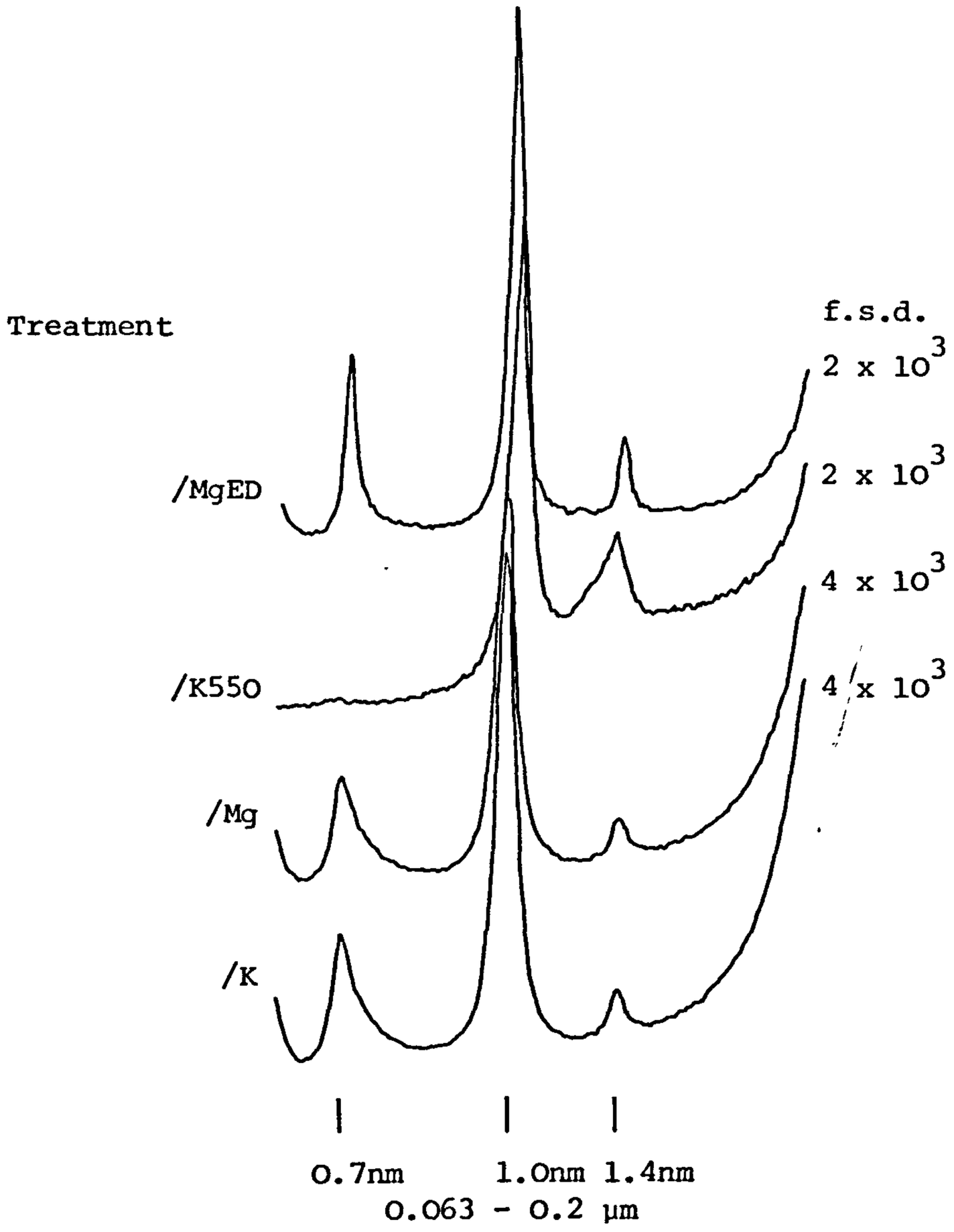


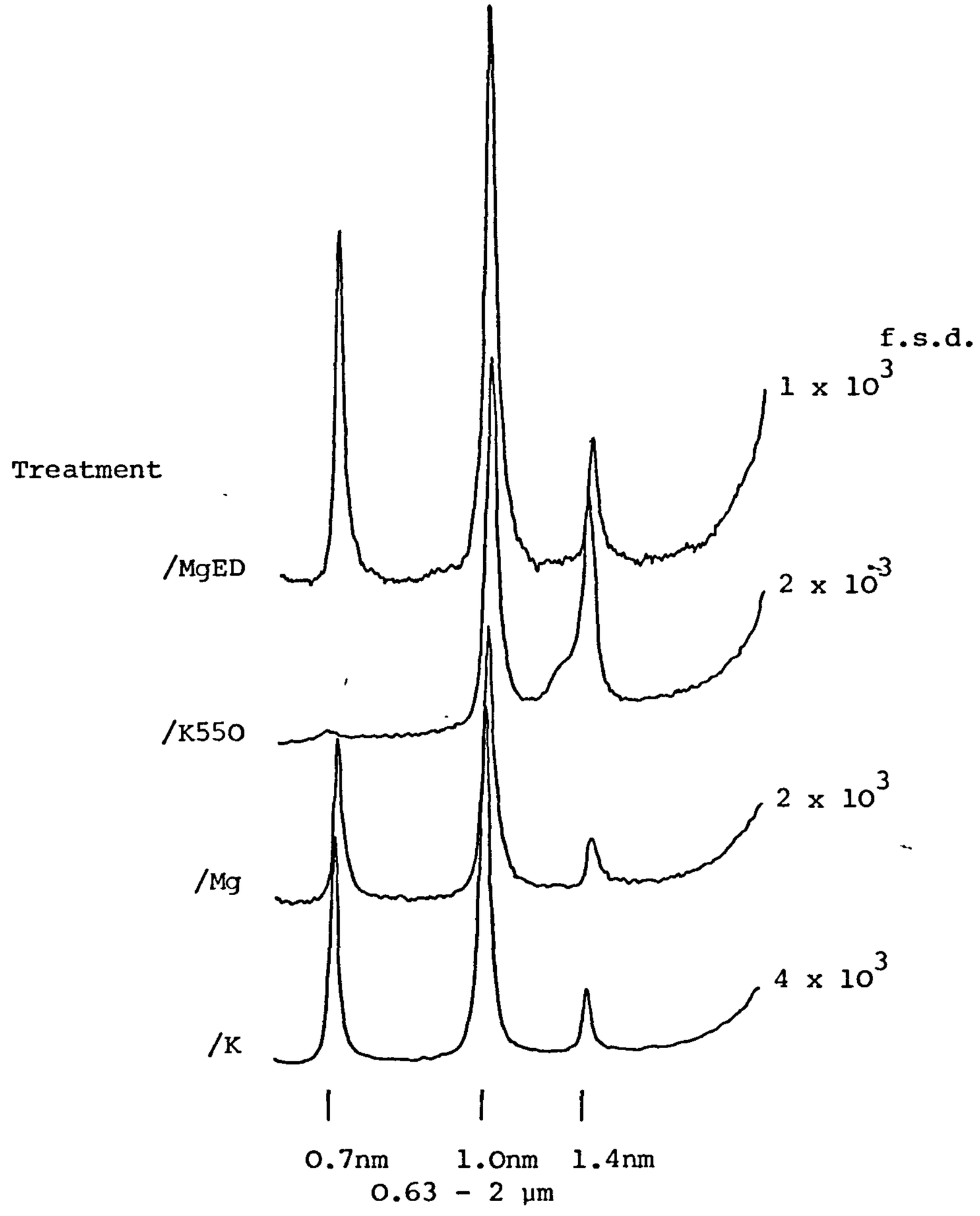


Figure A.12 X-ray Diffractometer Traces of 1087

## REFERENCES


1. Adams, W.A., L.J. Evans and H.H. Abdulla. 1971. Quantitative Pedological Studies on Soils Derived from Silurian Mudstones. III. Laboratory and In Situ Weathering of Chlorite. Journal of Soil Science, 22 (2) 158-165.

2. Albee, A.L. 1962. Relationships between the Mineral Association, Chemical Composition and Physical Properties of the Chlorite Series. American Mineralogist, 47 (7+8) 851-870.

3. Alexander, L.E. and H.P. Klug. 1948. Basic Aspects of X-ray Absorption in Quantitative Diffraction Analysis of Powder Mixtures. Analytical Chemistry, 20 (10) 886-889.

4. Alexiades, C.A. and M.L. Jackson. 1965. Quantitative Determination of Vermiculite in Soils. Proceedings of the Soil Science Society of America, 29 522-527.

5. Armstrong, L.C. 1940. Decomposition and Alteration of Feldspars and Spodumene by Water. American Mineralogist, 25 810-820.

6. Arnold, P.W. 1960. Nature and Mode of Weathering of Soil Potassium Reserves. Journal of the Science of Food and Agriculture, 11 285-292.

7. Aylmore, L.A.G. et al. 1970. Surface Area of Homoionic Illite and Montmorillonite Clay Minerals as Measured by the Sorption of Nitrogen and Carbon Dioxide. Clays and Clay Minerals, 18 (2) 91-96.

8. Bailey, S.W. 1972. Determination of Chlorite Compositions by X-ray Spacings and Intensities. Clays and Clay Minerals, 20 381-388.

9. Bailey, S.W. 1975. Chlorites. 191-263 in Gieseking, J.E. [105].

10. Bailey, S.W. 1980. Structures of Layer Silicates. 1-123 in Brindley, G. W. and G. Brown [40].

11. Bailey, S.W., G.W. Brindley, W.D. Johns, R.T. Martin and M. Ross. 1971. Summary of National and International Recommendations on Clay Mineral Nomenclature. 1969-70 CMS Nomenclature Committee. Clays and Clay Minerals, 19 129-132.

12. Bailey, S.W., G.W. Brindley, W.D. Johns, R.T. Martin and M. Ross. 1971. Clay Mineral Society Report of Nomenclature Committee 1969-1970. Clays and Clay Minerals, 19 132-133.

13. Bain, D.C. 1972. Oxidation of Chlorites in Soil Clays and Effect on DTA Curves. Nature (Physical Science), 238 142-143.

14. Bain, D.C. 1977. The Weathering of Ferruginous Chlorite in a Podzol from Argyllshire, Scotland. Geoderma, 17 193-208.

15. Bajwa, I. and D.A. Jenkins. 1978. A Technique for the Preparation of Clay Samples on Ceramic Slides for XRDA Using Pressure. Clay Minerals, 13 127-131.

16. Ball, D.F. 1966. Chlorite Clay Minerals in Ordovician Pumice-tuff and Derived Soils in Snowdonia, North Wales. Clay Minerals, 6 195-209.

17. Ball, D.F. 1966. Late-glacial Scree in Wales. Biuletyn Peryglacjalny, 15 151-163.

18. Barnhisel, R.I. 1977. Chlorites and Hydroxy Interlayered Vermiculite and Smectite. 321-356 in Dixon, J.B. and S.B. Weed [75].

19. Basset, W.A. 1960. Role of Hydroxyl Orientation in Mica Alteration. Bulletin of the Geological Society of America, 71 (4) 449-456.

20. Berner, R.A. 1978. Rate Control of Mineral Dissolution under Earth Surface Conditions. American Journal of Science, 278 1235-1252.

21. Berner, R.A. and G.R. Holdren Jr. 1977. Mechanism of Feldspar Weathering: Some Observational Evidence. Geology, 5 (6) 369-372.

22. Berner, R.A. and G.R. Holdren Jr. 1977. Mechanism of Feldspar Weathering - II. Observations of Feldspars from Soils. Geochimica et Cosmochimica Acta, 43 1173-1186.

23. Berner, R.A., E.J. Sjöberg, M.A. Velbel and M.D. Krom. 1980. Dissolution of Pyroxenes and Amphiboles during Weathering. Science, 207 (4436) 1205-1206.

24. Berry, R. and P. Jørgensen. 1969. Separation of Illite and Chlorite in Clays by Electromagnetic Techniques. Clay Minerals, 8 201-212.

25. Berthelin, J. and G. Belgy. 1979. A Microbial Degradation of Phyllosilicates during Simulated Podsolisation. Geoderma, 21 (4) 297-310.

26. Berthelin, J. and D. Boymond. 1978. Some Aspects of the Role of Heterotrophic Microorganisms in the Degradation of Minerals in Waterlogged Acid Soils. 659-673 in W.E. Krumbein, editor: Environmental Biogeochemistry and Geomicrobiology, 2: The Terrestrial Environment. Ann Arbor Science. ISBN 0-250-40219-2.

27. Biela, E.J. 1981. Personal Communication.

28. Bjørlykke, K. 1971. Petrology of Ordovician Sediments from Wales. Norsk Geologisk Tidsskrift, 51 123-139.

29. Blatt, H., G. Middleton and R. Murray. 1972. Origin of Sedimentary Rocks. 634pp. Prentice-Hall, Englewood Cliffs. ISBN 0-13-642702-2.

30. Blatt, H. and D.J. Schultz. 1976. Size Distribution of Quartz in Mudrocks. Sedimentology, 23 857-866.

31. Bohn, H.L., B.L. McNeal and G.A. O'Connor. 1979. Soil Chemistry. 329 pp. John Wiley and Sons, New York. ISBN 0-471-04082-7.

32. Bondam, J. 1969. Soxhlet Extraction of Albite. Proceedings of the 3rd International Clay Conference, Tokyo, 1 (2) 475-492.

33. Bower, C.A. and J.O. Goertzen. 1959. Surface Area of Soils and Clays by an Equilibrium Ethylene Glycol Method. Soil Science, 87 289-292.

34. Boyle, J.R., G.K. Voigt and B.L. Sawhney. 1967. Biotite Flakes: Alteration by Chemical and Biological Treatment. Science, 155 193-195.

35. Brady, N.C. 1974. The Nature and Properties of Soils, 8th edition. 639 pp. Macmillan, New York. ISBN 0-02-313350-3.

36. Bricker, O.P., A.E. Godfrey and E.T. Cleaves. 1968. Mineral-water Interaction during the Chemical Weathering of Silicates. 128-142 in R. A. Baker, editor: Trace Inorganics in Water. American Chemical Society - Advances in Chemistry Series, 73.

37. Brindley, G.W. 1966. Ethylene Glycol and Glycerol Complexes of Smectites and Vermiculites. Clay Minerals, 6 237-259.

38. Brindley, G.W. 1980. Order-disorder in Clay Mineral Structures. 125-195 in Brindley, G.W. and G. Brown [40].

39. Brindley, G.W. 1980. Quantitative X-ray Mineral Analysis of Clays. 411-438 in Brindley, G.W. and G. Brown [40].

40. Brindley, G.W. and G. Brown, editors. 1980. Crystal Structures of Clay Minerals and Their X-ray Identification. Mineralogical Society Monograph, 5. 495pp. Mineralogical Society, London. ISBN 0-903056-08-9.

41. Brindley, G.W. and F.H. Gillery. 1956. X-ray Identification of Chlorite Species. American Mineralogist, 41 (3+4) 169-186.

42. British Standards Insititution. 1975. BS1377. Methods of Test for Soils for Civil Engineering Purposes. 143pp. British Standards Institution, London. ISBN 0-580-08206-7.

43. Brown, B.E. and S.W. Bailey. 1962. Chlorite Polytypsim: 1. Regular and Semi-random One-layer Structures. American Mineralogist, 47 (7+8) 819-850.

44. Brown, G. 1955. The Effect of Isomorphous Substitutions on the Intensities of (001) Reflections of Mica- and Chlorite-type Structures. Mineralogical Magazine, 30 (229) 657-665.

45. Brown, G. and G.W. Brindley. 1980. X-ray Diffraction Procedures for Clay Mineral Identification. 305-360 in Brindley, G.W. and G. Brown [40].

46. Brunauer, S., P.H. Emmett and E. Teller. 1938. Adsorption of Gases in Multimolecular Layers. Journal of the American Chemical Society, 60 309-319.

47. Brydon, J.E., H. Kodama and G.J. Ross. 1968. Mineralogy and Weathering of the Clays in Orthic Podzols and Other Podzolic Soils in Canada. Proceedings of the 9th International Congress of Soil Science, Adelaide, 3 41-51.

48. Brydon, J.E. and G.J. Ross. 1966. Stability of Chlorite in Dilute Acid Solutions. Proceedings of the Soil Science Society of America, 30 740-744.

49. Burst, J.F. 1976. Argillaceous Sediment Dewatering. Annual Reviews of Earth and Planetary Sciences, 4 293-318.

50. Busenberg, E. 1978. The Products of the Interaction of Feldspars with Aqueous Solutions at 25°C. Geochimica et Cosmochimica Acta, 42 1679-1686.

51. Busenberg, E. and C.V. Clemency. 1976. The Dissolution Kinetics of Feldspars at 25°C and 1 Atm. $CO_2$ Partial Pressure. Geochimica et Cosmochimica Acta, 40 41-49.

52. Bustin, R.M. and W.H. Mathews. 1979. Selective Weathering of Granitic Clasts. Canadian Journal of Earth Sciences, 16 215-223.

53. Butler, J.R. 1953. The Geochemistry and Mineralogy of Rock Weathering. (1) The Lizard Area, Cornwall. Geochimica et Cosmochimica Acta, 4 157-178.

54. Butler, J.R. 1954. The Geochemistry and Mineralogy of Rock Weathering. (2) The Nordmarka Area, Oslo. Geochimica et Cosmochimica Acta, 6 268-281.

55. Buurman, P., L. Van Der Plas and S. Slager. 1976. A Toposequence of Alpine Soils on Calcareous Micaschists, Northern Adula Region, Switzerland. Journal of Soil Science, 27 395-410.

56. Carroll, D. 1970. Clay Minerals: a Guide to Their X-ray Identification. Geological Society of America Special Paper, 126.

57. Carter, D.L., M.D. Heilman and C.L. Gonzalez. 1965. Ethylene Glycol Monoethyl Ether for Determining Surface Area of Silicate Minerals. Soil Science, 100 (5) 356-360.

58. Chung, F.H. 1974. Quantitative Interpretation of X-ray Diffraction Patterns of Mixtures. I. Matrix-flushing Method for Quantitative Multicomponent Analysis. Journal of Applied Crystallography, 7 519-525.

59. Chung, F.H. 1974. Quantitative Interpretation of X-ray Diffraction Patterns of Mixtures. II. Adiabatic Principle of X-ray Diffraction Analysis of Mixtures. Journal of Applied Crystallography, 7 526-531.

60. Chung, F.H. 1975. Quantitative Interpretation of X-ray Diffraction Patterns of Mixtures. III. Simultaneous Determination of a Set of Reference Intensities. Journal of Applied Crystallography, 8 17-19.

61. Clarke, F.W. 1924. Data of Geochemistry. Bulletin of the United States Geological Survey, 770. 841pp.

62. Cluff, R.M. 1981. Mudrock Fabrics and Their Significance - Reply. Journal of Sedimentary Petrology, 51 1029-1031.

63. Coen, G.M. and R.W. Arnold. 1972. Clay Mineral Genesis of Some New York Spodosols. Proceedings of the Soil Science Society of America, 36 342-350.

64. Coffman, C.B. and D.S. Fanning. 1974. "Vermiculite" Determination on Whole Soils by Cation Exchange Capacity Methods. Clays and Clay Minerals, 22 271-283.

65. Coffman, C.B. and D.S. Fanning. 1975. Maryland Soils Developed in Residuum from Chloritic Metabasalt Having High Amounts of Vermiculite in Sand and Silt Fractions. Proceedings of the Soil Science Society of America, 39 (4) 723-732.

66. Copeland, R.A., F.A. Frey and D.R. Wones, 1971. Origin of Clay Minerals in a Mid-Atlantic Ridge Sediment. Earth and Planetary Science Letters, 10 186-192.

67. Courtois, C. and A. Desprairies. 1978. Les Terres Rares et Quelques Éléments de Transition dans les Minéraux Argileux Issus de Deux Processus d'Altération de Roches Basiques. Comptes Rendus Sommaires Société Géologique Français, 5 242-245.

68. Cubitt, J.M. 1975. A Regression Technique for the Analysis of Shales by X-ray Diffractometry. Journal of Sedimentary Petrology, 45 (2) 546-553.

69. Davis, B.L. 1980. "Standardless" X-ray Diffraction Quantitative Analysis. Atmospheric Environment, 14 (2) 217-220.

70. Davis, C.E., N. Ahmad and R.L. Jones. 1971. Effect of Exchangeable Cations on the Surface Areas of Clays. Clay Minerals, 9 258-261.

71. Deer, W.A., R.A. Howie and J. Zussman. 1966. An Introduction to the Rock-forming Minerals. 528pp. Longman, London. ISBN 0-582-44210-9.

72. De Kimpe, C.R. 1970. Chemical, Physical and Mineralogical Properties of a Podsol Soil with Fragipan Derived from Glacial Till in the Province of Quebec. Canadian Journal of Soil Science, 50 317-330.

73. De Kimpe, C.R., M.R. Laverdiere and Y.A. Martel. 1979. Surface Area and Exchange Capacity of Clay in Relation to the Mineralogical Composition of Gleysolic Soils. Canadian Journal of Soil Science, 59 (4) 341-347.

74. Dibble, W.E. Jr. and W.A. Tiller. 1981. Non-equilibrium Water/Rock Interactions - I. Model for Interface-controlled Reactions. Geochimica et Cosmochimica Acta, 45 (1) 79-92.

75. Dixon, J.B. and S.B. Weed, editors. 1977. Minerals in Soil Environments. 948pp. Soil Science Society of America, Madison. ISBN 0-89118-765-0.

76. Dominik, J. and A. Siwiec. 1975. Polygradient Electromagnetic Separation of Chlorites from Shales. Mineralogia Polonica, 6 (1) 91-96.

77. Douglas, L.A. 1977. Vermiculites. 259-292 in Dixon, J.B. and S.B. Weed [75].

78. Dragovich, D. 1978. Building Stone and Its Use in Rock Weathering Studies. Journal of Geological Education, 27 21-25.

79. Drever, J.I. 1969. The Separation of Clay Minerals by Continuous Particle Electrophoresis. American Mineralogist, 54 937-942.

80. Droste, J.B. 1956. Alteration of Clay Minerals by Weathering in Wisconsin Tills. Bulletin of the Geological Society of America, 67 911-918.

81. Droste, J.B., N. Bhattacharya and J.A. Sunderman. 1962. Clay Mineral Alteration in Some Indiana Soils. Clays and Clay Minerals, 9 329-342.

82. Droste, J.B. and J.C. Tharin. 1958. Alteration of Clay Minerals in Illinoian Till by Weathering. Bulletin of the Geological Society of America, 69 61-67.

83. Duddy, I.R. 1980. Redistribution and Fractionation of Rare-earth and Other Elements in a Weathering Profile. Chemical Geology, 30 (4) 363-381.

84. Dunoyer De Segonzac, G., J. Ferrero and B. Kubler. 1968. Sur la Cristallinité de l'Illite dans la Diagenèse et l'Anchimétamorphisme. Sedimentology, 10 137-143.

85. Dyal, R.A. and S.B. Hendricks. 1950. Total Surface of Clays in Polar Liquids as a Characteristic Index. Soil Science, 69 421-432.

86. Eckel, E.C. 1904. On the Chemical Composition of American Shales and Roofing Slates. Journal of Geology, 12 25-29.

87. Eggleton, R.A. and S.W. Bailey. 1967. Structural Aspects of Dioctahedral Chlorite. American Mineralogist, 52 673-689.

88. Eltantawy, I.M. and P.W. Arnold. 1973. Reappraisal of Ethylene Glycol Mono-ethyl Ether (EGME) Method for Surface Area Estimations of Clays. Journal of Soil Science, 24 (2) 232-238.

89. Englund, J-O. and P. Jørgensen. 1973. A Chemical Classification System for Argillaceous Sediments and Factors Affecting Their Composition. Geologiska Föreningens i Stockholm Förhandlingar, 95 (1) 87-97.

90. Eswaran, H. 1979. The Alteration of Plagioclases and Augites under Different Pedo-environmental Conditions. Journal of Soil Science, 30 547-555.

91. Evans, L.J. 1972. Mineralogical Changes in Lower Palaeozoic Mudstones during Pedogenesis in Mid Wales. Reports of the Welsh Soils Discussion Group, 13 91-105.

92. Evans, L.J. 1973. Clay Mineral Alteration and Elemental Redistribution during Pedogenesis in Mid-Wales. Unpublished Ph.D. Thesis, University College of Wales, Aberystwyth.

93. Evans, L.J. and W.A. Adams. 1975. Chlorite and Illite in Some Palaeozoic Mudstones of Mid-Wales. Clay Minerals, 10 387-397.

94. Evans, L.J. and W.A. Adams. 1975. Quantitative Pedological Studies on Soils Derived from Silurian Mudstones. IV. Uniformity of the Parent Material and Evaluation of Internal Standards. Journal of Soil Science, 26 (3) 319-326.

95. Evans, L.J. and W.A. Adams. 1975. Quantitative Pedological Studies on Soils Derived from Silurian Mudstones. V. Redistribution and Loss of Mobilized Constituents. Journal of Soil Science, 26 (3) 327-335.

96. Fagherazzi, G., G. Cocco, L. Schiffini, S. Enzo, A. Benedetti, R. Passerini and G.R. Tauszik. 1978. Particle Size Distribution and Surface Area of Supported Metal Catalysts. La Chimica e l'Industria, 60 (11) 892-900.

97. Fanning, D.S. and V.Z. Keramidas. 1977. Micas. 195-258 in Dixon, J.B. and S.B. Weed [75].

98. Farmer, V.C., J.D. Russell, W.J. McHardy, A.C.D. Newman, J.L. Ahlrichs and J.Y.H. Rimsaite. 1971. Evidence for Loss of Protons and Octahedral Iron from Oxidised Biotites and Vermiculites. Mineralogical Magazine, 38 (294) 121-137.

99. Foster, M.D. 1962. Interpretation of the Composition and a Classification of the Chlorites. United States Geological Survey Professional Paper, 414-A 1-33.

100. Gardner, L.R. 1980. Mobilisation of Al and Ti during Weathering - Isovolumetric Geochemical Evidence. Chemical Geology, 30 151-165.

101. Garrels, R.M. and P. Howard. 1957. Reactions of Feldspar and Mica with Water at Low Temperature and Pressure. Clays and Clay Minerals, 6 68-88.

102. Gibbs, R.J. 1965. Error Due to Segregation in Quantitative Clay Mineral X-ray Diffraction Mounting Techniques. American Mineralogist, 50 (5+6) 741-751.

103. Gibbs, R.J. 1967. Quantitative X-ray Diffraction Analysis Using Clay Mineral Standards Extracted from the Samples to be Analysed. Clay Minerals, 7 79-90.

104. Gibbs, R.J. 1968. Clay Mineral Mounting Techniques for X-ray Diffraction Analysis: a Discussion. Journal of Sedimentary Petrology, 38 242-244.

105. Gieseking, J.E., editor. 1975. Soil Components, 2 Inorganic Components. 684pp. Springer-Verlag, New York. ISBN 0-387-06862-7.

106. Giles, C.H., A.P. D'Silva and A.S. Trivedi. 1970. Use of Dyes for Specific Surface Measurement. 317-327 in D.H. Everett and R.H. Ottewill, editors: Surface Area Determination.

107. Gilkes, R.J. and I.P. Little. 1972. Weathering of Chlorite and Some Associations of Trace Elements in Permian Phyllites in Southeast Queensland. Geoderma, 7 233-247.

108. Gilkes, R.J. and A. Suddhiprakarn. 1979. Biotite Alteration in Deeply Weathered Granite: I. Morphological, Mineralogical, and Chemical Properties. Clays and Clay Minerals, 27 (5) 349-360.

109. Gilkes, R.J. and A. Suddhiprakarn. 1979. Magnetite Alteration in Deeply Weathered Adamellite. Journal of Soil Science, 30 357-361.

110. Gjems, O. 1967. Studies on Clay Minerals and Clay-mineral Formation in Soil Profiles in Scandinavia. Meddelelser fra det Norske Skogforsøksvesen, 21 (4) 299-415.

111. Goldich, S.S. 1938. A Study in Rock-weathering. Journal of Geology, 46 (1) 17-58.

112. Gottardi, G. 1967. On a Systematic Error in the X-ray Determination of the Iron Content of Chlorites and Biotites. American Mineralogist, 52 (9+10) 1573-1575.

113. Grainger, P. and M.C. George. 1978. Clay Mineral Studies of Crackington Formation Shales near Exeter. Proceedings of the Ussher Society, 4 145-155.

114. Griffiths, J.C. 1952. Reaction Relation in the Finer-grained Rocks. Clay Minerals Bulletin, 1 (8) 251-257.

115. Grim, R.E. 1968. Clay Mineralogy, 2nd edition. 596pp. McGraw Hill, New York. ISBN 0-07-024836-2.

116. Grossman, R.H., R.S. Liebling and H.S. Scherp. 1979. Chlorite and Its Relationship to Pyritization in Anoxic Marine Environments. Journal of Sedimentary Petrology, 49 611-614.

117. Grout, F.F. 1925. Relation of Texture and Composition of Clays. Bulletin of the Geological Society of America, 36 393-416.

118. Harriss, R.C. and J.A.S. Adams. 1966. Geochemical and Mineralogical Studies on the Weathering of Granitic Rocks. American Journal of Science, 264 146-173.

119. Hayes, J.B. 1970. Polytypism of Chlorite in Sedimentary Rocks. Clays and Clay Minerals, 18 285-306.

120. Heald, M.T., T.J. Hollingsworth and R.M. Smith. 1979. Alteration of Sandstone as Revealed by Spheroidal Weathering. Journal of Sedimentary Petrology, 49 (3) 901-910.

121. Heath, R.G. and N.G. Pisias. 1979. A Method for the Quantitative Estimation of Clay Minerals in North Pacific Deep-sea Sediments. Clays and Clay Minerals, 27 (3) 175-184.

122. Heilman, M.D., D.L. Carter and C.L. Gonzalez. 1965. The Ethylene Glycol Monoethyl Ether (EGME) Technique for Determining Soil-surface Area. Soil Science, 100 (6) 409-413.

123. Henin, S. and G. Pedro. 1965. The Laboratory Weathering of Rocks. 29-39 in E.G. Hallsworth and D.V. Crawford, editors: Experimental Pedology.

124. Hey, M.H. 1954. A New Review of the Chlorites. Mineralogical Magazine, 30 (224) 277-292.

125. Hoffman, J. and J. Hower. 1979. Clay Mineral Assemblages as Low Grade Metamorphic Geothermometers: Application to the Thrust Faulted Disturbed Belt of Montana, U.S.A. 55-79 in P.A. Scholle and P.R. Schluger, editors: Aspects of Diagenesis. Society of Economic Palaeontologists and Mineralogists Special Publication, 26.

126. Holdren, G.R. Jr. and R.A. Berner. 1979. Mechanism of Feldspar Weathering - I. Experimental Studies. Geochimica et Cosmochimica Acta, 49 1161-1171.

127. Hornung, M., B. Reynolds and A.A. Hatton. 1985. Land Management, Geological and Soil Effects on Streamwater Chemistry in Upland Mid-Wales. Applied Geography, 5 71-80.

128. Hower, J. and T.C. Mowatt. 1966. The Mineralogy of Illites and Mixed-layer Illite/Montmorillonites. American Mineralogist, 51 (5+6) 825-854.

129. Huang, P.M., L.S. Crosson and D.A. Rennie. 1968. Chemical Dynamics of Potassium Release from Potassium Minerals Common in Soils. Proceedings of the 9th International Congress of Soil Science, Adelaide, 2 705-712.

130. Huang, W.H. and W.D. Keller. 1973. Kinetics and Mechanisms of Dissolution of Fithian Illite in Two Complexing Organic Acids. Proceedings of the 4th International Clay Conference, 1972, Madrid, 385-396.

131. Hurd, D.C., C. Fraley and J.K. Fugate. 1979. Silica Apparent Solubilities and Rates of Dissolution and Precipitation for Ca. 25 Common Minerals at 1°-2°C, pH7.5-8.5 in Seawater. 413-445 in E.A. Jenne, editor: Chemical Modeling in Aqueous Systems. American Chemical Society Symposium Series, 93.

132. Imbrie, J. and A. Poldervaart. 1959. Mineral Compositions Calculated from Chemical Analyses of Sedimentary Rocks. Journal of Sedimentary Petrology, 29 (4) 588-595.

133. Jackson, M.L. 1963. Interlayering of Expansible Layer Silicates in Soils by Chemical Weathering. Clays and Clay Minerals, 11 29-46.

134. Jackson, M.L. 1968. Weathering of Primary and Secondary Minerals in Soils. Proceedings of the 9th International Congress of Soil Science, Adelaide, 4 281-291.

135. James, D.M.D. 1971. Petrography of the Plynlimon Group, West Central Wales. Sedimentary Geology, 6 255-270.

136. Johnson, L.J. 1964. Occurrence of Regularly Interstratified Chlorite-vermiculite as a Weathering Product of Chlorite in a Soil. American Mineralogist, 49 556-572.

137. Johnson, L.J. 1970. Clay Minerals in Pennsylvania Soils. Relation to Lithology of the Parent Rock and Other Factors - I. Clays and Clay Minerals, 18 247-260.

138. Jones, O.T. and W.J. Pugh. 1935. The Geology of the Districts around Machynlleth and Aberystwyth. Proceedings of the Geologists' Association, 46 (3) 247-300.

139. Jørgensen, P. 1965. Mineralogical Composition and Weathering of Some Late Pleistocene Marine Clays from the Kongsvinger Area, Southern Norway. Geologiska Föreningens i Stockholm Förhandlingar, 87 62-83.

140. Kaye, M.J., A.C. Dunham and D.M. Hirst. 1968. A Comparison of Two Methods of Quantitative Mineralogical Analysis of Sedimentary Rocks. Journal of Sedimentary Petrology, 38 675-678.

141. Keller, W.D. 1970. Environmental Aspects of Clay Minerals. Journal of Sedimentary Petrology, 40 (3) 788-813.

142. Keller, W.D. and A.F. Frederickson. 1952. Role of Plants and Colloidal Acids in the Mechanism of Weathering. American Journal of Science, 250 594-608.

143. Kepezhinskas, K.B. 1965. Composition of Chlorites as Determined from Their Physical Properties. Doklady Akademii Nauk SSSR, 164 126-129.

144. Kisch, H.J. 1980. Incipient Metamorphism of Cambro-Silurian Clastic Rocks from the Jämtland Supergroup, Central Scandinavian Caledonides, Western Sweden: Illite Crystallinity and 'Vitrinite' Reflectance. Journal of the Geological Society, 137 (3) 271-288.

145. Kittrick, J.A. 1973. Mica-derived Vermiculites as Unstable Intermediates. Clays and Clay Minerals, 21 479-488.

146. Kittrick, J.A. 1979. Ion Exchange and Mineral Stability: are the Reactions Linked or Separate? 401-412 in E.A. Jenne, editor: Chemical Modeling in Aqueous Systems. American Chemical Society Symposium Series, 93.

147. Kittrick, J.A. 1983. Chlorites Differentiated from Intergrade Smectites and Vermiculites by Solution Stability Criteria. Clays and Clay Minerals, 31 (4) 317-318.

148. Klug, H.P. and L.E. Alexander. 1974. X-ray Diffraction Procedures for Polycrystalline and Amorphous Materials, 2nd edition. 992pp. Wiley, New York. ISBN 0-471-49369-4.

149. Knapp, B.J. 1970. Problems of Water Movement on a Steep Upland Hillside, Plynlimon, Central Wales. Unpublished Ph.D. Thesis, University of Reading.

150. Knudsen, T. 1981. Quantitative X-ray Diffraction Analysis with Qualitative Control of Calibration Samples. X-ray Spectrometry, 10 (2) 54-56.

151. Kodama, H. and J.E. Brydon. 1968. A Study of Clay Minerals in Podzol Soils in New Brunswick, Eastern Canada. Clay Minerals, 7 295-309.

152. Krinsley, D.H. and J.C. Doornkamp. 1973. Atlas of Quartz Sand Surface Textures. x+91pp. Cambridge University Press. ISBN 0-521-08705-8.

153. Kronberg, B.I., W.S. Fyfe, O.H. Leonards Jr. and A.M. Satos. 1979. The Chemistry of Some Brazilian Soils: Element Mobility during Intense Weathering. Chemical Geology, 24 211-229.

154. Kubler, B. 1968. Évaluation Quantitative du Métamorphisme par la Cristallinité de l'Illite. État des Progrès Réalisés ces Dernières Années. Bulletin du Centre de Recherches de Pau - Société Nationale des Pétroles d'Aquitaine, 2 (2) 385-397.

155. Lawrence, J.R. and H.P. Taylor. 1972. Hydrogen and Oxygen Isotope Systematics in Weathering Profiles. Geochimica et Cosmochimica Acta, 36 1377-1393.

156. Lawrie, D.C. 1961. A Rapid Method for the Determination of Approximate Surface Areas of Clays. Soil Science, 92 188-191.

157. Leith, C.K. and W.J. Mead. 1915. Metamorphic Geology. 337pp. Holt, Rinehart and Winston, New York.

158. Leonard, R.A. and S.B. Weed. 1970. Mica Weathering Rates as Related to Mica Type and Composition. Clays and Clay Minerals, 18 187-195.

159. Lerman, A. 1979. Geochemical Processes: Water and Sediment Environments. 481pp. John Wiley, New York. ISBN 0-471-03263-8.

160. Leroux, J., D.H. Lennox and K. Kay. 1953. Direct Quantitative X-ray Analysis by Diffraction-absorption Technique. Analytical Chemistry, 25 (5) 740-743.

161. Levinson, A.A. 1955. Studies in the Mica Group: Polymorphism among Illites and Hydrous Micas. American Mineralogist, 40 (1) 41-49.

162. Lewan, M.D. 1978. Laboratory Classification of Very Fine Grained Sedimentary Rocks. Geology, 6 (12) 745-748.

163. Lin, F-C. and C.V. Clemency. 1981. The Kinetics of Dissolution of Muscovites at 25°C and 1 Atm. $CO_2$ Partial Pressure. Geochimica et Cosmochimica Acta, 45 (4) 571-576.

164. Loughnan, F.C. 1962. Some Considerations in the Weathering of the Silicate Minerals. Journal of Sedimentary Petrology, 32 (2) 284-290.

165. Ludden, J.N. and G. Thompson. 1978. Behaviour of Rare Earth Elements during Submarine Weathering of Tholeiitic Basalt. Nature, 274 147-149.

166. Ludden, J.N. and G. Thompson. 1979. An Evaluation of the Behaviour of the Rare Earth Elements during the Weathering of Sea Floor Basalt. Earth and Planetary Science Letters, 43 85-92.

167. Lyklema, J. and H.J. Van Den Hul. 1970. Specific Surface Area by Negative Adsorption. 341-356 in D.H. Everett and R.H. Ottewill, editors: Surface Area Determination.

168. MacEwan, D.M.C. and A. Ruiz-Amil. 1975. Interstratified Clay Minerals. 265-334 in Gieseking, J.E. [105].

169. McKeague, J.A., G.J. Ross and D.S. Gamble. 1978. Properties, Criteria of Classification and Concepts of Genesis of Podsolic Soils in Canada. 27-60 in W.C. Mahaney, editor: Quaternary Soils.

170. McKenzie, F.T. and R.M. Garrels. 1965. Silicates: Reactivity with Sea Water. Science, 150 (3692) 57-58.

171. ~~McKenzie~~ Mackenzie, R.C. 1975. The Classification of Soil Silicates and Oxides. 1-25 in Gieseking, J.E. [105].

172. Mackintosh, E.E. and D.G. Lewis. 1968. Displacement of Potassium from Micas by Dodecylammonium Chloride. Proceedings of the 9th International Congress of Soil Science, Adelaide, 2 695-703.

173. Madsen, F.T. 1977. Surface Area Measurements of Clay Minerals by Glycerol Sorption on a Thermobalance. Thermochimica Acta, 21 (1) 89-93.

174. Makumbi, L. and A.J. Herbillon. 1972. Vermiculitisation Expérimentale d'une Chlorite. Bulletin de la Groupe Française d'Argiles, 24 153-164.

175. Mamy, J. 1970. Extraction of Interlayer K from Phlogopite: Specific Effects of Cations; Role of Na and H Concentrations in Extraction Solutions. Clays and Clay Minerals, 18 157-163.

176. Martin, R.T. 1955. Ethylene Glycol Retention by Clays. Proceedings of the Soil Science Society of America, 19 160-164.

177. Mason, B. 1966. Principles of Geochemistry, 3rd edition. vii+329pp. John Wiley, New York.

178. Massey, B.S. 1970. Mechanics of Fluids, 2nd edition. 508pp. Van Nostrand Reinhold, London. ISBN 0-442-05176-X.

179. Mehra, O.P. and M.L. Jackson. 1960. Iron Oxide Removal from Soils and Clays by a Dithionite-citrate System Buffered with Sodium Bicarbonate. Clays and Clay Minerals, 7 317-327.

180. Melka, K. and J. Konta. 1973. X-ray Intensities of Muscovite, Kaolinite and Quartz of Various Size Fractions. Proceedings of the 4th International Clay Conference, 1972, Madrid, 817-825.

181. Meunier, A. and B. Velde. 1979. Weathering Mineral Facies in Altered Granites: the Importance of Local Small Scale Equilibria. Mineralogical Magazine, 43 261-268.

182. Millot, G. 1970. The Geology of Clays. xvi+429pp. Chapman and Hall, London.

183. Mitchell, W.A. 1960. A Method for Quantitative Mineralogical Analysis by X-ray Powder Diffraction. Mineralogical Magazine, 32 492-499.

184. Mohr, P.A. 1956. Trace Element Distribution in a Garnet-chlorite Rock from Foel Ddu, near Harlech, Merionethshire. Mineralogical Magazine, 31 (235) 319-327.

185. Moore, C.A. 1968. Quantitative Analysis of Naturally Occurring Multicomponent Mineral Systems by X-ray Diffraction. Clays and Clay Minerals, 16 325-336.

186. Moreira-Nordemann, L.M. 1980. Use of $^{234}U/^{238}U$ Disequilibrium in Measuring Chemical Weathering Rate of Rocks. Geochimica et Cosmochimica Acta, 44 103-108.

187. Morris, M.C., H.F. McMurdie, E.H. Evans, B. Paretzkin, J.H. De Groot, C.R. Hubbard and S.J. Carmel. 1979. Standard X-ray Diffraction Powder Patterns. United States Bureau of Standards Monograph, 25 (16).

188. Murad, E. and W.R. Fischer. 1978. Mineralogy and Heavy Metal Contents of Soils and Stream Sediments in a Rural Region of Western Germany. Geoderma, 21 133-145.

189. Naga, M.A., S.I. Abdel-Aal, I. Hosny and R.R. Shahin. 1977. Biotite Dissolution by Complexing Organic Acids. Egyptian Journal of Soil Science, 17 (2) 143-159.

190. Nanz, R.H. 1953. Chemical Composition of Pre-Cambrian Slates with Notes on the Geochemical Evolution of Lutites. Journal of Geology, 61 51-64.

191. Nelson, C.S. and R.H.A. Cochrane. 1970. A Rapid X-ray Method for the Quantitative Determination of Selected Minerals in Fine-grained and Altered Rocks. Tane, 16 151-162.

192. Nettleton, W.D., K.W. Flach and R.E. Nelson. 1970. Pedogenic Weathering of Tonalite in Southern California. Geoderma, 4 387-402.

193. Nicholls, G.D. 1962. A Scheme for Recalculating the Chemical Analyses of Argillaceous Rocks for Comparative Purposes. American Mineralogist, 47 (1+2) 34-46.

194. Nixon, R.A. 1979. Differences in Incongruent Weathering of Plagioclase and Microcline - Cation Leaching Versus Precipitates. Geology, 7 221-224.

195. Norrish, K. 1973. Factors in the Weathering of Mica to Vermiculite. Proceedings of the 4th International Clay Conference, 1972, Madrid, 83-101.

196. Norrish, K. and R.M. Taylor. 1962. Quantitative Analysis by X-ray Diffraction. Clay Minerals Bulletin, 5 98-109.

197. Nuhfer, E.B. 1981. Mudrock Fabrics and Their Significance - Discussion. Journal of Sedimentary Petrology, 51 1027-1029.

198. Odom, J.W. and P.F. Low. 1978. Relation between Swelling, Surface Area and b Dimension of Na-Montmorillonites. Clays and Clay Minerals, 26 (5) 345-351.

199. Oinuma, K. and K. Kobayashi. 1961. Problems of Rapid Clay Mineralogical Analysis of Sedimentary Rocks. Clay Science, 1 (1+2) 8-15.

200. Park, R.G. and G.C. Lewis 1969. Electrophoretic Separation and Fractionation of Clay Minerals. American Mineralogist, 54 1473-1476.

201. Park, R.G. and G.C. Lewis. 1971. Electrophoretic Separation of an Inorganic Amorphous Material from the Less Than 0.2μm Fraction of a Soil Clay Mixture. American Mineralogist, 56 603-612.

202. Parker, M. 1979. Personal Communication.

203. Pauling, L. 1930. The Structure of the Chlorites. Proceedings of the National Academy of Sciences, 16 578-582.

204. Petrović, R. 1976. Rate Control in Feldspar Dissolution - II. The Protective Effect of Precipitates. Geochimica et Cosmochimica Acta, 40 1509-1521.

205. Petruk, W. 1964. Determination of the Heavy Atom Content in Chlorite by Means of the X-ray Diffractometer. American Mineralogist, 49 (1+2) 61-71.

206. Pettijohn, F.J. 1975. Sedimentary Rocks, 3rd edition. 628pp. Harper and Row, New York. ISBN 0-06-045191-2.

207. Pollard, L.D. and C.E. Weaver. 1973. The Chemistry of Clay Minerals. Developments in Sedimentology, 15. 213pp. Elsevier Scientific, Amsterdam. ISBN 0-444-41043-0.

208. Post, J.L. and N.C. Janke. 1974. Properties of "Swelling" Chlorite in Some Mesozoic Formations of California. Clays and Clay Minerals, 22 67-77.

209. Potter, P.E., J.B. Maynard and W.A. Pryor. 1980. Sedimentology of Shale. Study Guide and Reference Source. 306pp. Springer-Verlag, New York. ISBN 0-387-90430-1.

210. Price, F.R. 1979. Personal Communication.

211. Quigley, R.M. and A. Dreimanis. 1972. Weathered Interstadial Green Clay at Port Talbot, Ontario. Canadian Journal of Earth Sciences, 9 991-1000.

212. Quirk, J.P. and J.H. Chute. 1968. Potassium Release from Mica-like Clay Minerals. Proceedings of the 9th International Congress of Soil Science, Adelaide, 2 671-681.

213. Rai, D. and W.T. Franklin. 1978. Effect of Moisture Content on Ethylene Glycol Retention by Clay Minerals. Geoderma, 21 (1) 75-79.

214. Rausell-Colom, J.A., T.R. Sweatman, C.B. Wells and K. Norrish. 1965. Studies in the Artificial Weathering of Mica. 40-72 in E.G. Hallsworth and D.V. Crawford, editors: Experimental Pedology.

215. Rawson, R.A.G. 1969. A Rapid Method for Determining the Surface Area of Aluminosilicates from the Adsorption Dynamics of Ethylene Glycol Vapour. Journal of Soil Science, 20 (2) 325-335.

216. Reesman, A.L. 1978. Extrapolation of Aqueous Dissolution Data to Determine Comparative Free Energies of Formation ($C\Delta G_f°$), and Relative Mineral Stabilities. Clays and Clay Minerals, 26 (3) 217-226.

217. Renouprez, A. 1970. Small Angle Scattering of X-rays. 361-367 in D.H. Everett and R.H. Ottewill, editors: Surface Area Determination.

218. Reynolds, R.C. 1980. Interstratified Clay Minerals. 249-303 in Brindley, G.W. and G. Brown [40].

219. Rezk, M.M.A.A. 1975. Studies on Chlorite in Soils Derived from Silurian Rocks in Denbighshire. Unpublished Ph.D. Thesis, University College of North Wales, Bangor.

220. Roaldset, E. 1972. Mineralogy and Geochemistry of Quaternary Clays in the Numedal Area, Southern Norway. Norsk Geologisk Tidsskrift, 52 (4) 335-369.

221. Robinson, D., R.A. Nicholls and L.J. Thomas. 1980. Clay Mineral Evidence for Low-grade Caledonian and Variscan Metamorphism in South-western Dyfed, South Wales. Mineralogical Magazine, 43 857-863.

222. Rogers, J.J.W., W.C. Kreuger and M. Krog. 1963. Sizes of Naturally Abraded Materials. Journal of Sedimentary Petrology, 33 (3) 628-632.

223. Ross, G.J. 1967. Kinetics of Acid Dissolution of an Orthochlorite Mineral. Canadian Journal of Chemistry, 45 3031-3034.

224. Ross, G.J. 1968. Structural Decomposition of an Orthochlorite during Its Acid Dissolution. Canadian Mineralogist, 9 522-530.

225. Ross, G.J. 1969. Acid Dissolution of Chlorites: Release of Magnesium, Iron and Aluminium and Mode of Acid Attack. Clays and Clay Minerals, 17 347-354.

226. Ross, G.J. 1975. Experimental Alteration of Chlorites into Vermiculites by Chemical Oxidation. Nature, 255 133-134.

227. Ross, G.J. and H. Kodama. 1974. Experimental Transformation of a Chlorite into a Vermiculite. Clays and Clay Minerals, 22 205-211.

228. Salyn, A.L. and V.A. Drits. 1973. On the Method of X-ray Quantitative Phase Analysis of Clays. Proceedings of the 4th International Clay Conference, 1972, Madrid, 797-806.

229. Sawhney, B.L. 1977. Interstratification in Layer Silicates. 405-434 in Dixon, J.B. and S.B. Weed [75].

230. Schoen, R. 1962. Semiquantitative Analysis of Chlorites by X-ray Diffraction. American Mineralogist, 47 (11+12) 1384-1392.

231. Schofield, R.K. 1949. Calculation of Surface Areas of Clays from Measurements of Negative Adsorption. Transactions of the British Ceramic Society, 48 207-213.

232. Schultz, L.G. 1964. Quantitative Interpretation of Mineralogical Composition from X-ray and Chemical Data for the Pierre Shale. United States Geological Survey Professional Paper, 391-C 1-31.

233. Schulze, D.G. and J.B. Dixon. 1979. High Gradient Magnetic Separation of Iron Oxides and Other Magnetic Minerals from Soil Clays. Journal of the Soil Science Society of America, 43 (4) 793-799.

234. Scott, A.D. 1968. Effect of Particle Size on Interlayer Potassium Exchange in Micas. Proceedings of the 9th International Congress of Soil Science, Adelaide, 2 649-660.

235. Seyfried, W.E. Jr. and J.L. Bischoff. 1979. Low Temperature Basalt Alteration by Seawater: an Experimental Study at 70°C and 150°C. Geochimica et Cosmochimica Acta, 43 1937-1947.

236. Shaw, D.B. and C.E. Weaver. 1965. The Mineralogical Composition of Shales. Journal of Sedimentary Petrology, 35 213-222.

237. Short, N.M. 1961. Geochemical Variations in Four Residual Soils. Journal of Geology, 69 (5) 534-571.

238. Siever, R. and N. Woodford. 1979. Dissolution Kinetics and the Weathering of Mafic Minerals. Geochimica et Cosmochimica Acta, 43 717-724.

239. Smalley, I.J. and C. Vita-Finzi. 1968. The Formation of Fine Particles in Sandy Deserts and the Nature of Desert Loess. Journal of Sedimentary Petrology, 38 (3) 766-774.

240. Smith, J.V. and H.S. Yoder. 1956. Experimental and Theoretical Studies of the Mica Polymorphs. Mineralogical Magazine, 31 209-235.

241. Smith, K. 1977. Catchment Area Experiments at Plynlimon. Water Services, 81 394-401.

242. Spyridakis, D.E., G. Chesters and S.A. Wilde. 1967. Kaolinization of Biotite as a Result of Coniferous and Deciduous Seedling Growth. Proceedings of the Soil Science Society of America, 31 203-210.

243. Srodon, J. 1984. X-ray Powder Diffraction Identification of Illitic Materials. Clays and Clay Minerals, 32 (5) 337-349.

244. Stewart, V.I., W.A. Adams and H.H. Abdulla. 1970. Quantitative Pedological Studies on Soils Derived from Silurian Mudstones. I. The Parent Material and the Significance of the Weathering Process. Journal of Soil Science, 21 (2) 242-247.

245. Stewart, V.I., W.A. Adams and H.H. Abdulla. 1970. Quantitative Pedological Studies on Soils Derived from Silurian Mudstones. II. The Relationship between Stone Content and the Apparent Density of the Fine Earth. Journal of Soil Science, 21 (2) 248-255.

246. Sulaiman, I. and W.E. Worrall. 1982. The Separation and Characterisation of the Micaceous Constituent of Sedimentary Clays. Transactions and Journal of the British Ceramic Society, 81 (4) 114-116.

247. Tsuzuki, Y. and K. Suzuki. 1980. Experimental Study of the Alteration Process of Labradorite in Acid Hydrothermal Solutions. Geochimica et Cosmochimica Acta, 44 673-683.

248. Van Olphen, H. 1970. Determination of Surface Areas of Clays - Evaluation of Methods. 255-269 in D.H. Everett and R.H. Ottewill, editors: Surface Area Determination.

249. Van Olphen, H. 1977. An Introduction to Clay Colloid Chemistry, 2nd edition. 318pp. John Wiley, New York. ISBN 0-471-01463-X.

250. Vedder, W. 1964. Correlations between Infrared Spectrum and Chemical Composition of Mica. American Mineralogist, 49 (5+6) 736-768.

251. Velde, B. 1965. Experimental Determination of Muscovite Polymorph Stabilites. American Mineralogist, 50 (3+4) 436-449.

252. Velde, B. and J. Hower. 1963. Petrological Significance of Illite Polymorphism in Palaeozoic Sedimentary Rocks. American Mineralogist, 48 (11+12) 1239-1254.

253. Verstraten, J.M. 1980. Water-rock Interaction. A Case Study in a Very Low Grade Metamorphic Shale Catchment in the Ardennes, NW Luxembourg. British Geomorphological Research Group Research Monograph, 2. 243pp. Geo Abstracts, Norwich. ISBN 0-86094-042-X.

254. Vita-Finzi, C. and I.J. Smalley. 1970. Origin of Quartz Silt: Comments on a Note by Ph. H. Kuenen. Journal of Sedimentary Petrology, 40 1367-1368.

255. Walker, G.F. 1975. Vermiculites. 155-189 in Gieseking, J.E. [105].

256. Walker, P.H. and J. Hutka. 1979. Size Characteristics of Soils and Sediments with Special Reference to Clay Fractions. Australian Journal of Soil Research, 17 383-404.

257. Waylen, M.J. 1979. Chemical Weathering in a Drainage Basin Underlain by Old Red Sandstone. Earth Surface Processes, 4 167-178.

258. Weaver, C.E. 1958. The Effects and Geologic Significance of Potassium "Fixation" by Expandable Clay Minerals Derived from Muscovite, Biotite, Chlorite and Volcanic Material. American Mineralogist, 43 (9+10) 839-861.

259. Weaver, C.E. 1960. Possible Uses of Clay Minerals in Search for Oil. Bulletin of the American Association of Petroleum Geologists, 44 (9) 1505-1518.

260. Weaver, C.E. 1960. Possible Uses of Clay Minerals in Search for Oil. Clays and Clay Minerals, 8 214-227.

261. Weaver, C.E. 1980. Fine-grained Rocks: Shales or Physilites. Sedimentary Geology, 27 301-313.

262. Weaver, R.M., M.L. Jackson and J.K. Syers. 1971. Magnesium and Silicon Activities in Matrix Solutions of Montmorillonite-containing Soils in Relation to Clay Mineral Stability. Proceedings of the Soil Science Society of America, 35 823-830.

263. Weber, K. 1972. Notes on Determination of Illite Crystallinity. Neues Jahrbuch für Mineralogie Monatschefte, 267-276.

264. Wells, C.B. and K. Norrish. 1968. Accelerated Rates of Release of Interlayer Potassium from Micas. Proceedings of the 9th International Congress of Soil Science, Adelaide, 2 683-694.

265. White, A.F. and H.C. Claassen. 1979. Dissolution Kinetics of Silicate Rocks - Application to Solute Modeling. 447-473 in E.A. Jenne, editor: Chemical Modeling in Aqueous Systems. American Chemical Society Symposium Series, 93.

266. White, A.F. and H.C. Claassen. 1980. Kinetic Model for the Short-term Dissolution of a Rhyolitic Glass. Chemical Geology, 28 (1+2) 91-109.

267. White, J.L., R.D. Bronson and G.W. Bailey. 1961. X-ray Diffraction Method for Determination of the Degree of Weathering of Micaceous Clay Minerals in Soils. Acta Universitatis Carolinae Geologica Supplementum, 1 351-359.

268. White, R.W. and C. Sarcia. 1978. Natural and Artificial Weathering of Basalt, Northwestern United States. Bulletin du Bureau de Recherches Geologiques et Minières, 2 (1) 1-29.

269. Wilson, M.J., D.C. Bain and W.J. McHardy. 1971. Clay Mineral Formation in a Deeply-weathered Boulder Conglomerate in North-east Scotland. Clays and Clay Minerals, 19 345-352.

270. Winer, B.J. 1971. Statistical Principles in Experimental Design, 2nd edition. 907 pp. McGraw-Hill Kogakusha, Tokyo. ISBN 0-07-070981-5.

271. Yaalon, D.H. 1962. Mineral Composition of the Average Shale. Clay Minerals Bulletin, 5 (27) 31-36.

272. Yaalon, D.H., I. Brenner and K. Koyumdjisky. 1974. Weathering and Mobility Sequence of Minor Elements on a Basaltic Pedomorphic Surface, Galilee, Israel. Geoderma, 12 233-244.

273. Yamasaki, K., C. Iida and H. Yokoi. 1955. A Spectrographic Determination of the Distribution of Trace Elements in a Granodiorite and in Its Weathering Products. Journal of Earth Sciences, Nagoya University, 3 (1) 58-64.

274. Yoder, H.S. and H.P. Eugster. 1955. Synthetic and Natural Muscovites. Geochimica et Cosmochimica Acta, 8 225-280.